

**NASA TECHNICAL  
MEMORANDUM**

**NASA TM X-64726**

**LARGE SPACE TELESCOPE  
PHASE A FINAL REPORT**

**Volume II — Mission Description and System  
Design Characteristics**

**By Program Development**

**December 15, 1972**

**CASE FILE  
COPY**

**NASA**

*George C. Marshall Space Flight Center  
Marshall Space Flight Center, Alabama*

## DOCUMENT CONTENTS

### Volume I – Executive Summary

- Chapter I – Introduction
- Chapter II – Mission Analysis
- Chapter III – LST Configuration and Systems Design
- Chapter IV – Maintenance Analysis
- Chapter V – Conclusions and Recommendations

### Volume II – Mission Description and System Design Characteristics

- Chapter I – Scientific Uses of the LST
- Chapter II – Phase A Study Approach
- Chapter III – Mission Analysis
- Chapter IV – LST Configuration and System Design
- Chapter V – Configurations and System Alternatives
- Chapter VI – Interfaces
- Chapter VII – Low Cost Considerations
- Chapter VIII – Program Implementation
- Chapter IX – Conclusions and Recommendations
- Appendix A – Alternate LST Structural Design Employing Graphite/Epoxy Shells
- Appendix B – Solar System Observations
- Appendix C – LST Configuration Concept Comparison

### Volume III – Optical Telescope Assembly

- Section A – Introduction
- Section B – System Considerations
- Section C – System Design

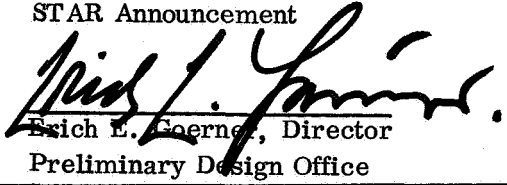
### Volume IV – Scientific Instrument Package

- Section 1 – Introduction
- Section 2 – General Scientific Objectives
- Section 3 – SIP System Analysis
- Section 4 – Scientific Instrumentation
- Section 5 – Ancillary Subsystems
- Section 6 – Imaging Photoelectric Sensors
- Section 7 – Environmental Considerations of the Scientific Instrumentation Design
- Section 8 – Scientific Instrument Package Physical Description
- Section 9 – Interface Considerations
- Section 10 – Reliability and Maintainability
- Section 11 – Program Planning
- Appendix A – Resolvable Element Size vs Pointing Parametric Analysis
- Appendix B – Signal-to-Noise Ratio

### Volume V – Support Systems Module

- Chapter I – Configuration and System Design
- Chapter II – Structures
- Chapter III – Thermal Control System
- Chapter IV – Electrical System
- Chapter V – Communication and Data Handling
- Chapter VI – Attitude Control System
- Chapter VII – Maintainability Analyses
- Chapter VIII – Reliability Analysis
- Chapter IX – Conclusions
- Appendix A – LST Contamination Control
- Appendix B – Scientific Data Gathering Efficiency
- Appendix C – Derivation of Optimum Readout Bandwidth for Preamplifier of SEC Vidicon

TECHNICAL REPORT STANDARD TITLE PAGE

1. REPORT NO. TM X- 64726	2. GOVERNMENT ACCESSION NO.	3. RECIPIENT'S CATALOG NO.	
4. TITLE AND SUBTITLE Large Space Telescope Phase A Final Report Volume II - Mission Description and System Design Characteristics		5. REPORT DATE December 15, 1972	6. PERFORMING ORGANIZATION CODE
		8. PERFORMING ORGANIZATION REPORT #	
7. AUTHOR(S) By Program Development		10. WORK UNIT NO.	
9. PERFORMING ORGANIZATION NAME AND ADDRESS  George C. Marshall Space Flight Center Marshall Space Flight Center, Alabama 35812		11. CONTRACT OR GRANT NO.	
		13. TYPE OF REPORT & PERIOD COVERED  Technical Memorandum	
12. SPONSORING AGENCY NAME AND ADDRESS  National Aeronautics and Space Administration Washington, D.C. 20546		14. SPONSORING AGENCY CODE	
15. SUPPLEMENTARY NOTES  Prepared by Program Development			
16. ABSTRACT <p>This document is a report of the Phase A study of the Large Space Telescope (LST). The study defines an LST concept based on the broad mission guidelines provided by the Office of Space Science (OSS), the scientific requirements developed by OSS with the scientific community, and an understanding of long range NASA planning current at the time the study was performed.</p> <p>The LST is an unmanned astronomical observatory facility, consisting of an optical telescope assembly (OTA), scientific instrument package (SIP), and a support systems module (SSM). The report consists of five volumes: Volume I is an executive summary, Volume II is a summary of the entire report, and Volumes III, IV, and V contain the analyses and conceptual designs of the OTA, SIP, and SSM, respectively. The report describes the constraints and trade off analyses that were performed to arrive at a reference design for each system and for the overall LST configuration.</p> <p>The LST will be launched into low earth orbit by the Space Shuttle and operated for 10 to 15 years. The Shuttle will also be used to maintain the LST and to update the scientific instrument complement. Several maintenance modes have been investigated, including on-orbit pressurization of the SSM to provide a shirtsleeve environment for maintenance, and earth return of the LST.</p> <p>The LST will provide the scientific community with several fundamentally unique capabilities which will permit the acquisition of new and important observational data. Its location in space permits observations over the entire spectrum from about 100 nm to the far infrared.</p> <p>A low cost design approach was followed in the Phase A study. This resulted in the use of standard spacecraft hardware, the provision for maintenance at the black box level, growth potential in systems designs, and the sharing of Shuttle maintenance flights with other payloads.</p>			
17. KEY WORDS Large Space Telescope Scientific Satellite Astronomy Payload High Resolution Astronomy Faint Object Detection Conceptual Satellite Design Shuttle Maintenance Spacecraft		18. DISTRIBUTION STATEMENT STAR Announcement  Erich E. Goerner, Director Preliminary Design Office	
19. SECURITY CLASSIF. (of this report) Unclassified	20. SECURITY CLASSIF. (of this page) Unclassified	21. NO. OF PAGES 632	22. PRICE NTIS

## LIST OF ACRONYMS

A/D	analog to digital
ACN	Ascension Island (tracking station)
ACS	attitude control system
AFO	Announcement for Flight Opportunity
AGC	automatic gain control
AGO	Santiago, Chili (tracking station)
ALU	arithmetic logic unit
AM	airlock module
AOS	acquisition of signal
APP	antenna position programmer
ASCS	attitude sensing and control system
ASR	automatic send/receive
ASTAM	automated system test and monitor
ATM	Apollo Telescope Mount
ATS	Applications Technology Satellite
AVE	Mojave, California (tracking station)
BDA	Bermuda (tracking station)
BECO	Teledyne-Brown Engineering Company
BER	bit error rate
BITE	built-in test equipment
BOL	beginning of life
BOM	basic operating module
BUR	Johannesburg, South Africa (tracking station)
C&DH	communications and data handling

## LIST OF ACRONYMS (Continued)

C&DHS	communications and data handling system
C&W	caution and warning
CAM	computer address matrix
CCD	charge couple device
CCS	contamination control system
CDR	critical design review
CG, C.G.	center of gravity
CMG	control moment gyro
CMOS	complementary metal oxide semiconductor
CPU	central processor unit
CRO	Carnarvon (tracking station)
CSS	coarse sun sensor
CTU	command and telemetry unit
CYI	Canary Islands (tracking station)
D/A	digital to analog
DAU	data acquisition unit
DDT&E	design, development, test, and engineering
DEA	drive electronics assembly
DG	double gimbal
DGCMG	double gimbal CMG
DOD	depth of discharge
DPA	digital processor assembly
DSIF	Deep Space Instrumentation Facility
DTPL	domain tip propagation logic

## LIST OF ACRONYMS (Continued)

DTU	data transmission unit
ECA	electrical control assembly
EC/LSS	environmental control/life support system
EDS	electrical distribution subsystem
EDU	electrical distribution unit
EIRP	effective isotropic radiated power
EM, em	electromagnet; engineering model
EMC	electromagnetic control
EMI	electromagnetic interference
EOL	end of life
EOM	end of mission
EPS	electrical power subsystem
ERTS	Earth Resources Technology Satellite
ESE	electrical support equipment
ETC	Engineering Training Center, Greenbelt, Maryland
EVA	extravehicular activity
EVLSS	extravehicular life support system
FGS	fine guidance system
FHST	fixed-head star tracker
FM	frequency modulated
FMEA	failure mode effects analysis
FOV	field of view
FRUSA	flexible, rollup solar array
FST	fixed star tracker

## LIST OF ACRONYMS (Continued)

GAC	Grumman Aerospace Corporation
GDN	ground data network
GDSX	Goldstone (tracking station)
GESE	ground electrical support equipment
ghu	gyro hang-up
GMT	Greenwich mean time
GRARR	Goddard range and range rate
GSE	ground support equipment
GSFC	Goddard Space Flight Center
GST	gimbaled star tracker
GWM	Guam (tracking station)
HAW	Hawaii (tracking station)
HEAO	High Energy Astronomy Observatory
HEPA	high efficiency particulate air
HPI	high performance insulation
HSK	Honeysuckle Creek, Australia (tracking station)
I/O	input/output
I. D.	inside diameter
IESE	in-space electrical support equipment
IOCC	integrated operations control console
IOP	in the orbit plane
ISA	interstage adapter; interface systems adapter
IVA	intravehicular activity
LCP	left circular polarized
LOHARR	Lockheed heat rate program
LOS	line of sight

## LIST OF ACRONYMS (Continued)

LSI	large scale integration
LST	Large Space Telescope
MAC	maximum allowable concentration
MAD	Madrid, Spain (tracking station)
MCC	mission control center
MCF	Mating/Checkout Facility
MIB	minimum impulse bit
MIL	Merritt Island, Florida (tracking station)
MMS	micrometeoroid shell
MNOS	metal nitride oxide silicon
MOJAVE	tracking station at Barstow
MOS/LSI	metal oxide semiconductor/large-scale integrated
MSFC	Marshall Space Flight Center
MSFN	Manned Space Flight Network
MSS	magnetometer sensing system
MT	magnetic torquer
MTBF	mean time between failures
MTE	magnetic torquer electronics
MTF	modulation transfer function
MTS	magnetic torquing system
MTU	magnetic tape unit
NASCOM	National Aeronautics and Space Administration Communications Network
NASO	National Astronomical Space Observatory
NDRO	nondestructive readout
NEA	noise equivalent angle



## LIST OF ACRONYMS (Continued)

NFL	St. John's, Newfoundland (tracking station)
OAAR	other activities as required
OAO	Orbiting Astronomical Observatory
OAS	Orbit Adjust Stage
OMS	orbit maneuvering system
OOC	observatory operation center
ORRX	Orroral Valley (tracking station)
OSR	optical solar reflector
OTA	optical telescope assembly
OWS	Orbital Workshop
PCM	phase change material; pulse code modulator
PCS	peripheral communication system
PCU	power converter unit
PDR	preliminary design review
PEP	perpendicular to the ecliptic plane
PGA	pressure garment assembly
PM	pulse modulated
POP	perpendicular to the orbit plane
PRR	preliminary requirements review
PSD	power spectral density
PSK	phase shift keyed
PSU	power switch unit
QUI	Quito, Equador (tracking station)
R&D	research and development
RAM	research applications module (studies); reference alignment mode

## LIST OF ACRONYMS (Continued)

RBV	return beam vidicon
RCD	remote command decoder
RCP	right circular polarized
RCS	reaction control system
REC	recurring costs
RF	radio frequency
RFI	radio frequency interference
RGA	reference gyro assembly
ROM	read-only-memory
ROS, ROSMAN	tracking station at Rosman, North Carolina
RSDP	remote site data processor
RTV	room temperature vulcanizing
RW	reaction wheel
SAA	South Atlantic anomaly
SBU	sensor buffer unit
SCAMA	switching, conferencing, and monitoring arrangement
SEC	secondary electron conduction
SFP	solicitation for proposal
SG	single gimbal
SGCMG	single gimbal CMG
SI	science instrument
SIP	scientific instrument package
SIT	silicon intensified target
SMS	secondary mirror sensor
SPD	solar power distributor

## LIST OF ACRONYMS (Continued)

SPEH	special purpose equipment handler
SPF	single-point failure
SPG	single-point ground
SSM	support systems module
SSP	Space Station prototype
STADAN	Space Tracking and Data Acquisition Network
STDN	Spaceflight Tracking and Data Network
2-SPEED	two scissored pair ensemble explicit distribution
TA	transfer assembly
TACS	thrust attitude control system
TAN	Tananarive, Malagasy Republic (tracking station)
TBC	The Boeing Company
TCS	thermal control system
TDRS	tracking and data relay satellite (network)
TEX	Corpus Christi, Texas (tracking station)
TMR	triple modular redundancy
TOOMBA	tracking station at Cooby Creek
TRW	TRW Systems, Incorporated
TTY	teletypewriter
TWT	traveling wave tube
ULA	Fairbanks, Alaska (tracking station)
UPD	update buffer
USB	unified S-band
USBE	unified S-band equipment
VAB	Vertical Assembly Building
VGP	vehicle ground point

## LIST OF ACRONYMS (Concluded)

VPM	variable permanent magnet
W-R	Wolf-Rayet
WASS	wide angle sun sensor
WFE	wavefront error
WNK	Winkfield, United Kingdom (tracking station)
XPDR	transponder

# INTRODUCTION

The Large Space Telescope (LST) is a 3-m aperture, near-diffraction-limited optical telescope which will be operated in earth orbit. The major elements of the LST are (1) the optical telescope assembly (OTA), which consists of the mirrors and other components of the telescope itself; (2) the scientific instrument package (SIP), which consists of the detectors at the focus of the telescope that record images and spectral data; and (3) the support systems module (SSM), which consists of the systems that are required to make the LST an unmanned, remotely operated spacecraft.

The Phase A report has been prepared in five volumes. The OTA and the SIP were studied under contract by Itek Optical Systems Division, Lexington, Mass., and by Kollsman Instrument Corporation, Long Island, New York, respectively, and are covered in detail in Volume III (OTA) and Volume IV (SIP). Volume I is an executive summary and Volume V is devoted exclusively to the SSM. Volume II is a summary of the other volumes, containing descriptions of the major elements and their components. It also contains the most detailed descriptions available of the interfaces between the LST elements and between the LST and the launch vehicle.

Volume II also contains information not presented elsewhere, such as descriptions of alternative system designs and approaches that were investigated in tradeoff studies to arrive at the present LST reference design; mission analysis and results such as orbit selection, launch vehicle performance, and ground contact opportunities; OTA light shield trade studies; instrument alignment tolerances; low cost considerations; and programmatic.

Maintenance mode analysis results are also presented in Volume II. On-orbit and return to earth maintenance modes have been considered. On-orbit maintenance alternatives included pressurization of the SSM to provide a shirt sleeve atmosphere for maintenance and the use of the Shuttle manipulators and other remote operating equipment for component and instrument replacement, with no pressurization of the SSM.

## CHAPTER I. SCIENTIFIC USES OF THE LST



# TABLE OF CONTENTS

	Page
A. Introduction .....	I-1
B. Scientific Objectives .....	I-1
1. Variation of Hubble Constant With Distance .....	I-1
2. Stellar Masses .....	I-2
3. Quasars, Seyfert Galaxies, and Peculiar Galaxies .....	I-3
4. Characteristics of Stellar Chromospheres and Coronae .....	I-3
5. Details of Intergalactic Medium .....	I-4
6. Globular Clusters and Nearby Galaxies .....	I-4
7. Distribution and Features of Matter in Interstellar Space .....	I-6
8. Star Formation .....	I-8
9. Planetary Nebulae and Wolf-Rayet-Type Stars .....	I-9
10. Optical Observations of X-ray Sources, Pulsars, and Neutron Stars .....	I-11
11. Detailed Studies of Planets .....	I-12
12. Studies of Asteroids, Comets, and Other Small Bodies .....	I-13
13. Helium-Rich Stars .....	I-15
14. Studies of Variable Stars .....	I-16
15. Infrared Studies of Stars and Galaxies .....	I-17
C. Instrument Growth Capability .....	I-17
D. Role of Principle Investigator (PI) Astronomers .....	I-18
E. Role of LST and Ground-Based Astronomy .....	I-19
REFERENCES .....	I-21
BIBLIOGRAPHY .....	I-23



# CHAPTER I. SCIENTIFIC USES OF THE LST

## A. Introduction

The LST provides the scientific community with several fundamentally unique capabilities which allow the acquisition of new and important observational data. Its location in space allows observations over the entire spectrum from about  $1000 \text{ \AA}$  to about  $5\mu$ . This represents roughly a sixfold increase in the continuous window available from earth. In addition the earth constraints on faint object detection and image resolution, which are atmospheric seeing and sky background brightness, are removed and much improved, respectively. Thus, the LST offers all of the observational advantages of a large aperture instrument operating at true diffraction-limited performance over a very large bandwidth.

Astronomy still is basically an empirical science, dependent on observations and the analysis and interpretation of new data. As such, it is therefore largely a science of discovery, development of new theories which fit and explain observations, and significant revisions to existing theories and concepts. In this context, it is to be expected that the observation targets of most interest, the type of data to be obtained, and the subsequent analysis process to be applied will vary a great deal over the lifetime of the LST. In part, the direction these variations will take will be dependent on the results of initial LST observations.

To illustrate the ways in which the LST can aid the advance of astronomical knowledge, several areas which are currently of high scientific interest are briefly discussed in the following sections. The areas chosen for discussion are not ordered by any criteria of importance, nor are they a complete list of current significant problems.

## B. Scientific Objectives

1. Variation of Hubble Constant With Distance. The spectra of distant galaxies are shifted toward the red, the amount of redshift being greater for the more distant objects. As far as is now known, the relation between redshift and distance is linear; the proportionality constant is known as the Hubble constant. The only physical mechanism now known that can produce the observed redshifts is Doppler shifting caused by relative recessional velocities of the galaxies. The Hubble constant is therefore expressed in units of velocity per unit of distance; generally, in kilometers per sec per megaparsec.

A question of the "constancy" of the Hubble constant arises in another connection. Some cosmological models predict an observed deceleration at very great distances, and different models predict different decelerations. No measurable deceleration has yet been found, but sufficient spectra have not yet been obtained for galaxies at the distances where the theories predict that deceleration begins. The ability of the LST to obtain high-dispersion, high-resolution spectra of very distant galaxies presents an opportunity to determine a value for the deceleration parameter.

The data required for calculation of the Hubble constant by the classical method are measured redshift values in the spectra of galaxies whose distances can be determined. The distances of such remote objects cannot be determined directly and may be found by measuring the apparent magnitude of each galaxy and assuming that its absolute magnitude is equal to the value most commonly possessed by galaxies having similar properties and known distances. The proper amount of correction for interstellar absorption is usually uncertain; therefore, the distance determination may be distorted for that reason also.

Ground-based spectrographs using image tubes can now achieve dispersions of 200 Å/mm or better for observations of faint galaxy spectra on a fairly routine basis [I-1]. "Faint" here signifies apparent magnitudes of the order of 15. LST dispersions should be at least as good.

2. Stellar Masses. It has been known [I-2] that the measured masses of stars are well correlated with their luminosities. The observed relationship, called the empirical mass-luminosity relation, is used to estimate masses of stars from their measured magnitudes. The luminosity in this relation is bolometric luminosity; i. e., the luminosity of a star over its entire spectral range. Only a portion of the stellar spectrum can be observed from the earth; therefore, the bolometric luminosity must be estimated by fitting the observed spectrum to a blackbody curve for the temperature which best represents the properties of the stellar atmosphere.

The fitting process could be done with more certainty if the observable spectral range could be extended. LST instruments will be capable of observing in the ultraviolet and near infrared, thus providing this extension. The observations required would be low to medium dispersion spectra or narrowband photometry in the ultraviolet and infrared, and some observations in the visible wavelength range for calibration and comparison with earlier ground-based data.

3. Quasars, Seyfert Galaxies, and Peculiar Galaxies. In recent years, interest existed in extragalactic objects that appear to be much more luminous than normal galaxies. These objects include quasars, Seyfert galaxies, exploding galaxies, radio galaxies, and X-ray galaxies. These objects are characterized by high nonthermal luminosities in the radio, infrared, and X-ray regions.

Quasars have been under intensive observational and theoretical study ever since their discovery in 1963. A large fraction of their radiation is emitted at radio and X-ray wavelengths, although spectral features are observed only in the optical region. These features are the most important measurable quantities for determining densities, temperatures, and other physical conditions. Because of the weak optical emission, high-resolution spectrograms of the fainter quasars cannot presently be obtained. It will be very useful to obtain spectra in the infrared region to which many of the lines normally in the visible region will be redshifted. Observations by the LST will be the only means to obtain these high-sensitivity measurements.

In 1943, Seyfert described a class of galaxies which appeared to separate them from other galaxies known at that time. They are characterized by bright, condensed nuclei which have broad emission lines.

Radio galaxies and the recently discovered X-ray galaxies are other examples of unusual galaxies which will be the subject of extensive studies in the future. The ability of the LST to obtain detailed spectroscopic and high-resolution image data on these objects of low surface brightness will give astronomers a unique chance to determine the origin and evolution of these objects.

4. Characteristics of Stellar Chromospheres and Coronae. Evidence of stellar chromospheres and coronae is obtained almost entirely from spectral studies. Generally speaking, the presence of both is indicated by emission lines in the stellar spectrum; chromospheric emission is usually from neutral or singly-ionized atoms, and coronal emission comes from highly-ionized atoms.

Prominent chromospheric stellar lines lie in the visible, the ultraviolet, and the near infrared wavelength ranges. Certain specific lines are considered to be indicators of chromospheric structure; this list may be extended in the future. Knowledge of stellar chromospheres is still incomplete, and detailed spectral studies offer the possibility of adding a great deal of information. Chromospheric studies require observations of stellar spectra over the entire spectral range available to LST. The dispersion should be

very high to permit detection of as many lines as possible, and the spectral resolution should also be very high to permit a chance of measuring the profiles of strong lines. Spectral line asymmetries and displacements should be measured if possible.

5. Details of Intergalactic Medium. The question of the existence of very large amounts of very diffuse matter distributed throughout intergalactic space has not yet been settled. The presence of such widely spread, diffuse material has been suggested for theoretical reasons. Based on our present knowledge, additional mass beyond what can be accounted for is required to stabilize clusters of galaxies. There is no direct observational evidence for the presence of such material.

Lyman- $\alpha$  absorption from intergalactic hydrogen might be observed if background levels were low enough. Intergalactic light extinction and reddening might be detected by methods analogous to those used for measuring interstellar extinction. These two observations would require photometry of a precision far higher than has previously been possible because the hypothetical intergalactic component must be separated from the hydrogen extinction in our own galaxy.

Another spectroscopic test has been proposed. It assumes that quasars are at immense distances and that their spectral redshifts are cosmological. The hydrogen in the intervening space would also have radial velocities caused by the expansion of the universe, and the Lyman- $\alpha$  line for the hydrogen would be Doppler shifted by varying amounts, depending upon the distance of the particular hydrogen cloud. The requirements for observing this phenomena from space are very high spectrophotometric precision and moderately high dispersion.

6. Globular Clusters and Nearby Galaxies. Globular clusters are dense groups of stars, roughly spherical in shape, which tend to occur in the central and halo regions of a galaxy. They are conspicuous in other galaxies, and those in the Magellanic Clouds are close enough to allow measurement of their colors [I-3]. There is very little interstellar gas in most globular clusters, so that star formation is presumably completed. In our galaxy, globular clusters are generally composed of old stars; a globular cluster thus represents a sample of stars which have roughly the same age; therefore, the differences between the stars are caused by the differences in their initial masses and by the different evolutionary paths they have followed. Studies of the stellar populations in globular clusters of different ages are the major source of information about the evolutionary processes in population II stars.

The clusters also reveal something about the history of the galaxy to which they belong. It is thought that the gas clouds from which each of the clusters formed separated from the rest of the galactic gas at an early stage in the development of the galaxy. The orbits of the globular clusters about the center of mass were slightly affected by the subsequent contraction and evolution of form of the remainder of the galactic gas, so that the orbits of the globular clusters provide a record of a part of the initial kinematic state of the galaxy. The relevant data for these studies are the positions and the radial velocities of the whole clusters.

Evolution studies are also based on Herzprung-Russell or color-magnitude diagrams, which relate the magnitude (luminosity) of a star to its color (temperature). These observations are incomplete or lacking for many clusters. Where these clusters exist, the magnitudes are often determined for a very wide wavelength range. The fainter limiting magnitudes attainable by LST should permit wideband photometry of stars in some of the fainter clusters. Such data would yield color-magnitude diagrams for previously unobserved clusters and improve the diagrams for some of the clusters which have been observed.

Another form of photometric data is equally important. Globular clusters contain RR Lyrae stars, a type of variable star whose period can be correlated with its luminosity. Therefore, if the periods and apparent magnitudes of RR Lyrae stars in clusters can be measured, the distances to the clusters can be determined. RR Lyrae observations are the source of much of our information about cluster distances. Much work remains to be done in this area.

One other spectroscopic observation can and should be made. The radial velocity of the cluster can be determined by measuring the Doppler shifts of prominent lines in the spectrum of the integrated light from the cluster. In the typical case, this would be comparable to measuring the Doppler shifts in the spectrum of a 12th to 14th magnitude star, although the cluster spectrum, being composed of the spectra of many stars, will be harder to analyze. Radial velocities of most clusters are of the order of 100 km/sec; therefore, a dispersion of 20 Å/mm should be adequate for such studies.

Our knowledge of the globular clusters in visible wavelengths is still incomplete and much might be learned from observations in the ultraviolet and infrared.

Our knowledge about the fainter and more distant members of the Local Group of galaxies is comparable to our knowledge of the fainter globular clusters, except a larger probability exists that more faint galaxies remain to be discovered. The undiscovered galaxies, if they exist, probably are dwarf galaxies, small and of low-luminosity and low-surface brightness.

Several of the known dwarf galaxies are difficult to observe because they are very close to bright stars. Some advantage may be gained by observing them with the LST, because light scattered by the earth's atmosphere will no longer be a problem.

The distances and masses of several of the dwarf galaxies are not well known. The apparent magnitudes of the integrated systems are difficult to measure accurately, and most of the existing mass estimates are based on tidal effects and assumed mass-to-light ratios [I-4].

Direct images of the galaxies will also be useful. From them, density estimates can be made by counting stars, and, from the intensity calibration, equal-light-intensity contours for the galaxy can be drawn. If possible, sets of isophotes should be made in both red and blue wavelengths, using broadband filters. Ultraviolet and infrared data would be interesting in addition to the visible-wavelength information.

7. Distribution and Features of Matter in Interstellar Space. The interstellar matter is composed of gas and dust. Gas is mostly neutral hydrogen, but contains other atomic, ionic, and simple molecular species. Dust is thought to be composed of clumps of molecules which form grains of the order of  $10^{-5}$  cm [I-5]. Most of our information about gas is derived from spectroscopy, especially at radio wavelengths. Dust can be studied only through its obscuration and scattering of starlight. This discussion will consider only the optical wavelengths.

In spiral galaxies, gas and dust tend to be concentrated in the spiral arms. Mapping the locations of large clouds of gas and dust therefore helps to provide information about the positions and dimensions of the spiral arms. Knowledge of the total mass of material in the galaxy is important to studies of galactic structure and evolution. A sizable fraction of the galactic mass appears to be in the form of interstellar matter which is not observable because its location and excitation are unfavorable. More information about the observable matter may suggest new observational approaches or at least improve our guesses about the quantity, distribution, and properties of the unobservable material. Some of the interstellar particles polarize the starlight they scatter, presumably because they are elongated in shape and are aligned

so the long axes are roughly parallel. This alignment is thought to be produced by the action of local magnetic fields so that studies of interstellar polarization can yield information about the magnetic fields in gas and dust clouds. The composition of the interstellar matter is important also for studies of cosmology and stellar evolution.

Interstellar material also directly affects other observations. Dust diminishes and reddens the starlight which passes through it. Distances of stars are often derived by comparing their apparent magnitudes with the absolute magnitudes which are normal for their spectral types. A star in a dust cloud may therefore be assumed to be more distant than it really is. The galactic distance scale is also based in part upon stellar distances derived from apparent magnitudes; therefore, improper corrections for interstellar extinction can yield a distorted picture of the galaxy.

Both photometric and spectroscopic observations provide information about the interstellar medium. Polarization observations are classed as photometric measurements.

Polarization measurements may be made for large-scale regions of the galaxy, where the scattered radiation originates from a number of sources so that the effective source of illumination is extended. In this case, the data give the direction of alignment of the interstellar particles; the strength and direction of the magnetic field in the observed region can then be estimated. Polarization observations are also made for reflection nebulae, which are localized clouds of dust and gas visible because they are illuminated by a nearby star. In these cases, the polarization can be measured at various distances from the single illuminating source in several wavelength bands. These values are determined by the details of the scattering process and provide information about the size, composition, and distribution of the scattering particles.

Information about interstellar extinction of starlight is most commonly obtained by observing the apparent colors of stars of known spectral type. The greatest addition to existing data would be narrow-band photometry of a large number of stars of known spectral type. The spectral types have already been determined from the ground for enough stars to make up an ambitious observing program. The LST instruments probably will be able to extend the ground-based photometric data by up to 5 magnitudes.

The interstellar matter produces absorption lines which appear superimposed on the spectra of bright stars, and these lines constitute an important source of information. The strengths of the interstellar lines can

be used to estimate the amount of absorbing material between the star and the earth. Often, the lines are Doppler-shifted by resolvable amounts. The radial velocities of the gas clouds can be determined from these shifts. If there is more than one cloud in the line of sight, the spectral lines may be double. In addition, the constituents of the interstellar matter can be identified from the wavelengths of some of the spectral lines.

The important quantities for interstellar spectroscopy are high spectral resolution and dispersion, since sufficient light can almost always be obtained by observing a bright-enough star. The line strengths are determined by measuring the equivalent widths of the profiles; therefore, dispersions should be high enough to allow for such measurement. Good resolution is required because the lines are often blurred by random motions in the cloud.

8. Star Formation. Star formation is thought to begin with the existence of a massive cloud of gas in interstellar space. For reasons which are not yet known, the cloud may begin to condense. It contracts more rapidly as the gravitational attraction by its denser parts increases. When the inner parts of the gas reach a sufficiently high density, nuclear processes begin to convert hydrogen into helium, releasing energy. The gas becomes self-luminous and is now a star. The newly-formed star continues to evolve as its internal conditions and composition are changed by the nuclear reactions. Gas in the contracting, preluminous phase is not identifiable on the basis of present knowledge. Therefore, deductions about star formation must be made from observations of the youngest known stars. Young stars generally exhibit variations in intensity and in their spectral characteristics. They are often found near clouds of gas or dust.

T-Tauri stars are thought to be examples of objects which are approaching the end of the contraction phase. T-Tauri characteristics seem to be adopted by objects of less than about 2 solar masses; essentially, nothing is known about the formation of the more massive stars [I-6, I-7]. There are other variable stars which are associated with nebulosity and show hydrogen emission lines in their spectra. These stars, which are otherwise spectroscopically distinct from T-Tauri stars, are at present grouped under the name of "Orion population" stars. (They may also be examples of very early evolutionary stages.) Other objects which may provide information on evolution are the Herbig-Haro objects and "flash" stars.

The objects to be observed are irregular variables; therefore, high-dispersion spectra at many different times are desirable. Both the infrared and ultraviolet ends of the spectra should be observed. The ultraviolet range is particularly interesting because the T-Tauri stars are much brighter in the blue and ultraviolet than normal stars of their spectral types.



Measurement of rotational velocities of these objects is important to theoretical studies of the early evolutionary stages. In addition, some of the stars appear to have expanding shells or to be ejecting material from their surfaces. All of these effects appear in the spectra as Doppler shifts, splittings, or broadenings of absorption or emission lines.

9. Planetary Nebulae and Wolf-Rayet-Type Stars. A planetary nebula is a star surrounded by a mass of gas which is excited to fluorescence by ultraviolet radiation from the central star. The spectra of both components sometimes show emission lines, and the nebular spectrum has a weak continuum. Within this description, individual planetary nebulae differ widely.

The central stars are generally quite hot, at least in our own galaxy. Some have absorption spectra which are classifiable as type O, some are of type Of, having an O-type spectrum with superimposed emission lines, and some are of Wolf-Rayet (W-R) type. Another group of fainter stars shows no absorption or emission lines at the low dispersions which are required to obtain their spectra from the earth. The strengths of the spectral lines vary over a wide range within all these classes. At least one central star may be a binary system.

The nebulosity is thought to be matter which was ejected from the central star. The radiating part of the gas may form a shell, or shells, which expand radially. The velocities vary, but the average is of the order of 20 km/sec. The nebulae often include structures such as knots, filaments, and gaps.

Although planetary nebulae have been studied for more than 100 years, surprisingly little is known about them. This is partly because of the great differences between individual objects and partly because they are difficult to observe.

The chemical composition, temperature, mass, density, and excitation conditions can, in principle, be determined from the spectra. Expansion velocities for the nebulosity can be found from Doppler shifts of spectral lines if they can be resolved. The observations should include spectral line strengths for as many of the stronger spectral lines as can be resolved. Because of the early spectral type of the central stars and their presumed high ultraviolet fluxes, ultraviolet observations of both stars and nebulae are important. The stellar continua should also be obtained, particularly in the ultraviolet, because many of them depart strongly from blackbody shape. In the cases of objects which are too faint for detailed spectra, narrow-band photometry would yield valuable information for approximate spectral studies. Even wideband photometry would help to provide refined luminosity data.

On the average, the central stars are almost 2 magnitudes fainter than the integrated magnitude of the surrounding nebulosity. Because the nebular continuum emission is nearly monochromatic, much of it can be removed with the proper filters. Even so, interference from the nebula often appears. The nebular hydrogen and helium lines usually mask the corresponding features in the stellar spectrum, and other absorption or emission lines formed in the nebulosity frequently appear superimposed on the stellar spectrum. It is usually easier to identify the nebular features on higher dispersion spectra. Short-term variations in the spectra of both stars and nebulae may exist.

W-R stars have spectra which are characteristic of very high temperatures. They are identified by the presence of prominent emission lines of neutral and ionized helium, carbon, and nitrogen. There are two major subclasses of W-R stars: (1) those whose spectra are dominated by nitrogen emission are called WN stars, and (2) those whose spectra are dominated by carbon emission are called WC stars. Besides these emission lines, the spectra of these stars differ considerably. Indeed, it would be difficult to name a "typical" W-R star.

It has been suggested that these objects may represent the final stages of formation of stars with masses about 4 to 10 times the solar mass [I-8, I-9]. More knowledge of W-R star properties may therefore be significant to studies of stellar evolution. Some central stars of planetary nebulae have W-R spectra. Even less is known about these than about the other W-R stars.

The W-R stars are assumed to have fairly compact atmospheres and to be surrounded by one or more extended shells of low density. The emission lines are broad and rounded, and few absorption lines are identifiable. In many cases, the observed broadening is greater than can be accounted for by known mechanisms and must be produced by some unknown cause.

Temperature estimates for the stellar atmospheres are uncertain because the continua depart from blackbody form, with the departures being larger in the blue part of the spectrum. Spectra extending further into the ultraviolet will help in understanding the radiation and absorption properties of the atmospheres.

The broadening of the spectral lines makes Doppler-shift determinations imprecise. Even so, enough evidence has accumulated to suggest that models of W-R stars which assume that all radial motion occurs in an

expanding shell outside the stellar atmosphere are too crude. More probably, the star has "a moderately extended, moderately dense atmosphere in chaotic motion above a compact photosphere" [I-8].

Because most W-R stars are faint, high-dispersion spectra can be made for only a few of them from the earth's surface.

High resolution and dispersion spectra are needed for all the objects in the ultraviolet, and in the visible and near infrared for the fainter stars. The intrinsic variability of most W-R stars appears to be slight or nonexistent. However, several W-R stars are known to be binaries, and at least four are eclipsing binaries. The presence of another component in the system provides opportunity to obtain at least approximate information about masses and radii. Photometric studies should be made in several wavelength ranges to see if other eclipsing binaries can be found and to check further on the possibilities of intrinsic variability. Also, the continua should be mapped in the ultraviolet down to the lower observable wavelength limit.

High dispersion spectra in the visible and infrared are also of interest. The amount of interstellar reddening of W-R stars is unknown in most cases, although it is probably large. Infrared spectra at high resolution may help to judge how large the reddening corrections to photometric data should be. Narrowband photometry of W-R stars in galactic clusters outside the plane of the galaxy will also help to determine the intrinsic colors of these objects [I-9].

Distances of most W-R stars are uncertain, since they must usually be derived from the strengths of the interstellar absorption lines in the spectra. Studies of the colors of W-R stars in the Magellanic Clouds and in galactic clusters of known distance can be used to improve the distance estimates by refining the estimated amounts of interstellar reddening and extinction.

10. Optical Observations of X-ray Sources, Pulsars, and Neutron Stars. During the past 10 years, various astronomical objects have been discovered which were completely unexpected and unlike celestial objects known previously. These new objects include X-ray stars, pulsars, quasars, neutron stars, and possibly black holes. They form the basis of the new field of high-energy astronomy where the energy densities are far greater than their normal counterparts. Because of their high luminosity and largely nonthermal emission, these objects were, for the most part, discovered by rocket and space-borne observations. These observations have continued to be the principal means of studying high-energy objects.

Although the major portion of the energy of these objects is emitted in the X-ray, gamma-ray, and radio regions of the spectrum, additional information about their nature has been derived from infrared, optical, and ultraviolet observations. The LST is expected to be an important part of future observations in this new branch of astronomy.

No high-resolution spectra are yet available for X-ray sources other than Sco X-1, but these data will be extremely valuable in determining distance, temperature, and atmospheric characteristics of these sources and thus obtaining these spectra will be an important assignment for the LST.

Pulsars are thought to be rotating neutron stars, objects of nuclear density only 10 km in diameter and at least as massive as the sun. Of the three X-ray pulsars and over 40 radio pulsars which have been found, only one of them has thus far been identified optically, NP 0532. This pulsar is at the center of the crab nebula. NP 0532 pulses 30 times per sec and its characteristic pulse profile has been observed from the radio through the hard gamma-ray region. No spectral features are apparent at optical wavelengths. Many unsuccessful attempts have been made to observe other pulsars. Due to their precisely known pulse period, the limit of detection for these objects is considerably below that of a continuous optical source.

Dedicated observations by the LST could result in detection of other pulsars or place even lower limits on their optical emission.

11. Detailed Studies of Planets. Extensive observations of planets are now made with instruments other than optical telescopes. Radar, radio, orbiters, and atmospheric probes are being used more for studies of planetary atmospheres and surfaces. Nevertheless, there is still need for detailed optical observations. The earth's atmosphere is troublesome in planetary work, where the observer usually wants to obtain the finest possible detail within the image of the disk; therefore, a space-borne telescope provides a distinct advantage.

Interesting properties of planetary atmospheres include composition, temperature, density, barometric pressure, size and distribution of atmospheric particles, and atmospheric circulation. The interesting properties for planetary surfaces are composition and topography, as well as the form of small-scale surface structures. Very little information about the surfaces of planets with dense atmospheres can be obtained at optical wavelengths.

The observations required are unpolarized photometric, polarization, and spectroscopic measurements at different times. LST observations should concentrate on the ultraviolet and the infrared. Most of the dense planetary atmospheres absorb strongly in the red and infrared wavelengths, and photometric observations in different infrared bands may give information about the height structure of the atmosphere. Ultraviolet wavelengths are required to penetrate to the lower levels of the atmospheres. Photometric observations are needed at as many different points on the planetary disk as possible, because the distribution of the reflected sunlight depends upon the scattering properties of the surface or atmosphere as well as upon the planet's angular distance from the sun [I-10]. The disk photometry thus provides information about particle sizes and densities. The measured polarization provides additional information about particle sizes and distributions and also allow the elimination of some proposed compositions which do not produce the observed polarization. The data are required for the same wavelengths as the unpolarized photometry. The internal precision of the measurements should be  $\pm 0.001$  degree polarization ( $\pm 0.1$  percent) or better [I-11].

Because the planets are illuminated by the sun, their spectra resemble the solar spectrum with additional absorption lines corresponding to the absorption in the planetary atmospheres. The major absorption bands are molecular bands and lie in the infrared [I-12]. The strengths and positions of these bands are determined by the number and type of molecules which produce the absorption; therefore, they can be used to study the composition of the atmosphere. The strengths also give clues to the atmospheric temperature and pressure.

A second application of spectroscopic observations is in estimating the rotation period of the planet from the Doppler shifts of the absorption lines. This requires measuring the spectra at the limbs to obtain the radial Doppler shifts.

12. Studies of Asteroids, Comets, and Other Small Bodies. Comets are thought to be conglomerate masses consisting of dust and metallic particles embedded in an ice of organic and water molecules; the ice forms about 75 percent of the comet mass [I-13]. Their orbits about the sun are usually highly eccentric; therefore, most comets spend most of their time far out in the solar system and are usually invisible. As the comets approach perihelion, the frozen gas vaporizes and forms the head or coma, a diffuse, which is roughly spherical cloud around the frozen nucleus. Often a tail appears.

Comet spectra consist of the reflected solar spectrum with superimposed emission bands. These bands are the primary source of observational information about comets. Identification of the bands provides information about the composition and about the excitation conditions (in particular, the temperature and pressure) in different parts of the comet. At dispersions of the order of 20 Å/mm, many of the molecular bands can be resolved.

High spatial resolution is also very important to comet spectrum studies since it permits isolating the spectra of different parts of each structure. It may thus be possible to study variations in the intensities of the emission lines at different parts of the head and tail. A focal plane scale of 25 to 50 arc-sec per millimeter permits distinguishing regions of the order of several hundred to a thousand kilometers at a distance of 1 AU from the earth [I-14].

High dispersion spectra of good spectral and spatial resolution should be made for as many comets as possible. Such observations will be of assistance for theoretical and spectrum studies of both the molecular emission and the scattered solar absorption spectrum. Line profiles should be obtained, since they would be particularly valuable for studies of the internal motions of the material. The ability to choose the location and orientation of the spectrograph slit on the image would be valuable. The observations should be made in all available spectral ranges and at as many points in the comet's orbit as possible.

Observational studies of asteroids are based on photometry. The asteroids are small irregular chunks of solid material in orbit about the sun. Most of them are in the asteroid belt between Mars and Jupiter. All information about the physical properties of these objects must be derived from the light they reflect. The observable quantities are the apparent magnitudes and the degree of polarization of the reflected light in various wavelength bands. From apparent magnitudes and colors measured at different times, it is possible to derive light curves which allow estimation of the reflectivity of the surface and the shape, size, and rotation period of the body. Measurements of polarization at different phase angles to the sun can provide more information about the surface properties. Because the objects are so irregularly shaped and because their orbits are generally inclined to the earth's orbit, the combined effects of precession and changing relative positions of the earth and the asteroids mean that two observations made at the same solar phase angle may in fact refer to very different portions of the asteroid surface. None of the physical properties are well known, and there are puzzling variations between some of the objects. Some unexplained phenomena are consistently observed; e.g., the colors of some asteroids depend on their solar phase angles.

Most modern asteroid photometry is done in the UBV system. Studies at comparable wavelengths should be continued with the best possible precision, and corresponding polarization measurements should be made. The photometry and polarimetry should be extended to the ultraviolet. Gehrels [I-15] gives a list of suggestions for specific future asteroid studies which also includes observations of high dispersion spectra to search for absorption features and possible emission.

Saturn's rings are another assemblage of very small particles. Photometric measurements include brightness at different solar phase angles and ring inclination angles. The rings are not of equal brightness; therefore, good spatial discrimination is required. The necessary amounts depend on the angle at which the rings are seen. In addition, the brightness within a ring appears to vary in the east-west direction. The rings show a tendency toward a dependence of color on solar phase angle; therefore, color and brightness observations should be made at a number of different times. Polarization measurements at various positions in the rings and angles to the sun are also of interest. All of these observations should be made in the visible, the ultraviolet, and the near infrared. Spectra should be obtained, especially in the near infrared where molecular bands tend to occur.

13. Helium-Rich Stars. A number of stars show helium abundances which are unusual for their spectral types, but the term "helium star" is usually reserved for the members of a very small class of stars with abnormally strong helium lines and abnormally weak hydrogen lines. They may be the helium cores of stars which have lost their hydrogen shells. In that case, they would be an important source of information about energy generation and evolutionary processes [I-16]. Even if they prove to have a more commonplace explanation, they are still important for studies of abundances and evolution.

On the basis of present knowledge, little photometry is required. Wideband observations could be made at different times to search for evidence of variability. Narrowband photometry in the ultraviolet and near infrared would give a quick check of possible abnormalities in the spectral continuum. Most of the required observations are spectroscopic. High resolution (at least  $0.1 \text{ \AA}$ ) spectra should be made at dispersions of  $10 \text{ \AA/mm}$  or better. Line profiles should be obtained wherever possible. Because these are early type stars, their ultraviolet spectra are particularly interesting. The visible region and the near infrared should also be studied. Spectra should be made at different times to check for spectrum variability.

14. Studies of Variable Stars. Variable stars, by definition, are stars whose magnitudes appear to vary. They may be multiple-star systems in which one component eclipses another, or they may be intrinsic variables, whose luminosity variations are caused by internal changes. In the optical wavelengths, the time scale for variability may extend from the order of minutes to hundreds of years. Changes appear in the spectra as well as in the luminosities of many intrinsic variables, and these spectrum changes provide clues to the physical processes which cause the variations.

Observations provide data on such stellar characteristics as size, mass, surface temperature, shape, internal density distribution, and composition and extent of the stellar atmosphere [I-17]. In addition, they furnish data on galactic structure. Many of the intrinsic variables are highly luminous and can be detected relatively easily. Some types of variables have well-defined relations between luminosity and some other easily-determined characteristic (e.g., length of period or shape of light curve) and these stars can be used as luminosity standards for determining distances, dimensions, and structures of our own and other galaxies [I-17].

After a star has been identified as a variable, its light curve must be determined. This process requires precise photometric observations made repeatedly over a sufficient length of time to determine the period, if the variable is periodic, or to establish with reasonable probability that no regular period exists.

For some types of stars, the observations must be spaced carefully to prevent the determination of spurious periods [I-18]. Novae and supernovae stars increase in brightness suddenly and then decline until their brightness returns roughly to its initial value; the rate and pattern of the decline are different for different types of novae. The brightness increase in the eruptive stage is very great; a total increase of about 10 to 11 magnitudes can be considered typical [I-19]. The spectrum changes throughout the process.

Detailed photometric data and spectra in all accessible wavelength ranges, from the beginning of a nova eruption to the final decline stages, would be of great value. The spectra should be taken at the highest available resolution and dispersion.

The required observations for other types of variables are similar: wideband photometry or, for the brighter and more thoroughly studied variables, narrowband photometry; and spectra of the highest possible dispersion and resolution.



15. Infrared Studies of Stars and Galaxies. Ground-based observations have revealed a large number of objects whose radiation is emitted almost entirely in the infrared or whose infrared radiation is anomalous in that it deviates markedly from predictions based on visual or radio data. These observations have been limited to a few "windows" or wavelength intervals in which the earth's atmosphere is transparent, and observations from space should increase the amount of accessible infrared data by 30 percent or more.

The vast majority of infrared sources so far observed can be identified with late type giant stars. Many galactic sources radiate much more intensely in the infrared than would be inferred from a blackbody distribution for the appropriate spectral type. This infrared excess is currently assumed to represent thermal radiation from a dust shell or cloud surrounding a central star. The evidence for this is still largely circumstantial, and their spectra have not yet been scanned in the region of the excess with sufficient resolution to distinguish between continuous and many-line emission.

The origin of the inferred dust shells has been the subject of much speculation. Some may have been formed from material ejected from the central stars, whereas others may represent the remnants of the original dust cloud from which the star was formed. Although the mechanism responsible for the infrared excesses is considered to be well understood, observations in the infrared are the only known method for determining which stars have dust shells.

There are many reasons for observing stellar spectra in the infrared. Certain abundant molecules can be observed only in the infrared and others have their strongest transitions in this region. Thus, infrared observations can provide important information concerning the abundances of relatively light elements, and many molecules never before observed in an astrophysical source may become available for study through their infrared rotation-vibration bands. Measured line strengths can be used to evaluate the infrared opacity of late-type stars, which, in turn, is needed for the construction of realistic model stellar atmospheres. Further studies of infrared lines in early-type stars will be useful in illuminating the structure of their outer layers, and infrared spectroscopy can be used to investigate the chromospheres of cool stars.

### C. Instrument Growth Capability

The concept of scientific instrumentation modularity for ease of removal and replacement has permeated the Phase-A design. Maintenance on an instrument "blackbox" level provides for singularity of design and relatively simple interfaces, the most critical being the optical tolerances

and thermal control designs. The ability to establish universal mechanical interfaces leaves the surrounding design of the instrument to expand or take on any required shape which would house an instrument with improved investigative powers for the LST.

The development over the years of scientific instrumentation located at the most advanced ground-based observatory reveals that the early periods at a new ground site are spent in developing a familiarity with equipment. Next comes the improvement of existing equipment, then the use of innovative unique equipment and modern technological schemes using digital solid-state devices for system operation and data gathering. The LST will be initiated at the third level; however, it will probably experience a remarkable variation by using the Shuttle to update and upgrade the scientific instrumentation periodically.

#### D. Role of Principle Investigator (PI) Astronomers

To guarantee that the community of astronomers realize their goal of a large diffraction-limited performance telescope in space, NASA is establishing the ways and means to involve a sufficient number of non-NASA astronomers to establish sufficient astronomical expertise to provide the necessary scientific judgement. The LST must reflect their opinions of relevance in design and must be widely available to the best astronomers.

The structure to be developed is divided into LST science groups. The LST program and project scientist and managers from MSFC, GSFC, and NASA Headquarters will work with five individual astronomers (experimentalist, users, and theoreticians) and five instrument definition team leaders. The team leaders will represent a five-man instrument(s) development effort, one for diffraction-limited camera instrument, low dispersion spectrograph, high dispersion spectrograph, and two other undefined instrument(s) assigned to two additional groups.

The procedure for selection of instrument definition teams and flight instrument and science teams for the national facility LST is being developed around the following guidelines:

1. A solicitation for proposal (SFP) is planned for early December 1972. The purpose is to solicit scientific community participation in scientific instrument definition. Proposals in response to the SFP will include conceptual definition of the proposed instrument, proposed scientific uses for the instrument, and a discussion of how the proposer can contribute to the instrument

definition team in manpower, technical expertise, and/or resources. A selection committee will be established by OSS, NASA Headquarters, to select the individuals for the instrument definition teams. For planning purposes, it is assumed that five teams will be selected consisting of five members each. NASA will appoint the team leaders with the concurrence of team members and will establish milestones for revised proposed instrumentation submittals, which will include objectives of the proposed instrumentation, design drivers, technology development areas, interface definition, performance requirements, and technical guidelines for preliminary design of the instruments.

2. Instrumentation selection for flight will be made by an OSS-appointed committee. The development of the selected instruments will be procured directly by NASA. This concept does not exclude the unique instrument developed by a single PI; however, the team effort and broadly accepted instrument will be more easily and readily approved. The definition teams will be dissolved at the conclusion of the definition activities.

3. The Announcement for Flight Opportunity (AFO) will be released by OSS in mid-1974 requesting proposals from potential users of the instruments which may include proposals from members of definition teams. A user selection committee will be established by OSS to select the individuals for the science teams; a team will be selected for each instrument selected for flight. The science team leader will be appointed by OSS with concurrence of the team members. The science team will be in the most advantageous position to be a prime user of the instrument and will be given appropriate consideration.

## E. Role of LST and Ground-Based Astronomy

In no sense does the LST compete with, or supplant, earth-based astronomy. Instead it is a tool to amplify on-going ground observational programs and to fill in data gaps in certain areas of research. Because of its potential for faint object detection and the expanded spectral window, the total available viewing time can be productively consumed many times over, solely in gathering data in the spectral and brightness ranges which are inaccessible from the earth.

For this latter reason, the LST observing program will be largely determined by the status of ground observational programs and research during its operating lifetime. In general, the observations will be confined to specific objects using instruments selected to provide data to answer

questions or resolve problems raised in the course of ground activities. Little work of a general survey nature will probably be done, with the possible exception of surveys for certain classes of faint objects. Even here, however, much work of this type can be accomplished as a secondary result of viewing specific target areas.

## REFERENCES

- I-1. Sargent, W. L. W.: The Spectra of 80 Galaxies in Markarian's Second List and the Space Density of the Markarian Galaxies. *Astrophysical Journal*, vol. 173, p. 7, 1972.
- I-2. Harris, D. L., Strand, K. Aa., and Worley, C. E.: Empirical Data on Stellar Masses, Luminosities, and Radii. *Basic Astronomical Data* (ed. K. Aa. Strand), University of Chicago, 1963.
- I-3. Bok, B. J.: The Magellanic Clouds. *Observational Aspects of Galactic Structure, Lecture Notes for NATO Summer Course*, (Eds., A. Blaauw and L. M. Mavridis), September 1964.
- I-4. Hodge, P. W.: Dwarf Galaxies. *Annual Review of Astronomy and Astrophysics*, vol. 9, 1971.
- I-5. Heiles, C.: Physical and Chemical Constitution of Dark Clouds. *Annual Review of Astronomy and Astrophysics*, vol. 9, 1971.
- I-6. Herbig, G. H.: Early Stellar Evolution at Intermediate Masses. *Spectroscopic Astrophysics* (Ed., G. H. Herbig), University of California Press, Berkeley, 1970.
- I-7. Herbig, G. H.: The Properties and Problems of T Tauri Stars and Related Objects. *Advances in Astronomy and Astrophysics*, vol. 1, 1962.
- I-8. Underhill, A. B.: *The Early Type Stars*. Reidel, 1966.
- I-9. Underhill, A. B.: The Wolf-Rayet Stars. *Annual Review of Astronomy and Astrophysics*. vol. 6, 1968.
- I-10. Harris, D. L.: Photometry and Colorimetry of Planets and Satellites. *Planets and Satellites* (eds., G. P. Kuiper and B. M. Middlehurst), University of Chicago, 1961.
- I-11. Dollfus, A.: Polarization Studies of Planets. *Planets and Satellites* (Eds. G. P. Kuiper and B. M. Middlehurst), University of Chicago, 1961.

## REFERENCES (Concluded)

- I-12. Adel, A.: Selected Topics in the Infrared Spectroscopy of the Solar System. The Atmospheres of the Earth and Planets, (Ed. G. P. Kuiper), University of Chicago, 1962.
- I-13. Donn, B.: Cosmic Chemistry. Introduction to Space Science (Ed. W. N. Hess), Goddard Space Flight Center, Gordon and Breach, 1965.
- I-14. Arpigny, C.: Spectra of Comets and Their Interpretation. Annual Review of Astronomy and Astrophysics, vol. 3, 1965.
- I-15. Gehrels, T.: Photometry of Asteroids. Surfaces and Interiors of Planets and Satellites (Ed. A. Dollfus), Academic Press, 1970.
- I-16. Cayrel, R., and Cayrel de Strobel, G.: Abundance Determinations from Stellar Spectra. Annual Review of Astronomy and Astrophysics, vol. 4, 1966.
- I-17. Kukarkin, B. V., and Parenago, P. P.: Surveys and Observations of Physical and Eclipsing Variable Stars. Basic Astronomical Data (ed. K. Aa. Strand), University of Chicago, 1963.
- I-18. Petrie, R. M.: The Determination of Orbital Elements of Spectroscopic Binaries. Astronomical Techniques (Ed. W. A. Hiltner), University of Chicago, 1962.
- I-19. Payne-Gaposchkin, C.: The Galactic Novae. Dover, 1964.

## BIBLIOGRAPHY

- Abell, G. O.: Clustering of Galaxies. Annual Review of Astronomy and Astrophysics, vol. 3, 1965.
- Allen, C. W.: Astrophysical Quantities. University of London, p. 155, 1963.
- Arp, H. C.: Globular Clusters in the Galaxy. Galactic Structure, (Eds. A. Blaauw and M. Schmidt), University of Chicago, 1965.
- Bobrov, M. S.: Physical Properties of Saturn's Rings. Surfaces and Interiors of Planets and Satellites.
- Brady, J. L.: Publications of the Astronomical Society of the Pacific. vol. 84, p. 314, 1972.
- Czyzak, S. J., Aller, L. H., and Kaler, J. H.: Spectrophotometric Studies of Gaseous Nebulae, XI. The Planetary NGC 6543. Astrophysical Journal, vol. 154, p. 543, 1968.
- Danziger, I. J.: The Cosmic Abundance of Helium. Annual Review of Astronomy and Astrophysics, vol. 8, 1970.
- Eckert, W. J., and Jones, R.: Measuring Engines. Astronomical Techniques (Ed. W. A. Hiltner), University of Chicago, 1962.
- Gould, R. J.: Intergalactic Matter. Annual Review of Astronomy and Astrophysics, vol. 6, 1968.
- Greenberg, J. M.: Interstellar Grains. Nebulae and Interstellar Matter (Eds. B. M. Middlehurst and L. H. Aller), University of Chicago, 1968.
- Gursky, H.: The Association of X-ray Sources with Bright Stars. Report ASE-2991 (to be published in the Astrophysical Journal), 1972.
- Hiltner, W. A.: Polarization Measurements. Astronomical Techniques (Ed. W. A. Hiltner), University of Chicago, 1962.
- Instrumentation Package for a Large Space Telescope (LST). GSFC Report X-670-70-480, November, 1970.

## BIBLIOGRAPHY (Continued)

- Johnson, H. L.: Interstellar Extinction. Nebulae and Interstellar Matter (Eds. B. M. Middlehurst and L. H. Aller), University of Chicago, 1968.
- Kuiper, G. P.: Limits of Completeness. Planets and Satellites (Eds. G. P. Kuiper and B. M. Middlehurst), University of Chicago, 1961.
- Munch, G.: Interstellar Absorption Lines. Nebulae and Interstellar Matter (Eds. B. M. Middlehurst and L. H. Aller), University of Chicago, 1968.
- Noonan, T. W.: Astrophysical Journal. vol. 171, p. 209, 1972.
- Nozawa, Y., and Davis, R. J.: Some Factors Affecting the Accuracy of a Space-Borne Astronomical Television Photometer. Astronomical Use of Television-Type Image Sensors (Ed. V. R. Boscarino), NASA SP-256, 1971.
- Plaut, L.: Variable Stars. Galactic Structure, (Eds. A. Blaauw and M. Schmidt), University of Chicago, 1965.
- Praderie, F.: What Do We Know Through Spectral Information on Stellar Chromospheres and Coronas. Spectrum Formation in Stars With Steady-State Extended Atmospheres, Proc. I.A.U. Colloquium No. 2, Commission 36, 1969 (N.B.S. Special Publication 332).
- Rosino, L.: Some Problems Concerning Globular Clusters. Observational Aspects of Galactic Structure.
- Russell, H. N., Dugan, R. S., and Stewart, J. Q.: Astronomy. vol. II, Ginn and Co., p. 688, 1927.
- Sandage, A.: The Redshift-Distance Relation. Astrophysical Journal, vol. 173, p. 485, 1972.
- Scarborough, J. M.: Large Space Telescope Contamination Study. TBE Interim Report ASD-PD-1527, May 1972.
- Scientific Uses of the Large Space Telescope. National Academy of Sciences, 1969.



## BIBLIOGRAPHY (Concluded)

Scott, F. P.: The System of Fundamental Proper Motions. Basic Astronomical Data (Ed. K. Aa. Strand), University of Chicago, 1963.

Sky and Telescope. vol. 43, p. 990, 1972.

Strand, K. Aa.: Trigonometric Stellar Parallaxes. Basic Astronomical Data (ed. K. Aa. Strand), University of Chicago, 1963.

Strom, S. E., and Strom, K. M.: An Analysis of the Bright O Star in the Globular Cluster M3. Astrophysical Journal, vol. 159, p. 195, 1970.

Van de Kamp, P.: Astrometry with Long-Focus Telescopes. Astronomical Techniques (Ed. W. A. Hiltner), University of Chicago, 1962.

Vasilevskis, S.: The Accuracy of Trigonometric Parallaxes of Stars. Annual Review of Astronomy and Astrophysics, vol. 4, 1966.

Westphal, J. A., Sandage, A., and Kristian, J.: Astrophysical Journal. vol. 154, p. 139, 1968.

## CHAPTER II. PHASE A STUDY APPROACH



# TABLE OF CONTENTS

	Page
A. Study Approach and General Guidelines . . . . .	II-1
B. LST Study Guidelines . . . . .	II-2
1. General Study Guidelines . . . . .	II-2
2. Structure Guidelines . . . . .	II-5
3. Thermal Control Guidelines . . . . .	II-7
4. Communications and Data Management Guidelines . . . . .	II-7
5. Attitude Control System (ACS) Guidelines . . . . .	II-8
6. Electrical System Guidelines . . . . .	II-9

## CHAPTER II. PHASE A STUDY APPROACH

### A. Study Approach and General Guidelines

The Marshall Space Flight Center (MSFC) report, Large Space Telescope (LST) Preliminary Study, dated February 25, 1972, was used as the beginning point of reference for the Phase A study. The primary objective of the Phase A study was to evolve to a reference design LST configuration which could achieve the precision accuracy and stability desired for large space telescopes.

During the Phase A study activity, participant responsibility was allocated as follows:

1. ITEK was responsible for the analysis and design of the Optical Telescope Assembly (OTA), which is defined in Volume III. This responsibility included review, analysis, and utilization of the results from the light shield study performed by the University of Arizona. It also included insuring satisfactory interfaces between the OTA and the other major elements of the LST.

2. Kollsman Instrument Corporation was responsible for the analysis and design of the Scientific Instrument Package (SIP), which is defined in Volume IV. This responsibility included insuring satisfactory interfaces between the SIP and the other major elements of the LST.

3. MSFC was responsible for the analysis and design of the Support Systems Module (SSM), which is defined in Volume V, and for integration of the overall LST.

The study approach employed during Phase A was to investigate technically, in some depth, a variety of promising LST configurations, systems, and subsystems. Technical analyses and trade studies were conducted to select the more promising concepts. Analyses and trade studies were continued on these concepts until the reference design LST configuration was defined.

This resulting reference design configuration provides an overall integrated mechanical, thermal, and structural design concept. Analyses indicate that this reference design concept minimizes launch and environment

loads to the primary optics, minimizes thermal distortions of the telescope, and isolates spacecraft disturbances from the primary mirror and telescope structural assembly. This design also provides for on-orbit maintenance for subsystem replacement and instrument update.

The selection of the Phase A LST reference design configuration as discussed in this document is meant to serve as a starting point for Phase B activities and should in no way constrain the option to investigate other concepts, systems, and subsystems.

## B. LST Study Guidelines

### 1. General Study Guidelines

1. The LST launch date is late 1980.
2. The LST must be designed for Shuttle initial launch and eventual return (either for maintenance or at end of life). In addition, the LST, including a 20 percent mass contingency as a design goal, must be compatible with launch on the Titan IIIE with the 17 m (56-ft) Viking shroud as a backup mode. Other backup launch vehicles will be analyzed during the study.
3. Total mission duration (on-orbit operation) will be a minimum of 5 years.
4. The nominal orbit will be a 28.5 degree inclination, 611 km (330 n.mi.) altitude; parametric data will be generated to show the impacts of other orbital altitudes and inclinations.
5. The time of the nominal initial maintenance visit will be determined during the study.
6. The telescope aperture is 3 m or as close thereto as possible. Performance shall be diffraction-limited. Wavefront error sensing and control should be done no more than once per month as a goal.
7. The MSFC LST Preliminary Study Report, dated February 25, 1972, will be utilized as the reference document for the OTA and SIP definition; SSM requirements will be revised based on that document and additional requirements stated herein.

8. In its normal operating mode, the spacecraft will have the capability of viewing targets within the entire celestial sphere except for targets within 45 degrees from the center of the sun and within 15 degrees from the center of the moon; data will not normally be taken within 15 degrees of the limb of the earth. Viewing capability during daytime and nighttime is required; the parameter to be optimized is total mission viewing time, with star magnitude contributing to the trade in a weighted manner to be determined in the study.

9. Integrated viewing time per target will vary from a few seconds to approximately 10 hours. Experiment interruption due to alignment and focus of the telescope or instruments should not be required more often than once per orbit as a goal.

10. The telescope instruments and attitude sensors will have automatic protective devices for protection against inadvertent viewing of the sun, moon, etc.

11. Reliability requirements for the LST will be determined in the study. There will be no single point failure of critical systems and ground diagnosis/failure correction commands will be used whenever possible. Failure rate data on existing equipment will be empirical data as adjusted for the environment; when this is not possible, the RADC Reliability Notebook, Volume II, will be used for basic failure rate data. An autonomous attitude-hold capability with a high reliability shall be provided.

12. Failures will be isolated to at least the "black box" level.

13. Docking port internal clearance must be 1 m in diameter and compatible with the Shuttle and Docking Module. The international docking mechanism concept will be used.

14. During all on-orbit operations involving the Shuttle, impingement/contamination of effluents from the Shuttle on the LST will be minimized. During deployment, retrieval, and when docked to the Shuttle, the LST appendages will nominally be retracted and all protective covers closed.

15. The Shuttle will provide the hardware necessary to deploy the LST from the cargo bay and release it and to rendezvous and dock with the LST.

16. Maximum utilization shall be made of hardware and designs from other programs which are expected to be operational in the same general time period as the LST [High Energy Astronomy Observatory (HEAO) for example] to reduce costs and improve confidence.

17. For purposes of defining mass locations, the axes shown in Figure II-1 will be utilized. The origin is at the aft surface of the docking ring.

18. At least the following three approaches to maintenance will be analyzed and compared:

- a. On-orbit Pressurized Maintenance.
- b. On-orbit Unpressurized Maintenance.
- c. Earth Return Maintenance.

Note: For pressurized maintenance, pressurization gases are assumed to be aboard the support vehicle. The LST internal pressure for this mode should be  $1.01 \times 10^5 \text{ N/m}^2$  (14.7 psi) during maintenance and 0 during other periods of operation.

19. A moderate amount of extravehicular activity (EVA) will be permitted during Shuttle visits.

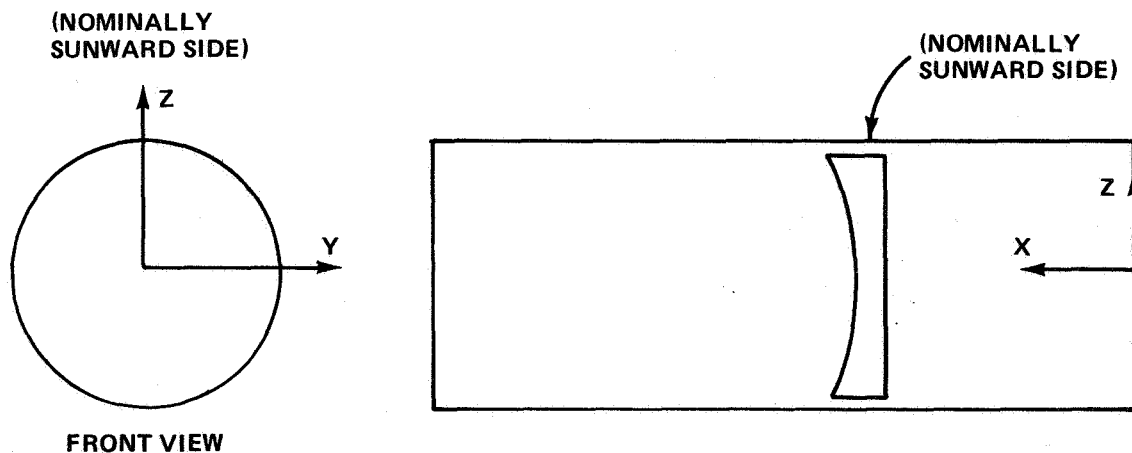


Figure II-1. Mass locations reference axes.



20. The maintenance vehicle will have the capability of providing attitude control and other necessary functions to the LST while docked. The LST will normally be dormant while docked. (The required active LST equipment will be defined in the study.)

21. The general philosophy of design of the LST will be one of low cost, with the capability of easily updating instruments and critical systems as more accurate or more sensitive hardware becomes available.

## 2. Structure Guidelines

1. The maximum allowable LST dynamic envelope is 3.7 m (147 in.). The 17 m (56-ft) Viking shroud dynamic envelope is shown in Figure II-2.

2. The structure interface between the SSM and the OTA will be at the aft surface of the OTA main ring. Structural design and thermal control design of at least the first 1 m (40 in.) of the SSM immediately aft of the OTA interface will require concurrence of the OTA design group.

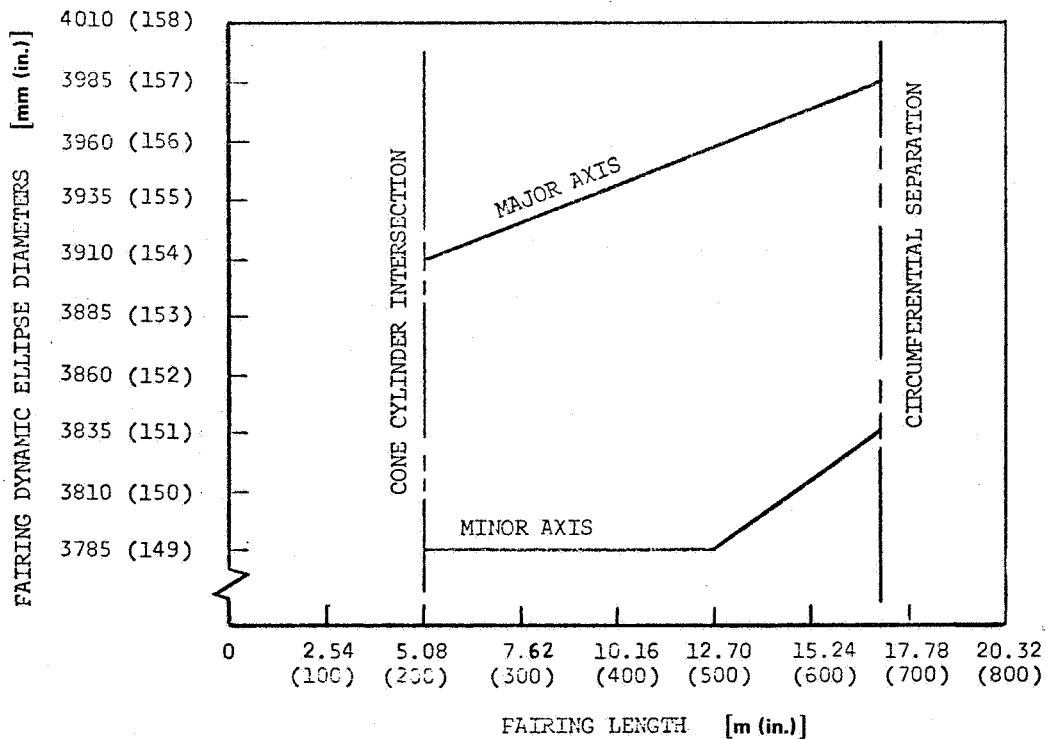


Figure II-2. Fairing dynamic envelopes.

3. The probability of no meteoroid penetration will be or exceed:

- a. 0.95 for 5 years — System
- b. 0.98 for 5 years — Pressurizable, inhabited volumes
- c. 0.995 for 5 days — pressurizable inhabited volumes that are inhabited during periods of maintenance.

4. Fluid pressure vessel (bottles) safety factors will be in accordance with Structural Strength Design and Verification Program Requirements, MSFC Handbook 505, June 1, 1971.

5. The telescope structure will be designed to allow a cradle support to be utilized in the primary mirror support ring area for Shuttle launch and retrieval.

6. A safety factor of 1.4 will be applied to limit loads to obtain ultimate loads. A safety factor of 2.0 will be applied to the pressure in pressurized volumes.

7. The add-on structure necessary to accomplish a Shuttle launch and/or return will be defined.

8. Structural Linearity — The structural design will minimize coulomb-friction-producing points where possible.

9. The LST will be designed to be capable of launch in the upright or inverted orientation in the Shuttle and in the upright orientation in the Titan.

10. Structural panels containing thermal control coatings will be designed with sufficient rigidity to eliminate the probability of flaking.

11. Limit load factors

- a. Titan launch — 6.0 g axial + 1.5 g pitch.

- b. Shuttle launch

- (1) 3.3 g axial + 0.6 g pitch + 0.6 g yaw at cutoff.
- (2) -0.5 g axial -4.0 g pitch  $\pm$  1.0 g yaw at reentry.
- (3) -1.3 g axial -3.2 g pitch  $\pm$  0.5 g yaw at landing.

### 3. Thermal Control Guidelines

1. See the preceding heading, Structure Guidelines, item 2.
2. The power required for thermal control of the OTA will be assumed initially to be 400 watts. The power to be dissipated from the SIP and SSM are 300 watts and 786 watts, respectively (initial assumptions).
3. The baseline OTA/SIP interface will be designed to be adiabatic. The thermal interfaces between the SSM and the SIP are the radiative surfaces of each instrument. SIP waste heat is to be dissipated through the SSM walls.
4. The thermal control design will be as passive as possible to insure high reliability, long life, low cost, minimum interference with other systems, and minimum maintenance requirements.
5. See the heading, General Study Guidelines, item 9.
6. See the heading, Structure Guidelines, item 10.

### 4. Communications and Data Management Guidelines

1. The Spaceflight Tracking and Data Network (STDN) will be the primary data network for early missions. The maximum data rate capability of the stations is assumed to be as follows:
  - a. Uplink — 1 kbs
  - b. Downlink — 1 megabit/sec
2. Baseline communications and data systems will be designed to be independent of the Tracking and Data Relay Satellite System (TDRSS).
3. Bit error rates are as follow:

a. Downlink —  $P_e^b = 10^{-5}$ ,

b. Uplink —  $P_e^b = 10^{-9}$

4. The time resolution for the command execution is 5 minutes  
24 hours.

5. Clock stability:  $1 \times 10^{-7}$  in 24 hours  
Clock resolution: 16 kHz

6. One quick-look picture per orbit displayed at a control center is required to locate a spectrograph slit with respect to an object star. Alternatives to provide this capability will be investigated.

7. The control center is assumed to be in the continental United States for the purpose of this study.

5. Attitude Control System (ACS) Guidelines

1. Guide star acquisition accuracy (SSM trackers) will be as follows:

a.  $\pm 30$  arc sec (2 axis),  $3\sigma$

b.  $\pm 0.1$  degrees about line of sight (LOS),  $3\sigma$ .

2. LST coarse pointing accuracy (offset fine guidance sensors + SSM actuators) will be  $\pm 1$  arc sec (3-axis),  $3\sigma$ . Note: Body stabilization capability will be studied to as fine an accuracy as possible.

3. LST fine pointing accuracy (offset fine guidance sensors + SSM actuators + secondary mirror control) is  $\pm 0.1$  arc sec (2-axis).

4. Image motion stabilization (offset fine guidance sensors + SSM actuators + secondary mirror control) is 0.005 arc sec rms (2-axis).

5. Maneuvering: at least 60 degrees in 40 minutes required; up to 90 degrees in 5 minutes will be considered, depending on actuator selection.

6. LST motion settling time after maneuver should be no greater than 5 minutes (including OTA coarse/fine guidance handoff).

7. Occasional off-sun roll orientation about the viewing axis during daylight or dark times may be required (up to three orbits duration, no more often than once per month) for spectrograph slit orientation. This should not be allowed to drive the design inordinately.

6. Electrical System Guidelines

1. The baseline electrical power design will be a solar array-rechargeable battery system.

2. Solar arrays should be capable of being oriented so that the LST might view the entire celestial sphere. Arrays should be retractable and/or jettisonable for compatibility with Shuttle visits and return to earth.

3. System voltage shall be a nominal  $29 \pm 1$  Vdc, with regulation.

4. See the heading, Attitude Control System Guideline, item 7.

## CHAPTER III. MISSION ANALYSIS



# TABLE OF CONTENTS

	Page
A. Reference Design Mission Analysis . . . . .	III-1
B. Orbit Selection and Lifetime Analysis* . . . . .	III-5
C. Launch Vehicle Analysis . . . . .	III-7
1. Space Shuttle . . . . .	III-7
2. Alternate Expendable Launch Vehicles . . . . .	III-10
a. Shroud Considerations . . . . .	III-10
b. Configuration Characteristics . . . . .	III-12
c. Performance . . . . .	III-14
d. Payload Characteristics Summary . . . . .	III-20
e. Cost Considerations . . . . .	III-28
f. Conclusions . . . . .	III-28
D. On-Orbit Operations* . . . . .	III-31
1. Source Viewing Requirements . . . . .	III-31
2. Orbital Environment . . . . .	III-31
a. Trapped Particle Radiation . . . . .	III-31
b. Magnetic Field . . . . .	III-33
c. External Disturbances . . . . .	III-33
d. Micrometeoroid Flux . . . . .	III-33
e. Contamination . . . . .	III-34
f. Stray Light . . . . .	III-34
3. Operational Constraints . . . . .	III-34
a. General . . . . .	III-34
b. Viewing Constraints . . . . .	III-35
c. Light Shield and Solar Panel Orientation Constraints . . . . .	III-37
d. Spectrograph Slit Orientation Requirements . . . . .	III-38
e. Spacecraft Maneuver Rate Capability . . . . .	III-38
f. Data Integration Limitations . . . . .	III-40

---

\*Results of the analysis performed in these areas by Program Development in the LST Preliminary Design Study and the present study and Martin Marietta's results appearing in Itek's "LST Phase A Study, Volume III - Design Analysis and Trade Studies" have been combined.



## TABLE OF CONTENTS (Concluded)

	Page
g. Scientific Data Storage and Transmission Capability .....	III-40
h. Observation Scheduling .....	III-40
4. Stellar Viewing Opportunities .....	III-51
a. General Viewing Opportunities .....	III-51
b. Earth Shadow Viewing .....	III-54
c. Two-Object Viewing .....	III-55
d. Instrument Checkout and Calibration Timeline ...	III-66
e. Typical Observation Day of UV Galactic Faint Objects .....	III-68
f. Typical Observation Day of UV Galactic Bright Stars .....	III-71
5. Conclusions .....	III-76
6. Operating Modes .....	III-79
E. Coverage Contact Statistics .....	III-80
1. Preliminary LST Mission Coverage .....	III-80
2. Coverage Assessment .....	III-81
F. Support Operations .....	III-95
1. Facilities/Equipment Required .....	III-95
2. Titan Launch Facilities .....	III-100
3. Shuttle Maintenance/Revisit .....	III-103
References .....	III-106

# LIST OF ILLUSTRATIONS

Figure	Title	Page
III- 1.	LST deployment profile . . . . .	III-2
III- 2.	LST viewing and contact opportunities . . . . .	III-3
III- 3.	Shuttle performance . . . . .	III-8
III- 4.	LST launch vehicle configurations comparison. . . . .	III-11
III- 5.	Titan IIIE/OAS and Titan IIIC-IA payload mass as a function of perigee altitude . . . . .	III-16
III- 6.	LST launch vehicle performance mass comparison to 28.5 degree circular orbit. . . . .	III-19
III- 7.	Nominal Titan IIIE/OAS LST flight profile . . . . .	III-21
III- 8.	Titan IIIE/OAS LST mission timeline . . . . .	III-22
III- 9.	Titan IIID/Burner II LST flight profile . . . . .	III-23
III-10.	Titan IIID/Agena LST flight profile . . . . .	III-24
III-11.	Power generating efficiency. . . . .	III-39
III-12.	Maneuver time. . . . .	III-39
III-13.	Solar projection on celestial sphere. . . . .	III-41
III-14.	Projection of 45 degree solar and 15 degree lunar avoid- ance cone on celestial sphere on March 21, 1978 . . . . .	III-42
III-15.	Projection of 45 degree solar and 15 degree lunar avoidance cone on celestial sphere on June 21, 1978. . . . .	III-43
III-16.	Projection of 45 degree solar and 15 degree lunar avoidance cone on celestial sphere on September 21, 1978 . . . . .	III-44

## LIST OF ILLUSTRATIONS (Continued)

Figure	Title	Page
III-17.	Projection of 45 degree solar and 15 degree lunar avoidance cone on celestial sphere on December 21, 1978 . . . . .	III-45
III-18.	Estimated faint object observation constraints for LST . . . . .	III-46
III-19.	Concurrent existence of constraints. . . . .	III-48
III-20.	Existence of favorable condition . . . . .	III-49
III-21.	Various degrees of favorability. . . . .	III-50
III-22.	Source observation time as a function of target angle . . . . .	III-52
III-23.	Unconstrained stellar viewing time . . . . .	III-53
III-24.	Constrained viewing time. . . . .	III-54
III-25.	Typical viewing opportunities at T + 0 (Dec 21). . . . .	III-56
III-26.	Typical viewing opportunities at T + 2 weeks. . . . .	III-57
III-27.	Typical viewing opportunities at T + 4 weeks . . . . .	III-58
III-28.	Typical viewing opportunities at T + 6 weeks . . . . .	III-59
III-29.	Observation time per orbit of a second source when a previous one located 90 degrees away is viewed for its full accessibility time. . . . .	III-60
III-30.	Situation for the observation of a second source (B) when a previous source (A) is viewed for its full accessibility time. . . . .	III-61
III-31.	Situation for the observation of a second source (C) when a previous source (A) is viewed for its full accessibility time . . . . .	III-62

## LIST OF ILLUSTRATIONS (Continued)

Figure	Title	Page
III-32.	Observation time per orbit of a second source when a previous one located 180 degrees away is viewed for its full accessibility time . . . . .	III-63
III-33.	Observation time per source when n are viewed for an equal amount of time and located $\Delta\alpha$ apart versus slew rate . . . . .	III-64
III-34.	Observation time per source when n are viewed for an equal amount of time and located $\Delta\alpha$ apart versus slew rate . . . . .	III-64
III-35.	Observation time per source when n are viewed for an equal amount of time and located $\Delta\alpha$ apart versus slew rate . . . . .	III-65
III-36.	Observation time per source when n are viewed for an equal amount of time and located $\Delta\alpha$ apart versus slew rate. . . . .	III-65
III-37.	Calibration timeline for high speed spectrograph . . . . .	III-67
III-38.	30-day overview of LST observational activities . . . . .	III-69
III-39.	Typical day observation for UV galactic faint objects . . .	III-70
III-40.	Distribution of UV galactic faint sources . . . . .	III-72
III-41.	Distribution of UV bright sources . . . . .	III-73
III-42.	Typical day observation of UV galactic bright objects . . .	III-75
III-43.	Distribution of bright UV galactic bright sources . . . . .	III-77
III-44.	LST observation of bright UV sources . . . . .	III-78

## LIST OF ILLUSTRATIONS (Concluded)

Figure	Title	Page
III-45.	Ground traces and coverages for LST; STDN Network Configuration A; H = 611 km (330 n.mi.) and 741 km (400 n.mi.), i = 28.5 deg . . . . .	III-87
III-46.	STDN station coverage for H = 611 km (330 n.mi.) and 741 km (400 n.mi.). . . . .	III-88
III-47.	Ground traces and coverages for LST; STDN (ATS) Network Configuration; H = 611 km (330 n.mi.) and 741 km (400 n.mi.), i = 28.5 deg . . . . .	III-89
III-48.	Ground contact and gap statistics for STDN Network Configuration A [Altitude = 611 km (330 n.mi.), Inclination = 28.5 deg]. . . . .	III-90
III-49.	Ground contact and gap statistics for STDN (ATS) Network Configuration [Altitude = 611 km (330 n.mi.), Inclination = 28.5 deg] . . . . .	III-91
III-50.	LST prelaunch/ground operations phase timeline . . . . .	III-97
III-51.	LST revisit/on-orbit maintenance . . . . .	III-104

## LIST OF TABLES

Table	Title	Page
III- 1.	Large Space Telescope Deployment Events Sequence . . . . .	III- 4
III- 2.	LST Altitude Selection Parameters . . . . .	III- 9
III- 3.	Modification and Adapter Mass [in kg (lb)] . . . . .	III-15
III- 4.	Orbital Lifetime for 28.5 Degree Inclination with Launch Date of June 1, 1980. . . . .	III-17
III- 5.	Titan IIIE/OAS Vehicle Performance for Final Orbit of 611 km (330 n.mi.) . . . . .	III-18
III- 6.	LST Launch Vehicle Operating Characteristics for a 611 km (330 n.mi.), 28.5 Degree Orbit . . . . .	III-25
III- 7.	LST Launch Vehicle Payload Comparison for 611 km (330 n.mi.), 28.5 Degree Orbit . . . . .	III-26
III- 8.	Payload Characteristics . . . . .	III-27
III- 9.	LST Launch Vehicle Trade Study, 1972 Dollars in Millions . . . . .	III-29
III-10.	Configuration Evaluation Summary . . . . .	III-30
III-11.	Source Viewing Requirements . . . . .	III-32
III-12.	Viewing Constraints . . . . .	III-36
III-13.	Characteristics of 208 G Eridani and 145 G Eridani . . . . .	III-71
III-14.	UV Galactic Bright Stars . . . . .	III-74
III-15.	STDN and STDN (ATS) Coverage Summary for LST . . . . .	III-83
III-16.	Summary of Station Cumulative Contact Time per 24 Hours . . . . .	III-84

## LIST OF TABLES (Concluded)

Table	Title	Page
III-17.	Summary of Average Net Contact Time Per Day . . . . .	III- 86
III-18.	Contact Summary of Tracking Stations with LST Space- craft STDN Network Configuration A . . . . .	III- 92
III-19.	Contact Summary of Tracking Stations with LST-Space- craft STDN Network Configuration B . . . . .	III- 93
III-20.	Contact Summary of Tracking Stations with LST Space- craft STDN (ATS) Network Configuration . . . . .	III- 94
III-21.	Postflight Ground Operations Timeline. . . . .	III-101

## CHAPTER III. MISSION ANALYSIS

### A. Reference Design Mission Analysis

Results of the LST Preliminary Study conducted by MSFC's Program Development impacted the Phase A Study reference design mission definition. The recommended orbit (611 km altitude, 28.5 degree inclination) was selected on the basis of launch vehicle performance and space environmental considerations for this Phase A Study. The Space Shuttle will be the primary launch vehicle and means for emergency and/or end-of-life LST retrieval.

An LST delivery flight profile for Space Shuttle delivery of the LST to the final orbit is presented in Table III-1 and Figure III-1. The major events required for LST deployment and system activation are described. The Shuttle ascent profile checkout sequence in the 185.2 km (100 n. mi.) orbit, transfer to the LST orbit, LST deployment operation, Shuttle phasing for reentry, deorbit, and landing are defined with their duration and  $\Delta V$  requirement. The orbital coast time for deorbit phasing was scheduled to allow a period for Shuttle systems checkout and crew rest prior to initiation of the deorbit maneuver (Event 23). The deorbit phasing and reentry times specified are consistent with Shuttle cross-range and atmospheric maneuvering capability. The availability of dark-time viewing opportunities for checkout, calibration, and tracking station contact during the 7 day deployment mission duration is shown in Figure III-2. Tracking station contact for the six stations listed is represented by the single vertical bars. The width of these bars is the length of contact as read from the abscissa of the figure. The abscissa is scaled from time of launch ("0 hours") to 160 hours, which encompasses LST activation and deployment as shown in Table III-1. The time spent on the sunlight portion of the orbit is depicted similarly with the dark-time viewing opportunities indicated between sunlight periods.

Once the LST is in its operating orbit, there will be a period of preparation for normal operations. Solar arrays will have been deployed and the support systems module (SSM) subsystems activated prior to release from the Shuttle. A series of maneuvers will be performed to check the functioning of the attitude control system (ACS). Once the SSM maneuvering capability has been verified, the optical telescope assemblies (OTA) and scientific instrument package (SIP) will be checked. Also, what has been termed "relative calibration" will be performed on each instrument in the SIP, and the calibration data will be analyzed to verify the functioning of those instruments. This type of calibration will essentially compare on-orbit instrument



readings utilizing an artificial source with those received on the ground from the same source prior to launch. This calibration will identify any changes in instrument performance due to launch vibrations.

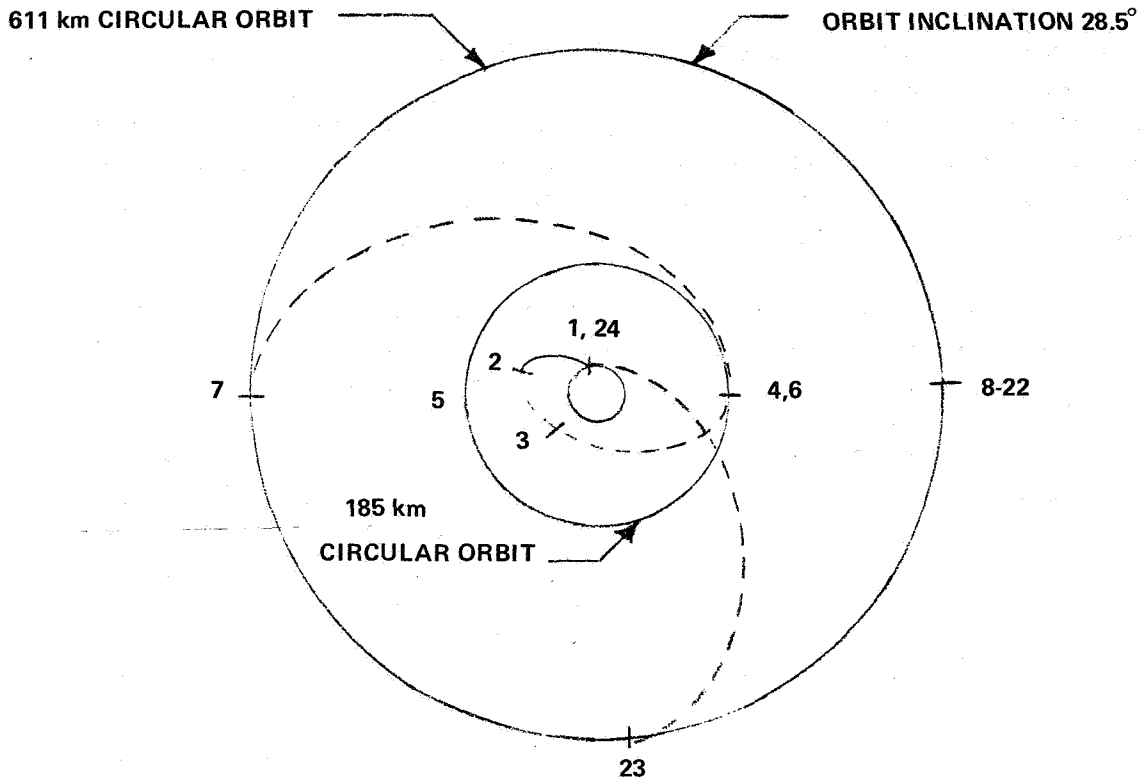
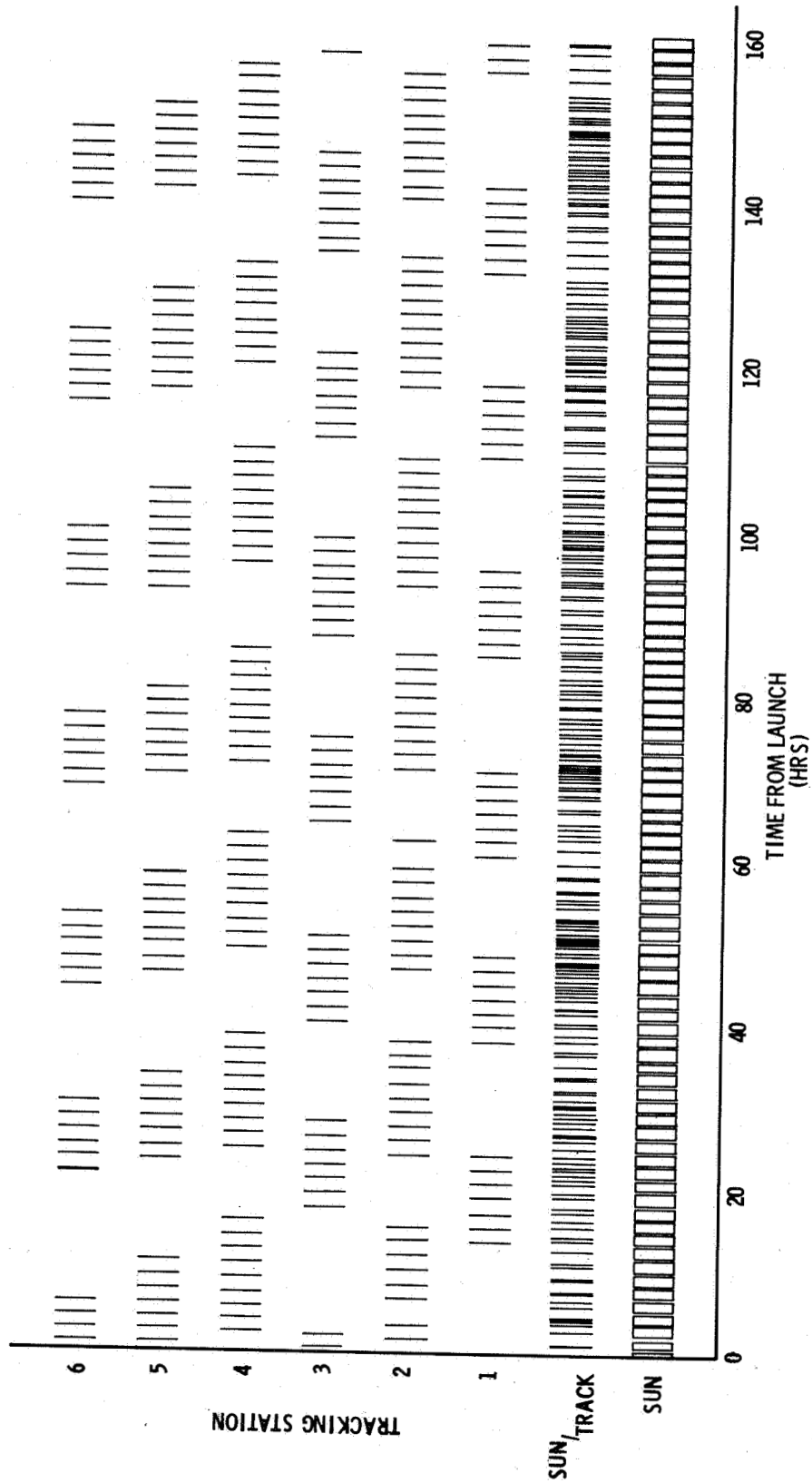


Figure III-1. LST deployment profile.

When the postlaunch checkout of the LST functions has been completed, an inactive period of approximately 48 hours will be provided to permit the clearing of contamination (e.g., engine exhaust, outgassing) and to allow the LST to reach thermal equilibrium. At the end of the contamination clearing period, a series of observations will be made using selected celestial objects in order to check the functioning of the LST subsystems in an operating environment and to measure the stability of telescope pointing.

The observation sequence will be initiated by maneuvering the line of sight (LOS) to a known standard calibration star for the desired instrument and, if required, the alignment of the instrument and telescope optics.



TRACKING STATIONS: 1 - GRAND CANARY ISLAND, 2 - ASCENSION, 3 - CARNARVON, 4 - GUAM, 5 - HAWAII, 6 - GOLDSTONE  
 NOTE: TRACKING FACILITY AT CARNARVON IS TO BE PHASED OUT IN 1974; HOWEVER, PARTICIPATION OF ORRORAL VALLEY  
 WAS CONSIDERED.

Figure III-2. LST viewing and contact opportunities.

TABLE III-1. LARGE SPACE TELESCOPE DEPLOYMENT EVENTS SEQUENCE

Start Time		Event Duration		Event Description	$\Delta V$ (m/s)
Days	Hours	Hours	No.		
0.00	0.00	0.00	1	Launch	
0.00	0.00	0.11	2	Inject into 185.2 km, 28.5° ascent orbit	
0.00	0.11	0.33	3	Separate from drop-tanks	
0.02	0.44	0.40	4	Coast to 185.2 km apogee and circularize	28.
0.04	0.84	4.41	5	Checkout Shuttle systems (3 revs)	
0.23	5.45	0.13	6	Burn and inject into 185.2 x 611 km transfer orbit	121.
0.23	5.58	0.77	7	Coast to 611 km apogee and circularize	120.
0.26	6.35	5.65	8	Open cargo bay, erect LST, begin systems check	
0.50	12.00	11.00	9	Crew rest and miscellaneous activities	
0.96	23.00	12.00	10	Continue LST systems checkout	
1.46	35.00	11.00	11	Crew rest and miscellaneous activities	
1.92	46.00	12.00	12	Continue LST systems checkout	
2.42	58.00	11.00	13	Crew rest and miscellaneous activities	
2.88	69.00	12.00	14	Continue LST systems checkout	
3.38	81.00	11.00	15	Crew rest and miscellaneous activities	
3.83	92.00	12.00	16	Continue LST systems checkout	
4.33	104.00	11.00	17	Crew rest and miscellaneous activities	
4.79	115.00	12.00	18	Continue LST systems checkout	
5.29	127.00	11.00	19	Crew rest and miscellaneous activities	
5.75	138.00	12.00	20	Calibration checks completed, eject LST and begin station keeping	
6.25	150.00	11.00	21	Crew rest, LST begins normal operations	
6.71	161.00	6.45	22	Shuttle systems check and phasing for deorbit opportunity	178.
6.98	167.45	0.17	23	Deorbit	
6.98	167.62	1.56	24	Reentry and landing	
				Total $\Delta V$ Required	447.

MSFC - Form 3304 (July 1969)

Following alignment, what has been termed "absolute calibration" will be performed. Specifically, this type of calibration will require that the specific instrument be calibrated against the known standard calibration star. No specific amount of time will be allocated at the beginning of the mission to perform this type of calibration on each instrument contained in the SIP, rather an instrument will be calibrated immediately prior to its use by the principal investigator who will be using it.

Following calibration, the two guide stars to be used during the observation will be acquired, the object to be observed will be centered in the field of the instrument, and the appropriate fine adjustment in telescope focus will be made. Once the object has been acquired, the data taking period will be initiated. During this interval, frames of data will be periodically read out of the instrument for transmission to ground. These frames result from integration (and storage) of the light energy from the object in the instrument camera tube.

When maintenance is required, a manned Shuttle will rendezvous with the LST to service and repair the LST subsystems. Periodic checkout and ground control monitoring of the LST will identify failures and degraded components and will provide a basis for the maintenance plan and spares inventory for the flight. Maintenance will be performed with the LST docked to an airlock module extended from the payload bay to the Shuttle Orbiter. The maintenance crew will consist of at least two men in addition to the two-man Shuttle crew.

## B. Orbit Selection and Lifetime Analysis

For a given LST design and a given set of objectives, the main elements that influence orbital operations are the orbit, the orbital environment, operational constraints, and target viewing opportunities. Complete knowledge of these factors allows development of typical operational concepts and sequences that can be used to measure performance and to perform tradeoffs of alternative systems and operations. One of the first tasks in planning an earth orbital mission is the selection of the orbit which maximizes mission performance and simplifies subsystem design. Program constraints include the use of the Shuttle as the primary launch vehicle with the Titan III E/OAS as an alternate, use of Kennedy Space Center (KSC) as the launch site, orbital accessibility by the Shuttle for maintenance or return, and minimum lifetime of 5 years. (The Titan IID is designated Titan III E when flown out of the Eastern Test Range with the OAS, the Integral, or the Centaur stage.) Mission performance parameters that are a function of the orbital elements are:

1. Payload capability.
2. Orbit decay rate.
3. Ground station contact time.
4. Target visibility.
5. Target viewing time.

Orbital environments that affect subsystem design are:

1. Trapped particle radiation.
2. Magnetic fields.
3. External disturbances.
4. Micrometeoroid flux.
5. Contamination.
6. Stray light.

A parametric orbit selection analysis was performed for the LST design study. Included in the analysis was the determination of minimum orbital altitude requirements for nominal mission conditions, lifetime and decay histories for the reference orbit, assessment of the effects of spacecraft configuration and mass changes on orbital lifetime, Space Shuttle performance capabilities, tracking network coverage, and mission timelines.

Consideration of all of the above performance and environmental parameters led to the selection of a circular orbit with an inclination of 28.5 degrees and an initial altitude of 611 km (330 n. mi.). A quantitative summary of most of these parameters and their sensitivities to change in altitude is given in Table III-2. A circular orbit was selected because no significant benefits can be derived from any elliptical orbit that can be attained, given the capabilities of the Shuttle or Titan launch vehicle. An orbital inclination of 28.5 degrees attained with a due-east launch from KSC was selected for the following reasons:

1. Lower inclinations require yaw steering and a significant loss in payload capability.
2. Higher inclinations quickly reduce the prime earth shadow viewing time.
3. Most of the other Shuttle delivery missions that can be combined with LST maintenance visits are located in 28.5 degree orbits.

The sensitivity of other performance parameters to inclinations between 28.5 and 40 degrees is negligible. The most significant parameters involved in the selection of an orbital altitude (see Table III-2) are (1) Titan payload capability, (2) orbital decay rate, and (3) trapped particle radiation environment. Payload capability and radiation environment make a low orbit desirable, whereas the decay rate makes a high orbit preferable. A good compromise occurs at an orbital altitude of 611 km. This selection was originally based on a 1978 launch date. The lower atmospheric density associated with the planned 1980 launch would enable an altitude reduction to approximately 556 km (300 n. mi.) if either a 181.5 kg (400 lb) increase in Titan payload capability or a 30 percent reduction in radiation environment is required. LST performance degradation due to residual atmospheric elements may become a significant factor in final orbit selection when this effect is better understood. Possible significance of increased ground station contact time with increased altitude must await a more complete evaluation of orbital operations and the design of the data and communication system to determine current network utilization at 611 km.

## C. Launch Vehicle Analysis

1. Space Shuttle. The Space Shuttle was designated as the design reference LST launch vehicle. Therefore, the result of the LST orbit selection had to be compatible with Space Shuttle performance capability. The Shuttle performance capability to low-earth orbit with and without the addition of OMS kits to the cargo bay is shown in Figure III-3. These data are for a 040C-2 orbiter-parallel burn, solid rocket motor launch assuming an OMS  $\Delta V$  reserve of 15.2 m/sec (50 ft/sec) and were taken from the "Space Shuttle Performance Capabilities" document<sup>1</sup>. The Shuttle has the capability to deliver approximately 23 587 kg (52 000 lb) to the 611 km (330 n. mi.) design reference orbit with one OMS tank set added to the cargo bay.

---

1. Space Shuttle Performance Capabilities, Revision 1, MSC-04813, May 16, 1972.

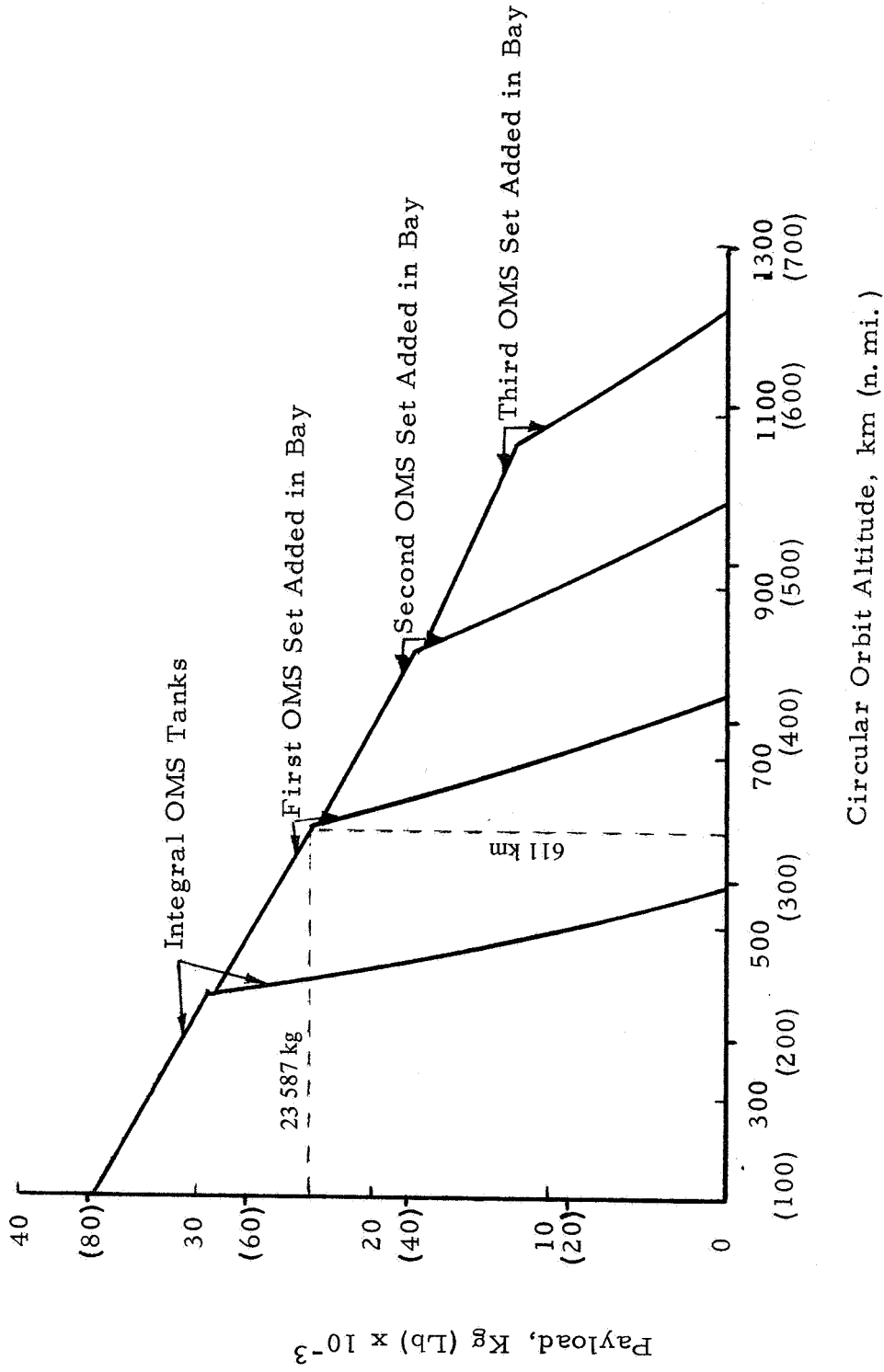


Figure III-3. Shuttle performance.

TABLE III-2. LST ALTITUDE SELECTION PARAMETERS

Parameter	Value <sup>f</sup>	Altitude Sensitivity <sup>i</sup>		Sensitivity Significance <sup>j</sup>
		Percent/n, mi.	Percent/km	
Shuttle Payload Capability	$1.82 \times 10^4$ kg, (40 000 lb) <sup>g</sup>	-16/+185	-16/+100	No
Titan III Payload Capability	$1.03 \times 10^4$ kg, (22 700 lb)	-6/+185	-6/+100	Yes
Orbit Lifetime	24 years <sup>h</sup>	-70/-93	-70/-50	No
Five-Year Orbit Decay <sup>a</sup>	16.70 km (9 n. mi.)	+700/-93	+700/-50	Yes
Maximum External Disturbance <sup>b</sup>	502 ±163 joule-sec, (370 ±120 ft-lb-sec)	+2/-93	+2/-50	No
Radiation Dose <sup>c</sup>				
Average	1.0 rad/day	+90/+185	+90/+100	Yes
Maximum	4.5 rad/day	+90/+185	+90/+100	Yes
Ground Station Contact <sup>d</sup>				
Average	26 min/orbit	-16/-93	-16/-50	No
Minimum	7 min/orbit	-16/-93	-16/-50	No
Earth Shadow Viewing Time	33 min/orbit	-2/+185	-2/+100	No
Target Viewing Time <sup>e</sup>	53 min/orbit	-2/-93	-2/-50	No

a. 1980 to 1983 density and ballistic coefficient = 427 N/m<sup>2</sup> (8.9 lb/ft<sup>2</sup>).

b. Maximum gravity gradient momentum (secular/orbit ± periodic).

c. Aluminum shielding = 0.71 cm (0.28 in.) maximum rate in South Atlantic anomaly.

d. Six-station set (ACN, CYL, GDS, GWM, HAW, HSK).

e. In-orbit plane, 0.26 rad (15 degrees) from earth limb.

f. At selected orbit of 611 km (330 n. mi.) and 28.5 degrees.

g. Orbit maneuvering system (OMS) ΔV reserve = 36.6 m/sec (120 ft/s) for rendezvous. Payload capability = 23 587 kg (52 000 lb) with OMS ΔV reserve = 15.2 m/sec (50 ft/s).

h. Orbit lifetime = 11 years for +2 σ solar density.

i. In adverse direction.

j. Relative to requirements and capabilities.



A single OMS tank set requires 1.52 m (5 ft) of the 18.29 m (60 ft) long cargo bay. The docking module which will be carried in the cargo bay on the LST delivery and maintenance flights requires 2.13 m (7 ft) of the cargo bay length and has a mass of 907.2 to 1360.8 kg (2000 to 3000 lb). A drawing of the Shuttle cargo bay configuration is shown in Volume V, Chapter VII. The Shuttle offers ample performance capability and payload cargo bay volume.

2. Alternate Expendable Launch Vehicles. An alternative expendable launch vehicle comparison study was performed to select a backup LST launch vehicle. The study also identified the optimum ascent profile for obtaining the mission orbit with an expendable vehicle, defined operational timelines, and investigated ways of increasing vehicle performance. The following launch vehicles were considered (Fig. III-4):

1. Titan IIIC.
2. Titan IIIC IA.
3. Titan IIIE/Centaur.
4. Titan IIID/Agena.
5. Titan IIIE/OAS.
6. Titan IIID/Burner II.
7. Titan IIIE/Integral.

a. Shroud Considerations. All of the configurations have the standard 17.1 m (56 ft) shroud except the Titan IIIC with the transtage inside the shroud (Configuration IA). An additional 1.9 m (75 in.) shroud section is required for this configuration. The Titan IIIE/Centaur (Configuration III) utilizes the standard Viking shroud but supports it on a new payload/shroud/transtage adapter. This structure supports both the shroud and LST loads.

For the purpose of this evaluation, the standard 17.1 m (56 ft) shroud mass was taken to be 2371 kg (5226 lb) total. Of this, 2124 kg (4673 lb) are dropped when the shroud jettisoned, and 251 kg (553 lb), which is the shroud adapter mass, are retained in orbit.

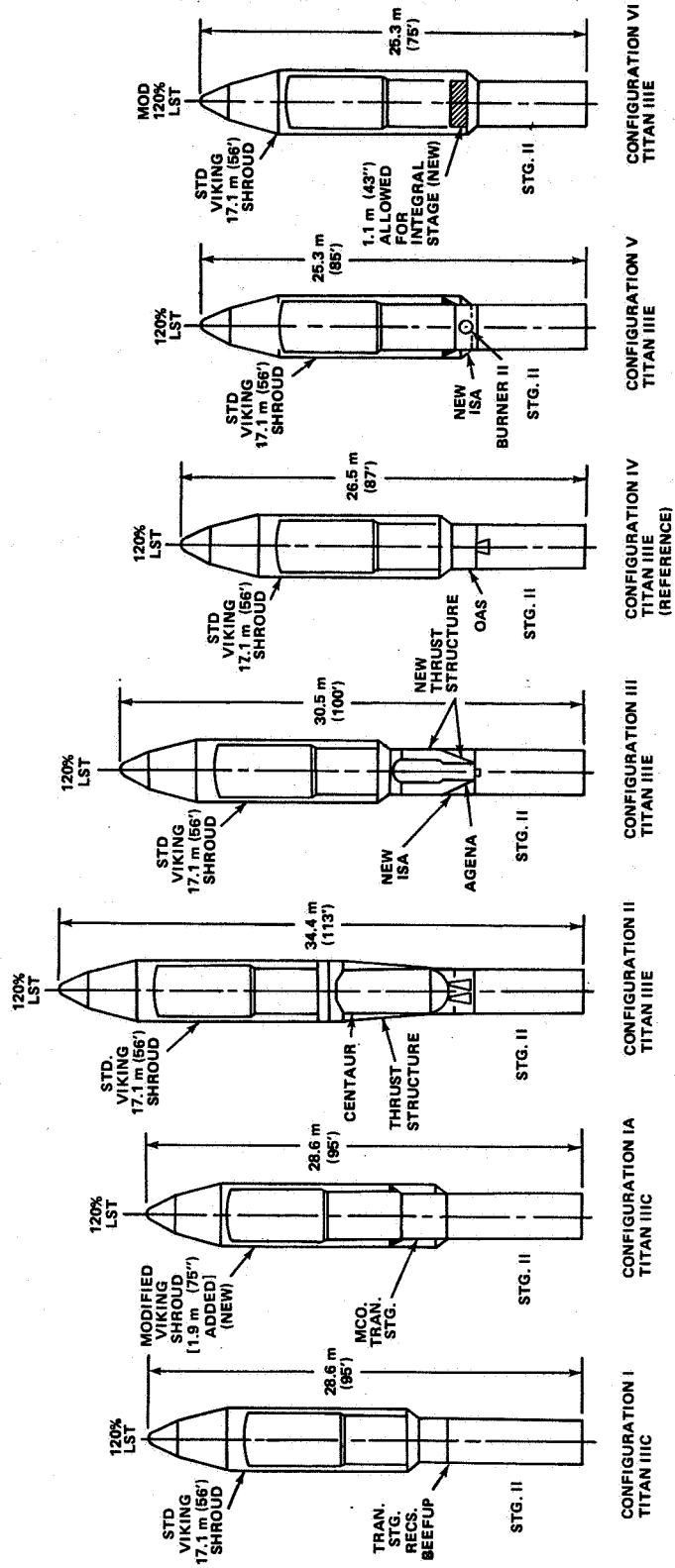


Figure III-4. LST launch vehicle configurations comparison.

## b. Configuration Characteristics

(1) Configuration I, Titan III C with Transtage. In this configuration, the shroud/payload/transtage adapter is attached at the top of the transtage. When the shroud separates, the adapter is carried with the LST payload into orbit. This adapter has a mass of 251 kg (553 lb). Beef-up of the transtage is required since it does not have sufficient strength to support the LST during boost. This beef-up imposes a 1406 kg (3100 lb) mass penalty (see Table III-3).

(2) Configuration IA, Titan III C with Transtage. This configuration is similar to Configuration I except that the shroud is attached to the aft end of the transtage. By enclosing the transtage, an extra 1.9 m (75 in.) section has to be added to the shroud. This means that the spacecraft has been snubbed in the shroud, requiring 181 kg (400 lb) of snubbing structure and spacecraft beef-up. The extra shroud segment and shroud snubbing hardware require 284 kg (624 lb).

At the outset of this study, the Martin Company was contacted about the two transtage configurations (Configurations I and IA). It was indicated that the transtage could not be strengthened sufficiently to carry the launch loads. It was established that Configuration I is not feasible on the basis of the recommendation from the Martin Company.

(3) Configuration II, Titan III E/Centaur. Since the Centaur will not carry the loads imposed by the LST, (either during Titan burn or during its own burn), it becomes necessary to provide a new interstage adapter (ISA) which serves to support the shroud, LST, and Centaur stage. After Core II separation, the structure above the adapter kick ring is retained so that the LST load is transmitted to the bottom of the Centaur; the structure below the kick ring is dropped. After Centaur burn is complete, the entire ISA is separated. The ISA has a mass of 2563 kg (5650 lb) and the interstage adapter below the kick ring has a mass of 454 kg (1000 lb).

The Centaur interstage adapter required is a unique and complex structural assembly. The adapter must include a conical external thrust structure including another separation system. This structure would be a sheet and stringer (with ring frames) design and would include the A-frame links and ring required to react the lateral loads from the Centaur.

Since these structural items are new and untested, at least a minimum proof test would be required; however, the separation system will have to be completely tested.

(4) Configuration III, Titan IIID/Agena. This configuration is identical to Configuration II except the Centaur has been replaced with the Agena. In this case the new ISA results in a 998 kg (2200 lb) penalty. At Core II separation, 272 kg (600 lb) of the ISA mass are dropped. Another 703 kg (1550 lb) are dropped at separation of the Agena.

The Agena interstage adapter is a unique and complex structural assembly. A new cylindrical interstage, including a separation system, would be required and an external thrust structure consisting of a conical shell, cylindrical shell, a kick ring at their juncture, and a separation system at the forward end would also be required.

Certain minor Agena modifications would be required to provide for the conical shell attachment. Since these structural items are new and untested, a minimum proof testing would be required and the separation system will have to be completely tested.

(5) Configuration IV, Titan IIIE/OAS. This configuration is the current reference. The Lockheed OAS supports the shroud and LST mass. No modifications are required to the shroud or OAS.

(6) Configuration V, Titan IIID/Burner II. This configuration utilizes the Burner II in the same manner as the OAS. However, a new ISA will be required to carry the LST loads to the Core II. The ISA has a mass of 438 kg (965 lb) and 136.1 kg (300 lb) of LST modification are required.

A new Burner II structural assembly including two separation systems is required to attach the LST, shroud, and Burner II to the Titan Stage II. This structure would be of sheet and stringer (with ring frames) design, with the Burner II attached by a link mechanism. Since these structural items are new and untested, at least minimum proof testing would be required; however, the separation systems will have to be completely tested. This structure would be less complex than either the Centaur or Agena structures.

(7) Configuration VI, Titan IIIE/Integral. In this configuration, the orbit adjust stage is integrated with the SSM of the LST. After separation of the Core II, the engine is separated, exposing the docking port. No modification is required to the shroud. The integral RCS hardware adds 697 (1536 lb) to the reference SSM structure.

Table III-3 establishes the distribution of the modification mass and also indicates which mass is dropped during staging and which mass remains with the LST as it is boosted into orbit. The latter must be subtracted from the gross payload capability to obtain the net payload capability.

c. Performance. The operations and performance capabilities of each of these launch vehicles are based on the latest launch vehicle characteristics given in References III-1 and III-2.

There are two general types of Titan launch vehicles considered for this study. These are launch vehicles flown with either open or closed loop guidance. For this study, the OAS and the Integral are flown to parking orbit on the Titan IIIE. The Titan IIIE is flown open loop with three sigma dispersion [ III-2]. The nominal parking orbit assumed a 232 by 445 km (125 by 240 n. mi.) ellipse with the OAS or the Integral stage making three burns to achieve the 611 km (330 n. mi.) mission orbit.

For the Titan IIIE/Burner II, the Titan IIIE is assumed to fly closed-loop and inject the Burner II into a 185 by 611 km (100 by 330 n. mi.) parking ellipse. The Burner II can make only one burn, which is made at a 611 km (330 n. mi.) apogee, to circularize into the mission orbit. It was assumed that all the other vehicles considered were flown closed loop and injected into a 185 by 611 km (100 by 330 n. mi.) parking orbit, coasted to a 611 km (330 n. mi.) apogee, upper stage restarted and circularized into the mission orbit.

The launch vehicle payload capability versus the perigee altitude is shown in Figure III-5. Note that the payload capability decreases as the altitude increases. These two launch vehicle configurations (III E/OAS and III C-IA) are typical launch vehicles used in the LST launch vehicle trade study. The III E/OAS is a typical configuration flown with open loop guidance and the III C/IA is a typical launch vehicle flown with closed loop guidance. The desired parking orbit is one having the lowest perigee altitude and a sufficient orbital lifetime that would cause no heating problems for the payload while it waits in orbit.

The lifetimes of various orbits having perigee altitudes in the range of 148 to 296 km (80 to 160 n. mi.) are given in Table III-4. It is shown that an orbit 148 by 611 km (180 by 330 n. mi.) has a lifetime of 3.1 days. This orbital lifetime is sufficient to allow for orbit adjustment to reach the LST mission orbit.

TABLE III-3. MODIFICATION AND ADAPTER MASS [in kg (lb)]

Configuration	Shroud Adapter	Core II Adapter	LST <sup>a</sup> Adapter	Kick Stage Modification	LST Modification	Shroud Modification	Mass Lost at Core II Separation	Mass Lost at LST Separation	Mass Remaining With LST
Titan IIC	250.8 (553)	96.2 (212)	--	1406.2 (3100)	--	--	96.2 (212)	1406.2 (3100)	250.8 (553)
Titan IIC (Configuration IA)	250.8 (553)	96.2 (212)	--	--	181.4 (400)	283. (624)	96.2 (212)	250.8 (553)	181.4 (400)
Titan IIIE/Centaur	--	453.6 (1000)	2562.8 (5650)	--	--	--	299.4 (660)	2331.5 (5140)	385.6 (850)
Titan IIID/Agona	250.8 (553)	306.2 (675)	691.7 (1525)	--	--	--	272.2 (600)	703.1 (1550)	273.5 (603)
Titan IIIE/OAS	250.8 (553)	96.2 (212)	11.3 (25)	--	--	--	96.2 (212)	--	262.2 (578)
Titan IIID/Burner II	250.8 (553)	49.9 (110)	40.8 (90)	210.9 (465)	136.1 (300)	--	22.7 (50)	504.9 (1113)	161. (355)
Titan IIIE/Integral	250.8 (553)	--	11.3 (25)	--	685.4 (1511)	--	508. (1120)	--	439.5 (969)

a. Where not listed separately, this mass is included in the other adapter masses or the kick stage modification mass.

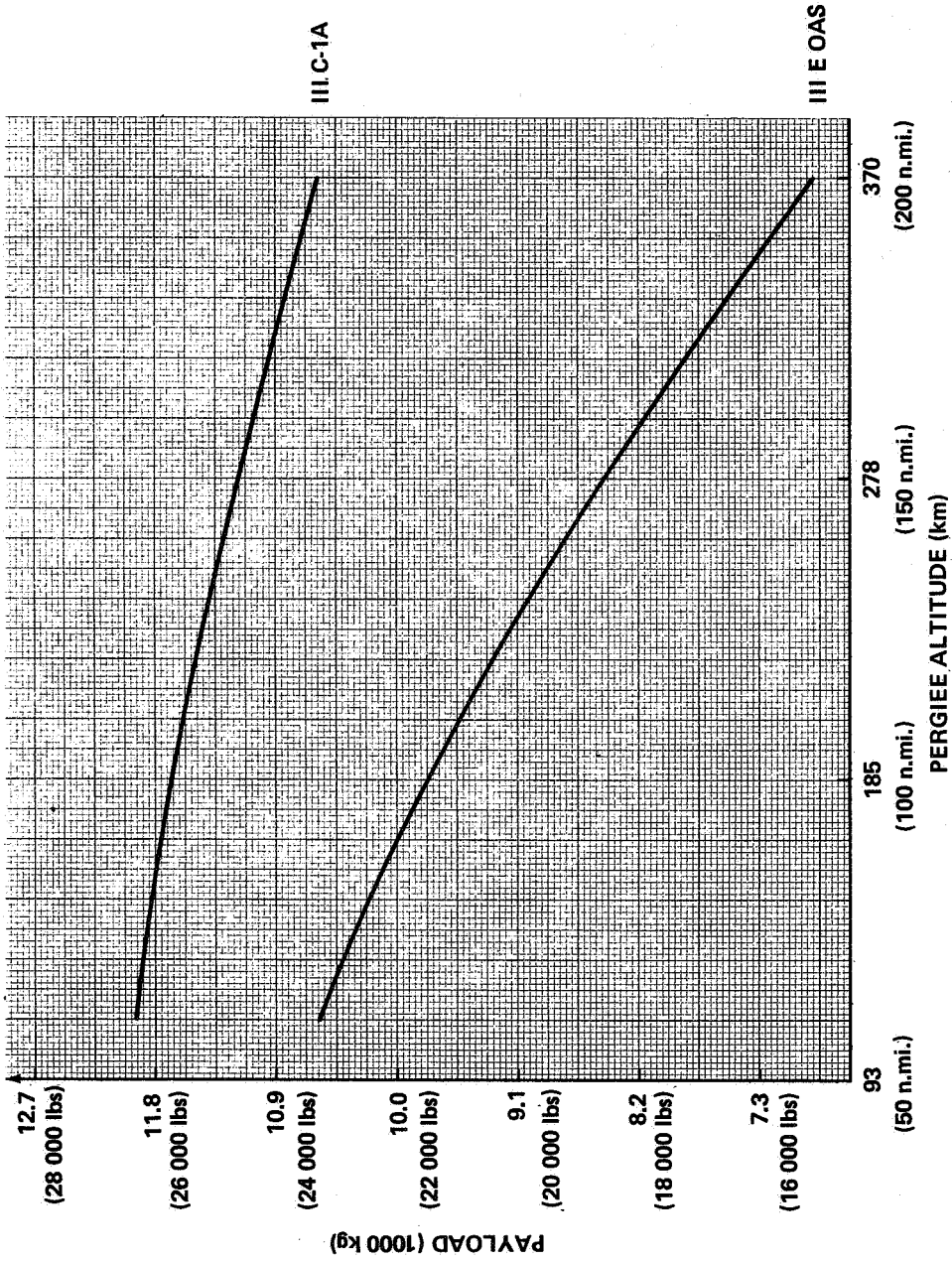


Figure III-5. Titan III E/OAS and Titan III C-1A payload mass as a function of perigee altitude.

The IIIE/OAS payload capability for a 611 km (330 n.mi.) circular orbit is given in Table III-5. The OAS is flown on the Titan IIIE open loop with three sigma dispersion to parking orbit. For details on IIIE open loop dispersion see Reference III-2. The OAS is required to make three burns to adjust the LST into the final orbit. Three nominal orbit injections — 232 by 491 km (125 by 265 n.mi.), 232 by 546 km (125 by 295 n.mi.), and 232 by 445 km (125 by 240 n.mi.) — are given in this table. Because of the IIIE dispersions [III-2], it is possible for the IIIE to inject the OAS into one of the orbits associated with its nominal given in the table instead of the nominal orbit. Based on the lifetime data, performance data, and dispersion data, the preferred parking orbit for the Titan IIIE/OAS is through a 232- by 445-km (125 by 240 n.mi.) orbit. For this parking orbit, the IIIE/OAS could put 9701 kg (21 386 lb) into a 611 km (330 n.mi.) circular orbit.

TABLE III-4. ORBITAL LIFETIME FOR 28.5 DEGREE INCLINATION WITH LAUNCH DATE OF JUNE 1, 1980

Orbit [km (n.mi.)]	Approximate Lifetime (Days)
148 × 611 (80 × 330)	3.1
148 × 667 (80 × 360)	3.6
195 × 583 (105 × 315)	12.9
232 × 491 (125 × 265)	19.1
232 × 546 (125 × 295)	24.8
259 × 463 (140 × 250)	27.3
269 × 391 (145 × 215)	20.9
269 × 454 (145 × 245)	30.3
296 × 370 (160 × 200)	25.5



Payload comparisons for the Titan IIIE/OAS, the Titan IIIE/Integral, the Titan IIID/Burner II, the Titan IIIE/Centaur, the Titan IIIE/Agena, the Titan IIIC, and the Titan IIIC-IA are given in Figure III-6. They are compared for circular orbits in the altitude range of 370 to 741 km (200 to 400 n. mi.). For each of the vehicles listed, the shroud was dropped at 280.5 sec after lift-off, the Q max was less than 4394 kg/m<sup>2</sup> (900 psf), and the integral of Qvt (aerodynamic heating indicator) was less than 4.549 × 10<sup>9</sup> N-m/m<sup>2</sup> (95 000 ft-lb/ft<sup>2</sup>).

TABLE III-5. TITAN IIIE/OAS VEHICLE PERFORMANCE  
FOR FINAL ORBIT OF 611 km (330 n. mi.)

Transfer Orbit		Payload	
km	n. mi.	kg	lb
232 × 491 <sup>a</sup>	125 × 265	9786	21 575
148 × 611 <sup>b</sup>	80 × 330	9838	21 690
269 × 472 <sup>b</sup>	145 × 255	9697	21 379
232 × 546 <sup>a</sup>	125 × 295	9783	21 569
148 × 667 <sup>b</sup>	80 × 360	9661	21 298
269 × 454 <sup>b</sup>	145 × 245	9695	21 375
232 × 445 <sup>a</sup>	125 × 240	9828	21 668
148 × 565 <sup>b</sup>	80 × 305	9883	21 790
269 × 352 <sup>b</sup>	145 × 190	9701	21 386

a. Titan IIIE nominal injected orbit.

b. Titan IIIE off-nominal three sigma dispersion orbit.

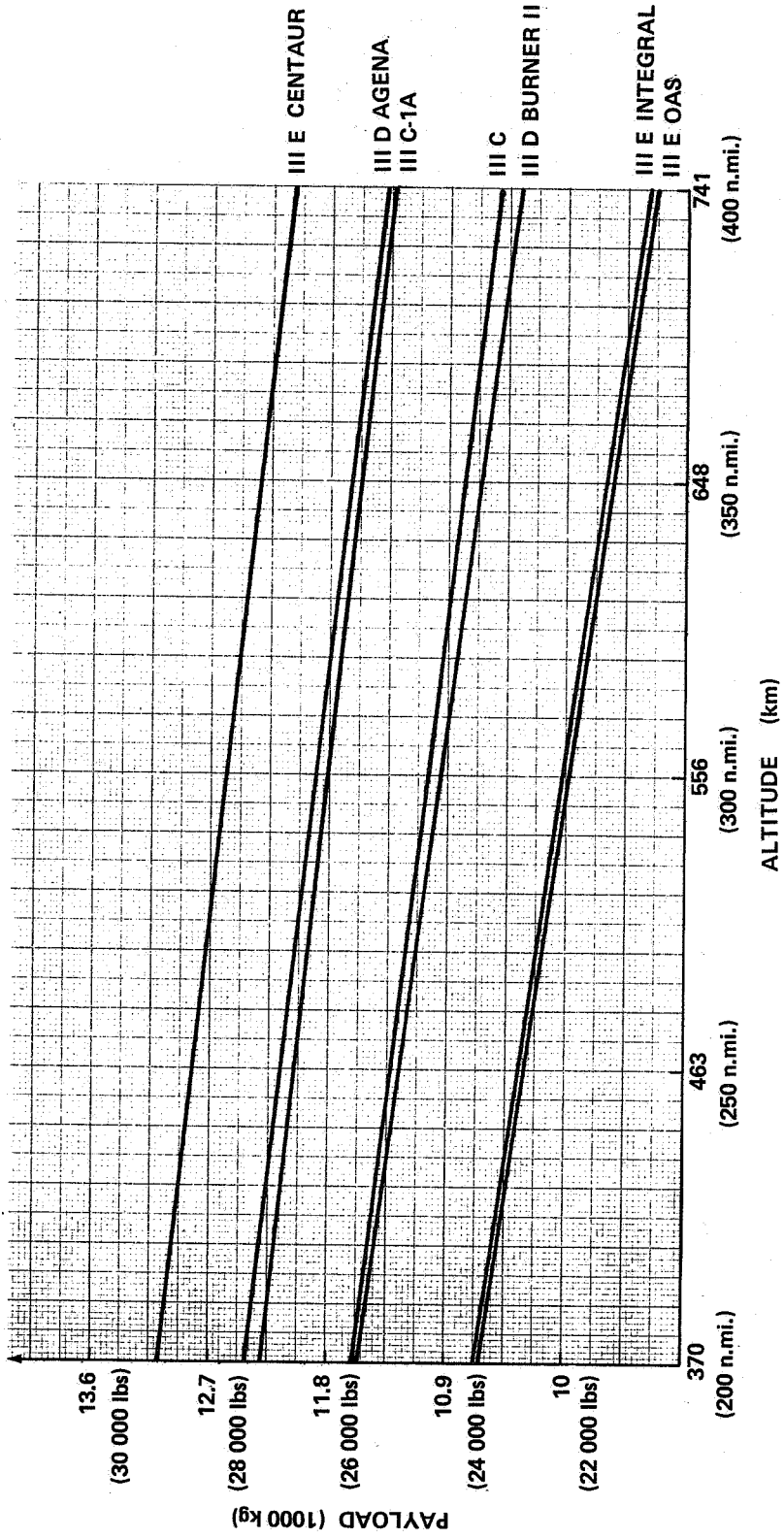


Figure III-6. LST launch vehicle performance mass comparison to 28.5 degree circular orbit.

For each launch vehicle listed in the LST trade study a flight profile schematic and a general timeline was prepared (Figures 7 through 10 are examples). Flight profile schematic shows a flight profile and events sequence for the launch vehicle from lift-off to mission objective. The general timeline describes the events, time required, the delta velocity required to perform the event shown on the flight profile schematic, and the total time required of the launch vehicle from lift-off to injection into the mission orbit.

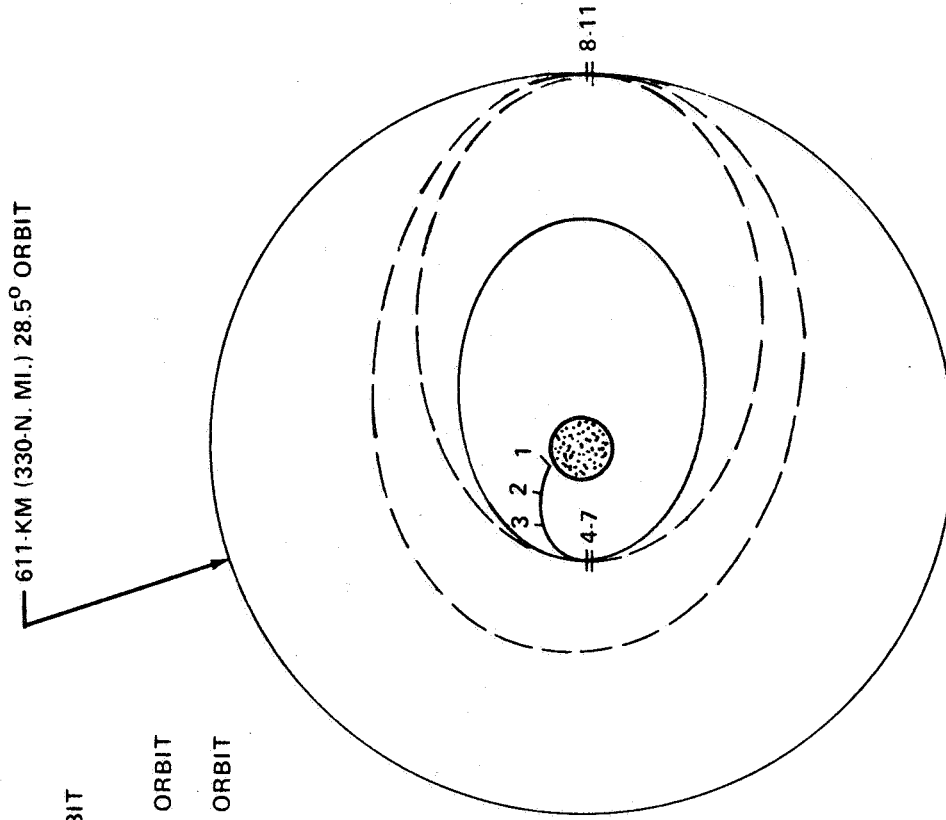
Table III-6 is a summary of the vehicle operating characteristics. It gives a comparison of the operations, propulsion, performance, and payload capabilities. It is shown that Burner II has only one burn capability; from an operational standpoint, this is a disadvantage. A good guidance capability would be required for the IIIE to insure injection of the Burner II into the proper transfer orbit. If the IIIE did not achieve the proper transfer orbit, there would be no way for the Burner II to inject the LST into the mission orbit.

The OAS and the Integral both have low thrust and must be over a tracking station when the 611 km (330 n.mi.) injection burn is made. A long burn time is required to adjust the payload to the proper orbit because the thrust is low. The OAS and the Integral are required to make three burns before achieving LST mission orbit. About 21 hours of phasing time are required. The Centaur has a lifetime of 0.5 hour. This means that after 0.5 hour, the restarting of the Centaur stage cannot be relied upon. The lifetime is sufficient for the LST mission, but for other future missions the 0.5 hour lifetime would not be sufficient.

d. Payload Characteristics Summary. A comparison of the launch vehicle payload capabilities is given in Table III-7. The payload characteristics are given in Table III-8. Gross payload is the total mass which the launch vehicle (including kick stage) can boost to orbit. However, all of this performance is not available as payload; the mass which remains with the LST on orbit must be subtracted. The result is the net payload capability available to be used for LST design. The contingency is computed on the basis of the net payload capability and the reference LST mass.

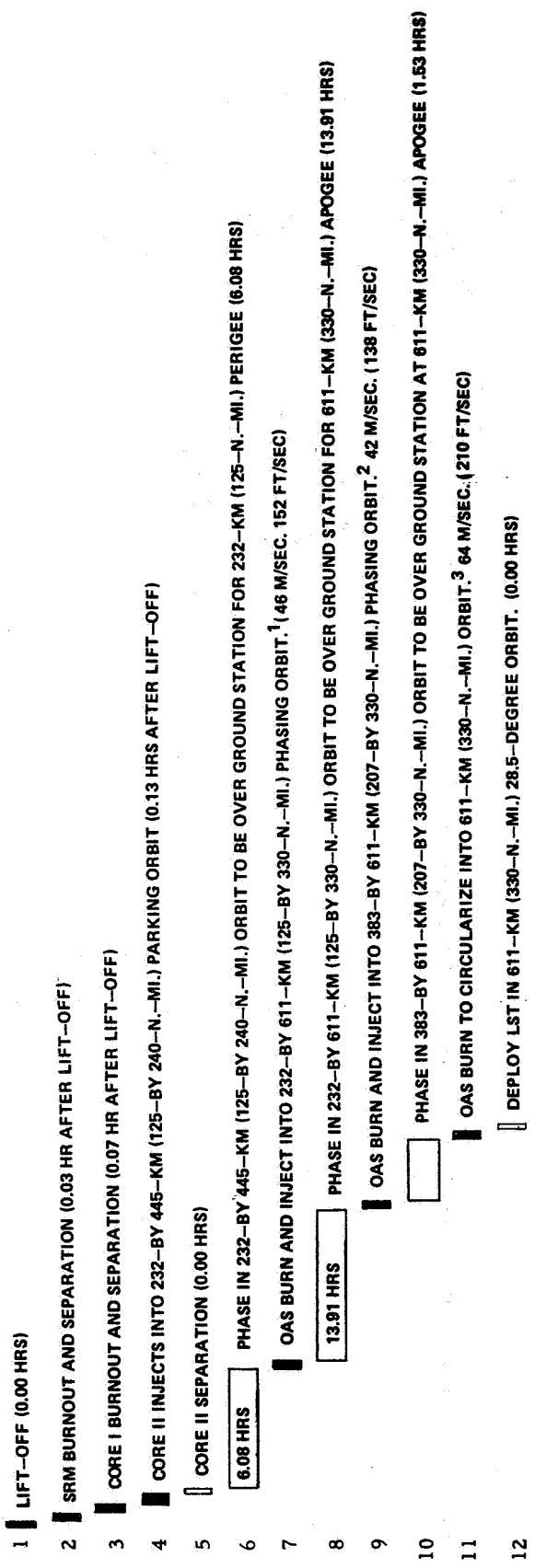
A contingency was not computed for the integral configuration since a baseline mass was not established for the integral configuration. It is felt that a 20 percent contingency is required at this point in time in the program, due to softness of these early numbers and the normal mass growth trend experienced in past programs.

1. LIFT-OFF
2. SRM BURN-OUT AND SEPARATION
3. CORE I BURN-OUT AND SEPARATION
4. INJECT INTO 232-BY 445-KM (125-BY 240-N. MI.) PARKING ORBIT
5. SEPARATE CORE STAGE II
6. COAST TO 232-KM (125-N. MI.) PERIGEE
7. BURN OAS TO INJECT INTO 232-BY 611-KM (125-BY 330-N. MI.) ORBIT
8. COAST TO 611-KM (330-N. MI.) APOGEE
9. BURN OAS TO INJECT INTO 383-BY 611-KM (207-BY 330-N. MI.) ORBIT
10. COAST TO 611-KM (330-N. MI.) APOGEE
11. BURN OAS TO CIRCULARIZE INTO 611-KM (330-N. MI.) ORBIT



NOTE: IDENTICAL LST FLIGHT PROFILE FLOWN BY TITAN IIIE/INTEGRAL

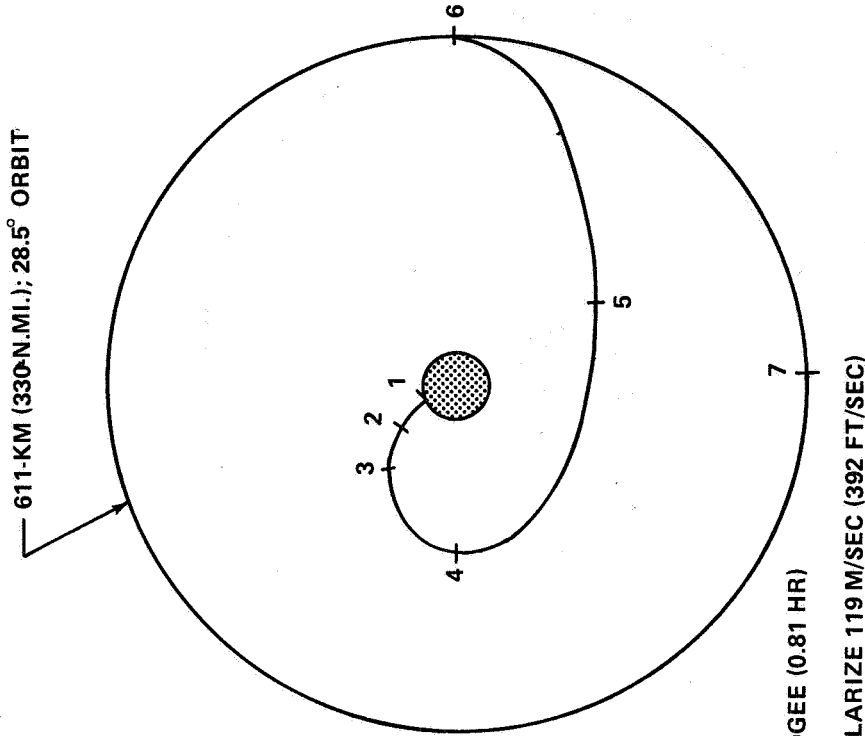
Figure III-7. Nominal Titan IIIE/OAS LST flight profile.




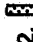





1. OAS BURN 9.90 MIN TO CHANGE ORBIT TO 232-BY 611-KM (125-BY 330-N.-MI.)
2. OAS BURN 8.81 MIN TO CHANGE ORBIT TO 383-BY 611-KM (207-BY 330-N.-MI.)
3. OAS BURN 13.10 MIN TO CIRCULARIZE INTO 611-KM (330-N.-MI.) ORBIT

NOTE: IDENTICAL LST MISSION TIMELINE FOR TITAN IIIE/INTEGRAL

Figure III-8. Titan IIIE/OAS LST mission timeline.



**EVENT:**









1.  LIFT-OFF (0.00 HR)
2.  SRM BURNOUT AND SEPARATION (0.03 HR AFTER LIFT-OFF)
3.  CORE I BURNOUT AND SEPARATION (0.07 HR AFTER LIFT-OFF)
4.  CORE II INJECT INTO 185- BY 611-KM (100- BY 330-N.MI.) TRANSFER ORBIT (0.13 HR AFTER LIFT-OFF)
5.  CORE II SEPARATION AND COST TO 611-KM (330-N.MI.) APOGEE (0.81 HR)
6.  BURNER II BURN AT 611-KM (330-N.MI.) APOGEE TO CIRCULARIZE 119 M/SEC (392 FT/SEC)
7.  DEPLOY LST IN 611-KM (330-N.MI.) 28.5-DEGREE ORBIT

ITEM 1-7 = 0.94 HR

Figure III-9. Titan IID/Burner II LST flight profile.

NOTE: FLIGHT PROFILES AND TIMELINES FOR THE TITAN IIIE/CENTAUR, TITAN IIIC, TITAN IIIC-1A ARE SIMILAR

EVENT:

1.  LIFT-OFF (0.00 HR)
2.  SRM BURNOUT AND SEPARATION (0.03 HR AFTER LIFT-OFF)
3.  CORE I BURNOUT AND SEPARATION (0.07 HR AFTER LIFT-OFF)
4.  CORE II BURNOUT AND SEPARATION (0.13 HR AFTER LIFT-OFF)
5.  AGENA INJECT INTO 185- BY 611-KM (100-BY 300-N.MI.) TRANSFER ORBIT (0.20 HR AFTER LIFT-OFF)
6.  COAST TO 611-KM (330-N.MI.) APOGEE (0.81 HR)
7.  BURN AGENA AT 611-KM (330-N.MI.) APOGEE TO CIRCULARIZE 119 M/SEC (392 FT/SEC)
8.  DEPLOY LST IN 611-KM (330-N.MI.) 28.5 DEGREE ORBIT (0.00 HR)

ITEM 1-8 = 1.01 HRS

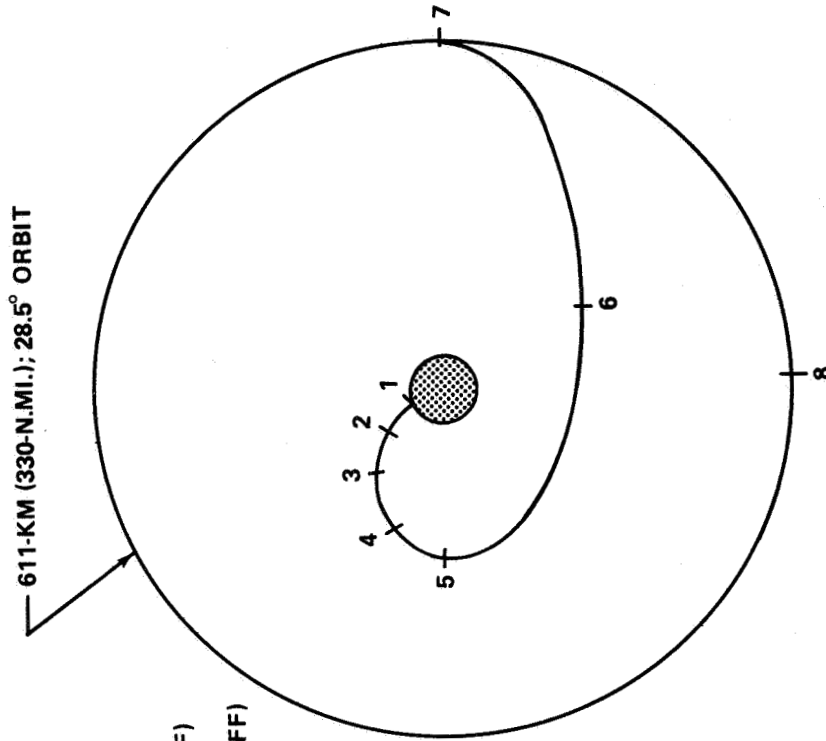


Figure III-10. Titan IIIE/Agena LST flight profile.

TABLE III-6. LST LAUNCH VEHICLE OPERATING CHARACTERISTICS FOR  
A 611 km (330 n. mi.), 28.5 DEGREE ORBIT

Parameter	Transtage	Transtage IA	Centaur	Agena	OAS	Burner II	Integral
Thrust (kg) (lb)	7257 (16 000)	7257 (16 000)	13 608 (30 000)	7257 (16 000)	98 (215)	4436 (9780)	98 (215)
I <sub>sp</sub> (sec)	302	302	442	293	230	290	230
Delta Velocity (m/sec) (ft/sec)	1778 (5834)	1778 (5834)	2470 (8104)	1185 (3889)	280 (918)	257 (843)	280 (918)
Burntime (sec)	401.9	401.9	439.9	245.2	1764.1	32.2	1764.1
Number of Burns Capability	Mult	Mult	2	3	Mult	1	Mult
Number of Burns Required	2	2	2	2	3	1	3
Must Burn Over Tracking Station	No	No	No	No	Yes	No	Yes
Launch Site Available ETR	Yes	Yes	Yes	Yes	Yes	Yes	Yes
Maximum g	3.75	3.75	3.76	3.88	4.46	4.43	4.46
Lifetime of Stage	7 hr	7 hr	0.5 hr	30 days	2 yr	14 days	2 yr
Mission Time (hr)	0.90	0.90	0.90	0.84	21.65	0.79	21.65
Payload kg to 611 km (330 n. mi.) (lb)	10 848 (23 916)	11 642 (25 667)	12 440 (27 425)	11 742 (25 886)	9701 (21 386)	10 783 (23 773)	9715 (21 418)
Shroud Separation Time (sec)	280.5	280.5	280.5	280.5	280.5	280.5	280.5



TABLE III-7. LST LAUNCH VEHICLE PAYLOAD COMPARISON  
FOR 611 km (330 n. mi.), 28.5 DEGREE ORBIT

Parameter	IIC/Transtage	IIC/Transtage I-A	III/Centaur	III/Agena	III/OAS	III/Burner II	III/Integral
Mass at Stage Cutoff Core II	25 637 (56 520)	25 207 (55 571)	34 841 (76 811)	23 116 (50 962)	15 303 (33 738)	15 937 (35 136)	15 276 (33 678)
Flight Performance Reserves	0 (0)	0 (0)	0 (0)	0 (0)	680 (1 500)	680 (1 500)	680 (1 500)
Core II Separation	96 (212)	96 (212)	299 (680)	272 (600)	96 (212)	23 (50)	508 (1120)
Core II Mass at Separation	2961 (6527)	2961 (6527)	3784 (8343)	3210 (7076)	2947 (6497)	3004 (6623)	2947 (6497)
Mass at Ignition	22 581 (49 781)	22 150 (48 832)	30 758 (67 808)	19 365 (43 287)	11 560 (25 529)	12 230 (26 963)	11 141 (24 561)
Prop. llant Consumed	7835 (17 274)	7825 (17 274)	13 055 (28 782)	5815 (12 820)	838 (1847)	537 (1183)	896 (1976)
Vehicle Mass at Cutoff	14 841 (32 507)	14 410 (31 558)	17 729 (39 026)	13 820 (30 467)	10 742 (23 682)	11 694 (25 780)	10 656 (22 585)
Stage Mass at Cutoff	1786 (3938)	1786 (3938)	2092 (4611)	648 (1428)	655 (1443)	191 (421)	0 0
Gross Payload	12 959 (28 569)	12 528 (27 620)	15 611 (34 415)	13 172 (29 039)	10 087 (22 239)	11 503 (25 359)	10 245 (22 585)
Mass To Be Subtracted:							
Flight Performance Reserves	454 (1000)	454 (1000)	454 (1000)	454 (1000)	125 <sup>a</sup> (275)	54 (118)	90 (198)
Payload Separation	1406 (3100)	251 (553)	2331 (5140)	703 (1550)	0 0	505 (1113)	0 0
Adapters and Mod. Mass Remaining with LST	251 (553)	181 (400)	386 (850)	274 (603)	263 (578)	161 (355)	440 (969)
Total Mass To Be Subtracted	2111 (4653)	886 (1953)	3171 (6990)	1430 (3155)	387 (853)	719 (1586)	529 (1167)
Net Allowable LST Mass	10 848 (23 916)	11 642 (25 667)	12 440 (27 425)	11 742 (25 886)	9701 (21 386)	10 783 (23 773)	9715 (21 418)

a. Includes 41 kg (90 lb) of RCS propellant.

TABLE III-8. PAYLOAD CHARACTERISTICS

Parameter	I T-III C	IA T-III C-IA	II Centaur	III Agena	IV OAS	V Burner II	VI Integral
Net Allowable LST Mass, kg (lb)	10 848 (23 916)	11 642 (25 667)	12 440 (27 425)	11 742 (25 886)	9701 (21 386)	10 783 (23 773)	9715 (21 418)
LST Design Reference Mass, kg (lb)	8163 (17 989)	8163 (17 989)	8163 (17 989)	8163 (17 989)	8163 (17 989)	8163 (17 989)	a
LST Growth Capability, kg (lb)	2685 (5927)	3479 (7678)	4277 (9436)	3579 (7897)	1538 (3397)	2620 (5784)	--
Percent Contingency	32.9	42.7	52.5	43.9	18.9	32.1	--

a. Not determined during Phase A study.

e. Cost Considerations. In making the cost trades, only the Titan IIIC and Titan IIIE or IIID launch vehicles were considered. Five different final stages were used with the Titan IIIE or Titan IIID and only the transtage was used with Titan IIIC vehicle. The final stage, final stage adapter, and the final stage launch services are the primary causes of the cost differences in the five options. The final stage adapters were costed using in-house CERs which were developed for the final stage adapters from historical programmatic data. The Centaur, Agena, and Burner II stages and final stage launch services cost data were taken from the "NASA Launch Vehicle & Propulsion Program Handbook" published by Office of Space Science Applications. The OAS and Integral final stage cost data, along with the Titan IIIC and Titan IIID launch vehicles, booster modification and integration, payload adapter, payload fairing, and launch services were furnished by Martin Marietta Corporation. Martin made the assumption that the cost of integrating the integral final stage to the support systems module (SSM) would be included in the overall SSM integration effort. No costs were included for modification or for a new guidance package for the Titan IIIE or IIID or final stage. Also, no costs were included for launch facilities modification. All cost data were normalized to 1972 dollars and do not include contractor fee. A summary of the cost data is given in Table III-9. Subsequent to this analysis, the cost of the IIIE/OAS has increased somewhat, and the differences between it and the IIIC have become smaller. MSFC has now selected the Titan IIIC rather than the IIIE/OAS as the HEAO launch vehicle.

f. Conclusions. Table III-10 is an overall summary of the key characteristics and feasibility of each configuration. Further study must be performed, particularly in the areas of programmatic considerations, facilities impacts, etc. Although the integral approach is slightly cheaper, it may have more cost risk associated with it since it is less off-the-shelf than the other two. Also, since the Shuttle is the primary launch vehicle, the IIIC and IIIE/OAS provide more flexibility to adapt from the primary to the backup launch vehicle with less impact on the basic LST design, since they are nonintegral. Commonality with the HEAO launch vehicle offers cost and other advantages, and should weigh heavily in the decision.

From a performance point of view, the Titan IIIC-IA (with transtage) has many advantages and is quite attractive as a backup launch vehicle for the LST mission. It has an excellent guidance system, multiple restart capability, long stage lifetime, no requirement for ground tracking, medium thrust, high  $I_{sp}$ , and good performance, and it is a potential candidate for other future missions.

TABLE III-9. LST LAUNCH VEHICLE TRADE STUDY, 1972 DOLLARS IN MILLIONS

Item	C-IA T-III C	C-II T-III E/Centaur	C-III T-III D/Agena	C-IV T-III E/OAS	C-V T-III D/Burner II	C-VI T-III E/Integral/SC
Basic Booster	15.00	12.00	12.00	12.00	12.00	12.00
Final Stage	--	7.49	4.04	1.90	.71	2.10
Booster Mod and Integ.	1.20	1.50	1.50	1.50	1.50	1.50
Payload Adapter	.60	.60	.60	.60	.60	.60
Payload Fairing (Shroud)	1.00	1.00	1.00	1.00	1.00	1.00
Final Stage (Adapter)	2.60	6.80	3.70	--	2.50	--
Launch Services	3.95	3.42	3.42	3.82	3.42	3.42
F/S Launch Services	--	2.94	.90	--	.16	--
Total	24.35	35.75	27.16	20.82	21.89	20.62
Cost Δ	+3.53	+14.93	+6.34	0	+1.07	--.20

TABLE III-10. CONFIGURATION EVALUATION SUMMARY

Configuration	Percent Contingency	Cost (\$M)	Modification	Feasibility	Recommendation For Future Study
T-III C/Transtage (I)	32.9	---	---	No <sup>a</sup>	No
T-III C/Transtage (I-A)	42.7	24.35	Enclosed Trans-Stage with Shroud	Yes	Yes
T-III E/Centaur (II)	52.5	35.75	New ISA and Support Structure	Questionable (Cost and Complexity)	No
T-III D/Agema (III)	43.9	27.16	New ISA and Support Structure	Questionable (Cost and Complexity)	No
T-III E/OAS (IV)	18.9	20.82	None	Yes	Yes
T-III D/Burner II (V)	32.1	21.89	New ISA and Support Structure	Questionable (Poor Guidance)	No
T-III E/Integral (VI)	---	20.62	Build New Stage Integrated With SSM	Yes	Possibly

a. Per recommendation from Martin.

Since the current HEAO launch vehicle at the time of this study was the Titan IIIE/OAS, it was selected as the backup launch vehicle for the LST. The HEAO project now utilizes the Titan IIIC rather than the IIIE/OAS, hence, reassessment of the LST trades between these two should be made at a later date if it is desirable to retain the Titan backup launch.

## D. On-Orbit Operations

1. Source Viewing Requirements. Source viewing requirements for the LST are presented in Table III-11. These activities are separated into two major categories of observation, ultraviolet (UV) and infrared (IR), each of which is further divided into subcategories of galactic faint, galactic bright, and extragalactic source observations. Bright sources will be observed for periods of time considerably less than those of faint sources. For example, viewing times for bright UV sources will be between a few seconds and 30 min each, while the viewing time for faint UV sources will be between 1 and 10 hours per source.

It is noted that the heading "Number of Sources per PI" refers to the approximate number of sources a principal investigator (PI) will want to observe before he relinquishes use of the telescope to another investigator.

2. Orbital Environment. The environment in the selected orbit is reviewed here to ascertain possible impacts on operational concepts.

a. Trapped Particle Radiation. The effects of trapped particle radiation on the operation of LST image tubes are of major concern for two reasons. The first potential problem is that passage through the heavy concentration of particles in the South Atlantic anomaly (SAA) may cause real-time degradation of the image stored on the tube faceplate. Second, the accumulated dosage over many orbits may permanently damage the tube or associated electronics. Calculations made at Princeton have predicted that the proton dose rate averaged over several orbits is  $2 \times 10^6$  protons/cm<sup>2</sup> per day, assuming aluminum skin thickness of 3.5 mm and an orbital altitude of 611 km (330 n. mi.), 28.5 degree inclination. Tests indicate that, if the photocathode is turned off during the South Atlantic anomaly portion of the orbit, a substantial reduction in tube background can be achieved. Further tests under a typical orbital environment indicate that there should be no problem with storing an image during the pass through the anomaly.

TABLE III-11. SOURCE VIEWING REQUIREMENTS

Object	Viewing Time per Object	No. of Source per PI
<u>Ultraviolet Observation</u>		
Galactic		
Faint Stars	1-10 hr	10
Bright Stars	Few sec - 30 min	20
Extra Galactic	1-10 hr	10
<u>Infrared Observation</u>		
Galactic		
Faint Stars	1-10 hr	10
Bright Stars	Few sec - 30 min	10
Extra Galactic	Few sec - 30 min	20

b. **Magnetic Field.** Another environmental concern is that magnetic field variations within the SIP will cause unwanted deflection of the electron beam during data readout of the image tube. Magnetic field generators include the earth, the momentum desaturation electromagnets, and adjacent tubes. With the electromagnets located on the telescope meteoroid shield (reference design), their field strength at the instruments is negligible with respect to the earth's field (0.23 to 0.35 gauss). The worst possible variation in the earth's field would occur if the LST were maneuvering to a new object during tube readout. This could result in a change of approximately 1.57 radians (90 degrees) in the flux vector during the scanning process. Inhibiting maneuvers during readout would have a significant operational impact. The amount of magnetic shielding required to prevent this restriction needs to be determined as soon as the scanning beam characteristics are defined. The effect of fields generated by adjacent tubes is a function of detail tube design and relative location. If this is shown to be significant in later analysis, the process of turning the focus coils of adjacent tubes on and off can be inhibited during data readout without restricting operations.

c. **External Disturbances.** The only significant external disturbance results from gravity gradient torques, which produce both a cyclic and a secular component of momentum. The cyclic component sizes the CMGs and thereby affects the amount of dynamic noise generated. The secular component sizes the magnetic desaturation system and determines the surrounding magnetic field strength. With the magnets located on the meteoroid shield, there is no direct operational impact resulting from the control of external disturbances. Continuous operation of the desaturation system can result in either smaller CMGs (less noise) or more momentum available for maneuvering to the next stellar object.

d. **Micrometeoroid Flux.** The basic LST structure will be designed to a low probability of micrometeoroid penetration over the duration of the mission. Analysis of micrometeoroids entering the telescope aperture indicates that about 2300 (meteoroid model NASA-SP-8013) can be expected to strike the primary mirror during a 5 year mission. Their mass varies from  $10^{-12}$  to  $10^{-5}$  gram. Even if they are all the largest size and produce a pit 10 times bigger than their cross-sectional area, only 0.03 percent of the reflecting area would be damaged. Thus, micrometeoroid environment will not impact operations.



e. Contamination. The LST contamination environment during orbital operations is of major concern. For several days after orbit insertion, or after an orbital maintenance visit, special procedures will be required in order to minimize contamination of sensitive surfaces. After outgassing rates have been reduced and contaminants dispersed, normal operation should not be influenced by contamination considerations. At 611 km (330 n.mi.) the residual atmosphere will disperse particles. Skylab study results, scaled for the change in density at the LST altitude and launch dates, indicate worst-case clearing times of 6 min for 1  $\mu\text{m}$  particles and 5 hours for 50  $\mu\text{m}$  particles. Orbital regression and atmospheric rotation will prevent buildup of contamination on successive orbits. The only contamination threat encountered during orbital operations is possible chemical or physical reactions of impacting ( $\sim 7$  km per/sec) atmospheric elements on the mirror surface. This is not expected to be a major problem because:

1. The mirror coating ( $\text{MgF}_2$ ) is fairly stable.
2. The velocities are much lower than experienced by interplanetary or reentry missions.
3. The aperture points along the velocity vector only a small part of the time due to earth shine constraints and the distribution of stellar objects.

f. Stray Light. The only environment that can produce stray light is secondary photon emission of ionized oxygen and hydrogen when they recombine with free electrons. However, this is not expected to be a problem since most of the emission lines and bands occur at wavelengths to which the LST instrumentation is insensitive. Another source of concern is sunlight reflection off contamination elements; however, relatively clean LST systems and fast particle clearing times should produce negligible contamination in this vicinity. All other stray light sources are discussed in the following section.

### 3. Operational Constraints

a. General. Planning LST astronomy observations requires a complete understanding of the operational constraints, their performance sensitivity, and their design impact sensitivity. Some of the limitations to unrestricted LST operation include:

1. Viewing constraints.
2. Light shield and solar panel orientation constraints.
3. Spectrograph slit orientation requirements.
4. Spacecraft maneuver rate capability.
5. Data integration limitations.
6. Data storage and transmission capability.

Each of these limitations is discussed in this section.

b. Viewing Constraints. A stellar viewing constraint is the condition that exists when a specific instrument can no longer see a specific stellar object. Since the characteristics of both the targets and the instruments vary over a wide range, the only firm viewing constraints are that the LST not look directly at the sun, at the moon, or through the earth's atmosphere. Looking progressively closer to these bodies increases the amount of unwanted stray light reaching the detector. This limits faint object detectability and increases the required integration time to obtain a desired photometric accuracy. A throughput analysis is required to determine true viewing constraints for a given stellar object and a given instrument. For planning purposes, pseudoviewing constraints are established at the point where there is an abrupt increase in stray light at the LST focal plane. These constraints have very recently been defined by a stray light suppression study.<sup>2</sup> Many of the results presented herein were generated using previously assumed constraints. A comparison of the constraints established by this study for two different truncation angles of the light shield are shown in Table III-12.

As the LST line of sight (LOS) approaches the sun, there is an abrupt increase in stray light at the detector when sunlight enters the tube and another increase when it strikes the secondary mirror support. For a truncated sunshade with the apex oriented toward the sun, the primary sun-viewing constraint is equal to the truncation angle. The fraction of the celestial sphere,  $r$ , within a cone of radius  $\theta$  is

$$r = 1/2 (1 - \cos\theta) \quad . \quad (1)$$

---

2. W. G. Tiff and B. B. Fannin, Stray Light Suppression Study for Large Space Telescope, Midterm Progress Report, University of Arizona, June 1, 1972.

For a 0.79 radian (45 degree) sunshade, 14.7 percent is excluded at one time, with any one stellar object excluded for a maximum of 3 months. For a 0.51 radian (30 degree) sunshade, the values reduce to 6.7 percent and 2 months, respectively. For short exposure times, objects can be viewed at angles up to 0.09 radian (5 degrees) from the sun LOS by using the earth limb as a shield. The small improvement in operational flexibility associated with a 0.51 radian (30 degree) sunshade does not appear to be worth any significant design penalty, e.g., a folding shade apex. The orbit periphery of the inner two planets (Mercury and Venus) are 0.40 radian (23 degrees) and 0.80 radian (46 degrees), respectively, from the sun. For the 0.77 radian sunshade, viewing of Mercury is limited to approximately 4 min per orbit just before sunrise. The adequacy of this duration requires a system throughout analysis. Stray light reflected by the bright earth will limit the observation of certain faint sources.

TABLE III-12. VIEWING CONSTRAINTS

Body	Constraint (Relative to Light Shield Apex)			
	90 Degree Truncation Angle		45 Degree Truncation Angle	
	Radian	Degree	Radian	Degree
Sun	±0.79	±45	±0.79 to 2.36	±45 to 135
Moon	±0.26	±15	±0.18	±10
Earth (Bright Side)	±0.26	±15	±0.90 to 1.69	±50 to 95
Earth (Dark Side)	±0.26	±15	±0.09	±5

A moon-viewing constraint of 0.18 radian (±10 degrees) is contingent upon obtaining an adequate nonreflecting surface on the secondary mirror structure. This presents less than 1 percent of the celestial sphere at one time. Also, since the moon has an orbital period of 27.3 days, it excludes a given object for a maximum of 1.5 days. The stray light from the full moon, although less than  $10^{-5}$  as bright as the sun, can, in certain situations, impact the observation of a source.

The earth's sensible atmosphere and air glow extend to an altitude of approximately 185 km (100 n. mi.), or approximately 0.09 radian (5 degrees) above the earth's limb when viewed from the LST orbit. This is the earth-viewing constraint on the dark side of the orbit for all stellar objects and, possibly, on the light side of the orbit for very bright objects. For other than very bright objects, a practical light-side viewing constraint is that there be no specular reflection of earth shine off the inside of the sunshade into the telescope tube [0.79 radian, -1.57 radian (+45 degrees, -90 degrees)]. Including 0.09 radian (5 degrees) for earth air glow, the light-side viewing constraint is 0.87 radian (50 degrees) for the shade directly toward the earth limb and 1.66 radian (95 degrees) for the shade directly away. During light-side viewing there is a conflict between orienting the shade toward the sun and toward the earth. The optimum viewing time may be achieved by an intermediate orientation without violating solar panel orientation constraints. For intermediate orientations, the viewing constraint,  $\gamma$ , is defined by the expression

$$\begin{aligned} \gamma &= 5^\circ + \cot^{-1} (\cos \phi / \tan 45^\circ) && \text{for } -90^\circ < \phi < 90^\circ \\ \gamma &= 95^\circ && \text{for } -90^\circ < \phi < 90^\circ \end{aligned} \quad (2)$$

where  $\phi$  is the roll angle of the vector to the closest earth limb measured from the sunshade apex.

c. Light Shield and Solar Panel Orientation Constraints. For observations while in the earth shadow, there are no constraints on the orientation of either the light shield or the solar panels. During light-side operation, the solar panels should be directed at the sun and the light shield oriented to produce maximum viewing time. The maximum viewing time occurs when the light shield is oriented toward the earth as much as possible without violating the solar viewing constraint. Considering the earth viewing constraints and worst-case conditions of 0.91 radian (52 degree) angle between the sun and the orbit plane, object declination of 0.33 radian (19 degrees), and the same right ascension as the sun, the largest roll angle required in order to optimize viewing time is 1.22 radians (70 degrees). For single-degree-of-freedom solar panels this would result in 0.47 radian (27 degree) incidence angle on the solar panels. This reduces the power generation rate to approximately 45 percent of maximum. For the average sun/orbit plane relationship, this increases to approximately 97 percent. The constraint on reduced power generation is usually a battery life constraint

associated with the number of cycles below a certain percent discharge. It appears that the reduction in predicted battery life associated with obtaining near-optimum viewing orientations is well within the uncertainty of the prediction and, thus, should not significantly restrict operations.

d. Spectrograph Slit Orientation Requirements. Several of the scientific objectives require specific spectrograph slit orientation in order to obtain the desired polarization effects or to position the slit to obtain only the desired portion of a diffuse object. The options available to meet this requirement are (1) rotation of the instrument, (2) rotation of the vehicle and acceptance of the power loss, (3) scheduling of the objects in the two periods each year when the vehicle can be rotated without excessive power loss, or (4) addition of a degree of freedom to the solar panel orientation system. At this point in the analysis a combination of (2) and (3) appears to be operationally feasible and is the design reference approach. For the optimum orientation of one-degree-of-freedom solar panels, the power generating efficiency is shown in Figure III-11. For a mean object location of 1.02 radians (60 degrees) from the sunline, and a mean slit rotation 0.79 radian (45 degrees) from optimum, the power generating efficiency is 79 percent. If the number of observations requiring specific slit orientations are not a large portion of the total, specific scheduling may not be required. For the worst-case ( $\phi = \delta_s = 90$  degrees), a 1 month scheduling delay will provide 50 percent generating efficiency.

e. Spacecraft Maneuver Rate Capability. The efficient utilization of the telescope requires the capability of maneuvering to a new object in a relatively small portion of the 97 min orbital period. The stated astronomical goal is 1.57 radians (90 degrees) in 5 min. Figure III-12 shows the 1.57 radian (90 degree) maneuver times as a function of momentum and torque available from the CMGs for performing maneuvers. This shows a diminishing return for momentums greater than 408 joule-sec (30 ft-lb-sec) and torques greater than 2.71 N-m (2 ft-lb). Current design concepts are capable of providing this output for maneuvering. A system designed for 1.57 radians (90 degrees) in 5 min would be much more massive, require more electrical power, and generate more vibration noise. For this system, two 1.57 radian (90 degree) maneuvers per orbit involve only 23 percent of the orbit period, and often one maneuver can be accomplished during the nonviewing time, i. e., when object occultation occurs or a viewing constraint is exceeded.

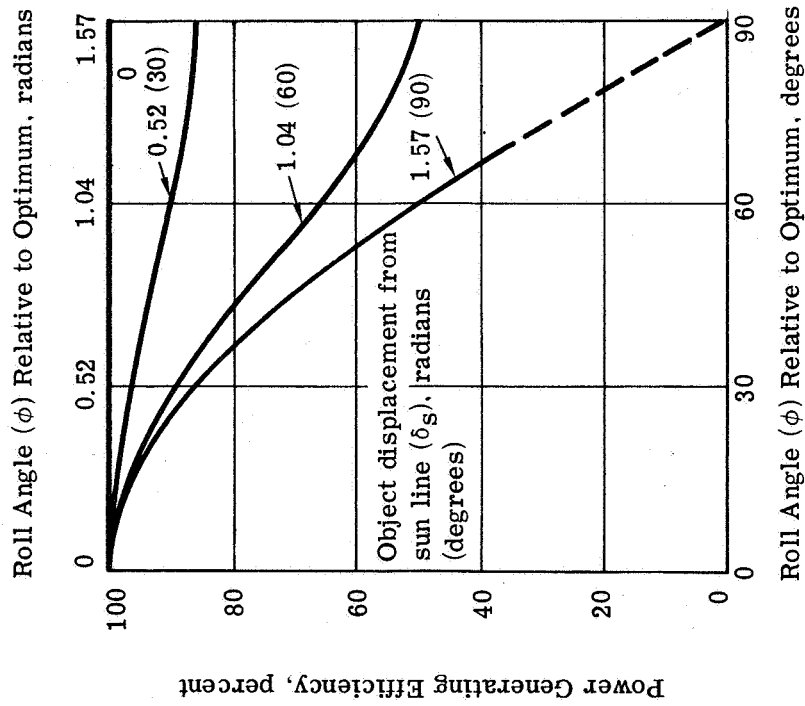


Figure III-11. Power generating efficiency.

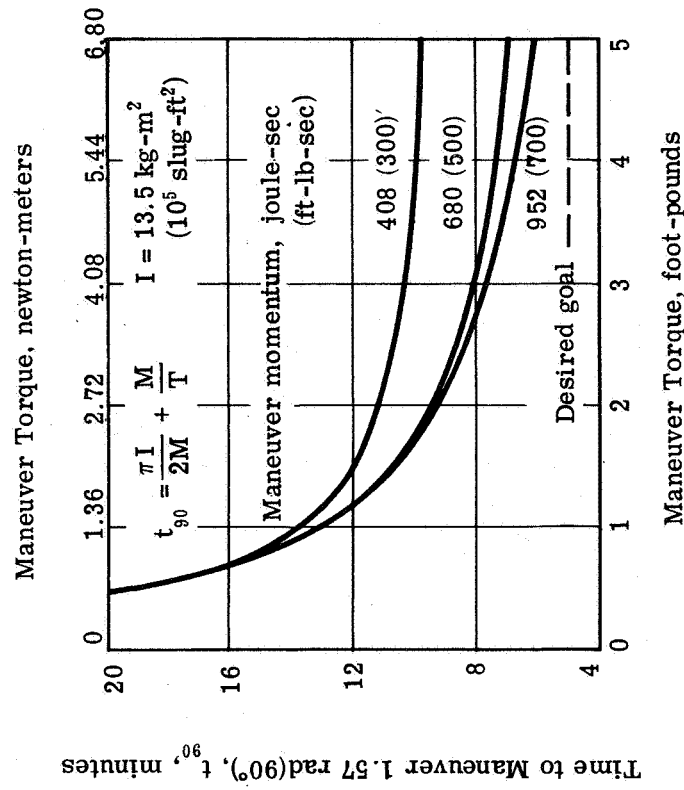


Figure III-12. Maneuver time.

f. **Data Integration Limitations.** Observation of very faint objects will require long integration times. A preliminary SEC-type image tube development specification calls for the capability to integrate for 10 hours and retain the image for an indefinite period prior to readout. The actual integration time required for a given object and a given instrument requires a throughput analysis of the signal and all the noise (stray light, dark current, etc.) sources. Viewing of faint objects may be restricted to the shadow portion of the orbit, which varies from 27 to 35 min. In this case a 10 hour exposure will require about 20 orbits and a lapse time of about 30 hours. The image accumulated each orbit will either have to be integrated external to the tube (if the readout noise is low enough to permit this approach) or, if integrated on the tube, the object will have to be reacquired within the stability tolerance of 0.024 microradian (0.005 arc-sec). Tube integration is the design reference approach and the reacquisition tolerance prevents any mechanical movement of the guide star sensors on the bright side of the orbit.

g. **Scientific Data Storage and Transmission Capability.** Two approaches to data storage and transmission are (1) tube storage and direct readout to the ground, and (2) onboard buffer storage prior to transmission. The first approach is the current design reference. It results in the simplest design but restricts operational flexibility. Each image tube can be used only once between ground station contacts, which for the proposed 6-station set can be as long as 90 min. The average contact time per station per revolution is approximately 12 min. Allowing 2 min for acquisition means that only 10 min are available for data transmission. For direct readout to ground, the tube readout beam scan time must be compatible with this 10 min period.

h. **Observation Scheduling.** To maximize the efficient utilization of the LST, various factors must be considered in the scheduling of sources for observation. These factors have been examined from a mission operations point of view with the objectives of determining the times when certain areas of the sky will be accessible for viewing and maximizing the length of time the sources within these areas can be observed by the telescope.

(1) **Source Accessibility.** The accessibility of certain sources to the telescope is determined by their relative location to the sun and moon, which are, in turn, dependent on specific times within a year. As the earth moves around the sun, the projections of the sun on the celestial sphere correspondingly move around the celestial sphere in a path described by the ecliptic plane (Fig. III-13). As the moon moves around the earth, its projection on the celestial sphere moves around the celestial sphere

correspondingly in the lunar plane. Sources which are located within 45 and 15 degrees from the center of the solar and lunar projections on the celestial sphere, respectively, cannot be observed. Thus the time of year is a prime factor which should be considered in the scheduling of various sources. This fact is illustrated in Figures III-14, III-15, III-16, and III-17. Figure III-14 shows the celestial sphere for the date March 21, 1978 (vernal equinox). Clearly from these data, one would not schedule sources whose right ascension and declination fall within either of these avoidance cones. A similar conclusion can be drawn from Figures III-15, III-16, and III-17 which show the solar and approximate lunar avoidance cones for the dates June 21, 1978 (summer solstice), September 21, 1978 (autumnal equinox), and December 21, 1978 (winter solstice), respectively.

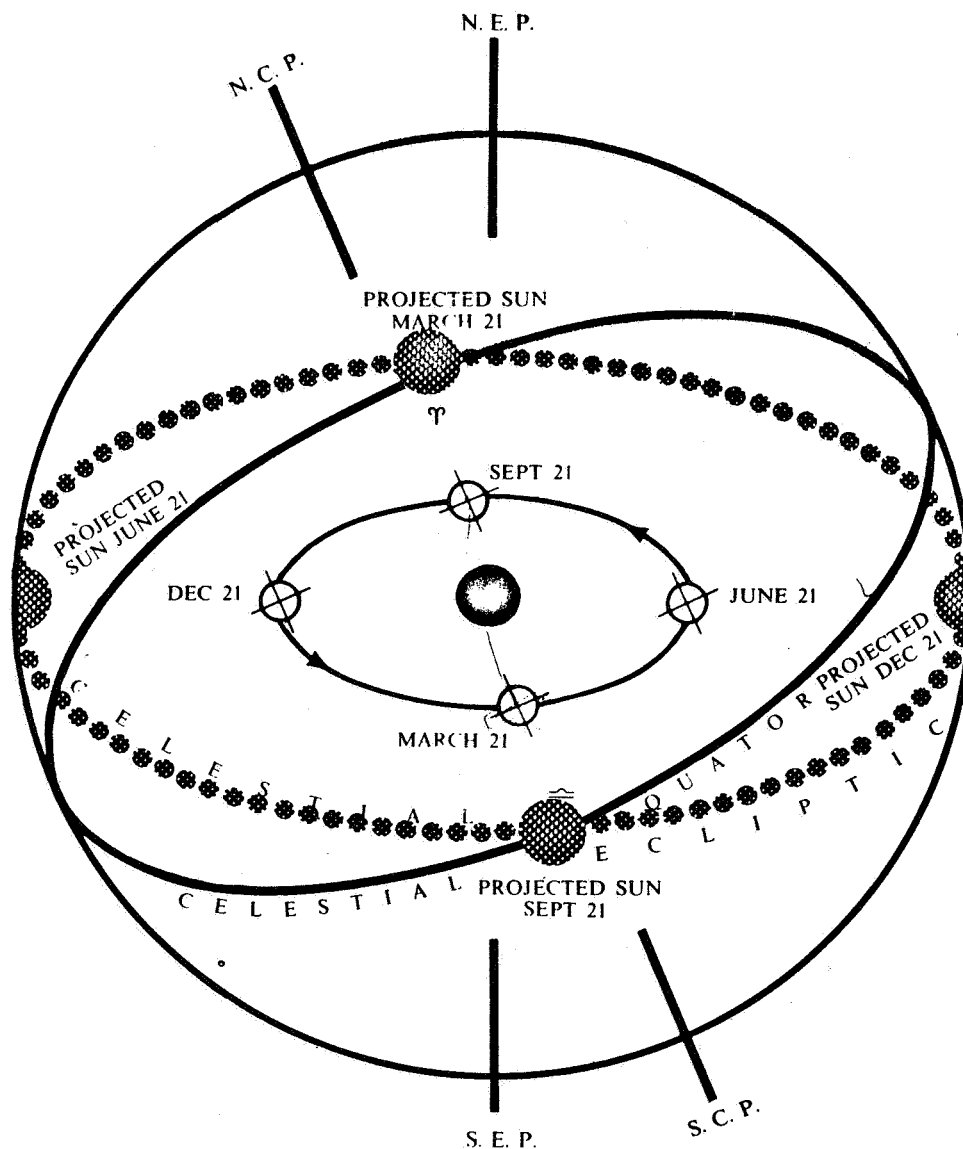


Figure III-13. Solar projection on celestial sphere.



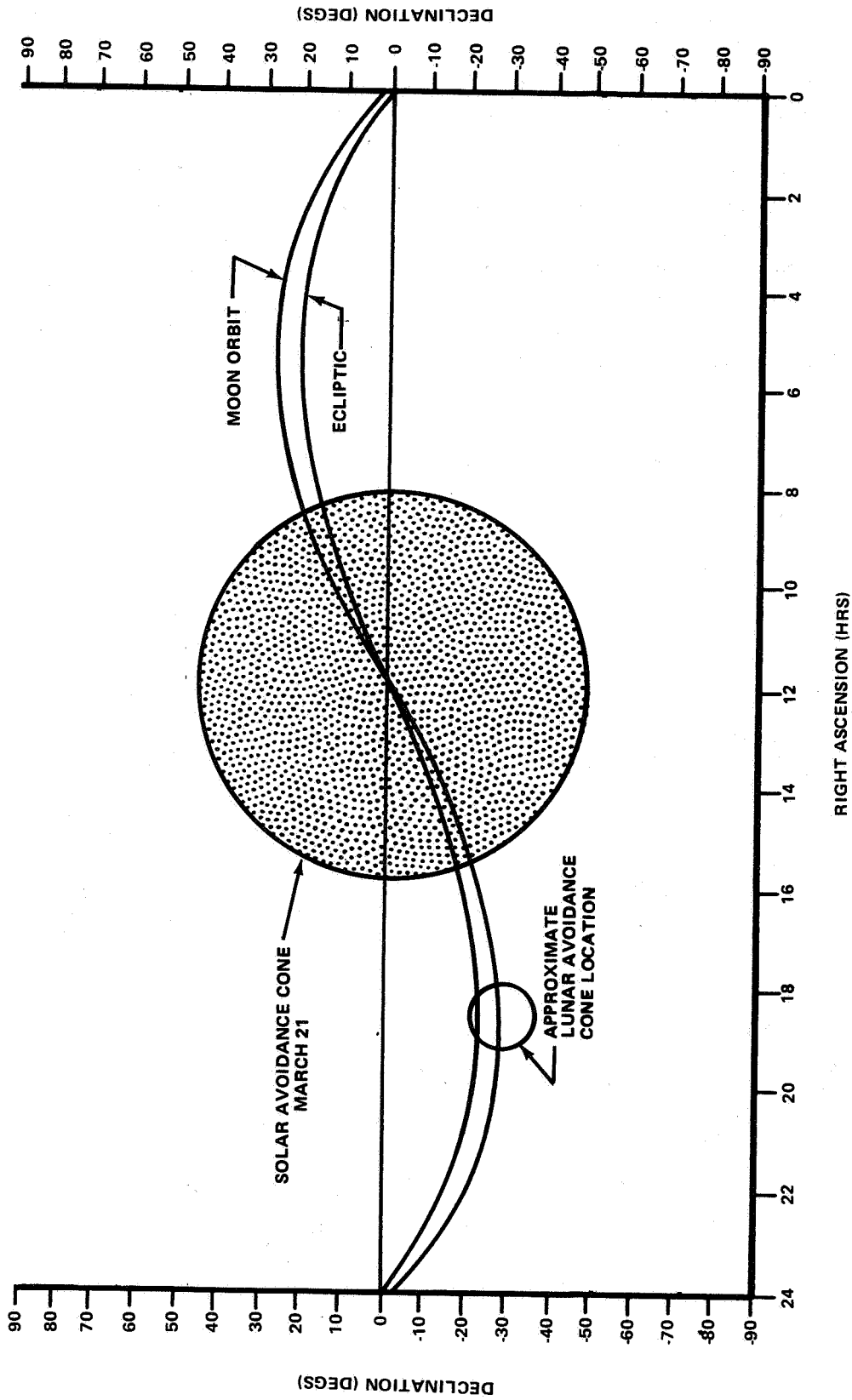


Figure III-14. Projection of 45 degree solar and 15 degree lunar avoidance cone on celestial sphere on March 21, 1978.

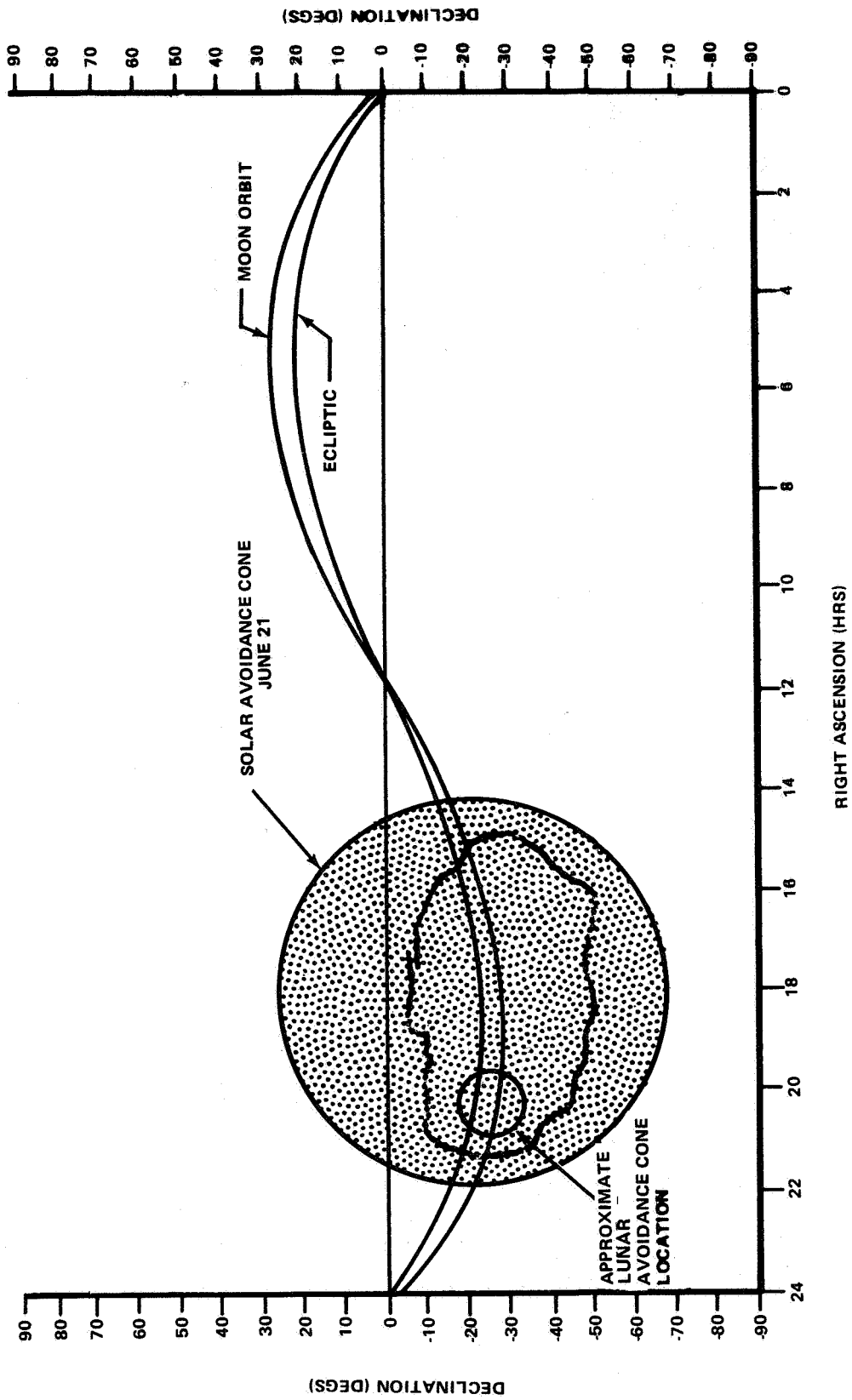


Figure III-15. Projection of 45 degree solar and 15 degree lunar avoidance cone on celestial sphere on June 21, 1978.

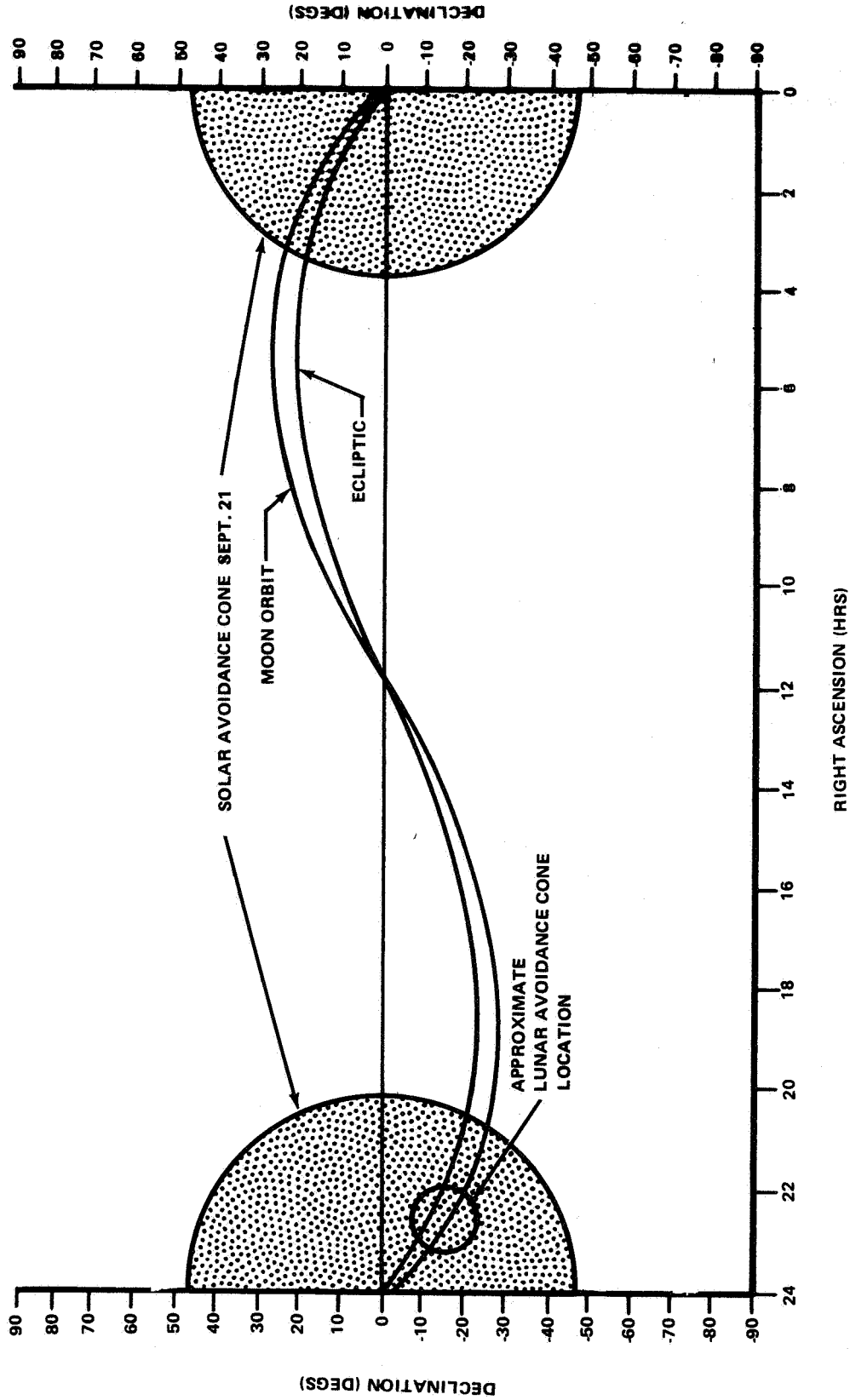


Figure III-16. Projection of 45 degree solar and 15 degree lunar avoidance cone on celestial sphere on September 21, 1978.

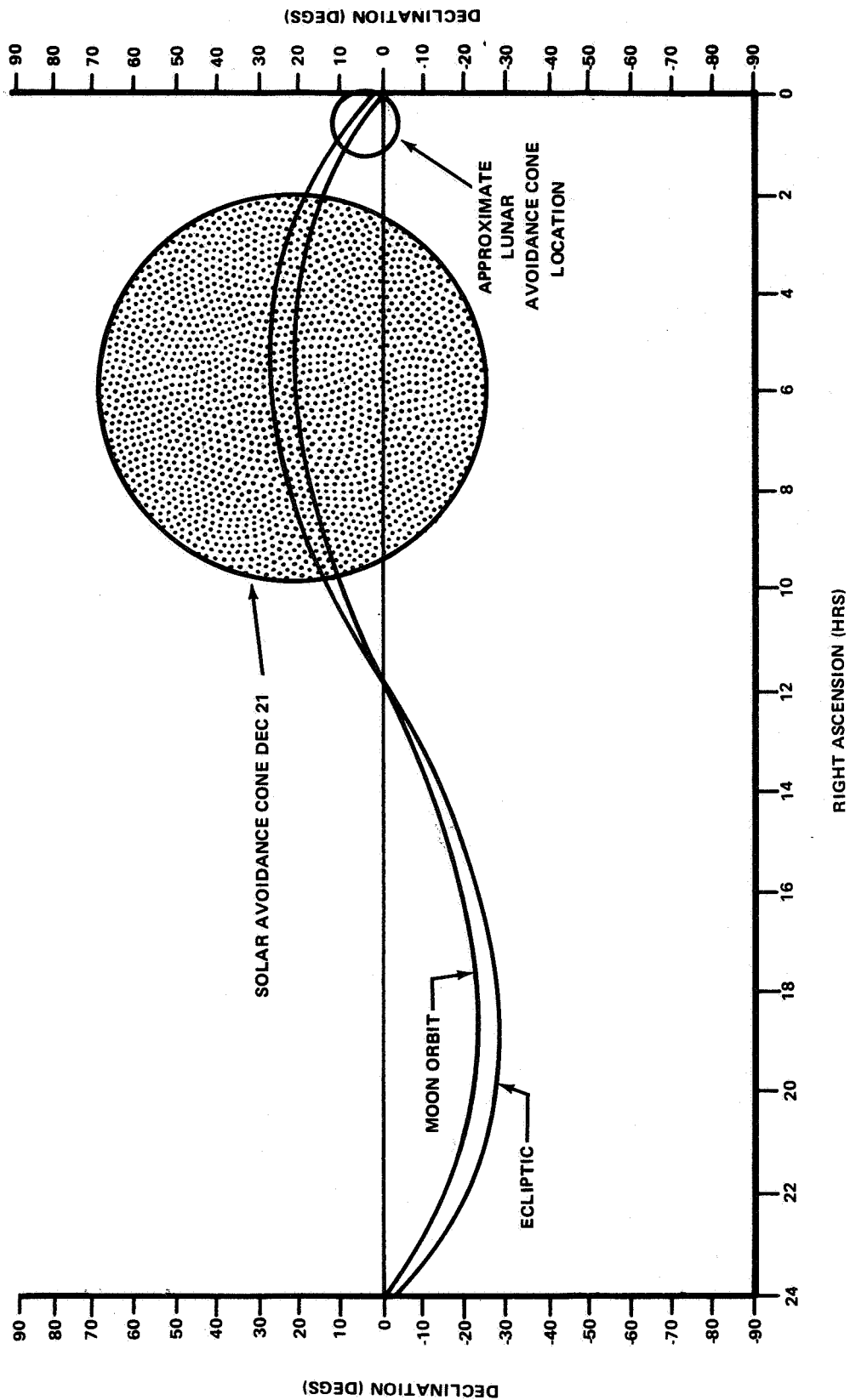


Figure III-17. Projection of 45 degree solar and 15 degree lunar avoidance cone on celestial sphere on December 21, 1978.

(2) Maximization of Observation Time. The question of how the observation times of sources located outside the solar and lunar avoidance cones can be maximized is one of prime consideration. The answer to this question can best be presented by the first separating sources according to their respective magnitudes. The magnitude of a source determines what orbital lighting conditions will allow it to be viewed. Consider, for example, the estimated faint object limits for the LST presented in Figure III-18. First this figure shows that 26.5 to 29th magnitude sources can only be viewed during the time the spacecraft is inside the dark portion of the orbit. On the other hand, a ninth magnitude source can be viewed during the time the spacecraft is on either the illuminated or dark side of the orbit.

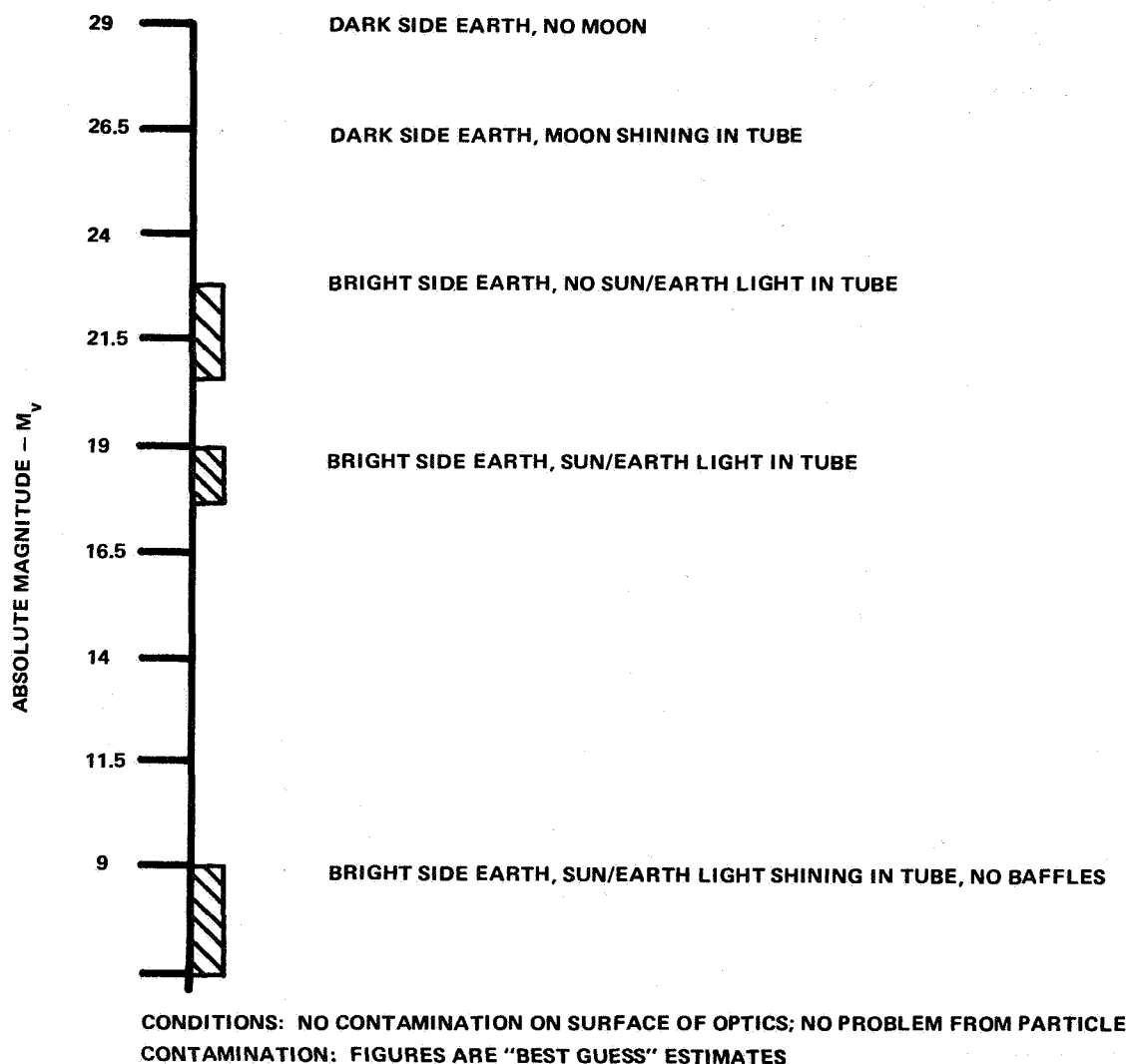


Figure III-18. Estimated faint object observation constraints for LST (see footnote 2).

The observation time of those sources which are constrained to being observed by the spacecraft only during the time the spacecraft is inside the shadow portion of its orbit can be increased tremendously if the sources are chosen such that as many of their environmental and observational constraints occur concurrently on the illuminated side of the orbit.

One environmental and two viewing constraints have been identified which should be considered in the maximization of observation time. First, there is the moon. Sunlight reflected by the moon, although less than  $10^{-5}$  as bright as the sun, detracts from the period of time a source can be observed during the time the spacecraft is in the dark portion of its orbit. The second constraint is more of an implied one; that is, if a source is observable only during the time the spacecraft is in the dark portion of the orbit, it cannot efficiently be observed during the time the spacecraft is on the illuminated side of the orbit. The principal stray light source for this constraint is light from the bright earth, which is about one-fifth as intense as that of the sun. The third constraint is the South Atlantic anomaly which may have an effect on those instruments which use photomultiplier tubes. When these three constraints exist concurrently outside the shadow portion of their respective orbits, a source can be observed during the full dark portion of the spacecraft's orbit. The meaning of this is enhanced by Figure III-19 which contrasts the existence and nonexistence of this condition for a coplanar source which can only be efficiently observed during the time the spacecraft is in the dark portion of its orbit. Example number one in this figure illustrates how the observation of this source has been maximized by choosing it such that, when it is occulted, the spacecraft, moon, and South Atlantic anomaly are in the illuminated portions of their orbits. From this example, it is clear that the spacecraft can view the source under observation during the entire time it is in the dark portion (spacecraft) of the orbit. Example number 2 shows a situation where a source cannot be observed during any portion of the spacecraft's orbit, because the source is occulted for approximately one-half of the dark portion of the spacecraft's orbit and would require the spacecraft to be inside the South Atlantic anomaly during the remaining portion of the orbit in order to make observations on the source. Example number 3 shows a more improved situation in that the source is observable during the latter dark portion of the spacecraft's orbit.

A projection of this favorable condition as it would appear looking from the earth on a rollout of the celestial sphere is shown by Figure III-20. The frequency of this favorable condition and the frequency of this favorable condition and the frequency of occurrence of lesser degrees of favorability are shown in Figure III-21. More specifically this figure shows that the total absolute time the spacecraft will be in the dark portion of its orbit will be about 116 days during a single year. This is without regard

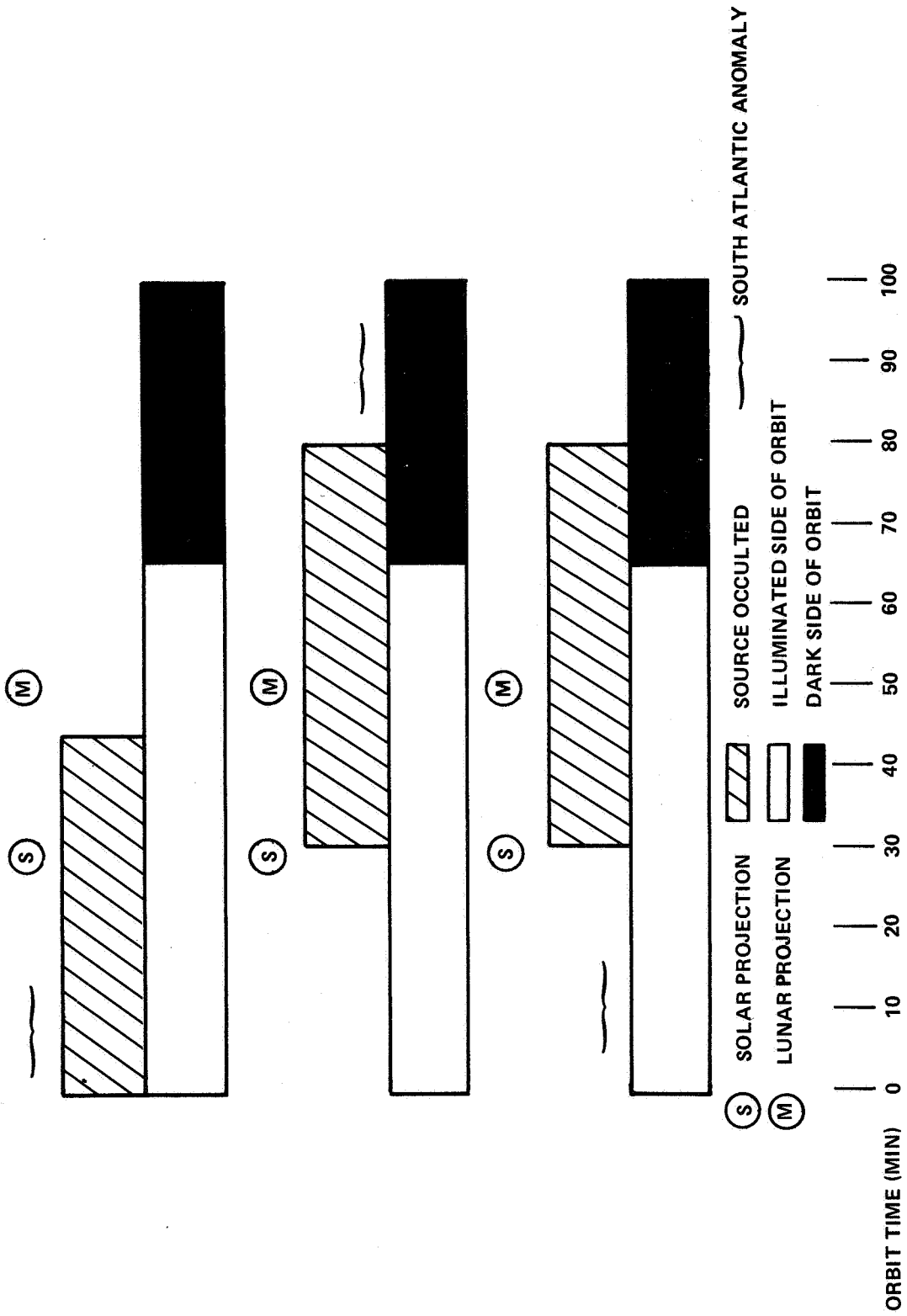


Figure III-19. Concurrent existence of constraints.

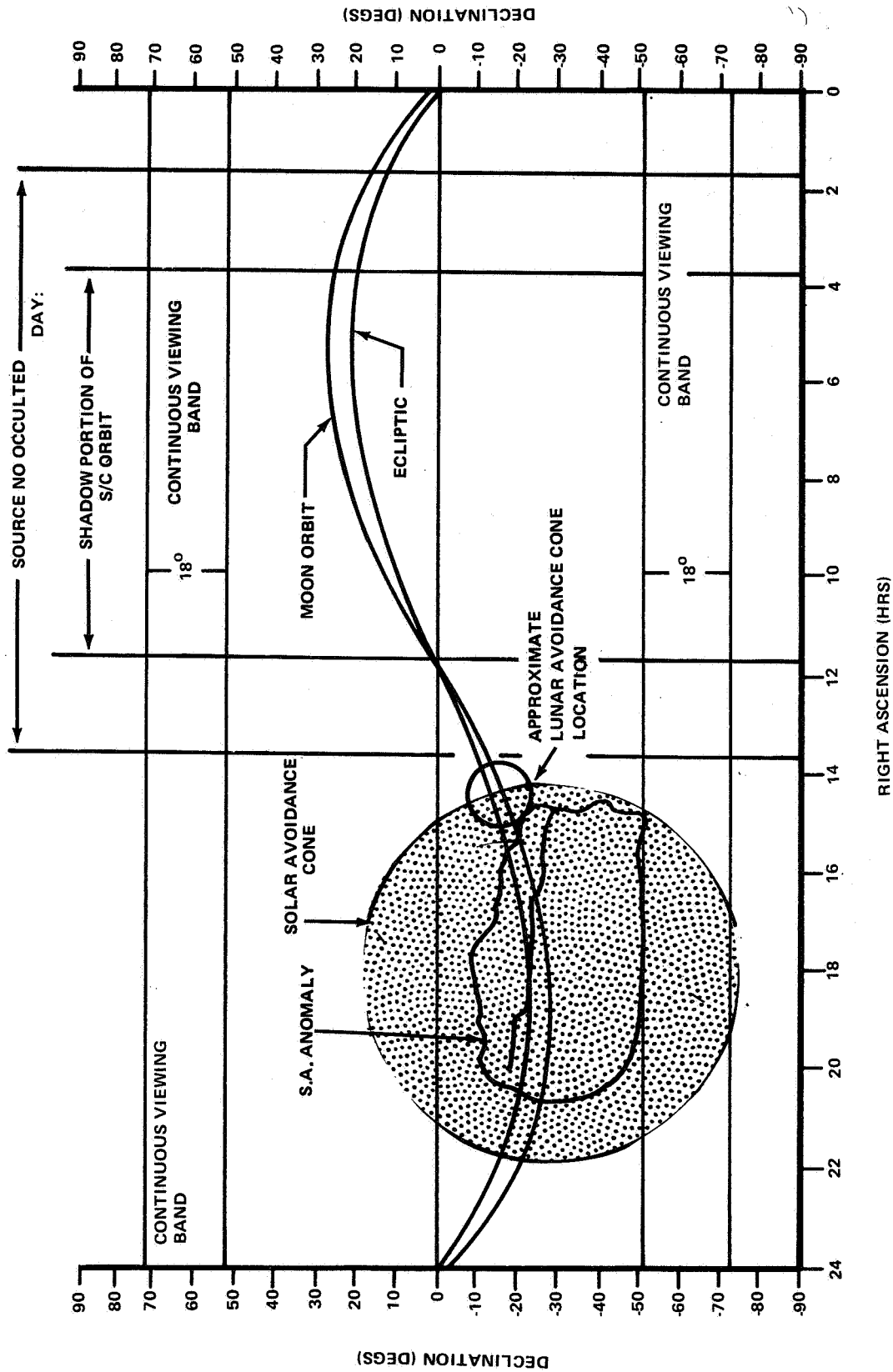


Figure III-20. Existence of favorable condition.



EXISTENCE OF FAVORABLE CONSTRAINT CONDITION  
(DAYS/YEAR) IN ABSOLUTE TIME

SHADOW SIDE OF ORBIT	MOON	SOUTH ATLANTIC ANOMALY	ILLUMINATED SIDE OF ORBIT MOON AND SOUTH ATLANTIC ANOMALY
116*	77	58	39

\*ABSOLUTE TIME (DAYS/YEAR) SPACECRAFT INSIDE SHADOW PORTION OF ORBIT.

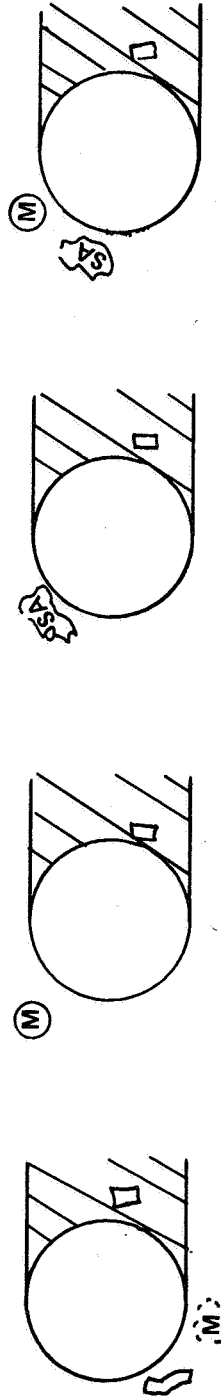


Figure III-21. Various degrees of favorability.

to when the moon and South Atlantic anomaly are located within their respective orbits. In addition, this chart also shows that the moon will be in the illuminated portion of its orbit while the spacecraft is in the dark portion of its respective orbit for approximately 77 days per year. This is without regard to the relative location of the South Atlantic anomaly. The figure also shows that the South Atlantic anomaly and spacecraft will be in the illuminated and dark portions of their respective orbits for an absolute time of approximately 58 days per year. This is without regard to the relative location of the moon. Lastly, the figure shows that the South Atlantic anomaly and moon will concurrently be in the illuminated portion of their orbits while the spacecraft is in the dark portion of its orbit for approximately 39 days per year in absolute time. This is of course the most favorable condition.

For those sources which can be observed during the time the spacecraft is in the illuminated portion of the orbit, source observation time can be maximized if the constraints associated with their observation occur concurrently at their farthest point away from the source. Figure III-22 illustrates this by showing that for various sunshade truncation angles, the length of time a source can be viewed increases as its distance from the sun increases. A discussion of the sunshade selection and design is presented in Chapter IV of this volume.

In summary, it is valid to state that maximum source observation time conditions exist for a source constrained to being observed only when the spacecraft is in the dark portion of the orbit when the South Atlantic anomaly and moon are located on the illuminated side of the orbit and the source's location is such that it can be viewed during the entire dark portion of the spacecraft's orbit. It is also valid to state that maximum source observation time conditions exist for sources not constrained to being observed only when the spacecraft is in the dark portion of the orbit, when the South Atlantic anomaly and sun exist concurrently at their farthest points away from the source under observation. It follows from this that in both cases source observation time can generally be enhanced if the source is located over the dark portion of the spacecraft's orbit.

#### 4. Stellar Viewing Opportunities

a. General Viewing Opportunities. Viewing opportunities are considered in two distinct categories, which should not be confused: (1) visibility — when can a stellar object be seen without violating constraints? and (2) viewing time — how long can a stellar object be seen without interruption? In addition to general viewing opportunities, viewing while in the earth shadow and two-object viewing are of prime importance for the LST. Object viewing time, measured in degrees of orbit travel in each direction from the object longitude, is given by the expression

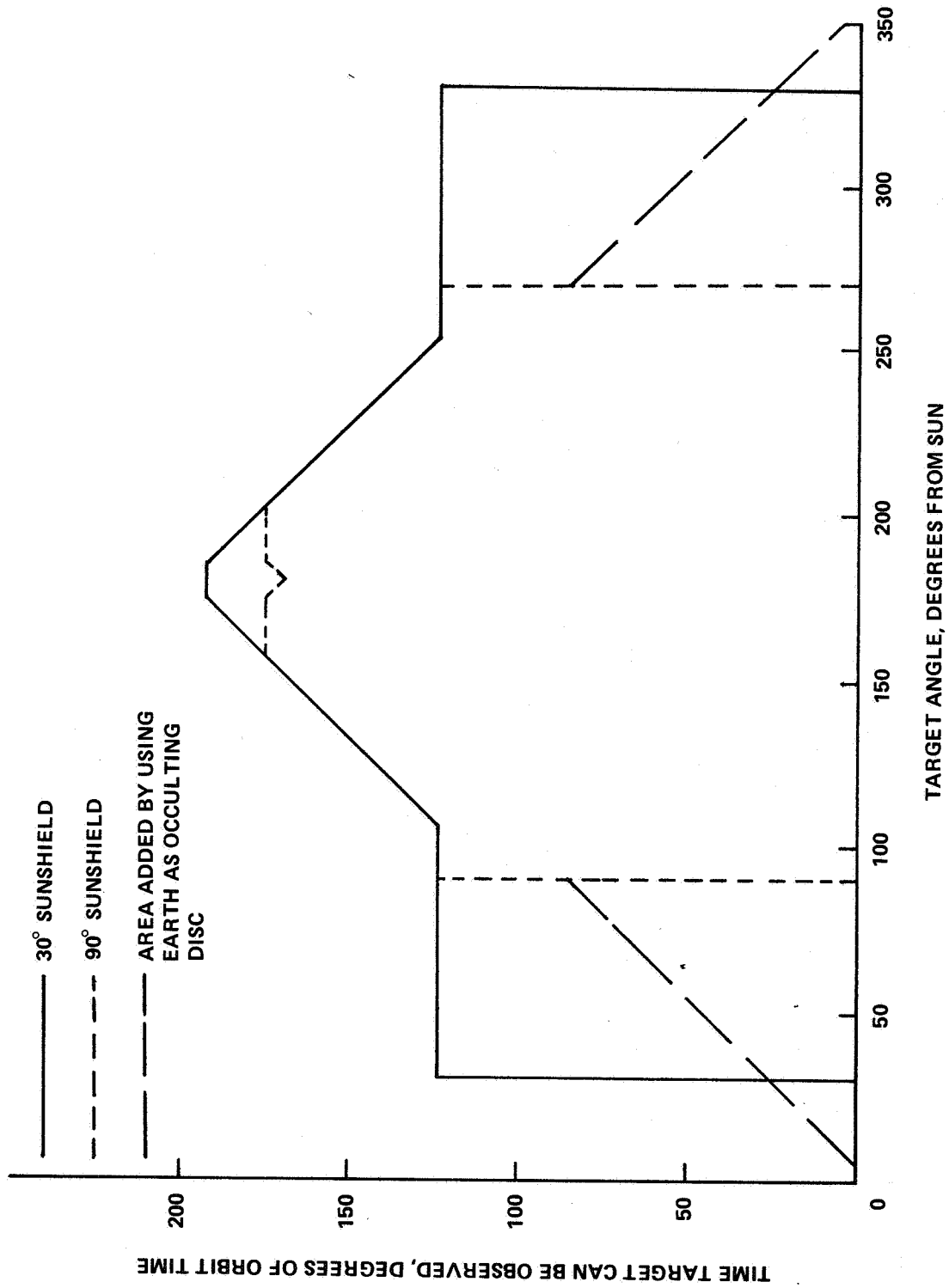


Figure III-22. Source observation time as a function of target angle.

$$\theta = \cos^{-1} \left\{ \frac{1}{\cos \zeta_0} \left[ \frac{r_e}{r_o} \sin \gamma - \frac{(r_o^2 - r_e^2)^{1/2}}{r_o} \cos \gamma \right] \right\} \quad (3)$$

where  $r_e$  is the earth's radius,  $r_o$  is the orbit's radius,  $\gamma$  is the viewing constraint relative to the earth limb, and  $\zeta$  is the object declination measured from the orbit plane. For the LST orbit and  $\gamma = 0.09$  radian (5 degrees),  $\theta$  is given by  $\cos^{-1} (-0.326/\cos \zeta_0)$ . This is the half angle viewing time, not considering constraints from earth shine stray light, and is shown in Figure III-23 as time contours on a stellar background. This shows that unconstrained viewing times do not change appreciably with object declination until the object approaches the orbit pole. Considering stray light, the viewing constraints vary with light shield orientation and brightness of the earth limb closest to the line of sight. The viewing constraint near the terminator is uncertain; however, approximate constrained viewing angles are shown in Figure III-24 for the sun and objects located in the orbit plane.

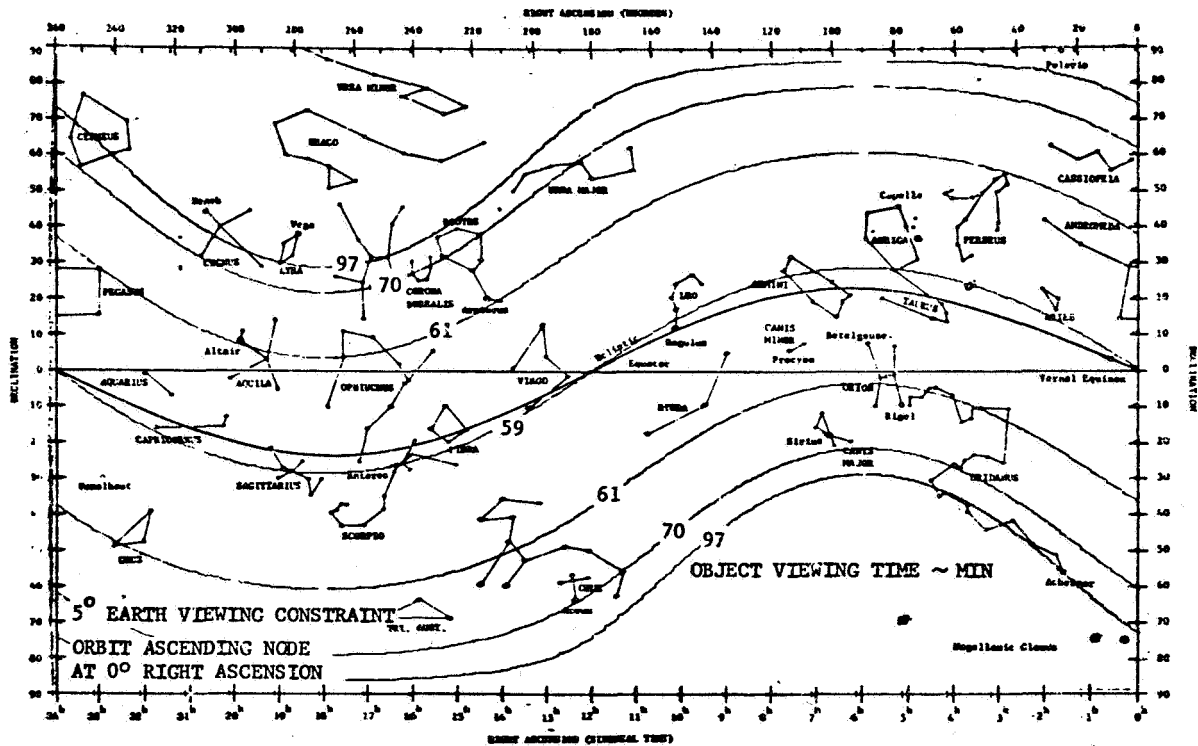


Figure III-23. Unconstrained stellar viewing time.

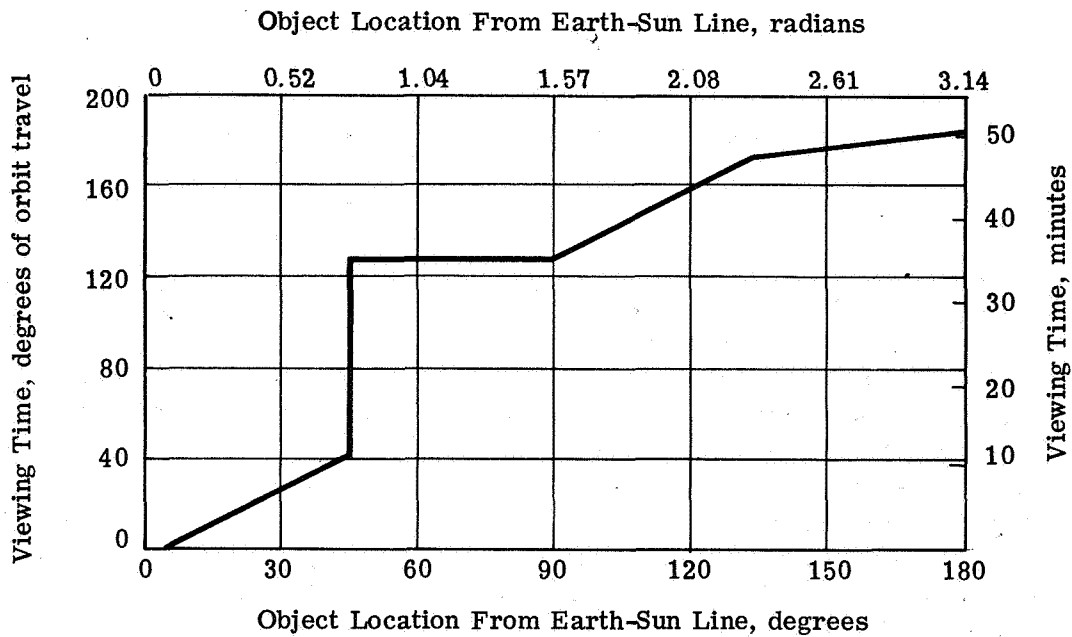


Figure III-24. Constrained viewing time.

b. Earth Shadow Viewing. At this time, stellar viewing while in the earth's shadow is considered to be the prime viewing time. This opinion is based primarily on the assumption that much less stray light reaches the detector when operating in the earth's shadow, even if none of the light-side viewing constraints are exceeded. More detailed stray light analysis may permit less restrictive viewing of faint objects, e.g., in the antisolar hemisphere. Additional advantages of shadow viewing are that there are no complex viewing constraints that are a function of light shield orientation, and there are no roll attitude constraints for power generation. For the LST orbit, the shadow viewing time varies from 35 to 27 min, depending on the angle,  $\beta$ , between the sunline and the orbit plane. Object limits for 100 percent shadow visibility, in terms of orbital longitude,  $\alpha_o$ , from the midshadow point, are defined by the expression

$$\alpha_o = \theta - \phi \quad (4)$$

where  $\theta$  is defined by equation (3) and  $\phi$  is the half shadow angle defined by

$$\phi = \cos^{-1} \left[ \frac{(r_o^2 - r_e^2)^{1/2}}{r_o \cos \beta} \right] \quad (5)$$

Figure III-25 shows these object visibility limits for shadow viewing transformed to celestial coordinates. These data were generated for an earth-viewing constraint of 0.26 radian (15 degrees) and was assumed to be independent of lighting conditions. Figures III-26, III-27, and III-28 illustrate the effect of orbital procession and sun motion in 2 week intervals. Faint objects requiring long shadow viewing times will have to be scheduled when they are in or near the 100 percent shadow visibility region. Objects near the celestial poles fall into this region approximately once every 9 weeks for a few days at a time, while objects near the celestial equator fall into this region once a year for about 3 months at a time. Efficient utilization of prime viewing time would thus require scheduling of faint stellar objects 1 year in advance.

c. Two-Object Viewing. The small portion of the orbit (approximately one-third) available for prime viewing, limited object visibility during prime viewing, and restricted operational flexibility make it highly desirable to have the capability to utilize the light side of the orbit as well as the dark side. Also, considering the long exposure times expected for prime viewing, it is desirable to be able to perform a light-side observation and then reacquire a dark-side object for continued exposure. If the total shadow time is used for primary object viewing, the time available for secondary object viewing is a function of object location, viewing constraints, maneuver rate, and settling time.

An analysis was performed to assess the feasibility of multiple-object viewing. Basically, this assessment is divided into three parts. The first part examines the feasibility of viewing two sources located 90 degrees apart when a first source is viewed during the entire period of time it is accessible. The second part examines the same situation but for sources located 180 degrees apart, and the third part examines the feasibility of viewing either 2, 3, or 4 sources per orbit for various relative source locations.

It is noted that each situation examined assumes the sources under consideration to be coplanar with the spacecraft's orbit plane. The coplanar case was examined because it represents a worst-case situation as far as source observation time is concerned.

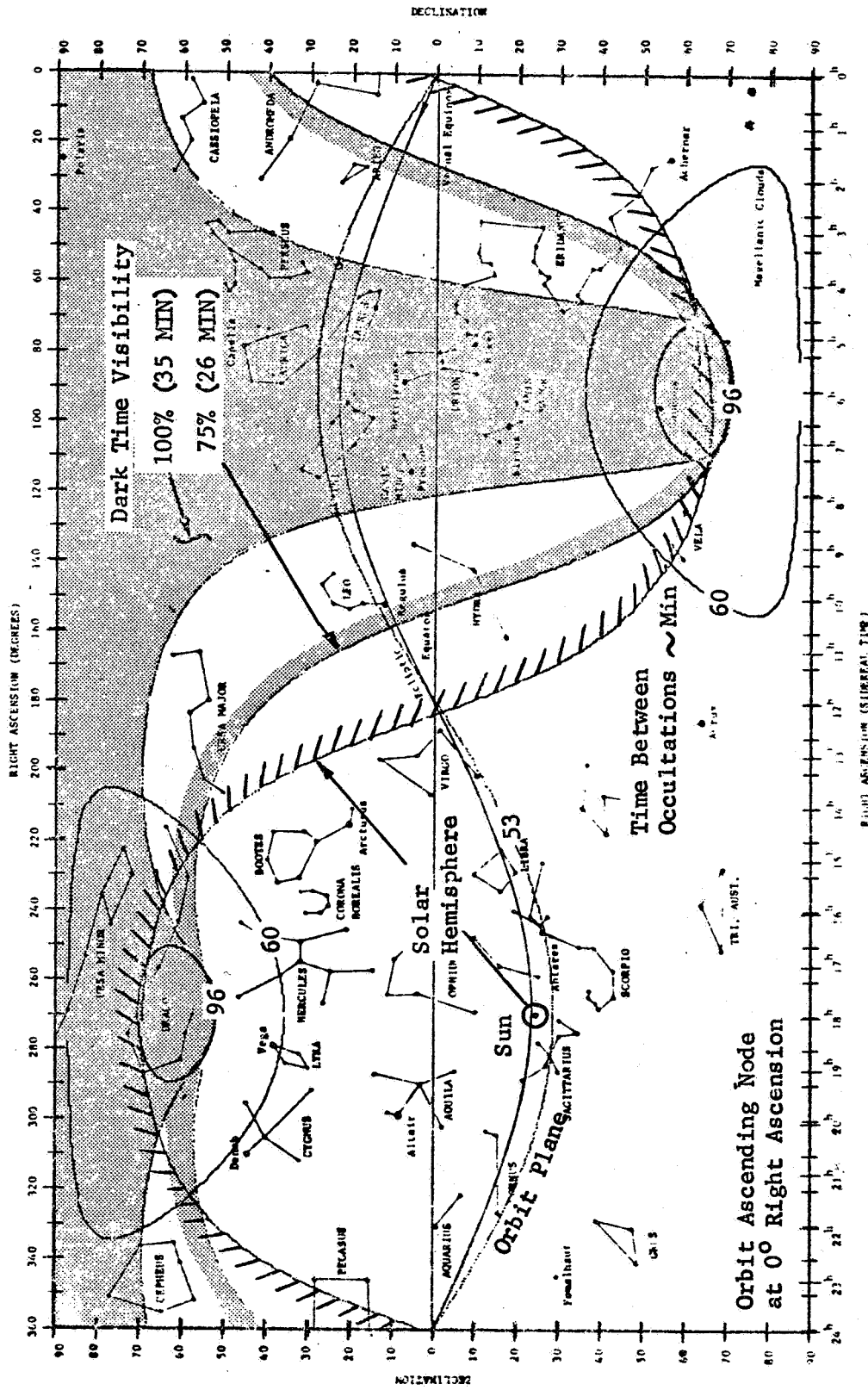


Figure III-25. Typical viewing opportunities at T + 0 ( Dec 21 ).

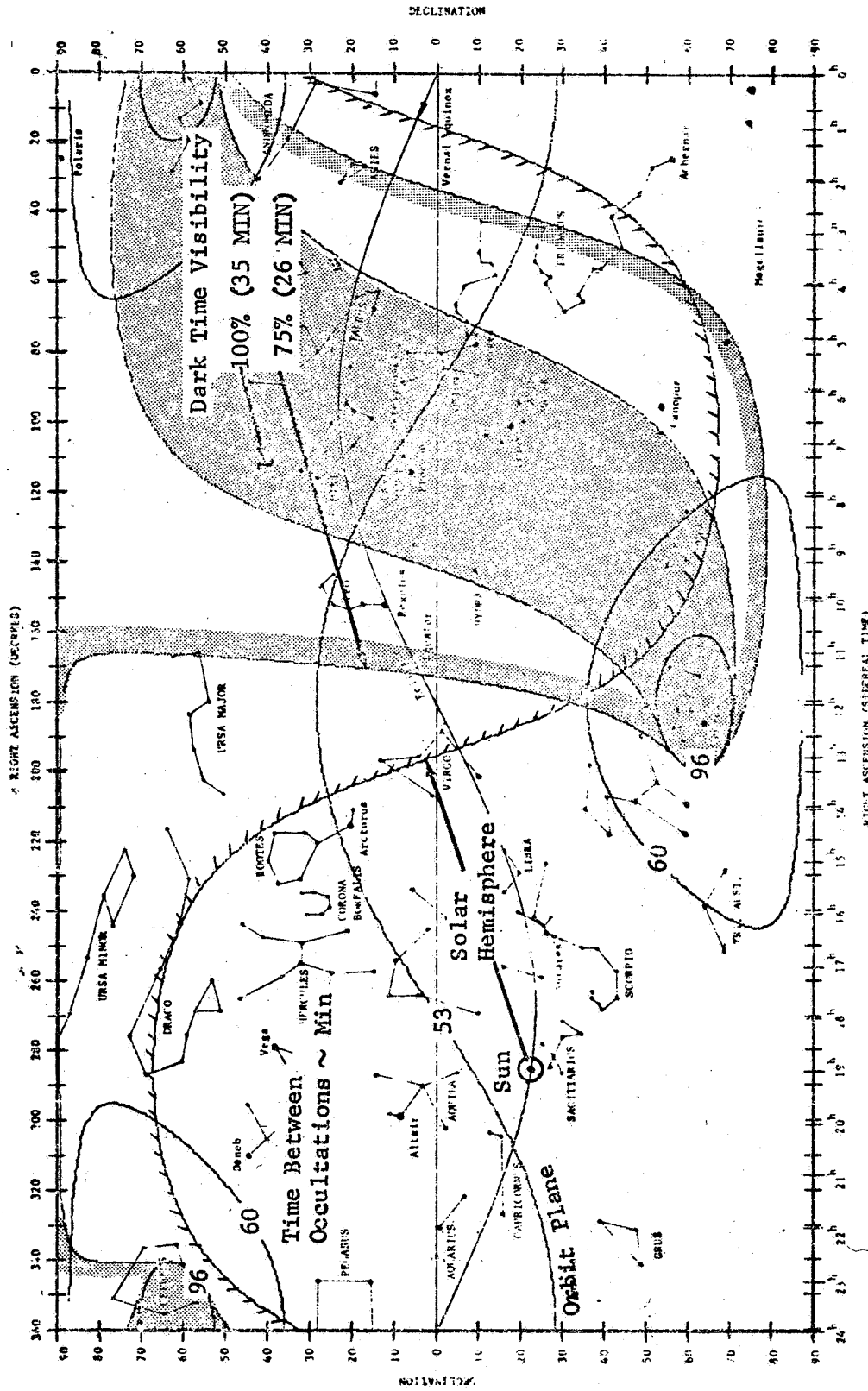


Figure III-26. Typical viewing opportunities at T + 2 weeks.



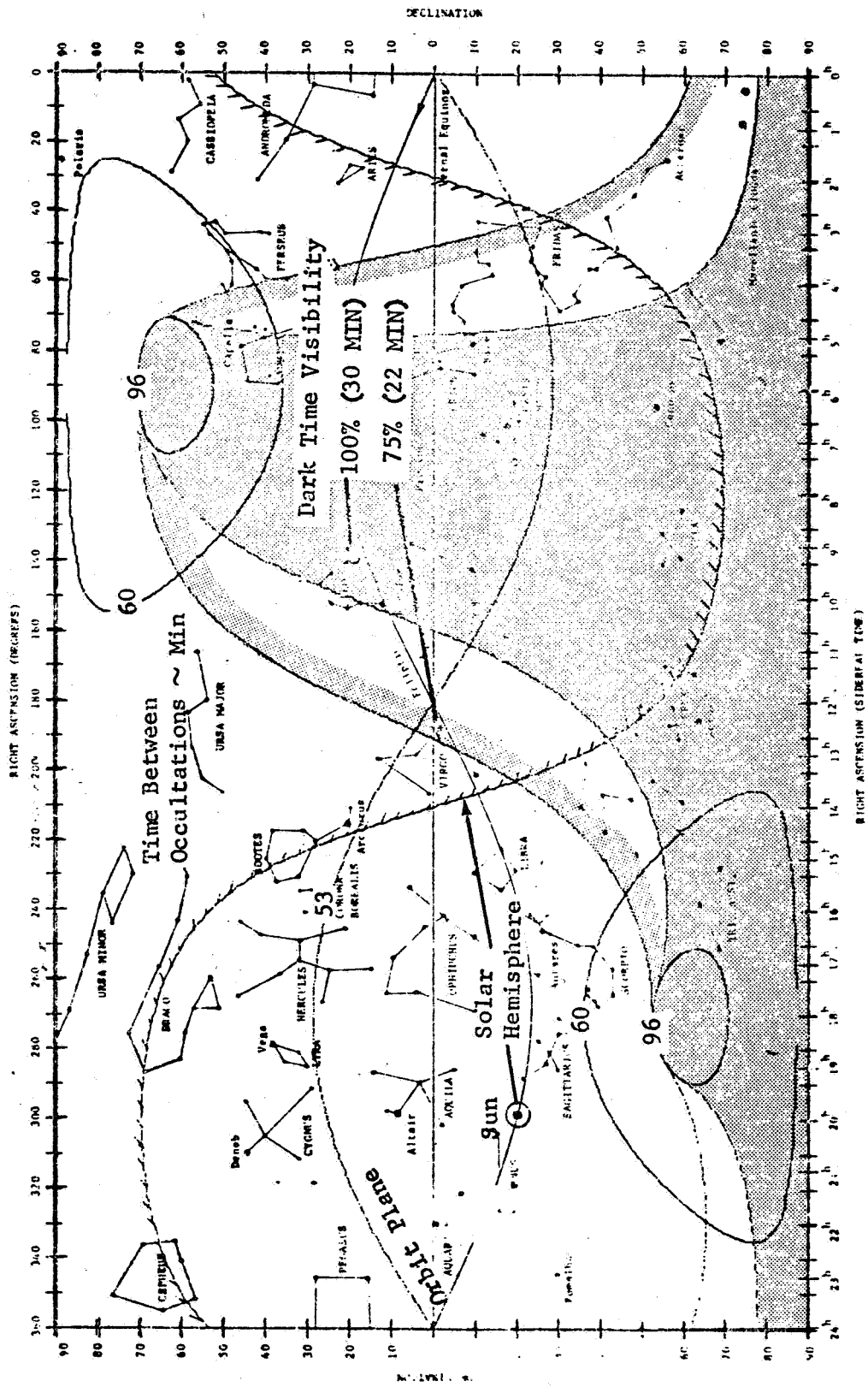


Figure III-27. Typical viewing opportunities at T + 4 weeks.

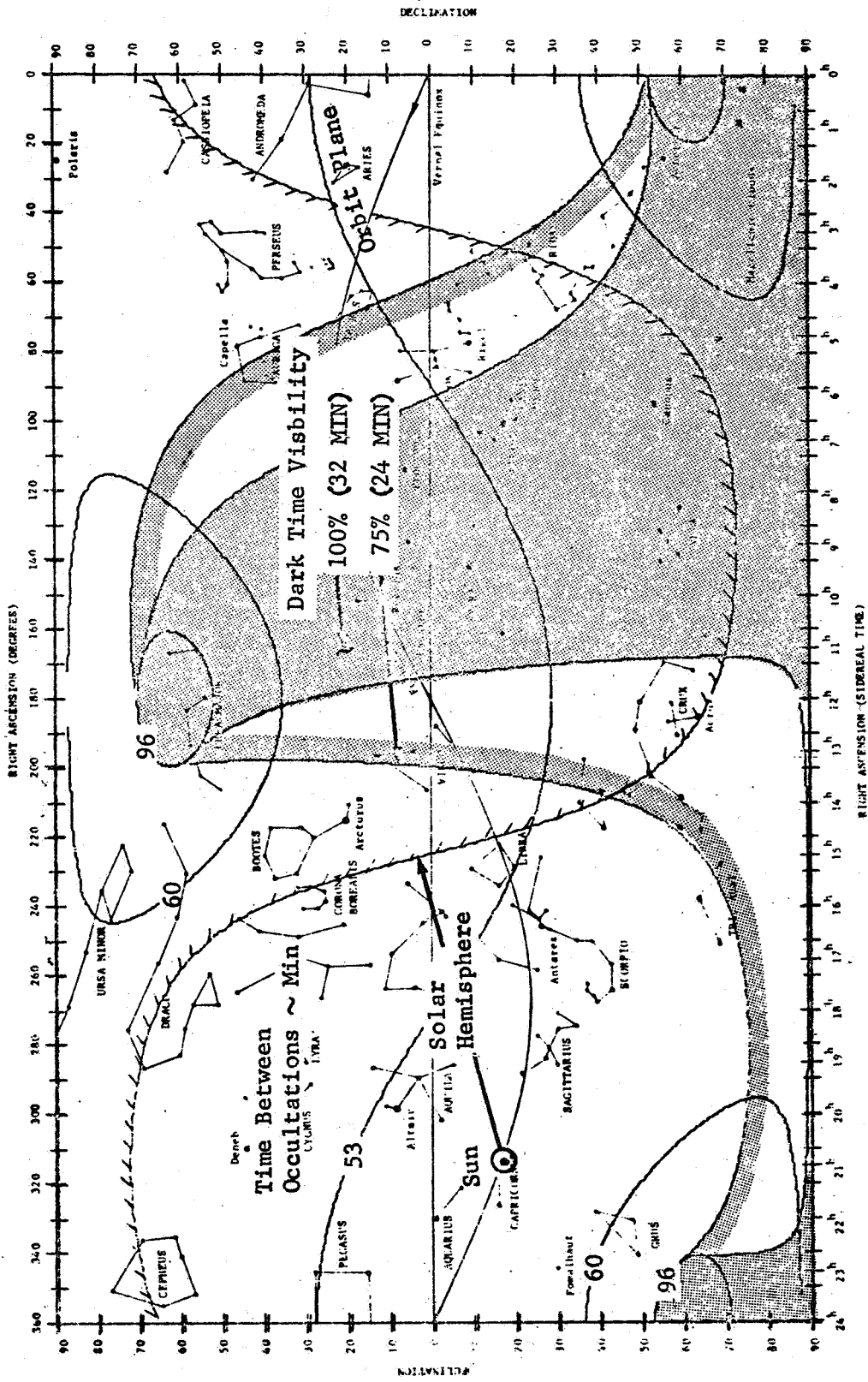


Figure III-28. Typical viewing opportunities at T + 6 weeks.

(1) Observation of Source B when Source A is Observed for its Full Accessibility Time. Figure III-29 shows for the situation shown in Figure III-30 the observation times for a source location in direction B (termed source B) when a source located 90 degrees to it in direction A (termed A) is viewed for the full time it is accessible as a function of vehicle slew rate. Both sources are assumed that the spacecraft has completed its maneuver to Source A. The spacecraft can perform its maneuver to a source although the source is occulted by the earth.

A source coplanar with the orbit plane is accessible to the spacecraft for approximately 53.45 min. Of this, approximately 3 minutes will be consumed for vehicle settle-out to 30 arc sec (using body-mounted star trackers), 1.0 min for vehicle settle-out to 1 arc sec (using OTA course signals), and 1 min for secondary mirror settle-out to 0.005 arc sec (using OTA fine signals). This results in a total settle-out time of about 5 min which must be taken away from the 53.45 min the source is accessible. Thus, source A can be viewed for approximately 48.45 min. At the end of this observation period, the spacecraft must maneuver to source B and settle out before it can begin viewing the source. Like source A, source B is accessible for 53.45 min. However, 29.2 min of this time is consumed viewing source A during the full time it is accessible. This, in effect, leaves 24.26 min for the spacecraft to perform a 90 degree maneuver and settle out. As indicated previously, approximately 5.0 min will be required for spacecraft settle-out and when taken away from 24.26 min leaves 19.26 min for the spacecraft to perform its 90 degree maneuver and view source B for a length of time dependent upon the spacecraft's slew rate. The length of time source B can be observed as a function of this required slew rate is shown in Figure III-29. From this curve it can be seen that, in order to view source B for 10 min, a spacecraft slew rate of 10 deg/min is required. Also, it can be seen that this observation time can be increased to 14 min if the spacecraft has the capability of slewing at a rate of 18 deg/min.

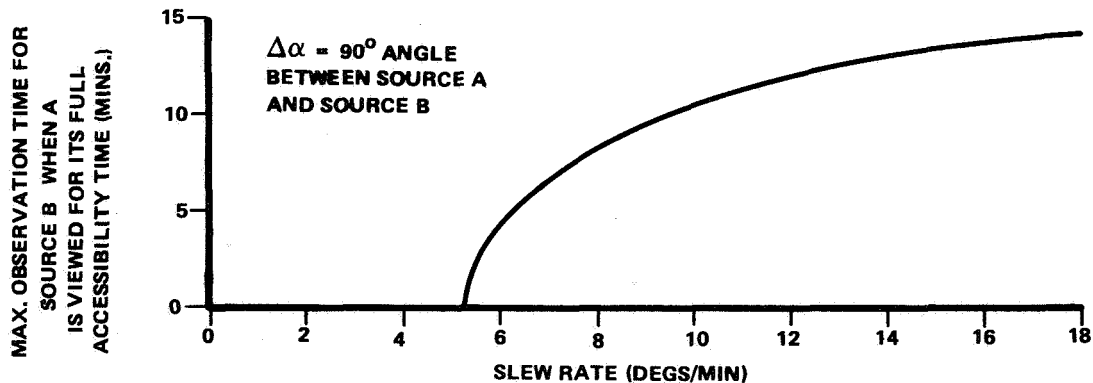


Figure III-29. Observation time per orbit of a second source when a previous one located 90 degrees away is viewed for its full accessibility time.

97 MIN PERIOD OF 611 KM ORBIT.  
 53.3 MIN MAXIMUM VIEWING OF COPLANAR ORBIT.  
 35.5 MIN MAXIMUM DARKNESS.  
 25.0 MIN MINIMUM DARKNESS.

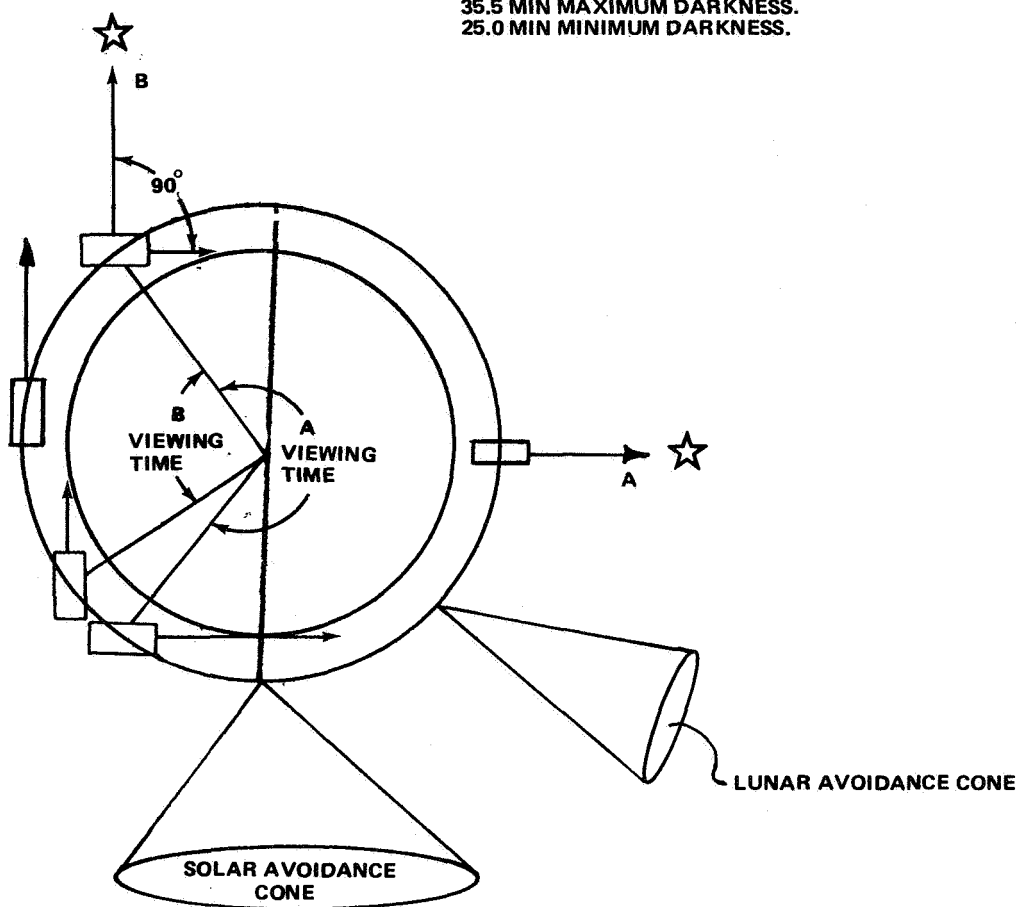


Figure III-30. Situation for the observation of a second source (B) when a previous source (A) is viewed for its full accessibility time.

(2) Observation of Source C When Source A is Observed for Its Full Accessibility Time. The second situation examined is presented in Figure III-31. It is similar to and based upon the same assumptions as the situation presented in Figure III-30 but for sources located 180 degrees apart rather than 90 degrees. The length of time source C can be observed as a function of slew rate when source A is viewed for the full time it is accessible is shown in Figure III-32. From this curve, it can be seen that, in order to view source C for 25 minutes, a slew rate of 10 deg/min is sufficient. A slew rate of 18 deg/min is required to increase this observation time to 33 min.

97 MIN PERIOD OF 611 KM ORBIT.  
53.5 MIN MAXIMUM VIEWING OF COPLANAR ORBIT.  
35.5 MIN MAXIMUM DARKNESS.  
25.0 MIN MINIMUM DARKNESS.

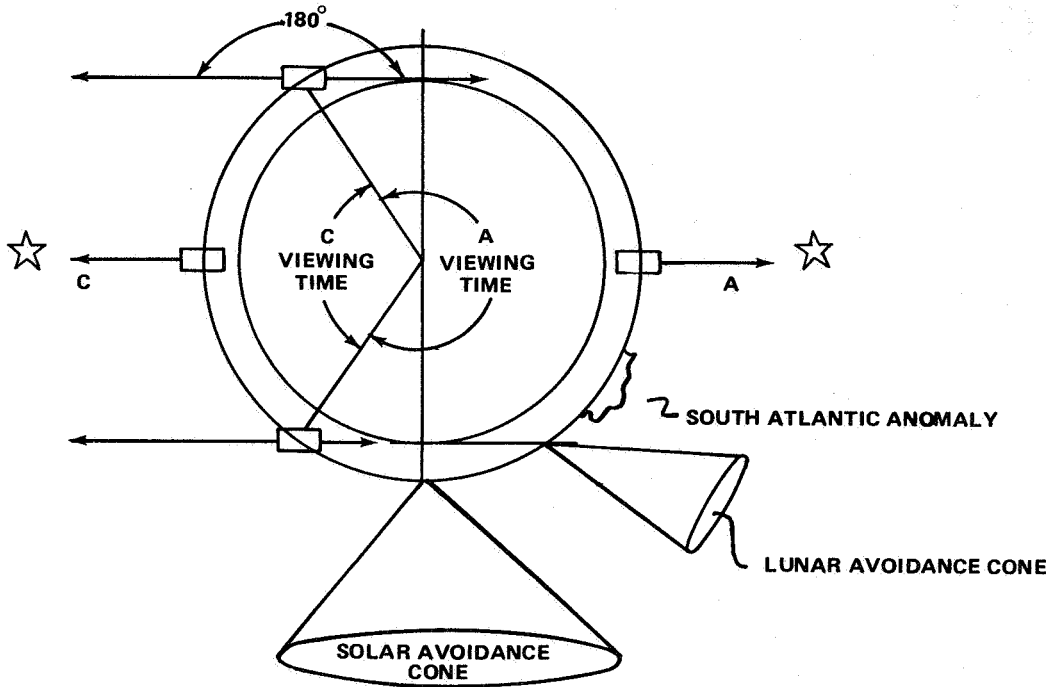


Figure III-31. Situation for the observation of a second source (C) when a previous source (A) is viewed for its full accessibility time.

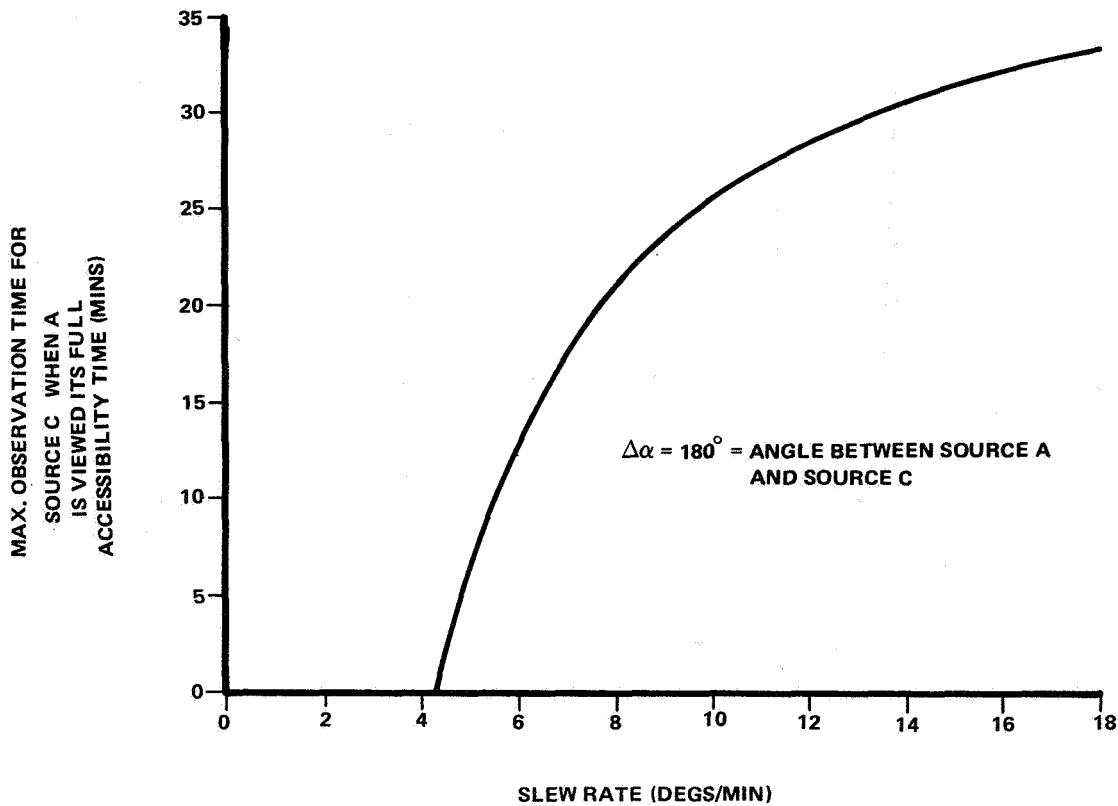


Figure III-32. Observation time per orbit of a second source when a previous one located 180 degrees away is viewed for its full accessibility time.

(3) Maximum Observation Time per Source for Various Sources Viewed for an Equal Period of Time. The final situation examined deals with the situation of viewing two or more sources per orbit for the maximum equal amount of time, each as a function of spacecraft slew rate. Figures III-33, III-34, and III-35 show the observation time per source if each of two, three, or four sources is viewed during a single orbit for relative source locations of 5, 15, and 25 degrees apart, respectively. Figure III-36 shows the same situation for two sources located 90 and 180 degrees apart, respectively. These charts assume, it is noted, that the spacecraft has completed its maneuver to its first source in each case. Figure III-33 shows that, in order to view two sources located 5 degrees apart for 22 min each, a slew rate capability of 6 deg/min is required. This slew rate will also allow three sources located the same distance apart to be viewed for 17 min each. Figure III-35 shows that two sources located 25 degrees apart can be viewed for 17 min each if the slew rate is 18 deg/min. Also, Figure III-36 shows that, for two sources located 90 and 180 degrees apart, a 10 deg/min slew rate will permit each source to be viewed for 29 min and 38 min, respectively.

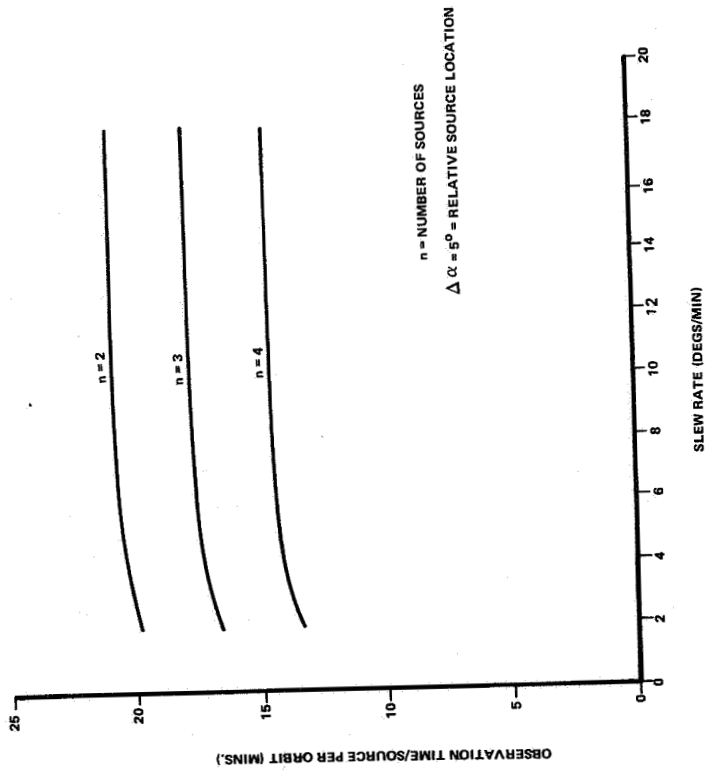


Figure III-33. Observation time per source when  $n$  are viewed for an equal amount of time and located  $\Delta\alpha$  apart versus slew rate.

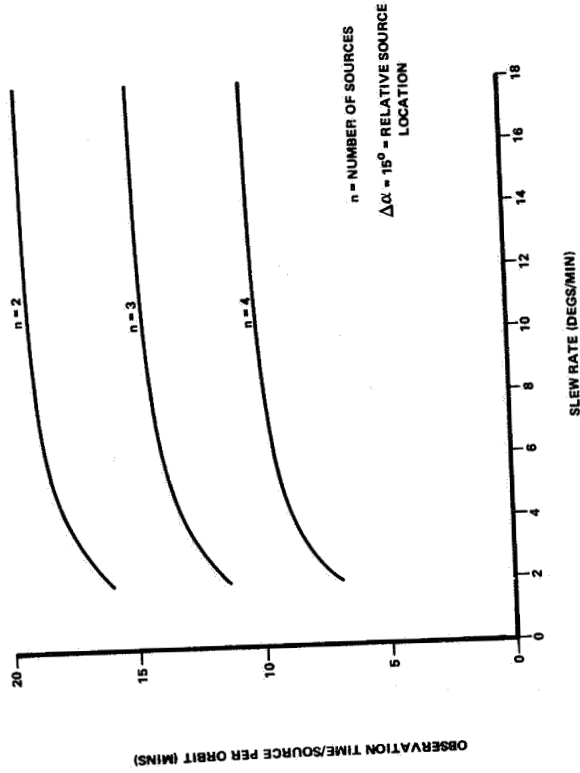


Figure III-34. Observation time per source when  $n$  are viewed for an equal amount of time and located  $\Delta\alpha$  apart versus slew rate.

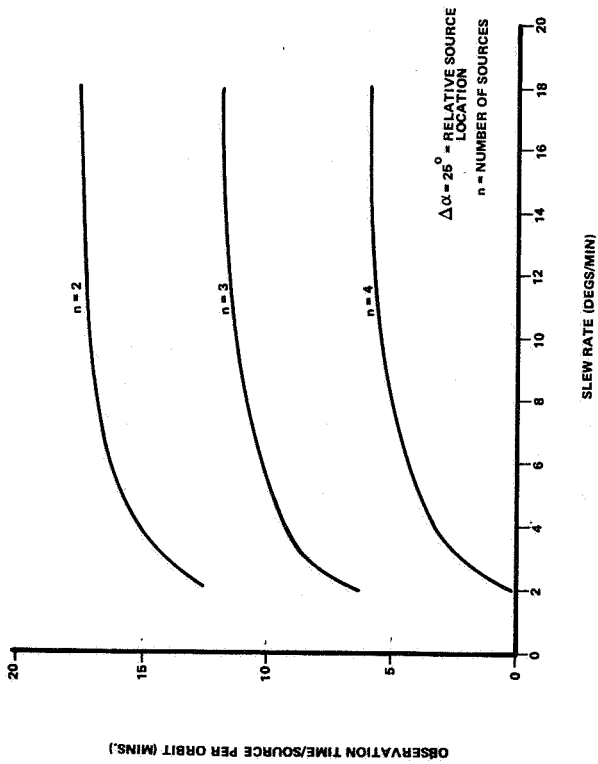


Figure III-35. Observation time per source when  $n$  are viewed for an equal amount of time and located  $\Delta\alpha$  apart versus slew rate.

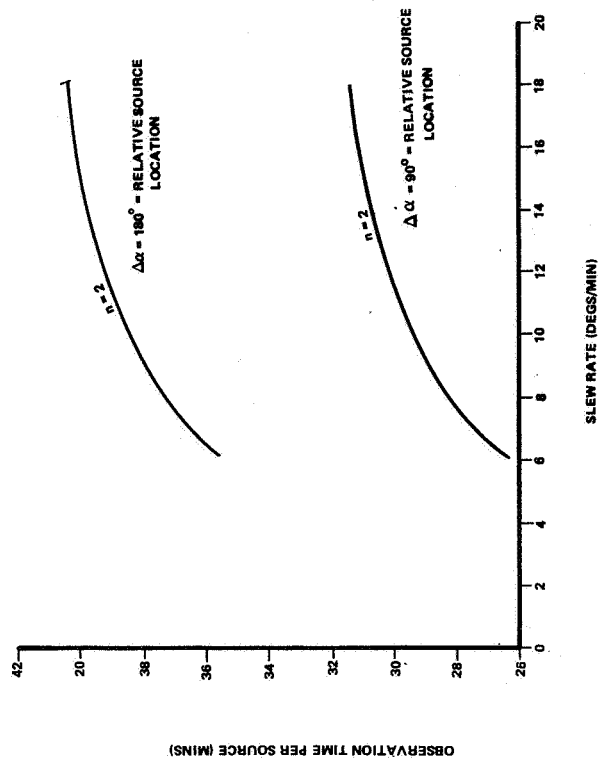


Figure III-36. Observation time per source when  $n$  are viewed for an equal amount of time and located  $\Delta\alpha$  apart versus slew rate.



This cursory analysis from a mission operations point of view shows that it is possible as well as feasible to program the observation of two sources per orbit when the sources are located near each other. The observation of a second source located 90 or 180 degrees apart from a first source observed for the full time it is accessible appears to be feasible only under ideal observing conditions and for sources requiring very short exposure times. The observation of two, three, or four sources per orbit appears encouraging if these sources are very near each other. The observation time of these sources becomes almost independent of slew rate for slew rates greater than about 10 deg/min.

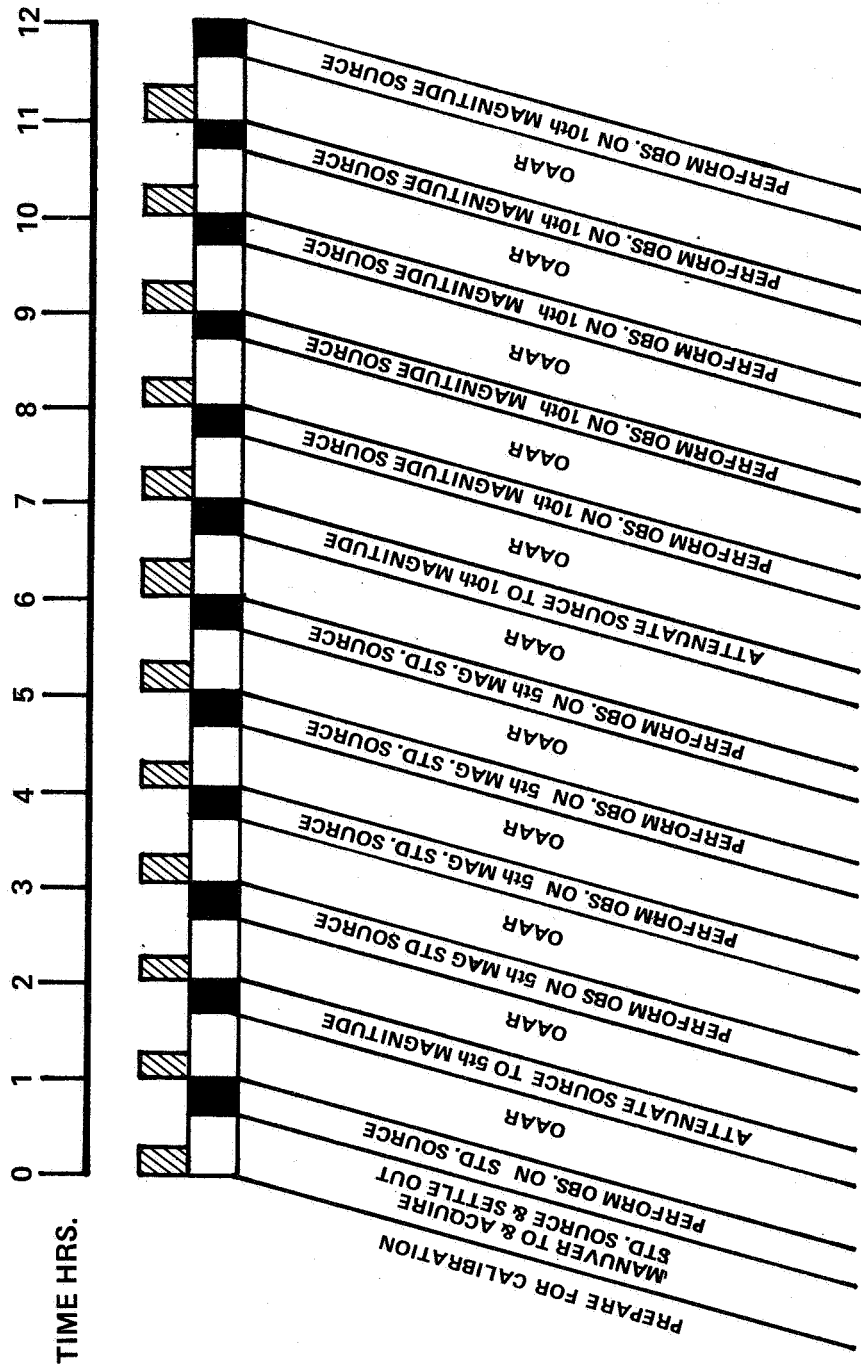
d. Instrument Checkout and Calibration Timeline. Prior to beginning the observation phase of the mission, several checks on the OTA should be performed. First, the primary and secondary mirrors should be aligned and focused. A figure check to verify the geometric characteristics of the primary mirror should then be performed. This is followed by checkout of the telescope transfer optics which is in turn followed by checkout of the telescope imaging systems.

Following this series of checks and corrections, each instrument will undergo a "relative calibration" check which can be performed in a total time of about 8 hours and will essentially compare on-orbit instrument readings utilizing an artificial source with those received on the ground from the same source prior to launch. This calibration will identify any changes in instrument performance due to launch vibrations.

Prior to its use by a principal investigator each instrument may undergo "absolute calibration". No specific amount of time will be allocated at the beginning of the mission to perform this type of calibration on each instrument contained in the SIP. Rather, an instrument may be calibrated immediately prior to its use by the principal investigator who will be using it. This is a calibration of the specific instrument against a known standard calibration star. Figure III-37 is a possible timeline for the high-speed spectrograph.

Source observation time is the most critical factor which contributes to calibration time. This is in turn related to source occultation. The timeline in Figure III-37 assumes that the source, as previously stated, is constrained to being observed only during the time the spacecraft is inside the shadow portion of its orbit and that the source is accessible during this complete time.

Alignment checks may be required about once per orbit and after maneuvers. Focus/figure checks may be required about once per month.



- DARK PORTION OF ORBIT
- ▨ SOURCE OCCULTATION
- ILLUMINATED SIDE OF ORBIT

"O.A.A.R." - OTHER ACTIVITIES AS REQUIRED.

Figure III-37. Calibration timeline for high speed spectrograph.

Figure III-38 gives an overview of the operational viewing activities which have been envisioned as representative of those the spacecraft will be involved in during a typical 30 day period. From this overview, timelines are included for the days indicated by the hash-marks. These timelines show how the spacecraft has been envisioned to operate on a daily basis under the various conditions created by the existence of the various constraints associated with the different source observation requirements. Specifically included in these timelines are such considerations as source observation time, source selection, instruments utilized, scheduling of housekeeping activities, observational constraints, and daylight and dark cycles. Associated with each timeline is a plot of the relative locations of the solar avoidance cone, lunar avoidance cone, and cones of continuous visibility due to their relative movements within the time periods allocated for the specific activities shown in Table III-11.

e. Typical Observation Day of UV Galactic Faint Objects. Two sources whose characteristics are faintness ( $M \geq 6$ ) and abnormally high emission of ultraviolet radiation are 208 G Eridani and 145 G Eridani. The specific characteristics of these sources are given in Table III-13. Figure III-39 shows how these two sources might possibly be observed during a given day for a period of about 4 hours integrated viewing time each. Specifically, it shows that, beginning with a starting orbit, 208 G Eridani is chosen such that when it is occulted; it is also on the illuminated side of the orbit. During this time, the high speed spectrograph is switched into the focal plane of the telescope. This is the instrument most likely to be used in making observations on this kind of sources. Also during this time, the spacecraft can possibly perform the maneuver required to achieve the attitude needed to observe 208 G Eridani. As 208 G Eridani becomes assessible, the spacecraft begins its settling out process followed by acquisition of the sources and the associated guide stars which are required for its observation. This followed by performing high speed spectrography on the source and by "other activities as required" (OAAR), such as momentum dumping or data readout for the observation of the same source during the next orbit.

As 208 G Eridani returns to view, the spacecraft begins its settling out process followed by reacquisition of 208 G Eridani and its associated guide stars. This procedure is continued through 7 orbits at the end of which time the spacecraft will maneuver to view the source 145 G Eridani using the same procedure that was used in observing the previous source for an approximate equal amount of time — 34 min per orbit for 7 orbits. The integrated viewing time for each of these sources translates about 4 hours observation time per source. This time, of course, reflects

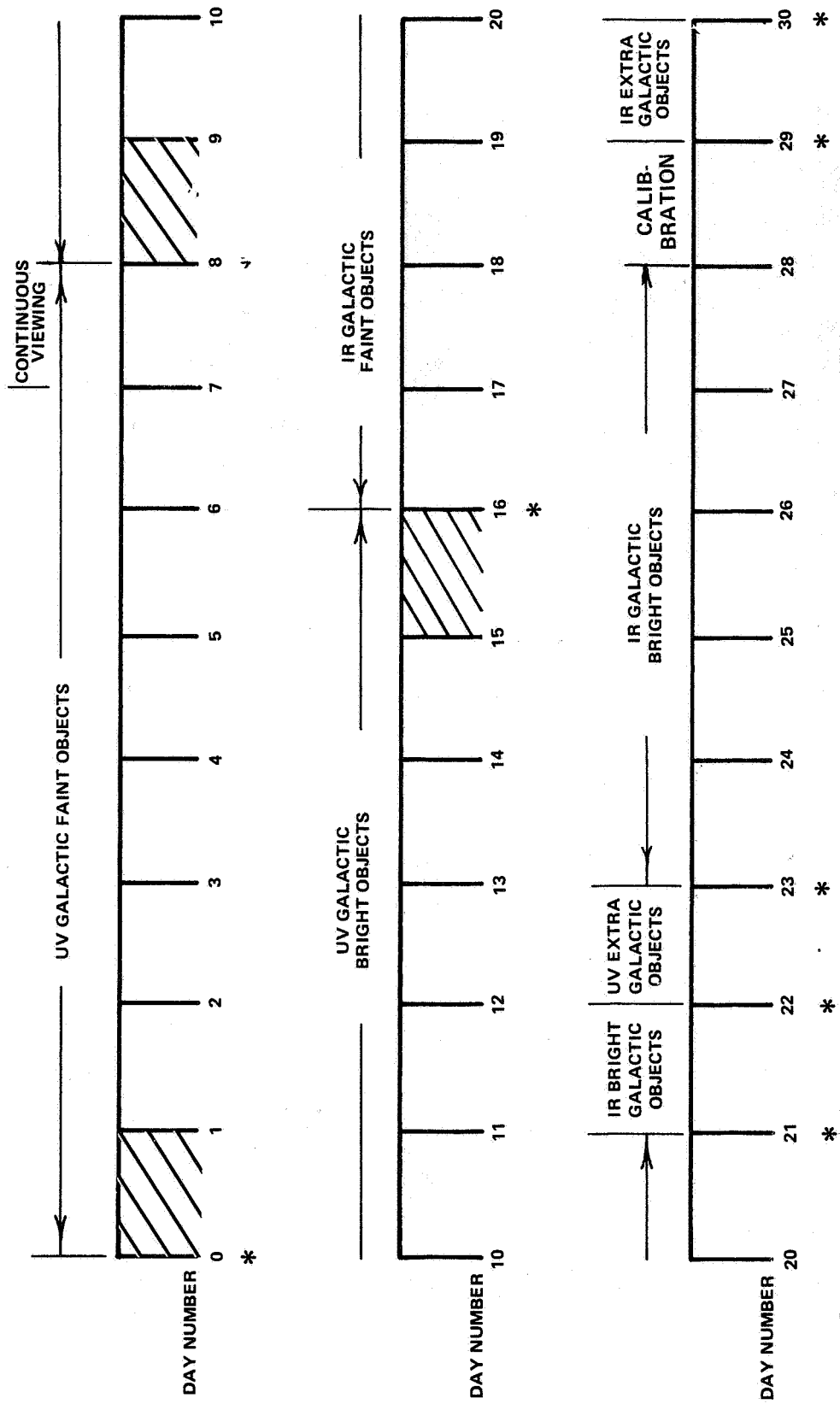


Figure III-38. 30-day overview of LST observational activities.

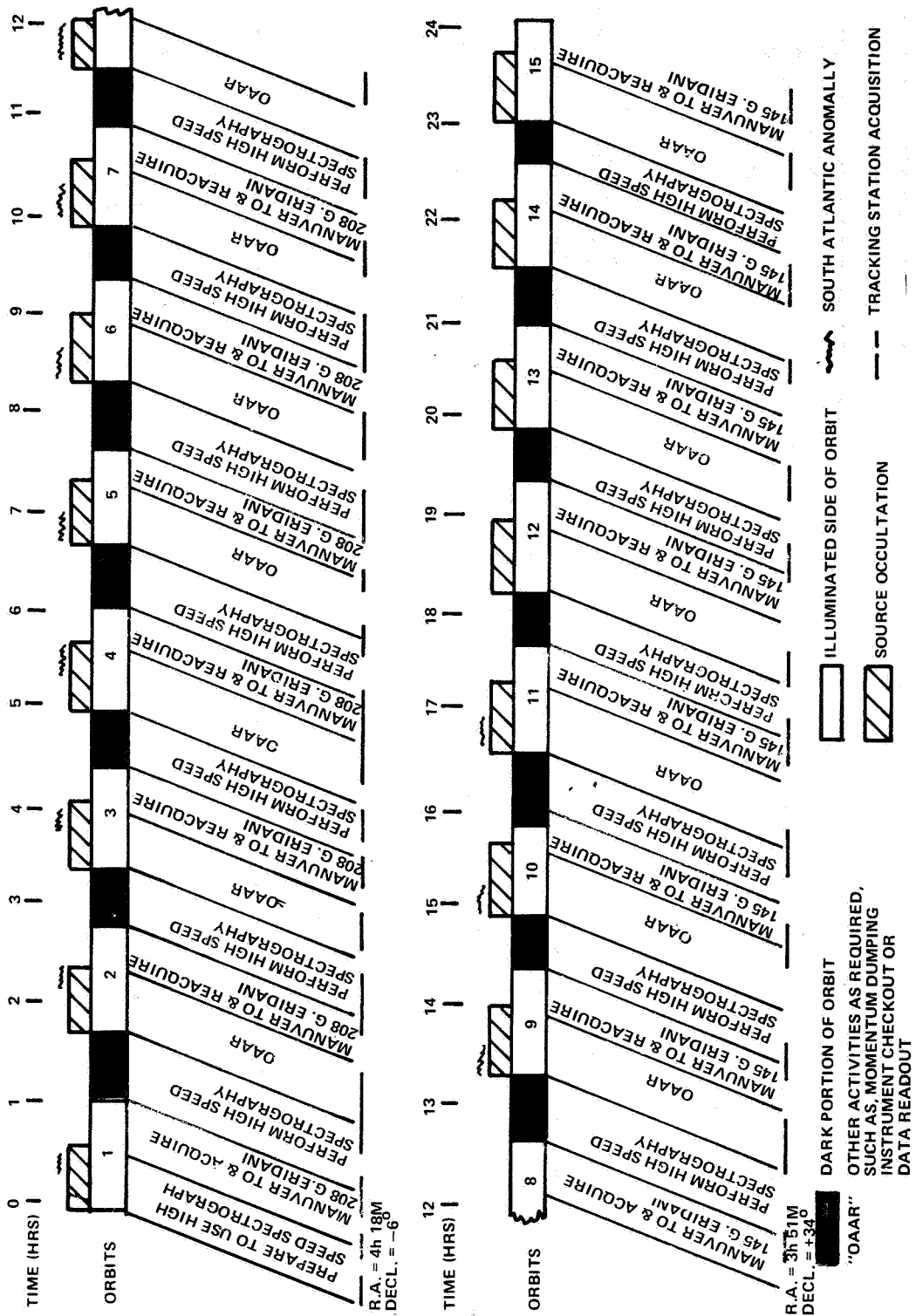


Figure III-39. Typical day observation for UV galactic faint objects.

observations made inside the shadow cone of the earth only, which varies as a function of the time of year. A plot of these sources on the celestial sphere is shown in Figure III-40. The relative projections of the solar avoidance cone, the lunar avoidance cone, and the cones of continuously accessibility are indicated also.

TABLE III-13. CHARACTERISTICS OF 208 G ERIDANI AND 145 G ERIDANI

Source	R. A. (hr:min)	Declination (deg/min)	Mag	Special Class
208 G Eridani	04:18	-6	6.7	B
145 G Eridani	03:51	+34	6.6	B

It is significant to note that, during the period of time indicated on the timelines by OAAR, the spacecraft can maneuver to and observe a second source if sufficient time permits. This, of course, depends upon slewing rate capability, possible instrument change-out requirements, type of source, etc.

f. Typical Observation Day of UV Galactic Bright Stars. The observation time of bright stars, as indicated by Table III-11 will be considerably less than that for faint stars. Consequently, about 14 bright stars should be observed by the LST during a given day. This implies the observation of about one source per orbit. The possibility of observing 14 sources per day depends upon several factors, such as the number of different instruments used, spacecraft slewing requirements, etc. However, to determine if 14 bright sources can be viewed by the LST during a given day, 14 sources were chosen (Table III-14) whose magnitudes were less than 6. A plot of these 14 sources is shown in Figure III-41 as a function of their right ascension and declination. It is significant to note that these sources belong to spectral class O or B, which implies that they are to some extent abnormally high emitters of UV radiation.

Figure III-42 presents a timeline showing how the LST might possibly go about making observations on these sources, in the order of their observation. Performing the observations in the order presented should have the effect of minimizing the extent of the individual spacecraft excursions.

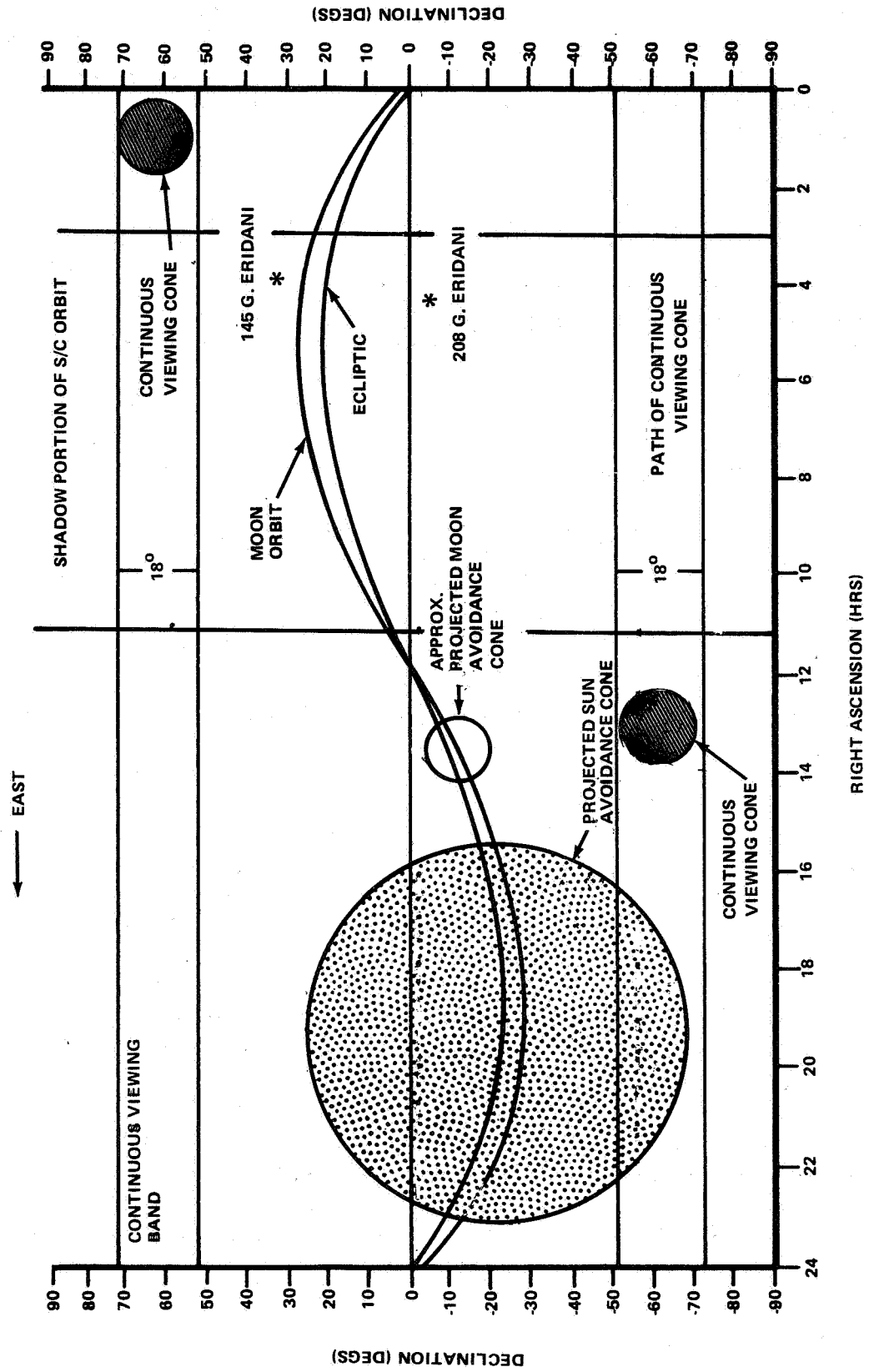


Figure III-40. Distribution of UV galactic faint sources.

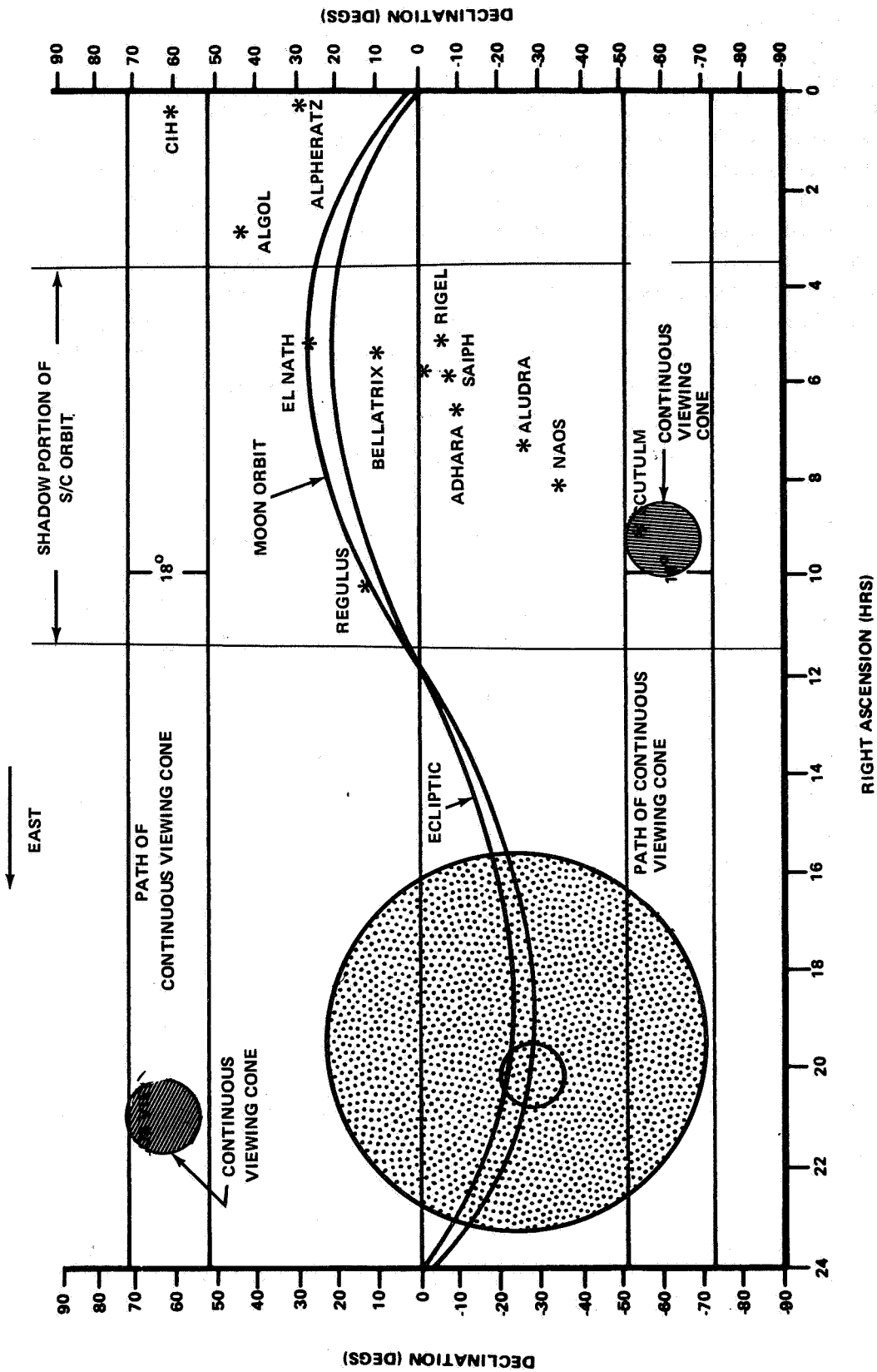


Figure III-41. Distribution of UV bright sources.



Specifically, Figure III-42 shows that first the sources are chosen such that they can be viewed during the time the spacecraft is inside the shadow portion of the orbit. Beginning with the first orbit, preparation for use of the Echelle spectrograph is achieved. Following this event, the spacecraft maneuvers to and acquires the first source, CIH, and its associated guide stars. Although the timeline shows the maneuver being performed during the time the source is accessible, the spacecraft can actually perform its maneuver concurrently with switching instruments during the time the source CIH is occulted. After guide star and source have been acquired, Echelle spectrography is performed on the source. Following this observation of the star, "other activities are required" to prepare for the observation of the second source, ALpheratz, are performed. As Alpheratz becomes accessible, the spacecraft settles out, and it and its associated guide stars are acquired. This general procedure is repeated for each orbit until all 14 sources are observed.

TABLE III-14. UV GALACTIC BRIGHT STARS

Source	R. A. (hr:min)	Declination (deg:min)	Magnitude
CIH	00:51	60:11	2.2
ALpheratz	00:03	28:32	2.1
AChernar	01:34	-57:45	2.2
ALgol	03:02	40:34	2.1
EL Nath	05:20	28:32	1.7
Bellatrix	05:20	6:16	1.6
Mintake	05:27	-0:22	2.2
Riquel	05:10	-8:19	.1
Saiph	05:43	-9:42	2.1
ADHARA	06:14	-16:35	-1.4
ALUDRA	07:20	-29:06	2.4
NAOS	08:00	-39:43	2.2
SCULTULUM	09:14	-58:51	2.2
REQULUS	10:03	12:27	1.3

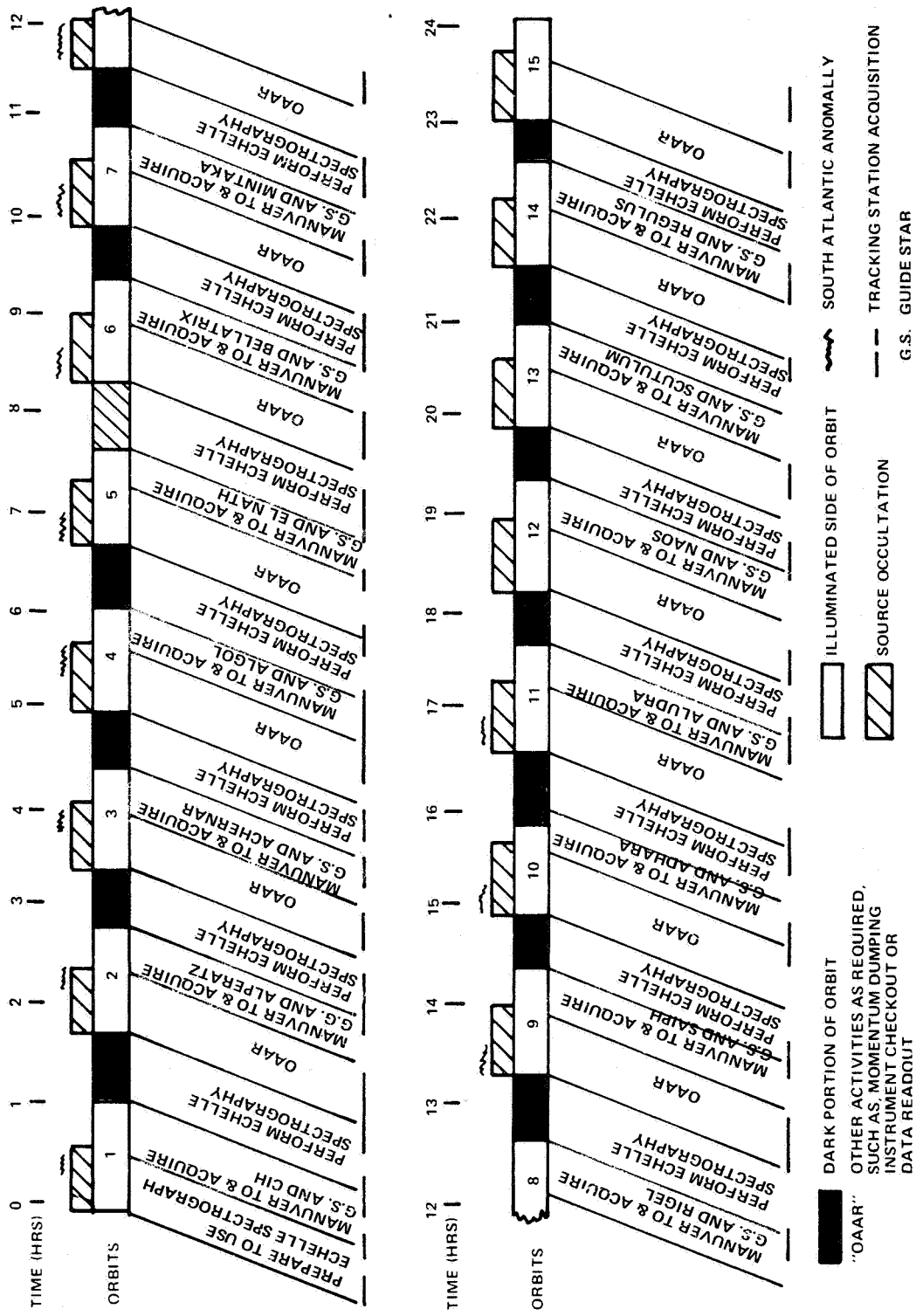


Figure III-42. Typical day observation of UV galactic bright objects.

Figure III-43 shows a plot of a group of sources which are representative of these which might possibly be observed during the final day of observing UV galactic bright sources for the 30 day time period. Also, this figure shows the relative locations of the solar avoidance cone, lunar avoidance cone, and cones of continuous visibility due to their relative movement from the relative locations shown in Figure III-41. Figure III-44 shows the timeline illustrating the observation of the sources plotted in Figure III-43.

5. Conclusions. This analysis has resulted in the identification of several interesting points. Source observation times for both faint and bright sources have been identified. It has been pointed out that faint sources will be observed from 1 to 10 hours each while bright sources from a few seconds to 1 hour each. Typically, an investigator will view from 10 to 20 sources before relenquishing the telescope to another investigator.

Several factors associated with source observation have been identified which definitely should be considered in the scheduling of certain observations. These factors are time of year, location of observational constraints, source location from the sun, and the location of the continuous observation cones.

A multiple-source viewing per orbit analysis was performed. This analysis indicates that more than one source per orbit appears feasible from a mission operations point of view. In addition, this analysis shows that equal observation time per source becomes almost independent of slew rates greater than 10 deg/min for sources located relatively close to each other.

Two types of calibration may be required for the instruments contained in the SIP. A "relative calibration" will be performed on each instrument before the observation portion of the mission is initiated. This calibration can be performed in a total time of about 8 hours and will essentially compare on-orbit instrument readings utilizing an artificial source with those received on the ground from the same source prior to launch. This calibration will identify any changes in instrument performance due to launch vibrations. Prior to its use by a principal investigator, each instrument may undergo "absolute calibration." Specifically, this type of calibration will require that the specific instrument be calibrated against a known standard calibration star.

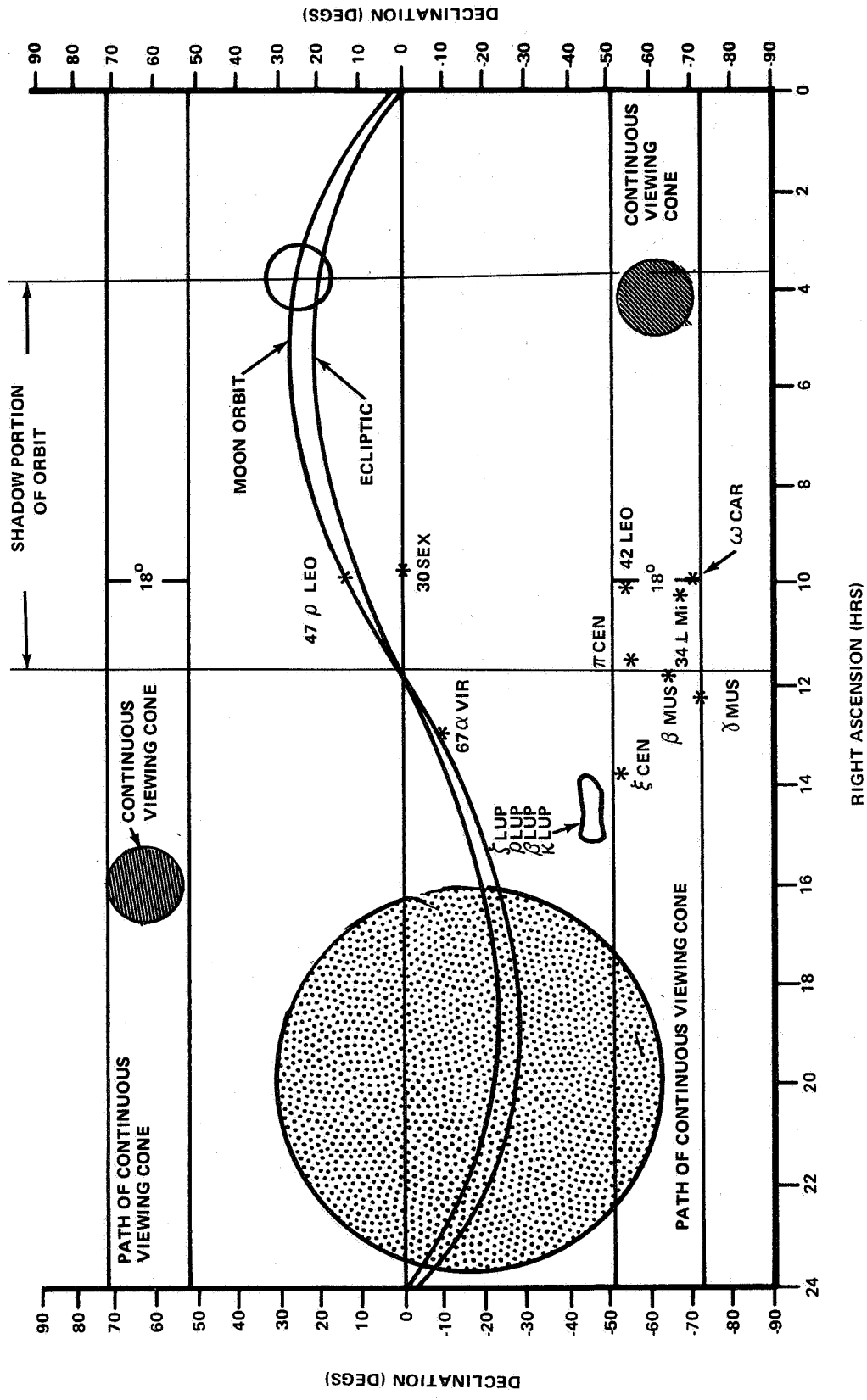


Figure III-43. Distribution of bright UV galactic bright sources.

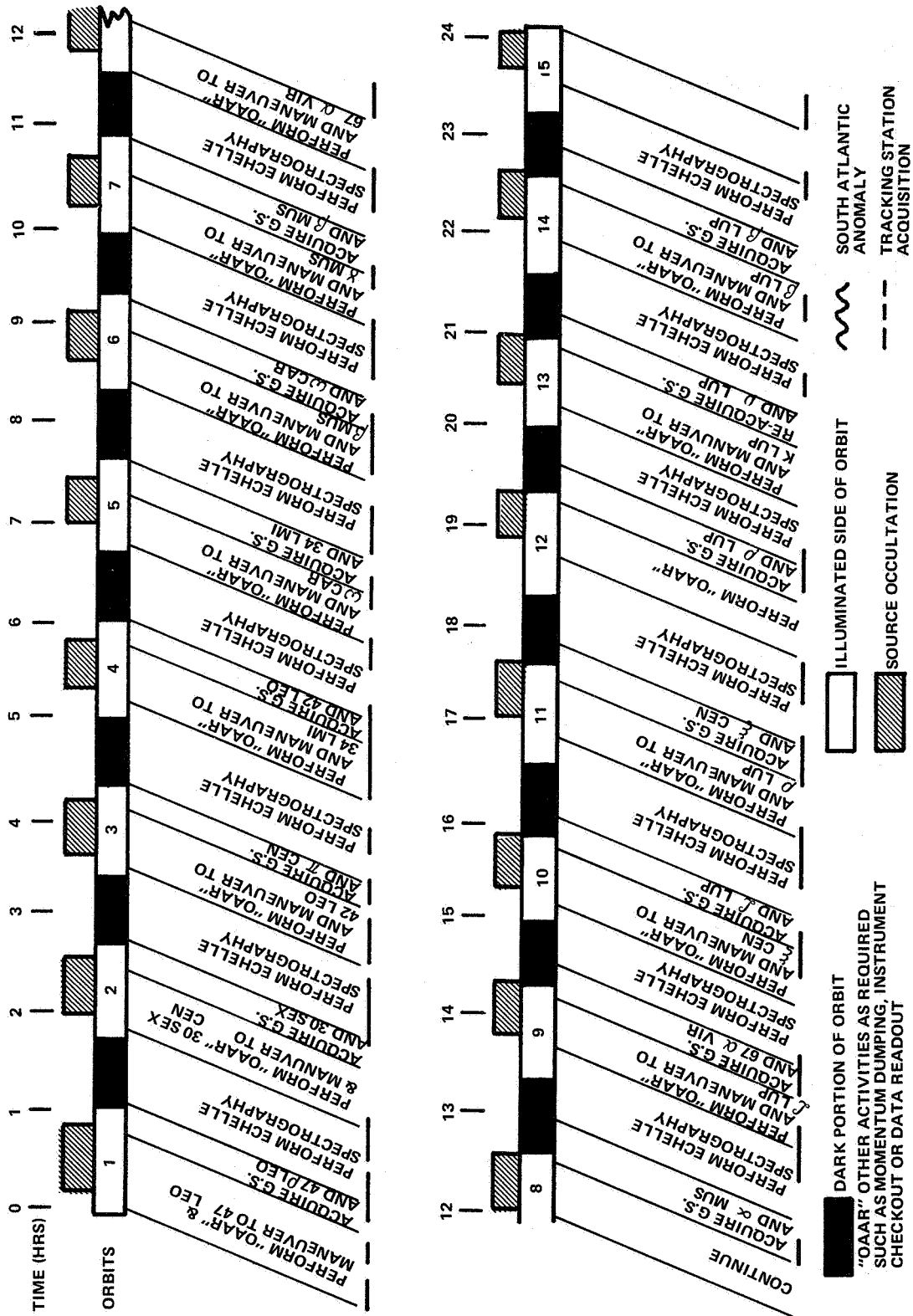


Figure III-44. LST observation of bright UV sources.

6. Operating Modes. During normal operation, the LST will view sources one at a time with one instrument until the viewing is completed; then, it will either select another instrument or another source, or both, and proceed with another observation. Optimization of the viewing program will contribute significantly to the overall viewing efficiency. Such optimization depends heavily on the slew rate and settle time capabilities, the thermal time constant of the system, warmup time of the instruments, observation time required to obtain the image, and ground contact frequency. Multiple-instrument simultaneous viewing is possible from a systems standpoint if the sources of interest are located properly.

Backup and emergency modes are provided in each system, in addition to considerable redundancy provided at the component (blackbox) level and below. In the portions of the systems which are mission-critical, these modes will be entered automatically, and in other systems, the modes will be entered upon detection of a failure or sufficiently degraded performance. Failures and performance degradation are detectable from the ground to the blackbox level.

An "on-orbit storage mode" is provided and is a very attractive capability for use in emergencies and/or in the event it is desired to shut down the LST temporarily to conserve lifetime or for programmatic reasons. This mode is effected by retracting the solar arrays, shutting down all systems except communications and thermal control heaters, and closing the aperture doors. The LST can tumble or assume any random orientation. The key features which permit lack of attitude control during this period are the wraparound solar panels and the antennae which provide near-omnidirectional coverage with arrays extended or retracted.

During the maintenance mode, the LST systems are dormant except for lights, thermal control heaters on the mirrors, and the hazardous warning/intercommunications box. Clean air is circulated through the SSM by a portable trace contaminant removal system, and the air temperature, relative humidity, and oxygen/CO<sub>2</sub> content is controlled by either a portable system or an isolatable portion of the Shuttle ECLSS.

In the on-orbit checkout mode after maintenance, the LST receives power from the Shuttle while all systems are turned on sequentially and verified via a coaxial link to the Shuttle cabin. Subsequently, the arrays are deployed and verified, and RF link is verified, and the LST is depressurized and released. The Shuttle remains in the area until communication with a ground station is verified, then it departs.

## E. Coverage Contact Statistics

1. Preliminary LST Mission Coverage. Preliminary mission coverage analysis, in terms of contact times, was undertaken to assess the capability of three selected ground network configurations of the Spaceflight Tracking and Data Network (STDN) in providing tracking coverage support to the LST mission. Another tracking concept, which initiates in geosynchronous orbit, has been retained to determine the feasibility of supporting the LST with the tracking and data relay satellite (TDRS) network. Ground and orbital contact statistics were generated by means of computer simulation to conform partly with current technical guidelines for communications and data handling for use in the LST design planning.

With the LST launch date programmed for 1980 from the Merritt Island launch area, general orbit requirements have dictated a circular orbit at an altitude of 611 km (330 n. mi.) and an inclination of 28.5 degrees. The selected orbit primarily reflects the expectations that the reference design altitude is considered compatible with the LST orbital lifetime requirements. Additionally, the altitude of 740 km (400 n. mi.) was examined during the early phase of the study on the basis of an assumed 1978 launch. The two altitudes have been compared as a possible means of providing tracking coverage to assess the sensitivity effects. Despite a reduction in station contact time, the lower altitude prevails with advantages of an increase in payload capability and a decrease in radiation environment when considering the significant variations within the altitude range.

To maintain the intensive communications and control links between earth and LST experiments, the STDN provides six ground tracking stations equipped with a 9.144 m (30 ft) diameter antenna (Configuration A). The selection was based on two criteria. The first was that the station had to be visible to the spacecraft and the second was that the ground station had to have the proper S-band equipment. The selected ground sites are Canary Islands (CYI), Ascension Island (ACN), Carnarvon (CRO), Guam (GWM), Hawaii (HAW), and Goldstone (GDSX). This configuration is used for evaluation in a simulation to determine the exact coverage provided for the mission.

The STDN is formed by combining the former Space Tracking and Data Acquisition Network (STADAN) and the former Manned Space Flight Network (MSFN) to achieve the overall support capability requirements. Current NASA studies have dictated a requirement that the tracking facilities

at Carnarvon (CRO) be phased out of the STDN in 1974. Since the LST is scheduled to operate initially in 1980, subsequent simulated analysis has assumed a possible participation of Orroral Valley (ORRX) instead of CRO. The new six station network is designated as the STDN Configuration B in the comparative analysis.

An alternate ground configuration, selected for further evaluation, consists of three ground stations located at Cooby Creek (TOOMBA), Barstow (MOJAVE), and Rosman (ROSMAN). Actually, AVE and ROS are relatively new acronyms and will be used in the ATS section of this report. The bandwidth capability of those stations would impose some constraints on the data transmission capability. The three stations demonstrate use of the Applications Technology Satellite (ATS) systems separately from the former standard STADAN antennas. The ATS facility at Rosman is equipped with a 25.908 m (85 ft) diameter antenna. The other two operate with 12.192 m (40 ft) diameter antennas. The three stations are considered redundant in establishing compatibility with the LST systems.

The TDRS concept uses two tracking and data relay satellites placed in geostationary orbit to simulate tracking of the LST spacecraft over long arcs in the circular orbit. This arbitrarily selected concept should be considered hypothetical and should not be construed as having been proposed by NASA/GSFC. Aim of the hypothetical concept is to primarily increase orbital and geographical coverage and to improve tracking accuracy requirements. With its unique capability for the continuous reception of data in real time, the TDRS objectively commands, tracks, and relays data from the LST to fewer ground stations. Although it would provide complete tracking coverage for the LST, the TDRS may pose a problem of accessibility since the scientific data generated on the LST orbital mission would not require continuous real-time data dumping or real-time ground control of experiment and subsystem operations. Nevertheless, the TDRS approach has been emphasized in the analysis of contact statistics.

2. Coverage Assessment. Computations of contact statistics have been carried out for three tracking configurations of STDN and TDRS networks to determine the capability of each one in supporting the communications and data handling requirements of the LST mission. Literally, from the statistics, the contact time achieved between the LST and the ground station or communications satellite can be identified as one informative source of ranging and range rate for use in performing orbit determination and in updating ephemeris data on subsequent orbits.



The purpose of the analysis phase of the study effort is to specify that reliable communications must be established at the 611. km orbit with each ground station or communications satellite. Therefore, each network configuration is evaluated to satisfy one contact per orbit with a 5 min minimal contact and to satisfy the minimum data hours that may be specified in the data handling requirements. Consequently, a representative trade-off evaluation in ground coverage statistics for two STDN configurations and one STDN (ATS) configuration is illustrated in Table III-15 for two altitudes. STDN Configuration B contains Orroral Valley instead of Carnarvon, the latter being in Configuration A. Contact conditions are shown for a length of computer simulation of 70 orbital revolutions; this is adequate to assure reasonably stable statistics. On this table, the conditions computed are externally constrained by a minimum 5 min contact time and elimination of ground station with shorter contact time in the event of station multiple coverage. Configuration B could acquire an average contact time of 26 min per revolution for the baseline altitude. An average contact time of 11 min per revolution is established for each STDN station when a contact is made.

Replacement of Carnarvon by Orroral Valley, according to the computer simulation results, has reduced total contact times and the total number of contacts made. This reduction is attributed to station latitude higher than orbital inclination and antenna obstructional data for Orroral Valley. The coverage summary cannot be considered fixed since orbital parameters and orbital insertion conditions might change as mission planning progresses. The coverage summary provides the required data for evaluation and the data should be treated as preliminary and representative. Table III-15 shows that Configurations A and B do not produce a big difference in the statistics for the 611. km orbit. Therefore, the six station configuration with the fewest gaps, greatest coverage, and smallest gap duration could satisfy LST mission requirements, assuming no implementation of the TDRS network.

Table III-16 is a summary of cumulative contact time per 24 hours for each STDN station, using the antenna horizon coverage limits as a constraining factor. Minimum zero-minute contact time is considered. The elimination requirement is not imposed on an overlapped station with a shorter contact time. A comparison of the individual station coverages in terms of minutes and seconds indicates that, when the overlapping elimination constraint applies, the ability to meet the one contact per orbit requirement decreases. Thus, replacement of CRO by ORRX has produced a substantial reduction in the total station cumulative contact time per 24 hours.

TABLE III-15. STDN AND STDN (ATS) COVERAGE SUMMARY FOR LST  
 [Orbital Count = 70 revolutions, Altitude = 611 km (330 n. mi.)  
 and 741 km (400 n. mi.), Inclination = 28.5 deg]

Contact Conditions	STDN Configuration A		STDN Configuration B		STDN (ATS) Configuration	
	611 Km Altitude	741 Km Altitude	611 Km Altitude	741 Km Altitude	611 Km Altitude	741 Km Altitude
Total contact time in 70 revs (min)	2070.37	2463.45	1796.97		503.72	543.30
Number of contacts in 70 revs	183	195	165		64	59
Percent of contact time in 70 revs	28.40	32.80	24.65		6.91	7.24
Average contact time per rev in 70 revs (min)	29.58	35.19	25.67		7.20	7.76
Avg. contact time per sta. per rev. with contact (min)	11.49	12.78	11.09		7.95	9.28
Min. time of combined contacts during any rev. (min)	13.28	14.85	13.28		5.35	6.10
Minimum station contact time achieved (min)	5.03	5.00	5.03		5.05	5.10
Maximum station contact time achieved (min)	47.07	52.02	47.07		24.42	18.97
	13.43	15.15	13.43		9.83	11.38
Average number of contacts per day	36	37	32		13	11
Minimum number of contacts per revolution	1	1	1		1	1
Number of revolutions without contact	0	0	0		30	27
Max. gap duration achieved in 70 revs (min)	89.77	91.55	89.73		697.23	714.60
Average gap duration in 70 revs (min)	28.59	25.78	33.39		105.49	117.25
Percent of coverage gap less than 1 hour long	92.86	99.49	92.07		53.12	45.76

Notes: (1) Minimum 5-minute contact time  
 (2) Elimination of overlapped station with shorter contact time  
 (3) Bias time for AOS and LOS not deducted from contact time

TABLE III-16. SUMMARY OF STATION CUMULATIVE CONTACT TIME PER 24 HOURS

STDN Network Configuration													
Tracking Station Alt(km)	CYI		ACN		CRO		GWM		HAW		GDSX		ORRX
	611	741	611	741	611	741	611	741	611	741	611	741	611
Duration	Cumulative Contact Time (min:sec)												
First 24 hours	82:38	99:26	74:47	107:24	83:34	101:15	93:21	107:48	87:18	90:47	49:49	54:01	32:34
Second 24 hours	79:32	83:31	75:52	103:26	83:07	85:22	92:10	101:41	87:02	105:13	42:21	62:57	29:45
Third 24 hours	83:32	96:42	83:47	109:33	84:26	102:30	93:52	108:08	77:05	90:57	49:11	51:56	29:57
Fourth 24 hours	79:23	87:25	84:56	98:24	80:28	87:21	92:44	104:37	85:51	106:32	49:24	65:25	29:03
Fifth 24 hours	77:54	98:18	81:25	116:39	80:26	100:20	90:43	109:17	84:41	89:32	52:15	54:20	28:43
70.3 revs	402:59	465:22	413:04	570:44	412:01	496:07	468:17	566:34	434:25	525:34	254:22	323:22	150:02

Notes: (1) Minimum zero-minute contact time.  
 (2) Elimination constraint not imposed upon overlapped station with shorter contact time.

STDN (ATS) Network Configuration												
Tracking Station Alt (km)	TOOMBA		MOJAVE		ROSMAN		CUMULATIVE CONTACT TIME (min:sec)		CUMULATIVE CONTACT TIME (min:sec)		CUMULATIVE CONTACT TIME (min:sec)	
	611	741	611	741	611	741	611	741	611	741	611	741
Duration	Cumulative Contact Time (min:sec)											
First 24 hours	45:08	46:49	33:10	38:06	27:20	37:03	45:08	46:49	33:10	38:06	27:20	37:03
Second 24 hours	47:03	59:15	25:11	45:46	30:38	47:11	47:03	59:15	25:11	45:46	30:38	47:11
Third 24 hours	47:42	53:41	32:50	34:00	35:18	33:18	47:42	53:41	32:50	34:00	35:18	33:18
Fourth 24 hours	44:22	60:07	32:57	47:40	34:35	47:42	44:22	60:07	32:57	47:40	34:35	47:42
Fifth 24 hours	41:02	47:06	32:16	35:27	35:21	36:20	41:02	47:06	32:16	35:27	35:21	36:20
70.3 revs	225:17	271:24	165:02	227:28	170:38	214:43	225:17	271:24	165:02	227:28	170:38	214:43

For each orbit under consideration, Table III-17 shows the impact in contact statistics for two to six sites in the STDN "A" network and for one to three sites in the ATS network on ground statistics. Hence, the average net contact time per day is computed with deduction of bias time which accounts for a total of 1.5 min for acquisition of signal and loss of signal. The computations are made within the constraints which specify minimum 5 min contact time and station overlapping elimination.

Figures III-45, III-46, and III-47 show worldwide coverage provided by the network configurations of STDN and STDN (ATS) for a 611 km spacecraft orbit. The coverage circles for all ground sites for orbital altitudes of 611 km (baseline) and 741 km have been calculated using the actual physical masking data on the antenna, considering terrain and antenna stops. Figure III-46 shows dashed coverages for three more stations which are added to the six station configuration. Also shown on the mercator maps are the ground traces for the first 8.3 orbital revolutions of the LST mission, based on the orbital parameters. All calculations are assumed to begin at insertion of a latitude of 28.5 degrees north and a longitude of 294.53 degrees east, with a trajectory originating in a southerly direction. Based on those figures, a longitude of 50 degrees east was designated as an orbital revolution counter, thus permitting easy counting of total contact time per orbital revolution without overlapping of contact time from one revolution to the next one. The orbital revolution time from the particular longitude to the same longitude is approximately 104 min.

For the first 70.3 revolutions, contact summaries are tabulated in Table III-18 for STDN Configuration A, Table III-19 for STDN Configuration B, and Table III-20 for STDN (ATS) Configuration for the 611 km/28.5 degree inclination orbit. The contact made with the LST by each ground station during any particular orbital revolution is indicated by an X, conforming to three external constraints. The orbital revolution "O" is normally one-third of an orbit, due to a fixed location of the revolution counter. Examination of Tables III-18 and III-19 shows that application of the constraints has degenerated the total contact time for each ground station, with the GDSX sustaining an 80 percent decrease.

Ground contact and gap statistics are compared in plot form: Figure III-48 for STDN Configuration A and Figure III-49 for STDN (ATS) configuration. To facilitate interpretation, the solid blocks, depicting the contact interval, indicate ground contacts equal to or greater than 5 min, using actual land masking data. Two parameters, orbital revolution number and time since insertion, identified in hours, are shown on top and bottom abscissas. On Figure III-49, in the first 70 revolutions after insertion into

TABLE III-17. SUMMARY OF AVERAGE NET CONTACT TIME PER DAY

STDN Network Configuration	Average Net Contact Time Per Day ~ Hrs	
	611 km/28.5 deg orbit	741 km/28.5 deg orbit
CYI, ACN, CRO, GWM, HAW, GDSX	5.9	6.9
CYI, GWM, HAW, GDSX	3.9	4.5
CYI, ACN	2.0	2.6
STDN(ATS) Network Configuration		
TOOMBA, MOJAVE, ROSMAN	1.3	1.4
MOJAVE, ROSMAN	0.7	0.7
ROSMAN	0.4	0.5

- Notes: (1) Minimum 5-minute contact time  
 (2) Elimination of overlapped station with shorter contact time  
 (3) Deduction of bias time of AOS and LOS from contact time

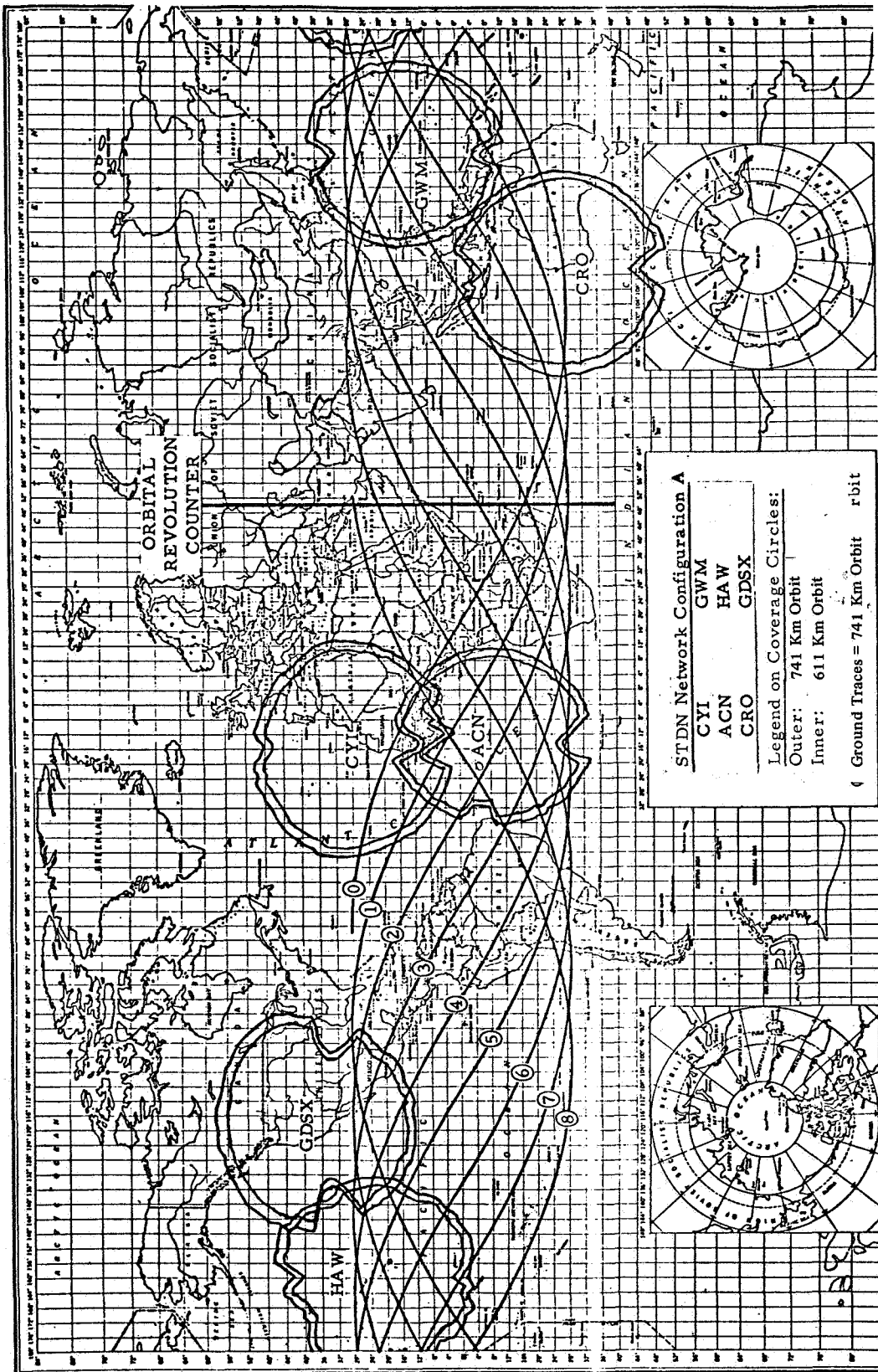


Figure III-45. Ground traces and coverages for LST; STDN Network Configuration A;  
 $H = 611 \text{ km (330 n.mi.)}$  and  $741 \text{ km (400 n.mi.)}$ ,  $i = 28.5 \text{ deg.}$

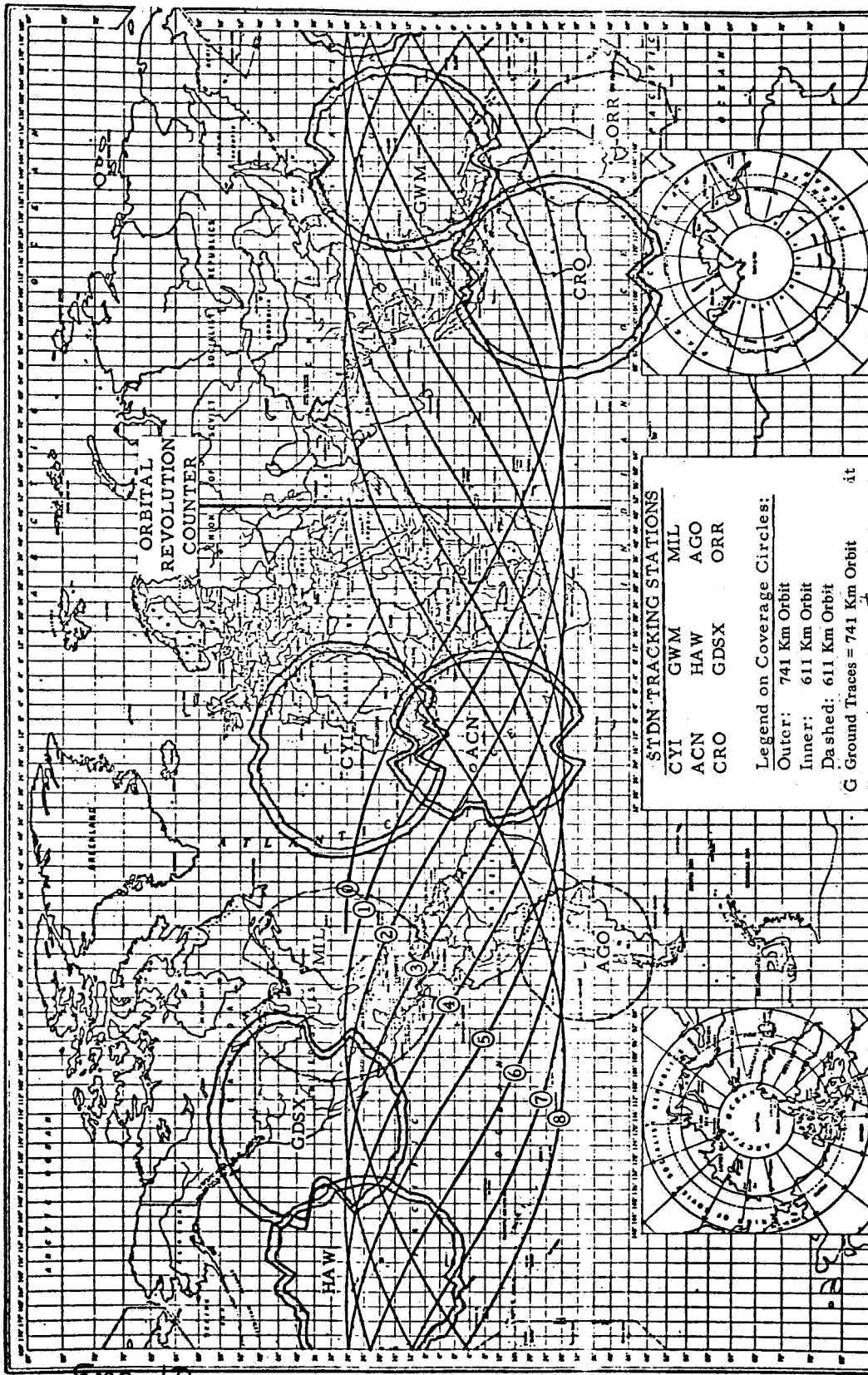
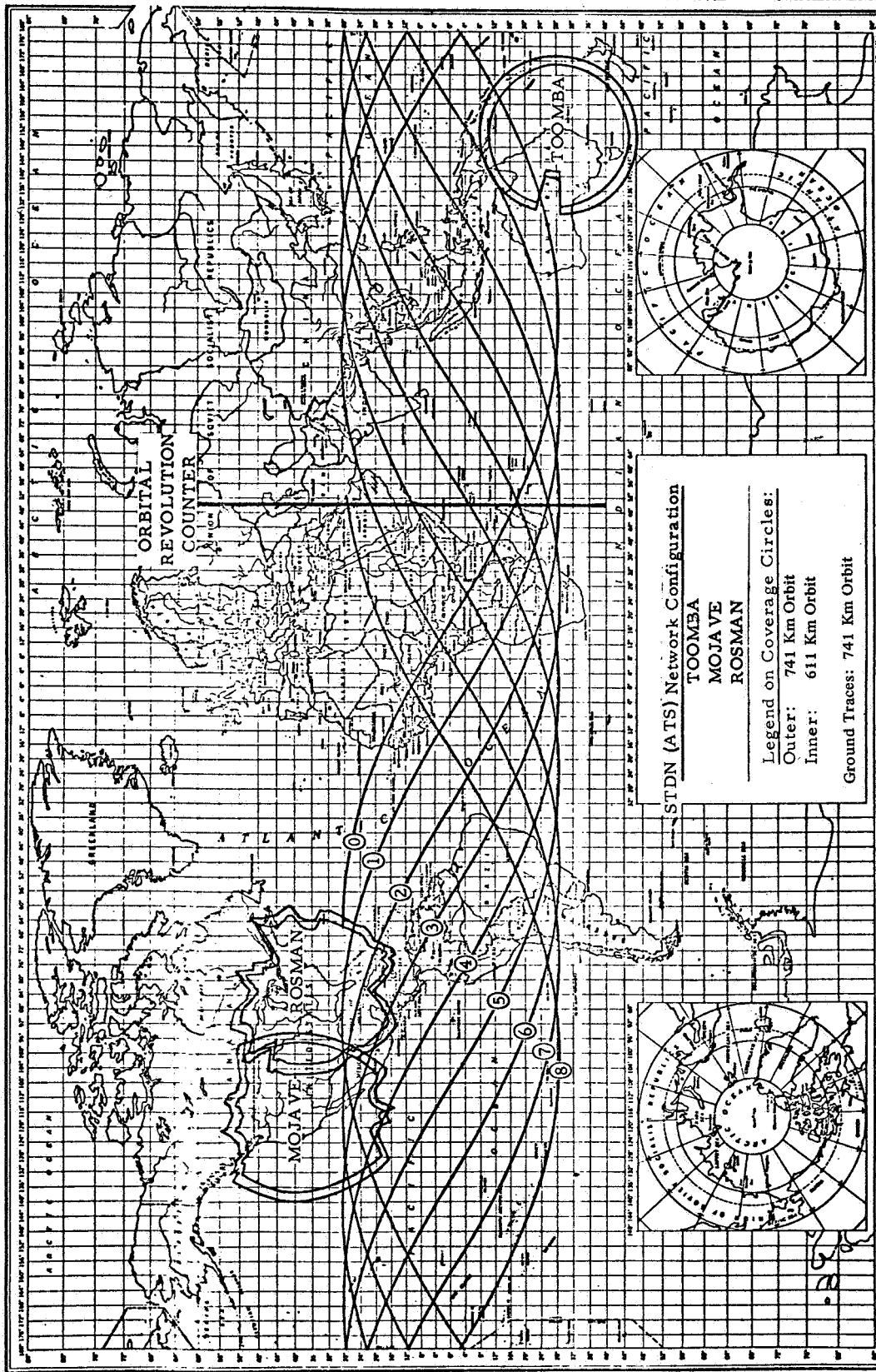


Figure III-46. STDN station coverage for H = 611 km (330 n.mi.) and 741 km (400 n.mi.).



Enc 13

Figure III-47. Ground traces and covers for LST; STDN (ATS) Network Configuration;  
 H = 611 km (330 n.mi.) and 741 km (400 n.mi.), i = 28.5 deg.



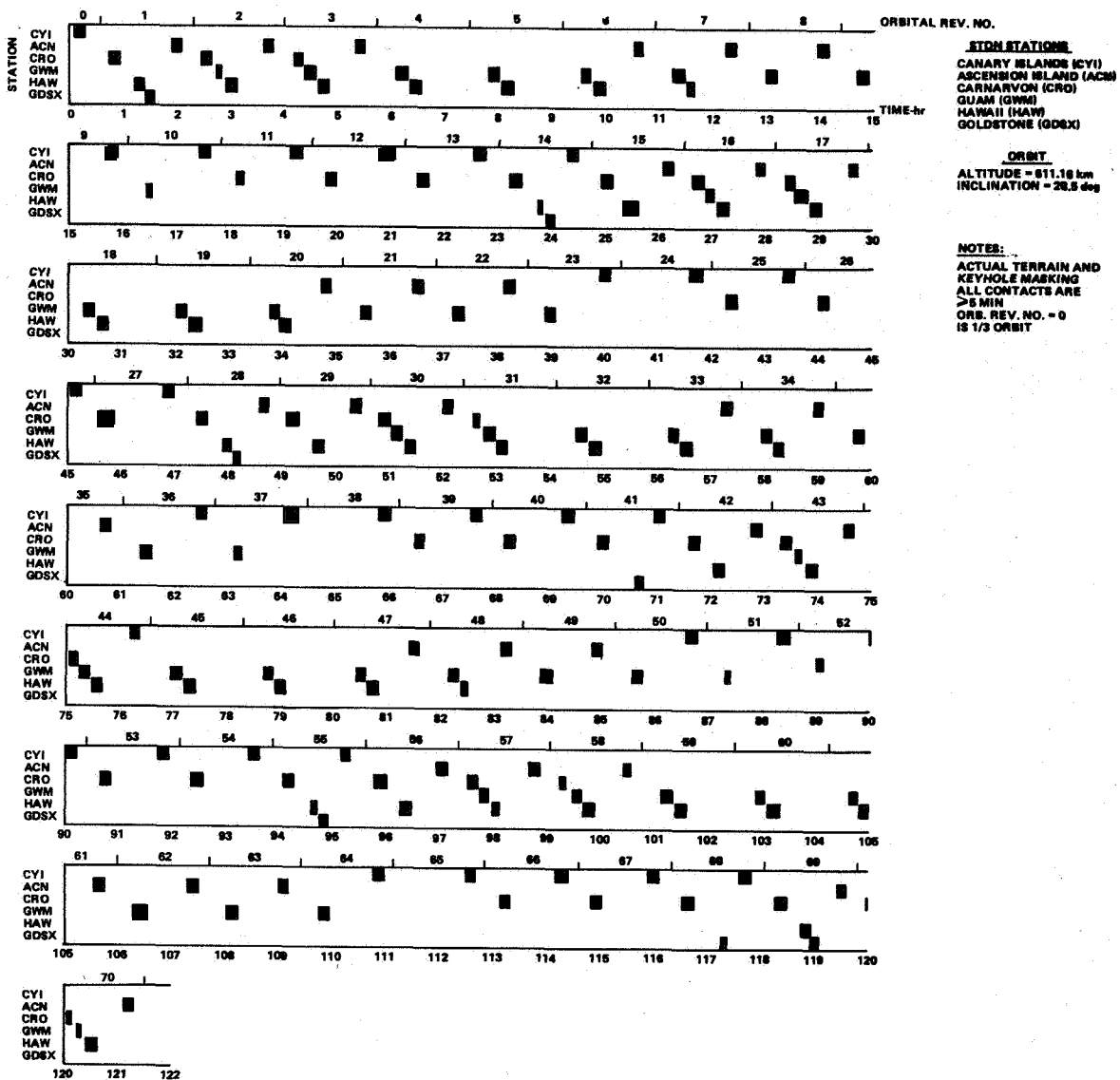


Figure III-48. Ground contact and gap statistics for STDN Network Configuration A. [Altitude = 611 km (330 n. mi.), Inclination = 28.5 deg].

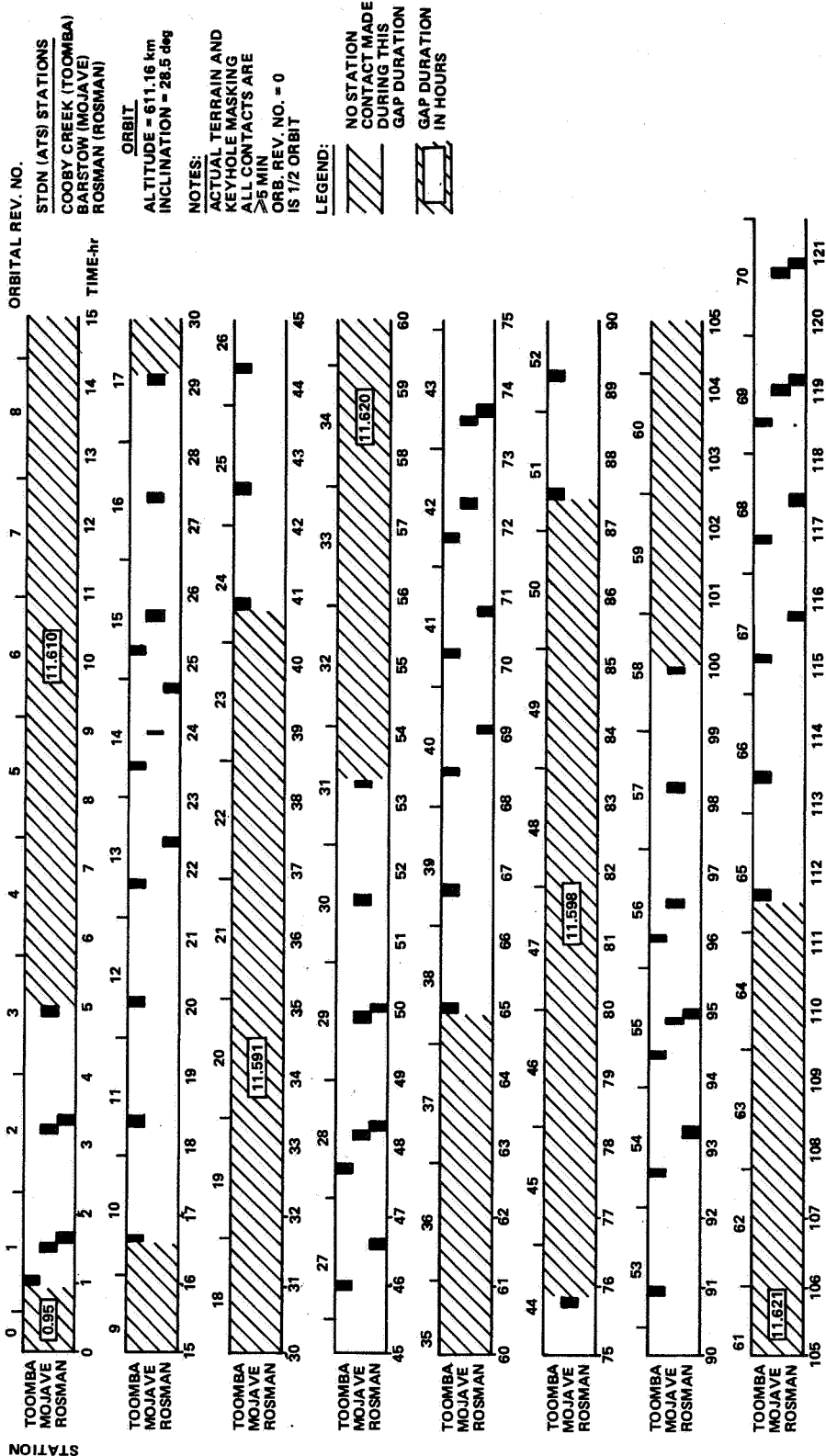


Figure III-49. Ground contact and gap statistics for STDN (ATS) Network Configuration [Altitude = 611 km (330 n. mi.), Inclination = 28.5 deg]

LST orbit, the 3 station configuration has provided 5 longest gap durations of 11.6 hours average produced by absence of additional ATS stations. The deficiencies in the ATS coverage could be corrected by adding more stations, which would require augmentation of the ATS equipment.

TABLE III-18. CONTACT SUMMARY OF TRACKING STATIONS WITH LST SPACECRAFT; STDN NETWORK CONFIGURATION A [Altitude = 611 km (330 n. mi.), Inclination = 28.5 deg]

Orb. Rev. No.	Tracking Station						Orb. Rev. No.	Tracking Station					
	CYI	ACN	CRO	GWM	HAW	GDSX		CYI	ACN	CRO	GWM	HAW	GDSX
0	X						36	X			X		
1		X	X		X	X	37	X			X		
2		X	X	X	X		38	X					
3		X	X	X	X		39	X		X			
4				X	X		40	X		X			
5				X	X		41	X		X			X
6		X		X	X		42		X	X		X	
7		X		X	X		43		X	X	X	X	
8		X		X			44		X	X	X	X	
9	X			X			45				X	X	
10	X			X			46				X	X	
11	X		X				47		X		X	X	
12	X		X				48		X		X	X	
13	X		X				49		X		X		
14	X		X		X	X	50	X			X		
15		X	X		X		51	X			X		
16		X	X	X	X		52	X		X			
17		X	X	X	X		53	X		X			
18				X	X		54	X		X			
19				X	X		55	X		X		X	X
20		X		X	X		56		X	X		X	
21		X		X			57		X	X	X	X	
22		X		X			58		X	X	X	X	
23	X			X			59				X	X	
24	X						60				X	X	
25	X		X				61		X		X	X	
26	X		X				62		X		X		
27	X		X				63		X		X		
28		X	X		X	X	64	X			X		
29		X	X		X		65	X					
30		X	X	X	X		66	X		X			
31			X	X	X		67	X		X			
32				X	X		68	X		X			X
33		X		X	X		69		X	X		X	X
34		X		X	X		70		X	X	X	X	
35		X		X									

Notes: (1) Minimum 5-minute contact time  
(2) Elimination of overlapped station with shorter contact time

To complement the STDN Configuration A in spearheading the improvement of gap distribution, three more STDN stations, namely, Merritt Island (MIL), ROS, and Santiago (AGO), were added. Coverage analysis, excluding the constraints, has been made of this nine station configuration. This analysis, within the external constraints, virtually eliminated GDSX since the stations overlapping the California site have attained greater contact times.

TABLE III-19. CONTACT SUMMARY OF TRACKING STATIONS WITH LST SPACECRAFT; STDN NETWORK CONFIGURATION B [Altitude = 611 km (330 n. mi.), Inclination = 28.5 deg]

Orb. Rev. No.	Tracking Station						Orb. Rev. No.	Tracking Station					
	CYI	ACN	ORRX	GWM	HAW	GDSX		CYI	ACN	ORRX	GWM	HAW	GDSX
0	X						36	X			X		
1		X					37	X			X		
2		X				X	38	X					
3		X		X	X		39	X		X			
4				X	X		40	X		X			
5				X	X		41	X		X			X
6		X		X	X		42		X			X	
7		X		X	X		43		X		X	X	
8		X		X			44		X		X	X	
9	X			X			45				X	X	
10	X			X			46				X	X	
11	X		X				47		X		X	X	
12	X		X				48		X		X	X	
13	X		X				49		X		X		
14	X		X		X	X	50	X			X		
15		X			X		51	X			X		
16		X		X	X		52	X		X			
17		X		X	X		53	X		X			
18				X	X		54	X		X			
19				X	X		55	X		X		X	X
20		X		X	X		56		X			X	
21		X		X			57		X		X	X	
22		X		X			58		X		X	X	
23	X			X			59				X	X	
24	X						60				X	X	
25	X		X				61		X		X	X	
26	X		X				62		X		X		
27	X		X				63		X		X		
28		X			X	X	64	X			X		
29		X			X		65	X					
30		X		X	X		66	X		X			
31				X	X		67	X		X			
32				X	X		68	X		X			X
33		X		X	X		69		X			X	X
34		X		X	X		70		X		X	X	
15		X		X									

Notes: (1) Minimum 5-minute contact time  
(2) Elimination of overlapped station with shorter contact time.

The TDRS network analysis assumes the hypothetical TDRS concept which uses two geostationary satellites to provide simultaneous tracking of the LST in its 611 km orbit. The ground stations are not considered in the TDRS satellite deployment. Orbital placement (subsattellite longitude) of two satellites on the equator is assumed to be 215 degrees east and 345 degrees east. The TDRS network was computer-simulated to determine the exact coverage it could provide for the LST mission. This simulation showed that each communications satellite tracked the LST constantly for about an hour during each revolution. Thus, a 611 km orbit gives an average TDRS network coverage of about 95 percent compared to 26 percent coverage for the STDN Configuration B. Based on the Julian date input, the time in sunlight for the LST in a 611 km/28.5 degree inclination orbit is determined to be about 1.07 hours during each revolution. At the 16th hour of the initial mission, the LST

has obtained 9.42 hours of accumulated contact time from communications satellite number 2, 9.09 hours from communications satellite number 3, and 10.48 hours of accumulated sunlight time.

TABLE III-20. CONTACT SUMMARY OF TRACKING STATIONS WITH LST SPACECRAFT; STDN (ATS) NETWORK CONFIGURATION [Altitude = 611 km (330 n. mi.), Inclination = 28.5 deg]

Orb. Rev. No.	Tracking Station			Orb. Rev. No.	Tracking Station		
	TOOMBA	MOJAVE	ROSMAN		TOOMBA	MOJAVE	ROSMAN
0				36			
1	X	X	X	37			
2		X	X	38	X		
3		X		39	X		
4				40	X		X
5				41	X		X
6				42	X	X	
7				43		X	X
8				44		X	
9				45			
10	X			46			
11	X			47			
12	X			48			
13	X		X	49			
14	X	X	X	50			
15	X	X		51	X		
16		X		52	X		
17		X		53	X		
18				54	X		X
19				55	X	X	X
20				56	X	X	
21				57		X	
22				58		X	
23				59			
24	X			60			
25	X			61			
26	X			62			
27	X		X	63			
28	X	X	X	64			
29		X	X	65	X		
30		X		66	X		
31		X		67	X		X
32				68	X		X
33				69	X	X	X
34				70		X	X
35							

Notes: (1) Minimum 5-minute contact time.  
(2) Elimination of overlapped station with shorter contact time.

The coverage statistics have emphasized that STDN and STDN (ATS) are hardly the primary competitive network candidates for support of the LST mission. The STDN Configuration B, which includes Orroral Valley instead of to-be-phased-out Carnarvon, may be adequate for the LST coverage requirements. The TDRS concept, when developed and deployed, should be designed to track a spacecraft such as the LST. Consideration of the STDN (ATS) configuration should be terminated in view of the fact that ATS-F and -G missions will, in all likelihood, preclude use of the ATS stations to support the LST mission.

## F. Support Operations

1. Facilities/Equipment Required. The following ground facilities and equipment will be required for the LST mission:

1. Processing Area (10K Clean Room) for OTA, SIP/SSM.
2. Optical Alignment Area.
3. Functional Checkout Area.
4. Shuttle Simulator.
5. Interface Checkout Area.
6. Interplant Transportation Equipment/Transporters.
7. Leak Testing/Test Area.
8. Work Bench Area.
9. Experiment Laboratory.
10. Storage Area.
11. Special Handling (Slings, Spread Bars, etc.).

The special ground support equipment will be received and inspected for damage, and the data package will be reviewed. It will then be transported to LST receiving, inspection, and processing area and will be installed.

Ground electrical support equipment (GESE) to be used for pre-delivery systems testing will be the same equipment to be used for checkout at the launch facility. In general, it will be standard racks of equipment typically used for payload checkout. Most of this equipment could be assembled from equipment previously used for HEAO, Skylab, etc., if made available. Adapters and interface units to be provided will assure that electrical interfaces are identical to those of the standardized, in-space electrical support equipment (IESE) to be located at the payload work station aboard the Shuttle Orbiter [III-3].

The ground support equipment will then go through the special checkout and acceptance testing as shown in the prelaunch/ground operation timelines (Figure III-50). Special calibration and self-checkout will be conducted.

Upon receipt of OTA/SI and SSM, the SSM docking interfaces will first be verified using the docking simulator supplied for physical and electrical interfaces. The mating interfaces of the SSM and OTA/SI would then be verified mechanically and electrically using the certified interface simulators. Upon satisfactory verification, the two elements would then be assembled into an integrated LST configuration. The OTA/SI electrical connections to the SSM are then completed.

The integrated LST will be connected to the verified electrical support equipment for checkout and functional testing of the entire integrated system. Alignment, calibration test of the telescope and instruments will be conducted. Then, the LST will be serviced and the integrated systems testing will be conducted.

The antennae and telescope covers are deployed and the required verification testing will be conducted. Then the panels, antennae, and telescope covers will be retracted and the LST transported to the Shuttle routing simulator for mating checkout and interface verification tests and mating. After Shuttle simulator mating tests have been completed the LST will be transported back to the test and processing area for final checkout and adjustment.

Then the data management, electrical power, and control interfaces will be verified between the OTA and SSM, and the coordinated functional verification of the OTA/SI and SSM will be conducted. The weight balance and prelaunch checkouts and verification will then be performed.

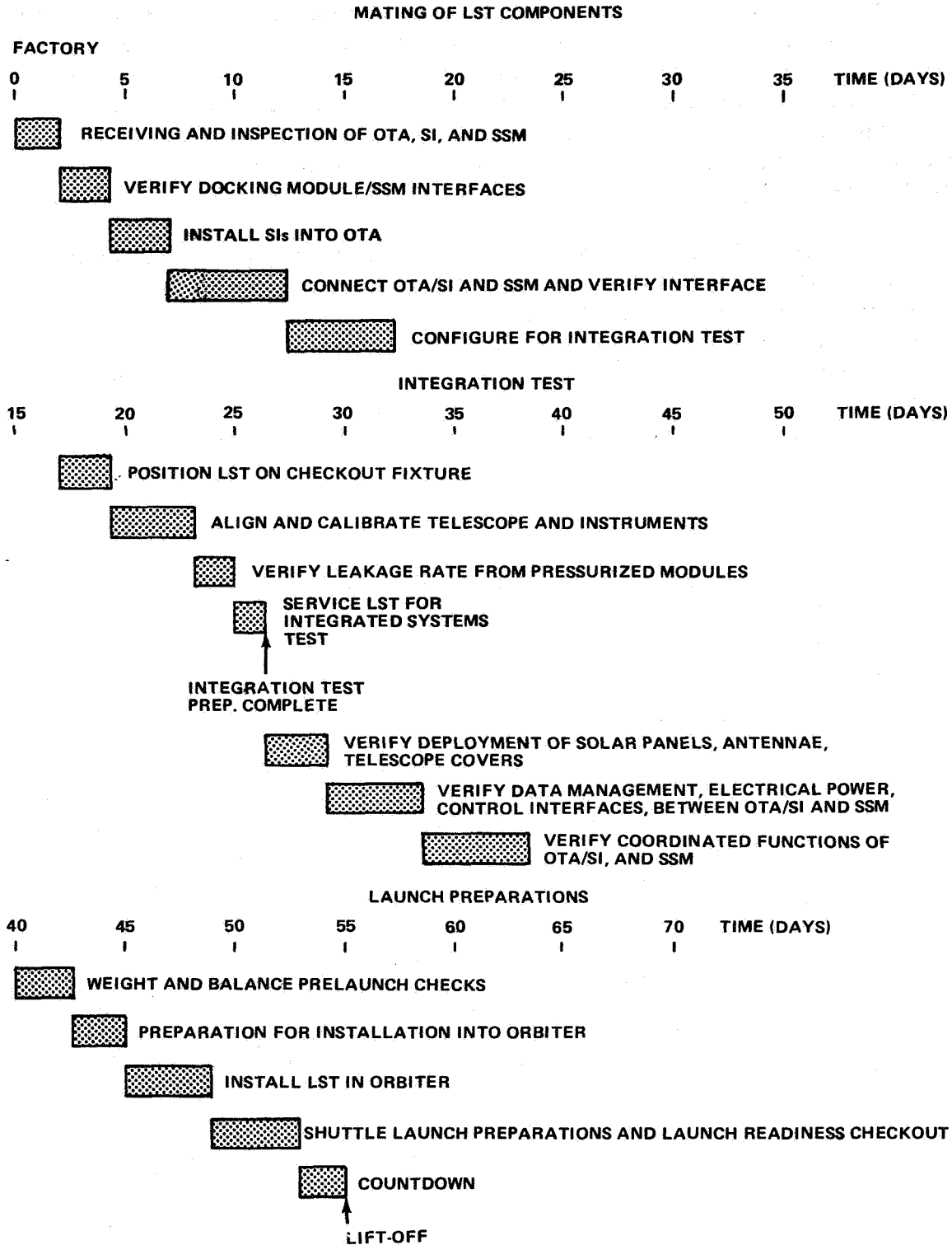


Figure III-50. LST prelaunch/ground operations phase timeline.



The LST will be transported to payload installation area for installation in the Orbiter cargo bay. The LST will be installed in the Shuttle cargo bay while the status of system and subsystems is monitored. Environmental control will be maintained from the time the LST leaves the processing and test area until it is installed in the cargo bay. After the cargo bay/LST interfaces are verified, the LST will be ready for the prelaunch checkouts required by its systems.

Once the LST has been assembled and checked out at the launch facility, it will proceed to a staging area for installation into the Shuttle Orbiter. From this point on, LST operations and checkouts will be made primarily with the IESE and the need for GESE minimized or eliminated. Operational support will be provided by the IESE. There will be no need for a control center complex at the Cape, unless desired, because the Orbiter controls operations and has "quick look" capabilities during launch and initial orbits. Normal ground control and tracking will begin when the payload is released from the Shuttle.

Carry-on cables to the IESE provide power and controls needed for prelaunch operation and checkout at the launch site. There will be provisions for RF data and command links. When the Orbiter is checked and made operational, it will provide power and will assume control of the payload until in-space checkout is completed.

The LST will be powered down at lift-off. The EPS and distribution buses will be energized and the data management equipment will be on to obtain sensor information. The OTA thermal system will be energized but will probably not draw power as long as the payload is in the Shuttle bay. The LST subsystem will be incrementally energized as in-space checkout proceeds. Such operations will most likely occur after the LST is erected out of the bay.

A conservative 2 day period will be allowed for operation and checkout of subsystems, assuming that 2 days may be needed for outgassing before high voltage supplies are turned on to operate scientific equipment. The ACS can be warmed up and operated but gyros and CMGs will have to be caged until the LST is free of the Orbiter.

When the Orbiter completes its navigation and control checks, payload checkout will commence. The Orbiter assumes an orientation to allow the LST to be erected from the bay without facing the optics sunward. As soon as it is erected and contamination protection is removed, the sunshade will be extended.

The solar array may be deployed soon after payload erection, offering the unprecedented advantage of being able to test retraction, orientation, and array performance before it assumes its critical operational function. After testing, the array may be used to supply power for subsequent operations. Only coarse attitude control is needed for such operations and this can be obtained by keeping the Shuttle properly oriented.

Since the arrays may be deployed, they can be used to supplement the energy needed for orbital checkout and maintenance operation.

It is also noted that the LST battery requirements are not dependent on launch phase requirements since the Orbiter furnishes the necessary power. In fact, it allows for trickle charge on the batteries, if needed, during launch.

The electrical system integrity and the operational capabilities of all subsystems can easily be verified within the 2 days assumed, allowing ample rest periods and a limited crew complement. Except for the ACS, the functional performance of the SSM subsystems will be verified before test and preliminary calibration of SIP instruments start. In addition to equipment operability, some of the AGS sensors can be verified during checkout. It is also possible to coarsely compare open-loop control signals with Shuttle control system information but final pointing and stabilization performance verification can occur only after the LST is released. For this reason and to permit better readiness verification of OTA and SIP equipment, it is desirable to allow a period of several orbits for the Shuttle to maintain station-keeping with the LST after release. This would permit vehicle recovery in the event that defects in the highly sensitive equipment were observed.

Subsequent to verification that outgassing and subsystem performance is adequate, scientific instrument tests and preliminary calibrations are made, as discussed in Section D of this chapter.

The postflight ground operations timelines (Table III-21) was prepared for the LST to be returned to the ground for maintenance. The same type of maintenance would be required for inflight maintenance with the exception of disassembling the LST.

2. Titan Launch Facilities. There are five basic areas of ETR that can be used for receiving and preparation of the LST for launch. These areas will require some modification to meet the LST particular requirements to be launched on a Titan III vehicle. Therefore, when the Space Shuttle retrieves the LST, it may be less costly to use the Titan facilities for the ground operations of the LST. If not, then like accommodations must be made in the KSC industrial area. The following is a list of areas for consideration:

1. Observatory operation center (OOC) (Class 10 000):

- a. Observatory control center.
- b. Experiment Laboratory
- c. Work bench area.
- d. Receiving area.
- e. Flight stores.
- f. Large equipment storage.
- g. High bay area.

2. Vertical Integration Building (VIB) (Class 10 000).

- a. Launch control center.
- b. Receiving, inspection, leak testing at test area.
- c. Storage area.
- d. Mating equipment and area.
- e. Work access stands.
- f. Crane.
- g. Air-conditioning.
- h. Special GSE.

TABLE III-21. POSTFLIGHT GROUND OPERATIONS TIMELINE

Event Description	Event Time					
	Start		Stop		Duration	
	hrs	min	hrs	min	hrs	min
Orbiter landing, taxi, turn onto travelway and stop	00	00	00	00	00	00
Install safing pins in ejection seats	00	03	03	03	03	00
Install down-lock pins in landing gear.	03	03	04	04	04	03
Power down all radios except ground communications	03	03	05	05	02	04
Power down all electronics (Tacan, radar, electronic compass, navigation, and guidance)	05	05	20	20	15	05
Power down de-icing heaters	05	05	07	07	03	06
Power down electric boost pumps and servos	07	07	10	10	03	07
Run performance checks on air-breathing engines	07	07	10	10	03	08
Shut down air-breathing engines	10	10	11	11	01	09
Hook up tow tractor	05	05	10	10	05	10
Deploy ground crew to wing tips and tail	10	10	12	12	02	11
Tow Orbiter to fuel servicing area	12	12	20	20	08	12
Hook up air-conditioning cart	20	20	22	22	02	13
Hook up ground power cart	27	27	32	32	05	14
Transfer power from internal to external	32	32	35	35	03	15
Power down onboard power source (fuel cells)	35	35	38	38	03	16
Power down propellant conditioners	38	38	40	40	02	17
Move personnel stairs to Orbiter	40	40	45	45	05	18
Flight crew egress/ground crew ingress	45	45	60	60	15	19
Remove flight performance recorders	60	60	10	10	10	20
Analyze flight data	10	10	5	00	50	21
Cool vehicle	60	60	4	00	00	22
Move access stands to vehicle	00	00	3	10	10	23
Open access doors	10	10	3	15	05	24
Move propellant service cart to vehicle	15	15	3	20	05	25
Connect propellant umbilicals	20	20	3	50	30	26
Leak check propellant umbilicals	50	50	4	30	40	27
Drain residual H <sub>2</sub> , O <sub>2</sub> , and JP <sub>4</sub>	30	30	5	15	45	28
Purge O <sub>2</sub> tanks and accumulators to 20 percent GO <sub>2</sub> (max)	15	15	8	15	00	29
Purge H <sub>2</sub> tanks and accumulators to 4 percent GH <sub>2</sub> (max)	15	15	8	15	00	30
Purge fuel cells (H <sub>2</sub> and O <sub>2</sub> ) same as above	15	15	8	15	00	31
Disconnect propellant umbilicals	8	15				32

FOLD-OUT #1

Fold-out #2

33	05	35	8	35	8	30	8
34	05	40	8	40	8	35	8
35	05	45	8	45	8	40	8
36	05	45	8	45	8	40	8
37	10	55	8	55	8	45	8
38	05	00	9	00	9	55	8
39	20	20	9	20	9	00	9
40	10	30	9	30	9	20	9
41	00	30	1	30	10	30	9
42	15	45		45	10	30	10
43	10	55		55	10	45	10
44	05	00		00	11	55	10
45	10	10		10	11	00	11
46	20	30		30	11	10	11
47	00	30	1	30	12	30	11
48	15	45		45	12	30	12
49	45	30		30	13	45	12
50	05	35		35	13	30	13
51	05	40		40	13	35	13
52	20	00		00	14	40	13
53	30	30		30	14	00	14
54	10	40		40	14	30	14
55	05	45		45	14	40	14
56	15	00		00	15	45	14
57	15	15		15	15	00	15
58	15	30		30	15	15	15
59	05	35		35	15	30	15
60	00	35	3	35	18	35	15
61	00	35	1	35	19	35	18
62	00	35	1	35	20	35	19
63	00	35	8	35	28	35	20
64	25	00	39	00	68	35	28
65	00	00	8	00	76	00	68
66	00	00	4	00	80	00	76
67	00	00	8	00	88	00	80
68	00	00	4	00	92	00	88
69	15	15		15	92	00	92
70	15	30		30	92	15	92
71	30	00		00	93	30	92
72	00	00	15	00	108	00	93
73	00	00	165	00	273	00	108
74	00	00	8	00	281	00	273
75	00	00	1	00	282	00	281
76	00	00	2	00	284	00	282

Fold-out #2

33	05	35	8	35	8	30	8
34	05	40	8	40	8	35	8
35	05	45	8	45	8	40	8
36	05	45	8	45	8	40	8
37	10	55	8	55	8	45	8
38	05	00	9	00	9	55	8
39	20	20	9	20	9	00	9
40	10	30	9	30	9	20	9
41	00	30	1	30	10	30	9
42	15	45		45	10	30	10
43	10	55		55	10	45	10
44	05	00		00	11	55	10
45	10	10		10	11	00	11
46	20	30		30	11	10	11
47	00	30	1	30	12	30	11
48	15	45		45	12	30	12
49	45	30		30	13	45	12
50	05	35		35	13	30	13
51	05	40		40	13	35	13
52	20	00		00	14	40	13
53	30	30		30	14	00	14
54	10	40		40	14	30	14
55	05	45		45	14	40	14
56	15	00		00	15	45	14
57	15	15		15	15	00	15
58	15	30		30	15	15	15
59	05	35		35	15	30	15
60	00	35	3	35	18	35	15
61	00	35	1	35	19	35	18
62	00	35	1	35	20	35	19
63	00	35	8	35	28	35	20
64	25	00	39	00	68	35	28
65	00	00	8	00	76	00	68
66	00	00	4	00	80	00	76
67	00	00	8	00	88	00	80
68	00	00	4	00	92	00	88
69	15	15		15	92	00	92
70	15	30		30	92	15	92
71	30	00		00	93	30	92
72	00	00	15	00	108	00	93
73	00	00	165	00	273	00	108
74	00	00	8	00	281	00	273
75	00	00	1	00	282	00	281
76	00	00	2	00	284	00	282



3. Launch Complex 41 (LC-41).
  - a. Crane.
  - b. Access.
  - c. Work space.
  - d. Power.
  - e. Communications.
  - f. Fuel.
  - g. Special GSE.
4. Ordnance.
  - a. Environmental control storage.
  - b. Appropriate handling equipment.
  - c. Checkout equipment.
5. Fuel Storage Area.
  - a. Fuel and other pressurants.

3. Shuttle Maintenance/Revisit. When maintenance is required, a manned Shuttle flight will rendezvous with the LST to service and repair the LST subsystems. (See Maintainability Analysis in Chapter VII, Volume V, for further details.) Periodic checkout and ground control monitoring of the LST will identify failures and degraded components and will provide a basis for the maintenance plan and spares inventory for the flight. Maintenance will be performed with the LST docked to the airlock module (AM) extended from the payload bay of the Shuttle Orbiter. The maintenance crew will be added to the two-man Shuttle crew. Maintenance flight, as required, will be repeated for the remainder of the life of the LST.

The timeline of a Shuttle maintenance flight is shown in Figure III-51. After being launched into an initial circular orbit, the Shuttle Orbiter transfers into the operating orbit of the LST. Prior to transfer, normal viewing operations of the LST are terminated and the OTA and SIP are secured.



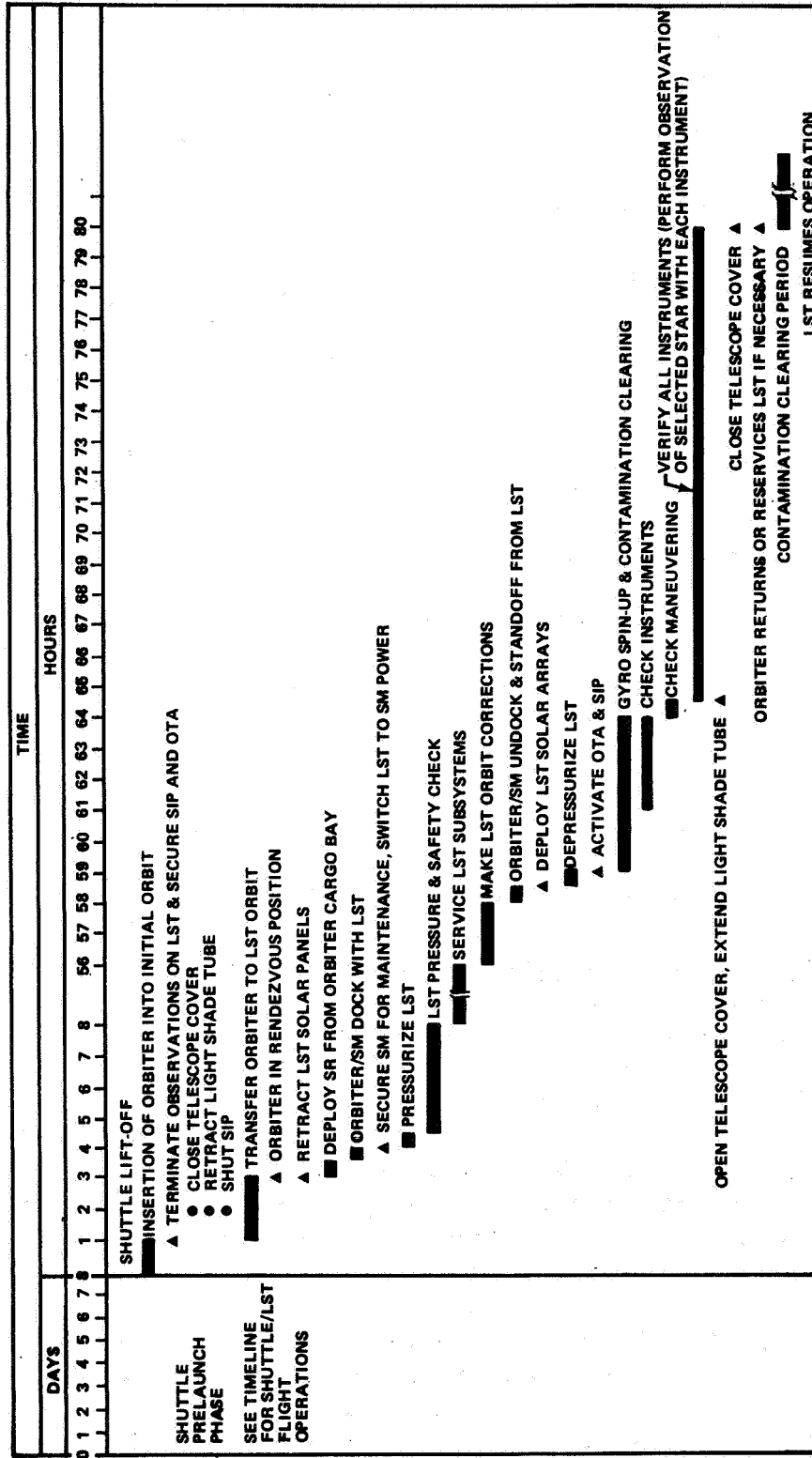


Figure III-51. LST revisit/on-orbit maintenance.

The AM extended from the Orbiter cargo bay and the LST is docked with the AM. After docking, the LST subsystems are switched to the AM power supply, the LST environmental control/life support system (EC/LSS) is activated, and the LST is pressurized. After the functions of the FC/LSS subsystem have been checked to insure the safety of the maintenance crew, the crewmen will enter the LST and begin the maintenance activities. Maintenance operation will include the replacing of failed, degraded or marginal units, and other servicing necessary for remotely controlled operations. After the maintenance operations have been completed, the maintenance crew will enter the Orbiter/AM and the Orbiter engines will be used to correct any degradation in the LST orbit which may have occurred. The Orbiter/AM will undock and stand off from the LST; the LST will be depressurized and the LST subsystems will be activated prior to undocking from the Shuttle. After the LST subsystems have reached the normal operating state, a series of tests will be performed to verify the functions of the instruments and the LST maneuvering system.

A period of contamination clearing may be required for open telescope tests. Finally, a series of observations of selected celestial objects using each of the instruments will be performed to verify the coordinated functioning of all LST subsystems. If any of these tests indicate that further maintenance operations are desirable, the Orbiter/AM will redock with the LST and the maintenance will be performed. If not, the Orbiter will return to earth, and the LST will resume normal operations.

## References

- III-1. Martin Marietta: Performance and Characteristics Basic Data Book Titan III Vehicle Family. Martin Company Report M-70-7, April 1972.
- III-2. Martin Marietta: Titan IID/OAS-HEAO Accuracy Analysis of 140- by 250- Nautical Mile Orbit. S71-41545-2 L.V. 104-71, February 17, 1971.
- III-3. KSC Large Space Telescope Launch Operations Plan, Phase A TR 1197, September 29, 1972.

## CHAPTER IV. LST CONFIGURATION AND SYSTEM DESIGN



# TABLE OF CONTENTS

	Page
A. Reference LST Configuration . . . . .	IV-1
1. Major Elements/Systems . . . . .	IV-1
2. Master Equipment List . . . . .	IV-5
3. LST Mass Characteristics . . . . .	IV-5
4. Configuration and Systems Description . . . . .	IV-11
a. LST Reference Configuration . . . . .	IV-11
b. Optical Telescope Assembly (OTA) . . . . .	IV-20
c. Scientific Instrument Package (SIP) . . . . .	IV-28
d. Support Systems Module (SSM) . . . . .	IV-34
5. Commonality . . . . .	IV-62
6. Maintenance Spares/Equipment . . . . .	IV-62
7. Contamination Control . . . . .	IV-64
8. Systems Reliability Summary . . . . .	IV-68
9. Man Rating Impacts . . . . .	IV-73
10. Error Budgets . . . . .	IV-76
a. Effect of WFE and Image Stabilization Errors on Image Size . . . . .	IV-76
b. Focus Error in WFE Budget . . . . .	IV-81
c. Alignment Error in WFE Budget . . . . .	IV-82
11. Focus and Alignment Tolerances . . . . .	IV-83
a. Effects of Secondary Mirror Repositioning . . . . .	IV-84
b. Instrument Replacement Tolerances . . . . .	IV-90
c. Conclusions . . . . .	IV-97
12. Overall Performance Trades . . . . .	IV-98
a. Introduction . . . . .	IV-98
b. Effect on Field Cameras of Pointing Stability Degradation . . . . .	IV-99
c. Spectrograph Exposure Time for Stellar Sources as a Function of Slit Width . . . . .	IV-106

## TABLE OF CONTENTS (Concluded)

	Page
d. Effect on Spectrographs of Pointing Error and Instability .....	IV-108
e. Conclusions .....	IV-118
B. Maintenance Mode Analysis and Trades .....	IV-118
1. Introduction .....	IV-118
2. Maintenance Trade Study Approach .....	IV-119
3. Maintenance Mode Study Results .....	IV-120
4. Flight Sharing .....	IV-120
a. Number of Flights Required .....	IV-125
b. Orbital Operations During Flight Sharing .....	IV-127
5. Scheduled Maintenance Cost Comparison .....	IV-129
6. Recommended Design Reference Maintenance Method...	IV-132

## LIST OF ILLUSTRATIONS

Figure	Title	Page
IV-1.	LST systems tree . . . . .	IV-2
IV-2.	Basic LST elements . . . . .	IV-3
IV-3.	SSM systems layout . . . . .	IV-6
IV-4.	LST mass characteristics . . . . .	IV-12
IV-5.	LST reference design longitudinal cross section . . . . .	IV-13
IV-6.	LST assembly operational configuration . . . . .	IV-14
IV-7.	LST launch configuration in payload bay . . . . .	IV-18
IV-8.	LST launch configuration deployed position . . . . .	IV-19
IV-9.	Optical telescope assembly . . . . .	IV-21
IV-10.	SIP configuration . . . . .	IV-29
IV-11.	Scientific instrument package functional block diagram . . . . .	IV-31
IV-12.	Support systems module reference design . . . . .	IV-35
IV-13.	LST assembly stowed configuration . . . . .	IV-37
IV-14.	LST Titan launch configuration . . . . .	IV-38
IV-15.	SSM reference design longitudinal cross section . . . . .	IV-39
IV-16.	LST thermal control features . . . . .	IV-41
IV-17.	SSM thermal control concept . . . . .	IV-45
IV-18.	Reference electrical system . . . . .	IV-47
IV-19.	LST communications and data handling system . . . . .	IV-54



## LIST OF ILLUSTRATIONS (Continued)

Figure	Title	Page
IV-20.	ACS block diagram and key interfaces for LST . . . . .	IV-57
IV-21.	LST star tracker configuration . . . . .	IV-59
IV-22.	System schematic of the LST reaction control system . . . . .	IV-61
IV-23.	LST potential commonality with other programs . . . . .	IV-63
IV-24.	Class 10 000/100 000 LST contamination control system layout . . . . .	IV-69
IV-25.	Contamination control system for class 10 000/100 000 LST . . . . .	IV-70
IV-26.	Relative fire hazard as a function of percentage of O <sub>2</sub> in the atmosphere . . . . .	IV-77
IV-27.	Percentage of O <sub>2</sub> required in habitable atmosphere as a function of total pressure . . . . .	IV-78
IV-28.	LST error budgets . . . . .	IV-79
IV-29.	LST encircled energy curve . . . . .	IV-80
IV-30.	Wavefront error caused by detector axial misposition at f/12 focal plane . . . . .	IV-85
IV-31.	Change in mirror separation distance to move image position . . . . .	IV-86
IV-32.	Movement of f/12 image as a function of change in mirror separation distance . . . . .	IV-88
IV-33.	Image movement due to secondary mirror decenter . . . . .	IV-89
IV-34.	WFE at f/12 focal plane due to secondary mirror decenter . . . . .	IV-91

## LIST OF ILLUSTRATIONS (Concluded)

Figure	Title	Page
IV-35.	Guidance error as a function of guide field defocus . . . . .	IV-92
IV-36.	Light path typical SLP instruments . . . . .	IV-93
IV-37.	Instrument misposition WFE at the f/12 focal plane and RSS WFE as a function of misposition distance in focus for $\lambda = 632.8 \text{ nm}$ . . . . .	IV-97
IV-38.	WFE caused by detector axial misposition at f/96 focal plane . . . . .	IV-98
IV-39.	Fit of the Gaussian approximation to the point spread function computed by Itek . . . . .	IV-101
IV-40.	Camera resolution as a function of pointing instability . .	IV-104
IV-41.	Strehl ratio as a function of pointing instability . . . . .	IV-105
IV-42.	Camera exposure time as a function of pointing instability for stellar sources . . . . .	IV-107
IV-43.	Spectrograph exposure time as a function of slit width . .	IV-109
IV-44.	Spectrograph exposure time as a function of pointing error . . . . .	IV-111
IV-45.	Spectrograph exposure time as a function of pointing instability . . . . .	IV-113
IV-46.	Spectrograph slit width as a function of pointing error for constant exposure time . . . . .	IV-115
IV-47.	Fractional increase in spectrograph slit width as a function of pointing instability for constant exposure time . . . . .	IV-117
IV-48.	Operational timeline for LST shared mission to synchronous orbit . . . . .	IV-128

# LIST OF TABLES

Table	Title	Page
IV-1.	Major LST Spacecraft Elements . . . . .	IV-4
IV-2.	LST Master Equipment List . . . . .	IV-7
IV-3.	LST Mass Moments of Inertia and Center of Gravity Locations . . . . .	IV-9
IV-4.	SSM Thermal Control Hardware Description . . . . .	IV-43
IV-5.	"Total" Maintenance Mission Equipment Load . . . . .	IV-65
IV-6.	"Typical" Unscheduled On-Orbit Maintenance Mission Equipment Load . . . . .	IV-66
IV-7.	Support Equipment Required for On-Orbit Pressurized Maintenance . . . . .	IV-67
IV-8.	LST Contamination Control System Mass and Power Breakdown: Onboard Requirements for Class 10 000/100 000 LST . . . . .	IV-71
IV-9.	LST Contamination Control System Mass and Power Breakdown: Support Requirements for Class 10 000/100 000 LST . . . . .	IV-72
IV-10.	SSM/OTA Reliability . . . . .	IV-73
IV-11.	Comparison of LST with Apollo and Skylab in Man-Rating and/or Man-Involvement Impacts . . . . .	IV-74
IV-12.	Focus Maintenance Budget . . . . .	IV-81
IV-13.	Secondary Mirror Alignment Budget . . . . .	IV-83
IV-14.	LST Focus Tolerances . . . . .	IV-94
IV-15.	SIP Instrument Alignment Tolerances . . . . .	IV-96

## LIST OF TABLES (Concluded)

Table	Title	Page
IV-16.	Maintenance Mode Comparisons . . . . .	IV-121
IV-17.	Flights Required for Various Scheduled Maintenance Methods . . . . .	IV-126
IV-18.	LST Scheduled Maintenance Cost Comparison . . . . .	IV-130
IV-19.	LST Maintenance Cost Impact Due to Additional Shuttle Flights . . . . .	IV-131

# CHAPTER IV. LST CONFIGURATION AND SYSTEM DESIGN

## A. Reference LST Configuration

1. Major Elements/Systems. The LST systems tree is shown in Figure IV-1. During the Phase A study, the LST was subdivided into three basic elements, as shown in Figure IV-2 and Table IV-1. The division between these elements was somewhat arbitrary and must be investigated further in the next phase of study. In general, the most difficult interface area at which to determine a satisfactory hardware division is between the optical telescope assembly (OTA) and scientific instrument package (SIP), since these two elements are more closely coupled than any of the other combinations. The SIP region is a hybrid one, containing telescope-peculiar instruments (figure sensor, focus sensor, fine guidance assembly, etc.) and scientific instruments; hence, the term Scientific Instrument Package is somewhat misleading. The general requirements for the SIP structure are very stringent and very similar to those for the OTA structure (very accurate positional stability, very small allowable thermal gradients, etc.). The solution to the structural design for the OTA should be in large part adaptable to the SIP structural design, resulting in cost and schedule advantages. This is particularly true if some of the more exotic structural materials and techniques are utilized, requiring some development effort in the LST program. Cost and schedule savings can also accrue by having one mathematical model and one structural/thermal analysis for the OTA/SIP structure. For the foregoing reasons, it was decided to include the SIP primary structure as part of the OTA in the Phase A study. The fact that the instruments must be capable of on-orbit removal and replacement without alignment degradation tends to support such a decision — the instruments and their structure cannot be a monolithic structure in any event. Since the SIP structure is removable from the OTA primary ring, it could be shipped to other locations for special tests or integration if schedules made this necessary.

Two of the key aspects of the decision on the interface divisions must be (1) the completeness of function of an end item and (2) its integrality into the next higher level with maximum efficiency. It seemed logical in the Phase A study to have a complete telescope as one of the second-level end items below the LST, rather than having several optical pieces and structural pieces which could not be mated and become a telescope until the entire LST was together. The buildup and integration of the OTA and SIP can proceed in parallel, and largely independently of each other, until a high level of buildup and testing has been achieved.

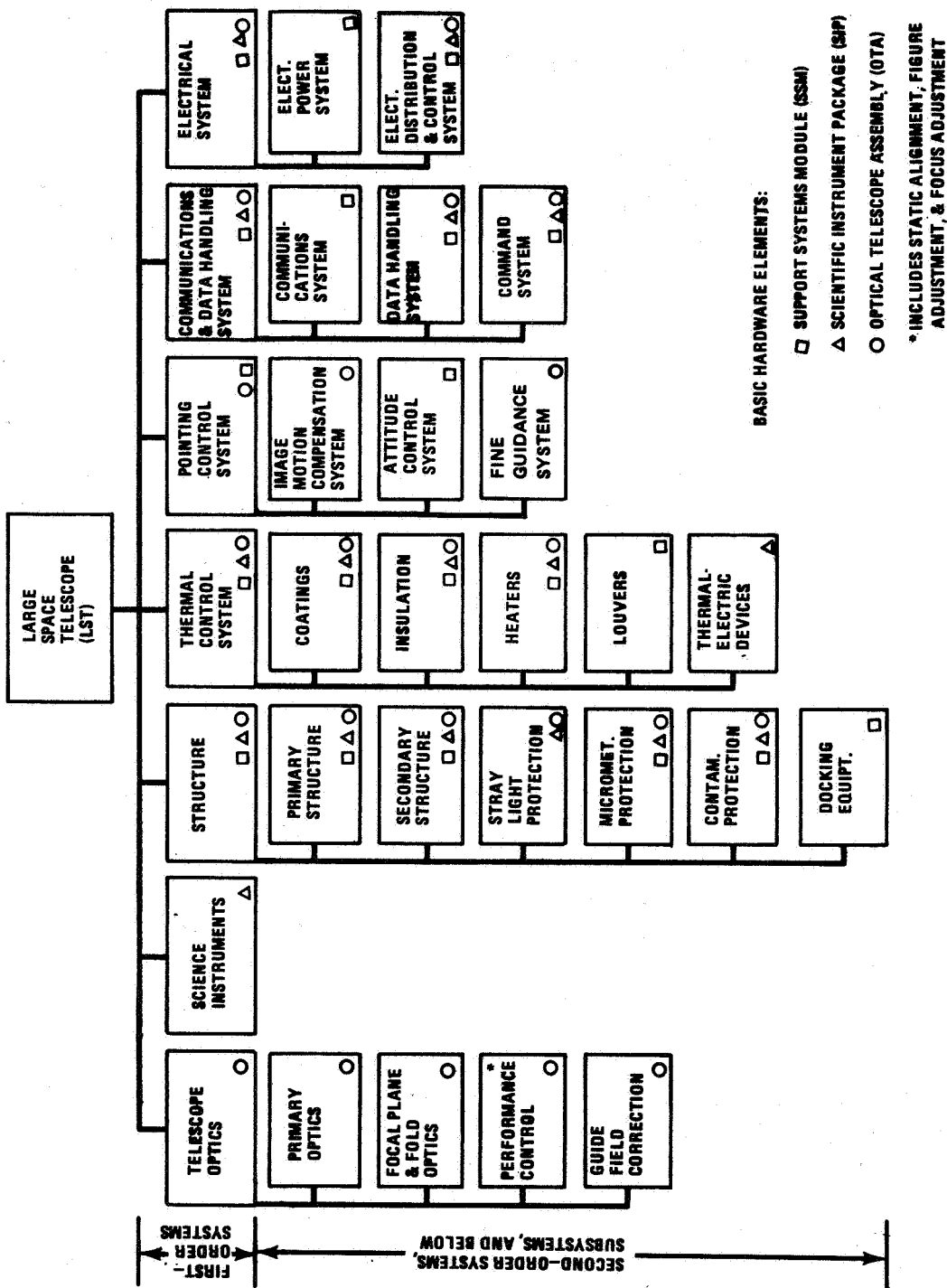
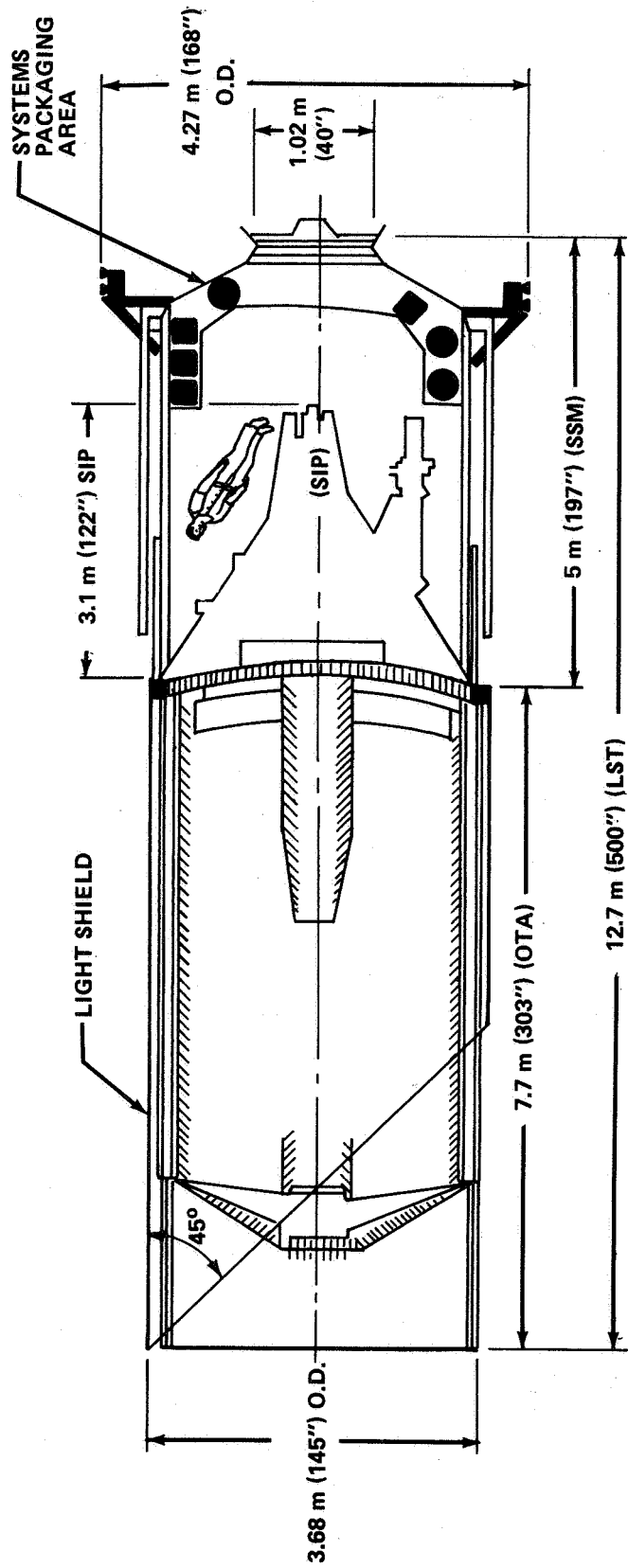


Figure IV-1. LST systems tree.



OTA: OPTICAL TELESCOPE ASSY.  
 SIP: SCIENTIFIC INSTRUMENT PKG.  
 SSM: SUPPORT SYSTEMS MODULE

Figure IV-2. Basic LST elements.

TABLE IV-1. MAJOR LST SPACECRAFT ELEMENTS

Optical Telescope Assembly	Scientific Instrument Package	Support Systems Module
<p>Telescope, Primary Ring, and Structure Forward of Primary Ring</p> <p>Light Shield</p> <p>Meteoroid Shield on Telescope (to 1.5 m or 59 in. behind primary ring)</p> <p>All the Primary Structure Supporting the Scientific Instruments</p> <p>All Pickoff Mirrors Which Produce The Initial Folds at the f/12 Plane</p> <p>Fine Guidance Equipment</p> <p>Telescope-Peculiar Sensors</p> <p>Image Motion Compensation</p> <p>Thermal Control for OTA Equipment and Structure</p>	<p>All Science Instruments</p> <p>Secondary Structure Supporting Each Instrument on Truss</p> <p>Slit Assemblies and Their Mechanisms</p> <p>Collimating Mirror Assemblies</p> <p>Filter Wheels and Shutters</p> <p>Secondary Fold Mirror and INCA for f/96 Plane</p> <p>Thermal Control for Science Instruments and Secondary Structure</p>	<p>All Primary Load-Carrying Structure Aft of Primary Ring (the most forward 1.5 m, or 59 in. must satisfy OTA requirements)</p> <p>Attitude Control Equipment</p> <p>Electrical Equipment</p> <p>Communication and Data Handling Equipment</p> <p>Thermal Control for Support Systems and Partial Control for SIP</p> <p>Contamination Control</p> <p>LST/Shuttle Interface</p>



The decision of how to divide the responsibilities for the focal plane and fold optics is not as straightforward as the structural decision. Since several key instrument design parameters are closely related to the fold optics (selection of coatings, astigmatic correction, field of view, and focal distance), it is logical to assume that the fold optics are extensions of the instruments. However, since the fold mirrors are upstream of the f/12 focal plane, it is also logical to assume that they are part of the telescope. Their curvature can be tailored to provide astigmatic correction for uncorrected telescope wavefront errors at that point. Their fields of view and mounting locations must be selected to best fit the overall instrument complement arrangement. The mounting to the structure, the thermal control, the maintainability/replacement, and the stray light control of the fold optics are closely coupled to the corresponding aspects of the SIP structure and to the overall instrument complement arrangement.

In the Phase A study, it was decided that the fold optics should be included with the OTA. This decision should be reevaluated during later phases of the study.

2. Master Equipment List. The LST master equipment list (Table IV-2) provides a summary of the total equipment on the LST reference design. The first column is used to key the equipment list to the layout drawing (Figure IV-3). The redundancy at the "component" level provided in the design can be determined by subtracting the "number of units required" from the "number of units provided."

3. LST Mass Characteristics. Table IV-3 is a summary of the LST mass moments of inertia and center-of-gravity locations.<sup>1</sup> Three configurations of the LST are considered:

1. Solar panels folded and light shield retracted.
2. Solar panels folded, light shield retracted, and orbital adjust stage (OAS) attached, (Titan configuration).
3. Solar panels deployed and light shield extended.

---

1. The moments of inertia used in Chapter VI of Volume V in the analysis of certain components of the attitude control system (ACS) were the values current at the time that work was done and are somewhat different from these values which reflect the latest updated estimates of mass characteristics. This in no way affects the validity of the control work because the values are well within the normal tolerances to which the ACS is designed.

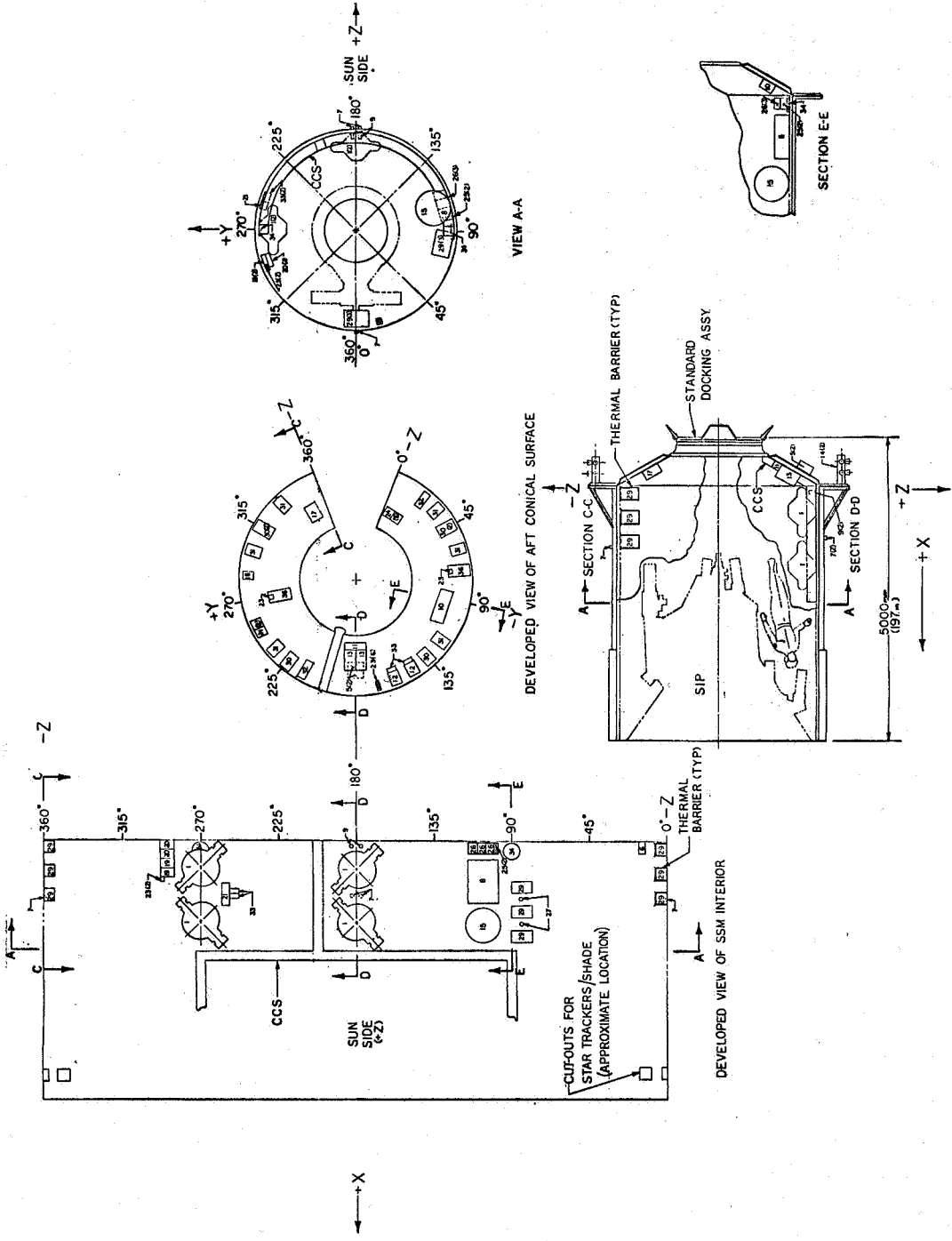


Figure IV-3. SSM systems layout.

TABLE IV-2. LST MASTER EQUIPMENT LIST

Ident. No.	System Component	No. of Units Required	No. of Units Provided	Unit Power (W)	Total Power (W)	Unit Heat Dissipated (W)	Size			Unit Mass (kg)	Total Mass (kg)	Allowable Operating Temperature (°C)
							mm	in.	lb			
1	CMCs and Digital Electronics Assembly	3	4	17 (pt.)	51	17	40.1X30.5X23	80.9	178	323.6	712	0 to 57
2	Magnetic Torque Assembly	6	6	22.5 (slew)	135	15	51DX1905	23.5	52	141	310	-18 to 54
3	Fixed Star Tracker (FST) and Reference Gyro Assembly, etc.	2	2	5	10	0	114X114X406	5.5	12	16.4	36	-35 to 70
4	3-Axis Magnetometer	1	1	36	36	36	44X173X152	10.45	23	10.5	23	0 to 57
5	Magnetic Torque Electronics	1	1	2	2	2	17X19X75.4	10.45	23	10.45	23	-35 to 70
6	Magnetic Torque Electronics	1	1	2	2	2	17X19X75.4	10.45	23	10.45	23	-35 to 70
7	Coarse Sun Sensors, B	1	1	0	0	0	48DX41	0.1	0.2	0.4	0.8	-84 to 51
8	Lines, Valves, and Regulator Set	1	1	0	0	0	711X508X178	96.7	13.7	96.7	13.7	-55 to 71
11	Digital Processor Assembly	1	1	16	16	16	107X130X366	6.2	13.7	6.2	13.7	-18 to 60
12	Transfer Assembly	1	1	26.5	26.5	26.5	152X203X246	6.2	13.7	6.2	13.7	-55 to 71
13	RCS Electronics	1	1	2	2	2	229X356X178	4.7	10.3	9.4	20.6	-55 to 71
14	RCS Thruster Module	2	2	4	8	4	274X127X160	2	4.5	8.2	18	-55 to 71
15	RCS Tank	1	1	1	1	1	274X127X160	32.4	71.3	32.4	71.3	-18 to 54
15	GN <sub>2</sub>	1	1	1	1	1	Sphere: 576D	32.4	71.3	32.4	71.3	-18 to 54
29	Batteries	3	6	6	18	21	406X279X178	22.4	49.3	134.4	296	+5 to 10
30	Charger	3	3	0.33	1	2	305X203X152	6.8	15	40.9	90	-18 to 52
31	Regulators	3	3	6	18	23	279X203X127	3.5	7.8	21.4	47	-18 to 52
32	Solar Power Distribution Units	2	2	5	10	10	325X165X152	5.5	12	10.9	24	-18 to 52
33	Solar Panel Mechanisms	4	8	2.5	10	3	152X102X76	1.1	2.5	9.1	20	-18 to 52
34	Solar Panel Deployment	2	2	2	4	2	28X20X76	48.2	106	96.4	212	TBD
35	Wing Orientation	2	2	2	4	2	3370X927X10	15.1	33.3	186.4	410	≤100
36	Solar Panel Electrical Control Assembly	1	1	5	5	6	356X203X203	7.3	16	14.5	32	-18 to 52
37	Cabling and Connect	1	1	2	2	2	14X8X8	7.3	16	14.5	32	-18 to 52
37	Subtotals	-	-	-	46	-	-	-	-	686.2	1510	-
9	Communications and Data Handling Switches	1	1	16	16	16	51DX105	0.5	1	0.9	2	-18 to 60
10	Apollo Transponder	1	1	5.3cc	5.3cc	5.3cc	22.2X9X6	14.5	32	14.5	32	-18 to 60
16	Antenna	1	1	2	2	2	565X229X152	10.9	24	10.9	24	-18 to 60
17	ERTS Transponder	1	1	9.3cc	9.3cc	9.3cc	88X6X13	10.9	24	10.9	24	-18 to 60
18	PSK Demodulator	1	1	4	4	4	203X152X330	10.9	24	10.9	24	-18 to 60
19	Data Control Unit	1	1	3	3	3	184X140X89	0.9	2	0.9	2	-18 to 60
20	Format Generator	1	1	2	2	2	152X229X152	1.8	4	3.6	8	-18 to 60
21	Command Processor	1	1	4	4	4	6X9X5.6	1.8	4	3.6	8	-18 to 60
23	Digital Acquisition Unit	1	1	1.34	1.34	1.34	107X130X366	6.2	13.7	6.2	13.7	-18 to 60
24	Remote Command	8	8	1.4	11.2	1.4	152X229X71	0.4	0.8	3.2	7	-18 to 60
25	Tape Control	1	1	1	1	1	157X185X41	1.4	3	2.7	6	-18 to 60
26	Tape Recorder	2	2	12 rec.	24 P.B.	20dd	246X203X147	5.5	12	16.4	36	-18 to 60
27	Clock	1	1	1.7	1.7	1.7	56DX114H	0.5	1	0.5	1	-18 to 60
9	Communications and Data Handling Switches	1	1	16	16	16	51DX105	0.5	1	0.9	2	-18 to 60
10	Apollo Transponder	1	1	5.3cc	5.3cc	5.3cc	22.2X9X6	14.5	32	14.5	32	-18 to 60
16	Antenna	1	1	2	2	2	565X229X152	10.9	24	10.9	24	-18 to 60
17	ERTS Transponder	1	1	9.3cc	9.3cc	9.3cc	88X6X13	10.9	24	10.9	24	-18 to 60
18	PSK Demodulator	1	1	4	4	4	203X152X330	10.9	24	10.9	24	-18 to 60
19	Data Control Unit	1	1	3	3	3	184X140X89	0.9	2	0.9	2	-18 to 60
20	Format Generator	1	1	2	2	2	152X229X152	1.8	4	3.6	8	-18 to 60
21	Command Processor	1	1	4	4	4	6X9X5.6	1.8	4	3.6	8	-18 to 60
23	Digital Acquisition Unit	1	1	1.34	1.34	1.34	107X130X366	6.2	13.7	6.2	13.7	-18 to 60
24	Remote Command	8	8	1.4	11.2	1.4	152X229X71	0.4	0.8	3.2	7	-18 to 60
25	Tape Control	1	1	1	1	1	157X185X41	1.4	3	2.7	6	-18 to 60
26	Tape Recorder	2	2	12 rec.	24 P.B.	20dd	246X203X147	5.5	12	16.4	36	-18 to 60
27	Clock	1	1	1.7	1.7	1.7	56DX114H	0.5	1	0.5	1	-18 to 60
9	Communications and Data Handling Switches	1	1	16	16	16	51DX105	0.5	1	0.9	2	-18 to 60
10	Apollo Transponder	1	1	5.3cc	5.3cc	5.3cc	22.2X9X6	14.5	32	14.5	32	-18 to 60
16	Antenna	1	1	2	2	2	565X229X152	10.9	24	10.9	24	-18 to 60
17	ERTS Transponder	1	1	9.3cc	9.3cc	9.3cc	88X6X13	10.9	24	10.9	24	-18 to 60
18	PSK Demodulator	1	1	4	4	4	203X152X330	10.9	24	10.9	24	-18 to 60
19	Data Control Unit	1	1	3	3	3	184X140X89	0.9	2	0.9	2	-18 to 60
20	Format Generator	1	1	2	2	2	152X229X152	1.8	4	3.6	8	-18 to 60
21	Command Processor	1	1	4	4	4	6X9X5.6	1.8	4	3.6	8	-18 to 60
23	Digital Acquisition Unit	1	1	1.34	1.34	1.34	107X130X366	6.2	13.7	6.2	13.7	-18 to 60
24	Remote Command	8	8	1.4	11.2	1.4	152X229X71	0.4	0.8	3.2	7	-18 to 60
25	Tape Control	1	1	1	1	1	157X185X41	1.4	3	2.7	6	-18 to 60
26	Tape Recorder	2	2	12 rec.	24 P.B.	20dd	246X203X147	5.5	12	16.4	36	-18 to 60
27	Clock	1	1	1.7	1.7	1.7	56DX114H	0.5	1	0.5	1	-18 to 60
9	Communications and Data Handling Switches	1	1	16	16	16	51DX105	0.5	1	0.9	2	-18 to 60
10	Apollo Transponder	1	1	5.3cc	5.3cc	5.3cc	22.2X9X6	14.5	32	14.5	32	-18 to 60
16	Antenna	1	1	2	2	2	565X229X152	10.9	24	10.9	24	-18 to 60
17	ERTS Transponder	1	1	9.3cc	9.3cc	9.3cc	88X6X13	10.9	24	10.9	24	-18 to 60
18	PSK Demodulator	1	1	4	4	4	203X152X330	10.9	24	10.9	24	-18 to 60
19	Data Control Unit	1	1	3	3	3	184X140X89	0.9	2	0.9	2	-18 to 60
20	Format Generator	1	1	2	2	2	152X229X152	1.8	4	3.6	8	-18 to 60
21	Command Processor	1	1	4	4	4	6X9X5.6	1.8	4	3.6	8	-18 to 60
23	Digital Acquisition Unit	1	1	1.34	1.34	1.34	107X130X366	6.2	13.7	6.2	13.7	-18 to 60
24	Remote Command	8	8	1.4	11.2	1.4	152X229X71	0.4	0.8	3.2	7	-18 to 60
25	Tape Control	1	1	1	1	1	157X185X41	1.4	3	2.7	6	-18 to 60
26	Tape Recorder	2	2	12 rec.	24 P.B.	20dd	246X203X147	5.5	12	16.4	36	-18 to 60
27	Clock	1	1	1.7	1.7	1.7	56DX114H	0.5	1	0.5	1	-18 to 60
9	Communications and Data Handling Switches	1	1	16	16	16	51DX105	0.5	1	0.9	2	-18 to 60
10	Apollo Transponder	1	1	5.3cc	5.3cc	5.3cc	22.2X9X6	14.5	32	14.5	32	-18 to 60
16	Antenna	1	1	2	2	2	565X229X152	10.9	24	10.9	24	-18 to 60
17	ERTS Transponder	1	1	9.3cc	9.3cc	9.3cc	88X6X13	10.9	24	10.9	24	-18 to 60
18	PSK Demodulator	1	1	4	4	4	203X152X330	10.9	24	10.9	24	-18 to 60
19	Data Control Unit	1	1	3	3	3	184X140X89	0.9	2	0.9	2	-18 to 60
20	Format Generator	1	1	2	2	2	152X229X152	1.8	4	3.6	8	-18 to 60
21	Command Processor	1	1	4	4	4	6X9X5.6	1.8	4	3.6	8	-18 to 60
23	Digital Acquisition Unit	1	1	1.34	1.34	1.34	107X130X366	6.2	13.7	6.2	13.7	-18 to 60
24	Remote Command	8	8	1.4	11.2	1.4	152X229X71	0.4	0.8	3.2	7	-18 to 60
25	Tape Control	1	1	1	1	1	157X185X41	1.4	3	2.7	6	-18 to 60
26	Tape Recorder	2	2	12 rec.	24 P.B.	20dd	246X203X147	5.5	12	16.4	36	-18 to 60
27	Clock	1	1	1.7	1.7	1.7	56DX114H	0.5	1	0.5	1	-18 to 60
9	Communications and Data Handling Switches	1	1	16	16	16	51DX105	0.5	1	0.9	2	-18 to 60
10	Apollo Transponder	1	1	5.3cc	5.3cc	5.3cc	22.2X9X6	14.5	32	14.5	32	-18 to 60
16	Antenna	1	1	2	2	2	565X229X152	10.9	24	10.9	24	-18 to 60
17	ERTS Transponder	1	1	9.3cc	9.3cc	9.3cc	88X6X13	10.9	24	10.9	24	-18 to 60
18	PSK Demodulator	1	1	4	4	4	203X152X330	10.9	24	10.9	24	-18 to 60
19	Data Control Unit	1	1	3	3	3	184X140X89	0.9	2	0.9	2	-18 to 60
20	Format Generator	1	1	2	2	2	152X229X152	1.8	4	3.6	8	-18 to 60
21	Command Processor	1	1	4	4	4	6X9X5.6	1.8	4	3.6	8	-18 to 60
23	Digital Acquisition Unit	1	1	1.34	1.34	1.34						



FOLD OUT #3

High Spectral Resolution Spectrographs	0.05-0.2X2 sec	110-180	4.5X10 <sup>4</sup>	25X25	Axial	62.4 (137.6)	16	3 Slit Sizes: 0.05X1.0 arc sec 0.1X0.1 arc sec 2.0 arc sec dia Same as above
Echelle Spectrograph	0.05-0.2X2 sec	180-350	3.0X10 <sup>4</sup>	25X25	Axial	62.4 (137.6)	16	3 Slit Sizes: 0.05X1.0 arc sec 0.1X0.1 arc sec 2.0 arc sec dia Same as above
Faint Object Spectrographs								
Czerny-Turner (Gratings A and B)	0.05-0.1X10 sec	A-110-160 B-160-220	A. 1.25X10 <sup>3</sup> B. 1.75X10 <sup>3</sup>	25X25	Axial	64.2 (141.5)	17	3 Slit Sizes: 1X1.5 arc sec 15X1.5 arc sec Other
Wadsworth (Dichronic Mirror)	0.05-0.1X10 sec	220-350 350-660	A. 1.23X10 <sup>3</sup> B. 0.75X10 <sup>3</sup>	25X25	Radial	49.2 (108.3)	17.5	3 Slit Sizes } Same as above 3 Slit Sizes } (mass and power in inst.) 3 Slit Sizes: Same as above (mass and power in inst.)
Slit Mechanism Czerny-Turner	0.05-0.1X10 sec	660-1μ	1.5X10 <sup>3</sup>	25X25	Radial	47.6 (104.8)	17.5	3 Slit Sizes: Same as above (mass and power in inst.)
Slit Mechanism	2.5-5.0 sec dia	1μ-5μ	3.3X10 <sup>4</sup>	25X25	Radial	50.0 (110.5)	10.0	2 Circular FOV openings
Fourier Interferometer	13 sec	115-550			Radial	47.7 (105.2)	20	
Slit Jaw Camera Assembly					Radial	36.9(81.3)	25	
Contingency Equipment <sup>v</sup>								
Support Equipment								
Collimating Mirrors and Axial Spectrograph Selector					Axial	7.0(17.4)	2.5	Serves 2 Echelles and F.O. Spectrographs
Axial Spectrograph Slit Selector Mechanism and Calibration					Axial	4.8(10.5)	3.5	
Source Assembly					Radial	38.1 (84.0)	22	
Support Electronics and Cabling					Radial	6.2 (13.7)	16	
Scientific Instrument Controller <sup>v</sup>					Radial	2.3 (5.0)	2	
Scientific Data Link Control Logic <sup>v</sup>						12.3 (27)	-	
Thermal Control Paint <sup>v</sup>						10.4 (23)	ee	
Strip Heaters <sup>v</sup>						189.3 (418.3)	80	Only needed for very faint sources (28th Magnitude) 50 Watts per tube max.
Secondary SIP Structure								
Thermo-Electro Devices (10 units)								
Totals						1000.8 (2208.6)	412.0 <sup>w</sup>	

- a. HEAO component  
b. Mounted on OTA  
c. New design (existing technology)  
d. Mounted on OTA main ring  
e. Nine watts per gyro  
f. Existing component of OAO  
g. Electronics in transfer assembly  
h. Existing component of Agena, Satellite Control Section, and others  
i. Software special for LST  
j. HEAO commonality possible if HEAO or LST concept is changed slightly  
k. Existing component of Agena thruster cluster  
l. Existing component of Lockheed Satellite Control Section backup RCS  
m. Existing component of ATM Skylab  
n. Existing commercial component  
o. Includes two PCM encoders, six ROMs  
p. Existing component of Gemint
- q. Existing component  
r. Duct work support straps, etc.  
s. Plug-in for air supply  
t. Cabin manifold; 150 CFM capacity  
u. SIP inlet; 200 CFM capacity  
v. Not included in list of instruments in Volume IV  
w. Based on earlier estimates; power used in estimating overall power requirements was 500W  
x. Six gyros per assembly (3 required)  
y. Internally redundant  
z. One active in record, one active in playback (P.B.) during contact  
aa. Power included in SSM electrical system.  
bb. Duty cycle is very small. Used only in emergency  
cc. On during ground contact only. Max ground contact estimated to be 33.3 percent  
dd. One unit active normally; second unit during ground contact. A max of 33.3 percent was assumed contact time  
ee. Heaters are on when some instruments are off; therefore, no additional power is required  
ff. Includes main ring and pressure bulkhead



TABLE IV-3. LST MASS MOMENTS OF INERTIA AND CENTER OF GRAVITY LOCATIONS

Item	Mass (Weight) [kg (lb)]	Center of Gravity Location <sup>a</sup> [mm (in.)]			Inertia (kg-m <sup>2</sup> )		
		X-axis	Y-axis	Z-axis	I <sub>x</sub>	I <sub>y</sub>	I <sub>z</sub>
OTA							
Structure <sup>b</sup>	1 707 (3 765)	6 919 (272.4)	-0.2 (-0.01)	22 (0.85)	3 689	11 735	11 588
Thermal Control	102 (226)	7 084 (278.9)	—	215 (8.46)	263	790	752
Primary Mirror	2 001 (4 413)	5 294 (208.4)	—	—	2 468	1 278	1 278
Secondary Mirror	40 (88)	11 044 (434.8)	—	—	2	1	1
Focal Plane and Fold Optics	40 (88)	4 067 (160.1)	-4 (-0.14)	31 (1.21)	1	1	1
Data Management	3 (7)	3 543 (139.5)	—	1 499 (59.0)	—	—	—
Power Distribution	34 (75)	7 258 (285.8)	—	107 (4.21)	5	58	53
Performance Control	308 (678)	6 154 (242.3)	16 (0.64)	742 (29.2)	168	3 740	3 599
SIP <sup>c</sup>	1 033 (2 278)	3 576 (140.8)	—	—	464	580	580
SSM							
Structure	635 (1 397)	2 604 (102.5)	—	—	1 472	1 966	1 966
Shroud Adapter <sup>d</sup>	251 (553)	813 (32.0)	—	—	849	445	445
Docking Port	199 (437)	190 (7.5)	—	—	100	207	207
Support Systems	1 139 (2 501)	1 374 (54.1)	—	—	2 009	1 359	1 359
Magnetic Torquers (6)	141 (310)	10 854 (427.3)	—	—	456	651	955
Subtotals	7 633 (16 821)	4 592 (180.8)	0.6 (0.02)	40 (1.59)	12 117	64 309	64 112
Light Shield (retracted)	344 (758)	8 103 (319.5)	—	-177 (-6.96)	1 088	2 079	2 030
Solar Panels (folded) (2)	186 (410)	3 048 (120.0)	—	—	650	503	503
Configuration I Totals (solar panels folded, light shield retracted)	8 163 (17 989)	4 709 (185.4)	0.6 (0.02)	30 (1.18)	13 870	71 479	71 217
Contingency	1 633 (3 598)	4 709 (185.4)	—	—	2 774	14 295	14 243
Configuration I Totals (with contingency)	9 796 (21 587)	4 709 (185.4)	0.5 (0.02)	25 (0.98)	16 645	85 776	85 460

TABLE IV-3. (Concluded)

Item	Mass (Weight) [ kg (lb) ]	Center of Gravity Location [ mm (in. ) ]			Inertia (kg-m <sup>3</sup> )		
		X-axis	Y-axis	Z-axis	I <sub>x</sub>	I <sub>y</sub>	I <sub>z</sub>
Subtotals	7 633 (16 821)	4 592 (180.8)	0.6 (0.02)	40 (1.59)	12 117	64 309	64 112
Light Shield (retracted)	344 (758)	8 103 (319.5)	—	-177 (-6.96)	1 088	2 079	2 030
Solar Panels (folded) (2)	186 (410)	3 048 (120.0)	—	—	650	503	503
Propulsion Module	1 631 (3 588)	- 889 (-35.0)	—	—	468	468	468
Configuration II Totals (Solar panels folded, light shield retracted, propulsion module attached)	9 794 (21 577)	3 732 (146.9)	0.5 (0.02)	25 (0.97)	14 340	115 115	114 852
Contingency	1 633 (3 598)	4 708 (185.4)	—	—	2 774	14 295	14 243
Configuration II Totals (with contingency)	11 427 (25 175)	3 870 (152.4)	0.4 (0.02)	21 (0.83)	17 114	130 704	130 388
Subtotals	7 633 (16 821)	4 592 (180.8)	0.6 (0.02)	40 (1.59)	12 117	64 309	64 112
Light Shield (extended)	344 (758)	14 643 (576.5)	—	-177 (-6.96)	1 088	2 079	2 030
Solar Panels (deployed) (2)	186 (410)	965 (38.0)	—	—	2 877	484	3 361
Configuration III Totals (solar panels deployed, light shield extended)	8 163 (17 989)	4 944 (194.7)	0.5 (0.02)	30 (1.18)	16 097	103 085	105 699
Contingency	1 633 (3 598)	4 944 (194.7)	—	—	3 219	20 620	21 140
Configuration III Totals (with contingency)	9 796 (21 587)	4 944 (194.7)	0.5 (0.02)	25 (0.98)	19 318	123 703	126 839

- a. Center-of-gravity reference located on IST longitudinal center line at the "docking plane."
- b. Includes electronics and SIP primary structure.
- c. Primary SIP structure included in OTA structure. Mass includes fixed star trackers (FSTs) and shades and reference gyro assembly (RGA).
- d. Required only for Titan launch.



Two totals are given for each configuration. The second total for each includes a 20 percent contingency factor. The mass distribution of the contingency is assumed to be the same as that without the contingency. Thus, the center of gravity of the contingency is taken as the center of gravity of the spacecraft without the contingency. Note that the contingency factor used for configuration II does not include a contribution from the OAS.

Figure IV-4 presents a major component breakdown and a summary of the totals including the contingency, along with a pictorial sketch for the three configurations.

#### 4. Configuration and Systems Description

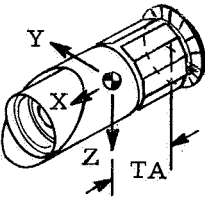
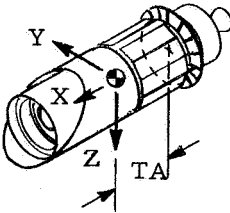
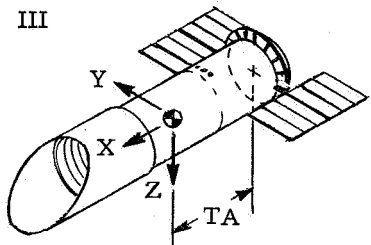
a. LST Reference Configuration. As discussed earlier, the reference LST consists of three basic elements: (1) the OTA, (2) the SIP, and (3) the SSM. The reference LST is discussed below, and alternative concepts are discussed later in this chapter. The reference LST in its launch mode (Fig. IV-5) is 12.7 m (500 in.) long and 3.68 m (145 in.) maximum outside diameter at the forward end. These dimensions are within the maximum allowable dynamic envelope of the Viking shroud on the Titan IIIE/OAS, which was a design constraint for backup launch in this study. The maximum diameter of the SSM across the retracted solar wings is within the shroud envelope. (The Shuttle tie points are slightly outside the solar wing envelope but can be designed to be removable, or the LST can be oriented so that they fit into the oblong portion of the shroud dynamic envelope.) The reaction control system (RCS) modules project slightly farther out and would be outside the shroud in the backup launch case. The degree of relief from Titan launch constraints if the backup launch is deleted is discussed in Chapter VII. The LST in its deployed mode is shown in Figure IV-6. The overall length in this mode is 19.55 m (770 in.).

The general shape is driven by the telescope optics and launch vehicle payload envelope to be something on the order of a long cylinder. The desire for as large a primary mirror as possible eliminates the space available for packaging systems or instruments around the periphery of the telescope. The need for multiple instruments at the focal plane, for access to them, and for minimum obscuration and reflections eliminates the possibility of packaging instruments or systems between the mirrors or in front of the telescope. Consequently, the systems and instruments must be located aft of the primary mirror. The long cylindrical shape of the LST causes unequal inertias, which causes unequal gravity gradient torques to act on the LST, necessitating a pointing control system of larger capability than would be

MAJOR COMPONENT

Mass Weight\*

Optical Telescope Assembly	4579	10 098
Scientific Instrument Package	1001	2 209
Support Systems Module	2583	5 682
Total	8163	17 989
Contingency (20 percent)	1633	3 598
Total with Contingency	9796	21 587

CONFIGURATION	CENTER OF GRAVITY (TA) mm (in.)	CENTROIDAL INERTIA** kg - m <sup>2</sup> (Slug - ft <sup>2</sup> )		
		I <sub>x</sub>	I <sub>y</sub>	I <sub>z</sub>
I 	4709 (185)	16 645 (12 284)	85 776 (63 303)	85 460 (63 069)
II 	3870 (152)	17 114 (12 630)	130 704 (96 460)	130 388 (96 226)
III 	4944 (195)	19 318 (14 257)	123 703 (91 293)	126 839 (93 607)

\* From master equipment list.

\*\* Includes a 20 percent contingency.

Figure IV-4. LST mass characteristics.

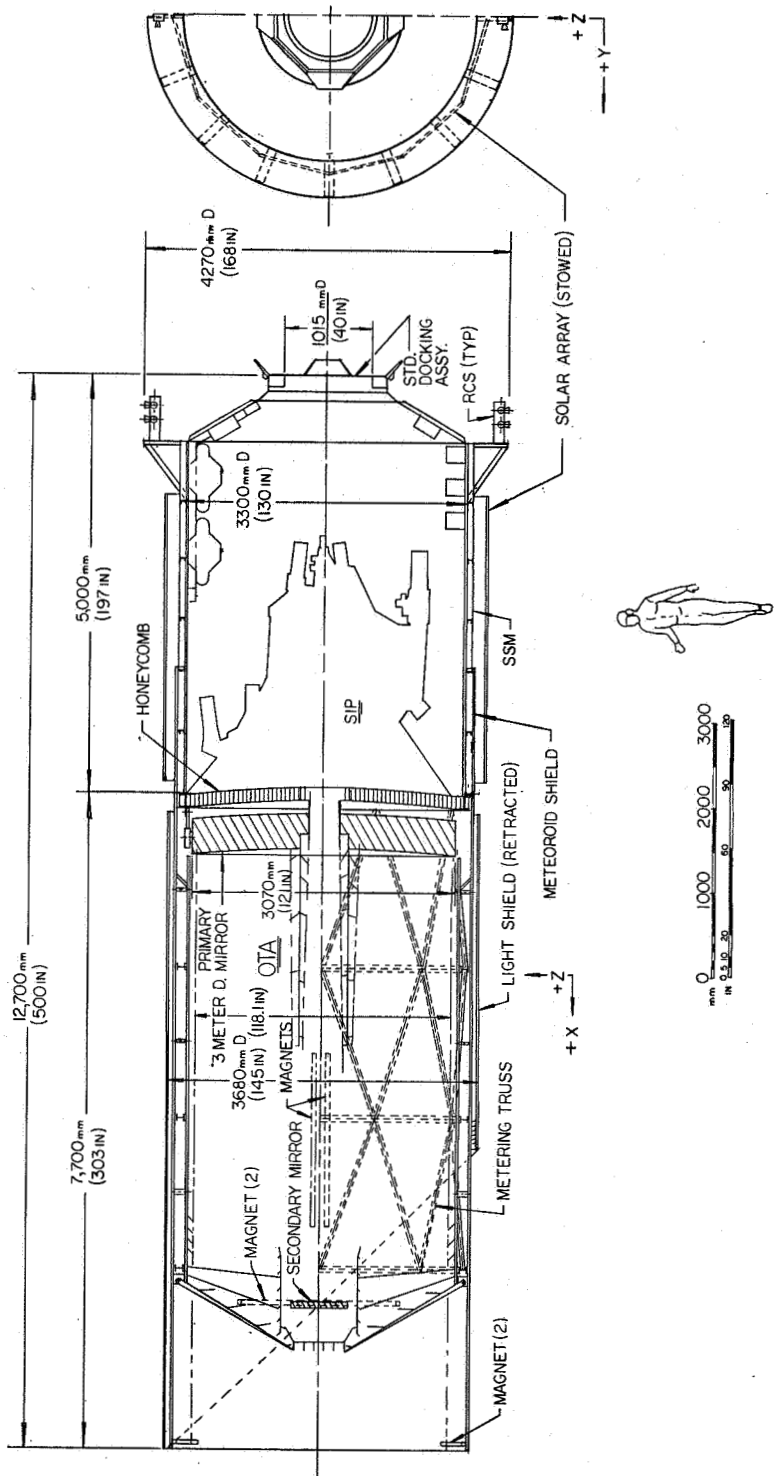


Figure IV-5. LST reference design longitudinal cross section.

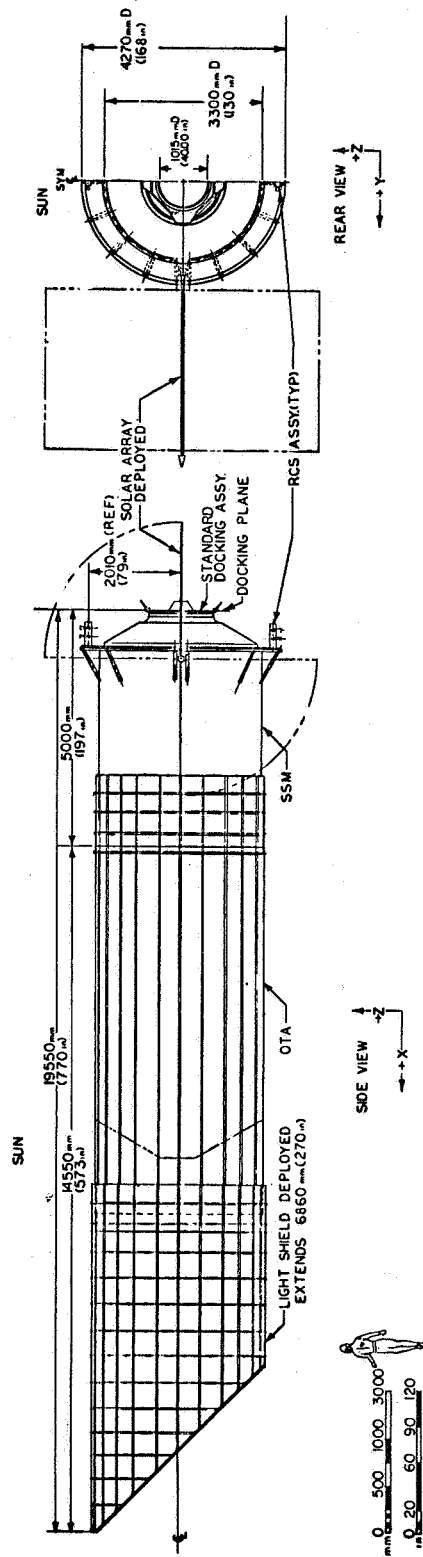


Figure IV-6. LST assembly operational configuration.

required if the inertias were more nearly balanced as, for example, in the Orbiting Astronomical Observatory (OAO). It was felt that mass balance booms would be so long and balance masses so large that structural interactions with the pointing control system would probably result.

The OTA and SSM are mated at the aft surface of the OTA titanium main (primary) ring, which is the reference for structural alignment of the entire LST. The primary mirror mounts are attached to it, as are the forward (optical) metering truss, which supports the secondary mirror, and the aft metering truss (SIP structure), which supports the telescope instruments and science instruments. Both portions of the metering truss are made of graphite-epoxy. The OTA meteoroid shield is attached to the SSM wall approximately 1.5 m (59 in.) aft of the main ring to provide better isolation of the ring from any structural vibrations of the shield. There are two main structural pickup points on the main ring for mounting the LST to the Shuttle and one point near the aft end of the LST.

The OTA light shield is aluminum alloy and the forward end is truncated at 45 degrees. It remains retracted during launch, earth return, or on-orbit storage and extends on-orbit to provide protection from undesirable light sources such as the sun, moon, or bright earth. The principle of operation and design details of the light shield and OTA baffle arrangement are discussed in Volume III. The results of the trade studies of the light shield truncation angle are discussed in Chapter V.

The OTA meteoroid shield is aluminum, as is the OTA baffle shell which is mounted to it. The forward metering truss lies between the meteoroid shield and baffle shell and is isolated from them structurally and thermally. The OTA motor-driven aperture doors are aluminum and are mounted and hinged to the OTA meteoroid shield. The doors protect the telescope and instruments from viewing dangerously bright objects and from contamination during nonviewing periods.

The secondary mirror has a 5-degree-of-freedom static alignment capability for ground or on-orbit use. In addition, there is a different set of actuators which provide dynamic image motion stabilization during observations. A four-legged spider was utilized to mount the secondary mirror to the metering truss because analysis showed that it provided less optical degradation at the image plane than a three-legged spider. The 3 m aperture primary mirror has 25 motor-driven adjustment jacks which react against the forward bulkhead to produce small amounts of force on the mirror to adjust its figure. The OTA bulkhead is aluminum honeycomb inside

titanium face sheets and is tied into the main ring so that it provides shear stiffness to the LST, as well as providing a reaction surface for the mirror jacks and a pressure wall for the SSM during maintenance. A motor-driven pressure bulkhead door remains open during observations but is closed during maintenance operations or for contamination protection of the mirrors during ground operations.

The scientific instruments are mounted to the aft metering truss (SIP structure), as are the three telescope instruments (figure sensor, focus sensor, and fine guidance assembly). Each instrument is removable on-orbit for maintenance. Guide rails and locking devices are provided to insure proper alignment and the secondary mirror can be utilized to provide some misalignment correction, if necessary (see paragraph A. 11, Focus and Alignment Tolerance). If it should become necessary, alignment devices could be provided on each instrument. Since maintenance is performed by a man in a shirtsleeve environment, maximum utilization of man's capabilities in this regard could be achieved. In addition to the capability to remove each instrument, the capability to remove only the sensor on each instrument is provided.

Since the SSM is pressurized at  $1.01 \times 10^5$  N/m<sup>2</sup> (14.7 psi) for maintenance, ducts and filters must be provided in the SSM for distributing and cleaning the air. The ducts are routed along the SSM walls and terminate in a ring at the forward end of the SSM. The airflow is directed toward the aft end of the SSM to provide as near laminar-flow conditions as possible across the instruments and systems. A contamination-control cover is provided around the outside of the aft metering truss to better enable a positive pressure differential to exist between the instruments and the SSM area. Removable panels are provided in this cover for access to accomplish maintenance.

The more alignment-critical items of the SSM systems (rate gyros and star trackers) are mounted on the aft metering truss for greater alignment accuracy and greater thermal stability because the SSM wall does not afford such accuracy and stability. The SSM wall is a cylinder of aluminum skin and stringer construction and provides a pressure shell for the maintenance operation at no additional weight penalty since launch loads determine the size of its members. The aluminum meteoroid shield is mounted to the outside of the shell and is thermally insulated from it. The 1-m clear-aperture docking ring and mechanism is located at the aft end of the SSM. A cover is provided over this opening for thermal, meteoroid, and contamination protection during normal LST operation. The cover is removable for maintenance.

An external ring with support struts is mounted near the aft end of the SSM and provides support to the solar array wings in the deployed mode and a mounting location for the RCS modules. The solar array is deployed and retracted by a motor-driven cable mechanism. In the retracted mode, the solar array cells face outward, thus allowing the generation of some power in this mode. This feature, along with the cam-operated antenna position-changing devices, allows an "on-orbit storage mode" to be available for emergency or programmatic reasons, which does not require attitude control. During operation each wing of the solar array is driven separately by a gimbal motor mounted inside the SSM. The wings are gimballed about one axis only, through a maximum angle of 135 degrees. This allows access to the full celestial sphere except for the  $\pm 45$  degree avoidance area about the sun with no degradation in power-generation capability. One antenna is mounted on each solar array boom and through the action of a cam during deployment and retraction of the arrays, the antenna pointing direction is maintained perpendicular to the body of the LST. Two coarse sun sensors (one per panel) are also mounted on the solar array and two magnetometers are mounted outside the aft end of the SSM.

The remainder of the SSM components are mounted inside the SSM. The smaller components are mounted on the aft cone and the others are arranged in four longitudinal columns to allow room for access to the systems and to the instruments.

The insulation used throughout the LST is high-performance multilayer aluminized Mylar. There is manual backup capability on all the mechanisms which are critical to mission success.

The LST in the launch mode in the Shuttle bay is shown in Figure IV-7 and in the on-orbit mode in Figure IV-8. It should be noted that this sketch excludes the orbital maneuvering system (OMS) propellant tanks which are necessary to achieve the 611 km (330 n. mi.) orbit. The OMS tanks would require 1.5 to 2.1 m (5 to 7 ft) of length in the aft end of the payload bay. A swing-table with bellows was used in the reference design since it was assumed that such a device would already be designed for such payloads as the Sortie Lab and would be available for use on the LST. The table allows the LST to be deployed outside the payload bay or to be retrieved into the bay with ease, and without depressurizing the SSM, if that is desired. The table is not a required item for LST utilization. Subsequent information on the Shuttle design indicates that there is no docking port on the Shuttle outer surface and that the one into the payload bay may be offset from the bay centerline. Consequently, a docking module which is carried in the payload bay may be required to be utilized with the reference LST. A sketch showing the LST in the bay with such a module and with the OMS tanks is shown in Figure VII-4 of Chapter VII.

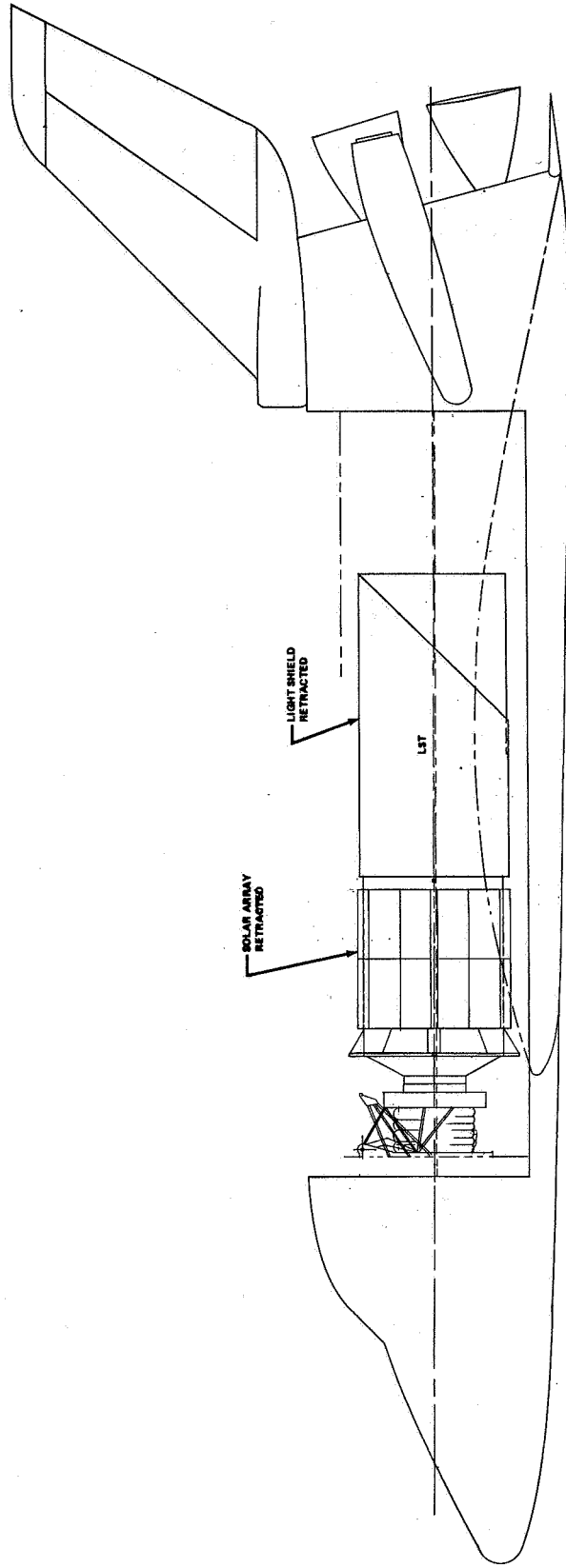


Figure IV-7. LST launch configuration in payload bay.



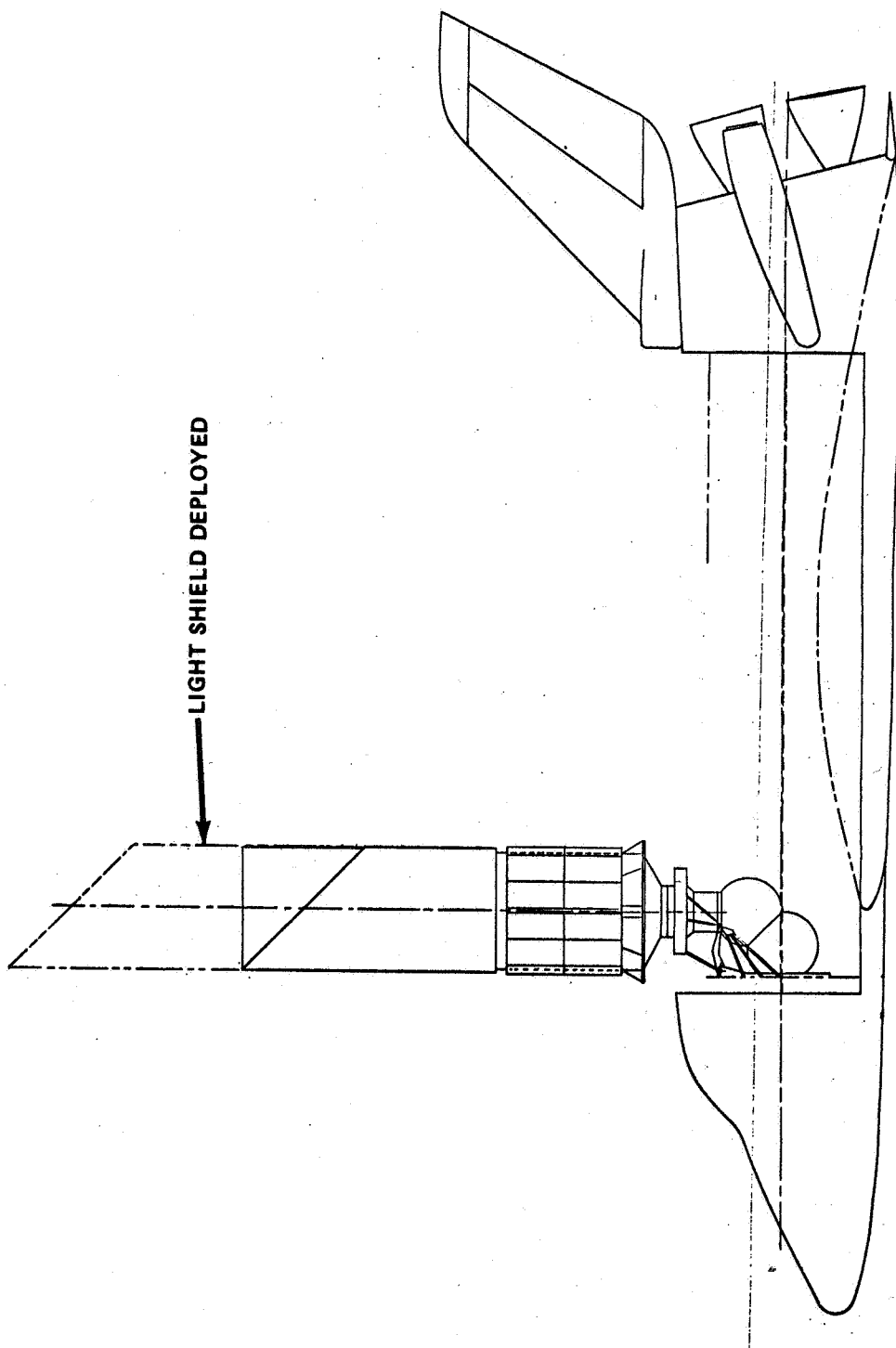


Figure IV-8. LST launch configuration deployed position.

The LST will be subjected to longitudinal launch g-loads in one direction during launch and in the opposite direction during reentry. This, however, does not appear to offer any significant design problem.

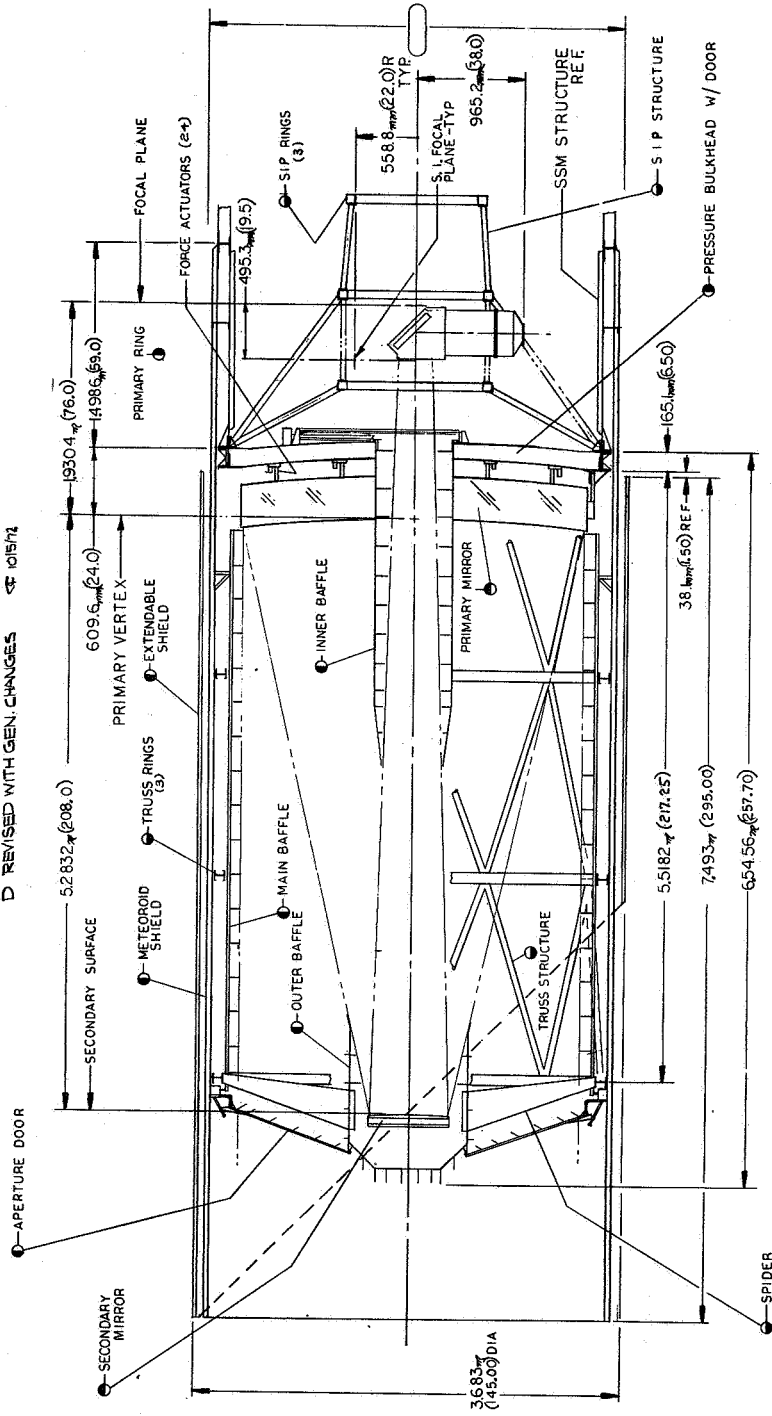
b. Optical Telescope Assembly (OTA). The reference concept that resulted from this study is a Ritchey-Chretien telescope, 3 m in aperture, with a primary focal ratio of  $f/2.2$  and a system focal ratio of  $f/12$  (Fig. IV-9). The primary mirror is a Cer-Vit monolith supported at three points with Invar leaf spring flexures attached to a titanium supporting bulkhead. A metering truss, manufactured from graphite-epoxy, supports the four-point spider and secondary mirror support ring, to which is attached the secondary mirror, its alignment system, and the fine guidance actuation and drive.

(1) Structural Design. The three structural systems that make up the OTA — (1) the optical metering truss, (2) SIP, and (3) telescope protective system — have been effectively designed to be structurally independent and thermally isolated from one another. The optical metering truss supports only the optics whereas the SIP structure supports the associated optical instrumentation. Thermal isolation of the metering truss and SIP is accomplished by both insulating the structure and using an athermalizing truss design. A three-bay, eight-point mount truss with graphite-epoxy members appears to be a most suitable design for the metering truss. The SIP truss structure is also governed by the same general requirements as the metering truss but to a lesser degree. Consequently, a graphite-epoxy composite truss design is also recommended. This truss has the added feature of satisfying the accessibility and maintainability requirements for the SIP. Structural isolation is accomplished by providing independent load paths. The pressure bulkhead and main ring form the main structural support base for both the metering truss and SIP.

The primary mirror, which serves as the optical reference, is the most critical component and has the greatest overall impact on the optical performance of the system. A series of force actuators is provided to augment the capability of the primary mirror in minimizing surface degradations caused by various unpredictable forces. Although uncertainties exist about the nature of the degrading forces, estimates can still be made as to the required corrective actuator forces.

The nonoptical protective system includes the meteoroid shield, sunshade, baffles, and aperture doors. The meteoroid shield acts as the main support member for the sunshade, baffles, and aperture doors and is itself supported by the SSM. In general, an aluminum semimonocoque construction is used except for the aperture doors, which are an eight-segmented

D REVISED WITH GEN. CHANGES 10/15/72



NOTE: DIMENSIONS SHOWN IN PARENTHESIS ARE ENGLISH EQUIV.

MATERIAL LEGEND	
SYMBOL	DESCRIPTION
●	ALUMINUM
○	GRAPHITE-EPOXY
◐	TITANIUM
◑	CER-VIT

Figure IV-9. Optical telescope assembly (OTA).

aluminum honeycomb design supported by the meteoroid shield and operated by screwjacks. The design concept for the sunshade is an open-ended circular shell truncated at 45 degrees which can be extended and retracted from the meteoroid shield. The pressurizable portion of the OTA structure includes the pressure bulkhead and SSM pressurized instrument bay, where servicing of instruments can readily be made by astronauts.

(2) Optical System Design. The LST will have the highest resolution of any telescope ever constructed. The space environment eliminates the atmospheric limitations to the system performance and makes it possible to build as large and as near perfect a telescope as desired. The theoretical factor governing the resolution is the aperture diameter, which has been set at 3 m. All other factors will be minimized or made insignificant to permit the entire system to take full advantage of that aperture.

The optical quality for a nearly perfect optical system is essentially diffraction-limited if the wavefront is perfect to  $1/4 \lambda$  peak to valley (J. W. Strutt, Lord Raleigh). The current goal is a value of  $0.05 \lambda$  rms, which is roughly equivalent to the  $1/4 \lambda$  peak to valley. For the LST, this has been taken a step farther by adding the unusually stringent requirement that all possible sources of image degradation be included, thereby developing a total imaging system that will give the best possible performance with a 3-m aperture.

If the wavefront is nearly perfect, the performance will then depend on the diffraction. The outside diameter of the aperture has the most influence, but obstructions inside the aperture also affect the image. The selected design is a Cassegrainian system but with an obscuration that is as small as feasible. The operational image quality of the LST will very closely match the diffraction pattern of the aperture geometry.

The telescope selected will achieve this near perfect performance. It has a basic Ritchey-Chretien optical design to give very good performance over a 5-arc-minute data field and adequate performance over a 24-arc-minute guide star tracking field. The telescope will have a relatively fast  $f/2.2$  primary to keep the structure short. The secondary will have a magnification of 5.5 to give a relative aperture of  $f/12$  at the primary image plane.

The primary mirror is one of the more critical elements in the LST. The choice of material for the primary mirror is Cer-Vit with an  $f/2.2$  hyperboloid surface shape. The secondary mirror is less demanding but it too is a critical optical element.

The reflective coating reference design is aluminum overcoated with magnesium fluoride. It is designed to last the life of the instrument rather than to be recoated periodically.

The techniques used to control stray light are a sunshade to permit use in sunlight and a well-designed but basically conventional interior baffling.

There are a number of mirrors near the image plane to direct the light to the various instruments. Some of these will have a nonflat shape to correct the small but finite astigmatism at the edge of the data field. Other aspects of the optical elements associated with the auxiliary optical devices are discussed in those appropriate sections.

(3) Thermal Design. To meet all of the system requirements, a reference design for thermal control has been developed. This concept consists of active and passive elements, described below.

(a) Active Elements. The principle of the reference design is to provide active thermal controls for the primary mirror, the secondary mirror, and the main support ring. Both the primary and secondary mirrors are actively controlled to maintain them at or near their manufacturing and figuring temperature. This approach is conservative; however, it reduces the potentially deleterious effects of coefficient of expansion variation over the 3-m aperture primary to values that are within the error budget. Active control of both optical elements is based on the use of multizone, thermostatically controlled electrical heaters bonded to the rear surface of the respective mirrors.

While not an optical element, the main support ring is considered to be sufficiently critical to telescope performance to warrant active thermal control. As it is the supporting member of the primary mirror and the instrument section and is fabricated from a more thermally sensitive material (titanium alloy), active control is necessary. As in the case of the optical elements, the thermal control is provided by multizone thermostatically controlled electrical heaters.

Although not part of the active thermal system, it should be noted that all of the active elements, the mirrors and the main ring, are thermally insulated from their surroundings to the maximum extent possible by means of multilayer insulation (aluminized Mylar film) known as superinsulation.

(b) Passive Elements. The reference design includes passive thermal control of two kinds, superinsulation and external thermal control finishes. The supporting structure between the primary and secondary mirrors consists of a three-bay graphite epoxy composite truss from the main support ring forward. At the upper end of this structure, a spider is positioned to support the secondary mirror. The passive baseline concept provides the maximum thermal isolation possible for this supporting structure. The effect of thermal isolation is to reduce the orbital variations in truss structural temperatures to a level compatible with the system fixed focus operational requirement (dictated by primary-secondary spacing change).

Thermal isolation of the truss is accomplished by sandwiching it between two superinsulation blankets that are themselves supported by the internal light baffle and by the external meteoroid shell. The spider supporting the secondary mirror and its 5-degree-of-freedom mount is not insulated since the use of a thermal blanket in this area is detrimental to system optical performance.

The thermal control finish on the exterior meteoroid shell will provide a cold external environment for the LST walls to maintain thermal control of the active elements within the system at all times regardless of solar orientation. However, it must be recognized that thermal finish property optimization has not been done. The allowable variation has been bracketed. Future study is necessary to establish an optimum finish that will reduce thermal power by increasing the external temperature level and provide a heat sink for the active elements under maximum thermal loads.

(4) Stabilization and Control. The present reference design provides within the telescope a fine tracking method capable of wider bandwidths than the vehicle itself. This approach has the secondary mirror of the telescope moved by means of actuators. There are two advantages to moving the secondary mirror for fine tracking system capable of wider band- including the offset guide field, is moved as a unit, preventing significant defocus or differential distortion; (2) the image position can be maintained in all  $f/12$  planes in a closed control loop via the offset guidance.

During the study program, the NASA Headquarters Astronomy Committee directed that the final image seen by the high resolution cameras have a means for structural drift compensation during long time exposures. Additionally, a means must be provided for positioning a fine spectrograph slit to at least 0.12 microradian (0.025 arc sec) with respect to any specific astronomical feature.

The present reticle concept replaced an earlier offset guidance concept, which relied upon mechanical devices such as lead screws with brakes to remember the guide star coordinates during the exposure. The mechanical approach limits the telescope system to observing one object at a time, unless duplicate guide heads and drivers are used. The present guide concept places its reliance for stability and repeatability upon an all-fused-silica structure so that it will be possible to repeat guide head settings to 0.005 microradian (0.001 arc sec), permitting two or more objects per orbit to be observed with full resolution.

The movable mechanical structures associated with the reticle guidance concept require only modest demands upon precision, the most precise being the tilting plate optical micrometer, which must resolve and repeat to one part in 4000. The reticle concept proposed has a sensitivity advantage since, unlike more conventional scanners that throw away half of the guide star's power, all the photons received are counted.

(5) Alignment, Focus and Figure Control Design.

(a) Alignment. In a classical Cassegrainian system with a parabolic primary and a hyperbolic secondary, the tilt of the secondary about the focus of the primary causes no aberration on axis (although the axis moves) because that point is also one focus of the hyperbolic secondary, and the secondary deflects any rays that would pass through that point to the other focus of the hyperbola. The equivalent neutral point for the Ritchey-Chretien design is found to be just inside the focus of the primary mirror. A tilt about that point gives no coma on axis, but astigmatism is introduced off axis. Thus, if the secondary positioning problem is perceived as one of keeping this coma-free point on the primary axis and keeping the axes of the two mirrors parallel, the penalty for decentering is coma and the penalty for tilt is off-axis astigmatism.

The effect of tilting the secondary about its vertex is almost equivalent to a decentering at the neutral point. If tilt and decenter are controlled by sensors with equal angular accuracy, the effect of tilt is an order of magnitude less than the effect of decenter. The calculated decenter sensitivity for the  $f/12$ - $f/2.2$  system is  $0.00055 \lambda$  rms per micrometer.

In terms of hardware components, because the tilt and decenter positioning of the secondary is critical relative to the primary mirror, the tilt and decenter sensors are mounted directly on the primary mirror and their targets are mounted directly on the secondary mirror.

These sensors are two-axis alignment telescopes that generate an error signal if the beam returned from a reflecting target on the secondary is offset from the beam as it originates at the alignment telescope. Stability of 1 micro-radian (0.2 arc sec) has been achieved for a space-hardened long-life device with an aperture of approximately 40 mm. As a tilt sensor, the device is used as an autocollimator reflecting from a flat mirror at the secondary.

As a decenter sensor, the device is focused at the neutral point of the system, and the beam is reflected back upon itself by a spherical mirror mounted on the secondary with its center of curvature at the neutral point. Relative motion between the primary and secondary at the neutral point is measured directly with a positional accuracy equal to the alignment telescope angular accuracy times the distance from the alignment telescope to the neutral point (approximately 6.6 m). Thus the centering accuracy of the alignment telescope can be expected to be  $6.6 \mu\text{m}$ . When multiplied by the  $0.00055 \lambda$  rms per micrometer decenter sensitivity of the optical system, this indicates a sensor-limited centering accuracy of  $0.0036 \lambda$  rms.

The alignment sensors will be used to realign the secondary mirror before each observation; the LST thermal design is such as to limit the thermal drift of the structure to acceptable values during the observation. The sensors and targets can be directly mounted to the mirrors. Initial alignment and calibration is determined as a final step in the mirror manufacturing process. Two sensors of each type are included for redundancy.

(b) Focus. The optical system is designed for certain spacing between the vertices on the primary and secondary mirrors. If this spacing changes, rotationally symmetric aberrations are introduced, but more important is the defocus. In the final figuring of the secondary (against the primary), the image is made aberration-free at the nominal image plane. After that time, if the spacing is changed, degradation due to defocus may be serious while the addition of rotationally symmetric aberration is negligible. Defocus caused by motion of the secondary relative to the primary is 30 times that caused by an equal motion of the instrument package, indicating that the critical focus problem is maintenance of the mirror spacing. Monitoring focus change at the focal plane, however, permits compensation of thermally induced power changes in the mirrors.

A lateral separation focus sensor in principle detects the absolute focus by autocollimation but in practice is suitable only for sensing changes in focus in a system such as the LST. Current devices



of this type measure focus changes of  $0.006 \lambda$  rms at the wavelength of the focus sensor light source. Assuming a 900-nm light source, the focus sensor limit for the system at 632.8 nm is about  $0.009 \lambda$  rms.

As in the case of the alignment sensors, it is expected that the focus change sensor will be used just before each observation. Other factors that limit the accuracy of focus are primarily thermal drift of the structure during an observation and the initial absolute focus accuracy.

Absolute focus may be accomplished by through-focus runs of the focus-sensitive instruments. On-orbit determination of absolute focus is considered necessary because of the difficulty in determining the residual power of the large autocollimating flat that will be used in the ground alignment of the telescope. A through-focus run for the particular focus-sensitive instrument in question will not establish the best focus position as accurately as it can be determined interferometrically but has the advantage of being directly related to the image plane of the data instrument.

(c) Figure Control. In regard to primary mirror figure control, the primary mirror is designed to retain its optical figure in space without the use of the figure control actuators that bridge the space between the back of the mirror and the pressure bulkhead. Nevertheless, should there be some degree of unpredicted creep in the mirror, or should the thermal control system fail in a way such as to cause a significant figure error in the mirror, these actuators can be used to apply correcting forces to the back of the mirror. The commands to the actuators are derived from the figure sensor information.

Concerning figure control under ground test conditions, when the OTA is assembled and subjected to the influence of gravity, the figures of the primary and secondary mirrors must be controlled to the extent of making ground tests of the system meaningful. The secondary mirror mount has nine points of axial support so that the gravity sag is controlled to a large extent. The primary mirror mount is a three-point support which will require augmentation during ground test. One means of achieving such augmentation is through the use of the figure control actuators.

(6) Light Shield. A light shield will be extended for orbital viewing to exclude direct sunlight from the telescope and to reduce the intensity of scattered light from all sources at the image plane. It was determined (see Chapter V) that a truncated light shield would be highly desirable for viewing in the solar hemisphere since the relatively large heat input from the

sun would overheat the primary mirror after relatively short observation periods and direct sunlight would interfere with faint source viewing.

The reference design 45 degree truncated light shield which extends 6.76 m (270 in.) forward of its stowed position was incorporated. The light shield is made of aluminum alloy; deployment is by means of motor-driven tubular members. These members are wrapped on storage drums; when they are extended, they form slotted tubes. There is no rotation of the light shield with respect to the OTA.

c. Scientific Instrument Package (SIP). The SIP is an energy selection, analyzing, and processing system that has been tailored to match a 3 m diameter, f/12 Ritchey-Chretien-type telescope. Energy reaching the focal plane is selectively imaged on a variety of detectors or spectrographs. The selection and design of the individual instruments is the result of preliminary tradeoff studies of several system configuration concepts.

(1) Configuration. The general SIP configuration is shown in Figure IV-10. The basic structure consists of three rings which are tied together by trusses to provide bending and torsional stability. All of the imaging detectors can be replaced and accurately repositioned without removing the associated optical elements or affecting any other subassembly of any instrument. The instruments located between the second and third rings are removed axially and the instruments between the first and second rings are removed radially. The configuration of the unit mounting pads is designed to allow for maximum variation of instrument configurations and growth. An additional instrument position is provided for adding a supplemental, redundant or "yet to be conceived" instrument.

(2) Instrument Package Effectiveness. The instruments are capable of operation for longer than the precursor LST mission lifetime of 5 years with maintenance of the life limited items. To facilitate the extended life of the LST instrumentation, the package has built-in features such as independence of instrument assemblies and subsystem accessibility despite the apparently dense packaging. The accessibility of the modules permits periodic maintenance and repair in orbit with the particular advantage of ready replacement of outmoded instruments. Peltier thermoelectric devices are utilized to cool the critical portions of the cameras.

(3) Instrument Complement. Current scientific objectives and technological capabilities — existing or anticipated — have, to a large extent, led to the tentative inclusion of the following instrumentation subsystems into the SIP:

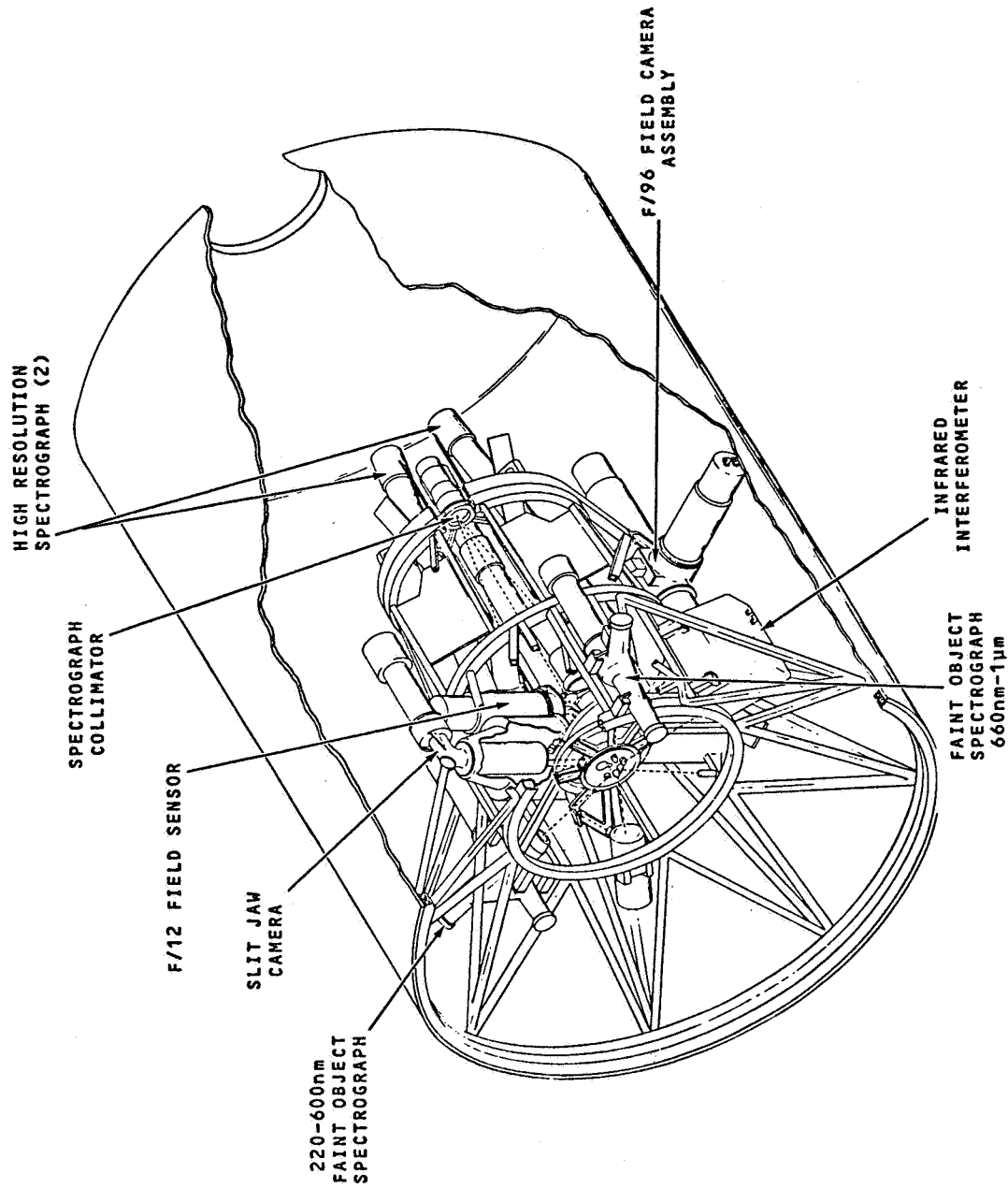


Figure IV-10. SIP configuration.

1. High spatial resolution camera, f/96.
2. Two high resolution spectrographs.
3. Three faint object spectrographs.
4. Fourier interferometer.
5. Wide field camera, f/12.

The instruments described here are not to be construed as the final choice of instrumentation for the LST. Rather, as chosen, they represent a reference design configuration.

A functional block diagram of the SIP is shown in Figure IV-11. The figure sensors and focus sensors are included in this diagram; however, their functions are associated with the OTA. The fine pointing sensor is also included under the control of the ACS system of the SSM.

(a) High Spatial Resolution Camera Assembly (f/96).

The f/96 camera is a cross-shaped cylinder mounted to the outboard side of the SIP structure. The camera contains three sensors from which the experimenter can choose for response in a particular spectral range of interest or, by successive observations, explore the total available spectral range. The spectral bands or ranges are as follows:

1. Range I — 115 to 300 nm.
2. Range II — 160 to 600 nm.
3. Range III — 500 to 1100 nm.

Each of the three sensors is provided with a filter select mechanism which permits the inclusion of up to four spectral filters. The positioning of the f/96 energy bundles on the desired sensor's cathode is controlled by the mirror select and drive assembly. A shutter capable of occulting the energy entering the sensor area is provided to protect the sensors and to permit measurement of sensor dark noise.

(b) High Resolution Spectrographs. The two high resolution spectrographs are nearly identical instruments; one covers the spectral range of from 110 to 180 nm and the other the spectral range of from 180 to 350 nm. The major differences in the instruments are the grating ruling frequencies and the photocathodes of the detectors.

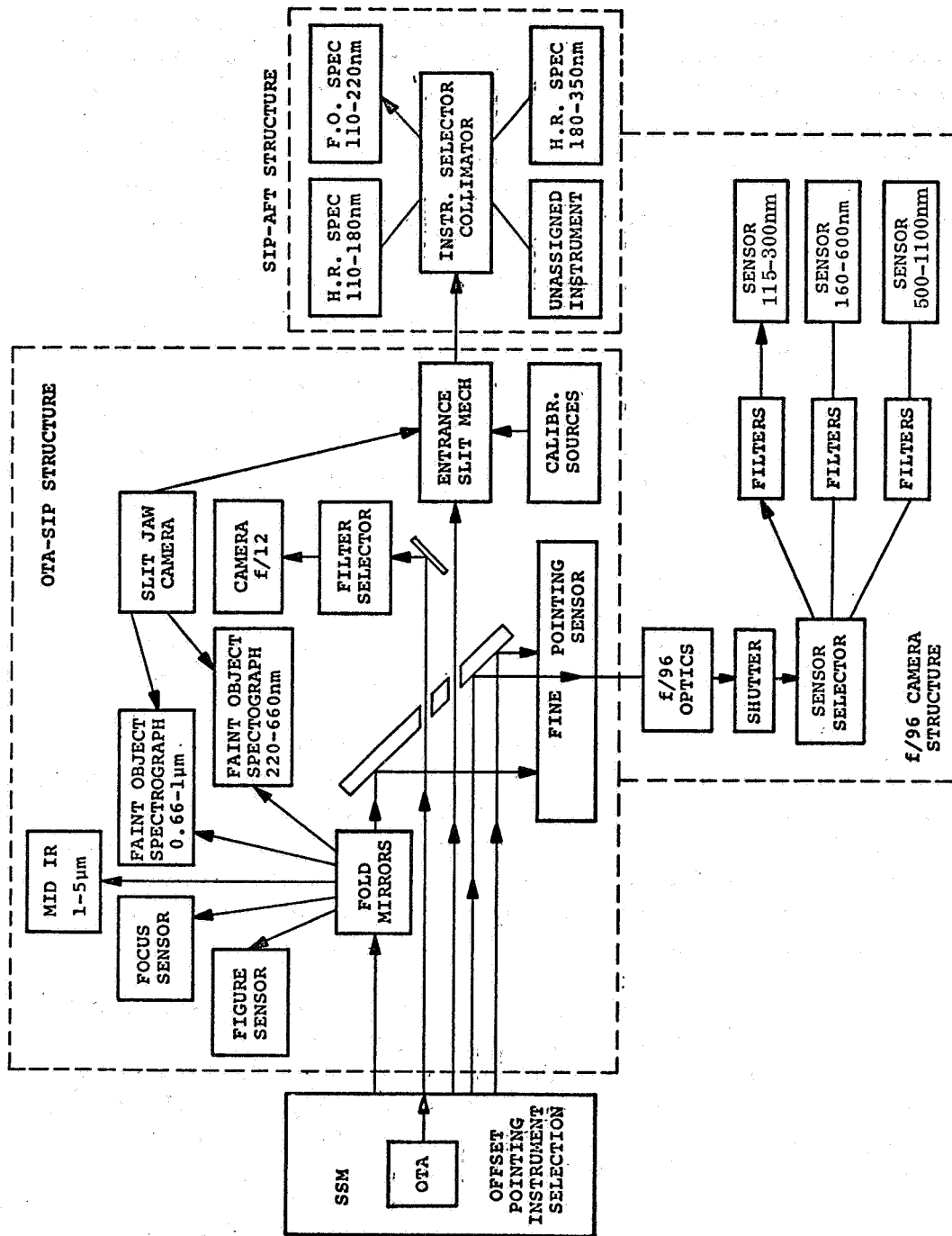


Figure IV-11. Scientific instrument package functional block diagram.

The two spectrographs are the largest of the instrument group and are located in the aft section of the SIP. Instrument selection in the aft section is accomplished by first offsetting the LST so that light from the object of interest passes through the slit. Then the off-axis collimator is rotated to the position which directs the light to the selected Echelle grating.

(c) Faint Object Spectrograph. The faint object spectrograph, with a resolving power of  $10^3$ , covers the spectral range from 110 to 1000 nm with three instruments. The first is a single dispersion instrument which covers the range from 110 to 220 nm using two interchangeable gratings to break up the spectrum into two intervals, 110 to 160 nm and 160 to 220 nm. This unit is located in the aft section of the SIP with the high resolution instruments and is accessed with the same collimator mirror.

The other two units which complete the faint object spectrograph use the same package outline and are smaller than the first. These instruments are located in the forward section of the SIP and each is accessed by a small pickoff mirror located about 0.3 mr off axis. The telescope is offset to select one of these mirrors. The second instrument covers the spectral range from 220 to 660 nm. It contains a dichroic beam splitter which reflects the light in the 220 to 350 nm range and transmits the light in the 350 to 660 nm range.

The third instrument of the faint object spectrograph is a single grating version of the previous instrument with a grating selected to cover the range of from 660 to 1000 nm. This instrument requires a III-V photocathode, which is presently early in the development cycle.

(d) Mid-IR Interferometer Assembly. The lack of non-cryogenic vidicon tubes capable of efficient operation in the middle infrared range (1 to 5  $\mu$ m) and the lack of efficient dispersive systems for that range lead to a choice of a modified Michelson interferometer. The interferometer is used to generate the interferogram of the source. A Fourier transform program, performed by ground computer, converts that interferogram into the power spectrum of the source.

(e) f/12 (Wide Field) Camera. The f/12 camera is a single instrument designed for the initial survey of the vicinity of the experiment target. This application dictates the largest possible field of view, permitting the observation of known constellations or star groups. For the purpose of mapping these targets, a second requirement evolves, which is sensitivity and resolution.

The wide field camera is at the Cassegrainian focus of the telescope and receives its light after only three reflections. The camera

is accessed by offsetting the telescope. The light passes through the large hole in the main diagonal to the second diagonal, which reflects the light to the 50 mm square photocathode.

(4) Ancillary Subsystems.

(a) Slit Jaw Camera. Neither of the three spectrographs is equipped to acquire a target's image nor to hold an image in its slit. With the aid of the field select mirror assembly, the latter image acquisition and maintenance is performed by the slit jaw camera. The camera views the target field, which has already been imaged in the immediate vicinity of the spectrographic slit, and displays that view at a remote (ground) station. The experimenter analyzes the display and, if necessary, originates the appropriate orientation commands to position the target's image into the slit, admitting light to the spectrograph.

(b) Field Select Mirror Assembly. Located near the telescope focal plane, the field select mirror assembly is an array of mirrors that apportions the field of view among the various instruments. The completely passive role of this assembly is its most important attribute. It consists of about a dozen different mirrors whose principal requirement is to stand perfectly still.

(c) Supporting Mechanisms. Supporting mechanisms located throughout the SIP serve a variety of functions. The following list gives these supporting mechanisms and their functions.

Instrument	Mechanism Function
1. Spectrograph Selector	Rotate off-axis paraboloid collimator; four positions
2. Faint Object Spectrograph 0.11 to 0.220 $\mu\text{m}$	Select grating for wavelength range; two positions
3. Three Slit Changers	Rotate slit discs; four positions
4. Four Filter Selectors	Select filters for three f/96 cameras and one f/12 camera; includes fail-safe return to open position
5. F/96 Camera	Camera select mirror; two at two positions (alternate design)

(5) SEC-Vidicon Camera Tube. The secondary electron conduction (SEC) vidicon is selected as the uniquely qualified camera tube type for LST/SIP applications. This tube has completed an extensive development cycle and environmental tests on the 50 by 50 mm format are in process. The efforts which remain are optimization of the tube and its electronics into a flight configuration or actually into two configurations for the 25 by 25 mm and 50 by 50 mm formats. Additional work is also required on target improvement, i. e., achievement of higher gain and greater capacity. The first reduces the effect of amplifier noise while operating on the dimmest targets; the second permits higher data quality in a single exposure by increasing the number of electrons collectable without target saturation.

d. Support Systems Module (SSM). The SSM interfaces structurally and electrically with the OTA and provides the OTA and the SIP with electrical power, communications and data handling, environmental control, course attitude sensing and control, launch vehicle structural and electrical interface, and docking structure for on-orbit servicing or retrieval by the Space Shuttle.

The SSM is primarily a cylindrical structure with a total length of 5000 mm (197 in.) and an inside diameter (ID) of 3300 mm (130 in.) (Fig. IV-12). The aft end is a shallow cone ending in a standard androgynous docking assembly.

The LST support systems contained in the SSM are structures, thermal control, electrical, communications and data handling, and attitude control. The components of these systems have been arranged so as to provide ease of astronaut maintenance while permitting adequate thermal control of these systems as well as the SIP.

#### (1) Structure

(a) Dimensions. All layout drawings give dimensions in both the International System of Units (SI) and English units; millimeters are given first, followed by inches in parentheses. It should be pointed out that in the layout drawings the basic dimensions are not given as a result of a direct mathematical conversion from millimeters into inches for the following reasons. To whatever measuring system a structure is designed and built, the basic dimensions, as a rule, will be selected to be reasonably round figures. A mathematical conversion from such figures into a secondary system will result in inconvenient and frequently even unrealistic figures in the latter. Furthermore, a structure can be built in one system only; any



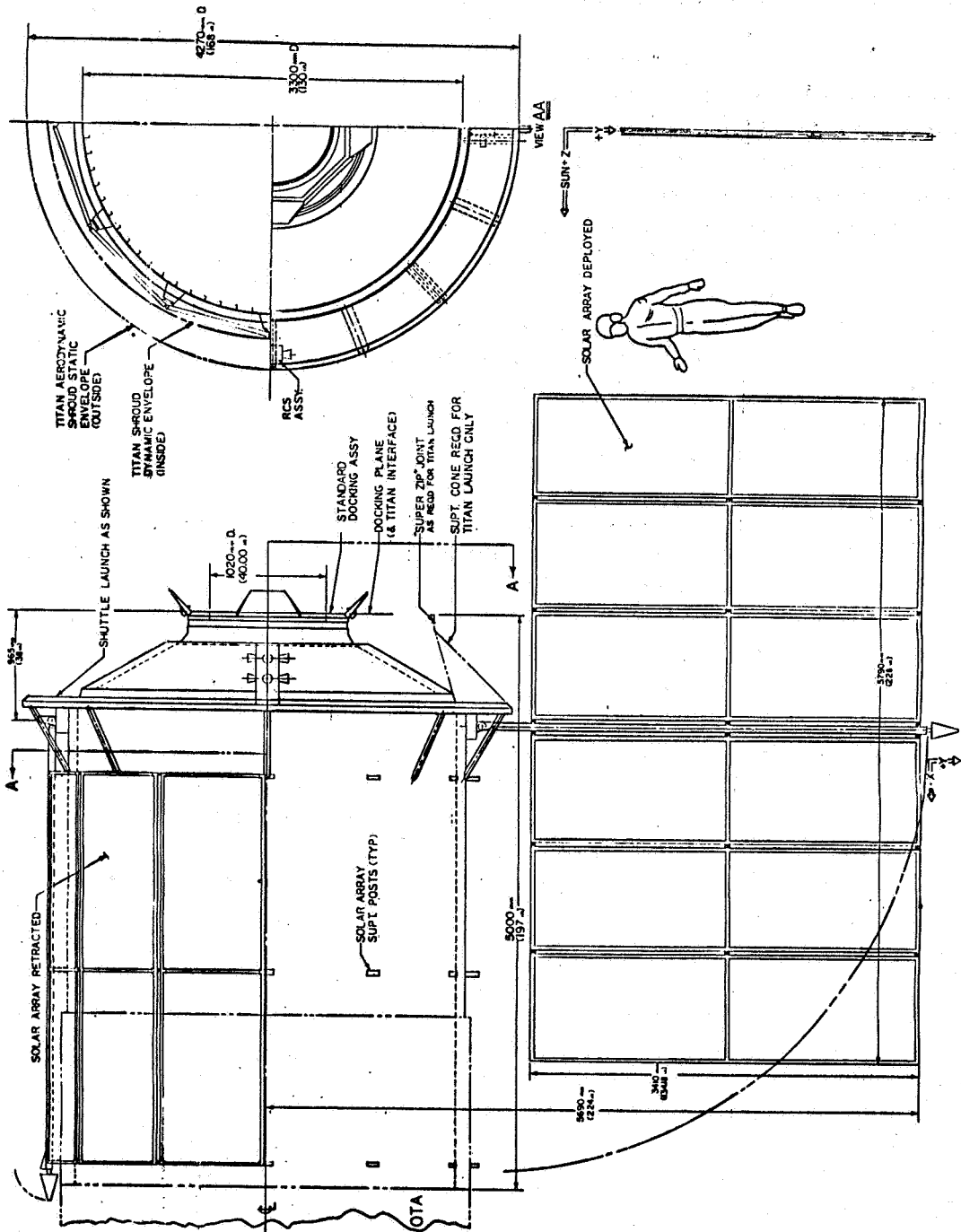


Figure IV-12. Support systems module reference design.

figures pertaining to a secondary system will only serve as a means for more general understanding. Therefore, the dimensions in the layouts are rounded off so as to give expectable figures in either system. The deviations from the mathematically correct conversions are held to less than 5 mm.

(b) Description. The SSM (see Fig. IV-6) provides a pressurized environment to allow SIP maintenance by two astronauts without space suits and is also used to carry forces and moments as required by the various flight and operational conditions. The SSM is essentially a cylinder of 5000 mm (197 in.) in length and 3300 mm (130 in.) ID (Fig. IV-13). It is an aluminum structure consisting of a stiffened, pressurizable shell protected by a meteoroid shield. Its forward end is bolted to a ring which, together with the honeycomb bulkhead, forms the structural base of the OTA. The aft end of the SSM is formed by a conical structure which also provides the tie-in to the docking structure. The conical section is protected by a meteoroid bumper. The hatch opening of the docking structure has a diameter of 1015 mm (40 in.). During orbital operations that opening is covered by a meteoroid shield for protection of the SSM interior.

A solar array, consisting of two wings of stiffened panels which fold around the SSM for launch, is mechanically extended upon deployment (see Fig. IV-6). The same mechanism that extends the wings may be used to retract them to permit the LST to be taken into the Shuttle payload bay for earth return. The solar array can be rotated about the Y-axis to maintain an optimum orientation to the sun.

The various systems components in the SSM have been arranged to provide the least interference with the astronaut during maintenance operations and to permit adequate thermal control of the SIP as well as the subsystems. As many components as practical were placed on the inside surface of the aft cone between the docking port and the cylindrical section. The remainder were placed in four longitudinal columns as far aft as possible along the wall of the cylindrical portion of the SSM. The locations of the components were determined by thermal requirements; those with higher allowable operating temperatures were placed on the sun side, while those with lower temperature limits were placed on the anti-sun side. The four columns are 45 degrees away from the instrument packages on the SIP so that the astronaut is provided a maximum clearance for package replacement. This arrangement also allows for heat radiation from the SIP with a minimum of interference from the support system components. Preliminary analysis indicates that the configuration shown provides adequate working space and acceptable system temperatures.

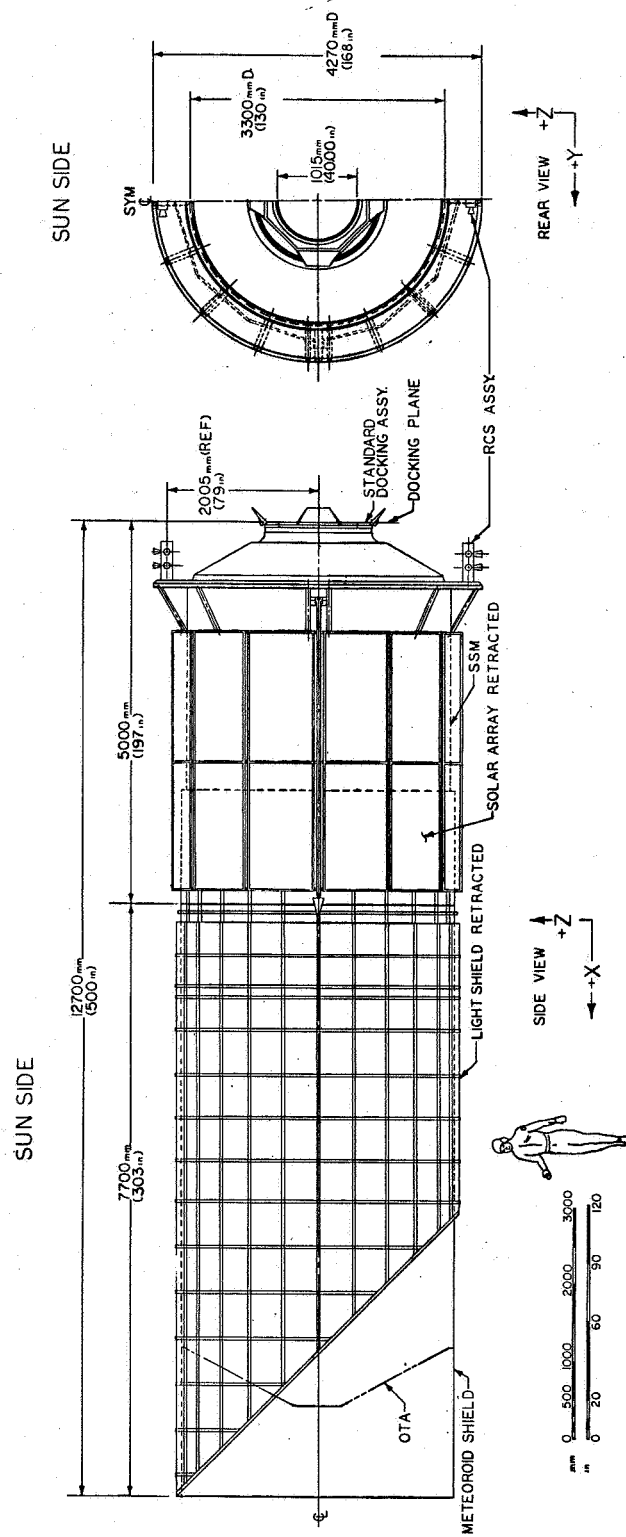


Figure IV-13. LST assembly stowed configuration.

(c) Titan Constraints Upon Reference Design. The aerodynamic shroud [Viking standard 17.06 m (56 ft) shroud] dynamic envelope limits a 3680 mm (145 in.) diameter LST to 12 700 mm (500 in.) length and also requires an aft cone for SSM stiffening and for support of the shroud. Figure IV-14 shows how the LST uses almost all of the available shroud volume. Figure IV-15 shows how the aft cone remains with the LST spacecraft. The Shuttle recovery requirement means that the fittings for such recovery must also be included for the Titan launch. If the Titan launch requirement were to be removed, the Shuttle launch, using a swing table, would permit a longer and more massive LST with a larger diameter. The Titan launch limits LST size and requires shroud/LST orientation to clear the Shuttle tie-points. The alternate graphite-epoxy shell OTA would permit a longer LST for Titan launch. The aft ring Shuttle tie-point probably must be provided with some thermal protection for the Titan launch because it extends clear of the shroud.

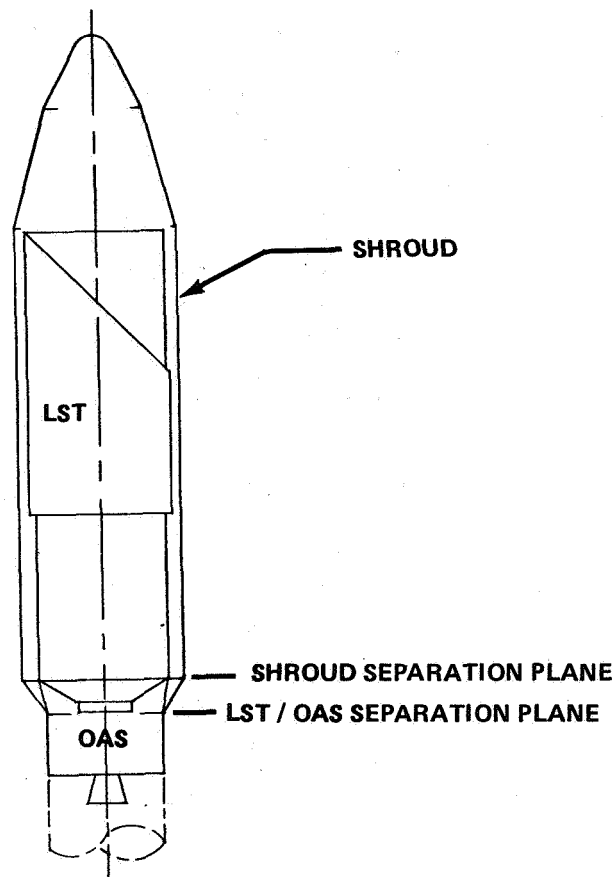


Figure IV-14. LST Titan launch configuration.

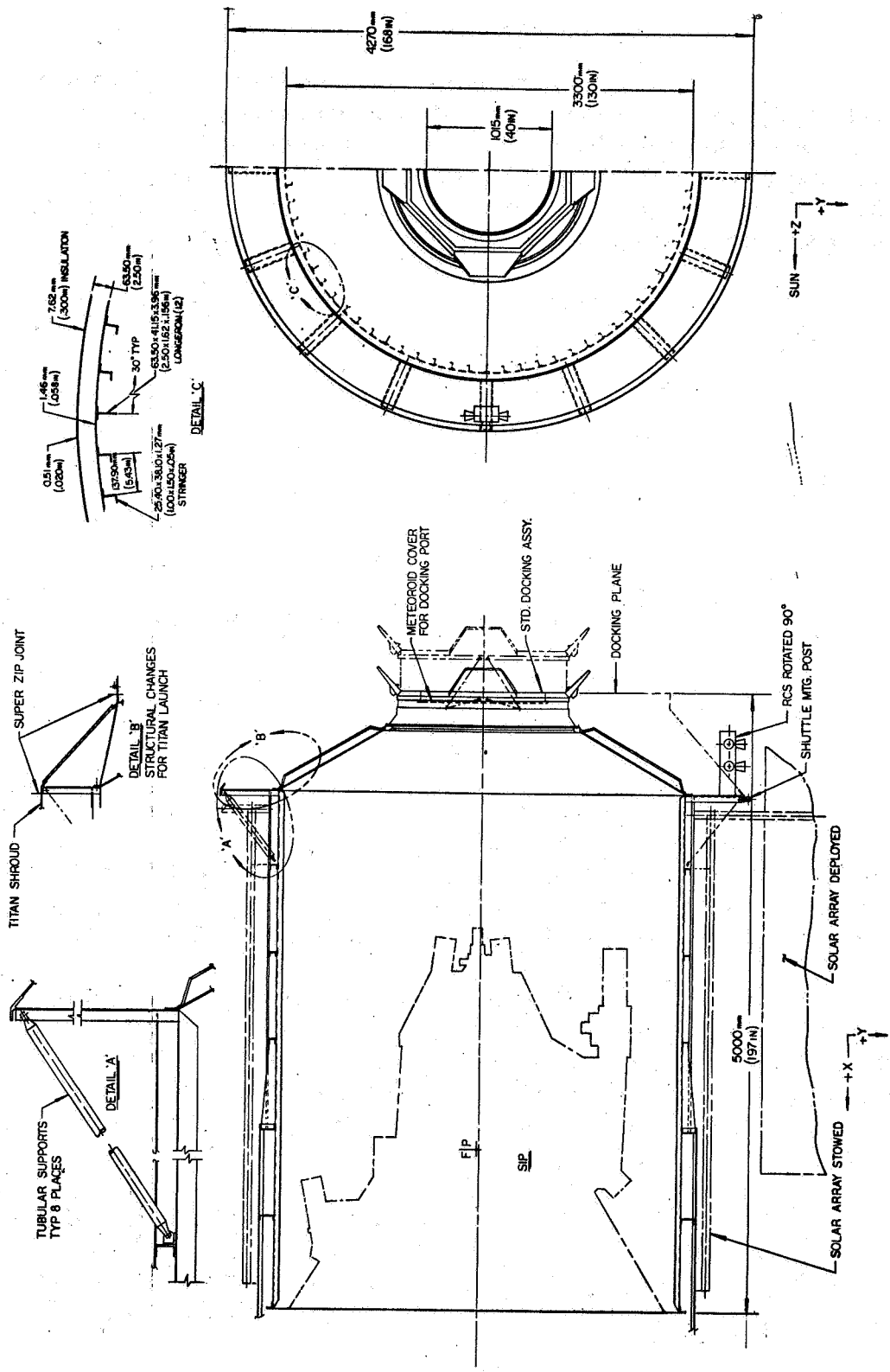


Figure IV-15. SSM reference design longitudinal cross section.

## (2) Thermal Control

(a) System Description. The function of the SSM thermal control system (TCS) is to maintain the equipment located in the SSM within prescribed temperature limits through all mission phases. System design must also allow for dissipation of heat from the SIP through the walls of the SSM. Thermal control is accomplished through the use of the following components and features (Fig. IV-16):

1. Paint.
2. Radiator Plates.
3. Louvers.
4. Twenty-four-layer External Insulation.
5. Polished-Aluminum Sheet.
6. Thermostatically Controlled Heaters.
7. Favorable System Component Grouping.
8. Isolated Battery Compartments.

Thermal control of the OTA is accomplished through the use of multilayer insulation, thermal control coatings, and thermostatically controlled heaters (Fig. IV-16). Thermal control of the SIP is achieved by the use of heaters and Peltier thermoelectric devices within the SIP and radiation of heat from the SIP to the walls of the SSM (Fig. IV-16).

Temperature control is achieved by establishing a heat balance between the absorbed radiation (solar, albedo, and earth), internal heat dissipation, and emitted energy. High efficiency multilayer insulation, thermal covers, and coatings minimize the effect of large variations in incident radiation caused by changes in orbital parameters or LST orientation.

Components such as the batteries that experience large variations in internal heat dissipation during an orbit are placed in compartments separated from the other electronic equipment. Their heat balance is closely controlled with separate louvers, radiating surfaces, and heaters.

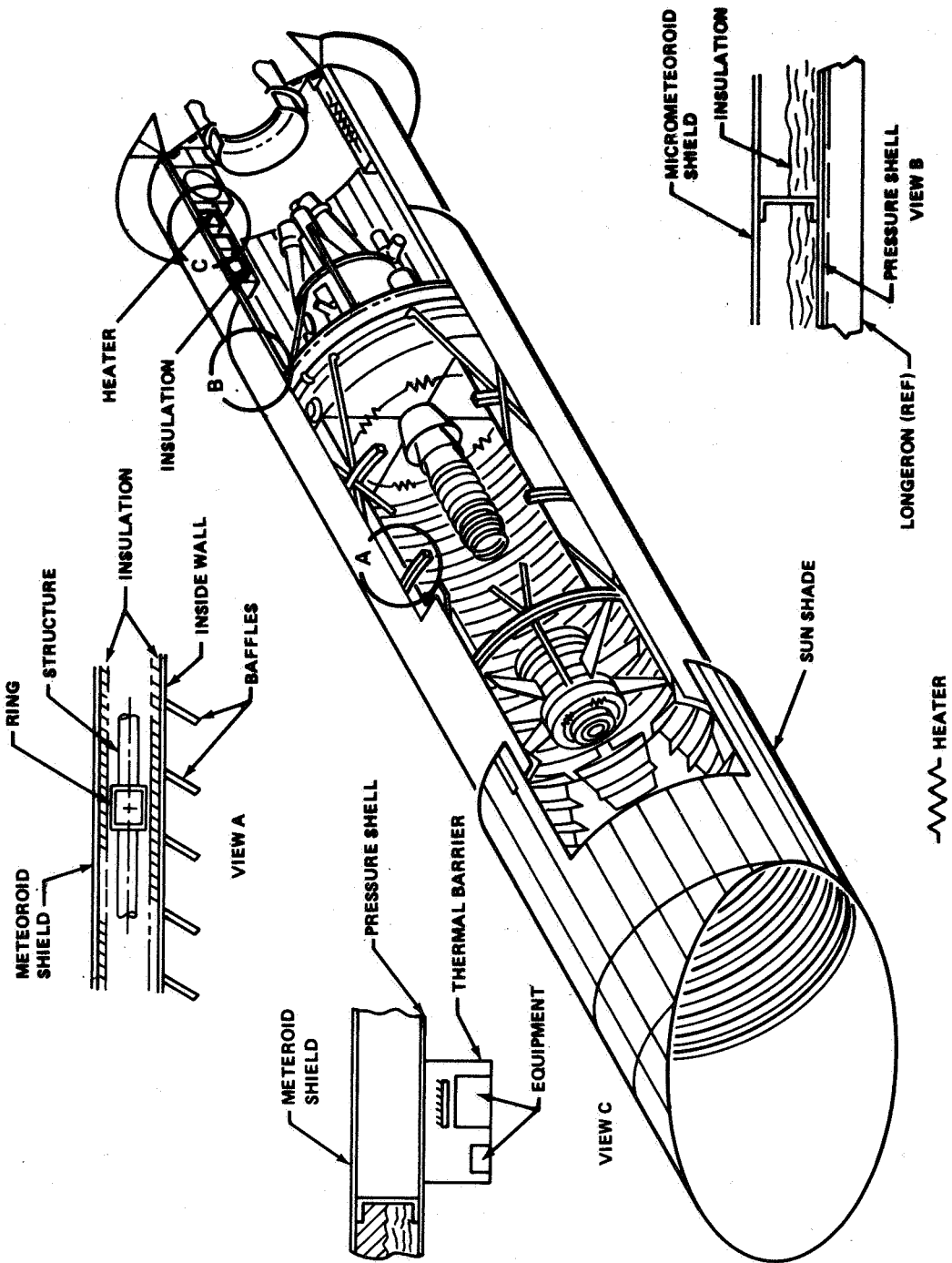


Figure IV-16. LST thermal control features.

A small amount of thermal control heater power is provided to certain components that may require a warmer environment than that provided by adjacent equipment. Commandable standby heaters are also placed on major heat dissipating system components to maintain a constant observatory heat dissipation, should it be necessary to turn off units for extended periods of time. The standby heaters do not impose an additional power load because they use power made available when components are turned off.

The amount of heat emitted from the SSM is controlled by the treatment of the surface on the pressure shell. Variations in heat absorption and dissipation that might result from orbital excursions are attenuated by these treated surfaces and by the meteoroid shield. The surfaces are designed to maintain the observatory thermal balance under long-term orbital, seasonal, and orientation conditions, as well as to provide flexibility to respond to changes in thermal requirements that may be identified during development.

During transient eclipse and short-term off-point modes, the thermal inertia of the LST greatly facilitates temperature control. This inertia also serves to maintain temperature control during short-term boost and transfer orbit conditions when incident heating and internal heat dissipation conditions are not within long-term orbital design values.

(b) Hardware Description. The items described as follows — louvers, insulation, paint, and heaters — represent the total thermal control hardware deliverables. Table IV-4 lists the SSM TCS hardware with corresponding descriptions and performance characteristics.

Each SSM louver assembly consists of four separate blades. The louver design is similar to that used on the High Energy Astronomy Observatory (HEAO). Each louver assembly is placed on the battery baseplate external surface and views the pressure shell. Bimetallic actuators sense the local battery baseplate temperature and provide the torque to rotate the louver blades. The bimetallic springs are thermally coupled to the baseplate by anchoring the frame to the baseplate, painting the bimetal, isolating the louvers with fiberglass shafts, and insulating the actuator housing.

The insulation installation techniques are similar to those of other spacecraft. The insulation material is 24-layer aluminized Mylar. All the blankets are made in sections to fit around the spacecraft between the pressure shell and the meteoroid shield. Venting occurs through the gaps and perforations in each layer. The perforations are staggered to avoid radiation heat loss.



TABLE IV-4. SSM THERMAL CONTROL HARDWARE DESCRIPTION

Item	Description	Location	Area (m <sup>2</sup> )	Mass (kg)	Performance
Louver Units	0.5 m x 0.33 m - Four blade unit, one per battery (1.12 m <sup>2</sup> /bat.), six total, sized to handle 35 W (max.) orbital average battery heat dissipation at 10°C	-Z, +Y, and -Y axes on pressure shell surface for each battery baseplate.	6.72	5.6	$\epsilon$ open = 0.7 at 14°C $\epsilon$ closed = 0.33 at 6°C
External Surface Insulation	24 layers of aluminized Mylar. (1) - 1-mil cover sheet aluminized side faces inward (22) - 1/4-mil crinkled filler sheets - aluminized side faces inward with 4 1/8 in. diam vent holes per square foot. (1) - 1-mil inner cover sheet - aluminized side faces inward	Outside of the pressure shell over the area used to dump heat from SIP	29.0	11.0	$\frac{K}{\Delta X} = 0.009 \frac{W}{m^2 \cdot C}$
Internal Insulation	Polished aluminum sheet	Covering all electronic equipment so SIP is not affected by SSM	6.0	3.3	$\epsilon = 0.04$ surface facing SIP
Paint	Zn <sub>2</sub> Ti O <sub>4</sub> (zinc orthotitanate) <sup>a</sup>	Outside cover of micro-meteoroid shell	39.1	16.0	$\alpha = 0.120$
	High emittance white Black	Inside pressure shell Inside micrometeoroid shield	38.0 39.0	15.1 15.8	$\epsilon = 0.92^b$ $\epsilon = 0.85^b$ $\epsilon = 0.85^b$
Heaters	Thermostatically controlled resistance type PT-4-B-13004	As required	4.0	5.5	≈ 250 W

a. This is a new paint. Research test data  $\alpha$  degrades 0.005/yr. Will be a test paint on Skylab.  
b. Recommended materials to meet NASA ATM 50M02442 (low outgassing specification).

A thermal barrier is maintained between the SIP and the SSM compartments by a polished aluminum sheet, with the polished surface facing the SIP (Fig. IV-17). This was used instead of a thermal blanket to eliminate the need for an insulation purge due to moisture contamination during manned maintenance.

Zinc orthotitanate ( $Zn_2TiO_4$ ), a high-emittance white paint, was selected as a design reference for use on the SSM external surface. This paint, one of many being tested on the Skylab program, was chosen because of its low  $\alpha/\epsilon$  ratio and low degradation alpha value of 0.005 per year. As a backup to the  $Zn_2TiO_4$  paint, a mosaic of optical solar reflectors (OSR) and white paint could be used.

The heaters are standard, flexible strip heaters that can be bonded to a conducting surface with a low outgassing room temperature vulcanizing (RTV) adhesive. The heaters are available in wattages from 1 to 10 at 28 volts. Heaters are enabled by command, after which turn-on is controlled automatically by a standard snap-acting thermostwitch. The number, size, and setting for the heaters are to be determined.

### (3) Electrical System

(a) General Concepts. The LST requires an electrical system to accomplish the functions necessary during the various phases of the mission. For this Phase A study it was assumed that the LST consists of three physically and electrically separable parts — the SSM, the SIP, and the OTA. Because of its role and position in the vehicle, the SSM section of the electrical system provides the primary system functions and accomplishes integration.

The electrical system includes two subsystems:

1. Electrical Power Subsystem (EPS).
2. Electrical Distribution Subsystem (EDS).

The electrical system also has intimate interfaces with the following systems and subsystems:

1. Communications and Data Handling System (C&DH).
2. ACS.

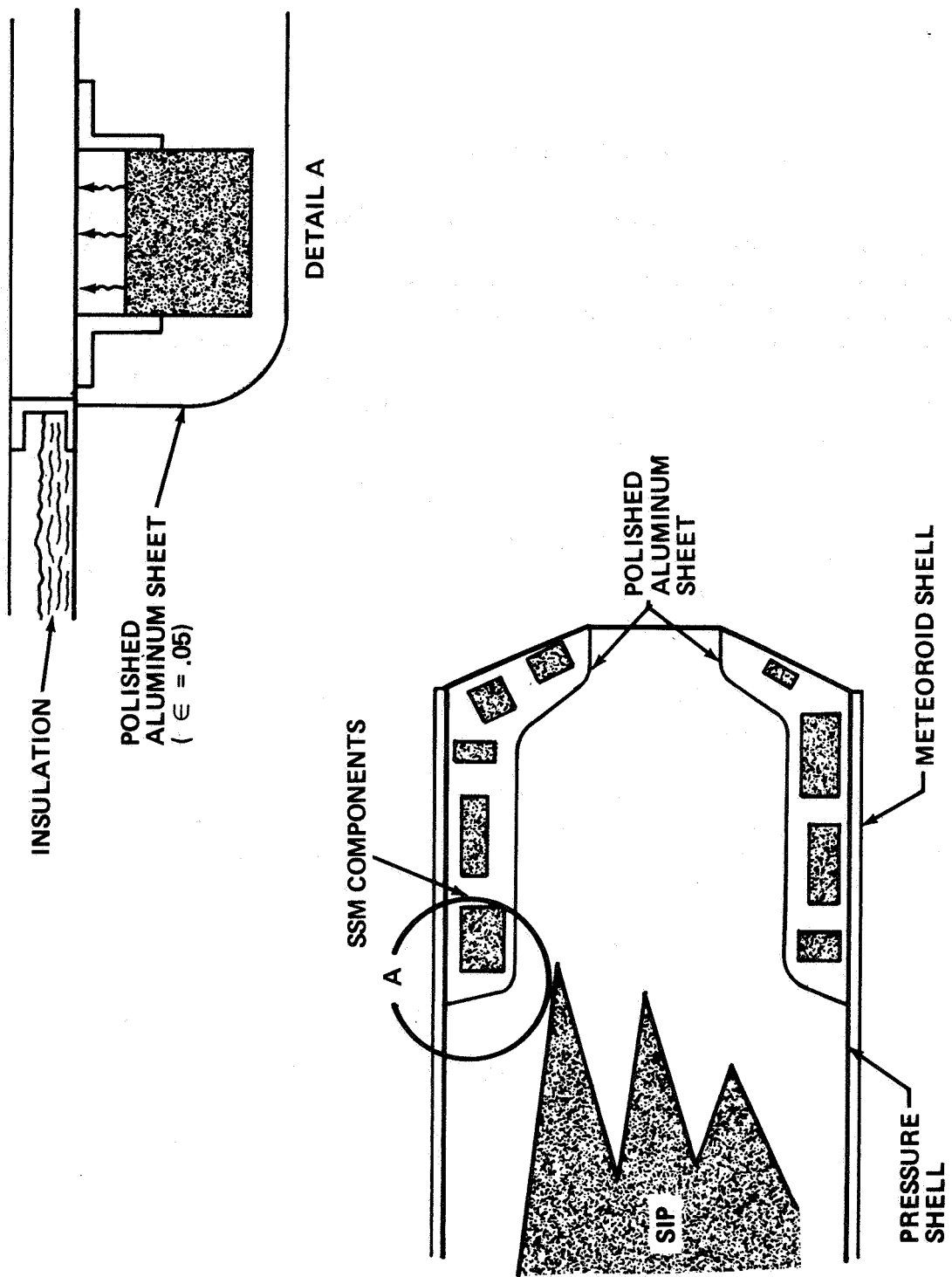


Figure IV-17. SSM thermal control concept.

3. TCS.
4. RCS.
5. OTA Electrical Subsystem.
6. SIP Electrical Subsystem.

The electrical system configuration was primarily influenced by the configuration and electrical requirements of the LST, the 5 year mission, the high reliability needed, and the considerations given to cost and maintenance. Critical components and networks were made redundant because they determine the probability of mission success based on the practicality of in-space maintenance. Low cost rather than mass and performance optimization was of primary importance in the selection of design concepts. Existing technology has been used throughout.

Since very little of the reference hardware has been qualified for the life and reliability required for the LST, maintenance is essential to achieve mission objectives, especially when components with known life limits are considered.

The simplified block diagram of the electrical system, given in Figure IV-18 shows the major components of the EPS and the EDS to be described.

(b) Electrical Power Subsystem. The EPS must furnish power to all the LST electrical loads and must satisfy system losses during orbital operations. The preliminary load analyses discussed in Chapter IV of Volume V determined the following requirements:

- |                            |              |
|----------------------------|--------------|
| 1. Orbital Average Power   | 1283 watts   |
| 2. Orbital Period          | 96.9 minutes |
| 3. Max. Occultation Time   | 35.5 minutes |
| 4. Peak Power (short term) | 1785 watts   |
| 5. Voltage at Loads        | 28±2% Vdc    |

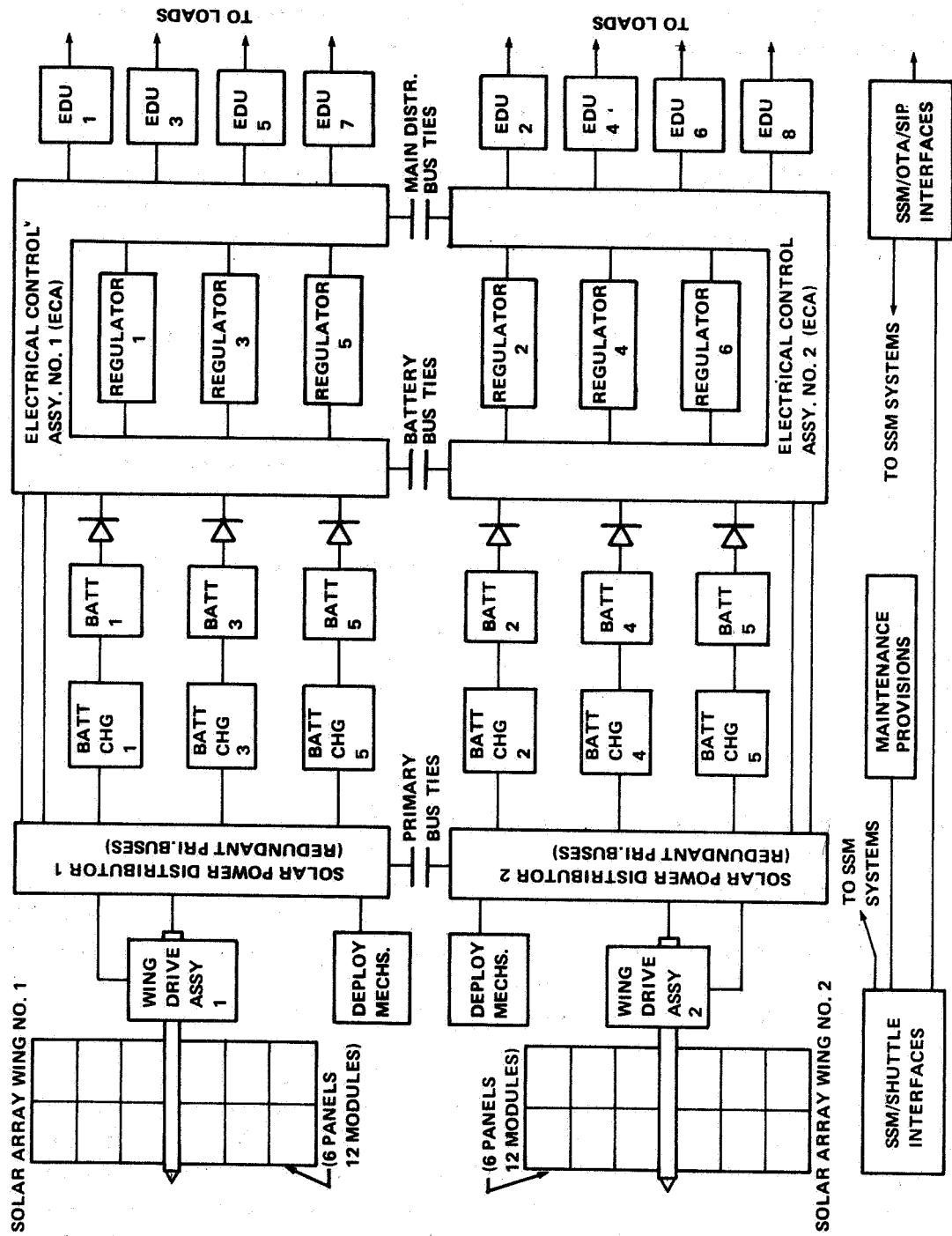


Figure IV-18. Reference electrical system.

The reference EPS has a peak power rating of 2700 watts and is designed for an orbital average of 1500 watts, which provides a margin of 217 watts for potential load growth. The system operates at an efficiency of 77.8 percent, including energy storage and distribution losses.

Except for its size and the features required for adaptation to the LST, the EPS is a conventional solar-array battery system, with power conditioning and output series regulators to control voltage. Design and performance criteria determined for existing hardware modules and qualified components have been used for establishing concepts and sizing the system.

The EPS configuration, power conditioning, energy storage, and the solar array are discussed in the following paragraphs.

A centralized series regulator configuration was used because it simplifies: (1) accounting for power conditioning losses during Phase A, (2) preliminary design of solar arrays and batteries, and (3) power management. Configuration tradeoffs indicated small differences in performance affecting battery and array size and costs. The advantages of a given configuration depended on subtle differences such as the ratio of regulated to unregulated loads, use of array maximum power, charge control, and the voltage tolerance of specific loads. Depending on power interface management, the centralized concept appears to be the most cost effective.

Six regulator assemblies, each rated at 750 watts and 28 Vdc, provide ample peak capacity and inherent overload protection of the primary power sources. Power regulated at  $28 \pm 2\%$  Vdc is delivered to the main buses for distribution to loads. These units are sized so that three can sustain the full LST load. In the event of more serious load or regulator faults, the EDS cross strapping favors the critical loads that could jeopardize recovery and maintenance. Considering the very remote chance of such conditions, one regulator assembly is sufficient to support critical loads.

Energy is stored during sunlight periods of the orbit by six rechargeable, nickel-cadmium battery assemblies. To assure reliable charge control for a wide range of load and environmental conditions, six charger assemblies — one dedicated to each battery — receive and condition power from the solar buses and deliver the necessary recharge power. Maximum power tracking networks permit the chargers to use the maximum power available from the array when needed. Should solar array power

become limited, as may occur during off-sun roll maneuvers, the chargers will assure that load demands are first met before recharging the batteries.

Each battery assembly consists of 24 series cells, and is nominally rated at 29 Vdc, 30 ampere-hours. Three cells in each assembly are four electrode types to provide redundant charge status information to the chargers. Temperature sensors incorporated in the battery assemblies provide telemetry information for power management and feedback to the chargers for compensation of charge control with temperature. The energy capacity of the six batteries is 5400 watt-hours compared with the normal LST design requirements of 1024 watt-hours per orbit when the array orientation to the sun is maintained. Thus the average depth of discharge will be 19 percent. With the temperature maintained at  $10^{\circ} \pm 5^{\circ}$  C by thermal control, a battery cycle life in excess of the 2 years is expected.

Polarimetry-type experiments requiring the vehicle to roll can cause the need for additional battery energy. Such requirements are discussed in Volume V, Chapter IV.

The LST mission and configuration constraints require a deployable solar array that can be sun oriented to minimize area and costs. The reference array consists of two boom-mounted wings attached to the aft end of the SSM. The location was selected because it provided the best thermal conditions, minimized reflection influence, and minimized interaction with the sensitive telescope structure. It was later determined that this location did not cause significant control problem or penalties.

Each wing is composed of 12 honeycomb substrate modules on which solar cells are mounted using flat laydown techniques. The modules are connected together to form six rigid, hinged panels which fold out when the boom is erected. Torsion rods effect foldout and a motor-cable system accomplishes retraction. The array configuration and mechanisms are highly sensitive to the LST configuration and the shroud constraints of the alternate Titan launch vehicle. For this reason the array panels wrap around the LST for launch storage and are secured to structural brackets which protrude from the SSM skin above the thermal and meteoroid shielding.

Two degrees of freedom are needed to orient the solar array to the sun. A solar array with a single degree of rotational freedom about the vehicle Y-axis was selected for simplicity and low cost. The second degree of freedom is provided by controlling the vehicle roll position about the X-axis. With a roll freedom of 180 degrees, the vehicle

Z-axis can be maintained sunward and the array can be oriented with a minimum rotational freedom of 135 degrees. Allowing a limit tolerance, the rotational freedom was set at 145 degrees to satisfy orientation requirements. Thus the positional limits of a vector normal to the array with respect to the X-axis will be 175 degrees to 320 degrees.

Orientation mechanisms are interlocked so they cannot be energized prior to array wing deployment. Once the wings are erected, controlled motor-gear drive assemblies attached to the cylindrical booms and located in the SSM achieve rotation. Dry impregnated, space-proven bearings, located within the drive assemblies and on the shroud and mounting support structure of the SSM, permit rotation and afford adequate support for the large wings.

Continuous orientation of the solar array is not required and is avoided to eliminate motional disturbance that could interact with the highly sensitive attitude and stabilization controls of the LST. Array orientation, therefore, is initiated by ground command via the transfer assembly prior to the start of an observational or experimental period. The array will then be positioned within  $\pm 5$  degrees of the sunline.

An average array power of 3054 watts is required to support the 1500 watt design load during maximum occultation orbits. The reference array has an end-of-mission (EOM) rating of 3161 watts at the average design temperature of 63° C. Using the most cost effective 2 by 4 cm silicon solar cells and protective coverslides, 40 440 cells were required for adaptation to the array configuration constraints. Symmetrical arrangement and standard modules were maintained in determining the number of cells required. Allowing adequate area for cell spacing and panel attachments, the total panel area of the array was 38.1 m<sup>2</sup>. The array was designed for a 5-year life because it is not a good, practical candidate for maintenance or replacement in space.

(c) Electrical Distribution Subsystem. The integration nature of the EDS requires it to be compatible with the subsystem concepts and the electrical and locational requirements of the items it services. The size of the EDS is primarily determined by the capacity required, the peak power, data, and control demands, the need for versatility and growth, and the redundancy provided for reliable operation. The maintenance and checkout accommodations also influence the configuration. The test and maintenance support network is discussed under interfaces.



The EDS provides three levels of distribution similar to a utilities system for protection, control, and versatility. The three power networks are as follows:

1. Power Transmission Network — Transmits and controls primary power between sources, primary buses, and power assemblies. This network consists of distribution and junction assemblies, power controls, protective devices, transmission cabling, and interface devices.

The two solar power distributors (SPDs) control the major part of the transmission network. Each SPD receives power from six cables servicing one solar wing. The wing is electrically segmented into 6 panels and 12 modules for redundancy, protection, and maintenance reasons. Controlled contactors within the SPDs direct primary power along redundant primary buses to EPS components, such as the chargers and array orientation power supplies, and to electrical control assemblies (ECAs), which service the main distribution network. Monitoring and protective features within the SPDs guard the integrity of the primary buses and provide the capability of routing primary power over alternate channels. Remote electrical management of the power transmission network is accomplished via the ECAs or, when in a maintenance or checkout status, by the SPD interfaces with the LST umbilicals. The remote command decoders (RCDs) providing commands to the EPS are located in the ECAs.

Signals from instrumentation provided to monitor the array performance, orientation, and network status are also accumulated by the SPDs. This information is transferred to the EPS data acquisition units (DAUs) for telemetry to ground.

2. Main Distribution Network — Receives and centralizes power from the EPS power assemblies and controls main power feeders. It distributes regulated power to decentralized secondary distribution units sectionalized on a subsystem basis.

The main distribution network centers about the two ECAs that house redundant buses, cross ties, switchgear, controls, and protective devices needed to assure reliable distribution and control of the network. Redundant cabling assures each subsystem access to power. Input switching provides several channels to redundant EPS power sources in the event an EPS assembly becomes faulty. Overload and low voltage protection is provided for EPS equipment and the loads are protected against open circuit and high voltage faults.

The decoders and data units in the ECAs provide the major command and data interfaces for the EPS and distribution networks, thus permitting remote operational control. Such provisions also enhance the protection afforded to assure a reliable life. System integrity is monitored in sections for the various possible faults. Should a fault be indicated, the network responds to isolate the faulty section immediately. Depending on the loads involved and system conditions, subsequent corrective action occurs. For loads considered critical to the survival or recovery of the spacecraft, the network establishes redundant channels and/or sources to sustain the load or its alternate, as the case dictates. For less critical loads, isolation occurs and is indicated by telemetry to ground, awaiting corrective action by remote command. Also, provisions are made to override isolation switching by command. This enables diagnosis of system conditions and assures that a fault in a protection device does not cause premature termination of operations.

Protection against RF and conducted interference is provided in all networks to assure trouble-free operation. The ECAs incorporate transient suppression devices, accommodate the shielding requirements of distribution cabling, and provide for insertion of additional network filtering as needed. Consistent with reliable grounding schemes, discussed in Chapter IV of Volume V, the ECAs provide the single-point ground for the entire system.

3. Secondary Distribution Network — Consists of Electrical Distribution Units (EDUs), cabling, and the test and control interfaces established to provide decentralized, highly adaptive distribution service for the various subsystem loads and requirements.

The LST subsystem power and hardwire interfaces with the EDS are primarily accommodated by the eight redundant EDUs. These are consistent with the system redundancy and subsystem requirements determined to date. However, system concepts allow the versatility of adding or subtracting EDU modules as the system design matures.

Each EDU consists of an input module and one or more output modules as required. The inputs are standardized for common interfaces with the electrical distribution subsystem. Electrical inputs from ECAs, RCDs, and test cable are provided. Output modules consist of a family of adaptable subassemblies selected to satisfy specific requirements of each subsystem. The modular construction of the EDUs is consistent with that of the RCDs and DAUs so that they may be grouped as one functional assembly when needed.

To complete the system protection scheme, the EDUs provide fault and electromagnetic interference protection for the major individual loads in the subsystem that interface with the power networks. Power items to be operated by command are energized by the EDUs. Such command received via the RCDs activate the proper power switching controls. Power semiconductors and relay matrices available in the EDU output modules can be used to produce parallel or subcontrolled stimuli from the serial commands.

(4) Communications and Data Handling. The design guidelines (Chapter II) for the C&DH system were derived from the system requirements of the OTA, and the SSM. The design reference C&DH system contains all the equipment required to manage the flow of data to and from the LST, SIP, and SSM. This includes the receipt, processing, and execution of real-time and stored commands; the processing, formatting, storage and forwarding for transmission of all diagnostic and status information from all LST systems and subsystems; and the routing of scientific data for transmission to ground stations. Primarily this system is concerned with accomplishing three functions:

1. Communications Link Between LST and Ground.
2. Command Distribution.
3. Data Acquisition and Storage.

(a) Communications Link. The ground network being utilized for the LST mission is called the spacecraft tracking and data network (STDN) and is composed of stations from the Manned Space Flight Network (MSFN) and the old Space Tracking and Data Acquisition Network (STADAN) system. Only stations with unified S-band (USB) capability were selected for this mission. Six stations were selected to provide support in tracking the spacecraft, commanding the spacecraft, and retrieving data from the spacecraft in real and near-real time. A block diagram of the LST onboard C&DH system is shown in Figure IV-19.

The reference communications system configuration shown consists of two transponders, a USB transponder called the engineering data transponder with a capability similar to that of the Apollo transponder and a modified ERTS transponder (proposed for the HEAO-C) called the scientific data transponder. The engineering data (PM-FM) transponder and scientific transponder combination provide a flexible communications system.

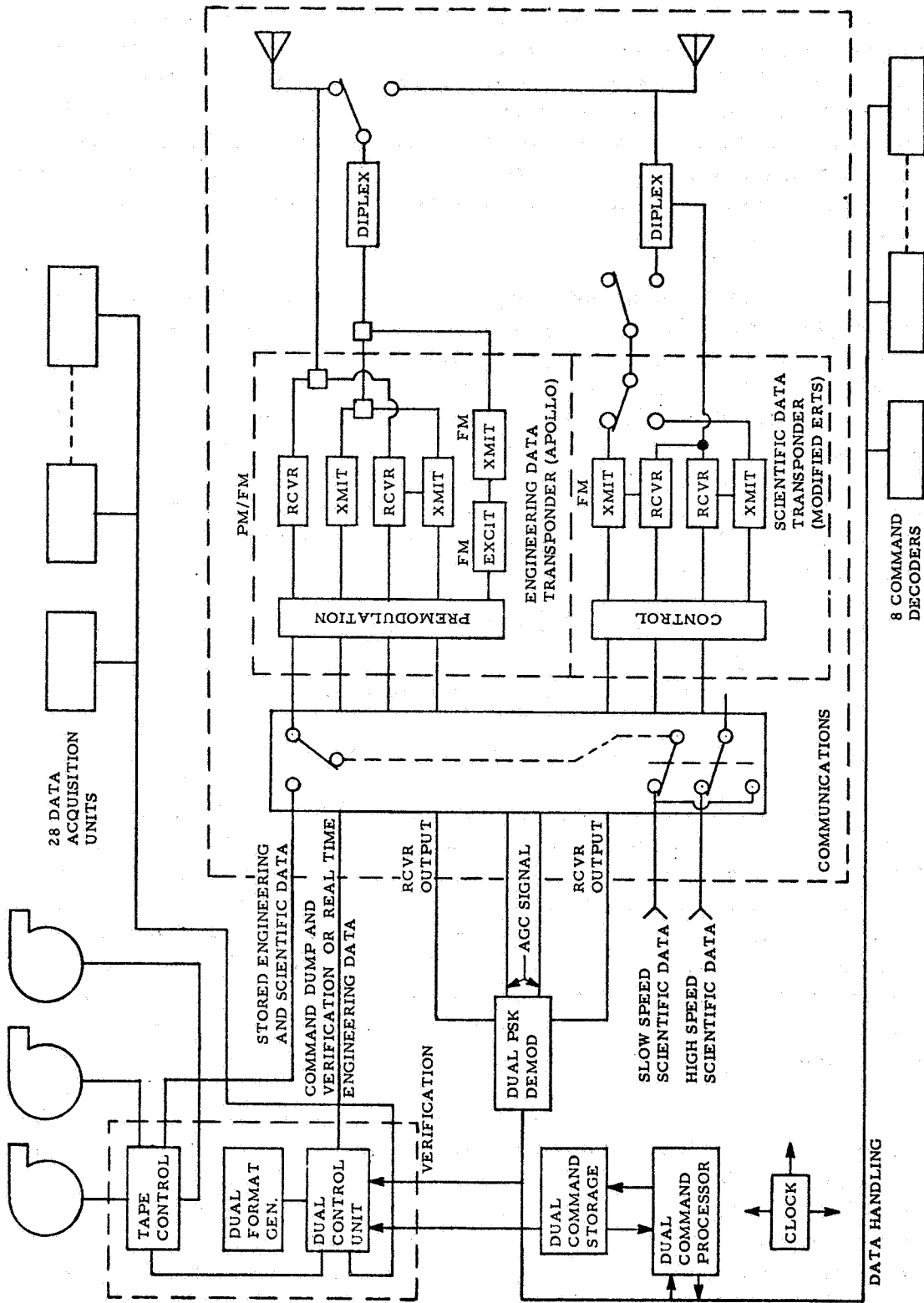


Figure IV-19. LST communications and data handling system.

The PM receiver-transmit capability of the engineering transponder is required for tracking to match the ground station PRN ranging capability in the PM mode. The transponder also provides the PM data downlink for command verification, spacecraft housekeeping and slow television. The scientific transponder provides the high data rate (1 megabit/sec) downlink for the star field camera data.

Two conical spiral antennas are utilized to provide  $4\pi$  sr coverage. One antenna is positioned on the end of each solar array.

(b) Command Distribution. The command distribution system of the LST consists of a command processor, a command memory, and eight addressable command decoders. This system is dedicated to processing two major types of commands: real-time and stored. Upon reception from the ground, real-time commands are sent directly to the command decoders for processing. The stored commands, however, are intercepted by the command processor and stored in the command memory. When the time tag of the stored command agrees with the real-time systems clock, the 11 bit command is put onto the command bus and acted upon as a real-time command.

(c) Data Acquisition and Storage. The Data Acquisition System accepts both analog and digital data (status and diagnostic) from the OTA, SIP, and SSM equipment. These data can be handled in one of two modes. In the real-time mode the data are taken directly from the DAU, formatted, and sent to ground at a rate of 51.2 kbs. In the stored mode, data are stored on magnetic tape at a rate of 1.6 kbs until time for transmission to the ground stations at the 51.2 kbs rate.

Scientific data are acquired in the majority of cases by utilizing SEC vidicons. The distinguishing characteristic of this tube is its ability to store images for several hours. This quality enables the SEC vidicon to integrate for hours on high magnitude (dim) stars and store the data until ground contact is acquired.

This tube storage capability negates the requirement of a mass memory for storing frames of scientific data. The information may be read directly from the tube and transmitted to ground. A single frame of data held on a tube possessing a 50 mm by 50 mm format with 60 cycle/mm resolution can be transmitted to ground in 10 minutes at an approximate rate of 1 megabit/sec.

(5) Attitude Control System. The LST/SSM spacecraft ACS has been configured to satisfy the following requirements:

1. To provide the capability for viewing any source on the celestial sphere at any time while satisfying sun, moon, and earth avoidance constraints. No observations will be made when the telescope line of sight (LOS) is within 45 degrees of the sun or within 15 degrees of the limb of the earth or moon.

2. Spacecraft coarse pointing accuracy

a. Two axes  $\pm 30$  arc seconds,  $3\sigma$ .

b. About LOS  $\pm 0.1$  degree,  $3\sigma$ .

3. Spacecraft fine pointing accuracy — Three axes  $\pm 1$  arc second,  $1\sigma$ , using the OTA offset find guidance sensing system.

4. Fine pointing accuracy (experiment LOS) — Two axes  $\pm 0.1$  arc second,  $1\sigma$  (LOS relative to guide star locations).

5. Image motion stabilization

a. Two axes  $0.005$  arc second,  $1\sigma$ , using OTA offset fine guidance system.

b. About LOS  $\pm 1$  arc second,  $1\sigma$ .

6. Maneuvering

a. 60 degrees in 40 minutes required.

b. 90 degrees in 5 minutes to be considered.

7. To provide momentum accumulation capability for a minimum of one orbit during experimentation without desaturation.

(a) Primary System. Figure IV-20 is a functional block diagram of the design reference ACS with a complete complement of sensors, actuators, and interface equipment to perform all phases of the LST mission. Also included in this block diagram are the key interfaces with the LST OTA/SIP system components. These interfaces are critical to establishing and maintaining LOS stability and are discussed further in Volume V.

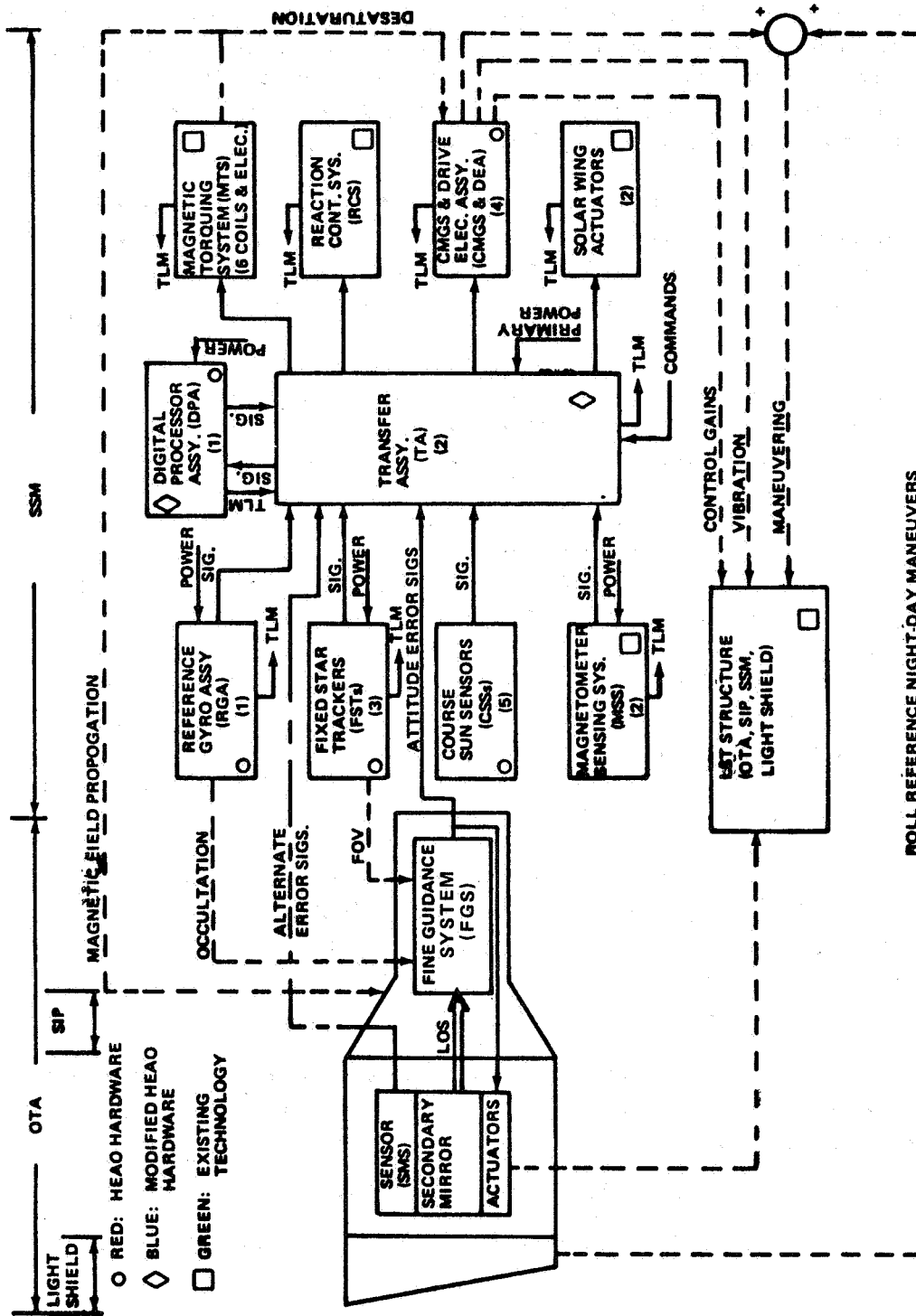


Figure IV-20. ACS block diagram and key interfaces for LST.

The three fixed star trackers (FSTs) are oriented in the Y-Z plane as shown in Figure IV-21. Normally, two are active with the third in a redundant standby status. When the FSTs are operated in this manner, approximately 99 percent coverage of the celestial sphere is attained with the capability of providing three-axis attitude error signals. The accuracy of the trackers has been selected to adequately align the telescope LOS so that preselected guide stars will appear within the coarse field of view (FOV) of the fine guidance system (FGS) located within the OTA.

Five coarse sun sensors (CSSs) are included. Coverage of  $4\pi$  sr is provided for sun acquisition and emergency sun acquisition. Two of the CSSs are located on the solar wings (one per wing) and provide monitoring of solar panel offset with respect to the sunline.

The reference gyro-assembly (RGA) consists of six gyros in a skewed dodecahedron configuration along with the necessary support electronics. In normal operation, four gyros are active and two are in a redundant standby mode.

A magnetic torque system (MTS) consisting of two 3-axis magnetometers (one redundant) mounted on the aft end of the SSM and six bar electromagnets mounted on the forward end of the OTA is used for momentum management. The magnetometers sense the vector components of the geomagnetic field in body coordinates. Voltage outputs proportional to the field strength are blended electronically with CMG momentum state to generate torquing currents for the bar electromagnets. A magnetic dipole is produced which reacts with the earth's ambient field to produce a torque on the LST. This torque continuously desaturates the CMGs, forcing them to remain near a preselected momentum state.

The transfer assembly (TA) serves as an interface assembly for all ACS components. It has a sensor buffer unit that places the required sensors on line for the control mode in use and routes signals between the sensors and digital processor assembly (DPA) via the computer input/output section of the TA.

The DPA receives data inputs from ground commands or the various sensors via the TA, processes the data, and provides the following outputs via the TA:

1. CMG gimbal commands.
2. Torque commands to the magnetic torquer system.
3. Gyro drift compensation.
4. Solar wing actuator commands.



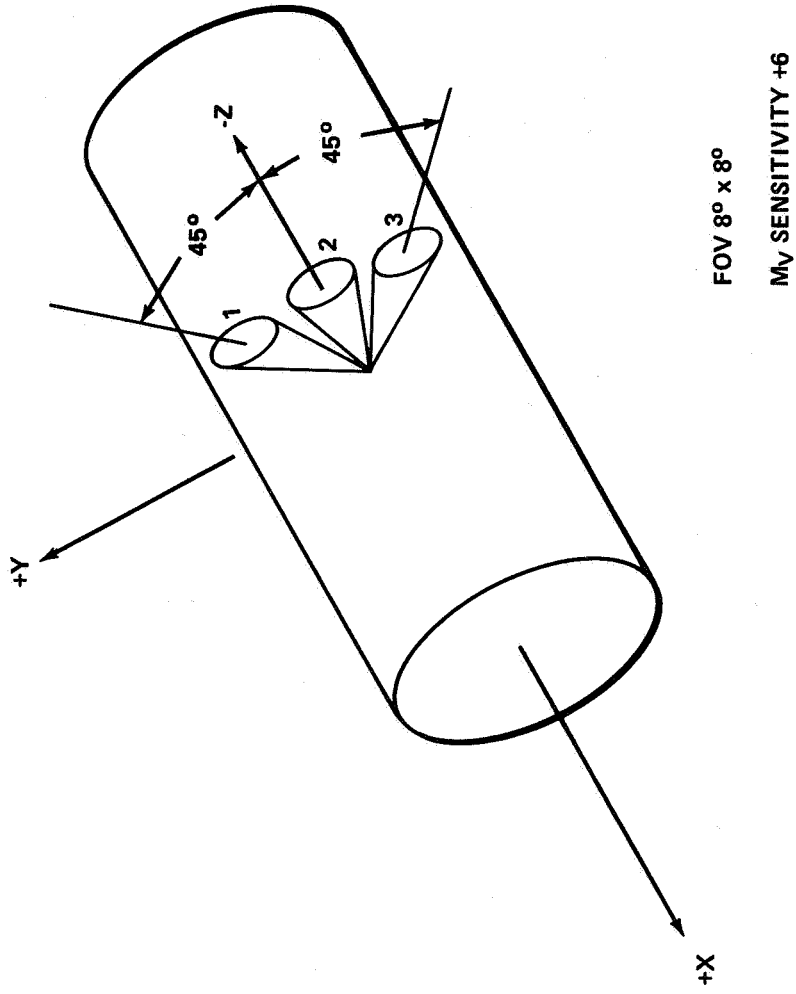


Figure IV-21. LST star tracker configuration.

Four single gimbal control moment gyro (CMG) assemblies, each complete with redundant drive electronics assemblies (DEAs) are mounted in a skewed configuration so that each CMG can provide a portion of the momentum requirements for each control axis. The CMGs provide the momentum storage capability required to maintain the LST in an accurate inertial hold attitude and supply the control torques required to maneuver the LST. The MTs supply control torques for CMG momentum desaturation.

(b) Reaction Control System. The primary requirement for an RCS on the LST is to serve as an emergency backup control system to the LST primary ACS. The RCS is to be in a standby "go" condition during certain critical LST maneuvers to aid the primary ACS if necessary. The RCS will also be required to provide control torques for the LST in the event of a complete or partial failure of the primary ACS. A functional schematic of the RCS selected for the LST is shown in Figure IV-22. The RCS is a pressure regulated, gaseous nitrogen, propulsion system modularized into three basic elements — a propellant tank, a black box, and two major thruster modules. Auxiliary items, most of which are contained in the black box, are latching solenoid isolation valves, filters, pressure regulators, check valves, pressure and temperature transducers, pressure gages, manual shutoff valves, pneumatic disconnects, propellant fill and drain valves, wire harness, and interconnecting plumbing. The RCS elements are assembled in the SSM of the LST. The total RCS mass, excluding electronics, is 104 kg (229 lb). Of this total mass, 19.5 kg (43.0 lb) is GN<sub>2</sub> propellant.

The RCS features of primary significance are as follows:

1. Twelve thrusters are used; six are active and six standby.
2. One tank is utilized to store the GN<sub>2</sub> propellant.
3. A dual-level pressure regulator is used. With the regulator operating in the high mode, the thrust level is 44.48 N (10 lb). With the regulator operating in the low mode, the thrust level is 2.22 N (0.5 lb).
4. With the exception of the tank, RCS component redundancy is available.

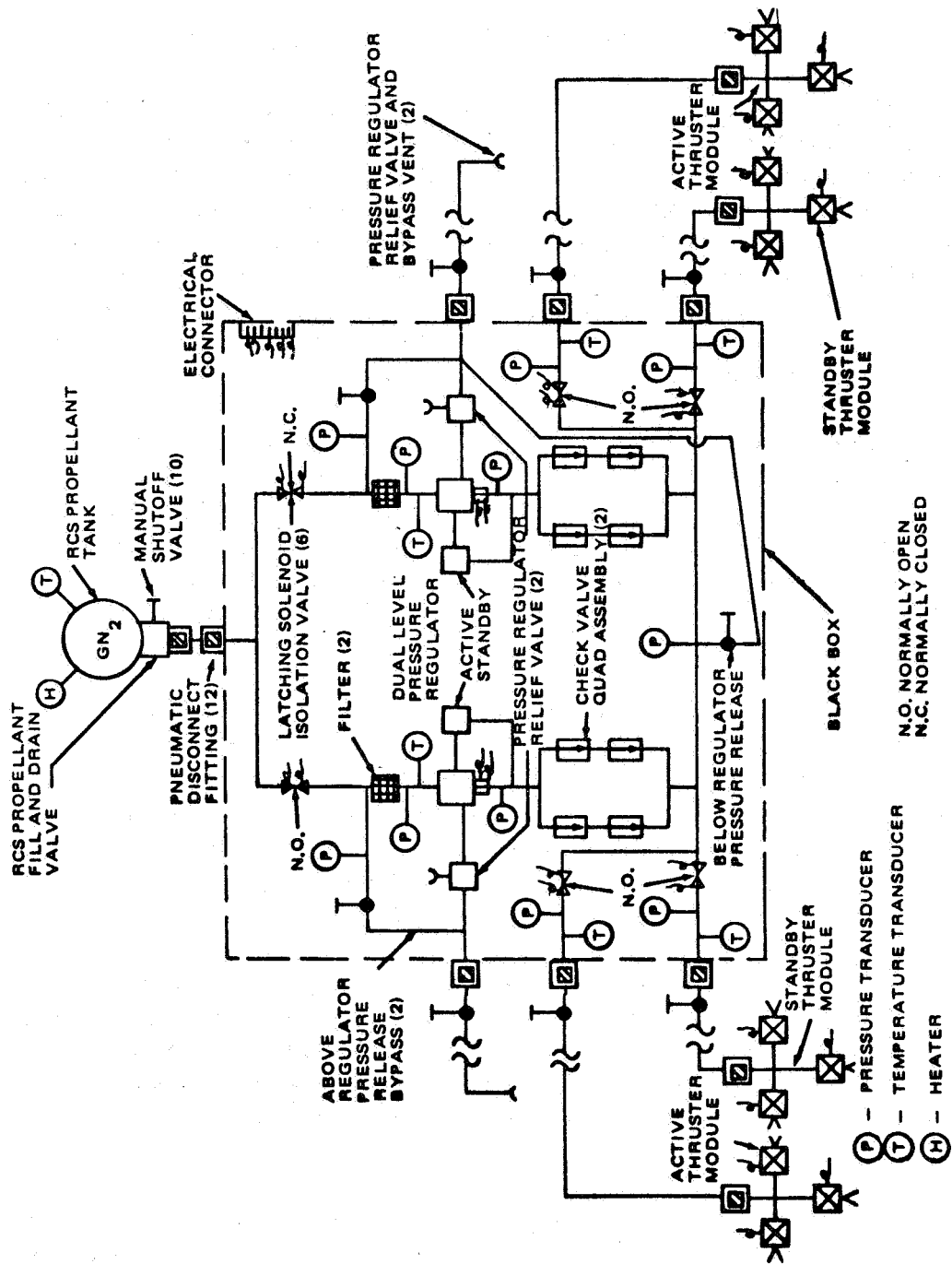


Figure IV-22. System schematic of the LST reaction control system.

5. Modularization of the RCS provides for ease in maintenance.

6. Most components are off-the-shelf items.

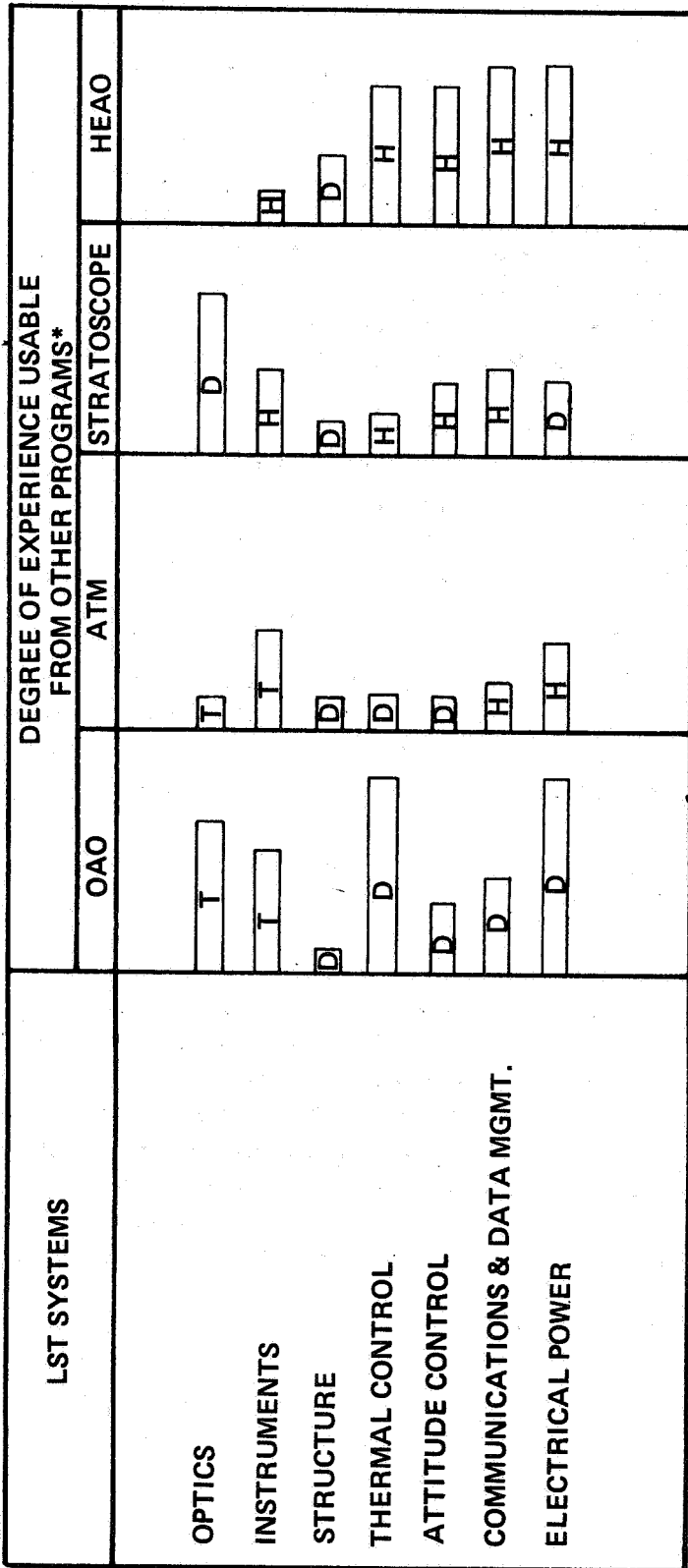
5. Commonality. The degree of commonality between the LST reference design and the hardware from other programs can be seen from the footnotes to the master equipment list (Table IV-2). There are approximately 67 components (47 percent total SSM components) which are identical to HEAO components, 24 components (17 percent) from other programs, 19 components (13 percent) which could probably be identical to HEAO components if it were shown to be cost-effective for these designs to be allowed to influence each other more, and 33 components (23 percent) which are new designs (requiring development, but no new technology).

There can be a considerable degree of commonality of LST hardware with the Stratoscope Program if the two programs are structured and funded to achieve such. For example, there could be hardware commonality in such areas as fine guidance, image tubes, cooling of image tubes, figure sensor, and focus sensor. In addition, there could be commonality in development of graphite-epoxy structures, secondary mirror sensing and control, and primary mirror figure control.

Figure IV-23 provides a rough estimate of the commonality which could be achieved between the LST and other programs in the areas of technology, development, and hardware. These are not the only programs with which commonality could be achieved, and it should also be emphasized that Figure IV-23 contains only potential commonalities and for this commonality to be fully realized, the programs probably would have to be structured to achieve it.

Only the highest order of obtainable commonality is shown in graph form. The highest degree of hardware commonality obtainable is expected to be with the HEAO hardware. This is logical since the HEAO and LST spacecraft have generally the same size, mass and orbit; the support systems requirements are roughly similar and the operational time frames are fairly close.

6. Maintenance Spares/Equipment. The reference LST design allows for on-orbit maintenance in the "black box" (component) level. The SSM and SIP components and the telescope-peculiar instruments and electronics packages which are mounted in the pressurizable volume can be replaced in a



\*COMMONALITY LEVELS (IN DECREASING ORDER OF VALUE):

- H = HARDWARE
- D = DEVELOPMENT
- T = TECHNOLOGY

NOTE: ONLY THE HIGHEST APPLICABLE LEVEL OF COMMONALITY IS SHOWN IN THE GRAPHS.

Figure IV-23. LST potential commonality with other programs.

shirtsleeve mode; in addition, some of the electronics and mechanisms which are mounted on the secondary mirror assembly and all of the externally mounted SSM black boxes can be replaced via extravehicular activity (EVA).

The equipment mounted externally to the pressurizable volume is designed to have a high reliability for 5 years and that mounted internally has a high reliability for at least 1 year. It is anticipated that the science and telescope instruments will be replaced at least once during the 5-year lifetime, and that the life-limited and randomly failed or degraded items would be replaced whenever required. Two lists were generated in an attempt to estimate the mass and volume of spares and other equipment required for a maintenance mission. The first one, shown in Table IV-5, is an estimate of the equipment which might be required to be replaced, assuming that it was desired to perform a total instrument update at the same time as a systems repair operation. This is an extreme case and is not expected to be a "typical" load. The masses of some components shown in these lists have been updated somewhat, as shown in the master equipment list (Table IV-2). The changes are not considered significant in the results of this section.

The second list, shown in Table IV-6, is what might be expected to be a more typical maintenance mission load. The life-limited and random failure items and support equipment are the same but the quantity of instruments to be replaced is more reasonable than that in the previous table.

Table IV-7 lists the support equipment required to be stowed in the Shuttle for the maintenance visit.

7. Contamination Control. Contamination control procedures and requirements have been investigated for the following phases of LST development and operations: design, manufacture, assembly, launch operation, and ground return. Specifically, the selection of materials during design has been considered. The procedures and facility requirements during manufacture and assembly have been addressed. The shroud, handling, and purge requirements have been considered during launch operations and ground return. The design impact and the equipment required on the LST and on the orbiter support volume during orbital maintenance have been studied and identified.

The requirements established for the control of contamination on the LST are 10 000 class particulate control in the SIP, 100 000 class particulate control in the SSM volume about the SIP, and 10 ppm trace contaminants for low vapor pressure constituents to 15 ppm for high vapor pressure constituents.

TABLE IV-5. "TOTAL" MAINTENANCE MISSION EQUIPMENT LOAD

Item	Mass		Volume	
	(kg)	(lb)	(m <sup>3</sup> )	(ft <sup>3</sup> )
<b>Life Limited Items</b>				
3 Tape Recorders	16.3	36	0.024	0.84
6 Batteries	<u>126.5</u>	<u>279</u>	<u>0.121</u>	<u>4.26</u>
Subtotal	142.8	315	0.145	5.1
+ 20% for packaging, etc., mass, and 50% volume	<u>28.1</u>	<u>62</u>	<u>0.072</u>	<u>2.55</u>
Total	<u>170.9</u>	<u>377</u>	<u>0.217</u>	<u>7.65</u>
<b>"Typical" Random Failure Items</b>				
1 RGA	10.4	23	0.011	0.4
1 DPA	6.3	14	0.006	0.2
1 CMG	80.7	178	0.462	16.3
1 Regulator	3.6	8	0.008	0.3
1 Remote Decoder	0.5	1	0.003	0.1
1 DAU	<u>0.5</u>	<u>1</u>	<u>0.0004</u>	<u>0.005</u>
Subtotal	102.0	225	0.4904	17.305
+ 20% for packaging, etc., mass, and 50%, volume	<u>20.4</u>	<u>45</u>	<u>0.245</u>	<u>8.65</u>
Total	<u>122.4</u>	<u>270</u>	<u>0.7354</u>	<u>25.955</u>
<b>Total Instrument Update Items</b>				
1 f/12 Camera and Filter Wheel	68.04	150	0.032	1.14
3 f/96 Camera and Filter Wheel	201.4	444	0.068	2.4
1 f/96 Camera and Selector Assembly	21.3	47	0.025	0.9
1 f/96 Magnifier and Housing	15.4	34	0.15	2.1
1 Fine Guidance Mechanism and Housing	116.6	257	0.091	3.2
1 Echelle Spectrograph	51.7	114	0.161	5.7
1 Echelle Spectrograph	51.7	114	0.147	5.2
1 Faint Object Spectrograph (UV)	55.8	123	0.100	3.5
1 Faint Object Spectrograph (IR)	45.4	100	0.184	6.5
1 Faint Object Spectrograph (IR)	44.4	98	0.074	2.6
1 Fourier Interferometer	18.1	40	0.100	3.5
1 Focus Sensor	10.9	24	0.006	0.2
1 Figure Sensor	17.2	38	0.006	0.2
1 Collimator Assembly (UV Spectrograph)	13.6	30	0.02	0.7
1 Slit Assembly (Axial Spectrograph Mechanism, etc.)	4.5	10	0.02	0.7
1 Slit Jaw Camera	<u>42.2</u>	<u>93</u>	<u>0.275</u>	<u>9.7</u>
Subtotal	778.24	1716	1.459	48.24
+ 20% for packaging, etc., mass, and 50%, volume	<u>155.6</u>	<u>343</u>	<u>0.68</u>	<u>24.12</u>
Total	<u>933.84</u>	<u>2059</u>	<u>2.139</u>	<u>72.36</u>
Subtotal, Spares and Instruments	1227.14	2706	3.0914	105.965
<b>Total Support Equipment (Contamination Removal and Miscellaneous)</b>				
Subtotal	408.6	900	2.3	82
+ 20% for packaging, mass, and 50%, volume, excluding contamination control package	<u>51.8</u>	<u>114</u>	<u>1.0</u>	<u>35</u>
	<u>460.4</u>	<u>1014</u>	<u>3.3</u>	<u>117</u>
Grand Total	1687.54	3720	6.391	222.965

TABLE IV-6. "TYPICAL" UNSCHEDULED ON-ORBIT MAINTENANCE MISSION EQUIPMENT LOAD

Item	Mass		Volume	
	(kg)	(lb)	(m <sup>3</sup> )	(ft <sup>3</sup> )
<b>Life Limited Items</b>				
3 Tape Recorders	16.3	36	0.024	0.84
6 Batteries	<u>126.5</u>	<u>279</u>	<u>0.121</u>	<u>4.26</u>
Subtotal	142.8	315	0.145	5.1
+ 20% for packaging, etc., mass, and 50%, volume	<u>28.1</u>	<u>62</u>	<u>0.072</u>	<u>2.55</u>
Total	<u>170.9</u>	<u>377</u>	<u>0.217</u>	<u>7.65</u>
<b>"Typical" Random Failure Items</b>				
1 RGA	10.4	23	0.011	0.4
1 DPA	6.3	14	0.006	0.2
1 CMG	80.7	178	0.462	16.3
1 Regulator	3.6	8	0.008	0.3
1 Remote Decoder	0.5	1	0.003	0.1
1 DAU	<u>0.5</u>	<u>1</u>	<u>0.00014</u>	<u>0.005</u>
Subtotal	102.0	225	0.49014	17.305
+ 20% for packaging, etc., mass, and 50%, volume	<u>20.4</u>	<u>45</u>	<u>0.245</u>	<u>8.65</u>
Total	<u>122.4</u>	<u>270</u>	<u>0.73514</u>	<u>25.955</u>
<b>"Typical" Instrument Update Items</b>				
3 f/96 Camera and Filter Wheel	201.4	444	0.068	2.4
1 Echelle Spectrograph	51.7	114	0.161	5.7
1 Faint Object Spectrograph (UV)	<u>55.8</u>	<u>123</u>	<u>0.1</u>	<u>3.5</u>
Subtotal	308.9	681	0.329	11.6
+ 20% for packaging, etc., mass, and 50%, volume	<u>61.7</u>	<u>136</u>	<u>0.06</u>	<u>5.8</u>
Total	<u>370.6</u>	<u>817</u>	<u>0.389</u>	<u>17.4</u>
Subtotal, Spares, and Instruments	663.9	1468	1.34114	51.005
<b>Total Support Equipment (Contamination Removal and Miscellaneous)</b>				
(Does not include contamination control package)				
Subtotal	405	900	2.2	82
+ 20% for packaging, etc., mass, and 50%, volume	<u>51.3</u>	<u>114</u>	<u>0.9</u>	<u>35</u>
Total	<u>456.3</u>	<u>1014</u>	<u>3.1</u>	<u>117</u>
Grand Totals for "Typical" Mission	1120.2	2478	4.44114	168.005



TABLE IV-7. SUPPORT EQUIPMENT (STOWED IN SHUTTLE)  
REQUIRED FOR ON-ORBIT PRESSURIZED MAINTENANCE

Item	Mass		Volume	
	(kg)	(lb)	(m <sup>3</sup> )	(ft <sup>3</sup> )
Contamination Control				
Contamination Control Equipment Package	150	330	0.36	12.6
Miscellaneous Ductings and Fittings	11.4	25	0.18	6.2
1 Quick Disconnect Joint	<u>2.3</u>	<u>5</u>	<u>0.0057</u>	<u>0.2</u>
Total	163.7	360	0.5457	19.0
EC/LSS <sup>a</sup>				
Miscellaneous				
Pressure Gas and Bottle (Capability, two pressurizations)	135.6	300	0.198	7
1 Tool Kit	13.6	30	0.085	3
1 Communications/Hazardous Warning Box	4.5	10	0.085	3
Checkout Equipment	<u>90.6</u>	<u>200</u>	<u>1.41</u>	<u>50</u>
Total Miscellaneous	244.3	540	1.778	63
Grand Totals for On-Orbit Pressurized Maintenance	408.0	900	2.3237	82

- a. It is assumed that the Shuttle environmental control and life support system (EC/LSS) is sized for the EC/LSS load of two maintenance personnel plus the moderate equipment loads of the LST during maintenance and that a portion of the EC/LSS can be isolated for LST servicing (no mixing of LST and Shuttle air in EC/LSS). Hence, no mass or volume is shown here.

Contamination control hardware located on the LST consists primarily of ducting and filters, as shown in the layout of Figure IV-24. The ducting conveys "clean air" from the SSM orbiter docking interface to the OTA/SSM interface plane and to the SIP for distribution from high efficiency particulate air (HEPA) filters. The flow of up to 0.189 m<sup>3</sup>/sec (400 cfm) to the SIP will provide 10 000 class particulate control and of 0.283 m<sup>3</sup>/sec (600 cfm) to the OTA/SSM interface plane will provide 100 000 class particulate control.

Contamination control equipment located in the orbiter support volume is schematically shown in Figure IV-25. This equipment consists of fans, trace contamination absorber beds, oxidizers, and filters. The trace contamination loop is located in the orbiter support volume, which is physically separated from the main environmentally controlled volume of the orbiter by a fabric partition, and requires a flow of 0.005 m<sup>3</sup>/sec (10 cfm) to the catalytic oxidizer and 0.189 m<sup>3</sup>/sec (400 cfm) to the primary sorbent bed to meet the trace contamination requirements stated above.

Equipment listings for the SSM and the orbiter support volume are presented in Tables IV-8 and IV-9, respectively. Electrical power, for contamination control during orbital maintenance, is provided by the orbiter.

8. Systems Reliability Summary. A detailed description of the LST reliability analyses and checkout approaches is given in Volume V, Chapter VIII. The SSM and OTA reliabilities are summarized in Table IV-10. "Failure" is defined as an event resulting in the loss of the LST or requiring a maintenance action.

The high reliability shown arises from the following factors:

1. Incorporation of "reasonable" redundancy.
2. Use of existing equipment or equipment common with the HEAO program. This, in some instances, implies acceptance of higher redundancy than would be planned in a new design.
3. Exclusion of noncritical and certain other system elements (because of a lack of credible data) from the reliability analyses.

Of these exclusions, the most significant is the exclusion of the battery/charger units, which have been identified as a possible reliability problem. Data collected during the Phase A study have led to inconsistent battery reliability predictions. A broader discussion of the battery problem is given in Volume V, Chapter VIII.

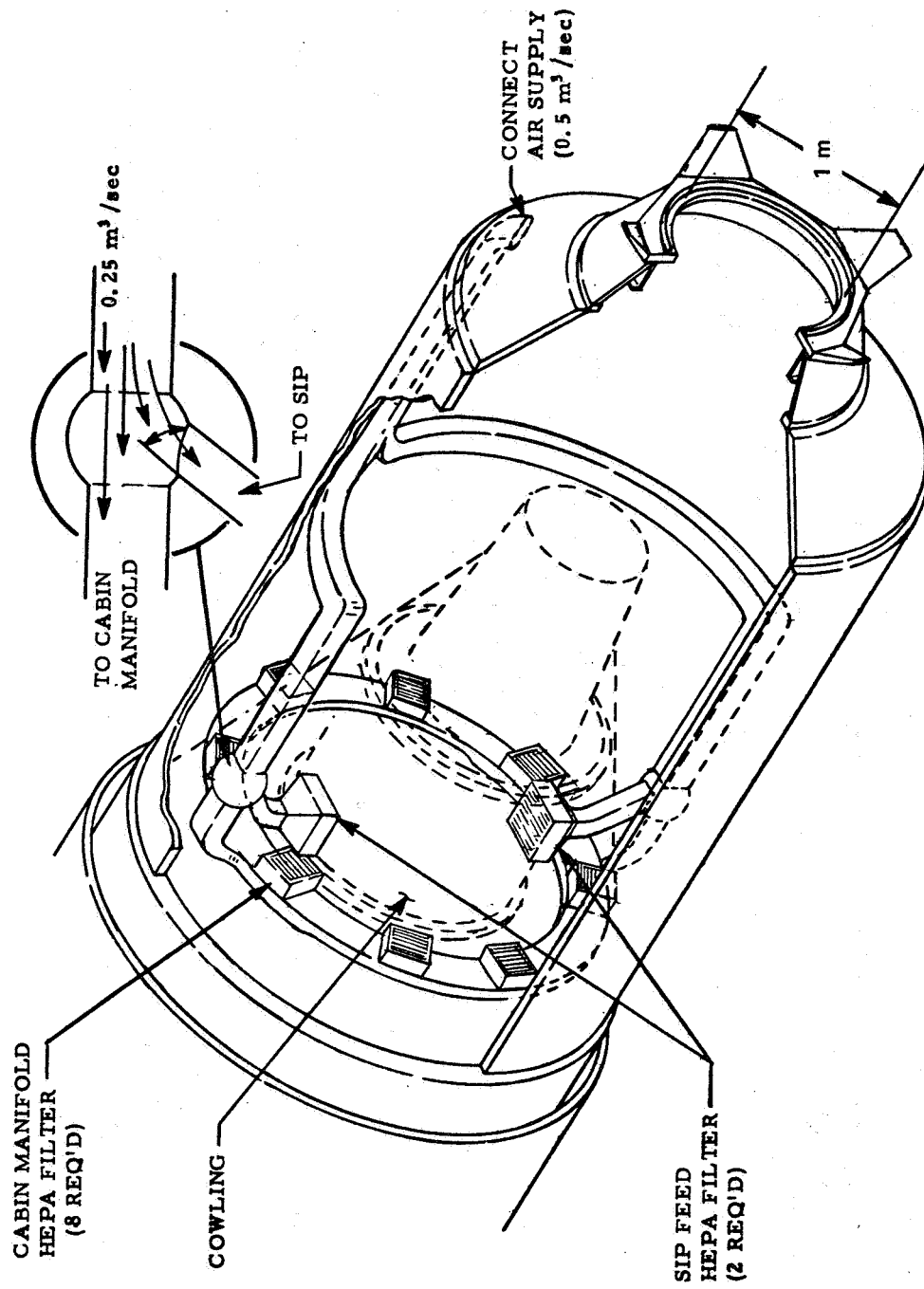


Figure IV-24. Class 10 000/100 000 LST contamination control system layout (hybrid version).

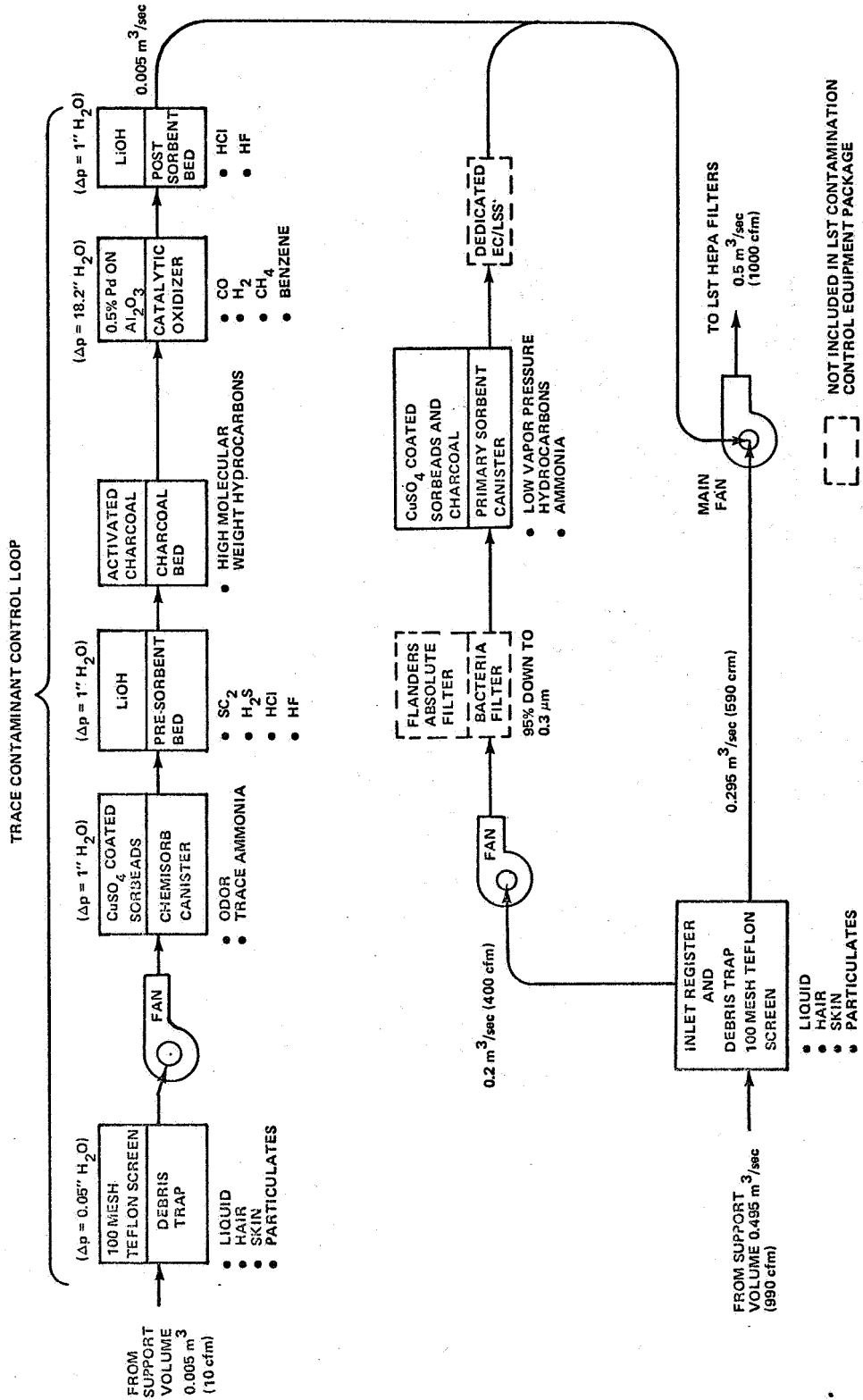


Figure IV-25. Contamination control system for class 10 000/100 000 LST.

TABLE IV-8. LST CONTAMINATION CONTROL SYSTEM MASS AND POWER BREAKDOWN:  
ONBOARD REQUIREMENTS FOR CLASS 10 000/100 000 LST

Item	No. of Units	Unit Mass (kg)	Unit Average Power (W)	Total Mass [kg (lb)]	Total Average Power (W)	Size (mm)	Remarks
Ducting	1 (15 m)	12.8 (0.85/m)	—	12.8 (29)	—	150 × 150 × 0.005	
Miscellaneous Fittings	—	—	—	1.8 (4)	—	—	Ductwork Support Straps, etc.
Quick-Disconnect Joint	1	0.9	—	0.9 (2)	—	150 Inside Diameter	Plug-In for Air Supply
HEPA Filters (Cabin Manifold)	8	1.4	—	11.2 (18)	—	300 × 300 × 150	Cabin Manifold 0.675 m <sup>3</sup> /sec (135 cfm) Capacity
HEPA Filters (SIP Feed)	2	1.8	—	3.6 (8)	—	350 × 350 × 150	SIP Inlet; 0.1 m <sup>3</sup> /sec (200 cfm) Capacity
Total				30.3 (67)			

TABLE IV-9. LST CONTAMINATION CONTROL SYSTEM MASS AND POWER BREAKDOWN:  
SUPPORT REQUIREMENTS FOR CLASS 10 000/100 000 LST

Item	No. of Units	Unit Mass (kg)	Unit Average Power (W)	Total Mass kg (lb)	Total Average Power (W)	Size (mm)
Miscellaneous Ducting and Fittings <sup>a</sup>	—	—	—	11.4 (27.4)	—	—
Quick-Disconnect Joint	1	2.3	—	2.3 (5.1)	—	150 Inside Diameter
Contamination Control Equipment Package	—	—	—	150 (330.4)	874	650 × 670 × 1170
Total				≈ 164 (362)	874	

a. Includes approximately 150 × 150 × 0.005 mm of ducting.

TABLE IV-10. SSM/OTA RELIABILITY

System	1-Year Reliability
Attitude Control (SSM)	0.9880
Communications and Data Handling (SSM)	0.9981
Electrical (SSM)	0.9980 <sup>a</sup>
Thermal Control (SSM/OTA)	0.9991
Main Optics & Structures (OTA/SSM)	0.9998
Data Handling and Control (OTA)	0.9988
Electrical (OTA)	0.9983
Pointing & Stabilization (OTA)	0.9860
Alignment Sensors and Logic	0.9898
Harmonic Drive Actuators & Control	0.9999
Light Shield	0.9958
Aperture Door	0.9952
SSM/OTA	0.9478

a. Does not include battery/charger units, solar array drive mechanisms, and solar arrays

No estimate for the SIP reliability can be given as those failure conditions justifying a maintenance action were not identified during the Phase A study. This identification should be an early objective of future studies.

9. Man Rating Impacts. Some of the key impacts of man rating the LST are listed in Table IV-11. It is significant to note some of the key differences between the LST in this regard and the Apollo or Skylab which should make the LST significantly less expensive than those programs. The

TABLE IV-11. COMPARISON OF LST WITH APOLLO AND SKYLAB IN MAN-RATING AND/OR MAN-INVOLVEMENT IMPACTS

Consideration	Apollo/Skylab	LST	Consequence
Duration of On-Orbit Manned Inhabitation	Weeks (56 days max. continuous)	2-5 days per year or less	Design can be less conservative in some areas, e.g., degree of long-term protection against micrometeoroid puncture of pressure shell (if punctured and not feasible to repair on-orbit, pressure suit can be utilized, or can supply makeup gas and withstand small leakages for this short a time).
Systems and Experiments Operating During Manned Occupancy	All	None	Hazards during manned occupancy greatly reduced. LST is dormant during maintenance. The limited checkout after maintenance is done remotely from Shuttle cabin. (See item below also.)
Atmosphere Pressure Level	$3.45 \times 10^4$ N/m <sup>2</sup> (5 psi)	$1.01 \times 10^5$ N/m <sup>2</sup> (14.7 psi)	The percentage of O <sub>2</sub> in atmosphere is greatly reduced, thus allowing fire hazard to be no greater than that on ground. The costs associated with imposing the stringent flammability specifications, designing for more exotic materials, and performing extensive testing on Apollo can be reduced or eliminated.



TABLE IV-11. (Concluded)

Consideration	Apollo/Skylab	LST	Consequence
Atmosphere Pressure Level (Continued)			<p>Data from checkout and calibration on ground is correlatable with that in orbit at <math>1.01 \times 10^5</math> N/m<sup>2</sup> (14.7 psi)</p> <p>Problems and costs of selecting and training on-orbit maintenance personnel might be reduced somewhat, since sea level pressure eliminates physiological impacts of reduced pressure.</p>
Knowledge, Experience and Efficiency of In-Orbit Operations	Good	Improved	<p>The experience in Apollo, Skylab, and early Shuttle flights will take place prior to LST operations in orbit. It should be expected that man will be able to do considerably more things in orbit, and do them better, by the time of LST operations.</p>
Equipment Peculiar to Man-in-Space Operations	Good	Improved (already developed)	<p>The equipment utilized in Apollo, Skylab, and Shuttle will have been more fully developed and tested, and should be improved considerably by the time of LST operations. This should allow elimination of new designs in this area for LST, as well as lower costs and greater efficiency.</p>

relative fire hazard is a function of the percentage of oxygen in the atmosphere, rather than the total pressure of the atmosphere. This can be seen in Figure IV-26. Figure IV-27 shows the relationship of the minimum required partial pressure, due to man's physiological needs, to the total pressure in a two-gas mixture. Since the LST would be at  $1.01 \times 10^5$  N/m<sup>2</sup> (14.7 psia), fire hazards would be no greater than ground operations. This should be a significant advantage in keeping costs down.

The degree of usefulness of man in space and the penalty for keeping him there are two important factors in the design of space flight hardware. It is anticipated that the ability of man to perform will increase and his needs for extensive human factors equipment will decrease greatly. A "new philosophy of man in space" must be developed, no matter what the final concept of the LST becomes.

This philosophy must be based on an evaluation of Apollo/Skylab experience and a projection of this experience to applications in the realm of unmanned, man-maintained spacecraft, combined with a heavy mixture of cost consciousness. This new philosophy will probably include a more lenient approach to the quantity of EVA activities allowed. Whatever its nature, the philosophy should be established in the very near future to permit an evaluation of its impact in trades of various LST concepts in the Phase B studies.

10. Error Budgets. Three error budgets have been prepared for the LST:

1. Wavefront Error (WFE).
2. Image Stabilization or Guidance Error.
3. Absolute Pointing Error.

These error budgets are given in Figure IV-28.

a. Effect of WFE and Image Stabilization Errors on Image Size. The WFE is a measure of the quality of the image produced by the telescope — the smaller the WFE, the higher the quality of the image. The WFE also results in increased image size, as shown in Figure IV-29. A convenient measure of image size is the radius of the circle that contains 60 percent of the image energy. As shown in Figure IV-29, a telescope obscuration ratio of 30 percent increases the 60 percent encircled energy radius from 0.024 arc sec for a perfect image to 0.028 arc sec. A WFE of 0.05 wavelength rms, at

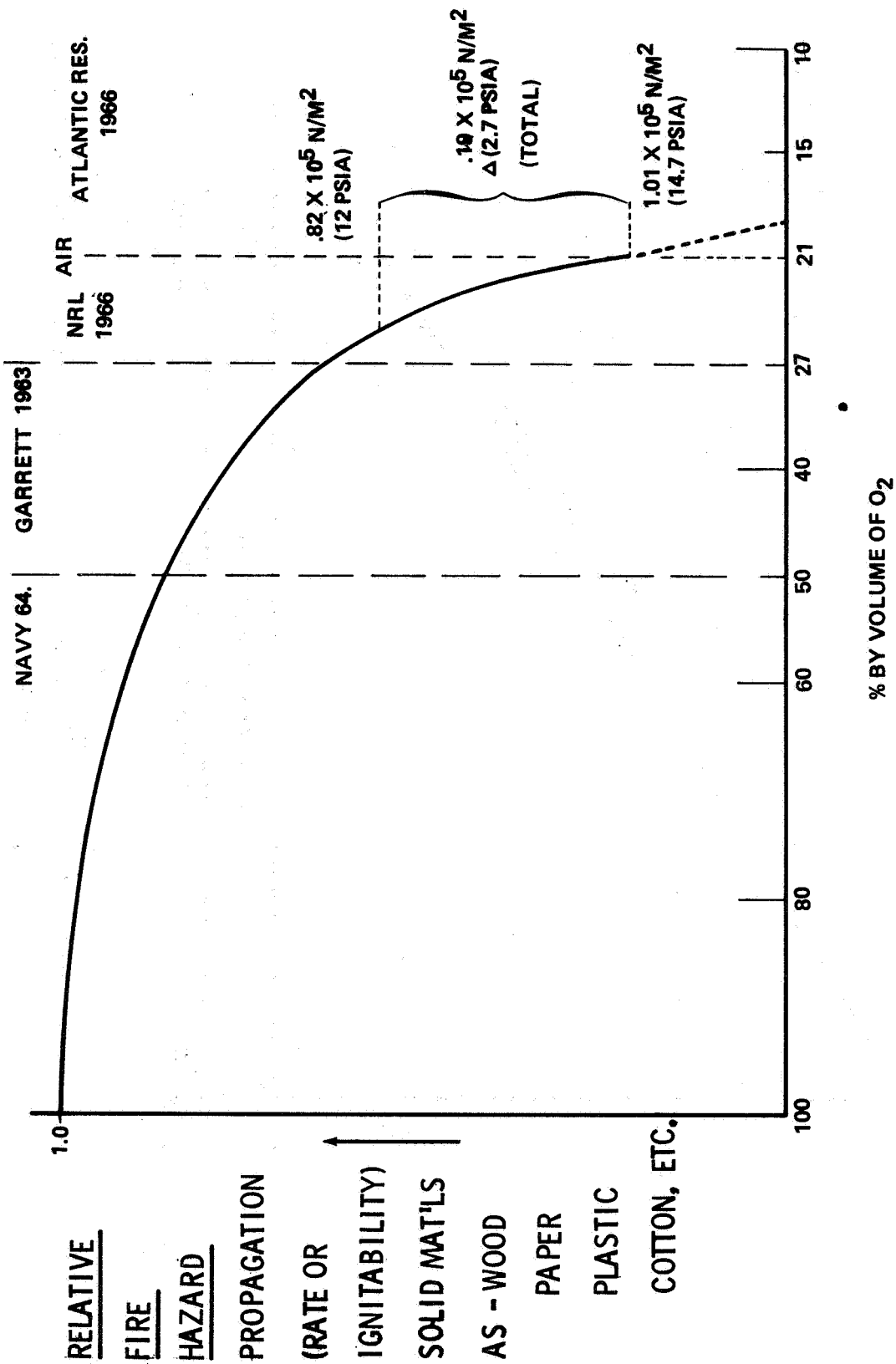


Figure IV-26. Relative fire hazard as a function of percentage of O<sub>2</sub> in the atmosphere.

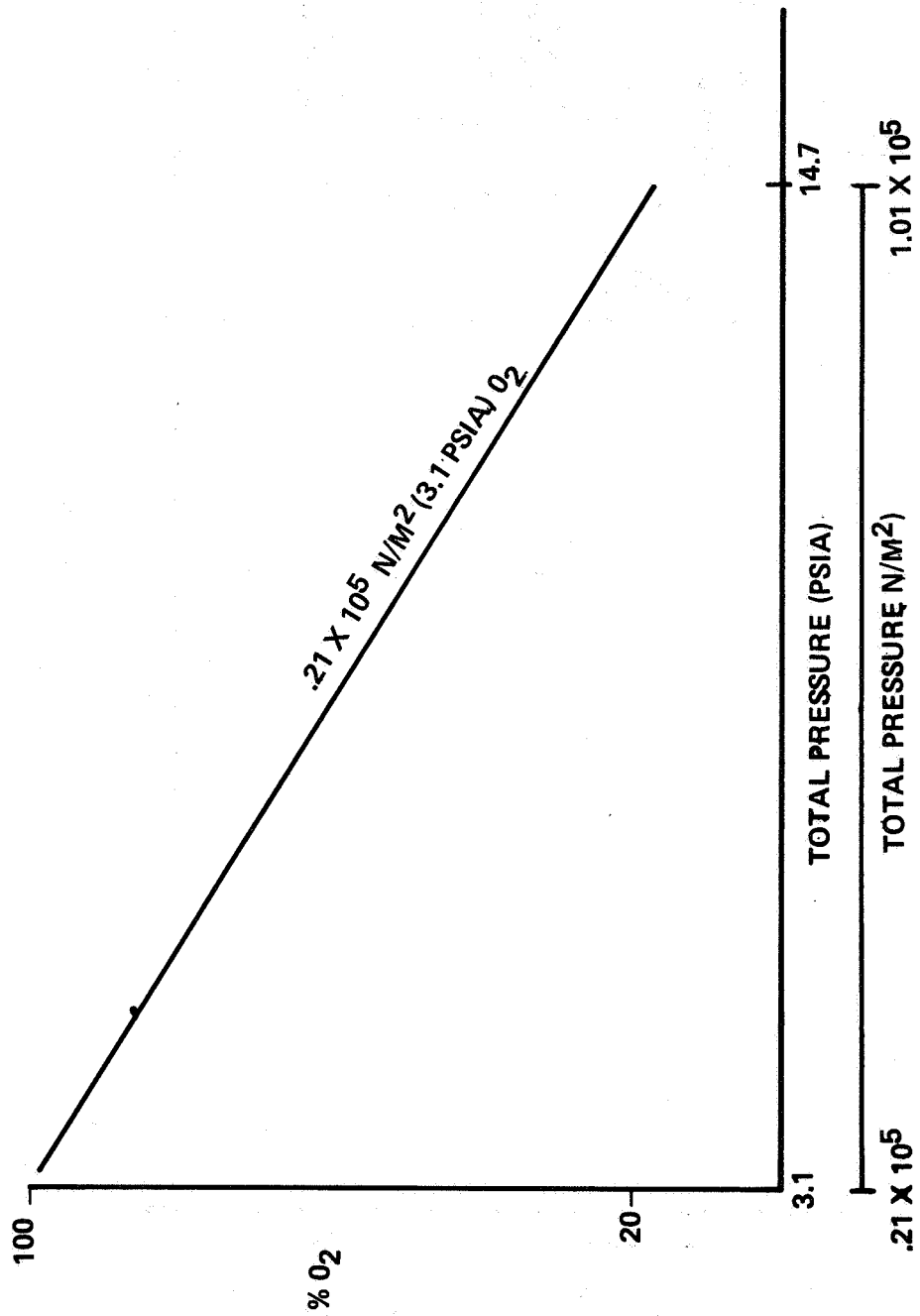


Figure IV-27. Percentage of O<sub>2</sub> required in habitable atmosphere as a function of total pressure.

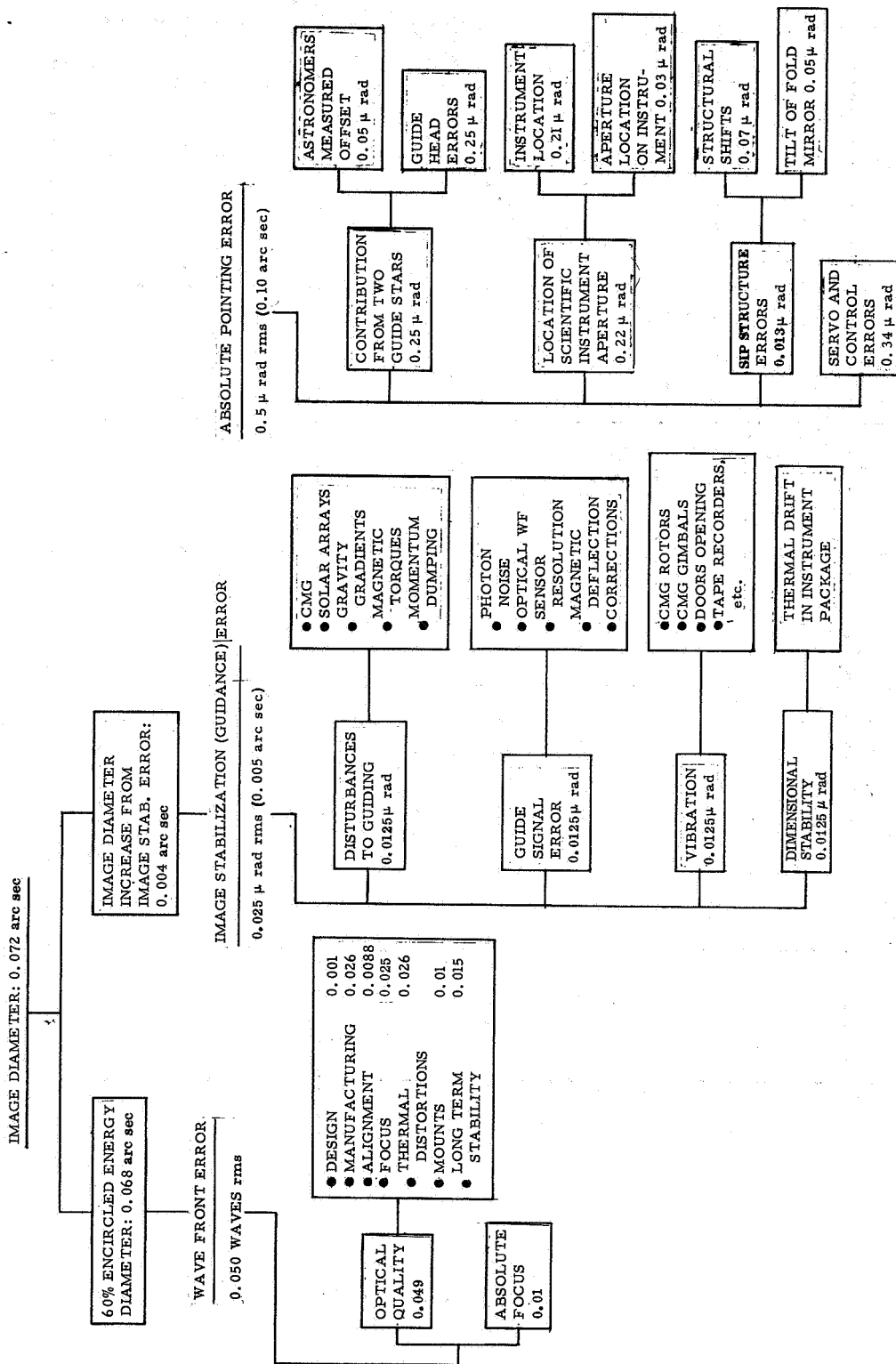


Figure IV-28. LST error budgets.

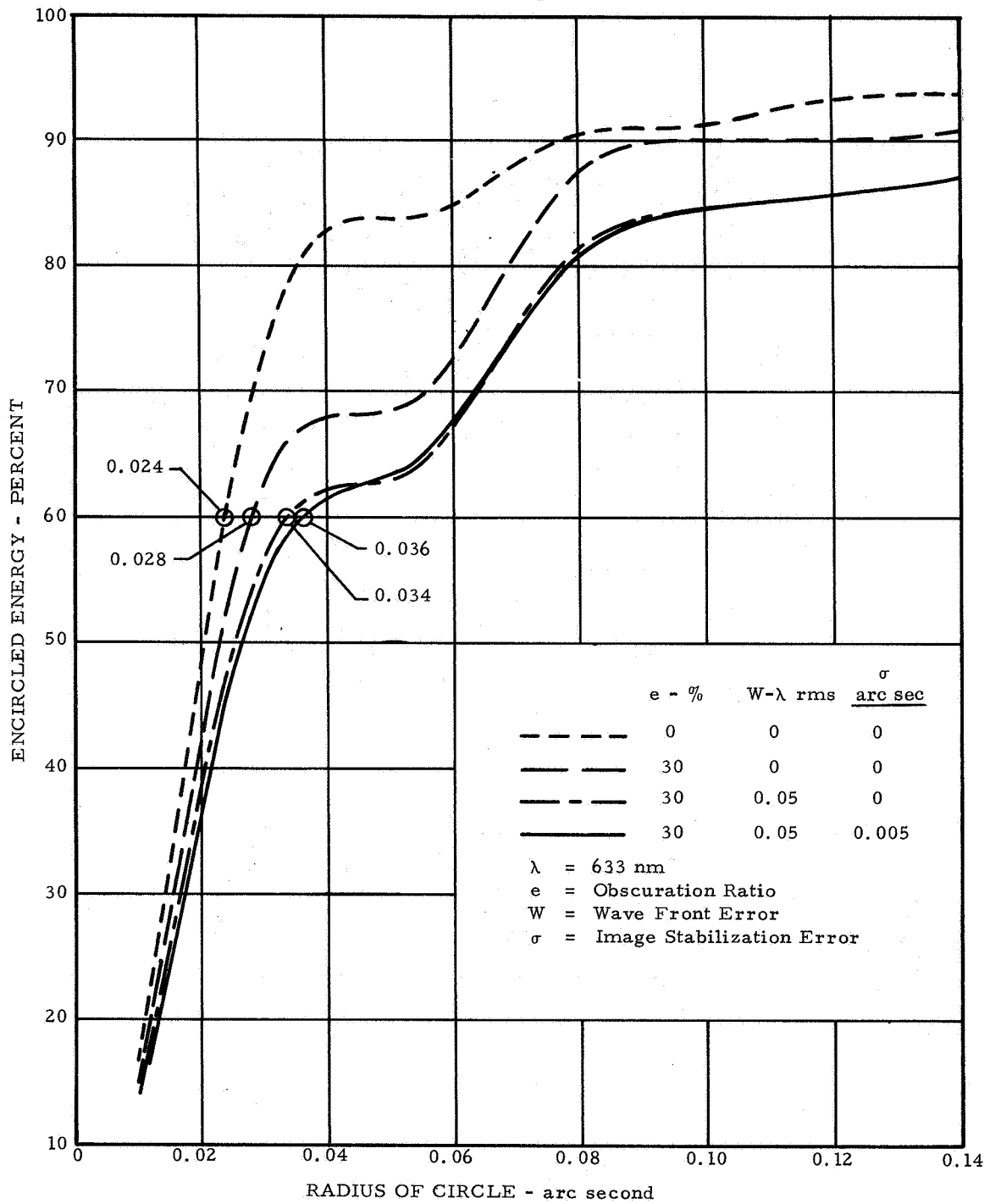


Figure IV-29. LST encircled energy curve.

a reference wavelength of 633 nm, increases the image radius from 0.028 to 0.034 arc sec. Motion of the telescope, i. e., image stabilization (guidance) error, also produces a larger image size. An image stabilization error of 0.005 arc sec rms increases image size from 0.034 to 0.036 arc sec. Larger WFE and image stabilization errors would increase the image size further.

The WFE and image stabilization error budgets are joined in Figure IV-28 to indicate their contribution to the image size. The absolute pointing error has no effect on image quality or size. It is a measure of the accuracy with which the telescope can be pointed.

b. Focus Error in WFE Budget. An identification of the components of the WFE budget, together with their numerical values, is given in Figure IV-28. A breakdown of the sources of the focus maintenance component of the WFE budget is given in Table IV-12. The sensor threshold error is the error contribution from the focus sensor when it is in a nulled condition.

TABLE IV-12. FOCUS MAINTENANCE BUDGET

Source	Error ( $\mu$ m)	Sensitivity ( $\lambda$ rms/ m)	WFE <sup>a</sup> ( $\lambda$ rms)
Sensor Calibration			0.009
Sensor Threshold			0.009
Sensor Location Error	5	0.00036	0.0018
Secondary Mirror Adjust Mechanism	0.47	0.0105	0.005
Thermal Drift During an Observation	2	0.0105	0.021
RSS error			0.025

a. Reference wavelength ( $\lambda$ ) = 632.8 nm.

The focus sensor location error is caused by the fact that the sensor and other instruments are located at the f/12 focal plane, which is in the SIP region of the SSM rather than on either the primary or secondary

mirror. Therefore, motion of the sensor and the f/12 focal plane relative to the mirrors may occur without an actual change in mirror separation distance. The equation for calculating the resulting WFE is

$$\text{Focal plane location WFE} = \frac{0.25 \Delta x_s}{8\lambda (F_{\text{syst}})^2} \quad (1)$$

where  $\lambda$  is the wavelength of light source = 632.8 nm for Table IV-12;  $F_{\text{syst}}$  = focal ratio of the telescope system = 12, and  $\Delta x_s$  = separation error between focus sensor, or focal plane, and secondary mirror. Note that it is the distance between the sensor and the secondary mirror that is in error and not the separation distance between the primary and secondary mirror.

The secondary mirror adjustment mechanism error is caused by the inability of the mechanism to position the mirror in the precise location dictated by the focus sensor. The equation for calculating the resulting WFE is

$$\text{Mirror separation WFE} = \frac{0.25 \Delta s}{8\lambda (F_p)^2} \quad (2)$$

where  $F_p$  = focal ratio of primary mirror = 2.2 and  $\Delta s$  = error in mirror separation distance. The error due to thermal drift is caused by the change in mirror separation resulting from a temperature change during the observation period. Equation (2) is also used to calculate this error.

c. Alignment Error in WFE Budget. Alignment error is produced when the secondary mirror is improperly positioned in a plane perpendicular to the telescope line of sight and/or when it is tipped or tilted about an axis perpendicular to the telescope line of sight. A breakdown of the sources of the secondary mirror alignment component of the WFE budget is given in Table IV-13. The equation for calculating the WFE is

$$\text{Mirror decenter WFE} = \frac{0.0037 \Delta y}{\lambda (F_p)^3} \quad (3)$$

where  $\Delta y$  = the decenter distance of the secondary mirror.



TABLE IV-13. SECONDARY MIRROR ALIGNMENT BUDGET

Source	Error	Sensitivity <sup>a</sup> ( $\lambda$ rms/ $\mu$ m)	WFE <sup>a</sup> ( $\lambda$ rms)
Initial Alignment	6.6 $\mu$ m	0.00054	0.0036
Sensor Threshold	6.6 $\mu$ m	0.00054	0.0036
Secondary Mirror Adjust Mechanism	3.5 $\mu$ m	0.00054	0.0019
Tilt of Secondary for 1 Arc Sec Line of Sight Correction	1 arc sec	0.00408 per arc sec	0.0040
Thermal Drift During an Observation	10 $\mu$ m-decenter; 5 $\mu$ rad-tip	0.00055 0.00032 per $\mu$ rad	0.0055 0.0016
RSS error			0.0088

a. Reference wavelength ( $\lambda$ ) = 632.8 nm.

The secondary mirror adjustment mechanism error is caused by the inability of the mirror transverse positioning mechanism to locate the mirror at the position dictated by the decenter sensor. The expected error is 3.5  $\mu$ m, which produces a WFE of 0.0019 wavelength in accordance with equation (3).

Image stabilization during an observation will be accomplished in part by movement of the secondary mirror. Maximum tilt for this purpose will be 1 arc sec. This will introduce a WFE of 0.0040 wavelength, as shown in Table IV-13. Temperature changes in the telescope structure during an observation are expected to cause a decentering of 10  $\mu$ m and a mirror tip of 5  $\mu$ rad. These misalignments will introduce WFEs of 0.0054 and 0.0016 wavelength, respectively.

11. Focus and Alignment Tolerances. It is anticipated that instruments within the SIP of the LST spacecraft will be replaced during on-orbit maintenance. Instruments may be replaced as an entire unit, or image tubes

only may be replaced. In either event, it is expected that the replacement units will have some residual position errors in both the axial and the transverse directions. Misposition of an instrument in the axial direction will introduce WFE and cause the image to be out of focus. WFE as a function of instrument detector misposition is shown in Figure IV-30. Transverse misposition of an instrument or image tube will cause the image to be moved on the face of the tube and may result in loss of a portion of the image; however, there will be no degradation of the image that is present on the image tube. In the case of axial misposition resulting in defocus, the secondary mirror may be repositioned to produce the best focus on the face of the image tube.

a. Effects of Secondary Mirror Repositioning. When the secondary mirror is in its design reference position relative to the primary mirror, an image having minimum WFE is produced at the optimum focus plane. This minimum WFE is expected to be 0.050 wavelength rms, as shown in Figure IV-28. If the secondary mirror is moved along the telescope axis from its design reference position, three things occur:

1. The plane of best focus, i. e., the image, moves and is no longer at the optimum focus plane.
2. A very minor additional WFE is introduced at the repositioned best focus plane because it is not coincident with the optimum focus plane.
3. The WFE at the optimum focus plane location is greatly increased.

Figure IV-31 is an illustration of moving the image (plane of best focus) onto the image tube by repositioning the secondary mirror. This eliminates the defocus caused by image tube (detector) axial misposition.

Image movement resulting from a change in the primary-secondary mirror separation distance change is expressed by the relationship:

$$\Delta x = -m^2 \Delta S \quad (4)$$

where  $\Delta x$  is the image motion distance,  $m$  is the amplification of the secondary mirror, and  $\Delta S$  is the change in the mirror separation distance. The value of  $m$  for the LST, which has a primary focal ratio of 2.2 and a

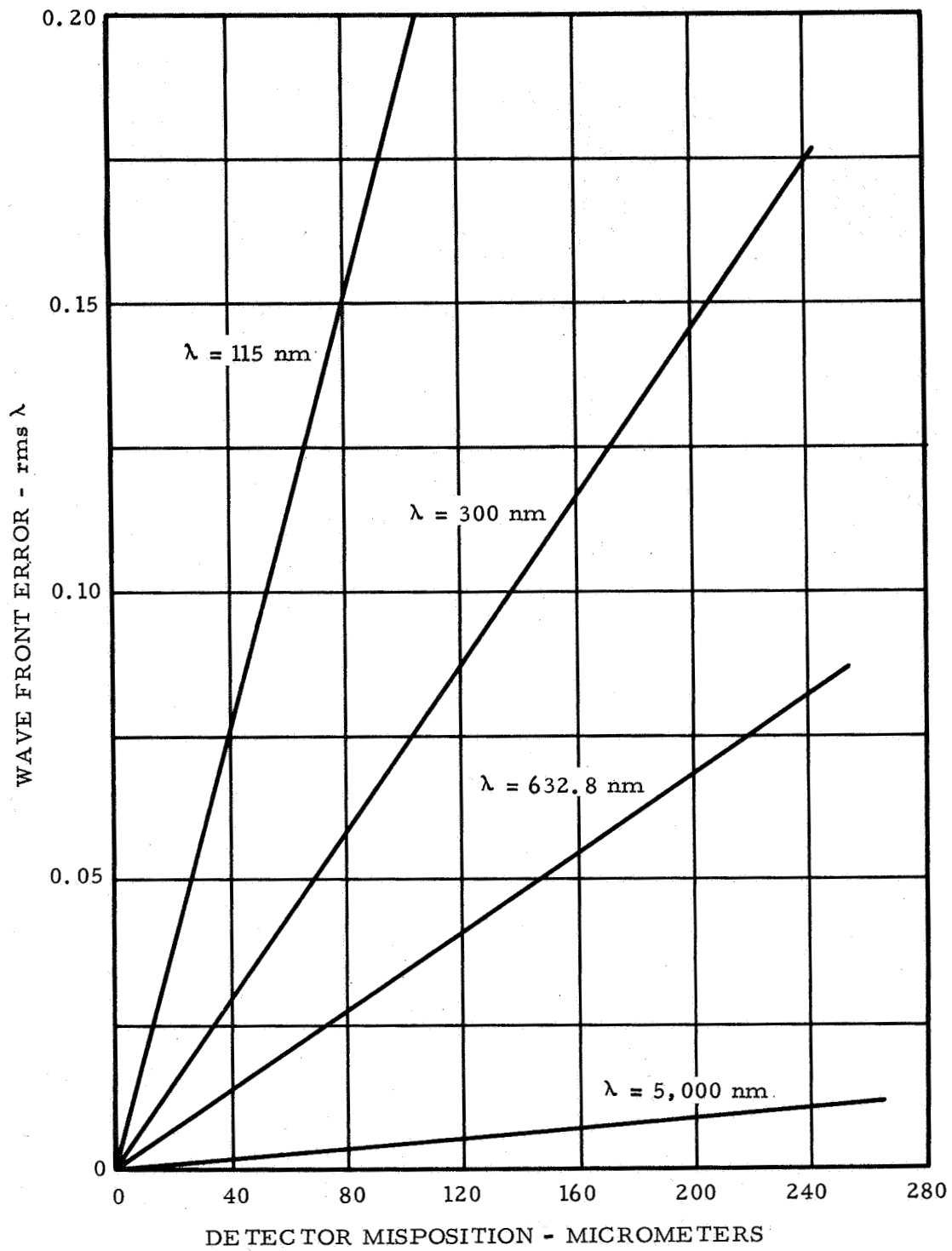


Figure IV-30. Wavefront error (WFE) caused by detector axial misposition (defocus) at  $f/12$  focal plane.

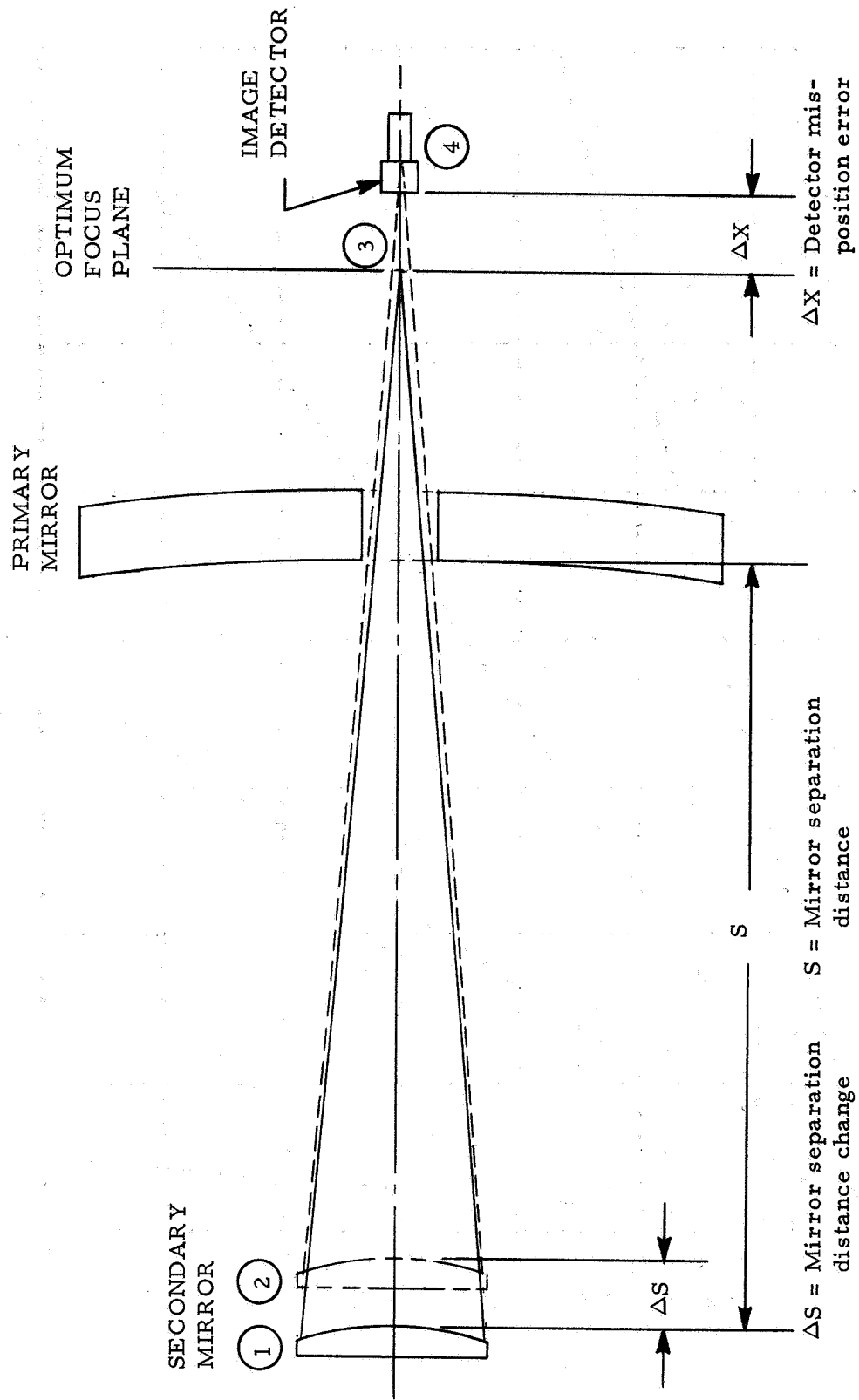


Figure IV-31. Change in mirror separation distance (refocus) to move image position.

system focal ratio of 12, is 5.45. Therefore, image motion is 29.7 times the change in mirror separation distance. This equation is plotted in Figure IV-32.

The WFE at the best focus plane caused by the fact that the secondary mirror is not at its design reference position is insignificant for the mirror movement tolerances of the LST. The fact that the plane of best focus can be moved axially without introducing any significant error can be utilized to compensate for instrument misposition. Figure IV-31 illustrates the case where the image detector has some axial misposition error,  $\Delta X$ , and is at neither the optimum focus plane nor the plane of best focus. The WFE at the detector is rather large for this reason (Figure IV-31). Movement of the secondary mirror from position (1) to position (2) results in movement of the plane of best focus from position (3) to position (4). The WFE caused by the detector not being at the plane of best focus is thereby eliminated.

When the secondary mirror is moved in a direction normal to the telescope axis, the image moves and WFE is introduced. The motion of the image at the telescope  $f/12$  focal plane as a function of secondary mirror decenter is

$$\Delta y' = (1-m) \Delta y_{cc} \quad (5)$$

where  $\Delta y'$  is the image motion at the telescope focal plane and  $\Delta y_{cc}$  is the decenter distance of the secondary mirror measured at the image motion neutral point.

The telescope image serves as the object for the 8X inverse Cassegrainian relay mirror system used with the  $f/96$  field cameras. Motion of the telescope focal plane image is amplified eight times by the relay system. Image motion at the  $f/96$  focal plane caused by motion of the secondary mirror is given by

$$\Delta y'' = (1-m) M \Delta y_{cc} \quad (6)$$

where  $\Delta y''$  is the image motion at the  $f/96$  focal plane and  $M$  is the amplification of the relay mirror system. Equations (5) and (6) are plotted in Figure IV-33.

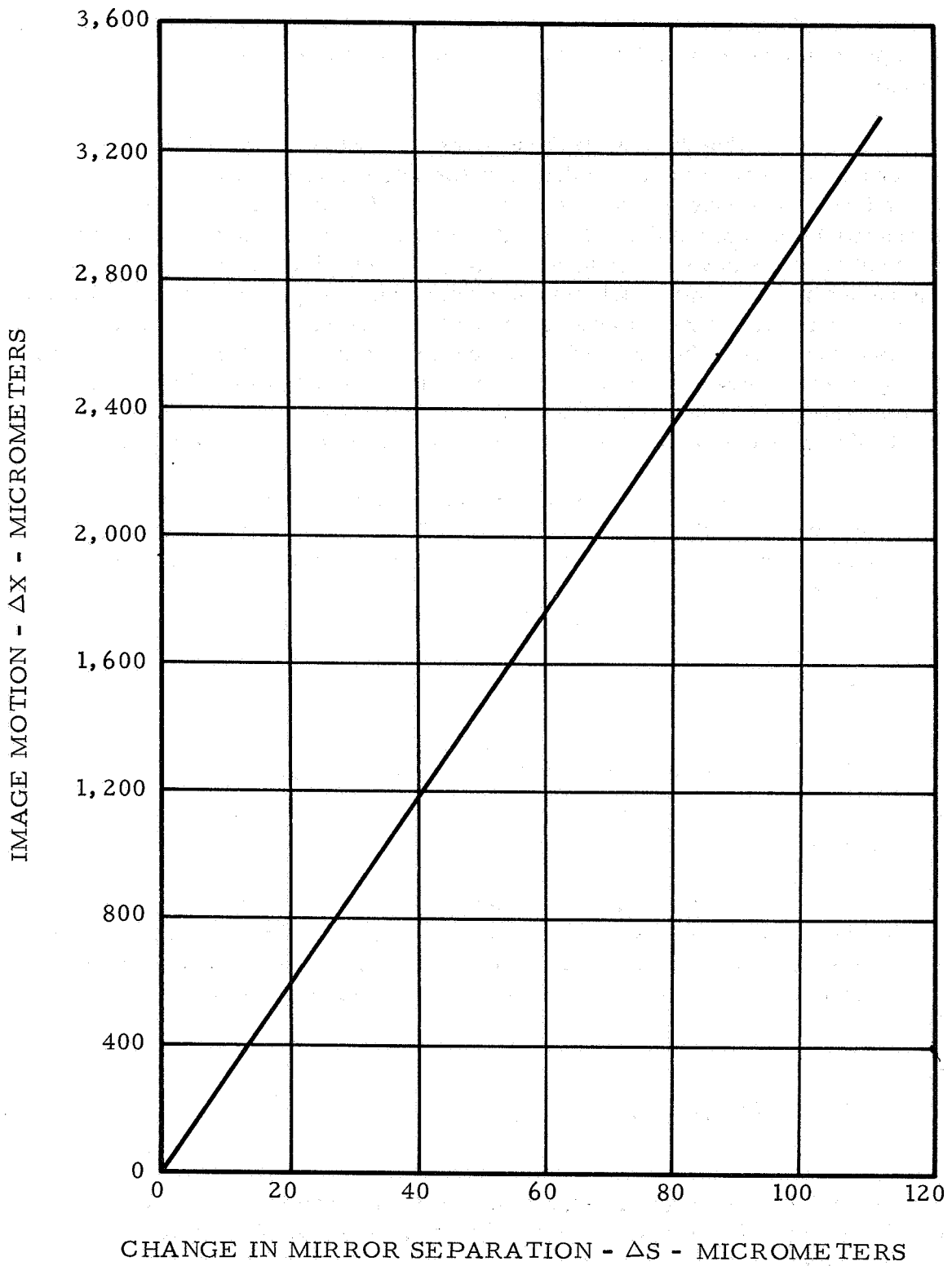


Figure IV-32. Movement of  $f/12$  image as a function of change in mirror separation distance (defocus).

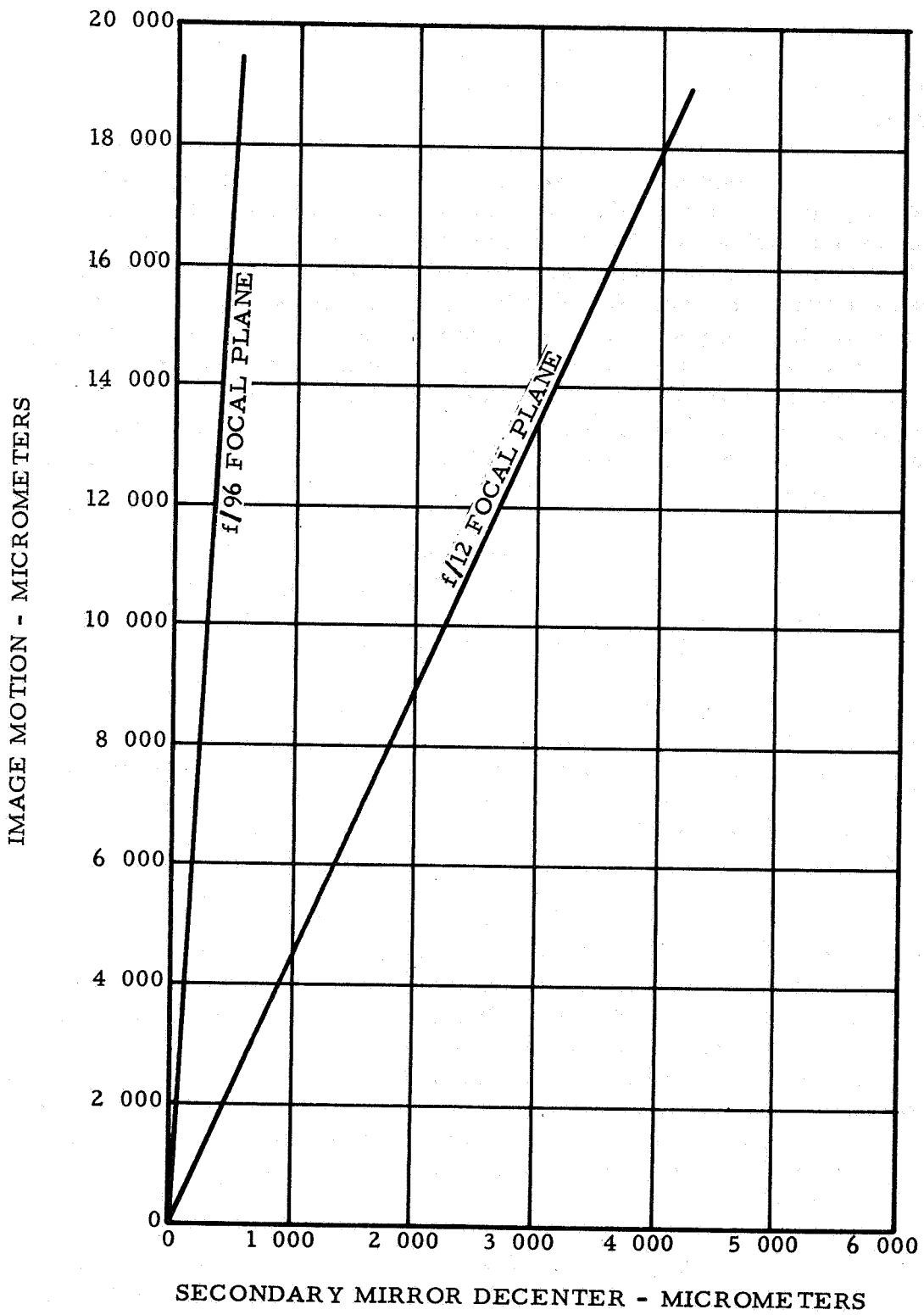


Figure IV-33. Image movement due to secondary mirror decenter.

Transverse movement of the secondary mirror also produces a wavefront error at the focal plane. The magnitude of this error is given by equation (3). This equation is plotted in Figure IV-34 for various wavelengths.

b. Instrument Replacement Tolerances. Adjustment of the secondary mirror to move the plane of best focus to a mispositioned instrument detector will also move the plane of best focus away from the fine guidance sensor and introduce the WFE eliminated at the instrument detector into the guidance sensor. This will increase the guidance error, as shown in Figure IV-35. The guide error is greater for dimmer guide stars. However, the slope of the curve is very shallow for even rather large defocus distances. A guide field defocus of  $100\ \mu\text{m}$  has a negligible effect on the guide system line-of-sight error. Defocus distances of 210 and  $250\ \mu\text{m}$  only increase the system line-of-sight error from its anticipated minimum error of  $0.025\ \mu\text{rad}$  to  $0.026$  and  $0.027\ \mu\text{rad}$  respectively.

Figure IV-36 is a schematic of the LST telescope indicating the  $f/12$  and  $f/96$  focal planes, the fine guidance sensor, and typical instrument locations. Table IV-14 gives the focus tolerances for various allowable resulting WFE values for a reference wavelength of  $632.8\ \text{nm}$ . Separation planes A-A, B-B, and C-C of Figure IV-36 and Table IV-14 represent axial misposition errors of image tubes that might be caused by their replacement during maintenance. The resulting WFE is caused by the misposition of the image tube; no repositioning (refocusing) of the secondary mirror has been considered for these cases. Since there is no repositioning of the secondary mirror, no additional WFE is introduced at the fine guidance sensor.

Separation plane D-D is the same physical location as plane A-A; however, it represents the case where refocusing of the secondary mirror is performed to minimize WFE at the image tube. A change in mirror separation distance (refocusing) can eliminate WFE caused by axial mispositioning of the image tube. However, this defocuses the fine guidance field, increases WFE at the guidance field, and thereby increases the guidance error, as shown in the last column of Table IV-14. The WFE values for equal misposition errors would be equal for cases A-A and D-D, although the errors would be at different focal planes. The slight differences in the numerical values of resulting WFE shown in Table IV-14 for the two cases are due to round-off errors in the sensitivities.

Separation plane E-E represents the case where the fine guidance sensor and the  $f/96$  cameras are replaced as a unit. There is an



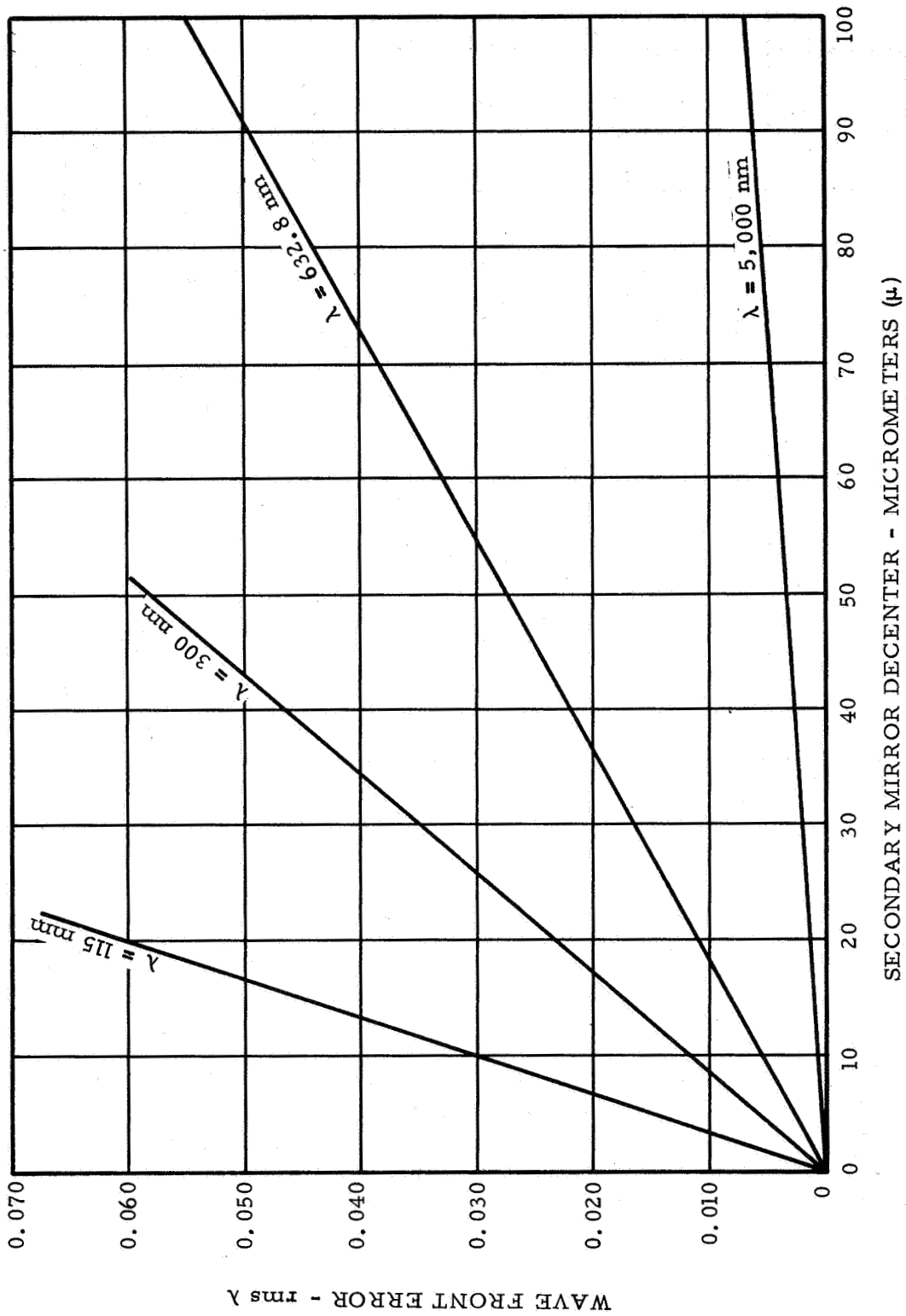


Figure IV-34. WFE at f/12 focal plane due to secondary mirror decenter.

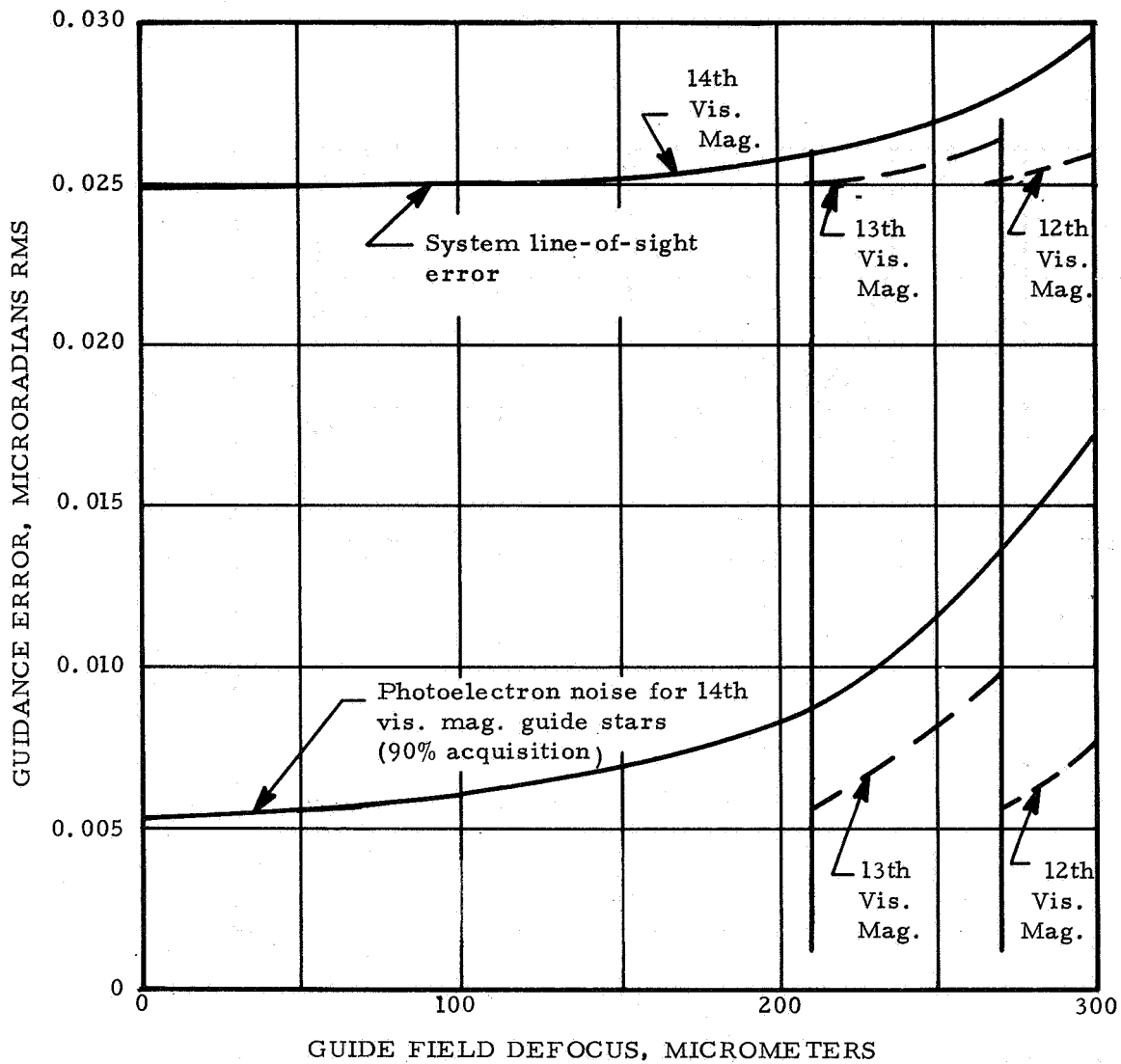


Figure IV-35. Guidance error as a function of guide field defocus.

axial misposition error between this unit and the f/12 focal plane, but there is no misposition error between the fine guidance sensor and the f/96 cameras. Repositioning the secondary mirror eliminates the WFE due to mispositioning, both at the fine guidance field and at the f/96 cameras; however, it does introduce additional WFE at the f/12 focal plane. Thus, any instrument other than the f/96 cameras would be out of focus with this mirror spacing.

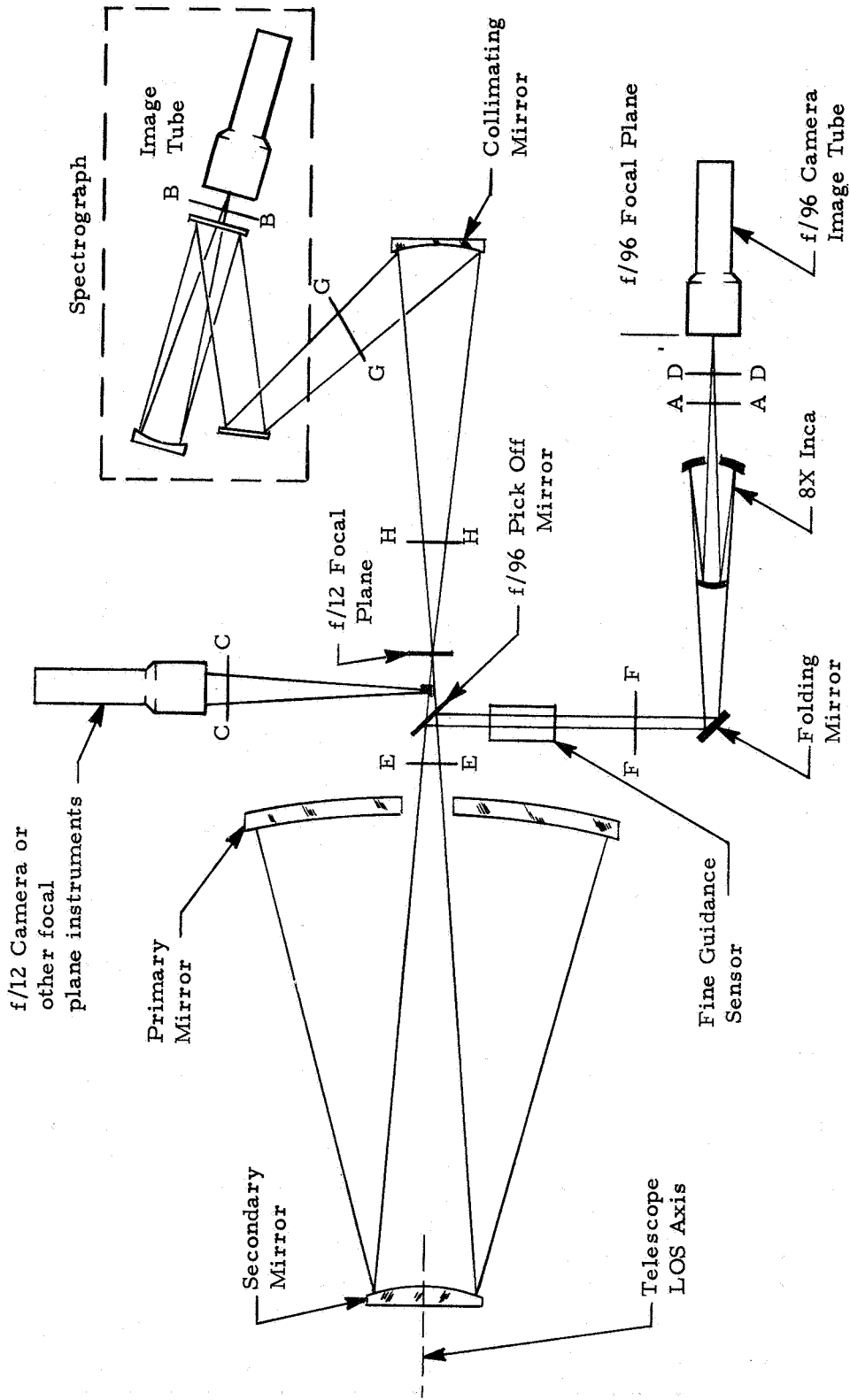


Figure IV-36. Light path typical SIP instruments.

TABLE IV-14. LST FOCUS TOLERANCES

Separation Plane (Fig. IV-36)	Item Replaced	Axial Misposition		No Change in Mirror Separation Distance		Change in Mirror Separation Distance					Location of WFE	Guide Error ( $\mu$ rad)				
		$(\mu\text{m})$	(in.)	Sensitivity to Axial Misposition WFE per $\mu\text{m}$		Required Image Motion		Sensitivity to Mirror $\Delta$ S					Resulting WFE ( $\lambda$ rms)			
				$(\mu\text{m})$	(in.)	Image Motion	WFE - $\lambda$ rms per $\mu\text{m}$ $\Delta$ S	Needed $\Delta$ S ( $\mu\text{m}$ )								
A-A	f/96 camera image tube	25	0.001	$5.36 \times 10^{-4}$								0.000	f/96 camera image tube	0.0250		
		254	0.010									0.001				
		2 540	0.100									0.014				
		25 400	1.000									0.136				
B-B	Spectrograph image tube	25	0.001	$3.43 \times 10^{-4}$								0.009	Spectrograph image tube	0.0250		
		254	0.010									0.087				
C-C	Image tube of f/12 focal plane instrument	25	0.001	$3.43 \times 10^{-4}$									0.009	Image tube of f/12 focal plane instrument	0.0250	
		60	0.002										0.021			
D-D	f/96 camera image tube	80	0.003	$5.36 \times 10^{-4}$												
		100	0.004													0.027
		120	0.005													0.034
		160	0.006													0.041
		190	0.007													0.055
		250	0.010													0.065
E-E	Fine guidance sensor, 8 X Inca, and f/96 cameras	25	0.001	$5.36 \times 10^{-4}$												
		254	0.010													0.001
		2 540	0.100													0.134
		25 400	1.000													0.134
F-F	8 X Inca and f/96 cameras or any instrument of f/12 focal plane	25	0.001	$5.36 \times 10^{-4}$												
		254	0.010													0.001
		2 540	0.100													0.013
		25 400	1.000													0.134
G-G	Spectrograph	25	0.001	$5.36 \times 10^{-4}$												
		254	0.010													0.001
H-H	Collimating mirror	25	0.001	$5.36 \times 10^{-4}$												
		254	0.010													0.001

Not sensitive to variation in instrument location along light path, since light is collimated.  
 Axial misposition of collimating mirror results in loss of spectrograph resolution because light is not collimated. Secondary mirror adjustment for misposition could produce collimation of light to spectrograph for a stellar image, but other factors would cause loss of resolution.

Separation plane F-F represents the case of axial misposition of the 8X Inca and f/96 camera system. Refocusing of the secondary mirror can eliminate the WFE caused by this misposition, but additional WFE is thereby introduced at the fine guidance sensor and guide error is increased. This is shown in the last column of Table IV-14.

Separation plane G-G represents axial misposition of a spectrograph. Misposition in this direction does not introduce additional WFE because the light is collimated and operation of the instrument is not affected.

Separation plane H-H represents axial misposition of the collimating mirror. This will result in the light reflected from this mirror not being collimated. This will cause a loss of spectral resolution in the spectrograph. If the secondary mirror is refocused, the light from the collimating mirror will be collimated if the viewing object is a star. However, other factors will cause loss of resolution and no advantage will be realized by refocusing.

The data given in Table IV-14 show that instrument misposition tolerances depend upon the WFE and guidance error that are acceptable. Refocusing of the secondary mirror can compensate for misposition errors at one plane but this will increase WFE at some other plane.

Preliminary SIP instrument alignment tolerances have been specified by Kollsman Instrument Corporation. These tolerances are given in Table IV-15 together with the WFEs that will result from these maximum allowable defocus mispositions. The WFE data in Table IV-15 are for a reference wavelength of 632.8 nm. WFEs for other wavelengths may be obtained from Figure IV-30. The root sum square WFE of the telescope WFE of 0.050 wavelength and the focus misposition WFE are also shown for each instrument in Table IV-15. The instrument misposition WFE and the root sum square WFE are plotted in Figure IV-37 as a function of instrument misposition error in focus. The reference wavelength for Figure IV-37 is 632.8 nm.

The misposition tolerance in focus of the f/96 camera at the f/96 focal plane is much greater than the other instrument tolerances. This fact is illustrated in Figure IV-38. The last line of Table IV-15 gives the tolerance at the f/96 focal plane for the same misposition WFE that would be created by the given position tolerance at the f/12 focal plane.

TABLE IV-15. SIP INSTRUMENT ALIGNMENT TOLERANCES

Instrument and Operating Range	Focus Tolerance X-Axis + or - ( $\mu\text{m}$ ) (in.)	Slit Location in Y-Z Plane + or - ( $\mu\text{m}$ ) (in.)	Resulting WFE at $\lambda = 632.8 \text{ nm}$	
			Axial Mis- alignment (defocus)	RSS of Instrument + Telescope <sup>a</sup> WFE
Echelle Spectrograph No. 1 115 to 180 nm	80 0.0032	400 0.016	0.027	0.057
Echelle Spectrograph No. 2 180 to 350 nm	100 0.0040	400 0.016	0.034	0.061
Faint Object Spectrographs 1A: 115 to 160 nm	80 0.0032	400 0.016	0.027	0.057
1B: 160 to 220 nm	100 0.0040	400 0.016	0.034	0.061
2A: 220 to 352 nm	120 0.0048	400 0.016	0.041	0.065
2B: 352 to 660 nm	190 0.0076	400 0.016	0.065	0.082
3: 660 to 1 000 nm	250 0.0100	400 0.016	0.086	0.100
Field Cameras				
f/12 Camera	160 0.0064	1 000 0.040	0.055	0.075
f/96 Camera at f/12 Interface	160 0.0064	1 000 0.040	0.055	0.075
f/96 Camera at f/96 Interface	160 0.0064	1 000 0.040	0.00085	0.050
	10 200 0.409	1 000 0.040	0.055	0.075

a. Based upon an assumed WFE of 0.050 at the telescope principal focus.

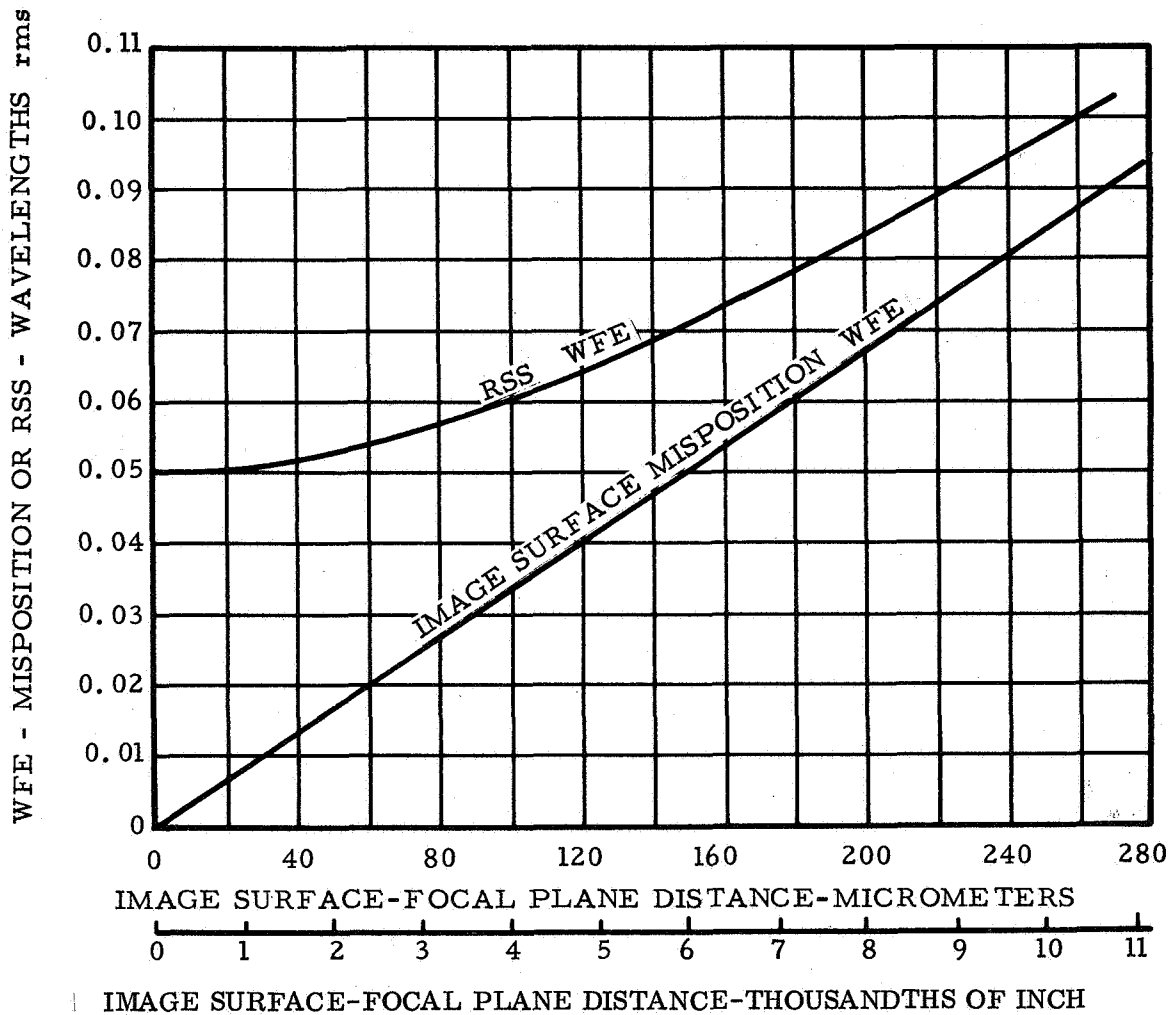


Figure IV-37. Instrument misposition WFE at the f/12 focal plane and RSS WFE as a function of misposition distance in focus for  $\lambda = 632.8 \text{ nm}$ .

Lateral misalignment of instruments will not create WFE but will simply cause a portion of the data field to fall outside the instrument field of view. The image could be moved by moving the secondary mirror laterally, but this would introduce WFE at the focal plane.

c. Conclusions. It should be possible to locate instruments replaced during on-orbit maintenance within the tolerances listed in Table IV-15. Even if these tolerances are exceeded, the instruments will still function but performance will be degraded. Replacement of the f/96 camera tubes will require the least precision.

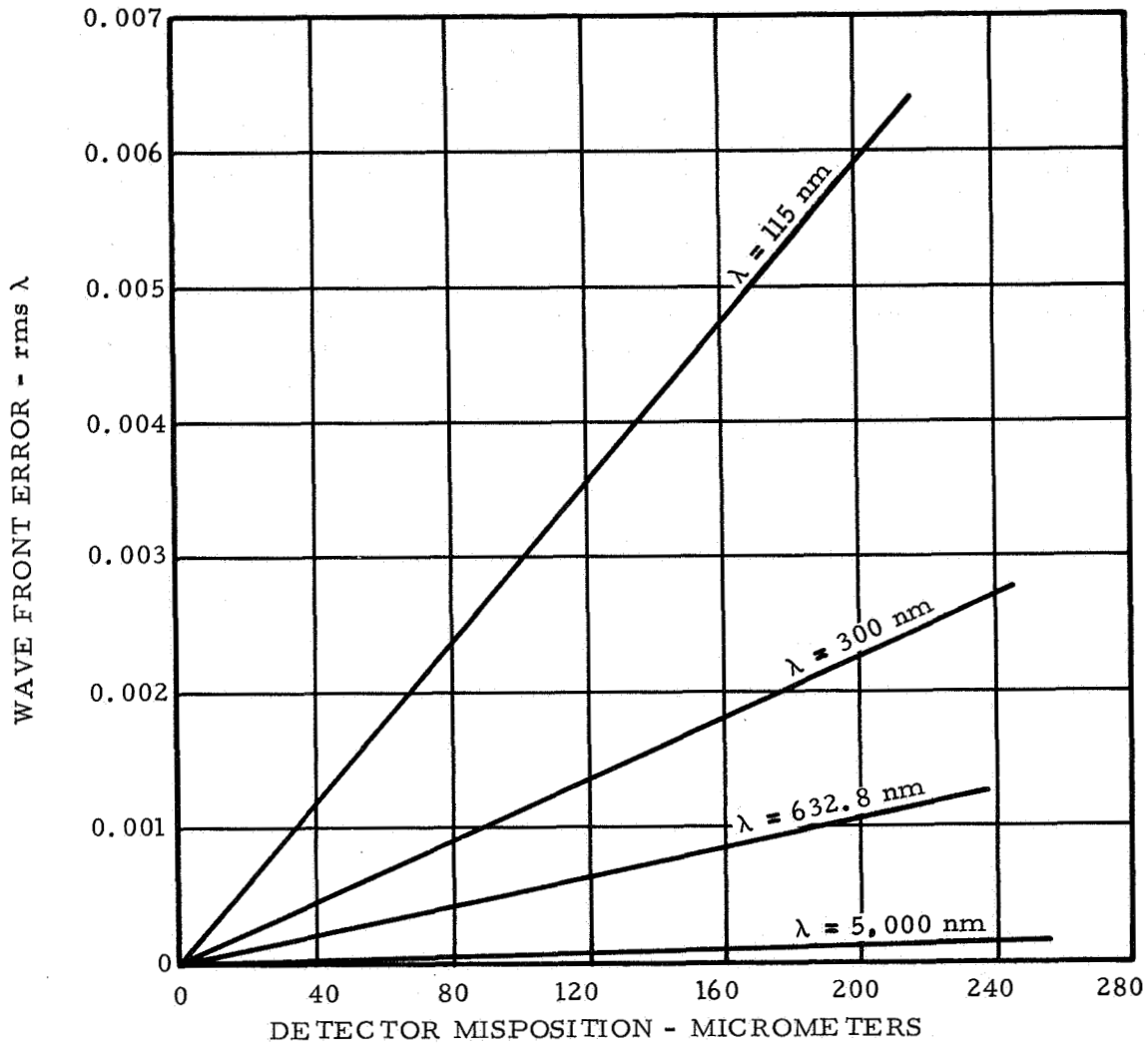


Figure IV-38. WFE caused by detector axial misposition (defocus) at f/96 focal plane.

## 12. Overall Performance Trades

a. Introduction. Pointing instability and error relative to the instrument field of view in the LST will degrade instrument performance. It is, of course, unreasonable to expect absolute zero pointing instability or error, and a certain amount of each must be anticipated. In Volume III, Itek presents values for pointing instability and error which it anticipates. In addition, it is possible that the pointing parameters could exceed these values for any one of the following reasons:



1. Failure of the SSM to meet its pointing requirements so that the FGS could not handle the errors.

2. Failure of the FGS to meet its pointing specifications.

3. Mechanical flexure within the instrument package.

The field cameras will be affected by pointing instability. Instability of the spacecraft will result in the smearing of images over time exposures, which will in turn cause lower resolution and require longer exposure times. Spectrograph performance will be affected principally by pointing error but also by pointing instability. The spectrograph entrance slit may be widened to accommodate these errors on stellar sources but at the expense of wavelength resolution. If the width of this slit is not increased, degradation of pointing parameters will result in longer exposure time requirements.

The dependence of spectrograph performance has been considered separately for pointing instability and pointing error for this preliminary analysis. While separate treatment is desirable for assessment of the relative importance of the two pointing parameters, in reality both parameters will occur simultaneously. An investigation of the combined effect of both parameters would be desirable as a follow-on study. In addition, two of the graphs included here are presented for single values of slit width. Since the slit width will be adjustable, a determination of the effect of the pointing parameters for other slit values would be desirable.

b. Effect on Field Cameras of Pointing Stability Degradation.

Recording an image with any data sensor takes a finite amount of time and for some experiments conducted with the LST, the time required will be several hours. If the image moves during this time, the effect will be degradation of the image. Pointing instabilities will cause such motion.

Analytically, image motion is best handled by considering it a modification of the light distribution in the object point, i. e., the object point will be converted from a delta function (a mathematical point) to an image motion spread function,  $I_m$ , in which the value of  $I_m$  for each area increment is proportional to the time the object point dwells in that particular incremental area. This spread function may then be convolved with the telescope point spread function to derive the effective system point spread function.

The Itek Volume III contains a telescope point spread function for a WFE of 0.05 wavelength rms at 633 nm and a secondary mirror

obscuration ratio of 0.30. That company believes these values to be achievable and realistic. Their function may be approximated by the Gaussian function,

$$I_s(x, y) = 0.8 I_{sp}(0, 0) \exp\left(-\frac{x^2 + y^2}{\tau^2}\right) \quad (7)$$

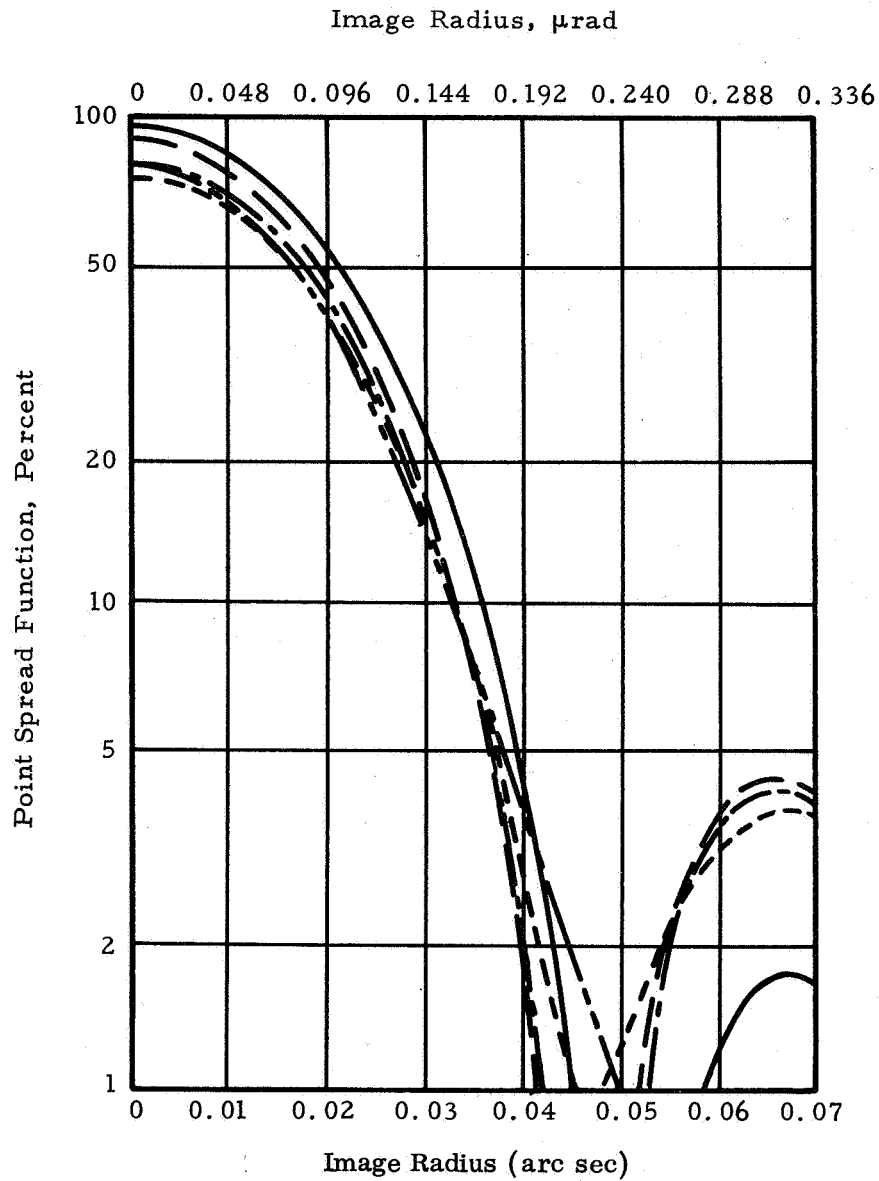
This function expresses the radiant power per unit area, which is the radiant flux  $I_s(x, y)$ , in the image at any point  $x, y$  in the image plane in terms of this quantity  $I_{sp}$  at the center of the image for a perfect, stationary telescope.

The quantity  $\tau$  is a measure of the image size and is the distance from the image center for which the radiant flux drops to  $1/e$  of its central value. For a perfect telescope, the Fraunhofer diffraction theory predicts that  $\tau$  is proportional to  $\lambda/D$ . A curve fitting to the point spread function computed by Itek for the above-quoted values of WFE and obscuration ratio indicates that, for the LST, the quantity  $\tau$  will be given approximately by  $0.000037 \lambda$  arc sec for the wavelength expressed in nanometers. Because of the WFE,  $\tau$  will deviate somewhat from this dependence at the wavelength extremes. Note that this relationship indicates a decrease in image size for a decrease in wavelength. The wavelength-dependent behavior of all of the following graphs is explained by this relationship. The fit of this approximation to the Itek point spread function curve is shown in Figure IV-39.

It should be noted that this approximation is made so that tractable, analytical solutions may be derived. These solutions should be useful for order-of-magnitude estimates. If exact solutions are desired, it would be necessary to numerically convolve the Itek point spread function for the stationary case with the image motion point spread function for each rms instability value and wavelength of interest. Subsequent integrations would also have to be performed numerically.

From equation (7) the radiant power falling into the elemental area  $dx dy$  at  $x, y$  is

$$dP_s = 0.8 I_{sp}(0, 0) \exp\left(-\frac{x^2 + y^2}{\tau^2}\right) dx dy \quad (8)$$



	$\epsilon\%$	$\omega, \lambda$ rms	$\theta$ , arc sec rms
—————	0	0	0
-----	30	0	0
- - - - -	30	0.05	0
- . - . -	30	0.05	0.005
.....	Gaussian Approximation		

NOTE: Gaussian Approximation fitted to curve for  
 $\epsilon = 30\%$ ,  $\omega = 0.05$ , and  $\theta = 0$

Figure IV-39. Fit of the Gaussian approximation to the point spread function computed by Itek.

For random image motion (LST motion) this radiant power will be spread out also as a Gaussian function. The image motion point spread function may be written as

$$d \text{ Im } (r) = \frac{d P_s}{\pi \rho^2} \exp \left( -\frac{r^2}{\rho^2} \right) \quad (9)$$

The parameter  $\rho$  denotes the amount of image motion (pointing instability) and represents the rms pointing deviation of the telescope. Substitution of equation (8) and the relation

$$r^2 = (x - x_0)^2 + y^2 \quad (10)$$

into equation (9) and integration over  $x$  and  $y$  leads to the convolution integral for the radiant flux at  $x_0, 0$ . It is

$$I_m(x_0, 0) = \frac{0.8 I_{sp}(0, 0)}{\pi \rho^2} \int_{-\infty}^{\infty} \int_{-\infty}^{\infty} \exp \left\{ - \left[ \frac{(x - x_0)^2 + y^2}{\rho^2} + \frac{x^2 + y^2}{\tau^2} \right] \right\} dy dx. \quad (11)$$

The integration over  $y$  may be performed at once with the aid of an integral table. After completion of the square of the terms in  $x$  followed by a change of variables, the integration over  $x$  is performed in the same manner. The result is

$$I_m(x_0, 0) = \frac{0.8 \tau^2}{\tau^2 + \rho^2} I_{sp}(0, 0) \exp \left( -\frac{x_0^2}{\tau^2 + \rho^2} \right) \quad (12)$$

This overall image point spread function, which includes the effects of WFE, secondary mirror obscuration, and image motion, is seen to be still another Gaussian function with new scale factors. The Strehl ratio follows as

$$\frac{I_m(0, 0)}{I_{sp}(0, 0)} = \frac{0.8 \tau^2}{\tau^2 + \rho^2} \quad (13)$$

The definition of resolution is quite arbitrary and for convenience may be taken as

$$\alpha = \left( \tau^2 + \rho^2 \right)^{1/2} , \quad (14)$$

which is the angular distance at which the radiant flux drops to 1/e of its central value. In the static case ( $\rho = 0$ ) the resolution  $\alpha = \tau$ . Resolution  $\alpha$  as a function of pointing instability  $\rho$  is presented in Figure IV-40 for  $\lambda = 100$  nm to  $\lambda = 1000$  nm. The variation of Strehl ratio as a function of  $\rho$  is presented in Figure IV-41 for the same wavelengths.

The behavior of the curves in Figures IV-40 and IV-41 is explained by the different stationary image sizes at the different wavelengths. At short wavelengths where the stationary image is small, the effective image size increases rapidly with increasing pointing instability and produces simultaneously a sharp drop in central flux and Strehl ratio. At longer wavelengths the stationary image is larger and image motion does not produce so striking an effect.

An important system performance parameter is the exposure time necessary to record stellar images with the camera to a given limiting magnitude. For a stellar image this exposure time is inversely proportional to the encircled radiant power incident in an area comparable to the tube resolution. The effect of pointing instability, and therefore image motion, will be to spread the radiant power in a stellar image over a larger area and require a longer exposure time. Thus, the exposure time to a given limiting magnitude is given by an expression of the form

$$\frac{1}{t} = C \int_0^{a/2} 2\pi x_0 I_m(x_0, 0) dx_0 \quad (15)$$

for a resolution element diameter of  $a$ . After substitution of equation (12) into equation (15) and evaluation of the integral, one obtains

$$\frac{1}{t} = 0.8\pi C \tau^2 I_{sp}(0,0) \left[ 1 - \exp\left(-\frac{a^2/4}{\tau^2 + \rho^2}\right) \right] . \quad (16)$$

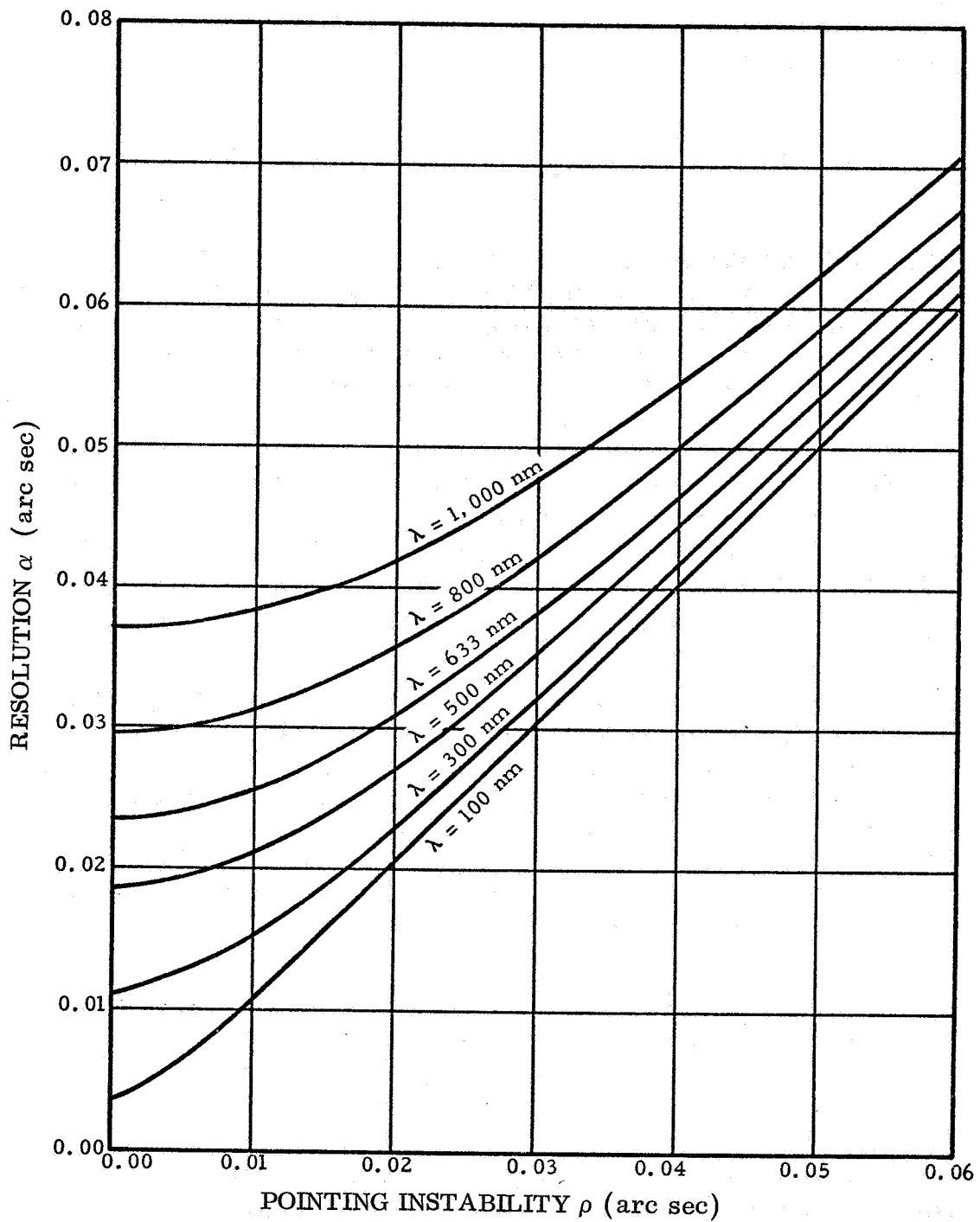


Figure IV-40. Camera resolution as a function of pointing instability.

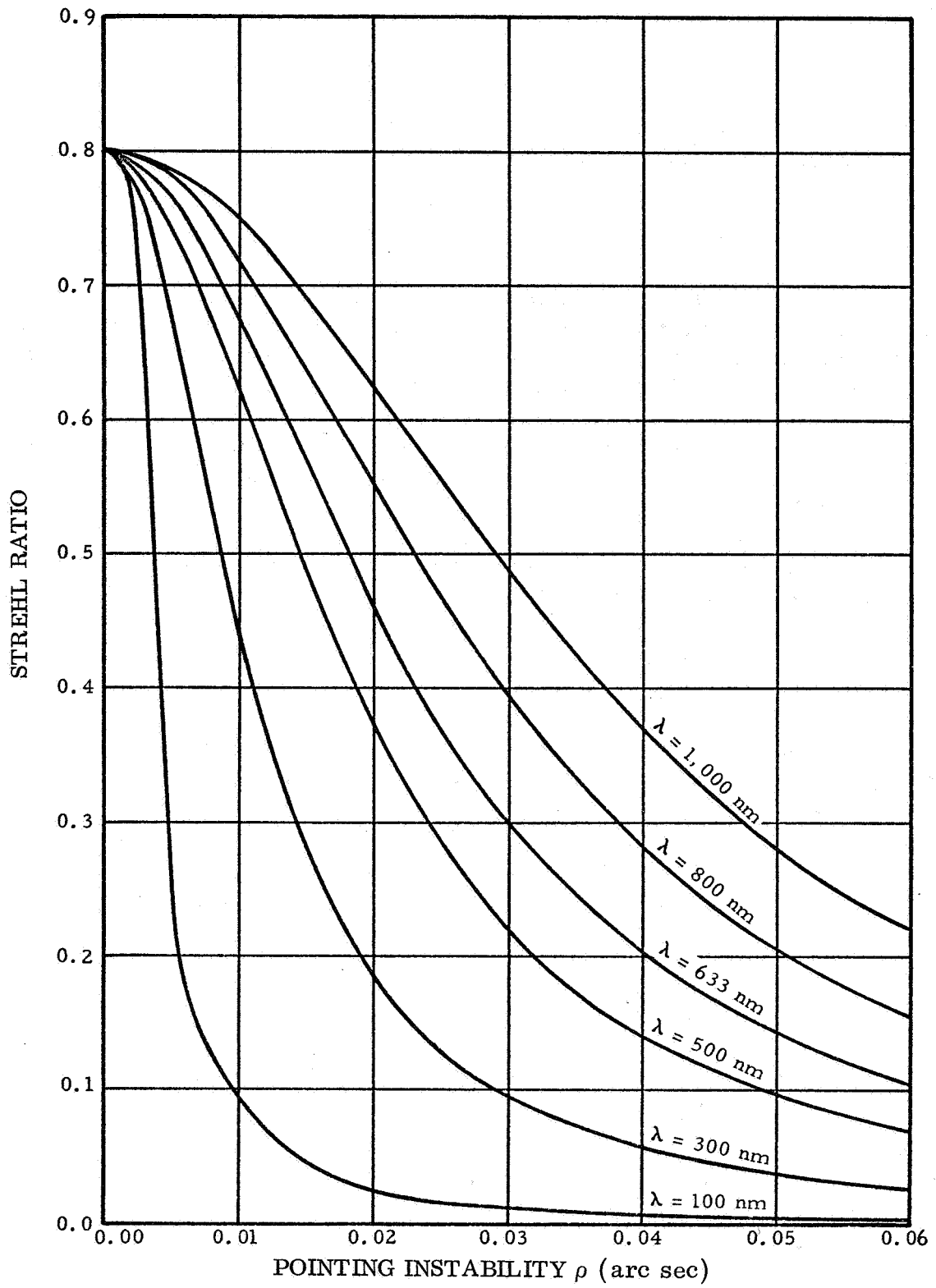


Figure IV-41. Strehl ratio as a function of pointing instability.

Now define  $t = t_0$  for  $\rho = 0$ . This leads to

$$\frac{t}{t_0} = \frac{1 - \exp\left(-\frac{a^2}{4\tau^2}\right)}{1 - \exp\left(-\frac{a^2/4}{\tau^2 + \rho^2}\right)} \quad (17)$$

This equation represents the exposure time in units of the exposure time for no motion. It is graphed as a function of pointing instability in Figure IV-42. The resolution size has been taken as 0.075 arc sec, which corresponds to a tube resolution of 20 line pairs/mm for a 3 m telescope at f/96.

In Figure IV-42, note that for short wavelengths the exposure time is practically unaffected by small values of pointing instability, but rises more rapidly at larger values. Here the stationary image is small and easily fills the resolution area at small instability values. The radiant power within the resolution area decreases rapidly after the motion smeared image has effectively exceeded the bounds of the resolution area. At longer wavelengths (larger stationary images) the stationary image (at  $\rho = 0$ ) may already effectively exceed the resolution area size, and the decrease in encircled radiant power with increasing pointing instability is not so marked.

c. Spectrograph Exposure Time for Stellar Sources as a Function of Slit Width. Before investigation of the effects of pointing degradation upon spectrograph performance, it is interesting to see how spectrograph exposure time depends on slit width. It is assumed that during an exposure the stellar image would be trailed along the slit so as to provide a sufficiently wide spectrum. Assume no pointing error or instability. The exposure time is given by

$$\frac{1}{t} = C \int_{-\infty}^{\infty} \int_{-\frac{\Delta S}{2}}^{\frac{\Delta S}{2}} 0.8 I_{sp}(0,0) \exp\left(-\frac{x^2 + y^2}{\tau^2}\right) dx dy \quad (18)$$

Upon evaluation of the integrals,



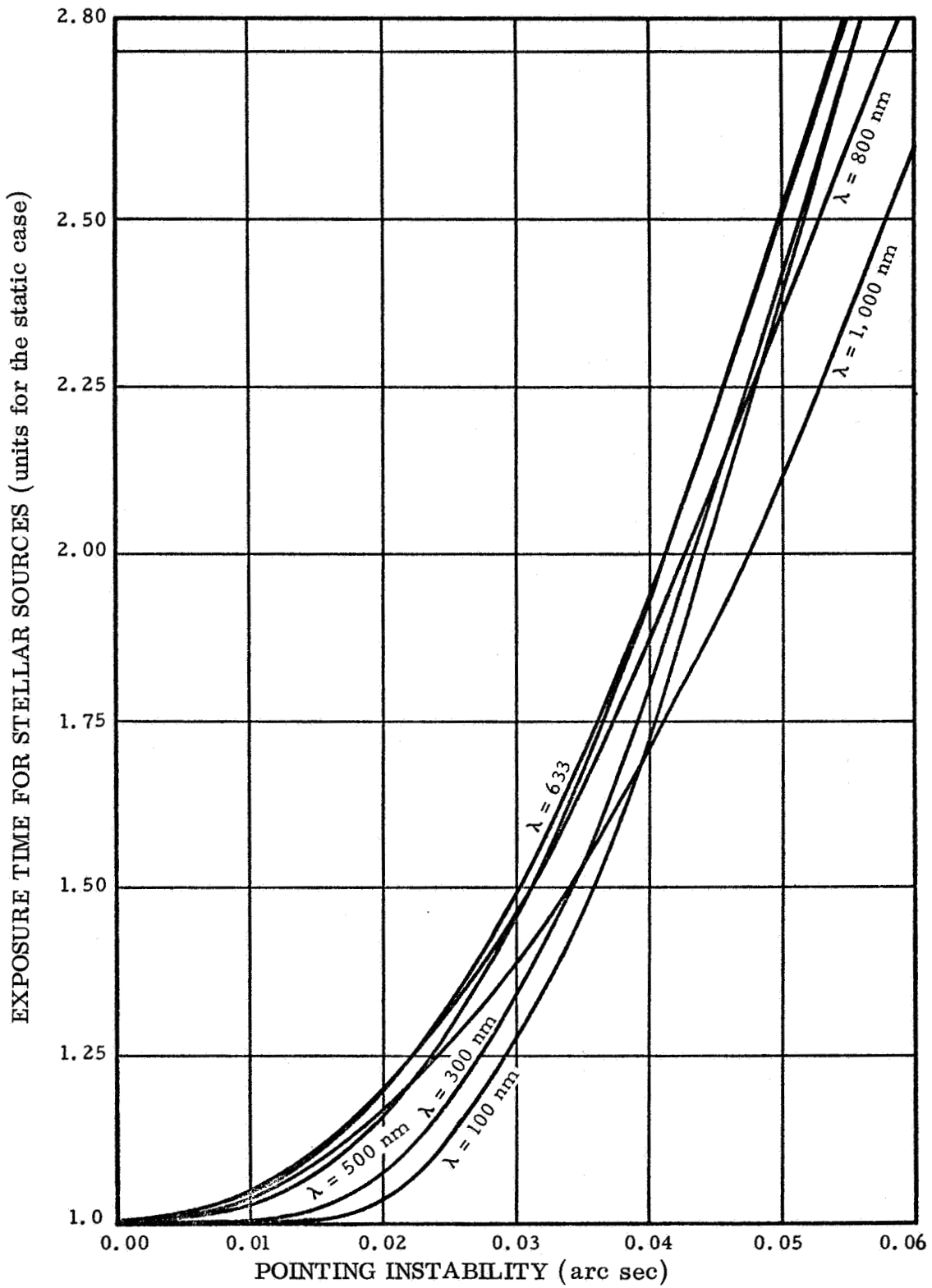


Figure IV-42. Camera exposure time as a function of pointing instability for stellar sources.

$$\frac{1}{t} = 0.8\pi C_T^2 I_{sp}(0,0) \operatorname{erf} \frac{\Delta S}{2\tau} \quad (19)$$

Define  $t = t_0$  for  $\Delta S \rightarrow \infty$ . By substitution and then division,

$$\frac{t}{t_0} = \frac{1}{\operatorname{erf} \left( \frac{\Delta S}{2\tau} \right)} \quad (20)$$

Exposure time  $t/t_0$  is a function of slit width  $\Delta S$ , as expressed by equation (20). This relationship is shown in Figure IV-43. At large slit widths, the exposure time approaches unity asymptotically. At short wavelengths the stellar image is small and easily fills the slit, even at small slit widths. The large image at long wavelengths overlaps the slit markedly at small slit widths.

d. Effect on Spectrographs of Pointing Error and Instability. For most spectrograph observations carried out aboard the LST, an entrance slit will probably be used. Conventionally, an entrance slit is required in spectrography to achieve wavelength resolution on extended images. In the case of spectrography of a sufficiently small individual stellar image, the entrance slit serves to exclude extraneous sources and radiation. During the exposure the star's image is trailed along the slit for a short distance so that the spectrum recorded will have sufficient width. Should pointing error or instability occur during such spectrograph exposures aboard the LST, three alternative results are possible.

1. If the spectrograph entrance slit is widened to accommodate the error or instability, reduced wavelength resolution will result.

2. If the slit width remains fixed, longer exposure times will be required because of the smaller amount of starlight passing through the slit.

3. The slit may be widened somewhat so that shorter exposure times are secured at the expense of some wavelength resolution.

The effect of pointing error and instability on spectrograph exposure times has been calculated. Let us consider pointing accuracy first.

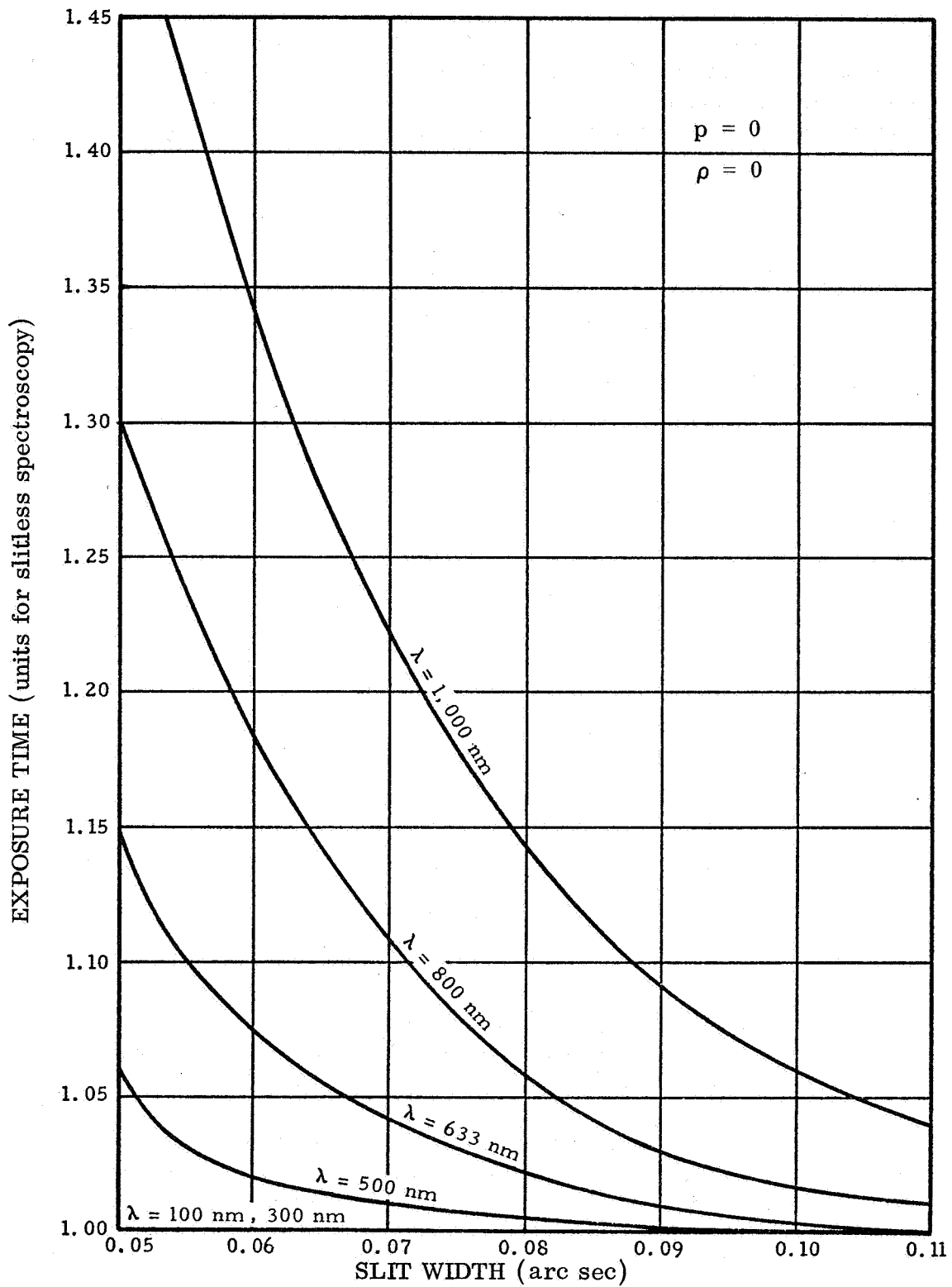


Figure IV-43. Spectrograph exposure time as a function of slit width.

If the reciprocity law holds, then exposure time will be inversely proportional to the amount of starlight passing through the slit. Perfect pointing stability is assumed, and this amount of light is obtained by integration of equation (7). For a pointing error  $p$  perpendicular to the slit, the exposure time is given by

$$\frac{1}{t} = C \int_{-\infty}^{\frac{\Delta S}{2} + p} \int_{-\left(\frac{\Delta S}{2} - p\right)}^{\infty} 0.8 I_{sp}(0,0) \exp\left(-\frac{x^2 + y^2}{\tau^2}\right) dx dy, \quad (21)$$

where  $C$  is a constant. For perfect pointing, one may define  $t_0$  by

$$\frac{1}{t_0} = \frac{1}{t}, \quad (p = 0) \quad (22)$$

After division of equation (22) by equation (21) and evaluation of the integrals, the result is

$$\frac{t}{t_0} = \frac{2 \operatorname{erf}\left(\frac{\Delta S}{2\tau}\right)}{\operatorname{erf}\left(\frac{\Delta S}{2\tau} + \frac{p}{\tau}\right) + \operatorname{erf}\left(\frac{\Delta S}{2\tau} - \frac{p}{\tau}\right)} \quad (23)$$

The error function  $\operatorname{erf}$  is the integral of the Gaussian distribution and is tabulated in the more extensive mathematical tables. Equation (23) is graphed in Figure IV-44 for  $\lambda = 100 \text{ nm}$  to  $\lambda = 1000 \text{ nm}$ .

Exposure time as a result of pointing instability is obtained similarly by integration of equation (12), where perfect pointing accuracy is assumed. For an instability  $\rho$ , the exposure time  $t$  is given by

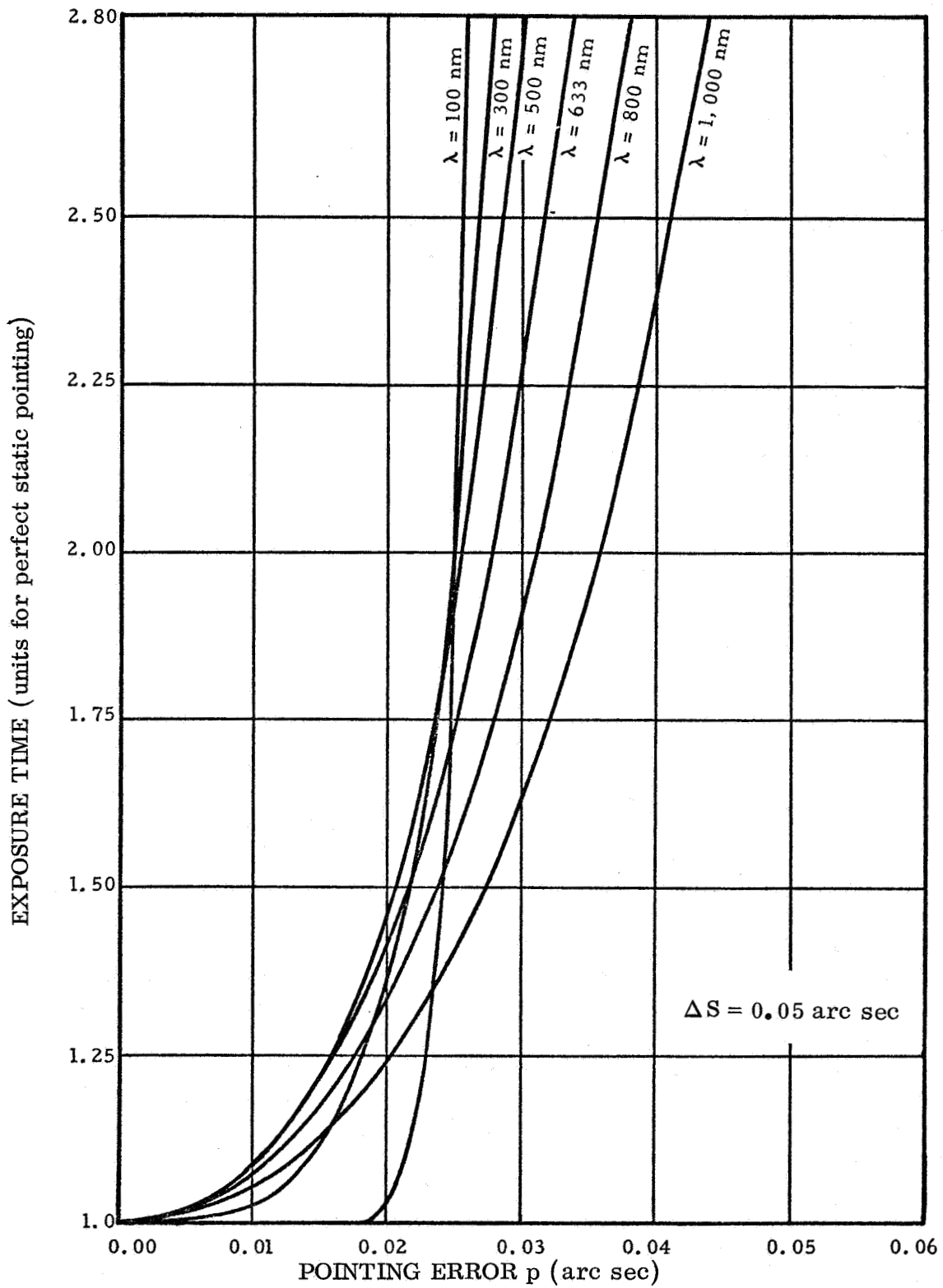


Figure IV-44. Spectrograph exposure time as a function of pointing error.

$$\frac{1}{t} = C \int_{-\infty}^{\infty} \int_{-\frac{\Delta S}{2}}^{\frac{\Delta S}{2}} \frac{0.8 \tau^2}{\tau^2 + \rho^2} I_{sp}(0,0) \exp\left(-\frac{x^2 + y^2}{\tau^2 + \rho^2}\right) dx dy \quad (24)$$

For no instability the exposure time  $t_0$  is given by

$$\frac{1}{t_0} = \frac{1}{t}, \quad (\rho = 0) \quad (25)$$

which is equivalent to equation (22). After division of equation (23) by equation (24) and evaluation of the integrals, one obtains.

$$\frac{t}{t_0} = \frac{\operatorname{erf} \frac{\Delta S}{2\tau}}{\operatorname{erf} \left[ \frac{\Delta S}{2(\tau^2 + \rho^2)^{1/2}} \right]} \quad (26)$$

This equation is graphed in Figure IV-45 for the same wavelength range.

Consider the effect of pointing error as shown by Figure IV-44. At short wavelengths where the image is small, the exposure time increases rapidly as the image passes behind a slit jaw. This exposure time increase is not as marked for the larger images at longer wavelengths. As shown in Figure IV-45, the effect of small amounts of pointing instability upon a small image at short wavelengths does not noticeably affect spectrograph exposure time until the image begins to fill the slit. As pointing instability increases to larger values and the effectively enlarged image overlaps the slit, the exposure time rapidly increases. These effects are not as marked at longer wavelengths. Note by comparison of Figures IV-44 and IV-45 that the pointing error becomes overwhelmingly important at large pointing parameter values.

As just mentioned, the spectrograph entrance slit may be widened to accommodate pointing degradation so that no increase in exposure

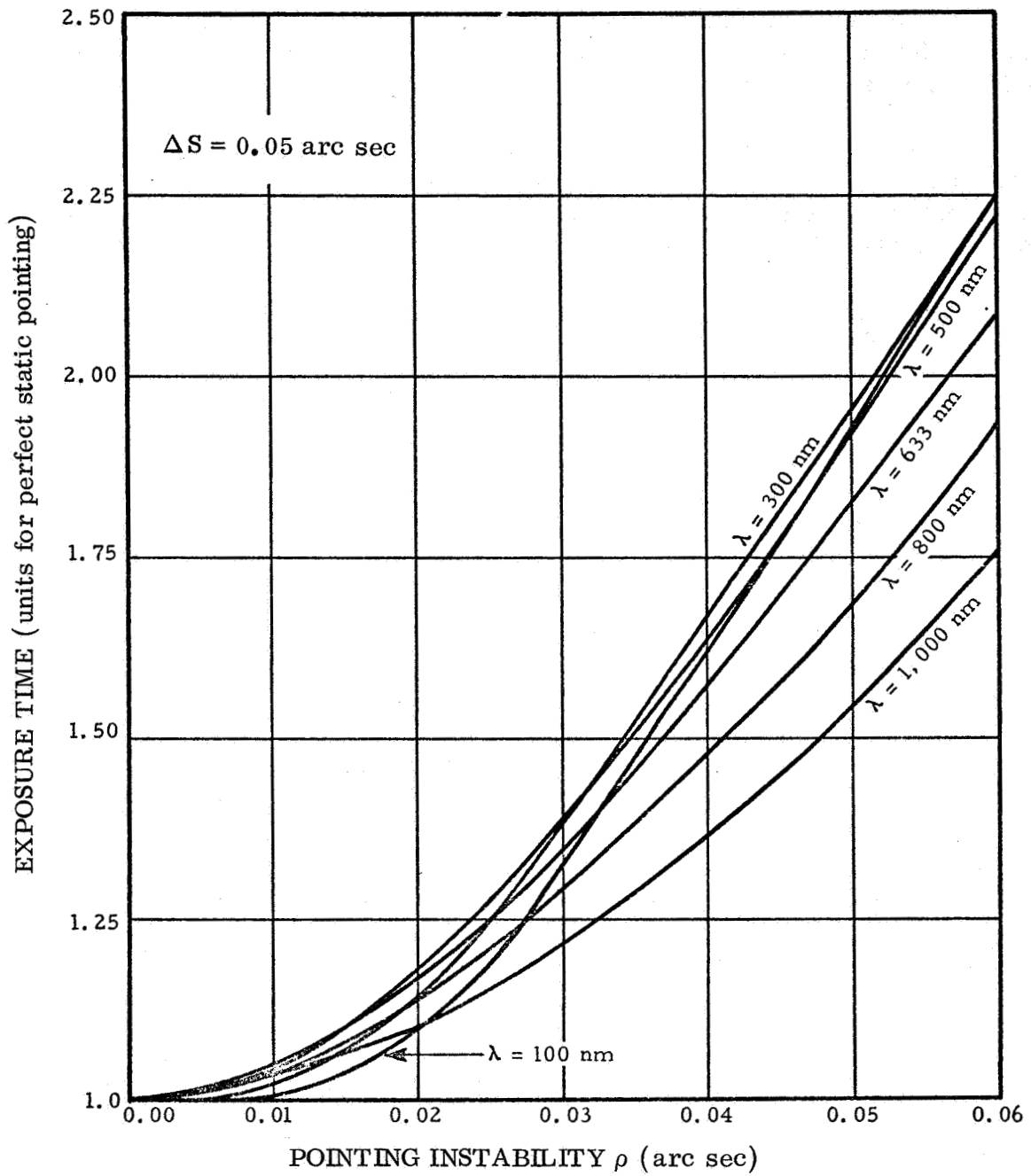


Figure IV-45. Spectrograph exposure time as a function of pointing instability.

time is required. Let  $\Delta S_0$  be the chosen slit width for no pointing degradation and let  $\Delta S$  be the widened value under degraded conditions. Let us consider pointing error first.

Pointing error will result in longer spectrograph exposure times caused by decentering of the stellar image in the slit. The slit width  $\Delta S$  which is necessary to accommodate a pointing error  $p$  perpendicular to the slit is given by

$$\int_{-\infty}^{\infty} \int_{-\frac{\Delta S}{2} - p}^{\frac{\Delta S}{2} + p} 0.8 I_{sp}(0,0) \exp\left(-\frac{x^2 + y^2}{\tau^2}\right) dx dy$$

$$= \int_{-\infty}^{\infty} \int_{-\frac{\Delta S_0}{2}}^{\frac{\Delta S_0}{2}} 0.8 I_{sp}(0,0) \exp\left(-\frac{x^2 + y^2}{\tau^2}\right) dx dy \quad (27)$$

for no pointing instability. The evaluation of the integrals leads to the expression

$$\operatorname{erf}\left(\frac{\Delta S}{2\tau} + \frac{p}{\tau}\right) + \operatorname{erf}\left(\frac{\Delta S}{2\tau} - \frac{p}{\tau}\right) = 2 \operatorname{erf}\left(\frac{\Delta S_0}{2\tau}\right) \quad (28)$$

The slit width  $\Delta S$  is thus related to the pointing error  $p$  by equation (28), and is graphed in Figure IV-46 for  $\Delta S_0 = 0.05$  arc sec. For large values of  $p$ ,  $\operatorname{erf}(\Delta S/2\tau + p/\tau) \rightarrow 1$ , and equation (28) becomes

$$\Delta S = 2p + 2\tau \operatorname{erf}^{-1}\left[2 \operatorname{erf}\left(\frac{\Delta S_0}{2\tau}\right) - 1\right] \quad (29)$$

Note that the curves for 100 nm and 300 nm are almost coincident straight lines in this figure. At these short wavelengths the image is



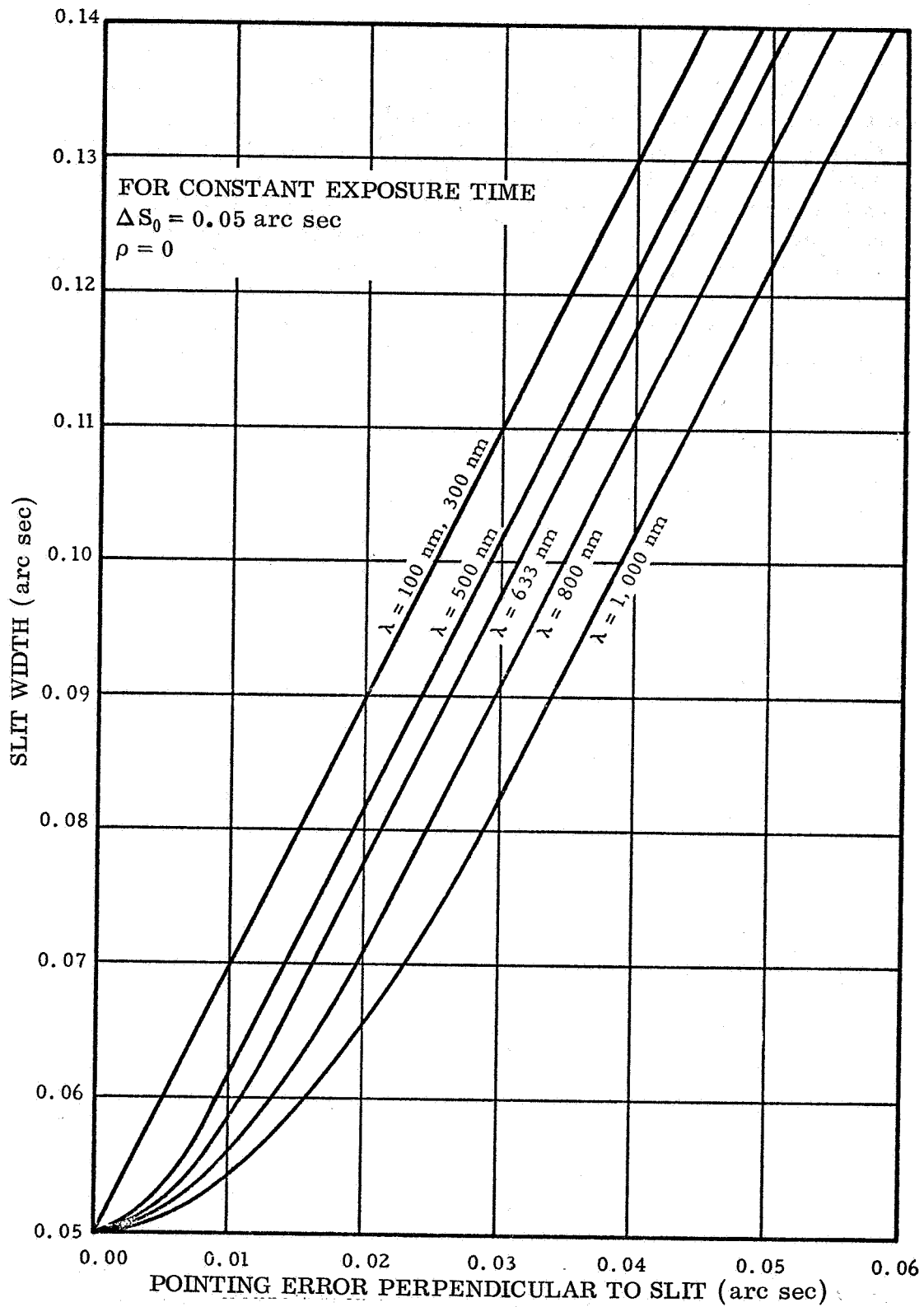


Figure IV-46. Spectrograph slit width as a function of pointing error for constant exposure time.

small relative to the slit width, and when the stellar image is decentered in the slit, the amount of light intercepted by the far slit jaw is small in comparison with that cut out by the near jaw. Thus, the slit half-width must increase nearly equally with the amount of decenter. For longer wavelengths and larger images, widening of the slit will increase the amount of light passed by the slit at the far jaw as well as the near jaw. In this case, for small pointing error, the slit does not have to be widened as much and thus these longer wavelengths curves do not rise as steeply near  $p = 0$ . At larger values of  $p$ , they approach the small image (short wavelength) behavior.

Consider now pointing instability. The slit width  $\Delta S$  which is necessary to accommodate a pointing instability  $\rho$  is given by

$$\int_{-\infty}^{\infty} \int_{-\frac{\Delta S}{2}}^{\frac{\Delta S}{2}} \frac{0.8\tau^2}{\tau^2 + \rho^2} I_{sp}(0,0) \exp\left(-\frac{x^2 + y^2}{\tau^2 + \rho^2}\right) dx dy$$

$$= \int_{-\infty}^{\infty} \int_{-\frac{\Delta S_0}{2}}^{\frac{\Delta S_0}{2}} 0.8 I_{sp}(0,0) \exp\left(-\frac{x^2 + y^2}{\tau^2}\right) dx dy \quad (30)$$

for no pointing error. Evaluation of the integrals leads to the expression

$$\operatorname{erf}\left[\frac{\Delta S}{2(\tau^2 + \rho^2)^{1/2}}\right] = \operatorname{erf}\left(\frac{\Delta S_0}{2\tau}\right), \quad (31)$$

which is true only if

$$\Delta S = \frac{(\tau^2 + \rho^2)^{1/2}}{\tau} \Delta S_0 \quad (32)$$

The slit width  $\Delta S$  is related to the pointing stability  $\rho$  by equation (32) and is graphed in Figure IV-47. For  $\rho \gg \tau$ , this relationship approaches the linear expression  $\Delta S = (\Delta S_0/\tau) \rho$ .

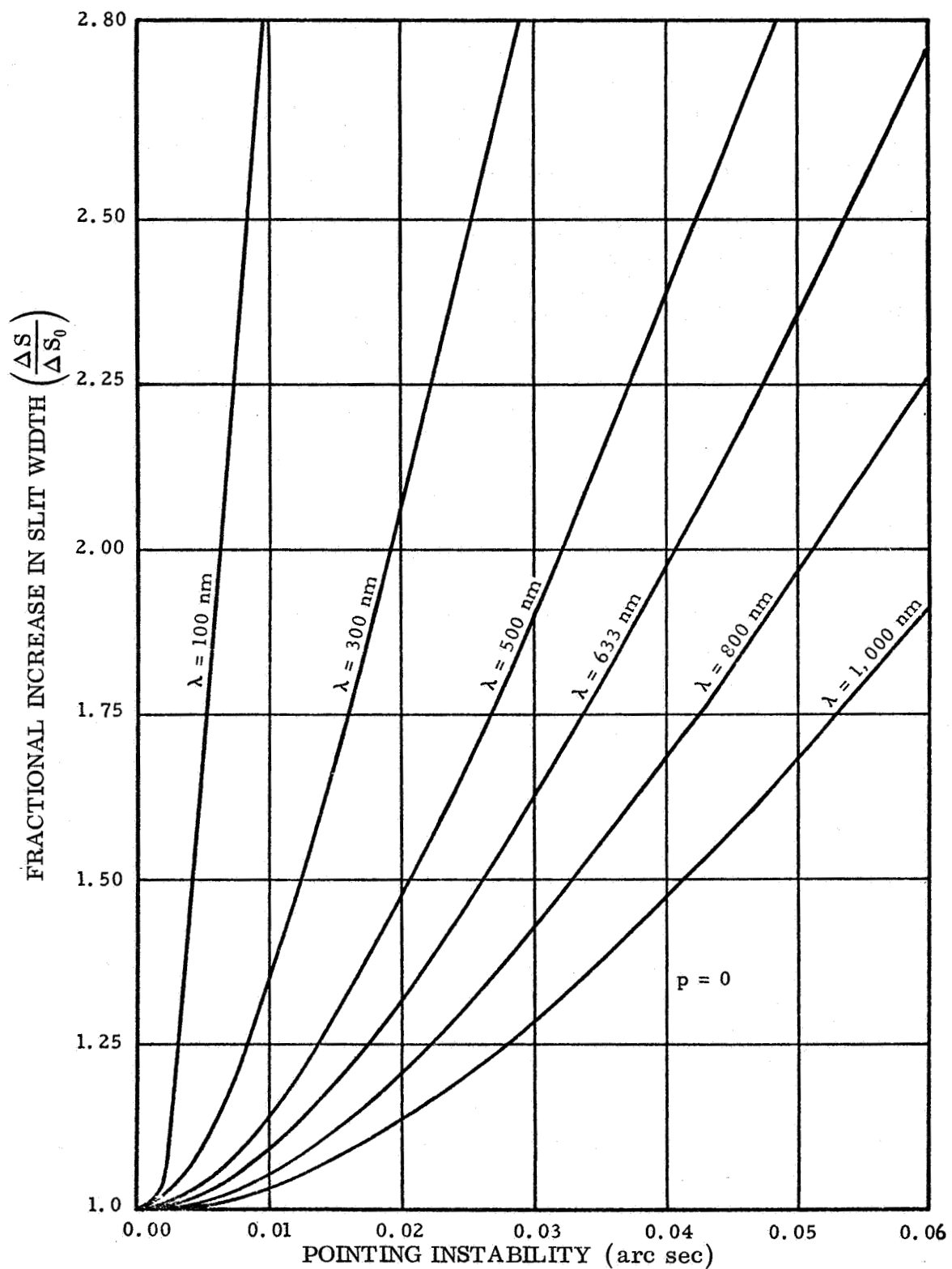


Figure IV-47. Fractional increase in spectrograph slit width as a function of pointing instability for constant exposure time.

The behavior of the curves in Figure IV-47 is explained by the action of the image motion spread function upon the various size stationary images. For small stationary images (short wavelengths), image motion has a relatively pronounced effect and necessitates relatively large slit width increases. For large stationary images (long wavelengths), image motion has a relatively lesser effect and requires smaller slit width increases.

e. **Conclusions.** An important conclusion drawn from this analysis is that for field camera exposures, pointing stability is more important than accuracy, whereas for spectrograph exposures, pointing accuracy is more important than stability. For field camera exposures, the pointing accuracy is often good enough if the object lies within the relatively large field of view. Here pointing instability will degrade the results, as evidenced by Figure IV-40. For spectrograph exposures, Figures IV-44 and IV-45 show the overwhelming importance of pointing accuracy.

Note also that in many cases, small amounts of pointing degradation will have almost nil effect upon instrument performance, whereas instrument performance degrades rapidly at large values of pointing error and instability. This follows from the near zero slope of many of the curves for an instability or pointing error near zero. It is true, for example, for Figures IV-40 and IV-41 at longer wavelengths and for Figures IV-42, IV-44, and IV-45 at shorter wavelengths.

A final conclusion is that extremely small spectrograph entrance slit widths should be avoided unless required for the highest wavelength resolution in some experiments. This is clear from Figure IV-43. Larger slit widths also lessen the sensitivity upon pointing error.

## B. Maintenance Mode Analysis and Trades

1. **Introduction.** The mission goal of the LST is to provide 15 years of on-orbit observation time. Present plans call for the initial 5 years of observation to be performed by the precursor LST, with the remaining 10 years of on-orbit operation being accomplished by the advanced LST.

To maintain an acceptably high level of operation performance during the entire 15-year LST mission duration, the following three inter-related factors must be considered:

1. Provide for instrument update when warranted by changing interest or advances in technology.
2. Assure system performance for long-time observatory operation.
3. Minimize total LST program cost.

The following two options exist to sustain the LST performance at the desired level for the 15-year mission duration:

1. Expendable LST — in this option a new LST is placed on orbit when the operational LST malfunctions.
2. Maintainable LST — this option provides for repair of the malfunctioning LST to return it to the desired performance level.

Presented as follows is a comparison of the relative payload and launch vehicle costs for both the expendable and maintainable LST options with the maintainable LST serving as a reference and assigned a relative total program cost of unity:

Configuration Option	Number of Flight Articles Required	Relative Total Payload Cost
Expendable LST	8	1.8
Maintainable LST	2	1.0

It is estimated that eight expendable flight vehicles would be required for the 15-year mission. This number is based on a component design lifetime of 2 years. The number of LST vehicles required for the maintainable option includes one precursor for the first 5 years and one advanced LST for the remaining 10 years. Because of the cost savings expected from building fewer vehicles, the maintainable LST option was selected and the expendable LST option was removed from further consideration.

2. Maintenance Trade Study Approach. A preliminary maintainability analysis was conducted for the LST mission to determine and define a feasible maintenance concept. The four following maintenance modes were initially considered for the LST spacecraft:

1. On-orbit manned maintenance - pressurized.
2. On-orbit manned maintenance - unpressurized.
3. On-orbit manipulator maintenance.
4. Ground-based maintenance.

The maximum design lifetime for life-limited subsystems and instruments has been assessed as being  $2\frac{1}{2}$  years. Consequently, initial maintenance trade studies were conducted assuming that scheduled maintenance is performed every  $2\frac{1}{2}$  years. Since the precursor LST is to have 5 years of service, one scheduled service mission was planned.

The trade study was accomplished by having specialists in the various discipline areas assess each maintenance mode with regard to the impact on the design of the LST configuration, design and operational flexibility, performance characteristics, complexity, and development and performance risks.

3. Maintenance Mode Study Results. Table IV-16 lists some 20 factors comparing and contrasting the four considered maintenance modes. The comparison, at this point in time, is qualitative, and as yet no attempt has been made to quantify or to arrive at "figures of merit" for the various comparison remarks. From a technical viewpoint, it can certainly be argued that all four maintenance options are feasible — each with certain attractive and detrimental features. A careful perusal of the table, however, does indicate that of the four maintenance options, the On-Orbit Manipulator Mode is the least attractive because of its shortcomings in the areas of (1) ease of maintenance tasks, (2) quantity/complexity of separate operations required, (3) growth potential and flexibility for design changes, (4) interconnection quantity and complexity, (5) ease of maintenance tasks, (6) logistics weight and volume requirements, (7) mission sharing possibilities, (8) alignment and calibration capability, and (9) special tool requirements.

4. Flight Sharing. Since the on-orbit maintenance mission does not utilize either the full mass or volume payload capability of the orbiter, LST costs could be reduced if some other mission shared the flight with the LST maintenance mission. Employing this premise, the Space Shuttle Mission Model was surveyed to locate compatible payloads to share flights with the LST maintenance mission.

TABLE IV-16. MAINTENANCE MODE COMPARISONS

Factor	Pressurized On-Orbit	Unpressurized On-Orbit	On-Orbit Manipulator System	Ground Serviced
Level of Maintenance	Black Box to Subsystem	Black Box to Subsystem	System	Any Desired Level
Quantity/Complexity of Separate Operations Required	Moderate quantity — complexity not a problem in shirtsleeve environment.	Moderate quantity — complexity slightly increased due to pressure-suited maintenance.	Greater quantity — considerable complexity imposed on automated carousel. Large bulky boxes are massive and fairly intricate maneuvers required.	Minimum
Time Required for Maintenance	Short	Longer due to pressure-suited maintenance	Considerable (2 carousels required)	Minimum
Turnaround Time	2-5 days	2-5 days	2-5 days	30 days minimum
Growth Potential and Flexibility for Design Changes	Excellent due to packaging freedom	Excellent due to packaging freedom	Box structures restrict growth and flexibility, especially pie-shaped radial instrument compartment. Interface at focal plane, lack of room for instrument growth, and lack of room for baffles.	Excellent due to packaging freedom
Interconnection Quantity and Complexity	Few per box. Shirtsleeve operation allows standard connections and uncomplicated operations.	Few per box. Standard connections, somewhat more complex operations due to pressure suit.	Moderate quantity. More complex due to automatic operations. Major concern.	Few per box. Shirtsleeve operation allows standard connections and uncomplicated operations.
Accessibility to Replaceable Units	Excellent — direct access to internally mounted components	Excellent — direct access to internally mounted components	Good for systems and radially mounted instruments. LST must be rotated on carousel. Poor for axially mounted instruments.	Excellent — direct access to all components

TABLE IV-16. (Continued)

Factor	Pressurized On-Orbit	Unpressurized On-Orbit	On-Orbit Manipulator	Ground Serviced
Ease of Maintenance Tasks	Good. Weightless condition requires use of handholds, foot or body restraints.	Good. Less than pressurized, due to pressure suit operation	Most difficult. High skill requirements for manipulator operator	Provides easiest accomplishment of maintenance tasks
Use of Man's Capabilities	Excellent	Good. Somewhat limited by retractions of the pressure suit.	Uses man for manipulator operation only	Excellent
Complex Remote Handling Maintenance Devices	None	None	One or two automated carousels	None
Spare for Refurbishment and Repair	Small subsystem or component modules mounted on racks in Shuttle bay or crew compartment	Small subsystem or component modules mounted on racks in Shuttle bay or crew compartment	Large system or subsystem modules mounted on racks in Shuttle bay. Must be transferred to and from Shuttle bay by manipulators.	Maximum flexibility due to spares availability and ready access
Logistics Mass/Volume to Orbit (Total life-limited item replacement plus total science update)	1687 kg (3720 lb) 6.3 m <sup>3</sup> (223 ft <sup>3</sup> ) Volume available in cargo bay, Sortie Lab, or crew compartment	1358 kg (2994 lb) 5.4 m <sup>3</sup> (190 ft <sup>3</sup> ) Volume available in cargo bay, Sortie Lab, or crew compartment	3652 kg (8050 lb) 127 m <sup>3</sup> (4487 ft <sup>3</sup> ) Note: The storage of system boxes and radial instruments apparently fills one carousel, and a second one must be designed and used for the on-axis instruments.	Not applicable
Mission Sharing Possibilities on Maintenance Flights	Excellent, especially with Tug flights, which predominate	Excellent, especially with Tug flights which predominate	Poor. Volume required by two carousels plus full spares/update complement is so great that LST could not be retrieved on same flight if ground service is required.	Poor



TABLE IV-16. (Continued)

Factor	Pressurized On-Orbit	Unpressurized On-Orbit	On-Orbit Manipulator	Ground Serviced
<p>LST Hardware Lifetime Requirements</p>	<p>Minimizes lifetime requirements and associated costs. Since mission sharing possibility is excellent, can have more frequent maintenance trips of shorter duration as failures dictate. (Unscheduled maintenance concept)</p>	<p>Same as pressurized maintenance</p>	<p>Maximum lifetime required due to large weight and volume of spares, science update items, and automated carousels</p>	<p>Long life required due to penalties accruing from unshared Shuttle flights and more extensive and expensive ground operations.</p>
<p>Science Down Time During Maintenance</p>	<p>2-5 days</p>	<p>2-5 days</p>	<p>2-10 days</p>	<p>1-6 months</p>
<p>Other Considerations</p>	<p>Possibly none. However, if "unscheduled maintenance" concept is used, traffic density, queuing, etc., must be considered. With a Shuttle launch rate of two per month, a reasonable worst case estimate is 1-2 months down time.</p>	<p>Same as pressurized maintenance</p>	<p>If two carousels are required for scheduled maintenance, two Shuttle launches are required. It is doubtful if one payload could schedule two consecutive Shuttle flights. For "unscheduled maintenance," flight sharing of this configuration is difficult. With a Shuttle launch rate of two per month, a reasonable worst case is 3-6 months for either case.</p>	<p>Possibly none (for scheduled ground return and re-launch). For "un-scheduled maintenance" a longer time is required to schedule the mostly unshared return trip than the 1-2 months shown in col. 1 for the shared up trip. Two to four months is probably more reasonable. The mostly unshared relaunch scheduling effort could begin at the time of failure, and if the wait is longer than 3-10 months from then, no additional wait would be required.</p>

TABLE IV-16. (Concluded)

Factor	Pressurized On-Orbit	Unpressurized On-Orbit	On-Orbit Manipulator	Ground Serviced
Hazard to Crew Due to Direct Involvement in Maintenance Operations	Minimum — safer than Apollo or Skylab EVA activities	Slightly more hazardous than pressurized maintenance mode due to IVA activities	None	None
Alignment and Calibration Capability	Excellent. Maximum accuracy possible due to man in shirtsleeve environment. Does not have to withstand relaunch.	Excellent but accuracy degraded slightly for suited operation. Does not have to withstand relaunch.	Probably feasible but with reduced accuracy. Does not have to withstand relaunch.	Excellent accuracy on ground, but has to withstand relaunch.
Tool Requirements	Standard hand tools would be required. Module alignment and quick release mechanisms are presently available.	Same as pressurized	Special manipulator tools would have to be designed to provide alignment of modules and power attachment and release	Standard shop tools would be required.
Contamination Protection During Maintenance	Active contamination control system required. Class 10 000/100 000 hybrid system recommended (see Appendix).	Contamination potential less than pressurized mode. Effluents from pressure suit may be area of concern.	Spares and automated carousel in Shuttle cargo bay must be maintained moisture and contaminant free	Entire LST must be maintained clean to prevent having to disassemble and clean on ground. This may be a major problem area.
Quantity of SSM Spares Inventory (cost must include purchase, storage, assembly into replaceable units, and testing)	16% (only failed and life-limited items)	16% (only failed and life-limited items)	100% Except for arrays. There will be some life-limited and failed items in each box. Therefore, many non-life-limited and nonfailed items must be replaced.	16% (only failed and life-limited items)

Currently, there are no ground rules as to how Shuttle flight costs are to be prorated for mission sharing. Costs could be prorated on payload mass ratio, payload volume ratio, on-orbit operations time ratio, etc., or a combination of some or all of the aforementioned factors. As a result of a discussion with engineering cost personnel, it was decided to select payload mass as the basis for prorating mission sharing costs for this study.

The selection of payload mass ratio as the basis of cost proration means that LST costs can be minimized by selecting the most massive payloads possible to share the LST maintenance mission flights. In this respect, Space Tug missions proved to be some of the best candidates for mission sharing.

It should be noted that down-flight flight sharing does not readily apply to the earth return maintenance mode. Since this mode requires retrieving the LST, which uses most of the orbiter payload bay volume, few payloads can be identified to share such down flights.

Servicing the LST at its orbit of 611 km (330 n. mi.) requires the orbiter to use an OMS propellant tank which is located in the aft end of the payload bay. The full OMS tank mass is 5443 kg (12 000 lb) and is chargeable to the LST maintenance mission as part of the required LST payload mass.

a. Number of Flights Required. Table IV-17 shows the number of shuttle flights chargeable to each of the candidate maintenance options. As an example, to determine the number of shuttle flights charged to on-orbit unpressurized (manipulator) maintenance, locate this maintenance mode in the far left column. The column to the immediate right describes the initial maintenance upflight. In this case, a Tug mission was selected to share the orbiter upflight costs. The current round-trip cost for a Shuttle flight is estimated at \$ 10.5 million. One-way flight was considered to be half the round-trip cost, or \$ 5.25 million. Recalling that costs are prorated on payload mass ratio, the LST portion of the cost is determined as follows:

1. LST Maintenance Mission Mass

Spares Plus Support Equipment	3 652 kg
OMS	<u>5 443 kg</u>
Total	9 095 kg

TABLE IV-17. FLIGHTS REQUIRED FOR VARIOUS SCHEDULED MAINTENANCE METHODS

Maintenance Mode	Initial Maintenance Upflight	Retrieval of LST	Return LST to Orbit	Orbiter Return Flight
On-Orbit Unpressurized (with manipulators) Ratio of LST Cost	LST Maintenance 3652 kg (8050 lb) Spares 5443 kg (12 000 lb) OMS Shared Payload 467 kg (1030 lb) Satellite 16 818 kg (37 077 lb) Tug 0.34	Not Applicable	Not Applicable	LST Maintenance 3652 kg Spares plus 544 kg Empty OMS Tank Shared Payload 2659 kg (5863 lb) Tug 0.61
On-Orbit Pressurized Ratio of LST Cost	LST Maintenance 1688 kg (3722 lb) Spares 5443 kg (12 000 lb) OMS Shared Payload 467 kg (1030 lb) Satellite 16 818 kg (37 077 lb) Tug 0.29	Not Applicable	Not Applicable	LST Maintenance 1688 kg Spares plus 544 kg Empty OMS Tank Shared Payload 2659 kg (5863 lb) Tug 0.46
Earth Return Ratio of LST Cost	Any Shuttle Ascent Flight  (No Charge to LST Program)	Retrieve LST (No Payload Sharing) 1.0	Return LST to Orbit (No Payload Sharing) 1.0	Orbiter Returns Empty; Few Payloads are Available to Share Return Flight 1.0

2. Shared Payload (Tug Mission)

Tug Payload	467 kg
Tug	<u>16 818 kg</u>
Total	17 285 kg

3. Total Flight Payload Mass 26 380 kg

The LST portion of the flight is

$$\$ 5.25 \text{ M} \frac{9\ 095}{26\ 380} = (0.345) \$ 5.25 \text{ M} = \$ 1.81 \text{ M.}$$

The next two columns, "Retrieval of LST" and "Return LST to Orbit," do not apply to this maintenance option. The next to last line contains the flight-sharing for the earth return flight. The procedure for calculating prorated costs is the same as previously described. The final result is that the LST program is charged for a portion of the cost of one round trip Shuttle flight for on-orbit unpressurized maintenance.

The on-orbit pressurized (manned) maintenance flight sharing is similar to the previously discussed case. It, too, is charged for a portion of one round-trip flight on the orbiter.

Earth return maintenance is not charged for the initial Shuttle upflight. The LST will be retrieved on the downleg of a mission to deploy a payload. Studying Table IV-17 reveals that the LST program is charged for one and one-half round-trip Shuttle flights (three one-way flights) for the earth return maintenance option. As will be discussed later, orbiter flight costs are a major discriminator when comparing maintenance options.

b. Orbital Operations During Flight Sharing. Thus far the discussion on flight-sharing has been devoted to the physical compatibility of payloads. The operational compatibility of shared payloads must also be considered. Figure IV-48 shows that it is operationally feasible to deploy a Tug at a 185 km (100 n. mi.) orbit, have the orbiter transfer to a 611 km (330 n. mi.) orbit, rendezvous with the LST, perform the LST maintenance mission, have the Tug rendezvous with the orbiter at the 611 km orbit and have the orbiter return to earth with the empty Tug. The upper timeline in Figure IV-48 illustrates the Tug events and the lower timeline presents concurrent LST maintenance activities. The 124 hours available for LST maintenance represents a minimum value due to a combination of worst case assumptions with respect to Tug phasing.

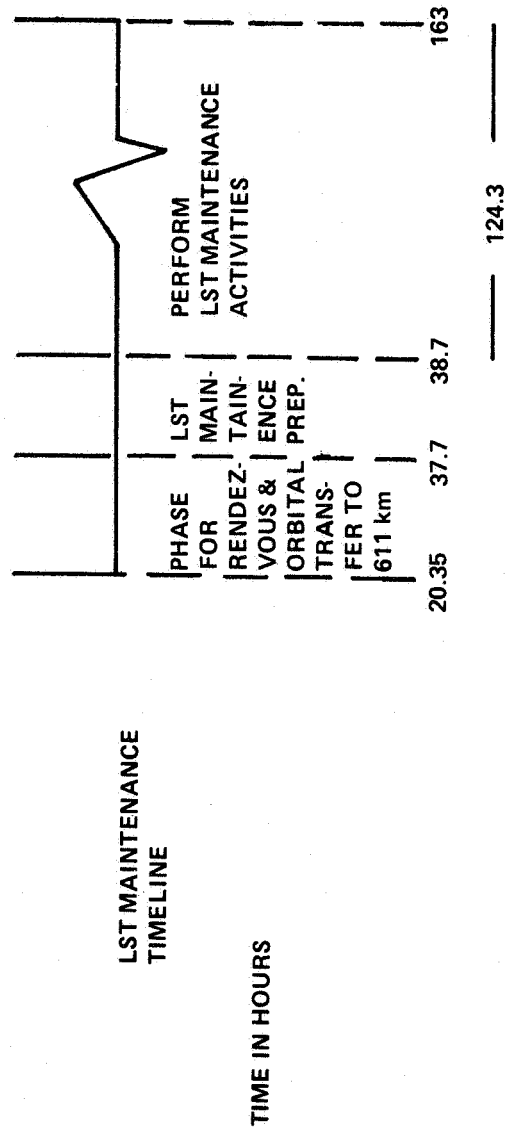
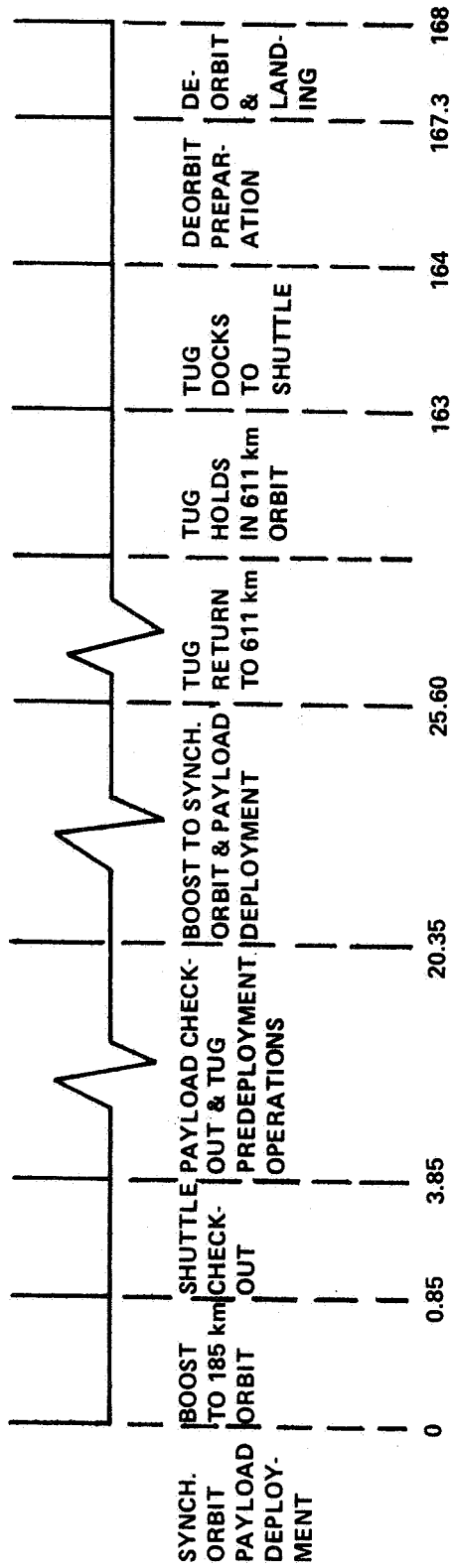


Figure IV-48. Operational timeline for LST shared mission to synchronous orbit.

Detailed crew activity schedules of the maintenance operations show that the required maintenance can be performed by two crewmen in 2 working days. Therefore, flight sharing with Tug missions provides ample time to conduct the LST maintenance.

5. Scheduled Maintenance Cost Comparison. The results of the cost comparison study of the three candidate scheduled maintenance methods are given in Table IV-18. On-orbit pressurized maintenance was selected as the cost study design reference, and costs are presented as millions of dollars difference ( $\Delta$ ) from the baseline. The four cost columns give delta costs for (1) shuttle flights, (2) design, development, test and engineering (DDT&E), (3) recurring cost (REC), and (4) total cost.

The Shuttle flight costs for the on-orbit pressurized maintenance and the on-orbit unpressurized maintenance using manipulators are essentially equal, since both missions were shared with a Tug flight. The earth return case is based on the cost of one and one-half round trips above the baseline mission.

Two sets of cost numbers are presented for the on-orbit unpressurized maintenance method using manipulators. These two cases bracket a range of estimates (NASA and industry) which results from an uncertainty as to the type and amount of required testing. From Table IV-18 on-orbit unpressurized maintenance using manipulators is seen to be the least attractive option from a cost standpoint and was eliminated from further consideration.

Although earth return maintenance appears to be more costly than on-orbit pressurized maintenance, the \$ 8.84 million is considered to be within the accuracy of the cost estimating techniques. Therefore, the earth return and on-orbit pressurized maintenance were considered equal competitors at this point.

Again referring to Table IV-18, the Shuttle flight cost for the earth return maintenance option is \$ 11.82 million greater than the baseline. With sharing effects included, the design reference maintenance mission Shuttle flight cost is \$ 3.93 million. Although scheduled maintenance may be planned, contingency or unplanned maintenance must be considered as a very realistic possibility. The cost impact of an additional maintenance visit during the 5-year precursor mission is presented in Table IV-19. Again the cost baseline is on-orbit manned maintenance with one maintenance mission. The costs shown are in millions of dollars difference from the baseline. It is clear that the earth return maintenance cost is highly sensitive to the number of maintenance missions required. As a result of these findings, the on-orbit manned maintenance concept was selected as the recommended maintenance mode for purposes of detailed study.

TABLE IV-18. LST SCHEDULED MAINTENANCE COST COMPARISON<sup>a, b</sup>

Maintenance Mode	Shuttle Flight Cost	DDT&E Cost	Recurring Cost	Total Cost
Pressurized On-Orbit Maintenance (design reference)	0	0	0	0
Unpressurized On-Orbit Maintenance Using Manipulators	1.09	31.93	1.93	34.95
Unpressurized On-Orbit Maintenance Using Manipulators (increased configuration and system testing)	1.09	55.27	1.93	58.29
Earth Return Maintenance	11.82	-(11.97)	8.99	8.84

a. Baseline maintenance mode for cost study is on-orbit pressurized.

b. Cost numbers are in \$ millions ( $\Delta$ ) from baseline.



TABLE IV-19. LST MAINTENANCE COST IMPACT DUE TO ADDITIONAL SHUTTLE FLIGHTS<sup>a, b</sup>

Maintenance Mode	Δ Cost for One Maintenance Mission	Δ Cost for Two Maintenance Missions
On-Orbit Manned Maintenance	0 (baseline)	5.9 <sup>c</sup>
Earth Return Maintenance	8.8	31.8 <sup>d</sup>

- a. Cost baseline is on-orbit manned maintenance with one mission.
- b. Cost comparison is in \$ millions Δ from baseline.
- c. Baseline maintenance Shuttle costs resulting from flight sharing plus \$ 2.0 M for spares.
- d. Includes \$ 7.19 M recurring costs and \$ 15.75 M for one and one-half additional Shuttle flights.

6. Recommended Design Reference Maintenance Method. The selection of on-orbit manned maintenance was made under the ground rule of one scheduled maintenance mission after  $2\frac{1}{2}$  years of LST operation. Perturbation of the schedule was accomplished by assessing the impact of a contingency maintenance flight. Therefore, inherent in the scheduled maintenance concept is the requirement for designing to accommodate unscheduled contingency maintenance. It follows that if the LST requires maintenance prior to the scheduled time, unscheduled maintenance will probably be performed. If the LST is performing at an acceptable level at the time for scheduled maintenance, maintenance will probably be postponed until required. Therefore, unscheduled maintenance better satisfies real-world requirements.

In summary, the selected maintenance concept is unscheduled, on-orbit manned maintenance. The necessary spares are packaged in the lower bay of the Shuttle crew compartment. Equipment will be replaced only when required because of failure or scientific update. Unscheduled maintenance will allow for a reduction in the design lifetime of equipment from  $2\frac{1}{2}$  years to some shorter time. Future studies will be required to determine the least cost design lifetime/maintenance frequency combination.

The LST maintenance mission will share Shuttle flights with other payloads to reduce costs. The LST may be returned to earth for major maintenance when dictated by complexity of repair or when major upgrading of optical or instrument systems is required.

**CHAPTER V. CONFIGURATION AND SYSTEM ALTERNATIVES**



# TABLE OF CONTENTS

	Page
A. Concept Comparisons .....	V-1
B. Telescope f-number Trades — Overall LST Effects .....	V-1
C. Light Shield Trades .....	V-13
1. Thermal Considerations .....	V-13
2. Viewing Considerations .....	V-13
3. Recommended Configuration .....	V-16
D. Optics .....	V-19
1. Aperture Selection .....	V-23
2. Choice of Telescope Type .....	V-23
3. Selection of Primary Mirror f-Number .....	V-23
4. Selection of System f-Number Optical Effects .....	V-24
5. Folding Optics .....	V-25
6. Mirror Material Selection .....	V-28
7. Optical Coatings .....	V-28
E. Structural Concepts .....	V-31
1. OTA Graphite Epoxy Shell Study .....	V-31
2. Pressure Bulkhead and Primary Ring .....	V-32
3. SIP Support Structure .....	V-32
4. Rollout Solar Array .....	V-36
5. Primary Mirror Support .....	V-36
6. Spider Beam .....	V-36
F. Thermal Control .....	V-38
1. OTA .....	V-38
2. SSM/SIP .....	V-40
G. Electrical Power and Distribution .....	V-41
H. Communications and Data Handling .....	V-42
1. Ground Station Selection .....	V-44
2. Antenna Configuration .....	V-44
3. Antenna Isolation .....	V-45
4. Image Tube Selection .....	V-45

## TABLE OF CONTENTS (Concluded)

	Page
5. Mass Memory Survey .....	V-45
6. Computer Configuration .....	V-45
7. Tracking and Data Relay Satellite System Data Return ..	V-46
I. Attitude Control .....	V-48
1. Reference Gyro Assembly .....	V-48
2. Star Trackers .....	V-49
3. Sun Sensors .....	V-49
4. Momentum Exchange System .....	V-49
5. RCS Concepts .....	V-50

## LIST OF ILLUSTRATIONS

Figure	Title	Page
V-1.	LST concepts comparison . . . . .	V-2
V-2.	LST length as a function of system focal ratio for the 3-m LST 20-percent thermal control margin . . . . .	V-5
V-3.	LST length as a function of system focal ratio for the 3-m LST minimum clearance case . . . . .	V-6
V-4.	LST length as a function of system focal ratio for the 2.5-m LST, 20-percent thermal control margin . . . . .	V-7
V-5.	LST candidate configuration . . . . .	V-8
V-6.	LST candidate configuration . . . . .	V-9
V-7.	LST candidate configuration . . . . .	V-10
V-8.	LST candidate configuration . . . . .	V-11
V-9.	LST length as a function of system focal ratio for the 3-m LST (reference configuration) . . . . .	V-12
V-10.	Effect of sun angle . . . . .	V-14
V-11.	Estimated faint object viewing limits . . . . .	V-15
V-12.	Light constraints for faint object viewing . . . . .	V-17
V-13.	Typical orbit: look angle 30 degrees from sun . . . . .	V-18
V-14.	Duration of faint source viewing conditions . . . . .	V-20
V-15.	Sky coverage increments as a function of minimum sun angle . . . . .	V-21
V-16.	Comparison of aplanatic Gregorians and design reference Cassegrain . . . . .	V-24

## LIST OF ILLUSTRATIONS (Concluded)

Figure	Title	Page
V-17.	An alternate focal plane layout that was not selected . . . . .	V-26
V-18.	Design reference f/12 image plane format . . . . .	V-27
V-19.	Spectral performance of MgF <sub>2</sub> and LiF overcoated aluminum . . . . .	V-30
V-20.	LST graphite/epoxy shell longitudinal cross section . . . . .	V-33
V-21.	LST structural concepts considered . . . . .	V-34
V-22.	LST alternate slip support schematic . . . . .	V-35
V-23.	LST alternate solar array . . . . .	V-37
V-24.	Alternate concept for LST primary mirror support . . . . .	V-38
V-25.	Spider beam configuration . . . . .	V-39
V-26.	Schematic of alternate thermal control system for SIP components . . . . .	V-40
V-27.	LST TDRSS terminal . . . . .	V-47



## LIST OF TABLES

Table	Title	Page
V-1.	Effects on LST Characteristics of f-Number Selection . . . . .	V-3
V-2.	Operational Advantages of Truncated Light Shield (for the Condition of Both Solar and Target Vectors in the Orbit Plane) . . . . .	V-22
V-3.	Mirror Material Selection Evaluation Matrix . . . . .	V-29
V-4.	General Appraisal of Solar Array Types . . . . .	V-43

## CHAPTER V. CONFIGURATION AND SYSTEM ALTERNATIVES

### A. Concept Comparisons

A comparison of several different concepts of the LST was made. Data from other sources were utilized, where available, including the Goddard Space Flight Center LST Preliminary Analysis and Design Report (Rev. A), dated December 1971. The basis of the configuration concepts is the method of performing maintenance on the LST, primarily on the support systems module (SSM) systems. The concepts which were compared are shown in Figure V-1. The three broad categories into which the concepts were divided are (1) on-orbit pressurized maintenance, (2) on-orbit unpressurized maintenance, and (3) ground-based maintenance concepts. All concepts except the "unpressurized concept with large external packages" are based on passive thermal control of the scientific instrument package (SIP) and SSM systems. The large external package concept is based on the utilization of heat pipes.

The unpressurized on-orbit maintenance configurations were divided into four subconcepts:

1. Replacement of small internal packages.
2. Replacement of small external packages.
3. Replacement of large external packages.
4. Replacement of the entire aft end of the LST.

All unpressurized maintenance concepts given above would utilize manipulators or special purpose handling equipment.

On the basis of a comparison of maintenance modes presented in Appendix C and the mission sharing and cost comparisons presented in Chapter IV, the on-orbit pressurized concept was selected as the design reference concept for more detailed analysis in Phase A.

### B. Telescope f-number Trades – Overall LST Effects

Parametric studies were made to determine the effects on the overall LST design of having "slower" or "faster" telescope systems. Table V-1 shows in qualitative terms the general effects of selecting slower or faster

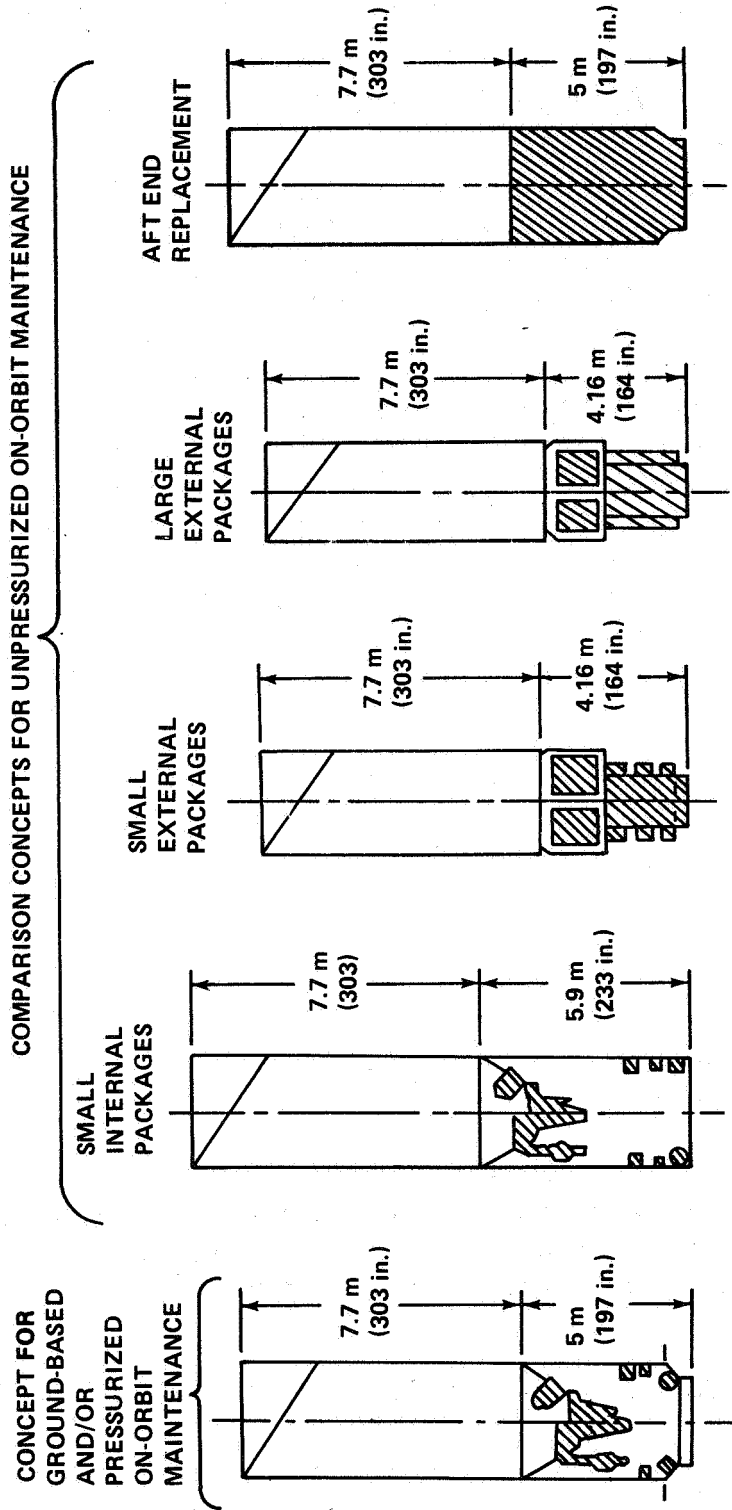


Figure V-1. LST concepts comparison.

TABLE V-1. EFFECTS ON LST CHARACTERISTICS OF f-NUMBER SELECTION

Function	"Fast" Optics (Toward $f_p/2.2, f_s/12$ )	"Slow Optics (Toward $f_p/3.0, f_s/30$ )
Optical Surface Manufacturing	More Difficult	Easier
Alignment Sensitivity	More Critical	Less Critical
Alignment Retention Ability	Easier	Harder
Secondary Mirror Movement Required for Adjustment	Smaller	Greater
Telescope-to-Instrument Direct Match	Worse (Requires Relay)	Better
Physical Separation of Fine Guidance and f/96 Imaging Equipment	Greater	Less
Instrument Packaging/Arrangement	Easier	More Difficult
Instrument Replacement During Maintenance	Easier	More Difficult
Volume Available for Instrument Growth	Good	Poor
Fine Guidance Field	Smaller and Less Curved	Larger and More Curved
Fine Guidance Optical Correction and Mechanism Implementation	Easier	More Difficult
LST Mass	Less	Greater
LST Volume	Less	Greater
LST Length	Less	Greater

optics. Several parametric curves were generated in the range between  $f_p/2.2$ ,  $f_s/12$  and  $f_p/3.0$ ,  $f_s/30$ , since this range seemed to be the most feasible to consider. Although telescopes anywhere within this range might be made to work, the faster systems appear to have more advantages. In the Phase A study, the guideline of having the Titan III launch as a backup to the Shuttle launch imposed mass and length constraints which excluded some choices of slower systems, as shown in Figure V-2. In this particular case, the primary mirror was 3.0 m in diameter, and the thermal control concept was constrained to be a passive one, with a 20-percent margin. The use of a passive thermal control system necessitates some minimum amount of area of the SSM walls for radiation of heat. It also imposes a limit on the density of component arrangement and resulting heat dissipation per unit area. The length of the SSM was determined by either the thermal control constraint or by the SIP length, whichever was larger. A second case which was run with a 3-m diameter primary mirror was a "minimum clearance" case (Fig. V-3), in which the clearance required to remove an SIP instrument dictated the SSM length, and the thermal control system was not constrained to be passive. The 20-percent thermal control margin case was run for a 2.5-m diameter primary mirror; the curve is shown in Figure V-4.

In all cases, it is felt that a 20-percent mass margin is the minimum that should be allowed at this early point in the LST program. Sketches showing the major LST elements (optical telescope assembly, SIP, and SSM) approximately to scale are provided for two choices of f-number in Figures V-5 through V-8. The first two of these would have ample clearance in shroud length, whereas the last two would exceed the shroud length. In these cases, the number of reflections for each instrument in the SIP was maintained constant, and the diameter of the collimating mirror for the spectrographs was maintained constant, to help provide a more common basis for comparison. Obviously, these design parameters could be changed to shorten the SIP, at the expense of instrument performance.

Subsequent to generating these data, the reference configuration for this study was selected, which had several significant differences from the configuration on which these data were based. Some of these differences are the selection of graphite-epoxy rather than invar-titanium for the optical telescope assembly (OTA) and SIP primary structures, reduction in size of the fine guidance field, reduction in size of the spectrographs, and reduction of reaction control system (RCS) requirements. A total mass reduction of about 770 kg (1700 lb) was achieved because of these changes. As a point of reference, the first case was rerun using the current reference LST design and updated launch

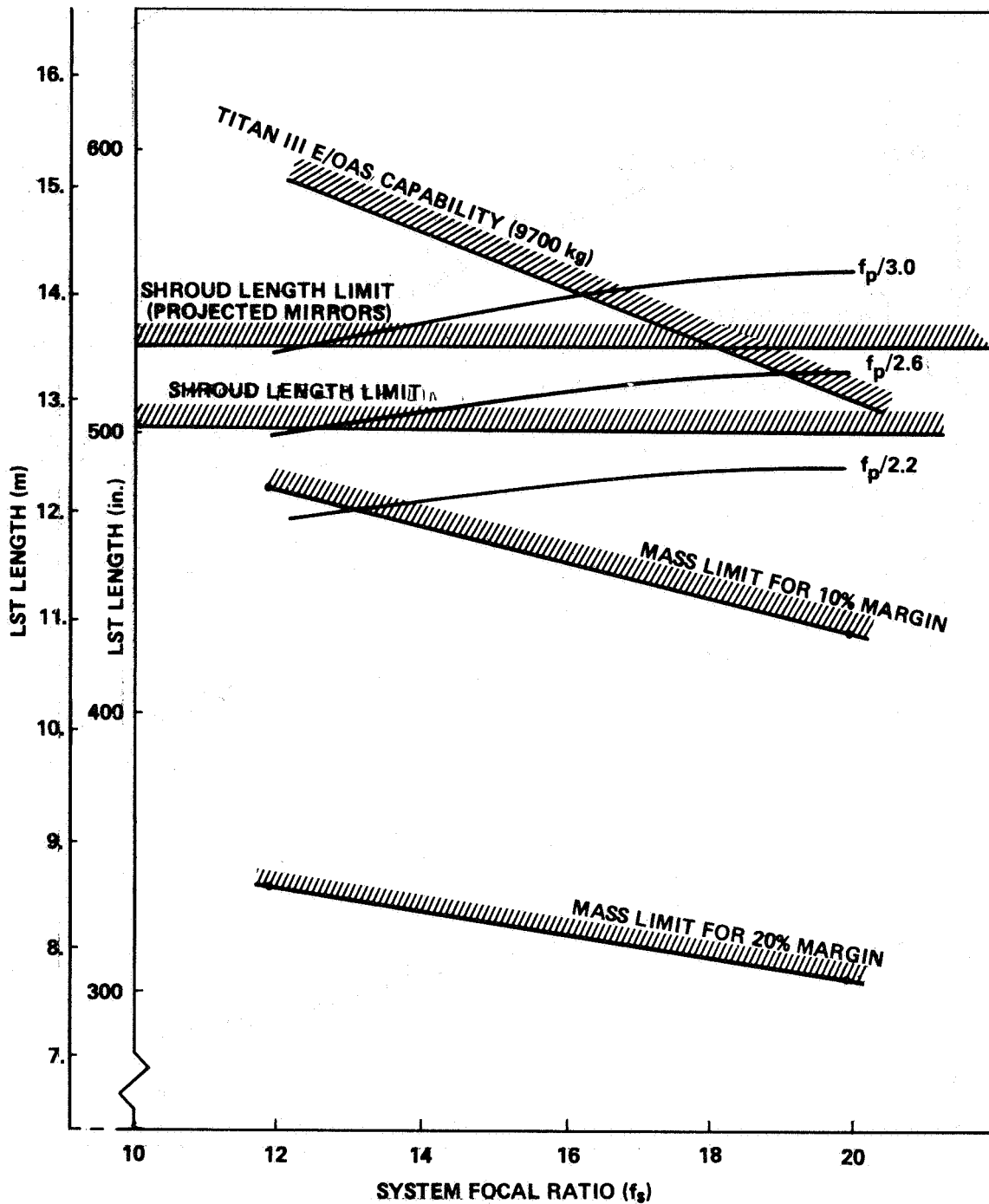


Figure V-2. LST length as a function of system focal ratio for the 3-m LST 20-percent thermal control margin.

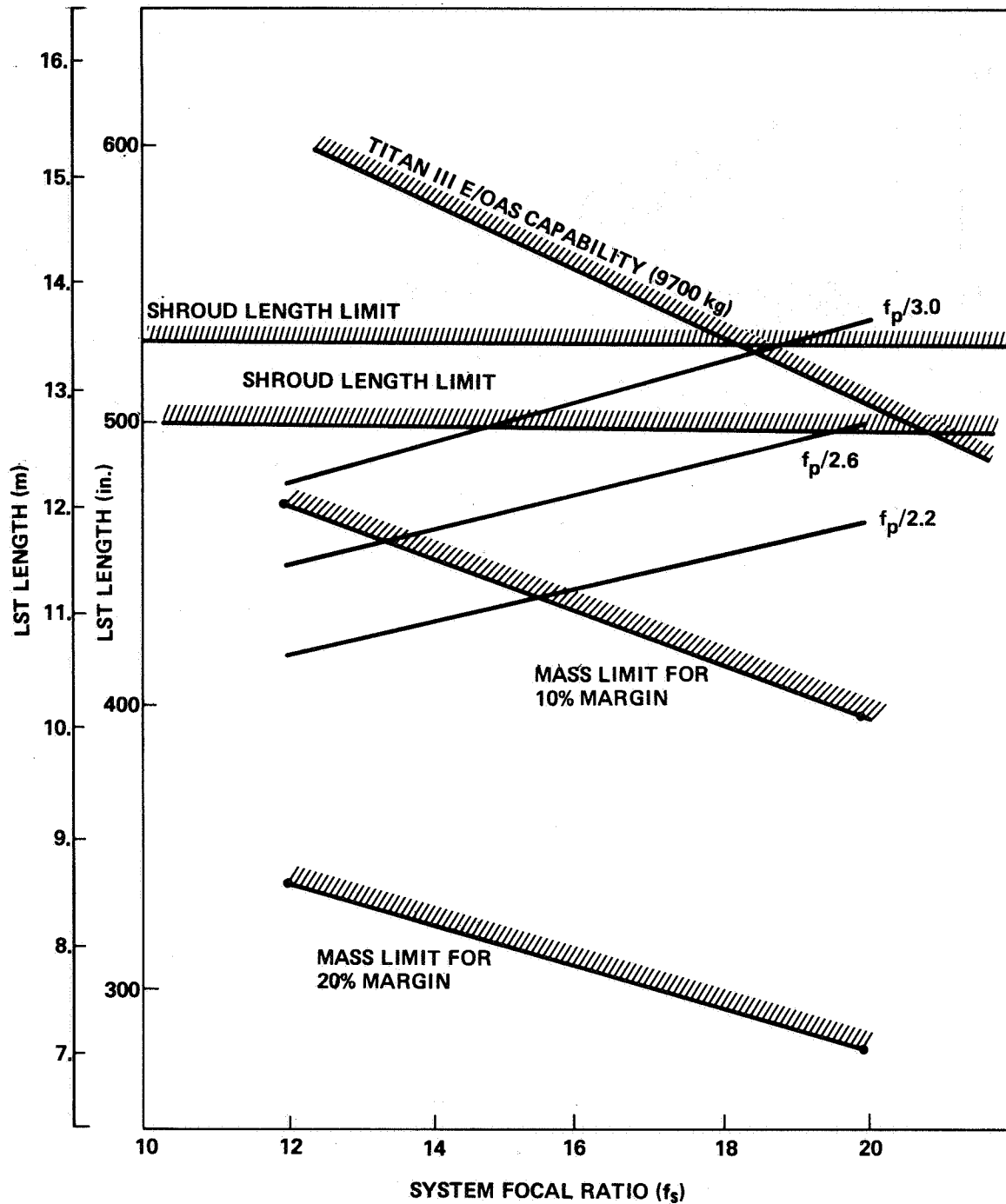


Figure V-3. LST length as a function of system focal ratio for the 3-m LST minimum clearance case.

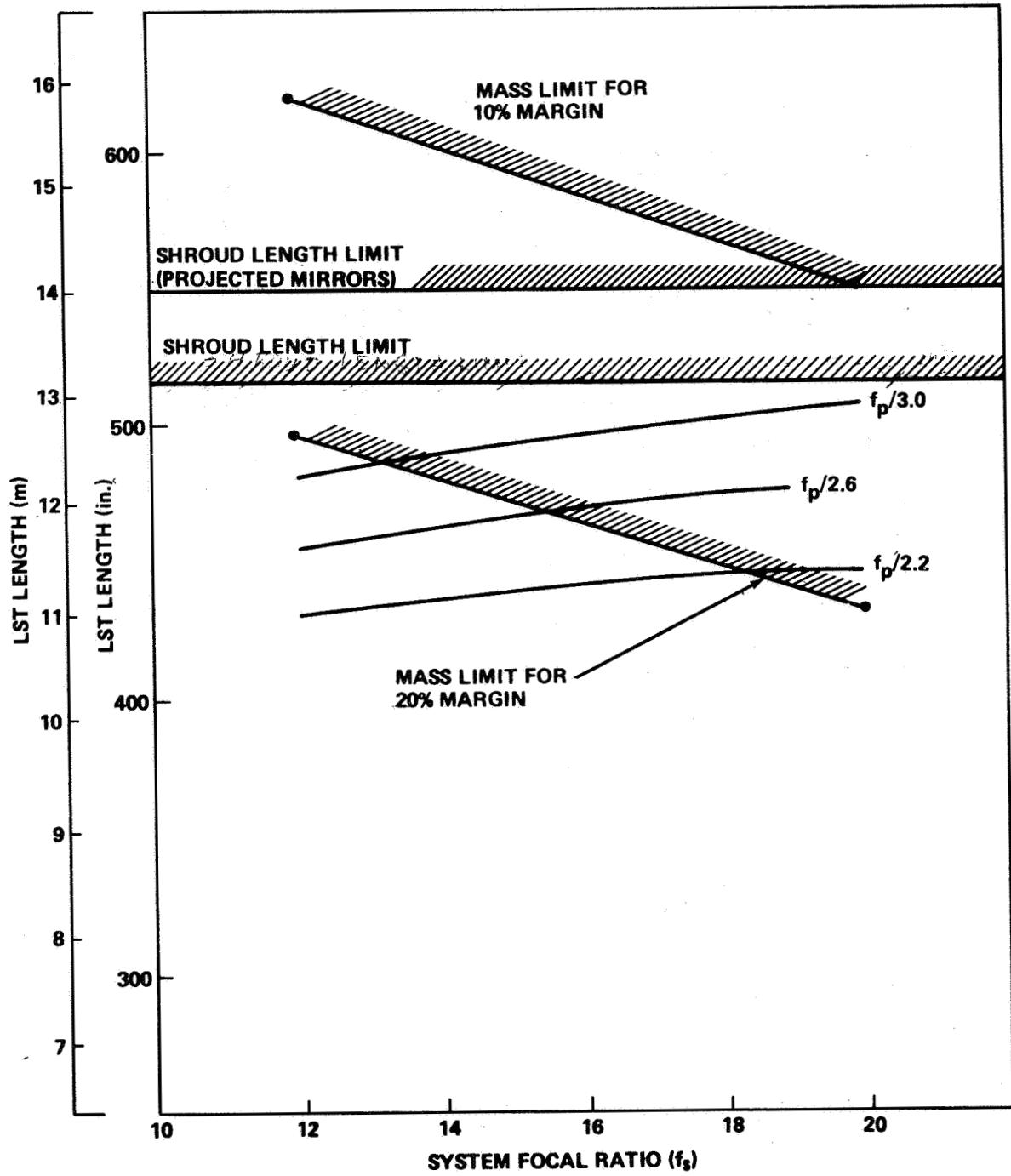
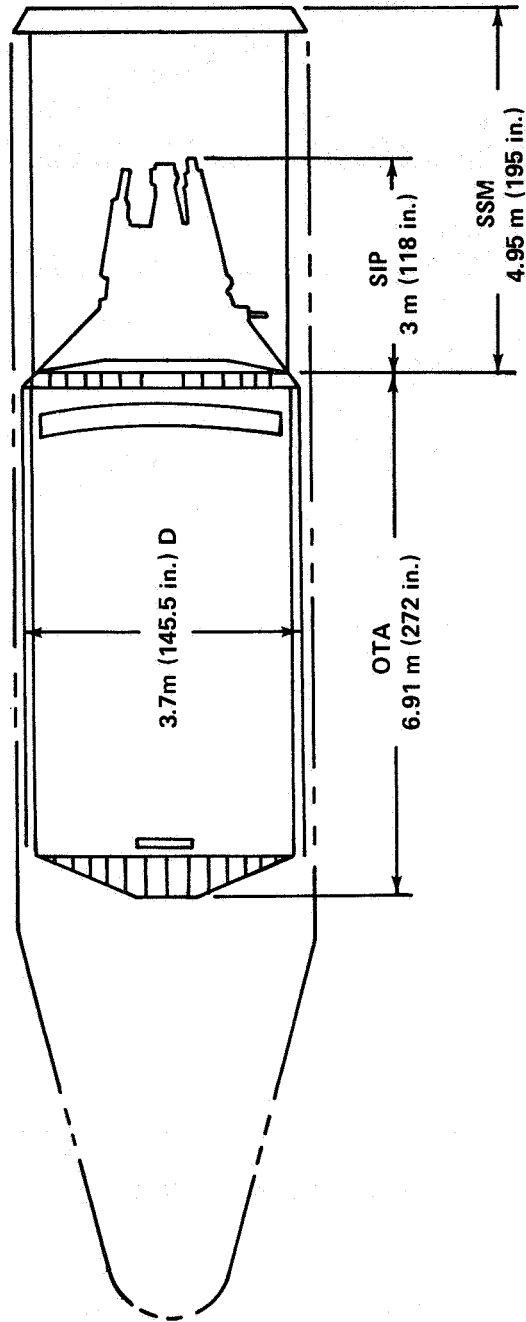


Figure V-4. LST length as a function of system focal ratio for the 2.5-m LST, 20-percent thermal control margin.



$f_p/2.2, f_s/12$   
**3-m LST, PASSIVE THERMAL CONTROL (20% MARGIN)**



OTA MASS	3960 kg	( 8 730 lb)
SIP MASS	1364 kg	( 3 008 lb)
SSM MASS	3569 kg	( 7 869 lb)
	<u>8893 kg</u>	<u>(19 607 lb)</u>

Figure V-5. LST candidate configuration.

$f_p/2.2, f_s/12$   
 3-m LST, MINIMUM CLEARANCE CASE

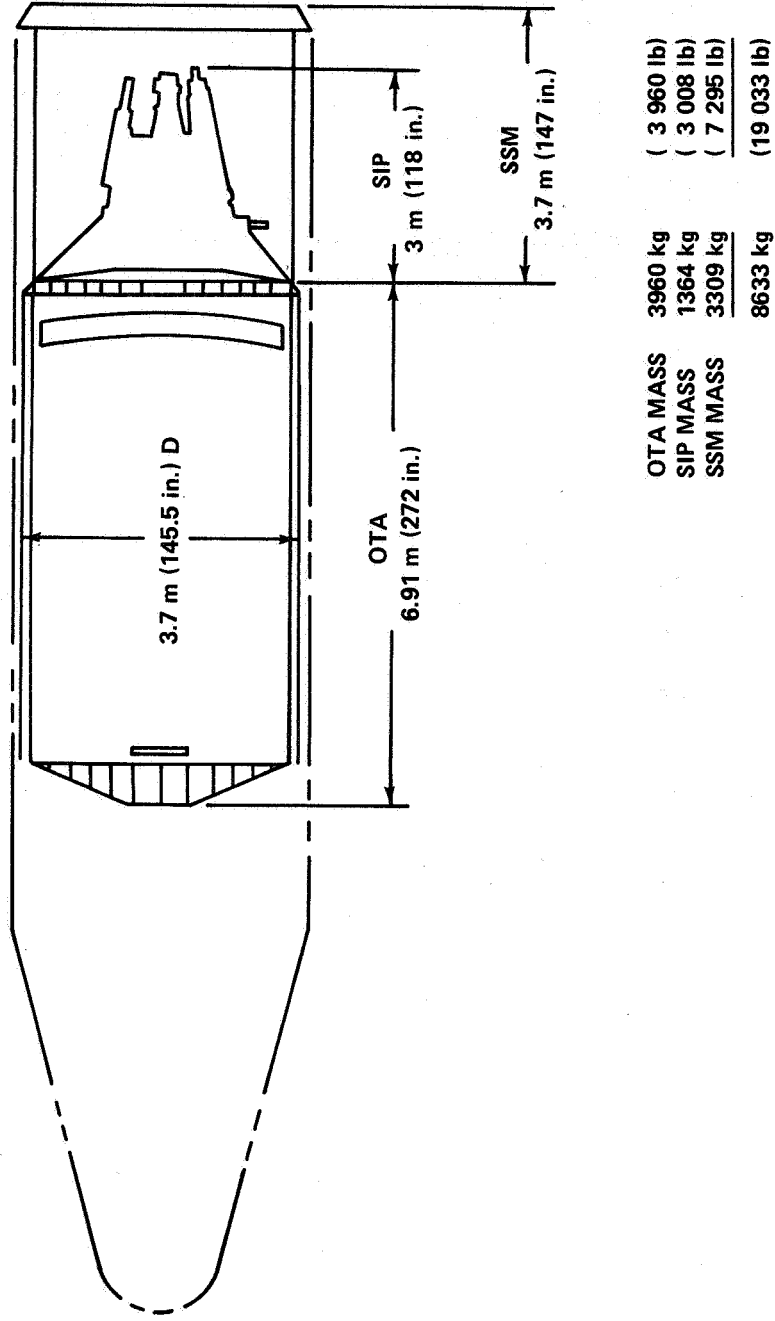
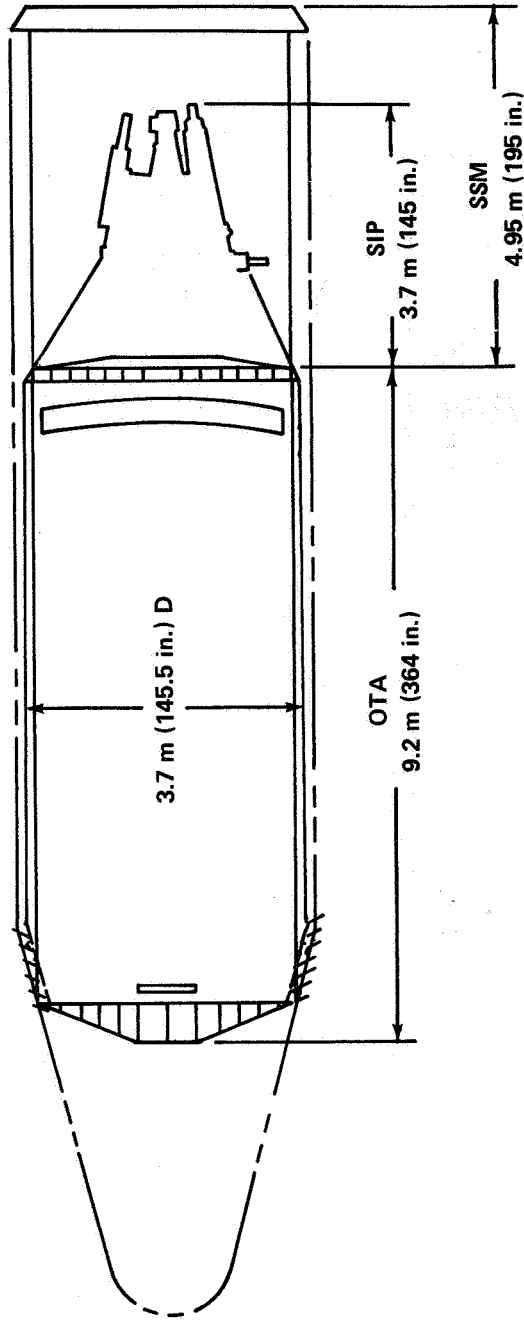


Figure V-6. LST candidate configuration.

$f_p/3.0, f_s/20$

3-m LST, PASSIVE THERMAL CONTROL (20% MARGIN)

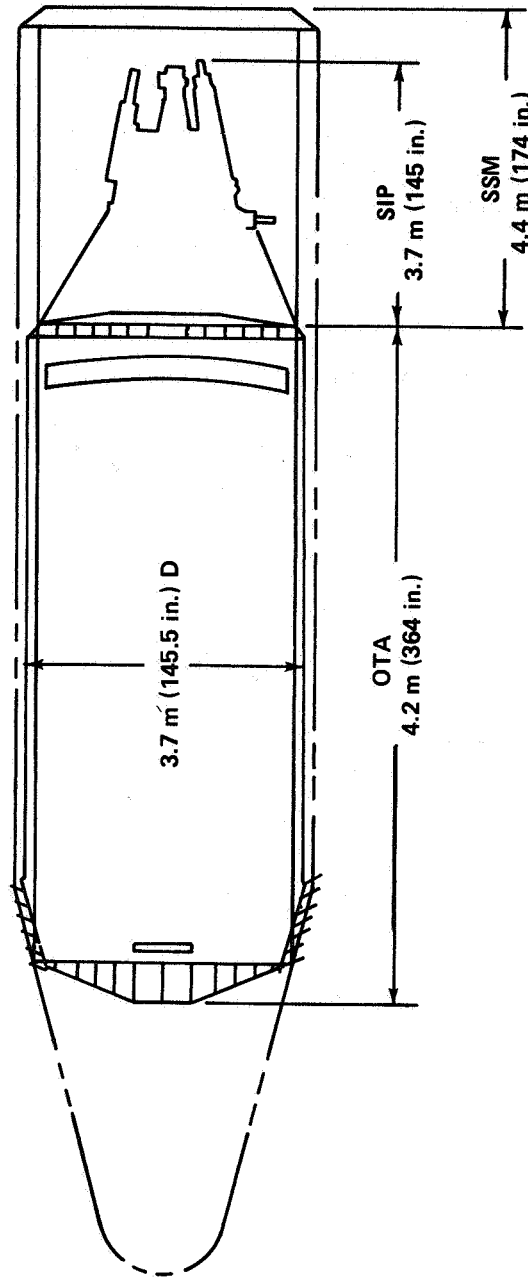


OTA MASS	4 563 kg	(10 060 lb)
SIP MASS	1 889 kg	( 4 164 lb)
SSM MASS	3 569 kg	( 7 869 lb)
	10 021 kg	(22 093 lb)

Figure V-7. LST candidate configuration.

$f_p/3.0, f_s/20$

3-m LST, MINIMUM CLEARANCE CASE



OTA MASS	4563 kg	(10 060 lb)
SIP MASS	1889 kg	( 4 164 lb)
SSM MASS	3464 kg	( 7 636 lb)
	<u>9916 kg</u>	<u>(21 860 lb)</u>

Figure V-8. LST candidate configuration.

vehicle performance numbers. The data are shown in Figure V-9. These data show that a slower system may now be selected than was feasible under the previous design parameters. It is anticipated that the selection of f-number will be reopened as a viable area of study in the Phase B studies.

Should the requirement for retaining the Titan backup launch capability be removed, the length and mass constraints would be significantly relieved as far as the LST design alone is concerned. However, since increased mass and length would make it more difficult for the LST to share Shuttle launches

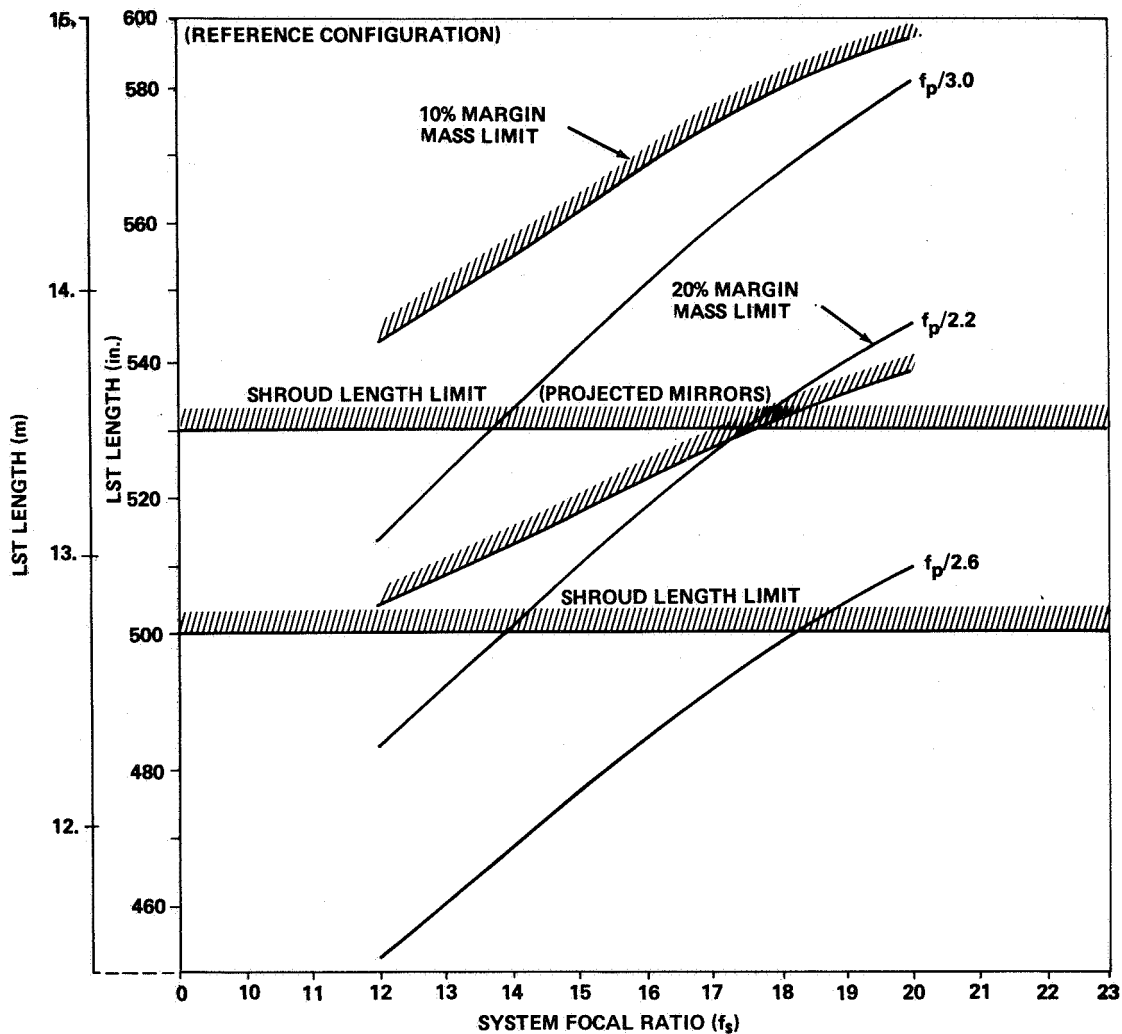


Figure V-9. LST length as a function of system focal ratio for the 3-m LST (reference configuration).

with other payloads (and thereby share costs), the choice of a longer and more massive LST would have to be traded against programmatic considerations. In general, it appears that there will always be a strong driver for the LST to have a low mass and be as short as is reasonably possible.

### C. Light Shield Trades

The LST will have a light shield (sunshade) that will be extended after the spacecraft attains orbit. The function of the light shield is to exclude direct sunlight from the telescope and to reduce the intensity of scattered light from all sources at the telescope image plane.

1. Thermal Considerations. To maintain the thermal balance of the OTA, it is necessary that the light shield be geometrically configured to eliminate the incidence of solar radiation onto the inner surfaces of the OTA. A thermal model of the OTA with a right circular cylindrical light shield (90-degree truncation angle) was analyzed at a number of orbit and spacecraft orientations relative to the solar vector. It was determined from this analysis that if the telescope were pointed at an object in the solar hemisphere, the relatively large heat input from the sun would cause the primary mirror to exceed its maximum allowable temperature. The time requirement for solar hemisphere observation with a cylindrical light shield was not strictly determined; however, it is expected to be on the order of a few hours.

A similar analysis was made using a cylindrical light shield which was truncated at a 45-degree angle. For this configuration it was shown that the LST could view any object located outside a 45-degree, half-cone angle centered on the sun for an unrestricted period of time. The impact on the thermal control of the OTA of additional energy from the earth entering through the truncated portion of the light shield was shown to be acceptable.

It was concluded that a truncated light shield is necessary to maintain the proper thermal balance of the OTA when viewing sources in the solar hemisphere.

2. Viewing Considerations. To maximize useful viewing time of the LST, it will be necessary to view sources during the daylight as well as the dark portion of the orbit. Figure V-10 gives an indication of the effect of sun angle on LST viewing capability for a 90-degree truncation of the light shield. As the telescope is pointed toward the sun, i. e., when the sun angle becomes

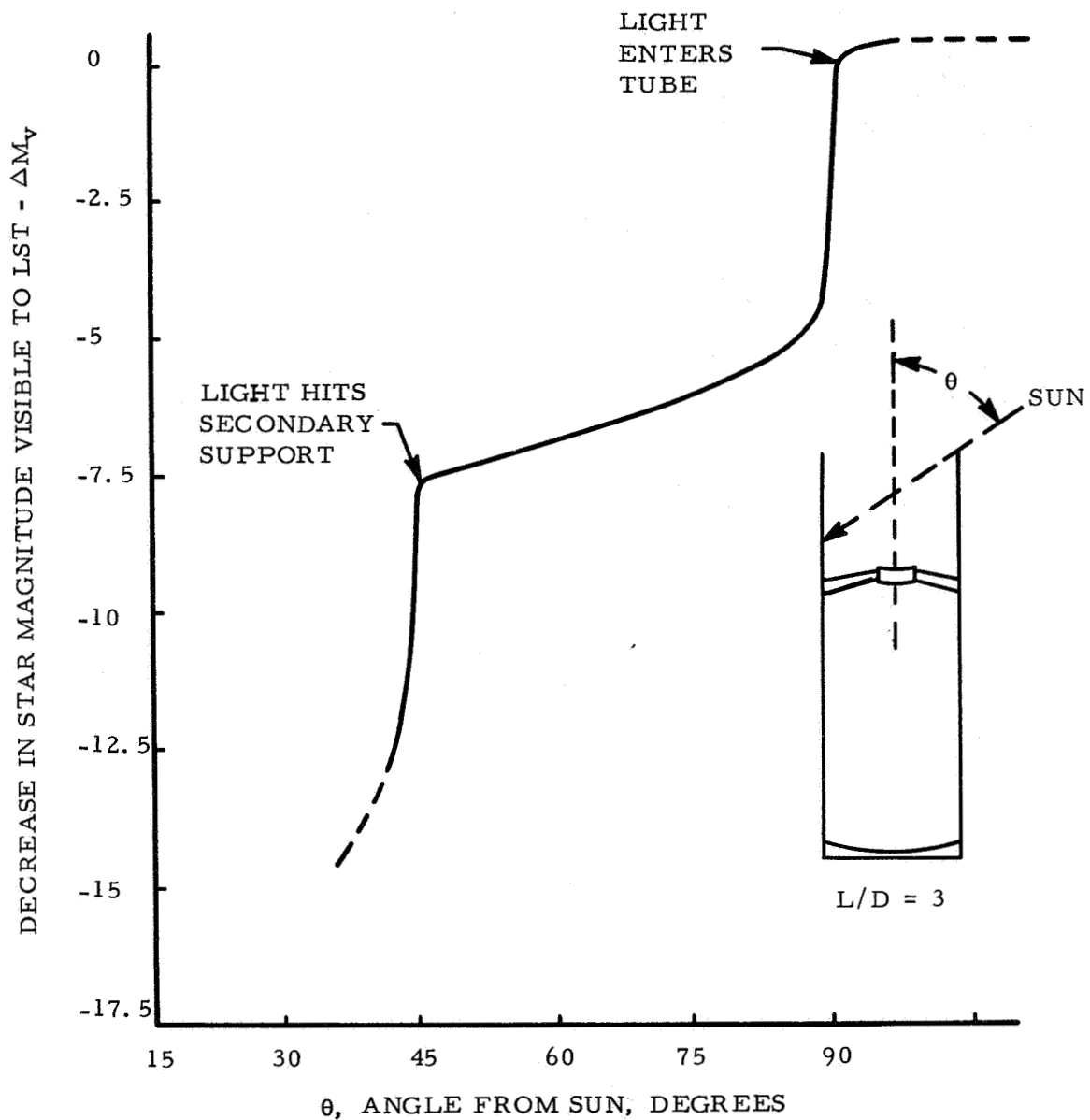


Figure V-10. Effect of sun angle.

less than 90 degrees, sunlight enters the telescope tube. The effect is an increase in the level of stray light and a loss of faint star viewing capability. Figure V-11 indicates the increase in near sun viewing capability that results from various light shield truncation angles. Viewing condition 3 is indicated in Figure V-11 to be the condition when the telescope is opposite a sunlit earth, but with no earthlight entering the tube. The limit of this condition is reached with a 90-degree truncated light shield whenever the telescope is pointed at an angle of less than 90 degrees to the sun. This same limit is not

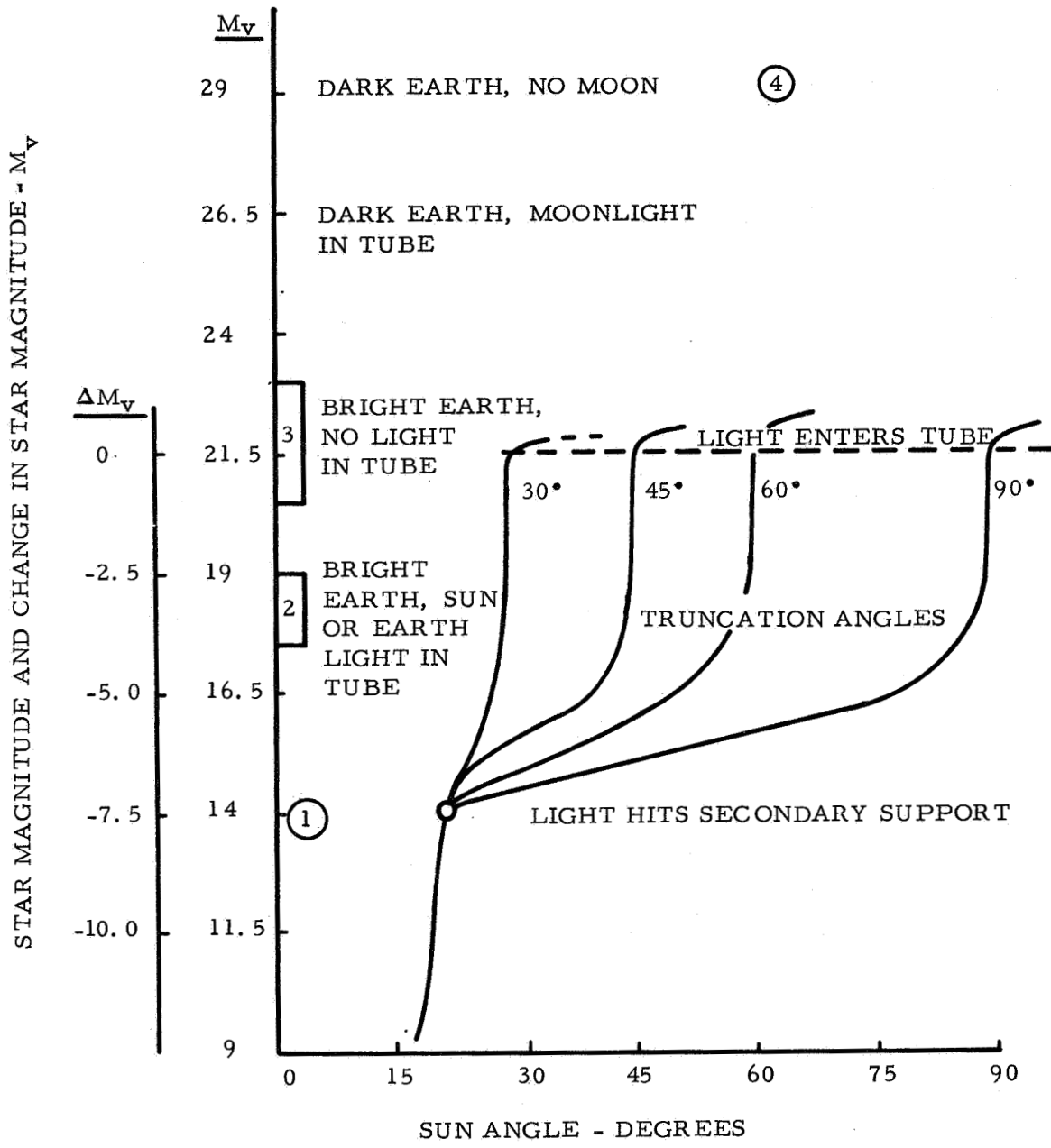


Figure V-11. Estimated faint object viewing limits.

reached with a 30-degree truncated light shield, however, until the telescope is pointed within 30 degrees of the sun. Therefore, the 30-degree truncation angle permits viewing of a much larger portion of the celestial sphere during the sunlit portion of an orbit than the 90-degree truncated light shield does.



The interior surface of the light shield is a polished optical surface. The constraints for faint object viewing are shown in Figure V-12. The sun angle,  $\alpha$ , must be greater than the truncation angle so that no sunlight can enter the telescope tube. Light from the bright earth must strike the inner surface of the light shield at an angle,  $\beta$ , less than 90 degrees, so that most of the light is reflected out of the tube. In addition, the polished optical inner surface of the light shield is coated with a "black mirror" thin film coating. This coating has the property of absorbing energy in the visible region of the spectrum, while reflecting energy in the infrared region. The reflection characteristic of the coating multiplies that of the optical substrate so that the earthlight entering the tube will be reduced to a level that can be handled effectively by the internal telescope baffles.

The operating constraints defined by the design of the light shield and specified in Figure V-12 determine the interval during an orbit when observations may be made and when they may not. Viewing conditions during an orbit are defined in Figure V-13 for the simplest case in which both the sun and the source being viewed lie in the orbit plane. The source is at an angle of 30 degrees away from the solar vector. Viewing condition 1, shown in Figure V-13 and in Figure V-11, is the condition where earthlight is shining into the telescope tube and strikes the secondary mirror support. Under this condition, the dimmest star that is visible in the telescope is visual magnitude ( $M_v$ ) 14. Condition 2 represents the case where earthlight is still shining into the telescope tube, but does not strike the secondary mirror support; dim star visibility has been increased from  $M_v$  14 to  $M_v$  17 to 19.

Viewing condition 3 (Figs. V-11 and V-13) is the limiting operating condition defined by the light shield design, as specified in Figure V-12. The angle between the limb of the bright earth and the telescope line of sight,  $\beta$ , is 90 degrees at this point in the orbit. This angle will decrease as the spacecraft continues around its orbit. The dimmest star visible in the telescope at viewing condition 3 is  $M_v$  20 to 23. Viewing conditions continue to improve from this point in the orbit until the spacecraft reaches the point where viewing condition 4 is defined. At this point, the source becomes occulted by the earth; limiting visible star magnitude is 26 to 29. The viewing conditions defined in Figure V-12 are met during 127 degrees of the orbit, as illustrated in Figure V-13.

3. Recommended Configuration. The duration during an orbit of faint source viewing conditions is a function of the truncation angle of the light shield and the angle between the solar vector and the source vector. This is shown

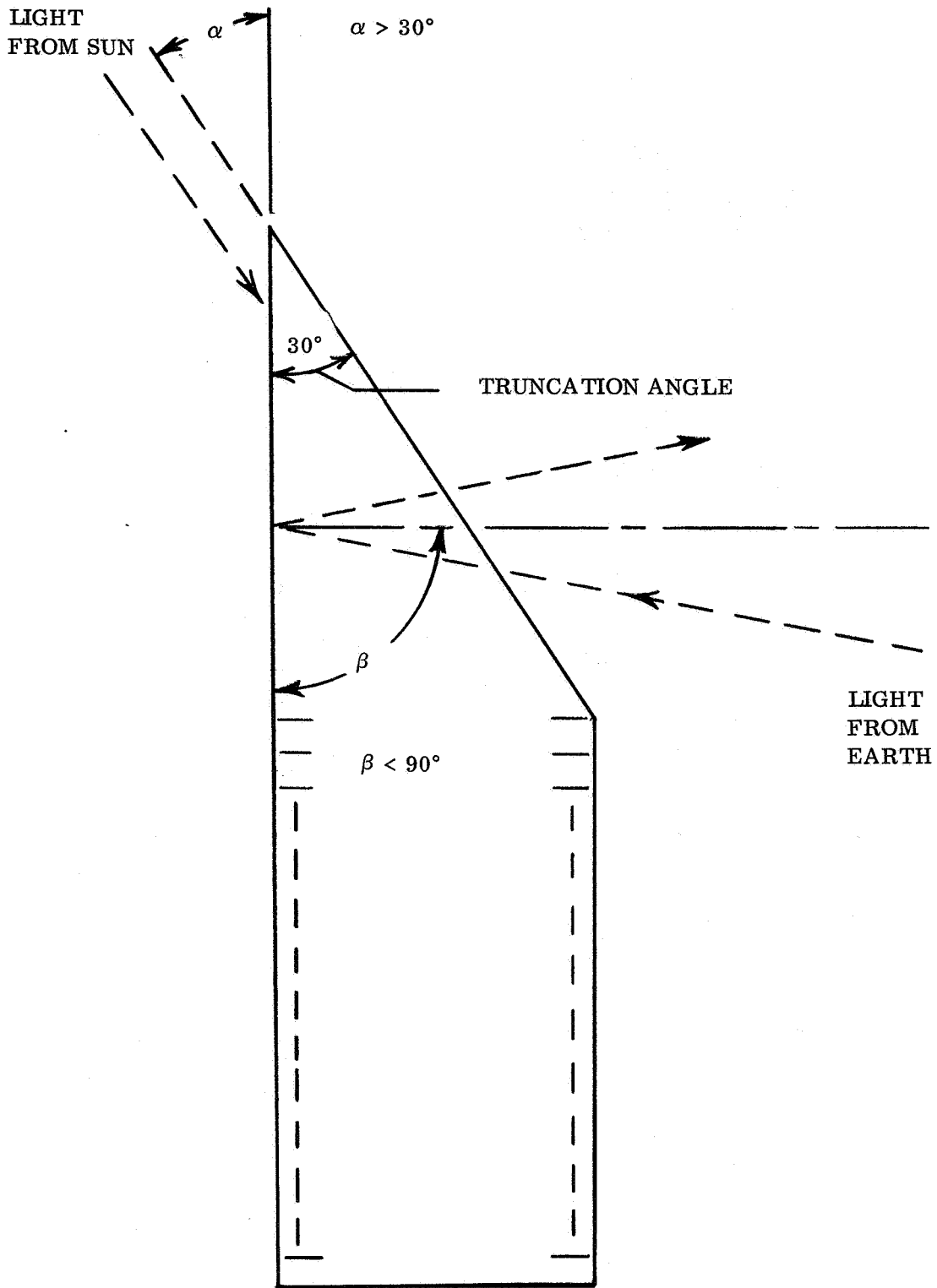


Figure V-12. Light constraints for faint object viewing.

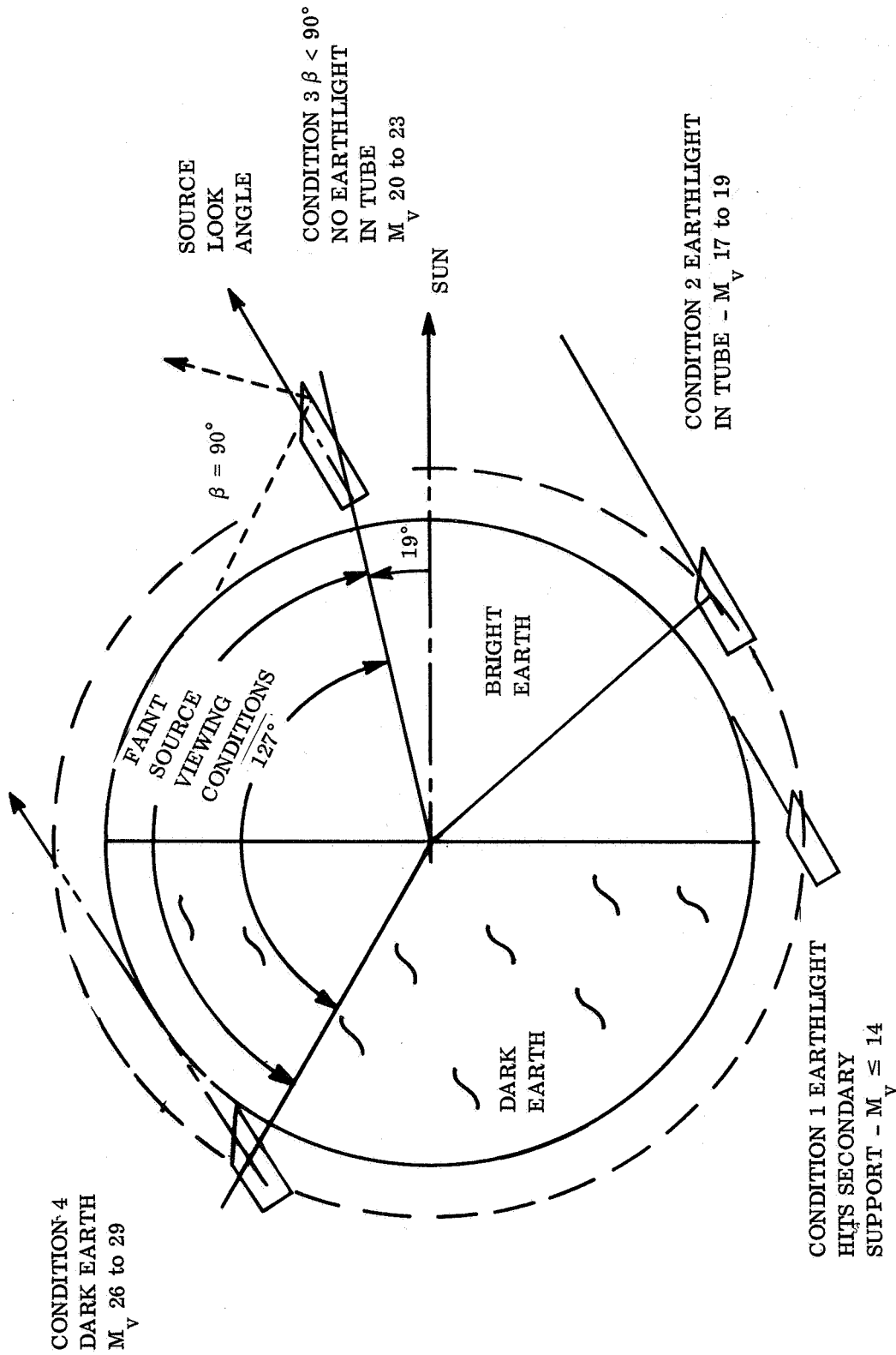


Figure V-13. Typical orbit: look angle 30 degrees from sun.

in Figure V-14. The truncation angle of the light shield does not have a significant effect on orbit viewing time for sources that are at angles greater than 90 degrees from the sun. However, a small truncation angle permits viewing sources that are located near the sun, and this results in a greater portion of the sky being visible to the telescope than if the truncation angle were large. The increase in percent of the celestial sphere visible to the LST as the light shield truncation angle is decreased is shown in Figure V-15 and Table V-2. If the truncation angle is 90 degrees, 50 percent of the celestial sphere cannot be viewed without violating the constraints defined in Figure V-12. Reducing the truncation angle from 90 to 60 degrees permits viewing in an additional 25 percent of the sky, for a total of 75 percent. Reducing the truncation angle from 60 to 45 degrees increases total sky visibility by an additional 10 percent and changing from 45 to 30 degrees increases visibility by an additional 8 percent.

Truncation of the light shield at a 30-degree angle makes the shield much longer on one side than on the opposite side. This produces problems in the structural design of the shield and shield deployment mechanism, and reduces the effectiveness of suppression of stray light from the bright earth. A truncation angle of 45 degrees for the LST design reference was chosen for the Phase A study as being a good compromise between providing maximum sky coverage and minimizing design problems.

## D. Optics

An important part of the activity of the Phase A study program was to establish the basic optical parameters that are most appropriate to the LST, that are compatible with the specified launch vehicles and that would enable the LST to perform the widest possible scientific mission. The speed (f-number) of the primary mirror was governed by the necessity of matching the length of the telescope to that of the secondary launch vehicle, the Titan IIIE/Orbit Adjust Stage (OAS), and by mass considerations. The chosen  $f/2.2$  speed yielded the lightest and shortest payload. The upper boundary for an acceptable primary f-number appeared to be about  $f/3$ . Study showed that optical performance (as measured by Strehl, for instance) varied very little over a wide range of primary mirror and system f-numbers. Indeed, the largest optical effect is obtained from the variation of the central obstruction with general system parameters, and during the progress of the study, substantial reductions in this factor were obtained by reducing the size of the annular field used for offset guidance. The improvement in performance due to this reduction in the size of the tracking field is much larger than the entire

NOTE: SOLAR VECTOR AND  
TARGET VECTOR LIE  
IN ORBIT PLANE

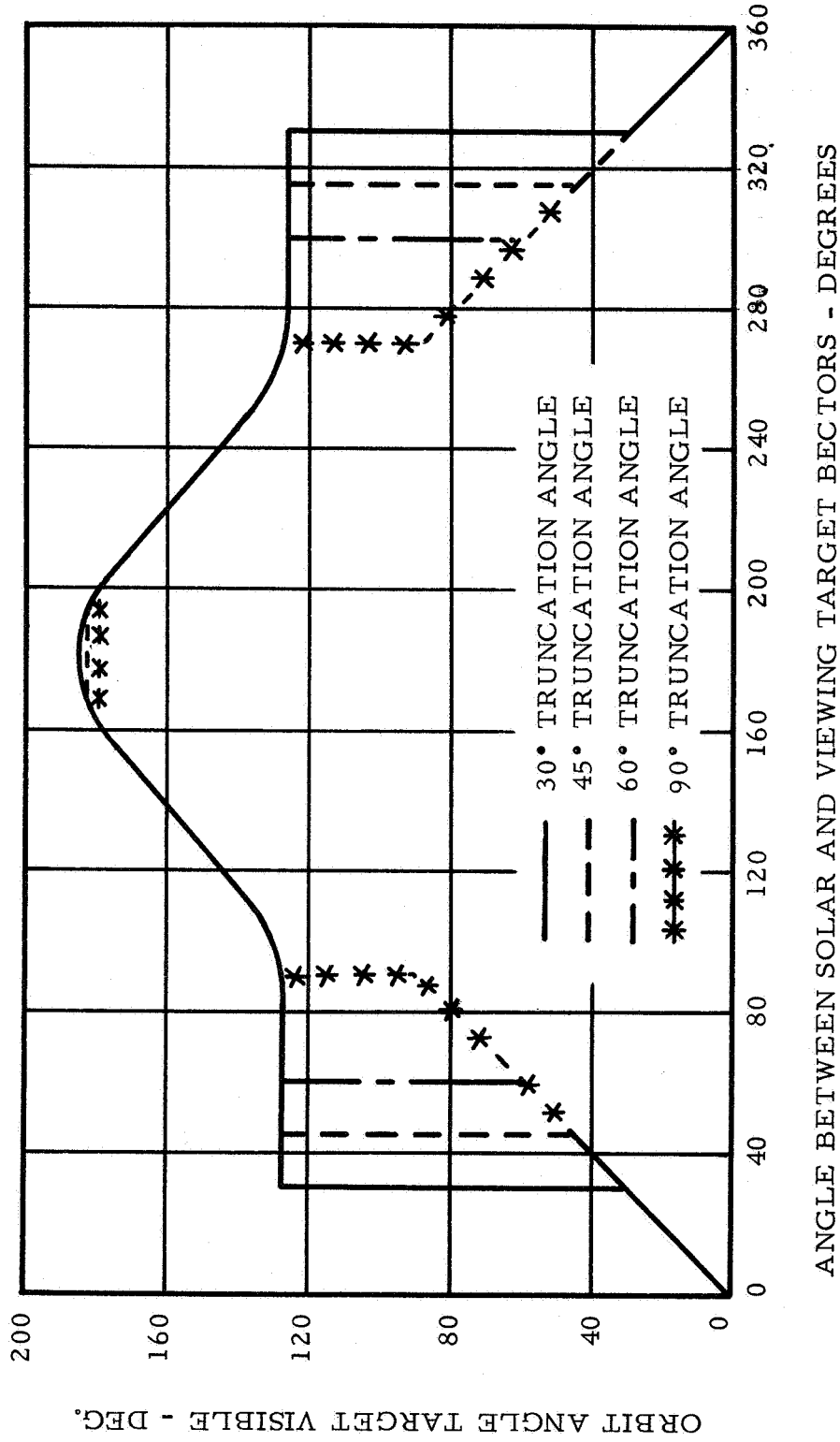


Figure V-14. Duration of faint source viewing conditions.

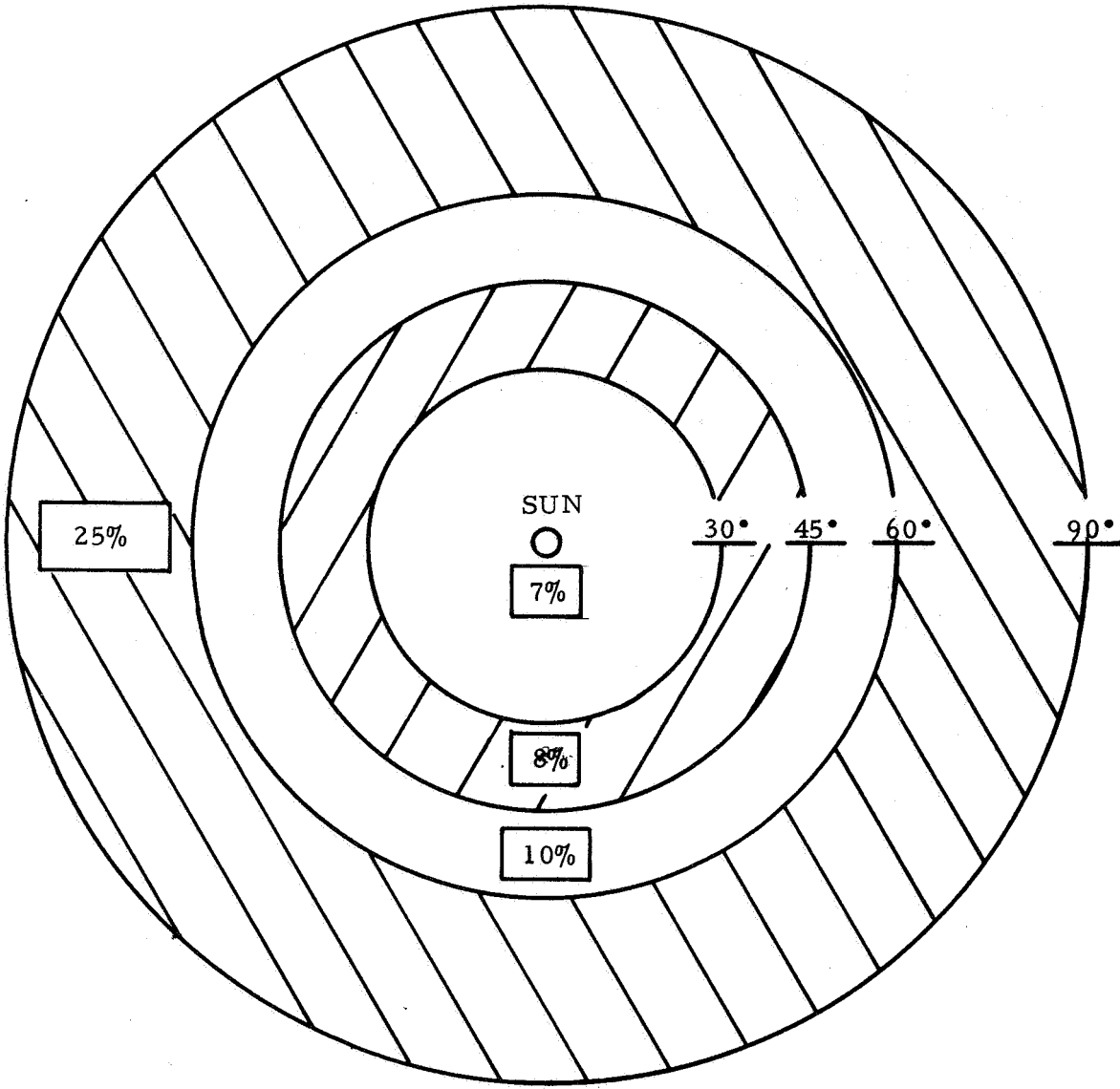


Figure V-15. Sky coverage increments as a function of minimum sun angle.

variation obtained by varying the f-numbers over ranges of 2.0 to 4.0, and 8 to 24, respectively. An additional benefit to be obtained from the reduced guide field is that the complex five-element refracting corrector is simplified and a fine guidance system is not needed in the reticle plate.

TABLE V-2. OPERATIONAL ADVANTAGES OF TRUNCATED LIGHT SHIELD (FOR THE CONDITION OF BOTH SOLAR AND TARGET VECTORS IN THE ORBIT PLANE),

Comparison With:	Target Angles	Additional Allowable View Area	Additional View Time Percent of Orbit	
			Range	Average
90-degree Truncation Angle		Percent of Sky		
60-degree Truncation	60-90	25%	10-18.5	14.3
45-degree Truncation	45-90	35%	10-23	16.5
30-degree Truncation	30-90	43%	10-27	18.5
60-degree Truncation Angle				
45-degree Truncation	45-60	10%	18.5-23	20.8
30-degree Truncation	30-60	18%	18.5-27	22.8
45-degree Truncation Angle				
30-degree Truncation	30-45	8%	23-27	25.0

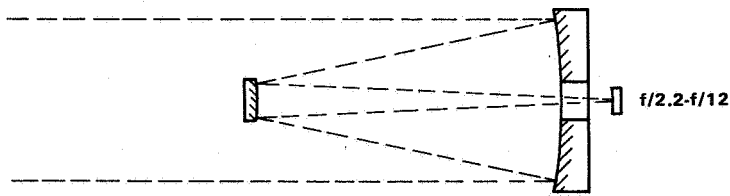
1. Aperture Selection. The scientific usefulness of a space-based telescope is most importantly related to the improvement in angular resolution that may be obtained by removal of atmospheric degradation and the consequent improvement in ability to detect dim objects. As the aperture of the space telescope decreases, its performance becomes comparable to earth-based instruments, and the only remaining justification for the instrument is the wider spectral response, free from atmospheric effects. To justify an LST, it is necessary that its performance be maximum, and therefore the maximum aperture that can be launched must be chosen. Since the secondary launch vehicle is the Titan IIIE/OAS, the outside diameter of the telescope is limited to 3.7 m (145 in.). The Space Shuttle has a larger aperture capacity, but the LST must be compatible with the secondary launch vehicle. When allowance has been made for light shield, meteoroid shield, metering structure, and baffles, the largest feasible aperture is 3 m (118 in.).

2. Choice of Telescope Type. Previous studies indicated that both the Ritchey-Chretien and Gregorian types of telescope should be considered for the LST application. During the beginning of the present Phase A study, a more detailed comparison of the Gregorian and Ritchey-Chretien telescope was carried out under the added constraint of a length-limited Titan III vehicle.

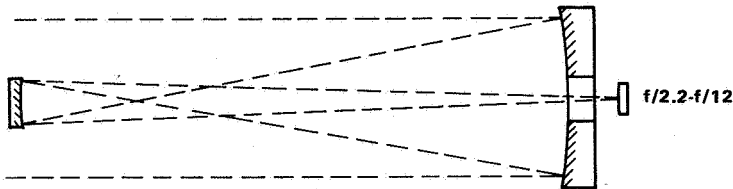
The length constraints imposed by the Titan IIIE on the selection of the telescope configuration quickly limited the selection to Cassegrain and Gregorian telescopes of equal length. A faster primary was required for the Gregorian,  $f/1.5$  versus  $f/2.2$  for the Cassegrain, as shown in Figure V-16. The departure from a spherical surface for the faster primary will be much greater; hence its manufacture will be much more difficult. The alignment tolerances are also tighter for the faster primary, further complicating the thermostructural design of the primary-secondary metering truss and requiring far more precise decenter measurement. The backward-curving focal plane would be an advantage with some imaging tubes, although present efforts at Princeton University are directed toward the development of flat surface, magnetic focused image tubes for the LST, and these are equally compatible with either system.

3. Selection of Primary Mirror f-Number. As mentioned above, the primary mirror f-number has been set by the compromise in length between the spacecraft (Support Systems Module) and telescope (OTA) portions of the LST. The optical factors relating to this choice are (1) manufacturing ease versus quality, (2) the ability to maintain alignment, (3) sensitivity to vibration, and (4) central obstruction. A previous detailed study showed that the above factors balanced in such a way that variation in optical quality was insignificant over the range of relevant values.



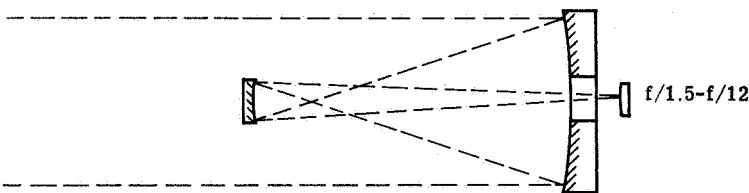


(a) Baseline Cassegrain



(b) Gregorian with equal  $f$ /numbers

45% longer  
 $\sim 2 \times$  greater WFE per unit decenter  
 10% larger high quality field  
 30% less field curvature, backward



(c) Gregorian with equal length

$3.4 \times$  greater WFE per unit decenter  
 $2 \times$  greater image motion per unit decenter  
 Possibly 10% less obscuration  
 20% smaller high quality field  
 70% more field curvature, backward

Figure V-16. Comparison of aplanatic Gregorians and design reference Cassegrain.

4. Selection of System  $f$ -Number Optical Effects. When the overall system  $f$ -number is faster than about  $f/15$ , greater care must be exercised in the design of such instrument accessories as the fine guidance or spectrograph slits, because the size of the diffraction limited star image becomes small (i.e., has point spread functions of the order of 7 to 14  $\mu\text{m}$ ) as compared to easily fabricated components. Furthermore, the small image scale makes it difficult to package several instruments in proximity. A faster system provides a larger field of view with a given image tube, which is usually limited by the ability to span distances with thin flimsy elements within the

tube or by the pixel throughput of the electron beam readout. A slower system decreases obscuration up to a point, beyond which it increases again. The most important potential of a slow system is the possibility of placing the image sensor surface directly into the first real image plane of the telescope. The state of the art of image tubes is presently such that spatial resolution of the order of 20 lines/mm is obtained at 50-percent modulation. If the tube resolution is not to significantly degrade the telescope optical resolution, a system f-number of the order of f/100 is required. Clearly, it is not feasible to build a telescope at f/100 without gravely compromising the fine guidance system, and there is the difficulty of staying within the vehicle length without an excessive number of folding mirrors. An intermediate alternative was investigated in which a stage of electronic magnification of the order of 2X to 3X is introduced into the tube. This method would require an optical focal plane of about f/30 to f/50. Such systems were investigated in the study, and it was found that the system length required for this configuration was excessive for the Titan III vehicle. By drastically altering the spacecraft configuration and using a side-mounted docking adapter, it was found to be conceptually possible to accommodate an f/30 system, but the drastic nature of the required alterations made this alternative unacceptable, since a possible incompatibility with the Shuttle and Space Tug programs was introduced. If the emphasis of the scientific community on far-ultraviolet observations were to be considerably increased, one might reconsider imaging in the first real image plane of the telescope because of the greatly increased optical system transmission below 110 nm.

The present choice of system f-number (f/12) has been made for reasons of system compactness and because it has been shown that existing sensing elements are compatible with the small scale images in the focal plane.

5. Folding Optics. To distribute the telescope image to the various instruments (spectrographs, guidance sensors, f/96 relay, etc.), one or several folding mirrors are used just in front of the primary image plane. These mirrors allow the instruments to be spread around the optical axis. To ensure that the mountings of these mirrors do not obstruct the guidance field, they are mounted directly to a glass plate that is normal to the telescope axis on the front side of the folding optics assembly. The glass plate is perforated and baffled to allow ultraviolet light to be transmitted without loss. Refractive effects of the plate on the guidance field are included in the optical design and are expected to be slight if low scatter surfacing techniques are used. This glass plate with its attached mirrors can be removed as a unit from the assembly.

An early concept that was considered consisted of one small mirror that rotated to fold the data field to selected instruments, or moved aside to allow the light to pass to other instruments. This is shown schematically in Figure V-17. Although this concept provides great flexibility, it has the significant shortcoming that a failure of the translating/rotating mirror in an intermediate position would prevent further observations.

A more reliable configuration, based on sharing of the available field, is shown in Figure V-18. At the center of the data field is a fixed fold mirror that brings a 0.174-mrad (0.6-arc min) image through a power changer to the f/96 cameras. This mirror is on the optic axis of the telescope to ensure that the image tube will not significantly degrade the resolution of the optical system.

By offsetting the telescope about 1.59 mrad (5.5 arc min), the beam is brought to the 1.39-mrad (4.8-arc min) f/12 cameras via a stationary fold mirror. The image quality is lower since it is off axis, but at f/12 the image tube will be the resolution-limiting factor.

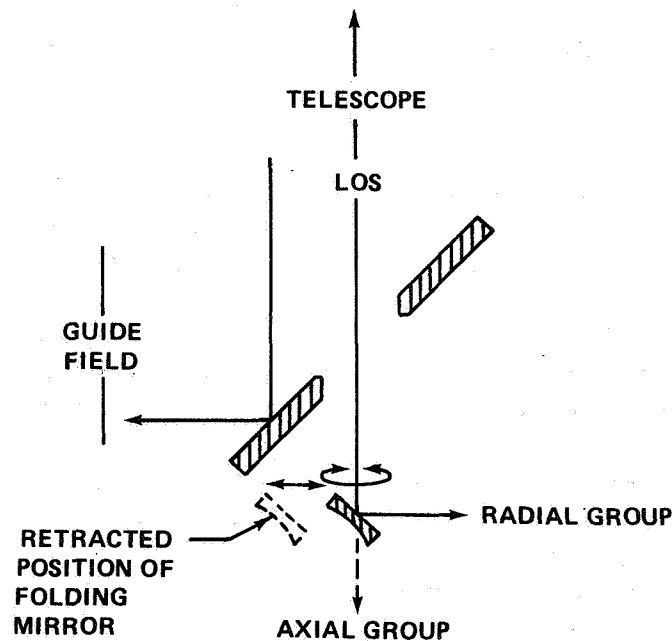


Figure V-17. An alternate focal plane layout that was not selected.

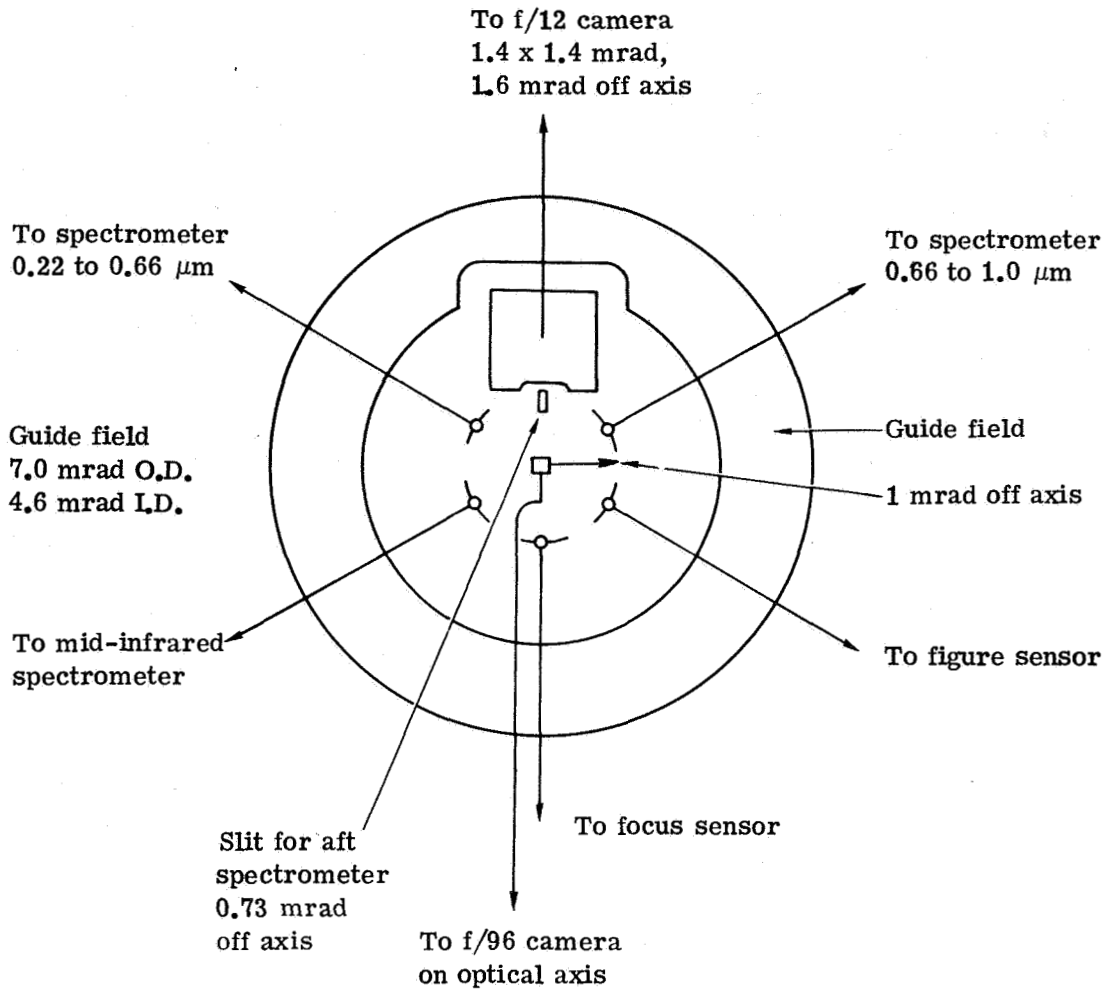


Figure V-18. Design reference f/12 image plane format.

Offsetting the telescope in the other direction allows the light to pass to the various spectrographs, and another offset (e.g., out of the plane of the page) illuminates other instruments.

Small stationary spherical mirrors are used to bring light to the infrared spectrographs and the focus and figure sensors, all of which require negligible field. The spherical surface, properly tilted, gives excellent correction over a small field, even though it may be several milliradians (arc-minutes) off axis.

6. Mirror Material Selection. Constant development in the technology of producing large diameter, lightweight mirror blanks demands a continuous surveillance of the industry in order to rationally select the appropriate material for any particular application. Specifically, the LST requires a primary mirror of 3-m (120-in.) diameter to be figured to a minimum surface error of  $\lambda/64$  rms, which quality is to be maintained for a 10-year orbital lifetime in a controlled thermal environment of  $\pm 3^\circ\text{C}$ .

Several materials were considered for this application: Corning ULE, titanium silicate, Owen-Illinois Cer-Vit, fused silica, Zero-Dur, and crystalline quartz. Due to the overall size requirement, the need for a lightweight blank, and the desire to minimize the sensitivity to thermal variation, the choice was reduced to two prime candidates, Cer-Vit and ULE.

A comparison of the relative merits of Cer-Vit and ULE is given in Table V-3 on the basis of the listed parameters. As can be seen from this evaluation matrix, Cer-Vit has the highest point total and is a major influence on the selection. While some of the weighting factors and influence coefficients values may be disputed, it is apparent the Cer-Vit does have a distinct edge for the LST application.

The primary basis for the selection is more influenced by the manufacturability problems and the resulting design latitude that it offers rather than by a material problem along with a substantial cost influence.

The general impression is that as a substrate material, ULE and Cer-Vit are acceptable. However, Cer-Vit offers a higher degree of confidence in producing an operational mirror of the described quality in the LST operational environment.

7. Optical Coatings. Since the large orbiting telescope is expected to operate as a general purpose instrument, optical coatings that would operate over as broad a wavelength range as possible were investigated. The usefulness of coating materials over the range of 0.1 to 100  $\mu\text{m}$  was evaluated; however, no materials transmit throughout this entire region. Since the optical system must be primarily reflective in form, efforts were concentrated on metallics. Data available in the literature show the reflectivity of the most commonly used metals over a 0.22- to 40- $\mu\text{m}$  region. Aluminum is the only metal that maintains a high ( $\geq 86$  percent) reflectivity in this region. The reflectivity of aluminum in the far infrared also shows it to be well behaved.

TABLE V-3. MIRROR MATERIAL SELECTION EVALUATION MATRIX

Parameter	ULE	Cer-Vit	Influence Coefficient 1 to 5	Evaluation Factor		Point Total	
				ULE	Cer-Vit	ULE	Cer-Vit
Coefficient of Expansion $\alpha$ , 0 to 35°C	$0.03 \times 10^{-6}$ in./in./°C	$0.02 \times 10^{-6}$ in./in./°C	5	4	5	20	25
$\alpha$ Confidence	95%	95%	2	4	4	8	8
$\alpha$ Measurement	$3.0 \times 10^{-9}$	$3.0 \times 10^{-9}$	3	4	4	12	12
$\Sigma$ Modulus	$9.7 \times 10^{-6}$	$13.0 \times 10^{-6}$	3	4	5	12	15
Birefringence	40 $\mu\text{m}/\text{cm}$	10 $\mu\text{m}/\text{cm}$	4	3	5	12	20
Inclusions	—	—	2	4	4	8	8
Material Stability	—	—	4	4	4	16	16
Manufacturing Risk	—	—	3	3	4	9	12
Mount Design Compatibility	—	—	2	2	3	4	6
Structural Determinant	—	—	2	3	4	6	8
Required Development	—	—	3	3	4	9	12
Cost	\$1700K	\$850K	3	3	5	9	15
Delivery	12 months	12 months	2	3	3	6	6
Totals						131	163

If reflectance below 200 nm is not required, an aluminum film overcoated with  $\text{Al}_2\text{O}_3$  or  $\text{SiO}_2$  can be used. These films are quite durable and can be cleaned without damage. For some components of the LST, this may be the coating of choice. When reflectance is required in the region below 200 nm,  $\text{MgF}_2$  or  $\text{LiF}$ -overcoated aluminum are the only choices. The spectral performance of these two combinations is shown in Figure V-19. The 250-nm thickness of the  $\text{MgF}_2$  represents the thinnest layer that provides adequate protection from degradation due to atmospheric oxygen. Neither of these coatings can be regarded as cleanable, and both require special handling precautions.  $\text{MgF}_2$  is normally thought of as a durable hard film because of its use as an antireflection coating. For this application, it is soft because it must be deposited at room temperature rather than at  $250^\circ\text{C}$ . Aluminum loses its reflectivity if it is heated and any protective coating must be deposited on an unheated substrate.

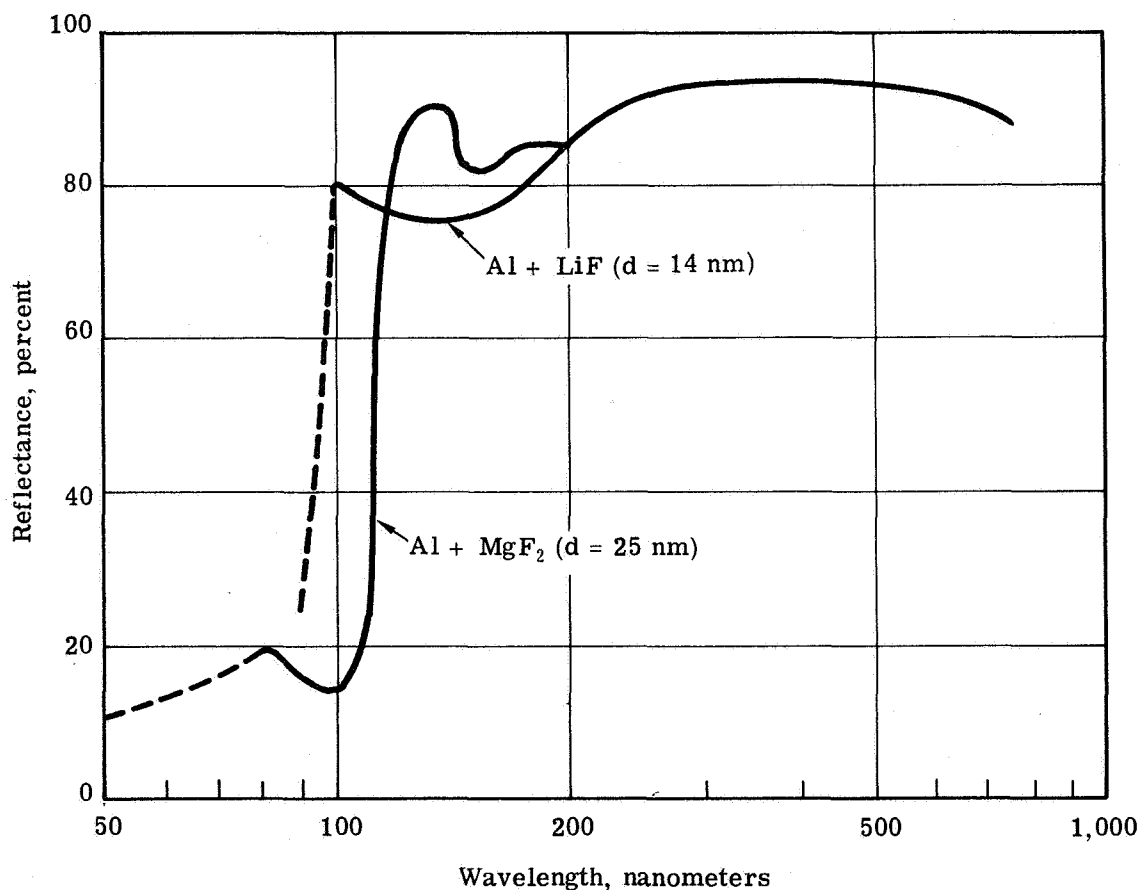


Figure V-19. Spectral performance of  $\text{MgF}_2$  and  $\text{LiF}$  overcoated aluminum.

The decision between these is almost automatic once the system requirements have been defined. Since  $MgF_2$  provides higher reflectance above 120 nm and has less tendency to degrade on exposure to atmospheric humidity, the decision to use LiF as an overcoating material would only be made if the region between 95.0 and 115 nm was of overriding importance.

## E. Structural Concepts

In several instances, alternate concepts are to be investigated before final determination of configurations and design can be made. The major items to be considered in that respect are the following:

1. OTA Graphite Epoxy Shell
2. Pressure Bulkhead and Primary Ring
3. SIP Support Structure
4. Rollout Solar Array
5. Primary Mirror Support
6. Spider Beam

1. OTA Graphite Epoxy Shell Study. The objective of this study was to assess the potential of advanced composite materials for certain major structural components of the optical telescope assembly of the LST. The technical approach taken was to redesign the OTA metering structure, primary light baffles, meteoroid shield, extendible light shield, and secondary mirror mounting beams to take advantage of the low coefficient of expansion, high strength, high stiffness, and low density of graphite epoxy materials.

Advanced composite materials differ greatly from metallic structural materials in basic mechanical and physical behavior, in optimum structural arrangement, and in fabrication processing. It was felt desirable, therefore, to reconfigure the all-metal OTA configuration (a combination of a truss and several shells) for the graphite epoxy shell study. The basic criteria for the two structural concepts are the same, of course, in terms of allowable distortion, environment, applied loads, and size constraints.



The configuration selected for study in graphite epoxy consists of an integrated metering shell structure and primary light baffle, surrounded by a very low mass light shield shell (Fig. V-20). This arrangement is not necessarily the lowest mass configuration, but it will save significant mass over the metal structure.

The cylindrical shell combines the functions of light baffle and metering structure, thus reducing the number of concentric cylinders from four (truss design) to three (shell design), Figure V-21. This allows reductions of the diameters of the meteoroid shield and the light shield so that the outside diameter of the LST could be reduced from 3680 mm (145 in.) to 3580 mm (141 in.). On the other hand, the outside diameter could be held constant and more radial clearance between the three cylinders could be provided. Additional advantages of the shell design are the improved interface to bulkhead and SSM and considerably simplified assembly procedures.

The final thermal distortion analysis results indicate that the graphite epoxy OTA structure is very stable during the worst thermal condition, because it handily meets all of the design criteria and constraints. The natural frequencies are high; therefore, launch dynamics are not expected to be significant and the on-orbit dynamics effects will be minimized.

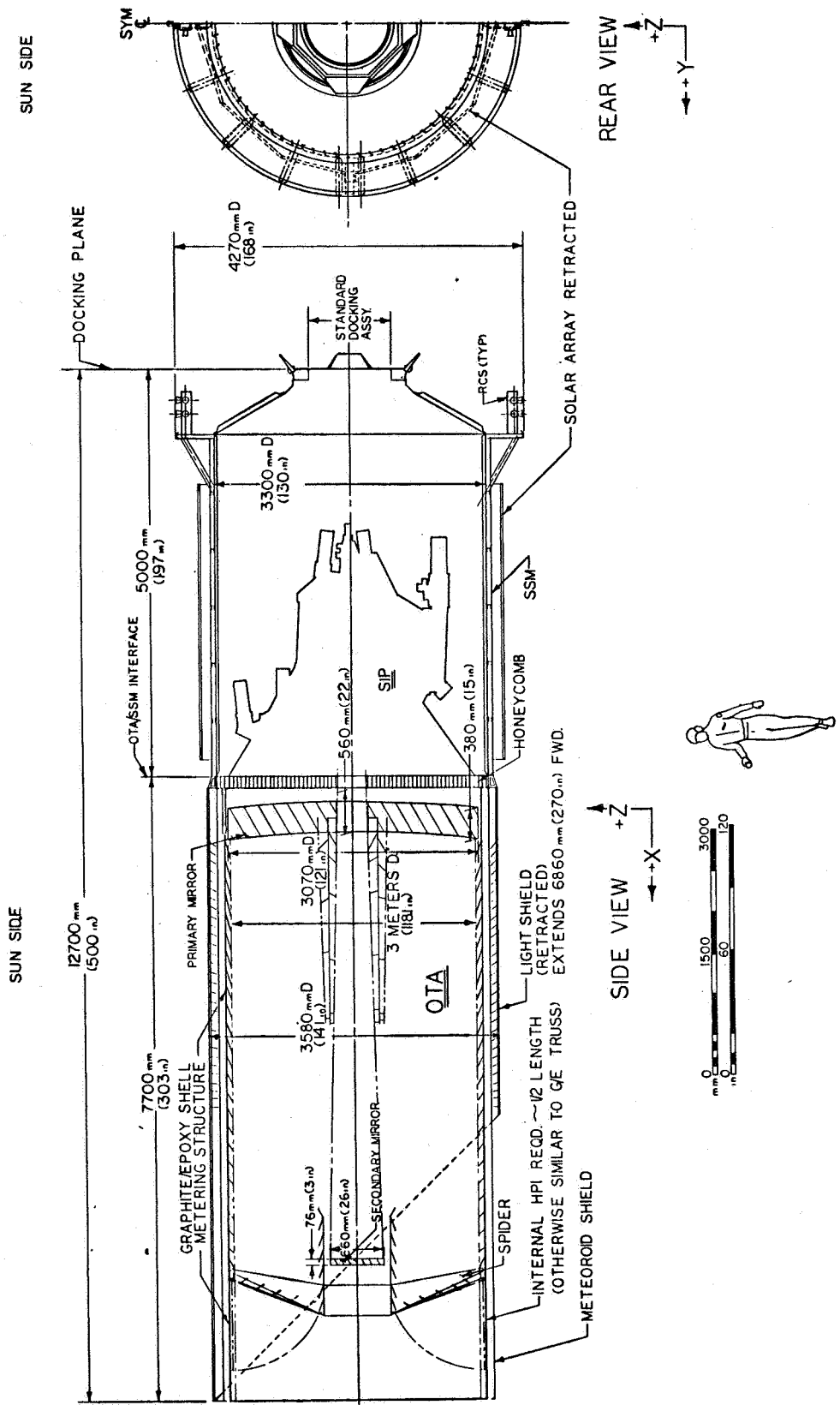
It was concluded from the study that the shell design is a viable concept and that it possesses most of the desirable structural features that the spacecraft should have.

Further detail discussion on this alternate design is given in Appendix A of this volume.

2. Pressure Bulkhead and Primary Ring. It would be advantageous to use a flat bulkhead rather than the expensive curved bulkhead at the forward end of the SSM, if it can be shown that this change has no adverse effect on the primary mirror. In that case the function of the primary ring can, to a large extent, be taken over by the stiff honeycomb bulkhead.

3. SIP Support Structure. As an alternate to the eight outrigger-type supports of the reference design, a statically determinate three-point design, as indicated in Figure V-22, is structurally feasible. It is noted that the distance,  $d$ , can be selected to satisfy the thermal requirements.

Although the advantages of this concept with regard to structural matters, analyses, and installation are obvious, its thermal conditions and alignment requirements need clarification.



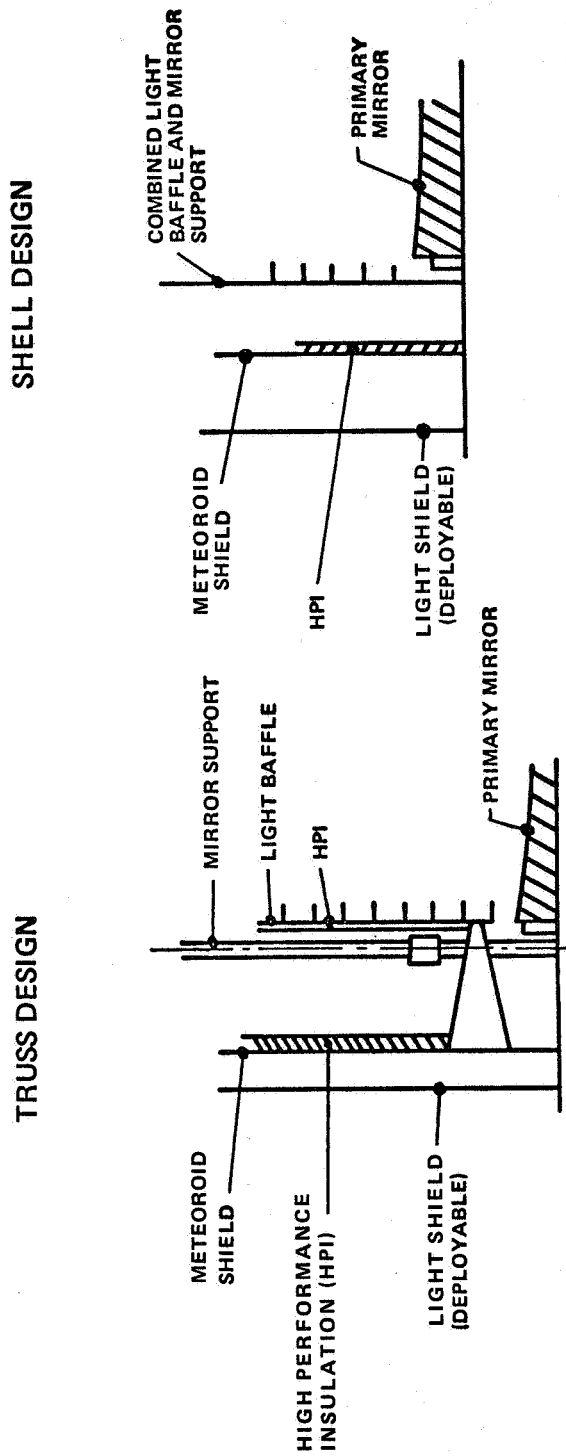
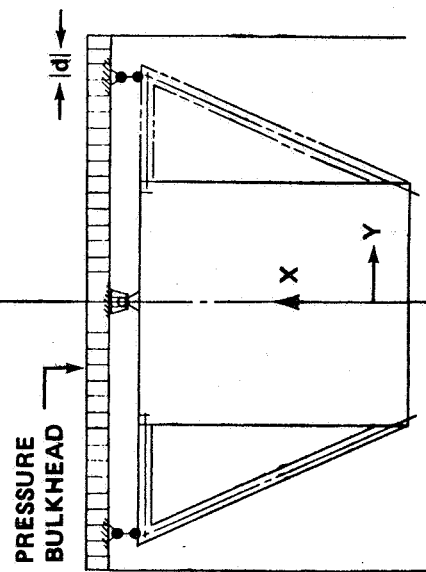
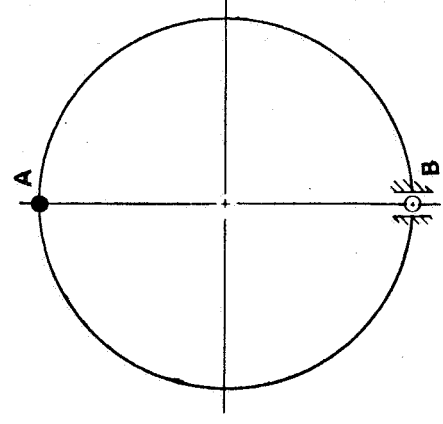
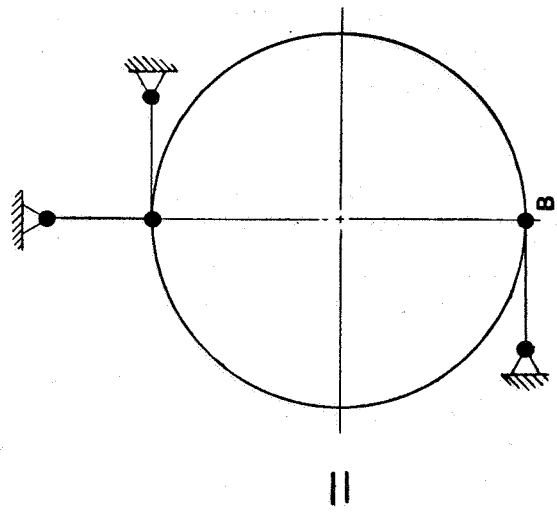
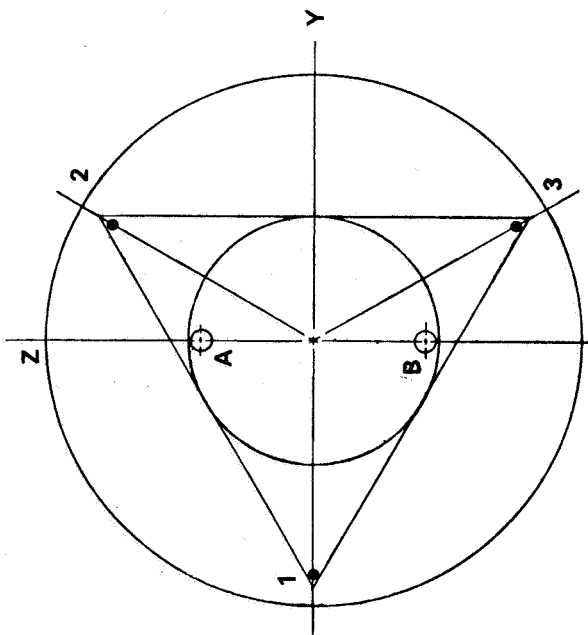


Figure V-21. LST structural concepts considered.



STATICALLY DETERMINE:  
 NO. 1-3 FOR X LOADS  
 NO. A-B FOR Y & Z LOADS

4. Rollout Solar Array. Rollout solar arrays offer some mass savings relative to the reference arrays. Such savings may well be offset, however, by the redesign required to avoid interference with the Titan shroud dynamic envelope. The interference of the current rollout array design is indicated by the crosshatched areas in Figure V-23.

In addition, a separate support structure and stiffer SSM longerons will be needed, since the aft ring of the SSM cannot be used for such purposes. These structural influences and potential dynamic problems require careful investigation if rollout arrays are to be considered.

5. Primary Mirror Support. The reference design shows the primary mirror supports to be clamped to the ring-bulkhead system. As a result, thermal effects cause radial loads to the mirror. Their assessment is complicated and time consuming. Such problems can be avoided by eliminating the clamping of the support brackets. This concept is outlined in Figure V-24. This concept is also expected to simplify the assembly procedure; however, its feasibility with regard to the optical performance has not yet been established.

6. Spider Beam. The reference design has the secondary mirror nested inside a circular ring frame. Beams extend radially from this ring frame to the metering structure, where all four are rigidly connected. The flexibility (spring action) inherent in this concept can be eliminated by an arrangement such as shown in Figure V-25. In this case the beams are located above (i.e., behind) the secondary mirror, which allows their arrangement in a simple and rigid cruciform structure. The secondary mirror is attached to the underside of the spiderbeam and there is no interference with the mirror adjustment mechanisms. A circular disk on the upper side is required to carry light baffles. In this case, the forward end of the metering structure can either be extended to achieve a rather flat profile of the spider beam arrangement, or it can remain at or near its present station, which would require steeper beams.

The connection between the four ends of the spider beam and the metering structure need not be a rigid attachment; a statically determinate support concept may be used instead.

Again, the feasibility with regard to the optical requirements is to be established.

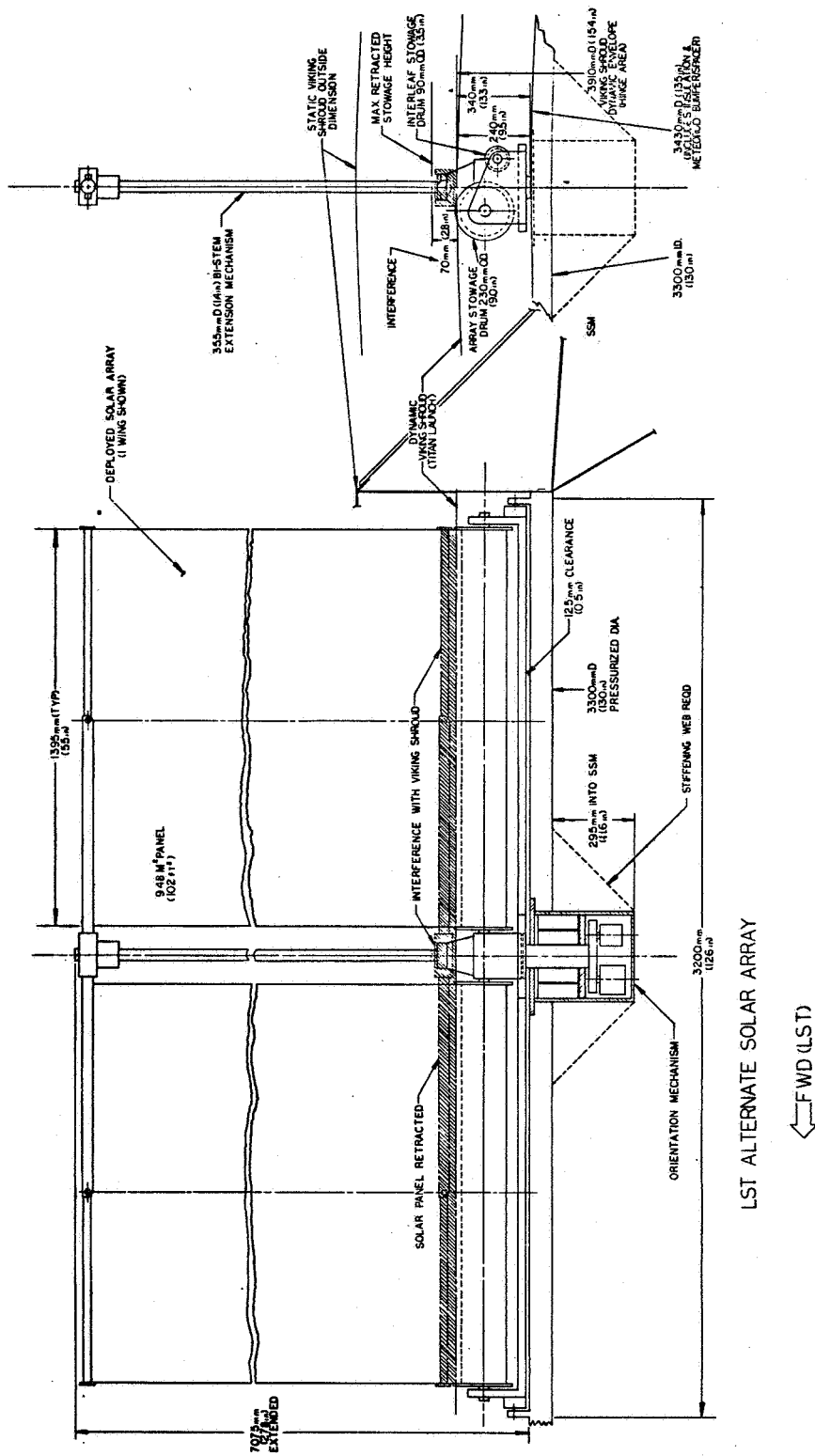
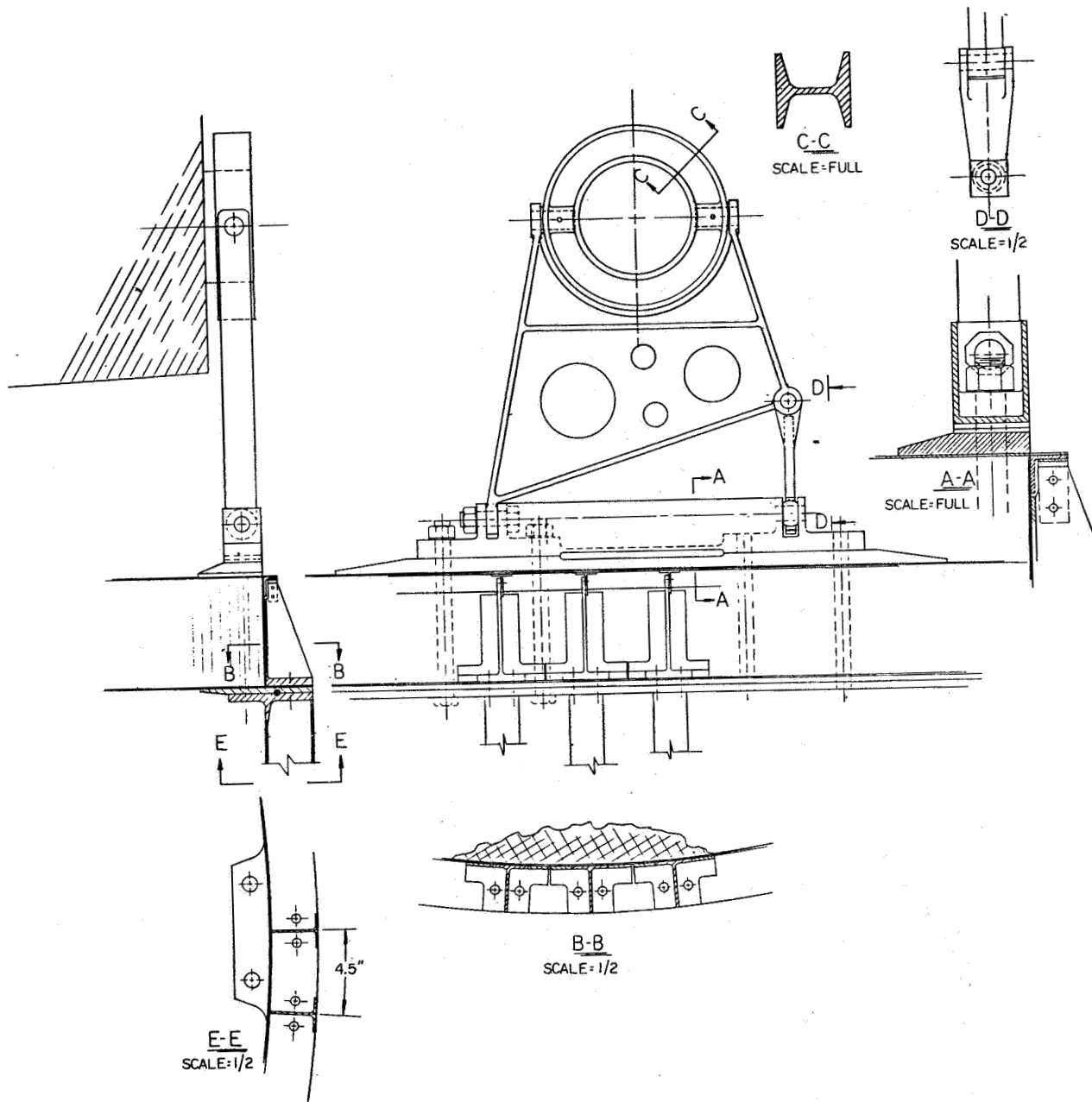


Figure V -23. LST alternate solar array.



LST primary mirror support.

## F. Thermal Control

1. OTA. A feasible alternate to the graphite epoxy athermalized truss metering structure of the OTA is a large cylindrical shell of the same material. The thermal system associated with the graphite epoxy shell, which satisfies all requirements, is virtually identical to that for the truss. The two systems are thermally very similar. Due to a somewhat lower mass, the thermal stability characteristics of the shell are less attractive than those of the truss, although they are acceptable.

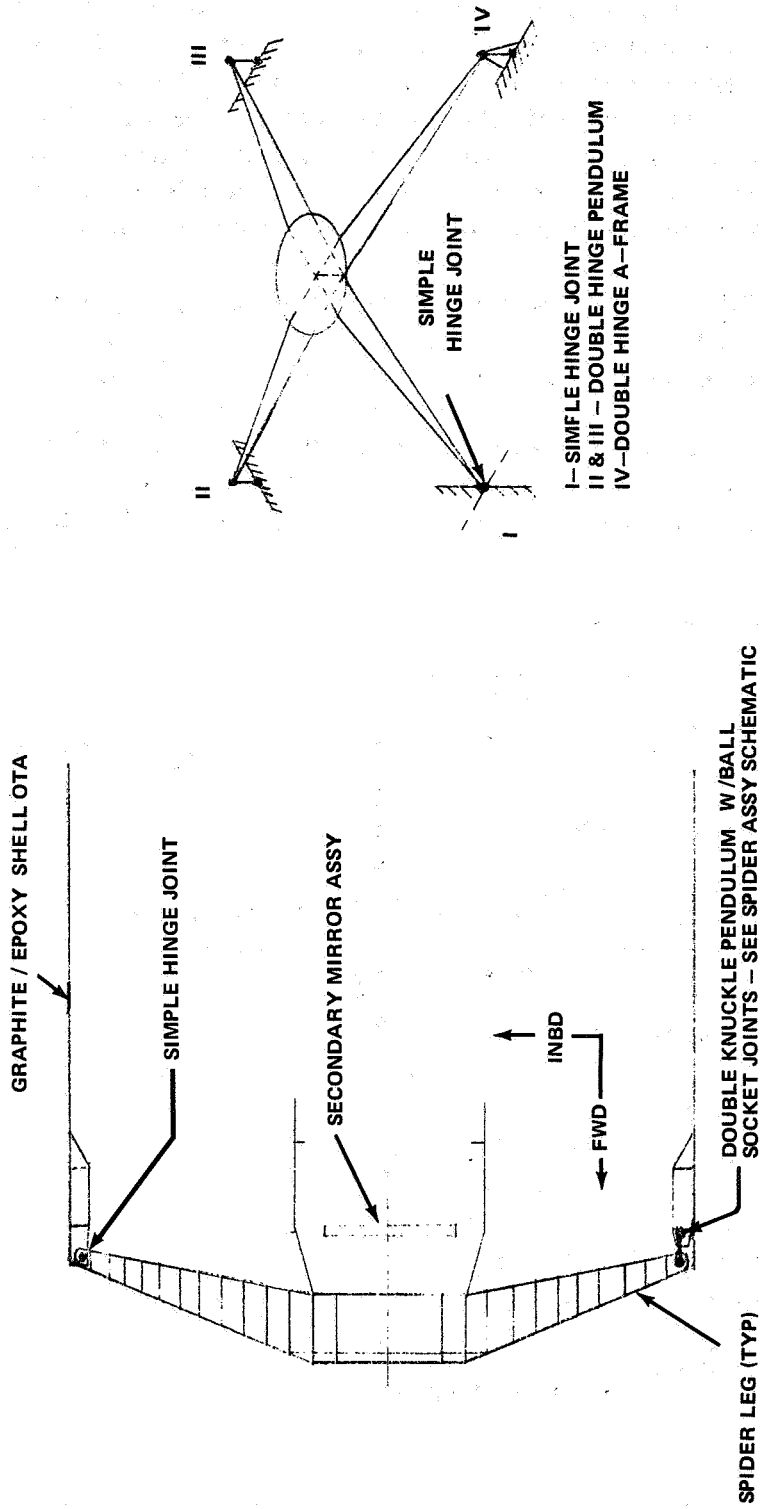


Figure V -25. Spider beam configuration.



One of the most attractive features of the graphite epoxy truss is that different types of the composite materials, having different coefficients of thermal expansion, can be used for the rings and struts. This will allow the design of an extremely thermally stable structure. The same concept of athermalization was explored with the use of titanium rings and invar struts. The results of the analysis were satisfactory with all requirements satisfied. However, mass magnetic properties, and thermal stability characteristics led to the choice of graphite epoxy over the titanium-invar combination.

2. SSM/SIP. An alternate to the reference design approach to providing SSM/SIP thermal control was studied. The fluid loop system shown in Figure V-26 was considered. The basic operating temperature of the components was to be  $20 \pm 4^\circ\text{C}$ . The temperature at which the heat energy is removed at the cold plates is determined by the efficiencies of the conductive and convective heat transport mechanisms in series. A double loop system was considered because of the working environment provided within the SSM

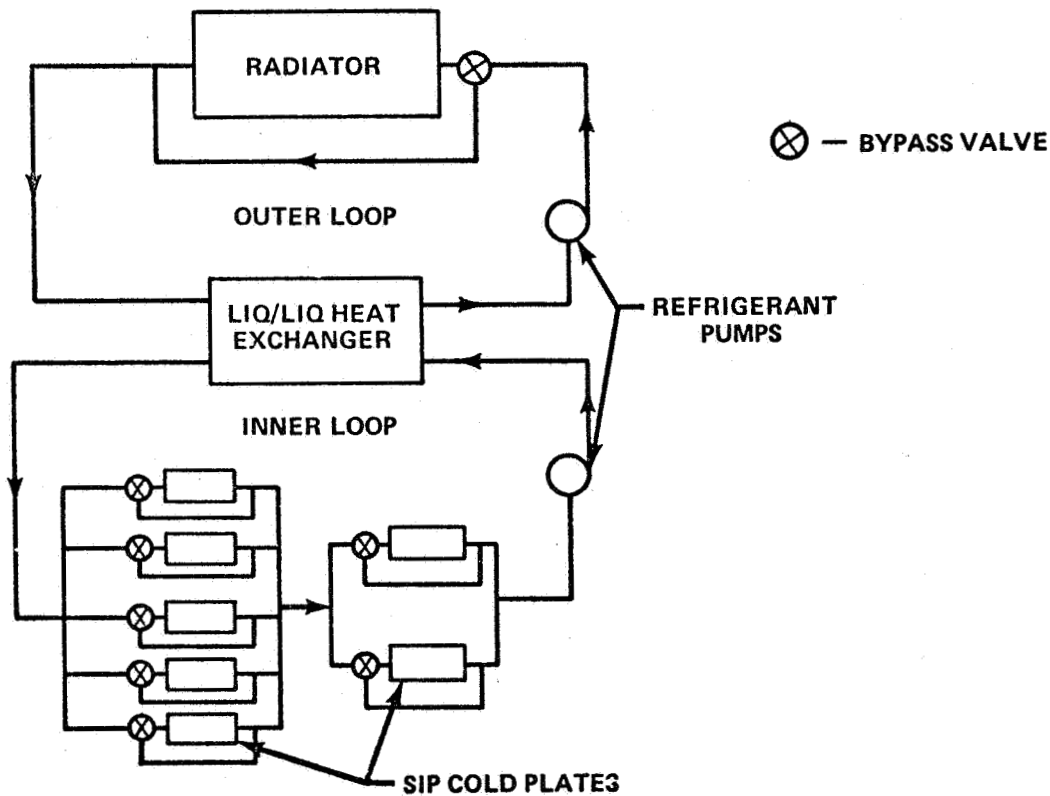


Figure V-26. Schematic of alternate thermal control system for SIP components.

during manned occupancy. No toxic working fluids, such as the common refrigerants, can be permitted to pass through the manned environment. Therefore, water was selected as the working fluid for the internal loop. Freon 21 was selected for the external loop to prevent freezing in the radiator during periods of low environmental heating and/or low internal heat load. The fluid loop system was shown to satisfy all SSM/SIP thermal design requirements. However, lower reliability, the possibility of telescope fine pointing interference, greater contamination potential, difficulty in maintenance, and cost led to rejection of this approach.

In addition to the fluid loop system for SSM/SIP thermal control, variable conductance heat pipes were considered. Reliability of a heat pipe system would theoretically be better than for the fluid loop, but the lack of previously demonstrated flight systems employing controllable heat pipes led to the rejection of this system.

## G. Electrical Power and Distribution

Before selecting the reference design electrical system, several alternate system configurations and subsystem concepts were considered. Numerous assembly and component designs were also studied for the application.

Centralized versus decentralized distribution schemes were evaluated with respect to design complexity, redundancy, reliable controls and protection, versatility, and cost. Centralized systems appear to cost less because the amount of hardware is less and design management is better. The versatility is poorer, however, and integration time is greater. The main distribution network of the reference system is centralized; secondary distribution is decentralized for versatility, fault isolation, and maintenance reasons.

Four electrical power subsystem (EPS) configurations were analyzed; and their performance, design, operational constraints, and potential costs were compared. Dedicated charge control for each battery was considered essential in all cases. EPS types 1, 2, and 4 were regulated approaches; type 3 was unregulated. These candidates included series and shunt regulator concepts as well. Type 1 was selected as the design reference. It was considered the best compromise of design and operational characteristics with efficiency and cost. The potential higher efficiency of the type 4 system makes it a candidate worthy of further in-depth study. It could be most cost effective.

Three basic types of solar arrays — rigid panel type, flexible panel type and semirigid type — were considered. In addition, several variations of these types were studied. The rationale for the selection of the design reference array was based on comparisons shown in Table V-4. The alternate launch vehicle constraints and preliminary cost estimates were the factors favoring the reference design. However, the flexible solar arrays offer significant design and operational advantages when Shuttle operations and maintenance are considered. In addition, the growing use of the flexible arrays could make them equal or lower in cost than the design reference panels in the near future.

Although the batteries to be used for Skylab, Mariner, and HEAO are feasible candidates for the LST, the reference battery is considered a low cost, high performance design concept for the future. Based on previous studies of low cost designs for future payloads, the concept offers ruggedness, commonality with commercial production tooling, and a high degree of standardization of cells and assemblies to effect lower cost. This can be done without sacrificing reliable performance or the versatility of selecting energy capacity.

Many of the tradeoffs considered at the assembly and component level were considered too detailed and lengthy for discussion in this report. For example, conventional cabling connectors were compared with zero-g types, flat conductor types, and automatic/remotely operated types. Semiconductor switching circuits were compared to relays or contactors for power switching. Although all candidates had specific advantages, conventional, proven hardware was adequate and was used. In some cases, alternates appeared to be equivalent to the reference design on a preliminary design and cost basis. For example, previously designed dc torque motors, gears, and controls could satisfy the array orientation drive requirements as well as the stepper-harmonic drive assembly selected. Since such assemblies must be adapted to the array requirements, cost differences would be insignificant.

## H. Communications and Data Handling

Alternatives were considered within the communications and data handling system in the following areas:

1. Ground Station Selection
2. Antenna Configuration

TABLE V-4. GENERAL APPRAISAL OF SOLAR ARRAY TYPES

Array Type	Advantages	Disadvantages
1. Rigid Foldout Panels	<p>Proven Technology                      Proven Fabrication Methods                      Presently Lowest Cost                      Conservative for Phase A                      Evaluation of LST                      High Natural Frequency                      (0.6 to 1.0 Hz)</p>	<p>High Mass                      Complex Retraction Restricts                      External Maintenance Concepts                      Very Difficult to Replace In-Space                      at Any Level</p>
2. Rigid Foldout Panels with Phase Change Material (PCM)	<p>Reduces Thermal Cycle                      Stresses                      Improves Reliability of                      Interconnects/Terminals                      Can Increase Output up                      to 6%</p>	<p>Most Massive                      Unproven Fabrication Techniques                      Compatibility with Adhesives not                      Verified                      Maintenance Diminishes                      Attractiveness</p>
3. Flexible Rollout Types	<p>Lowest Mass                      Compact Storage                      (Smallest Volume)                      One Successful Flight                      Easier Retraction                      Better Adapted to In-Space                      Maintenance Concept</p>	<p>Presently 15 to 20% Higher Cost                      (Could Change Before Phase C)                      Most Complex Design                      Low Natural Frequency (0.04 to                      0.1 Hz)                      Must be Retracted for Docking                      Compatibility with Shroud                      Envelope not Verified</p>
4. Semirigid Type (Rigid Module Frames with Flexible Substrates)	<p>Lower Mass than Type 1                      but not Type 3                      Efficiency Increase                      Possible</p>	<p>Has Most of the Disadvantages of                      Type 1                      Complex Fabrication</p>

3. Antenna Isolation
4. Image Tube Selection
5. Mass Memory Survey
6. Computer Configuration Analysis
7. TDRSS Data Return

The following discussion lists the alternatives within each of these areas together with the reasons for making the final selections.

1. Ground Station Selection. In the area of ground station selection, stations from two former networks were considered, MSFN and STADAN. Two criteria were used in selecting the stations. The first criterion was that the station had to be visible to the spacecraft from its orbit. The second ground station selection criterion pertained to equipment available at the station.

The ground network used in the reference design is composed of six stations selected from both the MSFN and STADAN systems. These six stations are now part of a larger net called the Spacecraft Tracking and Data Network (STDN). Only stations with unified S-band capability having 9.144-m (30-ft) antennas were selected. The selected ground sites were originally Canary Islands (CYI), Ascension Island (ACN), Carnarvon (CRO), Guam (GWM), Hawaii (HAW), and Goldstone (GDSX). Current NASA studies have dictated a requirement that the tracking facilities at CRO be phased out of the STDN in 1974. Since the LST is scheduled to operate initially in 1979, subsequent simulated analysis has assumed a possible participation of Orroral Valley (ORRX) instead of CRO.

2. Antenna Configuration. An antenna configuration tradeoff analysis was performed on four configurations. The first configuration consisted of six antennas, with four antennas located around the circumference of the LST body and two antennas located on the ends of the LST body. The second configuration had an antenna at either end of the LST, with at least one antenna on a boom. A third configuration had two antennas 180 degrees apart on the LST body, and one of the antennas was boom-mounted. The fourth configuration utilizes the solar arrays as antenna booms, and had one antenna on the end of each of the two solar panels. Configuration number four was chosen as the reference design because it provided the best overall antenna coverage with isolated antennas.

3. Antenna Isolation. Both frequency diversity and polarization diversity were considered as methods of isolating the two conical spiral antennas. Frequency diversity was chosen primarily for reasons of ground station compatibility.

4. Image Tube Selection. In the area of image tube selection, many candidates were considered. The three primary candidates were the return beam vidicon (RBV), the secondary electron conduction (SEC) vidicon, and the silicon intensified target (SIT) vidicon. The RBV was considered a doubtful candidate because of the absence of a suitable mass memory system needed for optimum utilization of this tube. SEC was chosen over the SIT tube for the majority of tube applications because of its long target storage capability.

5. Mass Memory Survey. A mass memory technology survey was performed to determine the feasibility of utilizing a mass memory with the RBV. The following memories were examined as candidates for the LST mass memory: ferrite core, tape recorders, magnetic bubble, DTPL, Dynabit, plated wire, surface wave acoustic delay lines, laminated ferrite, optical beam, oligatomic film, charge coupled devices, metal nitride oxide silicon (MNOS), complementary metal oxide semiconductor (CMOS), and Sonic Boram. It was concluded from this survey that no suitable mass memory system exists at this time for LST application because of the large mass and/or power requirements.

6. Computer Configuration. A computer configuration analysis was performed to determine how many computers were needed. Three primary LST functions were identified, initially as candidates for onboard computer support:

1. ACS system and solar array pointing.
2. Spacecraft data handling and the SIP and OTA housekeeping.
3. OTA and SIP control and computations.

To support these functions three computer configurations were considered:

1. Alternative I — Three separate computers, one for each function.

2. Alternative II — A single computer for all functions.
3. Alternative III — Two separate computers.

After examining the data handling and computational requirements of all LST functions, it was determined that two separate computers would be utilized, one for the ACS system and one for control of SIP operations.

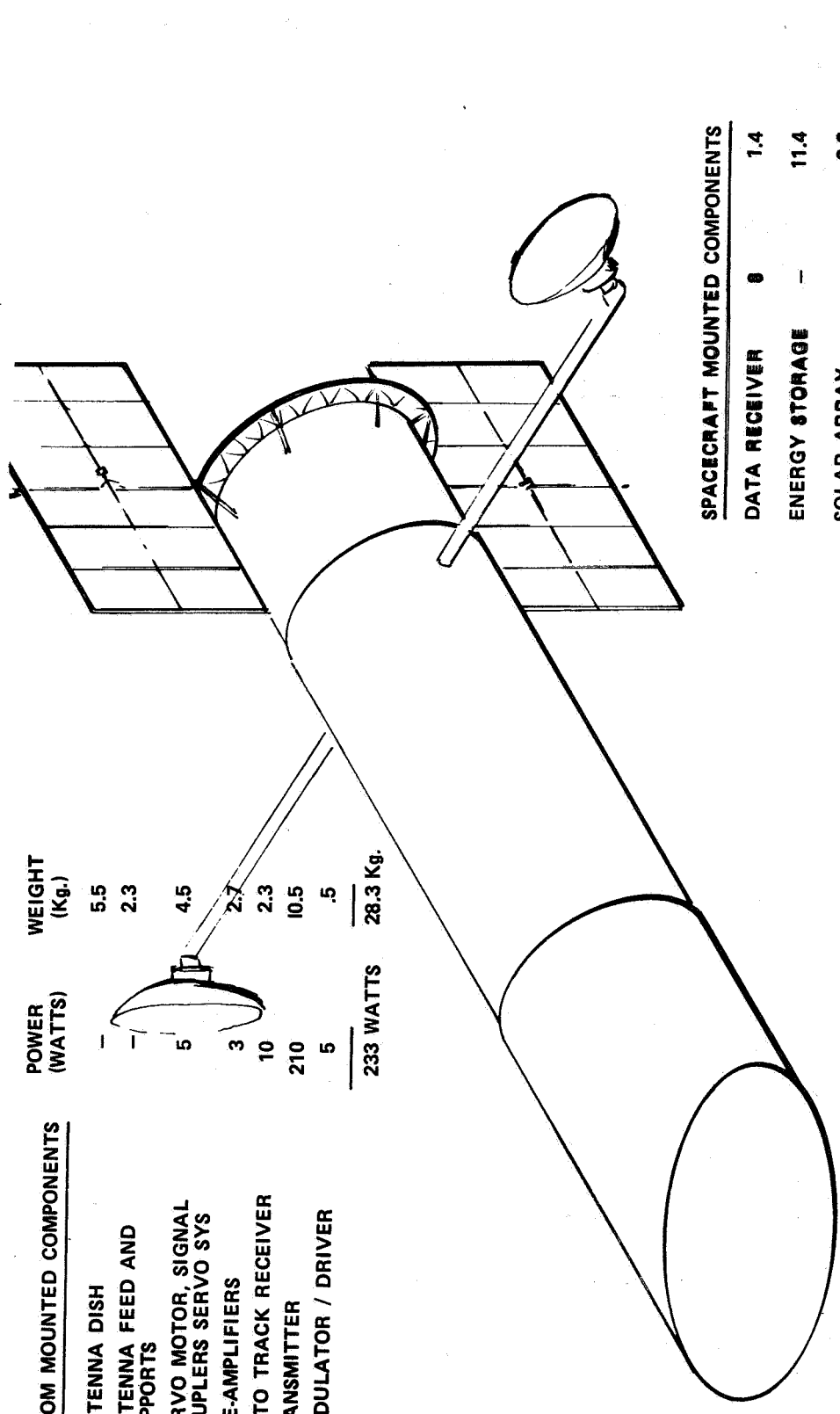
7. Tracking and Data Relay Satellite System Data Return. An alternative to the use of outlying tracking stations and National Aeronautics and Space Administration Communications Network (NASCOM) for returning scientific data to the central operations control station is the utilization of the synchronous orbit tracking and data relay satellite system (TDRSS).

An assessment was made of the impact upon the LST reference design configuration of utilizing a TDRSS system. A design of a spacecraft terminal was made that interfaced with the  $K_u$  band TDRSS under study by Goddard Spaceflight Center. Some of the proposed characteristics of this system are as follows:

1. Transmit frequency, 13.4 to 14.2 GHz.
2. Receive frequency, 14.4 to 15.35 GHz.
3. Antenna, 2.4-m (8-ft) dish.

The spacecraft terminal was designed to be capable of utilizing the 50-megabit capability of the TDRSS. The physical characteristics of the terminal are given in Figure V-27. The two antennas are 2.4-m (8-ft), steerable, 2 degree of rotary freedom, rigid dishes mounted on 8.6-m (338-in.) booms. A monopulse tracking loop maintains lock on the TDRSS. The spacecraft transmitter output power is 40 W. Except for the data receiver, all hardware (identified as "boom mounted components" in Figure V-27) is mounted on the antenna side of the gimbal joint. The frequency crossing the gimbal is thus reduced from  $K_u$  band down to approximately 100 MHz, and flexible cables rather than a rotary joint transmission line can be used.

An antenna boom design of a lock-alloy (62 Be-38AL) hollow circular tube of 8.9-cm (3.5-in.) outside diameter and 0.95-cm (0.374-in.) thickness was investigated in a dynamic analysis. It was found that pointing accuracy of 0.005 arc sec could be maintained even while slewing one antenna to acquire while the other was tracking.



BOOM MOUNTED COMPONENTS	POWER (WATTS)	WEIGHT (Kg.)
ANTENNA DISH	-	5.5
ANTENNA FEED AND SUPPORTS	-	2.3
SERVO MOTOR, SIGNAL COUPLERS SERVO SYS	5	4.5
PRE-AMPLIFIERS	3	2.7
AUTO TRACK RECEIVER	10	2.3
TRANSMITTER	210	10.5
MODULATOR / DRIVER	5	.5
	<b>233 WATTS</b>	<b>28.3 Kg.</b>

SPACECRAFT MOUNTED COMPONENTS	POWER (WATTS)	WEIGHT (Kg.)
DATA RECEIVER	8	1.4
ENERGY STORAGE	-	11.4
SOLAR ARRAY	-	8.2
	<b>8 WATTS</b>	<b>21.0</b>
<b>TOTAL</b>	<b>241 WATTS</b>	<b>49.3 Kg.</b>

Figure V-27. LST TDRSS terminal.



The TDRSS system will make real time data transmission back to the control center possible, but this capability must be carefully weighed against the impacts of the mass, power, and the large tracking antenna of the spacecraft terminal.

## I. Attitude Control

Alternate configurations for the attitude control system (ACS) were not considered on a complete system basis, but rather from an individual component standpoint. The alternates considered were further categorized into sensors, actuators, and signal processing.

1. Reference Gyro Assembly. Reference gyro assembly (RGA) alternates were considered primarily from the standpoint of the following configurations and operating concepts:

1. Dodecahedron
  - a. Three active plus three standby
  - b. Four active plus two standby
  - c. Six active
2. Tetrahedron
  - a. Three active plus one standby
  - b. Four active
3. Five-Pack
  - a. Three active plus two standby
  - b. Four active plus one standby
  - c. Five active
4. Dual Orthogonal Triad
  - a. Three active plus three standby
  - b. Six active

The dodecahedron configuration with four active and two standby gyros for normal operation was selected because of commonality with HEAO, better reliability, and ease of fault detection.

2. Star Trackers. The ACS star tracker alternates considered were classified as fixed star trackers (FST) or gimbaleed star trackers (GST). Secondary alternates for each classification are the number of trackers, installation geometry, and the required redundancy. The design reference selected was three FSTs arranged symmetrically about the minus Z-axis in the Y-Z plane with two active trackers and one standby tracker during normal operation. Alternate selections considered and their advantages are as follows:

1. Four to six FSTs — permits smaller field of view (FOV) with increased accuracy.
2. Two GSTs — larger effective FOV, smaller instantaneous FOV.
3. More than two GSTs.

The three FSTs selected provide the required accuracy and star coverage and have advantages in reliability, operational and mounting simplicity, cost, mass and power.

3. Sun Sensors. Alternates to the sun sensors selected are digital sun sensors and other types of analog sun sensors. The sun sensor selected is common to HEAO and has cost and reliability advantages over the digital sun sensor. There are other types of analog sun sensors that are competitive in price and reliability and a final selection will probably depend largely on commonality with HEAO.

4. Momentum Exchange System. The principal building blocks used in formulating the momentum exchange systems that were compared were reaction wheels (RWs), single gimbal control moment gyros (SGCMGs), and double gimbal control moment gyros (DGCMGs). The primary alternate systems and configurations that were evaluated were:

1. Three DGCMGs
2. Four skewed SGCMGs at skew angles of:

- a. 53.1 degrees (near spherical envelope)
  - b. 30.0 degrees
3. Two scissored pair ensemble explicit distribution (2-SPEED) SGCMG system
4. Four skewed RWs at skew angles of:
    - a. 63.1 degrees (near spherical envelope)
    - b. 76.0 degrees

The augmentation of any of the above basic systems by either a small RW or a small CMG system was also considered as a means of improving the pointing stability during experimentation. Complete details of the momentum exchange system trade study are contained in Volume V, Chapter VI.

CMGs were selected over RWs because of mass and power advantages and because of the larger dynamic range. The four-skewed SGCMG configuration was selected over DGCMGs for reliability purposes.

The 2-SPEED SGCMG system is considered to have excellent possibilities as an alternate system because of its singularity avoidance capability. It has the other basic advantages of the design reference system (four-skewed SGCMGs, 30-degree skew angle), but the 2-SPEED SGCMG was not selected because it is in a developmental stage and further evaluation is needed.

5. RCS Concepts. An alternate RCS considered for the LST during the Phase A study was a monopropellant hydrazine system. A monopropellant hydrazine RCS provides good performance (specific impulse 120 to 230 sec), and the total system mass when applied to the LST is low; i. e., 82 kg (180 lb). A hydrazine RCS is simple and reliable for long periods of operation. However, a hydrazine RCS for the LST is believed to be more expensive than a  $\text{GN}_2$  system. The exhaust of a hydrazine RCS is not considered to be a contamination-producing source, but hydrazine is toxic and may produce harmful effects due to ingestion, inhalation of vapors, or contact with the skin. The toxicity effects of hydrazine could prove fatal to man, and for this reason, a hydrazine RCS for the LST was rejected.

The RCS selected for the LST ( $\text{GN}_2$ ) is slightly heavier than the hydrazine system; i. e., 104 kg versus 82 kg (230 lb versus 180 lb). However, in sizing both systems, existing components were used. The performance of the  $\text{GN}_2$  system is less than the hydrazine system ( $\text{GN}_2$  specific impulse, 60 to 70 sec). The  $\text{GN}_2$  RCS is simple and highly reliable as the regulated  $\text{GN}_2$  RCS of the Mariner 64 spacecraft demonstrated a 2.5-year lifetime. A  $\text{GN}_2$  system requires the least cost for reliable hardware. The exhaust gas of a  $\text{GN}_2$  RCS is clean, and  $\text{GN}_2$  is not toxic unless, of course, the entire environment becomes saturated with nitrogen.

Two types of  $\text{GN}_2$  reaction control systems were considered for the LST — a blowdown system and a regulated system. The blowdown system was rejected primarily because the initial high thrust produced by such a system would cause the spacecraft to overshoot its deadband and initiate limit cycling. This would result in inefficient utilization of propellant. Also, since the thrust level is constantly decreasing, complexity is added to the guidance system in determining the thrust level at all times.

## CHAPTER VI. INTERFACES



# TABLE OF CONTENTS

	Page
A. LST/Launch Vehicle Interfaces . . . . .	VI- 2
1. Mechanical Interfaces . . . . .	VI- 2
a. LST/Shuttle Mechanical Interfaces . . . . .	VI- 2
b. LST/Titan Mechanical Interfaces . . . . .	VI- 2
c. LST/Shuttle-Titan Common Mechanical Interface . . . . .	VI- 6
2. LST/Shuttle Contamination Control Interfaces . . . . .	VI-10
3. LST/Shuttle Manned Maintenance Interfaces . . . . .	VI-11
4. LST/Launch Vehicle Thermal Interfaces . . . . .	VI-11
a. LST/Space Shuttle Interface . . . . .	VI-11
b. LST/Titan Thermal and Environmental Interfaces . . . . .	VI-12
5. Electrical Interfaces with Launch Vehicle . . . . .	VI-13
a. Electrical System Interface Summary . . . . .	VI-13
b. Shuttle/SSM Electrical Interfaces . . . . .	VI-13
c. Electrical Support Equipment Interfaces . . . . .	VI-16
d. Electrical Interfaces for Alternate Launch Vehicle . . . . .	VI-19
6. Pointing Control Interfaces with the Shuttle . . . . .	VI-19
7. Preliminary LST/Shuttle Interface Summary . . . . .	VI-21
 B. General LST Interfaces . . . . .	 VI-21
1. General Environmental Requirement . . . . .	VI-21
2. Electrical Interfaces . . . . .	VI-21
a. Test and Maintenance in Space . . . . .	VI-21
b. Standards and Hardware . . . . .	VI-38
c. Electromagnetic Control . . . . .	VI-38
3. SSM/SIP/OTA Manned Maintenance Interfaces . . . . .	VI-39
4. Support Requirements . . . . .	VI-41
 C. SSM/OTA Interfaces . . . . .	 VI-41
1. SSM/OTA Mechanical Interfaces . . . . .	VI-41
2. SSM/OTA Thermal Interface . . . . .	VI-42
3. Environmental Interfaces . . . . .	VI-42
4. SSM/OTA Electrical Interfaces . . . . .	VI-42
a. Separable Connectors . . . . .	VI-48
b. Electromagnetic Control . . . . .	VI-48
5. Pointing Control Interfaces . . . . .	VI-49

## TABLE OF CONTENTS (Concluded)

	Page
D. SSM/SIP Interfaces .....	VI-49
1. Mechanical/Structural Interface .....	VI-49
2. SSM/SIP Contamination Control Interfaces .....	VI-50
3. SSM/SIP Thermal Interface .....	VI-50
4. Pointing Control Interfaces .....	VI-50
5. SSM/SIP Electrical Interfaces .....	VI-50
a. Interface Implementation .....	VI-50
b. Separable Connectors .....	VI-51
c. Requirements of SSM and SIP .....	VI-51
E. OTA/SIP Interfaces .....	VI-52
1. OTA/SIP Optical/Physical Interface .....	VI-52
2. Structural Interfaces .....	VI-56
3. OTA/SIP Thermal and Environmental Interfaces .....	VI-58
4. Electrical Interfaces .....	VI-60
5. Pointing Control Interfaces .....	VI-60
6. Compatibility Tests .....	VI-60
F. Mission Control Operations Interface .....	VI-60



## LIST OF ILLUSTRATIONS

Figure	Title	Page
VI-1.	LST reference structural design . . . . .	VI- 3
VI-2.	Cradle for supporting LST in Shuttle . . . . .	VI- 4
VI-3.	Attachment of spacecraft to Shuttle . . . . .	VI- 5
VI-4.	LST-Titan launch configuration . . . . .	VI- 6
VI-5.	LST/SSM Titan adaptor and docking assembly provisions . . . . .	VI- 7
VI-6.	LST erected from Shuttle bay . . . . .	VI- 8
VI-7.	LST located in Shuttle payload bay . . . . .	VI- 9
VI-8.	LST docked to Shuttle with solar array deployed . . . . .	VI-10
VI-9.	LST electrical system interfaces . . . . .	VI-14
VI-10.	SSM/OTA structural interface . . . . .	VI-43
VI-11.	SSM/OTA structural provisions . . . . .	VI-45
VI-12.	SSM electrical interfaces . . . . .	VI-47
VI-13.	Location of f/12 image plane . . . . .	VI-53
VI-14.	f/12 image plane arrangement schematic . . . . .	VI-55
VI-15.	Instrument locations in SIP forward truss . . . . .	VI-58
VI-16.	OTA/SIP coordinate system . . . . .	VI-59

## LIST OF TABLES

Table	Title	Page
VI-1.	Payload Bay Thermal Environment . . . . .	VI-12
VI-2.	Environmental Requirements for a Titan Launch . . . . .	VI-12
VI-3.	LST Interface Connectors, SSM to Orbiter Docking Adaptor . . . . .	VI-15
VI-4.	LST Shuttle Power Interface . . . . .	VI-18
VI-5.	Caution and Warning Preliminary Interface . . . . .	VI-20
VI-6.	Preliminary LST/Shuttle Interface Requirements . . . . .	VI-22
VI-7.	Physical Characteristics for LST Launch . . . . .	VI-36

## CHAPTER VI. INTERFACES

The major program elements required for the LST missions are:

1. LST Spacecraft
2. Launch Vehicle
3. Mechanical and Electrical Support Equipment
4. Maintenance Support Equipment and Logistics
5. Tracking and Data Acquisition Network
6. Mission Control Center
7. Facilities

Only cursory consideration was given to facilities and logistics during the Phase A study. Facility interfaces with the LST and support equipment were not investigated. Logistics analyses were limited to potential spares and characteristics needed for in-space maintenance as discussed in Chapter VII of Volume V and Chapter IV of this volume.

Functional and accessibility interfaces with the ground tracking network were analyzed and are discussed in Chapter VI of Volume V and Chapter III of this volume.

Support equipment studies were limited primarily to in-space maintenance requirements and associated interfaces with the Shuttle systems. Unique mechanical ground support equipment, adapted to the LST configuration, will be required for interface tests, handling, and transporting the LST. Such equipment has not been specifically defined. The ground electrical support equipment (GESE) interfaces were considered on a general functional basis. The electrical interfaces that this equipment has with the LST will be made identical to those to be established with the in-space electrical support equipment (IESE) that will be used for launch, orbital checkout, and maintenance operations. Except for the adaptive sections and that required for special optical testing, the GESE is considered to be standard support hardware. Most of the GESE could be assembled from panels and racks of equipment produced for other programs such as Skylab, HEAO, and Apollo Telescope Mount (ATM), if made available.

The study ground rule to design for both a Shuttle launch and an alternate Titan launch has a moderate influence on the interfaces.

It was assumed that the LST spacecraft consisted of three separable major elements — optical telescope assembly (OTA), the scientific instrument package (SIP), and the support systems module (SSM). The interfaces and integration concepts between these elements and between the LST and launch vehicle are discussed in the following.

## A. LST/Launch Vehicle Interfaces

### 1. Mechanical Interfaces

a. LST/Shuttle Mechanical Interfaces. The LST reference design illustrated by Figure VI-1 is supported in the Shuttle by a statically determinate four-point cradle as shown in Figure VI-2. The cross-sectional schematic of this cradle, given in Figure VI-3, shows the load bearing attachment points.

The attachment point on the large aft ring of the SSM takes loads along the Shuttle pitch axis only, while the points in the yaw plane on the OTA primary ring take pitch and longitudinal loads only. The third point on the primary ring in the pitch plane takes loads along the yaw axis only. All of the attachments are designed so that moments are not transmitted to the LST from the Shuttle through the cradle. With this attachment arrangement, the LST structural system will thus be completely relieved of loads induced by structural deflections of the Shuttle during flight. The SSM structure was designed to withstand concentrated attachment interface loads.

The OTA primary ring was checked for Shuttle launch loads. It was found to be adequate and required only local modification to allow installation of the attach fittings.

b. LST/Titan Mechanical Interfaces. The LST-Titan launch configuration is shown in Figure VI-4. For the alternate Titan launch, a 4.3-mm (0.17-in.) thick conical adapter shown in Figure VI-5, Detail B, is provided to attach the spacecraft to the Orbit Adjust Stage (OAS) kick stage. "Super Zip" joints as shown in Figure VI-5 separate the LST from the OAS. "Super Zip" stands for a pyrotechnic method for cutting a seam through sheet metal. It is also used to separate the Titan-Viking shroud from the LST. The adaptor and aerodynamic fairing remain with the LST spacecraft.

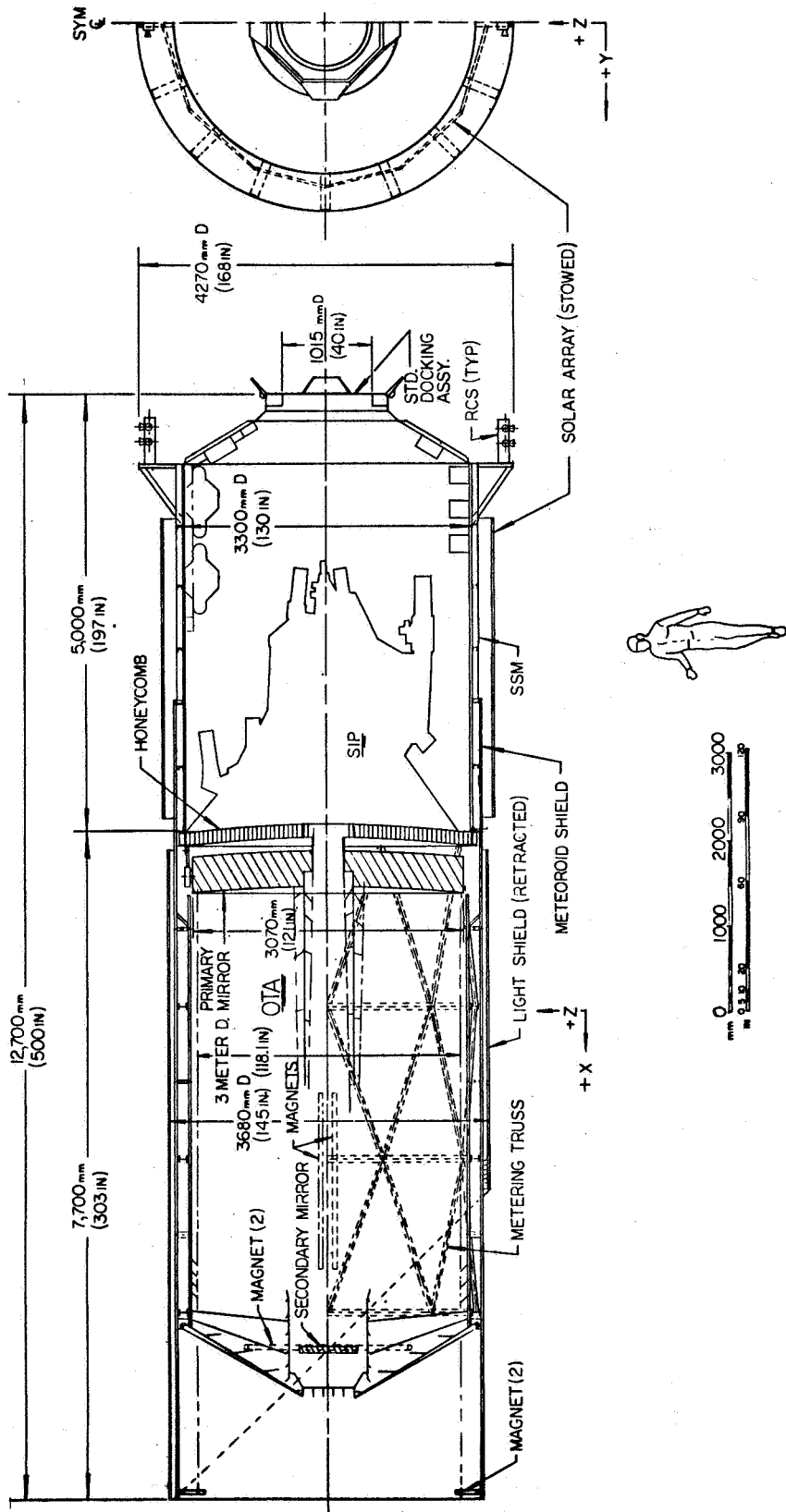


Figure VI-1. LST reference structural design.

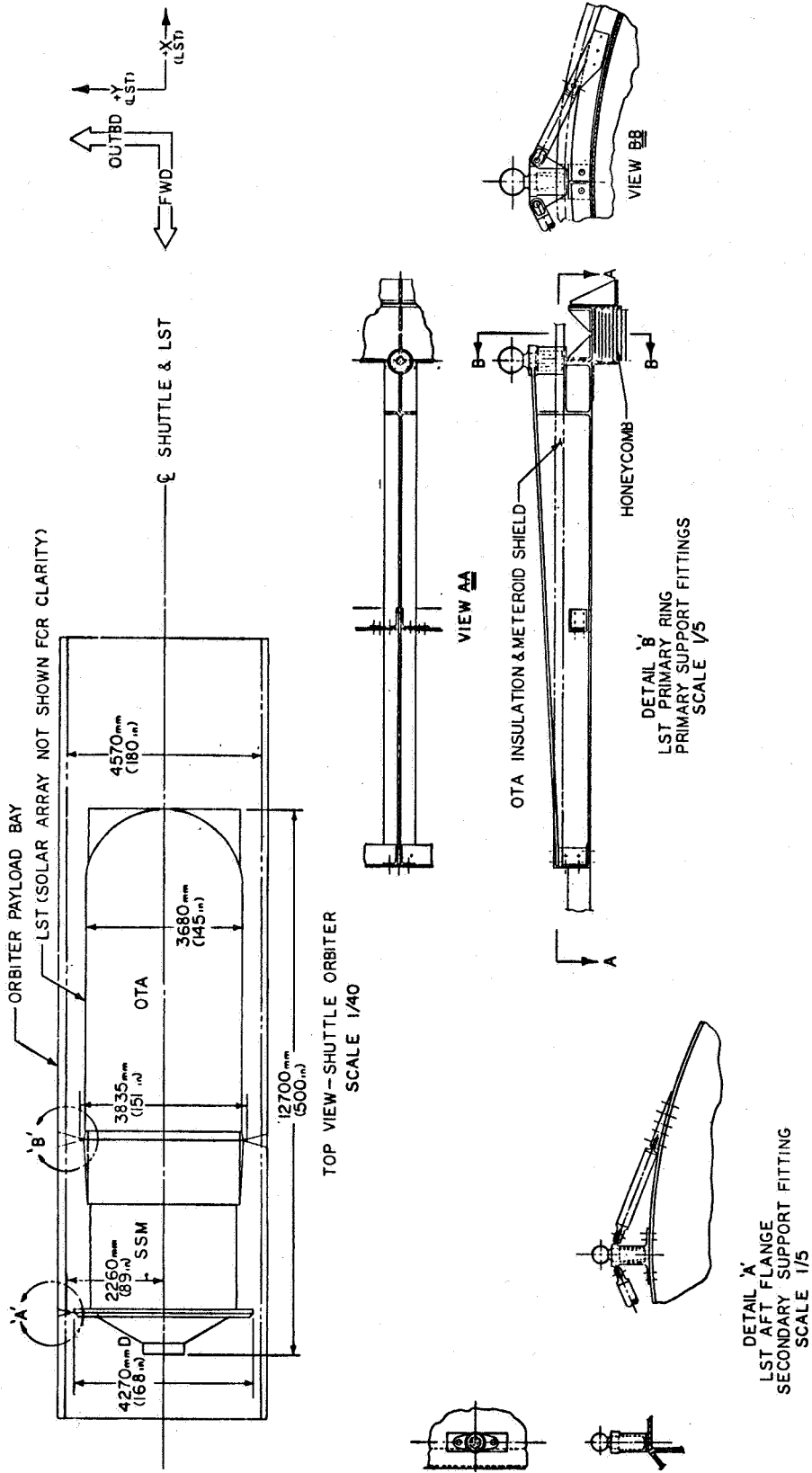


Figure VI-2. Cradle for supporting LST in Shuttle.

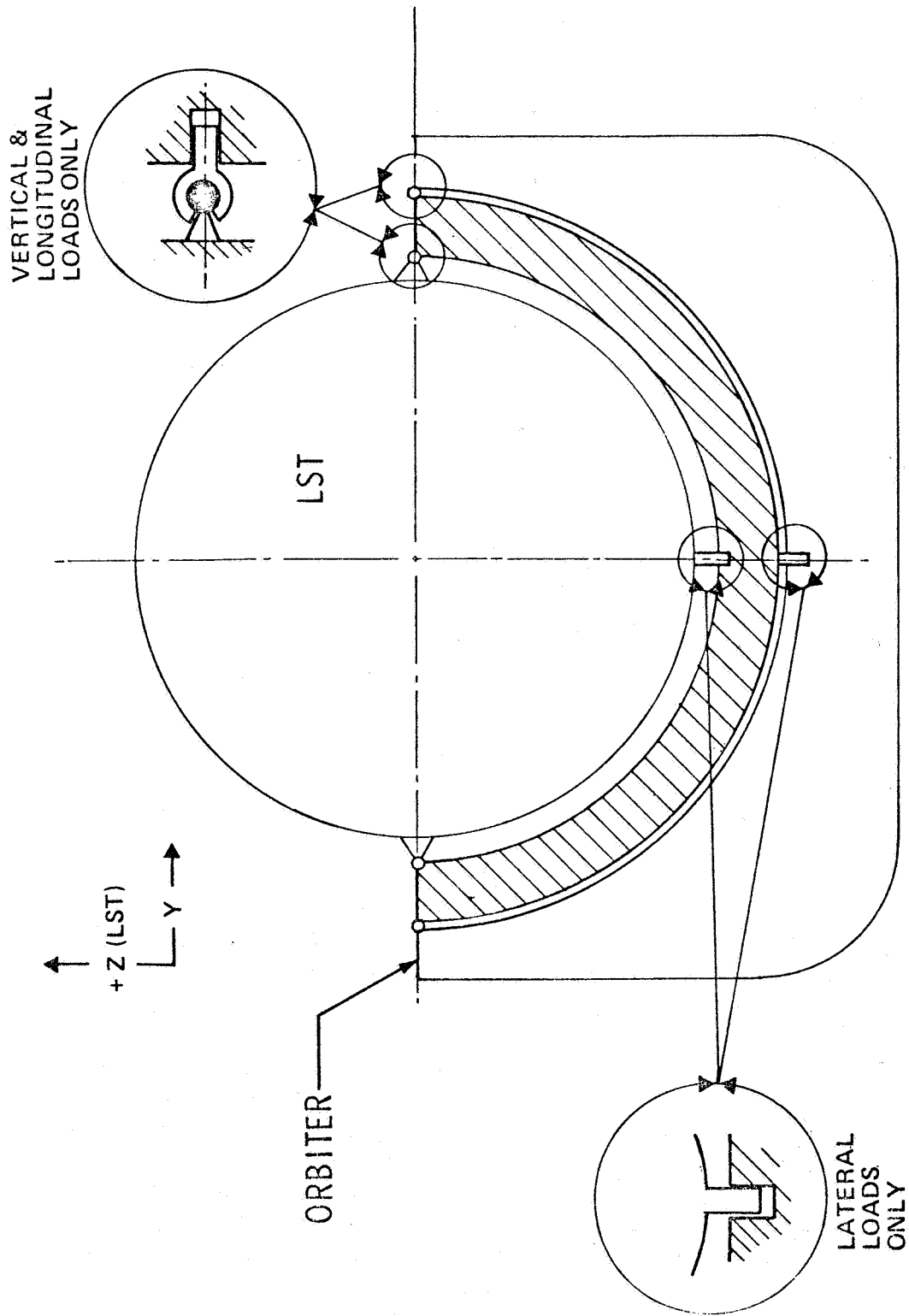


Figure VI-3. Attachment of spacecraft to Shuttle.

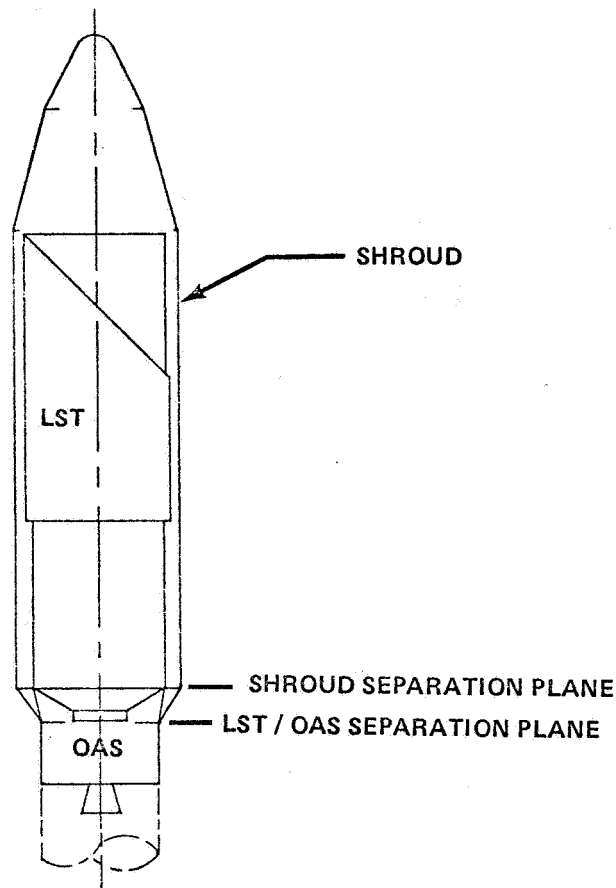


Figure VI-4. LST-Titan launch configuration.

c. LST/Shuttle-Titan Common Mechanical Interface. Since, for either the Shuttle-launched or Titan-launched LST, maintenance or recovery must be by the Shuttle, some items, of necessity, must be common to both launch modes. A docking mechanism must be provided for both, as well as a Shuttle-provided pressurization system. The reference design, shown in Figure VI-5, provides a docking system of at least 1-m opening based on the "International Docking System." The docked LST will be pressurized through the docking assembly by bottled gas provided by the Shuttle.

The reference design LST uses a Shuttle-mounted tilt-table for docking for retrieval/maintenance operations or for deploying the LST from the Orbiter. Figure VI-6 shows the LST in its erected position prior to release from the Orbiter. The tilt-table retracts the LST into the Shuttle bay as shown in Figure VI-7. Figure VI-8, with Figure VI-5, shows that the LST may be made operational by deploying the light shield and solar array and that all systems may be checked out before undocking the LST. There is adequate clearance to rotate the solar array as required.



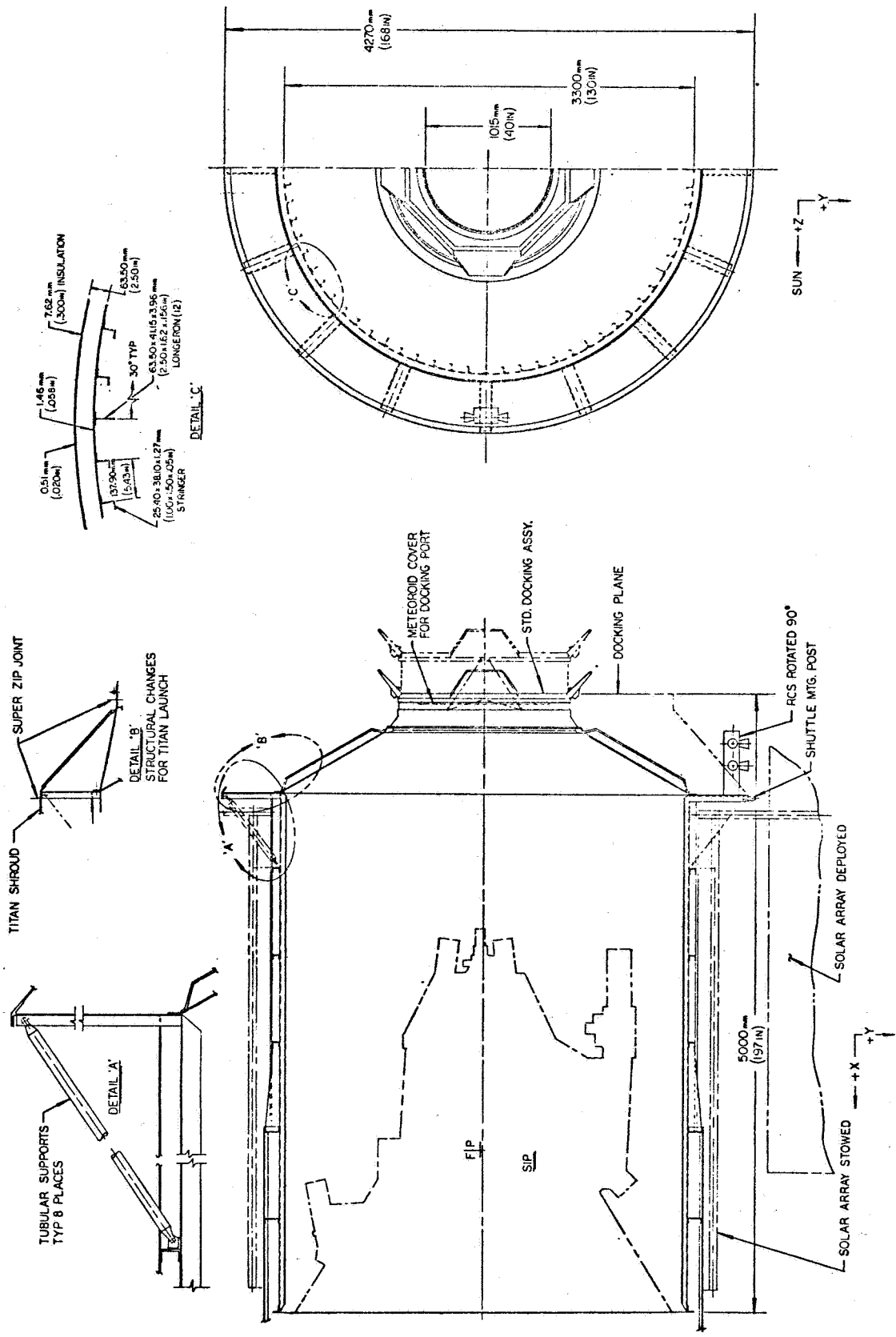


Figure VI-5. LST/SSM Titan adaptor and docking assembly provisions.

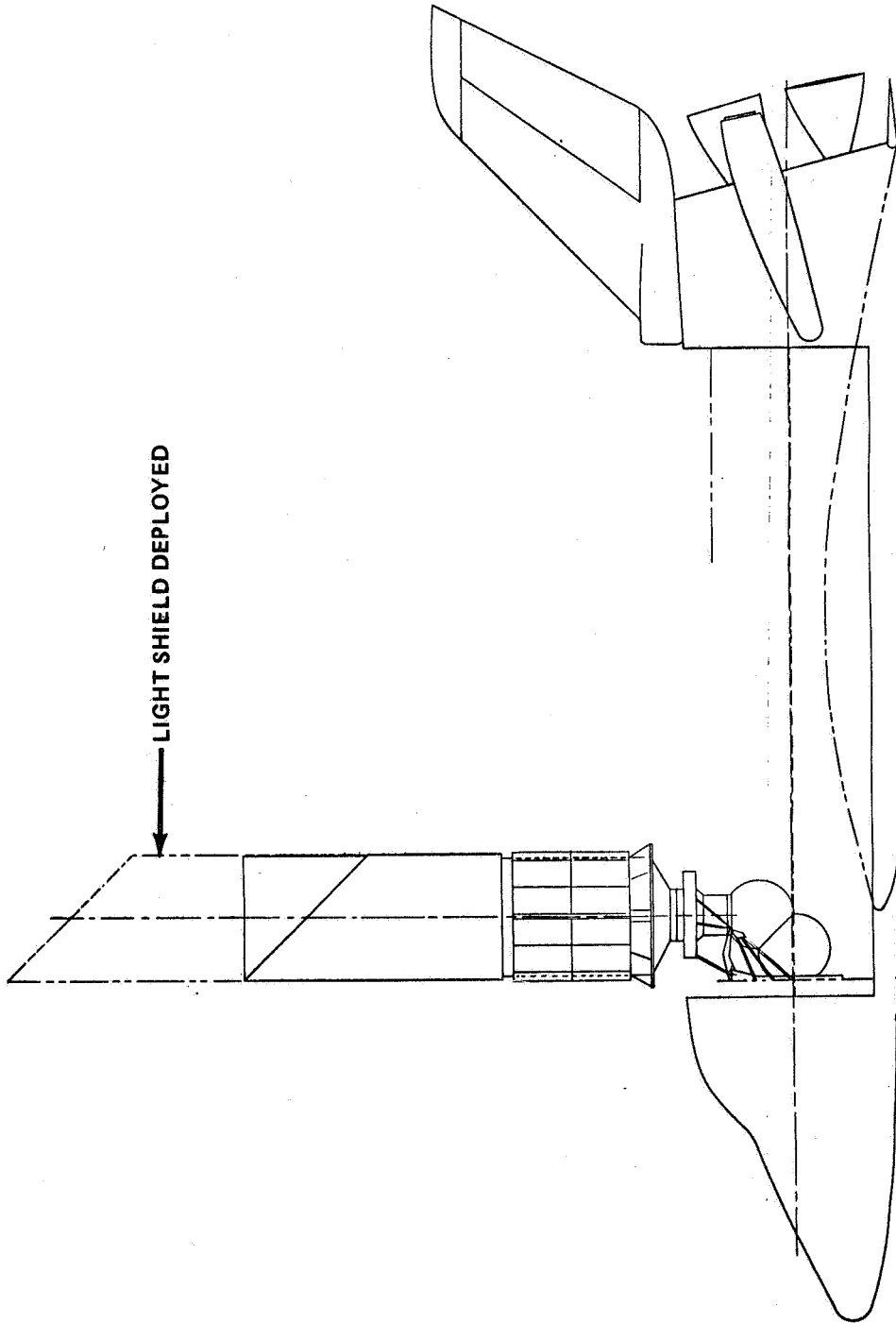


Figure VI-6. LST erected from Shuttle bay.

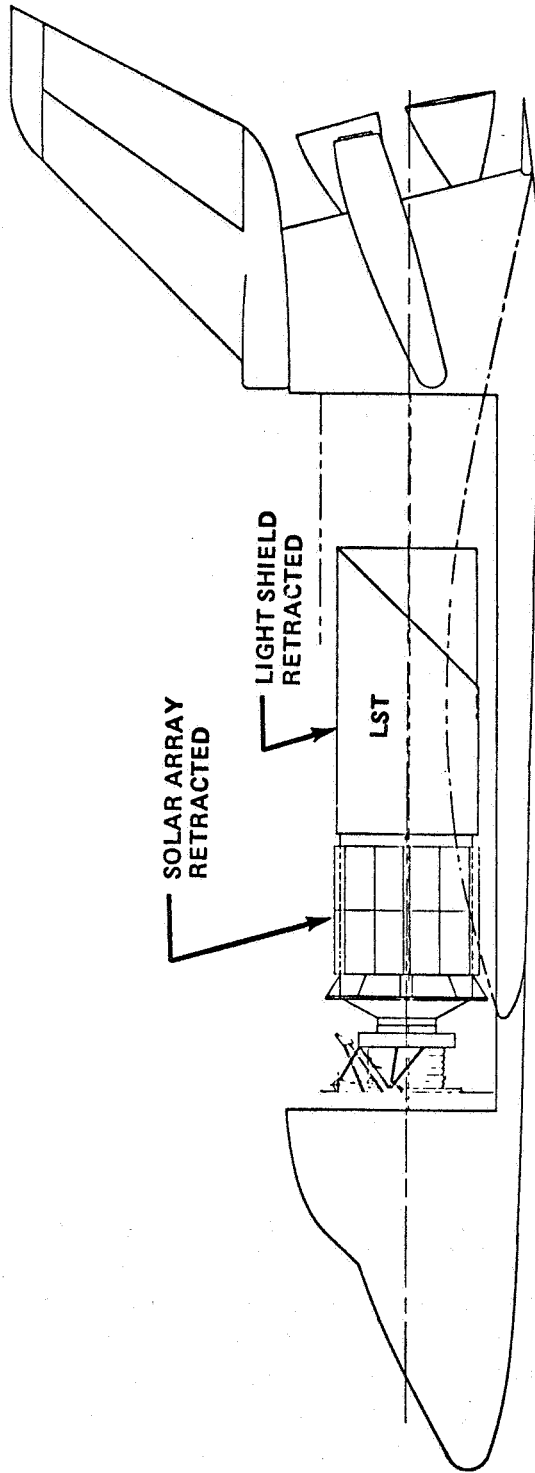


Figure VI-7. LST located in Shuttle payload bay.

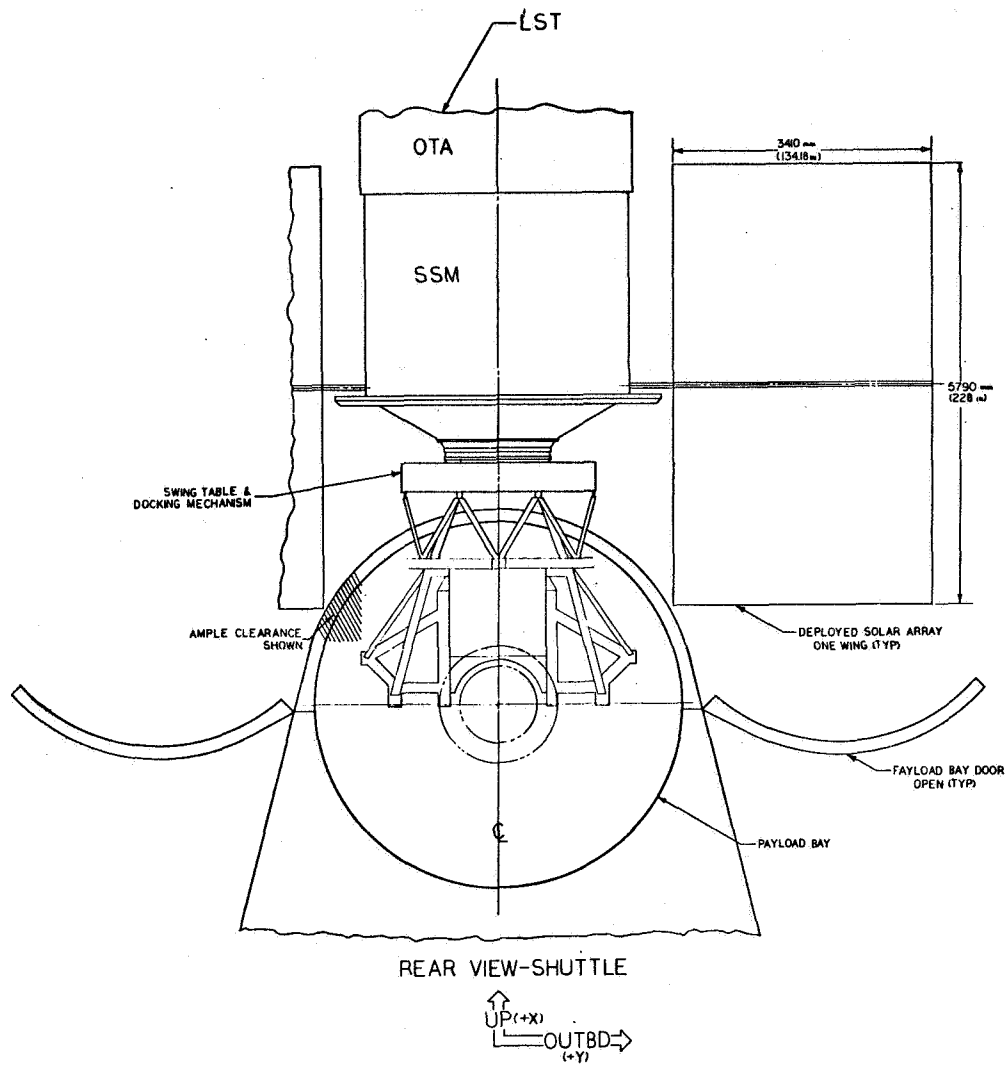


Figure VI-8. LST docked to Shuttle with solar array deployed.

2. LST/Shuttle Contamination Control Interfaces. The LST contamination control support equipment to be installed on board the Shuttle has a mass of 164 kg (362 lb), packaged dimensions of 650 mm by 670 mm by 1170 mm, and a total average power requirement of 870 W. In addition to the support equipment, approximately 30 m<sup>3</sup> (1000 ft<sup>3</sup>) of orbiter volume with an individually controlled clean environment sealed off from the contamination of the support vehicle is required for spares and work space for the maintenance crew. This space should be directly accessible to the docked and pressurized LST during maintenance operations and provide a plenum for the backflow of

high efficiency particulate air (HEPA) filtered from the SIP and SSM. To this volume will be connected the inlets of the contamination control equipment package which will, in turn, be interconnected with a separate dedicated environmental control/life support system (EC/LSS) loop operating independently from the support vehicle (Shuttle) EC/LSS during LST maintenance. The sealing-off of the control volume may be accomplished by an air-supported fabric that maintains a proper cleanliness/air flow barrier without imposing safety problems such as emergency egress, etc., which might accrue with hard structure.

3. LST/Shuttle Manned Maintenance Interfaces. The Shuttle Orbiter's EC/LSS atmospheric revitalization subsystem will provide for LST atmospheric revitalization during periods of manned maintenance by providing flow into and out of the LST.

The Orbiter's airlock support subsystem will provide the systems required for extravehicular activity (EVA), payload bay access, and access to the pressurized volume of the LST during manned maintenance activities.

Mobility aids are provided in the payload bay and Orbiter structure. These mobility aids include strategically located handholds, tether-attachment points, and foot restraints at work areas. Similar mobility aids will be provided on payloads that require EVA/intravehicular activity (IVA) crew operations such as maintenance, inspection, or deployment.

The EVA capability for a minimum of two crewmen is provided by the Orbiter. To support EVA, the Orbiter has an airlock, EVA equipment storage and donning area, extravehicular life support system (EVLSS) recharging station, crew mobility aids, and the necessary communication circuits and monitoring systems for on-orbit operations. The EVA equipment and expendables are available and are chargeable to the payload. This EVA equipment includes (1) pressure garment assemblies (PGAs), (2) EVLSSs, (3) maneuvering systems, (4) tool kits, (5) restraints, and (6) portable lights. Standard tools and a torquing device are included in the tool kit. Specialized tools and tool adapters are provided by the payload.

#### 4. LST/Launch Vehicle Thermal Interfaces

a. LST/Space Shuttle Interface. The thermal control interface between the LST and the Space Shuttle is specified by payload bay temperatures, LST/carrier hard-mounts, pressure equilization venting during ascent and descent, and LST internal heat sources. Table VI-1 summarizes the allowable internal payload bay wall temperature extremes for pre-launch, launch, and entry. The environment within the payload bay for on-orbit conditions depends on orientation and LST internal energy dissipation.

TABLE VI-1. PAYLOAD BAY THERMAL ENVIRONMENT

Mission Phase	Temperature Limits, °C
Pre-launch	24 ± 5.5 <sup>a</sup>
Launch/Ascent	-40 to 65.6
Entry	-78.9 to 93.3

a. Provided by ground support equipment gas purge.

During ascent the maximum temperature rise of the side wall of the SSM has been estimated at 41°C.

During orbital maintenance, a thermally controlled air environment is supplied from the Shuttle Orbiter, contributing to the thermal control scheme of the SSM.

b. LST/Titan Thermal and Environmental Interfaces. The thermal control interface between the LST and the Viking 17.07-m (56-ft) shroud (for Titan IIIE launch) is specified by the ascent trajectory and the insulation scheme on the internal surfaces of the shroud. This interface has not, to date, been quantitatively defined.

The LST will withstand without damage the boost environment maximum conditions listed in Table VI-2.

TABLE VI-2. ENVIRONMENTAL REQUIREMENTS FOR A TITAN LAUNCH

Local Factor	
Longitudinal	+6.0 ± 2.5 g
Lateral	±1.5 g
Vibration	4 g rms
Shock	2400 g at 4000 Hz
Acoustic Pressure	145 dB
Pressure Change	1.73 × 10 <sup>3</sup> N/m <sup>2</sup> /sec (0.25 psi/sec)
Temperature	57.3°C (135°F)
Heating Rate	346.5 W/m <sup>2</sup> (110 Btu/ft <sup>2</sup> hr)

The LST will not undergo transient excursions outside the boost dynamic envelope of 3.7-m (147-in.) diameter imposed by shroud separation.

## 5. Electrical Interfaces with Launch Vehicle

a. Electrical System Interface Summary. The electrical distribution system within the LST spacecraft integrates the subsystems into an overall functional system. Because of the SSM functional role and its position in the spacecraft, the electrical distribution subsystem (EDS) of the SSM must satisfy the interface requirements of the OTA and SIP. It must also accomplish the integration of the LST with the launch vehicle and support equipment.

The elementary block diagram of Figure VI-9 depicts the LST subsystem complement and shows the major electrical system interfaces.

b. Shuttle/SSM Electrical Interfaces. The Shuttle Orbiter assumes control of the LST during the launch, the orbital checkout, the in-space maintenance, or the retrieval operational phases of the mission. Whenever the LST is within the Orbiter payload bay, or attached to the docking adaptor, hardwire cabling links are established to service, monitor, and locally control the electrical functions of the spacecraft. The Orbiter also has receivers and transmitters capable of monitoring and commanding control of the LST by radio frequency (RF) links. The ground stations relinquish control of the free-flying LST to the Orbiter during checkout, station keeping, rendezvous, docking, and release periods of operational support. During in-space maintenance and support operations, the Orbiter provides two-way voice communications between ground stations and payload operations. The Orbiter RF equipment is also capable of sending LST data to, or receiving commands from, the ground station.

The external electrical connections provided for the LST will satisfy all the test, checkout, and control requirements and will be compatible with the IESE, the GESE, and with the Orbiter provisions. All external connectors will be located around the docking port of the SSM. These shall be easily accessible to either a suited or unsuited man within the pressurizable docking adaptor which will provide access to the spacecraft. Manual disconnects should satisfy the majority of the interface requirements for the reference LST. Since the LST can be made self-sustaining prior to release, by transferring power and controls, the interfaces can be de-energized and disconnected in advance of payload separation. Therefore, automatic flyaway umbilicals do not appear to be necessary. Table VI-3 lists the interface connectors allocated for location on the SSM.

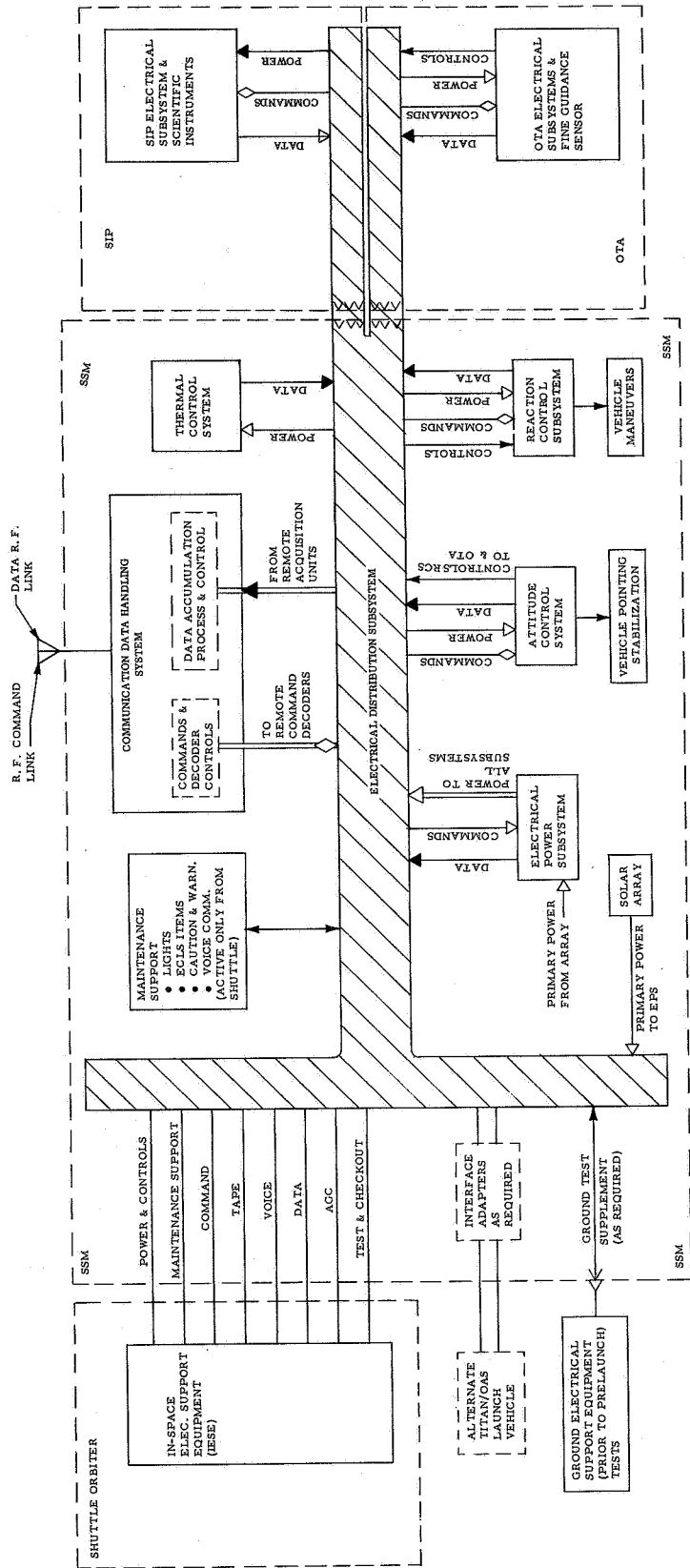


Figure VI-9. LST electrical system interfaces.



TABLE VI-3. LST INTERFACE CONNECTORS, SSM TO ORBITER DOCKING ADAPTOR

Connector Title	Quantity	Receptacle Type	Approximate Pins	MSFC Specification Number
Power and Distribution Control	1	Cir. Std.	60	40M39569
Audio Communications	1	Coax	—	40M38286
Caution and Warning	1	Cir. Std.	60	40M39569
Narrow Band Data	2	Coax	—	40M38286
Wide Band Data	2	Coax	—	40M38286
Command Input	2	Coax	—	40M38286
Data Handling and Communications Test	1	Cir. Std.	39	40M38277
Guidance, Navigation, and Control and Reaction Control System	1	Cir. Std.	39	40M39569
OTA/SIP Test	1	Cir. Std.	60	40M38569

Pre-installed cables will be provided in the pressurizable docking adaptor for mating with the SSM. They shall be routed to avoid interference with passageways and will not pass through doors or parts for safety reasons. All cabling will be protected against possible damage during manned access operations. Unless required for redundant equipment, cabling and hardware dedicated to test and checkout will not be redundant. Feedthrough connectors will provide electrical access to the IESE in the Orbiter.

To the extent possible, cabling and provisions for test and maintenance will be electrically isolated from the active LST systems to assure reliable, trouble-free operations. All cabling will be accessible and easily installed or replaced. Complex harnessing or installation strapping is to be avoided.

Cabling required to initiate release and separation of the LST does not interface with the SSM and is not routed through the docking adaptor. It originates from a connector panel provided in the cargo bay and terminates at the release devices located on the erection mechanism. Similarly, the cabling for the contamination control equipment originates from the same panel.

Other functional requirements for the SSM interface are given with the description of the IESE. Electrical interface requirements are also summarized later in Table VI-6.

c. Electrical Support Equipment Interfaces. The IESE will consist of space-hardened, versatile checkout equipment (to be used for other payloads) and adaptive LST dedicated equipment to assure that the electrical interfaces are identical to those of GESE used for LST pre-delivery and pre-launch checkout. When the LST is attached to the Orbiter, the cables from the SSM external connectors are routed to the IESE which will be located at the payload checkout station in the Shuttle.

The IESE will provide manual controls, visual indicators, instruments, power converters, signal supplies, patch distributors, CRTs and keyboard, recorders, encoders, decoders, electronic buffers, and adaptive circuitry needed to operate and test the LST. This equipment will be compatible with the Orbiter equipment. It will serve as the interface adaptor between the LST and the Orbiter subsystems that will provide power, data, and communications services during launch, in-orbit checkout, or maintenance operations. It will also have connections for contamination control equipment and for ground utilities and services, to be provided for installation checkout prior to the Orbiter being staged or made ready.

Once the Orbiter is made ready at the launch pad, it supplies services to the IESE for payload operation and checkout. The payload is then under local control of the crew from the payload checkout station or in some cases from the other Orbiter stations. From this point, RF command up-link or data down-links to the LST will be via the Orbiter system. For equipment and personnel safety during launch and orbital checkout, the payload command system will be interlocked so that only hardwire commands via the IESE can operate LST equipment. Normal checkout and exercising on the LST subsystems will be accomplished from the payload checkout station using the coax cables to LST equipment dedicated to command and data retrieval. When direct commands to an attached LST are permitted, potentially hazardous functions will be interlocked separately.

The IESE receives power at 28 Vdc from the Orbiter power subsystem. Manual controls, instrumentation, and converters in the IESE energize the LST buses and control distribution. Converters step up and control the voltage delivered to the primary (solar) buses. The IESE has special provisions for conditioning batteries and for load checks on the LST batteries and arrays during maintenance. Controls and instrumentation are also provided for energizing contamination control equipment and for internal lighting. Individual controls for each of the eight lights will be provided.

The LST power requirements are within the capability of the Orbiter electrical power system (EPS). The orbiter can supply between 3 and 6 kW depending on the mission phase. LST power requirements are summarized briefly in Table VI-4. The LST requires more energy than the 50 kW-h provided by the basic Orbiter when IESE and contamination control requirements are considered. However, the Shuttle can provide additional reactant tanks to provide additional energy. Only the mass and volume penalty is charged to the payload. The mass penalty would be about 1 kg/kW-h.

The voice communication link provides for possible maintenance and replacement operations within the LST. The crew member in the LST is in constant communication with the Shuttle crew. This enhances the safety of such operations. The Shuttle will provide audio sending and receiving stations at the commander/pilot consoles and at the payload checkout station. It is also expected that the Shuttle will provide the portable audio equipment to be used inside the LST spacecraft.

The caution and warning (C&W) assembly located in the SSM will interface with the IESE. Similar equipment will be located on the IESE console. The IESE will also provide interfaces with the Orbiter C&W system

TABLE VI-4. LST SHUTTLE POWER INTERFACE

Mission Phase	Launch <sup>a</sup>			Orbital Checkout			Maintenance <sup>b</sup>		
	Average Power, W	Peak Power, W	Energy, kW-h	Average Power <sup>c</sup> , W	Peak Power, W	Energy <sup>d</sup> , kW-h	Average Power <sup>c</sup> , W	Peak Power, W	Energy <sup>d</sup> , kW-h
Load									
LST Spacecraft	250	350	1.6	1800	2200	144	3000	3000	168
Voice/C&W	12	12	0.08	15	15	0.2	20	20	0.2
LST Lighting	-	-	-	-	-	-	120	240	10
IESE	300	400	2.5	500	500	60	5500	500	64
Contamination Control	-	-	-	-	-	e	874	1250	61

a. LST powered down for launch phase.

b. Maximum load configuration with battery cycling.

c. Averages do not indicate average over entire phase.

d. Assumes solar arrays are not deployed.

e. Assumes no power when LST is not manned.

to exchange the necessary C&W signals. Some payload signals may be directed to the commander's station. Potential caution and warning functions are listed in Table VI-5.

IESE test connectors provide access to special test points within the SSM/OTA/SIP subsystems for calibration of sensors, troubleshooting faults, and evaluating the status and redundancy of various critical assemblies and instruments. Dedicated and general purpose test instruments are provided in addition to the CRTs. Power supplies for special sensors and signal conditioning for analog signals are also provided in this equipment as needed.

d. Electrical Interfaces for Alternate Launch Vehicle. The external electrical interfaces of the LST spacecraft are designed for integration with the Shuttle. Should the alternate Titan launch vehicle be used, an add-on "mod-kit" consisting of junction assemblies and adaptor cables will be provided for easy adaptation to the launch vehicle interfaces.

To avoid complexity in the LST, active interfaces with the alternate launch vehicle were avoided. A complete injection stage is assumed that would provide its own power, guidance and control, communications, and data functions and would deliver the LST into the specified orbit. Since the shroud ejection is from the injection stage, signal lines related to shroud ejection and LST separation would be used to initiate LST functional sequences such as array deployment.

Electrical interfaces would also be required with the launch vehicle to provide access to the ground electrical support equipment necessary for pre-launch operations and checkout. Flyaway umbilicals for payload support are not provided at the Eastern Test Range; therefore, GESE cables are removed approximately 2 hours before launch. LST batteries must be sized for this additional period of self-sustained operation.

From T-2 hours through the launch phase, the LST is powered down to conserve energy. Equipment essential to initiating LST operations is energized from the SSM batteries. Initial LST functions are sequenced from shroud ejection and payload separation. Once the shroud is removed, LST operations can be controlled from the ground via the command link.

6. Pointing Control Interfaces with the Shuttle. Precision pointing and attitude control is not required to meet the LST/Shuttle interface requirements. The phases in the mission where attitude control is required for interfacing are at LST release into orbit, and during rendezvous and docking.

TABLE VI-5. CAUTION AND WARNING PRELIMINARY INTERFACE

LST Functions	No.	Phase Interface Applicable			Alert Location
		Launch	Return	Maintenance	
Cable/Umbilical Connected	4	X	X	X	C <sup>a</sup> /W <sup>b</sup> /L <sup>c</sup>
LST Pressure	3			X	C/W/L
LST Temperature	2			X	W/L
CO <sub>2</sub> Level	2			X	W/L
O <sub>2</sub> Partial Pressure	2			X	W/L
External Command Interlock	2	X	X	X	C/W/L
Ordnance Networks Armed	2	X	X	X	C/W/L
Emergency Suit Connection Ready	3			X	W/L
Battery Temperature/Pressure High	6	X	X	X	C/W/L
RCS Tank Pressure	2	X		X	C/W/L
RCS Tank Temperature	2	X		X	C/W/L
Distribution Buses Activated	3			X	L
Contamination Control	?	X	X	X	W
Shuttle Side Functions					
LST Overload/Reverse Current	3	X	X	X	C/W/L
EPS/Fuel Cells/Buses	5	X		X	C/W/L
Cryogenic Pressure/Temperature	6			X	C/W/L
ECLS Status	4			X	C/W/L
Stabilization and Control Status	1	X		X	C/W/L

a. C = Shuttle Commander Station

b. W = Shuttle Payload Work Station

c. L = LST SSM

When the Shuttle releases the LST into orbit, it is desirable, but not necessary, that the initial LST attitude be roughly that required for the sun acquisition mode. However, the Shuttle design should not be driven by any initial attitude requirements because the altitude control system (ACS) has been designed to stabilize the LST and acquire the sun acquisition mode attitude from any initial attitude.

For rendezvous and docking, transponders compatible with the Shuttle rendezvous and docking system will be available on the LST. The selection of transponders will be influenced by the Shuttle system and may be a system of passive corner reflector cubes for a laser radar docking system, or compatible transponders if a clockwise radar system is selected. The primary interface requirement for attitude control will be rate stabilization. A secondary requirement that could exist is for a specific attitude orientation to facilitate the rendezvous and docking maneuver. The reference ACS has sufficient attitude hold capability. If misdock occurs resulting in large impulses being applied to the LST, an RCS provides stabilization control torques.

7. Preliminary LST/Shuttle Interface Summary. The preliminary interfaces established for the LST/Shuttle are summarized in Tables VI-6 and VI-7.

## B. General LST Interfaces

This section describes interface requirements and provisions considered applicable to all elements of the LST.

1. General Environmental Requirement. The environmental requirements given for the LST launch vehicle interfaces in Sections A.4 and A.7 of this chapter are applicable to all elements of the LST.

### 2. Electrical Interfaces

a. Test and Maintenance in Space. The SSM will provide interfaces and electrical networks for LST in-space test and maintenance.

The test and maintenance support networks are to be activated only through external LST connections when electrical support equipment is available for the various test and maintenance operations. The test network will be common for, and made compatible with, both GESE and IESE. The

TABLE VI-6. PRELIMINARY LST/SHUTTLE INTERFACE REQUIREMENTS

Interfacing Areas	Operational Mode	
	On-Orbit	Other (Pre-Launch/Launch/Entry Landing/Post-Landing)
<u>Operational Requirements</u>		
Mission Support Crew Size/ Requirements	2	
Commander/Pilot Payload Specialist	- 2	- 2 (Ground Checkout)
Crew Access to Payload Bay		
Airlock Direct		None
IVA	Only for contingencies.	N/A
EVA	Only for contingencies.	N/A
Payload Handling	Only for contingencies.	N/A
Payload Deployment/ Release	0.7 g is maximum with arrays deployed; not critical with arrays retracted; low tumble rates (0.5 degree/sec) or so desired.	
Multiple Payload Deployment	No	



TABLE VI-6. (Continued)

Interfacing Areas	Operational Mode	
	On-Orbit	Other (Pre-Launch/Launch/Entry Landing/Post-Landing)
<p>Performance</p> <p>Orbit Altitude</p> <p>Inclination</p> <p><math>\Delta V</math> Capability</p> <p>&gt; 7-Day Mission</p> <p>Stability and Control</p> <p>Nonrestrictive Orientation</p>	<p>611 km (330 n.mi.)</p> <p>28.5 degrees</p> <p>For achieving above orbit.</p> <p>Not normally required but could be a desirable capability.</p> <p>Undesirable to point telescope within 45 degrees of sun; possible special checkout requirements are: (1) LST in shade of Shuttle, (2) LST arrays to sun (<math>\pm 7</math> degrees), (3) LST pointing at a star (checkout); during normal maintenance period (1 to 4 days), no special orientation required.</p>	<p>N/A</p> <p>N/A</p>

TABLE VI-6. (Continued)

Interfacing Areas	Operational Mode	
	On-Orbit	Other (Pre-Launch/Launch/Entry Landing/Post-Landing)
Orientation Hold Time (Maximum and Frequency)	Approximately 1 hour each orbit (~ 100 minute orbit) during checkout period (1 to 2 days maximum)	
Attitude Dead Band	See next item.	
Attitude Stability Rate	Not critical — possible requirement to hold on a star during checkout, but should not drive Shuttle design.	
<u>Physical and Functional Requirements</u>		
Mechanical/Structures		
Payload Size	See Table VI-7.	Same
Payload Mass	See Table VI-7.	
Type of Structural Supports	Cradle/Pallet	
Number and Location of Supports	4 total, 3 at main ring and 1 near aft end.	

TABLE VI-6. (Continued)

Interfacing Areas	Operational Mode	
	On-Orbit	Other (Pre-Launch/Launch/Entry Landing/Post-Landing)
Center of Gravity Envelope (Weight versus Station)	LST center of gravity (in launch configuration) is 454 mm (179 in.) from the docking plane; the net center of gravity of the payload must include the orbit maneuvering system and the equipment in the bay; these have not been calculated.	Same
Standard Orbiter to Payload Interface Plates/ Panels (Data, Power, Fluids, Communications, etc.)	No flyaway umbilicals defined. SSM connections to be manual and accessible from within docking adaptor; pressure tight feedthrough connectors into crew compartment needed for cables (Table VI-3); connector panels in payload bay services payload release and separation and contamination control equipment; payload furnishes cabling to IESE; no fluids flow across interface (except possibly air flow to EC/LSS).	Same

TABLE VI-6. (Continued)

Interfacing Areas	Operational Mode	
	On-Orbit	Other (Pre-Launch/Launch/Entry Landing/Post-Landing)
Consoles, Equipment, etc. in Crew Compartment (Volume and Support)	See listings under systems headings; dedicated in-space electrical support equipment (IESE) payload furnished to serve as payload adaptor; interface with Shuttle equipment and subsystems.	
Docking Hardware g-levels	Yes See "Payload Deployment/Release."	Payload requirements not defined yet — designing to meet Shuttle capabilities: ascent, 6 g long, 1.5 g; lateral descent, 1 g long, 2.7 g lateral.
Fluids (Gases) Transfer Between Orbiter/Payload (Types — LH <sub>2</sub> , N <sub>2</sub> , H <sub>2</sub> O, etc.) Transfer Between Payload/Ground (Types — LH <sub>2</sub> , N <sub>2</sub> , H <sub>2</sub> O, etc.)	None (GN <sub>2</sub> , RCS only used for emergency backup; entire bottle is replaced rather than refilled, if used; may be dropped from design.)	Same

TABLE VI-6. (Continued)

Interfacing Areas	Operational Mode	
	On-Orbit	Other (Pre-Launch/Launch/Entry Landing/Post-Landing)
Atmospheric Conditioning in Payload Bay	See "Contamination;" need relative humidity $\leq 40\%$ , and temperature as shown under "Payload Bay."	Same
Payload Bay Purge	None	Only as required to meet cleanli- ness and environmental require- ments.
EC/LSS	Required during maintenance. Assumed that part of basic Shuttle EC/LSS was isolatable and switchable to LST.	Supplied by ground support equipment.
Thermal Heat Rejection Support	Shuttle EC/LSS must handle CO <sub>2</sub> , humidity, and tempera- ture control for two payload specialists plus dissipation of some equipment heat [part of that listed under "Power (LST via IESE from Orbiter)"]	Unknown

TABLE VI-6. (Continued)

Interfacing Areas	Operational Mode	
	On-Orbit	Other (Pre-Launch/Launch/Entry Landing/Post-Landing)
Heat Rejection Support (Concluded)	and all of that listed under "Power for Consoles and Auxiliary"].	
Electrical	28 Vdc to IESE	28 Vdc to IESE
Voltage and Frequency	IESE furnishes 0 to 80 Vdc; 28 V, 15 V, 5 V, etc., to SSM. 115 V, 1 $\phi$ , 400 Hz desired for lighting but not required.	
Power (LST via IESE from Orbiter)	Assume array power not available. Normal checkout maximum: 1800-W average; 2200-W peak (144 kW-h) Full system operation with batteries: 3000-W average; 3000-W peak (168 kW-h)	250 to 350 W, ~ 1.7 kW-h.

TABLE VI-6. (Continued)

Interfacing Areas	Operational Mode	
	On-Orbit	Other (Pre-Launch/Launch/Entry Landing/Post-Landing)
Power (LST via IESE from Orbiter) (Concluded)	Add during manned maintenance Operations: 20 W for C&W and communications; 120-W average, 240-W peak for lighting 10 kW-h (maintenance only).	
Power for Consoles and Auxiliary In-Space Electrical Support Equipment (IESE)	500-W average for IESE, 64 kW-h (maintenance maximum).	300 to 400 W average, ~ 2.5 kW-h.
To Contamination Control	874-W average; 1250-W peak Maintenance visit, 61 kW-h maximum.	N/A
Data Handling	Orbiter interfaces with IESE; IESE receives data from LST.	Same
Data Formatting Prior to Transmission	Data received from LST are either formatted on board the LST or by IESE; wide-band	Same

TABLE VI-6. (Continued)

Interfacing Areas	Operational Mode	
	On-Orbit	Other (Pre-Launch/Launch/Entry Landing/Post-Landing)
Data Formatting Prior to Transmission (Concluded)	and narrow-band data serial data will be made compatible with Shuttle.	
Data Computation and Analysis (Operations, Speed)	Possible up to 16K word memory required for checkout; speed not critical.	Same
Data Recording (Type, Rates, etc.)	Diagnostic data for recording are serial at a 1.6 kbit/sec rate.	Same
RF links for Transmitting or Receiving	Shuttle should provide RF links equivalent to the LST transponders; LST uses one Apollo transponder and one ERTS transponder.	Same
Communication Transmission Rate	1 Mbit/sec for scientific data; 51.2 kbit/sec for engineering data.	Same
Number of Hardware Lines	~ 4 Coax	Same



TABLE VI-6. (Continued)

Interfacing Areas	Operational Mode	
	On-Orbit	Other (Pre-Launch/Launch/Entry Landing/Post-Landing)
Communications		
Two-Way Voice With Payload	Yes; portable transceiver and suitable communications; preinstalled cabling.	N/A
Two-Way Voice Payload to Ground	Desired	N/A
Two-Way Voice Payload Specialist to Ground	Desired	Desired
Displays and Control		
Caution and Warning	Yes; TBD	Same
Payload Checkout and Analysis	Payload-peculiar consoles; ~ 91 kg (200 lb) 1.42 x 10 <sup>9</sup> mm <sup>3</sup> (86 400 in. <sup>3</sup> ); 500 W estimated in addition to some "basic" capability provided by Shuttle.	Same

TABLE VI-6. (Continued)

Interfacing Areas	Operational Mode	
	On-Orbit	Other (Pre-Launch/Launch/Entry Landing/Post-Landing)
Physical Inspection (Illumination)	Internal lights are preinstalled in payload.	Same
TV Direct Viewing	External lighting, etc., to be provided by Shuttle.	Same
<u>Environmental Requirements</u>		
Payload Bay		
Temperature	Payload being designed to meet Shuttle-stated capabilities of -100° F to 200° F.	Same
Pressure	Not Critical	Not Critical
Maximum Vibration Levels	Not Defined	Same
Maximum Acoustic	Payload being designed to Shuttle-stated capability of 151 dB.	
Contamination (Cleanli- ness)	The cleanliness of the LST must be protected during all mission phases associated	Same

TABLE VI-6. (Continued)

Interfacing Areas	Operational Mode	
	On-Orbit	Other (Pre-Launch/Launch/Entry Landing/Post-Landing)
Contamination (Cleanliness) (Concluded)	with Shuttle operations; class 10 000 desired; can 'bag' payload for launch, but protection needed for earth-return mission phase; potentially a major problem.	
ECLS for Payload Operations Shuttle ECLS Support	Required for payload specialists station; required for manned operations within LST during maintenance.	
Contamination	Class 10 000 desired in LST payload contamination control equipment to be provided will have mechanical, environmental, and electrical interface with Orbiter.	Same

TABLE VI-6. (Continued)

Interfacing Areas	Operational Mode	
	On-Orbit	Other (Pre-Launch/Launch/Entry Landing/Post-Landing)
<u>Programmatic and Support Requirements</u> Logistics Storage Spares	See typical maintenance mission list.	
<u>Operational Availability</u>	Not Critical	
<u>Reliability</u>	Higher than payload which should be around 0.9 to 0.95.	
<u>Maintainability</u>	Desirable to have spares and tools stored in pressurized Orbiter compartments to avoid IVA; Contamination control in cabin, bay area, and within LST is of major importance; Shuttle EC/LSS interfaces between LST and Orbiter must be compatible; payload	Same

TABLE VI-6. (Concluded)

Interfacing Areas	Operational Mode	
	On-Orbit	Other (Pre-Launch/Launch/Entry Landing/Post-Landing)
<u>Maintainability (Concluded)</u>	will supply space, tools, and mechanical and electrical support equipment for maintenance operations; see power, data, and communications requirements applicable to payload maintainability.	

TABLE VI-7. PHYSICAL CHARACTERISTICS FOR LST LAUNCH

Item	Size, mm (in.)	Mass, kg (lb)
Basic LST	$3.68 \times 10^3$ diameter $\times 1.36 \times 10^4$ long (~ 145 diameter $\times 534$ long)	9520 (~ 21 000)
Delivery Mission		
Swing Table <sup>b</sup>	$3.05 \times 10^3$ diameter $\times 1.52 \times 10^3$ long (~ 120 diameter $\times 60$ long)	5442 (~ 12 000)
Spares	$3.05 \times 10^3$ diameter $\times 1.52 \times 10^3$ long (~ 120 diameter $\times 60$ long)	294 (~ 647)
Typical Maintenance Mission	$9.63 \times 10^8$ mm <sup>3</sup> volume (58 752 in. <sup>3</sup> volume)	371 (~ 817)
Scientific Update	$7.37 \times 10^8$ mm <sup>3</sup> volume (44 928 in. <sup>3</sup> volume)	461 (~ 1014)
Other	$3.32 \times 10^9$ mm <sup>3</sup> volume (202 176 in. <sup>3</sup> volume)	

a. OMS = orbit maneuvering system.

b. This concept was used in LST reference mission for basic delivery mission, but may not be required.

maintenance networks are only needed for in-space maintenance with the Shuttle. These provide for illumination, local communications, life support sensors and accommodations, and warning alerts necessary for manned maintenance operations.

Based on historical safety concepts and procedures, approximately 39 kg of electrical equipment is installed in the LST to satisfy estimated interface, test, and maintenance requirements. These accommodations will be dependent on the mechanization and equipment provisions of the Orbiter. The operational procedures and constraints, and safety requirements have not yet been fully defined for the Shuttle.

Eight 30-W fluorescent light fixtures are located in the vicinity of the OTA, SIP, and SSM equipment to be maintained. These units are powered and may be individually controlled from the IESE as necessary. The power necessary will be supplied from the Orbiter power source to the IESE.

A caution and warning assembly is installed to provide visual and audible alarms to a crew member working in the LST. He will be alerted to potential hazardous conditions that may develop in either the LST or the Shuttle. A separate cable to exchange safety signals exists between the LST and Shuttle so that the same alerts are displayed in the payload and in the Shuttle.

Three plug-in receptacles, cabling, and interface connectors provide a voice communications link to the Shuttle. This link is to be adapted to either suited or unsuited operations within the LST.

Separate test cables are provided for the OTA, SIP, EPS, ACS, and communications and data handling system (C&DHS) for easier integration and troubleshooting. This avoids complex harnesses and is consistent with modularization and maintenance concepts. They provide special hardwire access for checking redundancy, critical components, and for checkout and fault location in the event of failures such as nonoperative command or data equipment. Should the number of external connectors be constrained by the docking adaptor or the Shuttle system, a junction box will be added to the SSM to channel the internal test cabling to the interface connectors.

Coax cables provide data and command channels to the IESE for normal checkout and maintenance. Normally, the onboard LST data and command equipment will be used for maintenance and checkout.

The LST has provisions to accept power from the Shuttle via the IESE. Control of power distribution and major EPS assemblies may be effected from the IESE.

b. Standards and Hardware. To assure reliable, trouble-free operations, electrical system specifications, standards, and verification procedures will be established that will be applicable to the OTA, SIP, and SSM.

Qualified, proven system hardware and processes will be specified for all elements to assure system integrity and interface compatibility. Tentative Specifications for cabling, connectors, switching devices, etc., are given in Volume V, Chapter IV.

c. Electromagnetic Control. An electromagnetic control (EMC) plan based on existing specifications will be established. The requirements to be imposed shall be specifically adapted to the LST. To assure trouble-free operation, accuracy of controls, and high quality data, rigid controls will be imposed on the design and implementation of the LST system. Applicable concepts and standards are as follows:

1. System Design Requirements

a. Electrical Bonding

(1) The structure will be electrically bonded to provide a low impedance electrical ground reference plane.

(2) Provide an electrostatic discharge path between spacecraft, scientific instruments, and the boost vehicle.

b. Electrical Grounding — Single-point electrical ground concept with design implementation as specified in the EMC control plan to be established for LST.

2. System Compatibility Requirement — The spacecraft equipment, scientific instruments, and Shuttle-borne equipment will be designed such that an electromagnetic compatibility margin exists at the integrated Shuttle/spacecraft level with respect to the self-generated interference environment in accordance with MIL-E-6051D.



3. System EMC Verification — Verification that EMC requirements have been satisfied will be accomplished for the LST integration simulators, LST integrated spacecraft, IESE, and LST/Shuttle Integrated Vehicle.

4. Unit or Subsystem Requirements

a. Electrical Bonding — A dc resistance of 2.5 m $\Omega$  or less per joint (MIL-B-5087B, Class R); an impedance of 0.5  $\Omega$  or less up to a frequency of 1.0 MHz as a design goal.

b. Electrostatic Grounding — A dc resistance of 1.0  $\Omega$  or less per joint (MIL-B-5087B, Class S).

c. Electrical Grounding (implementation per Figure IV-35 of Volume V) — Primary dc power employs single-point ground (SPG) located near electrical control assemblies (ECAs of the SSM); secondary dc power employs dedicated transformer windings with internal vehicle ground point (VGP) for each applicable equipment load; signal circuits may employ the structure as a signal return path with current limited to "TBD" milliamperes, but this is not recommended in general.

d. Electrical dc Isolation — Primary dc power leads to unit case shall be a minimum dc resistance of 1.0 M $\Omega$  at 5.0 Vdc prior to electrical connection; primary to secondary dc circuitry isolation shall be greater than 1.0-M $\Omega$  dc resistance prior to electrical connection.

e. Interference Control Requirements — MIL-STD-461A requirements tailored specifically for the LST system, which integrates the MSFC power quality requirements.

3. SSM/SIP/OTA Manned Maintenance Interfaces. The configuration of each SSM, OTA, and SIP subsystem design will include modular arrangements which will permit those components identified to be readily replaced or refurbished in orbit by maintenance personnel in a "shirt sleeve" mode.

The LST subsystems will be configured so that replacement of components or instruments will not necessitate a complex alignment or calibration procedure by maintenance personnel.

The LST program will perform a reliability analysis of each of the subsystems which will identify those components that require replacement or refurbishment in orbit at each servicing visit by the logistics Shuttle.

Replacement components and refurbishment materials will be procured and stored and maintenance tasks will be identified so that execution of the planned servicing program in-orbit will restore the LST to essentially "as new" operating condition.

The LST/SSM spacecraft will be outfitted with restraints and handrails needed within the instrument compartment for maneuvering by maintenance personnel.

Astronaut maintenance personnel will be required to train in the LST servicing program in an LST simulator prior to performing a logistics mission.

Restrictions are listed below on variations of assemblies to insure their replaceability with others of the same kind and adherence to the same performance criteria as the original instruments.

Instrument and Location	Defocus Tolerance	Decentration Tolerance
f/96 Camera at f/12 Focus	0.07 mm	0.1 mm
Slit Assembly for Axial Bay Instruments	0.08 mm	0.3 mm
Spectrograph Select Collimator Assembly	0.17 mm	0.3 mm
Faint Object Spectrograph in Radial Bay	0.08 mm	0.5 mm
f/12 Camera	0.15 mm	0.5 mm
Sensor Tubes for Spectrographs	0.10 mm	0.5 mm
Sensor Tube for f/96 Camera	1.0 mm	1.0 mm
Axial Bay Instruments	Not Applicable	0.2 mrad tilt maximum

The tolerances given are for the coordinates of focal plane interfaces relative to mechanical mounting interfaces. The decentration limits are measured at the focal interface, which is often remote from the mechanical

interface. The projection of the focal plane centration to the mounting plane assumes that the measurement is made perpendicular to the mounting plane within 0.1 mrad.

4. Support Requirements. Each element (OTA, SSM, SIP) of the LST will require exchange of electrical and mechanical simulators, mating jigs, interface devices, etc., for compatibility tests and interface verification prior to integration of elements.

All LST elements will be delivered to an integration facility for integration and testing prior to delivery of the LST.

The SSM will furnish ground support equipment necessary to test, verify interfaces, and handle the entire LST.

The IESE cabling, mechanical devices and tools, integrating structures, and payload unique contamination control equipment necessary for integrating the LST with the launch vehicle systems and for maintenance operations will be verified and delivered to the launch site.

## C. SSM/OTA Interfaces

1. SSM/OTA Mechanical Interfaces. The mechanical interface between the OTA and the SSM is at the OTA primary ring. The cylindrical portion of the SSM consists of a stiffened shell surrounded by a meteoroid shield. As shown in Figure VI-5 the 3300 mm (130-in.) inside diameter shell is internally stiffened, longitudinally, with stringers and longerons. External stiffening is circumferential with formed channel rings. The rings are deep enough to support the meteoroid shield. The SSM extends 5000 mm (197 in.) from the docking plane to the OTA/SSM mechanical interface as illustrated in Figure VI-1.

The structural interface between the OTA and the SSM is detailed in Figure VI-10 which shows the pressure seals between the SSM pressure shell and the OTA primary ring. Brackets shown in Figure VI-11 provide flanges to bolt the SSM to the OTA primary ring for SSM/OTA pressure-tight assembly. External longitudinal brackets, shown in Figures VI-5 and VI-10, stiffen the SSM for longitudinal loads and moments for either Shuttle (tension) or Titan (compression) launch loads.

Although the structural interface between the OTA/SSM is at the OTA primary ring, the OTA meteoroid shield diameter is continued 1500 mm (59 in.) aft to provide the additional depth required for the OTA-designed longitudinal fittings as illustrated in Figure VI-11. From this plane aft, the lesser meteoroid shield depth required permits decreasing the meteoroid shield outside diameter to 3430 mm (135 in.) as shown in Figure VI-5. The 1500 mm (59 in.) section of the meteoroid shield transition between the OTA and SSM is made removable to provide for OTA/SSM disassembly. The entire OTA meteoroid shield is one structural unit of the same diameter to prevent inducing loads into the primary mirror through a structural connection at the primary ring.

2. SSM/OTA Thermal Interface. Mechanically, the SSM/OTA interface exists at the connection of the SSM and the primary ring. The thermal interface at this point is to be as adiabatic as practicable, making use of insulation and low conductivity connectors.

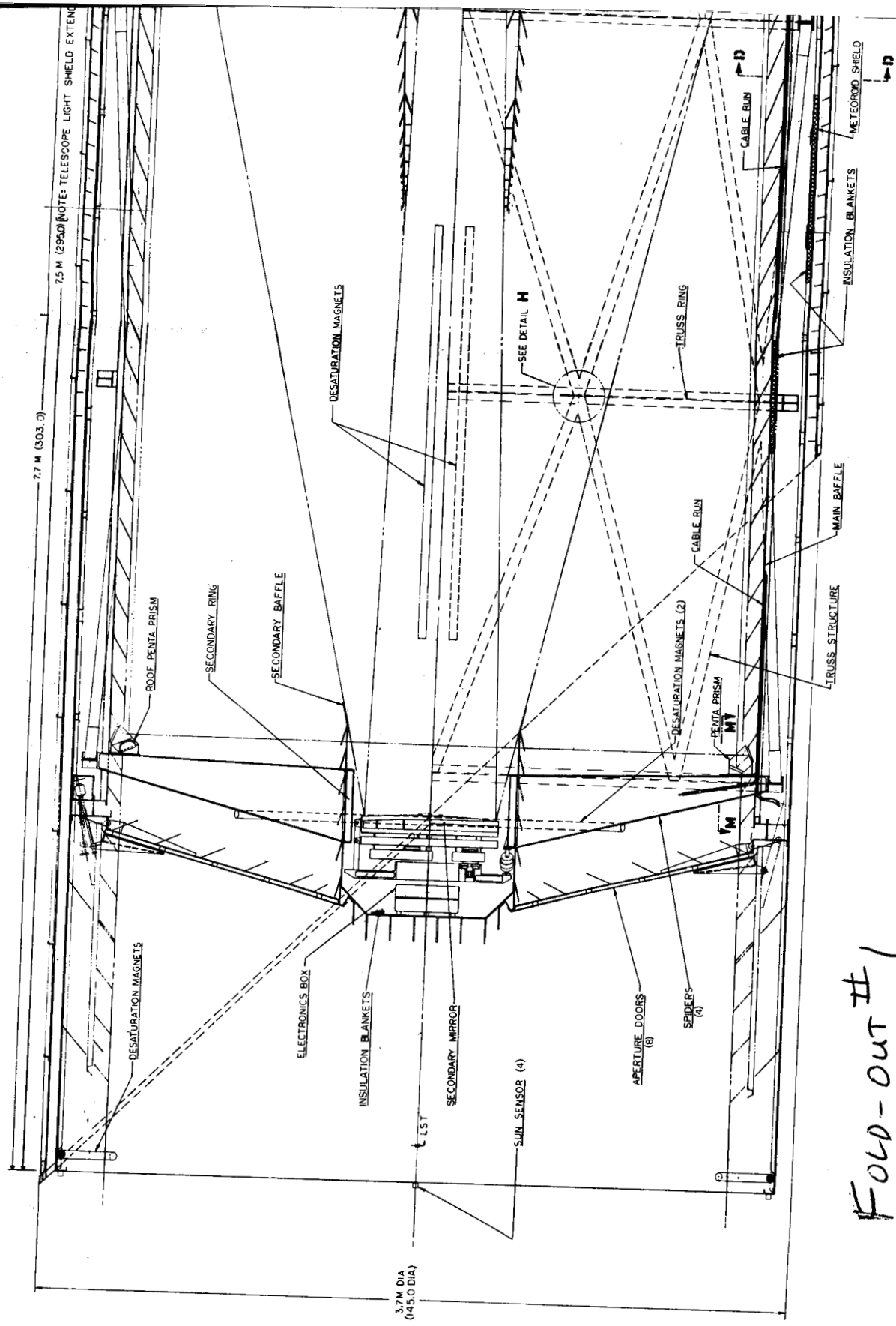
3. Environmental Interfaces. The SSM equipment will generate electromagnetic fields in the vicinity of OTA equipment.

Both the OTA and SSM equipment in the instrument compartment are potential sources and recipients of contamination material. The design of all subsystems will avoid use of nonapproved material and will provide protection against introduction of contaminating substances.

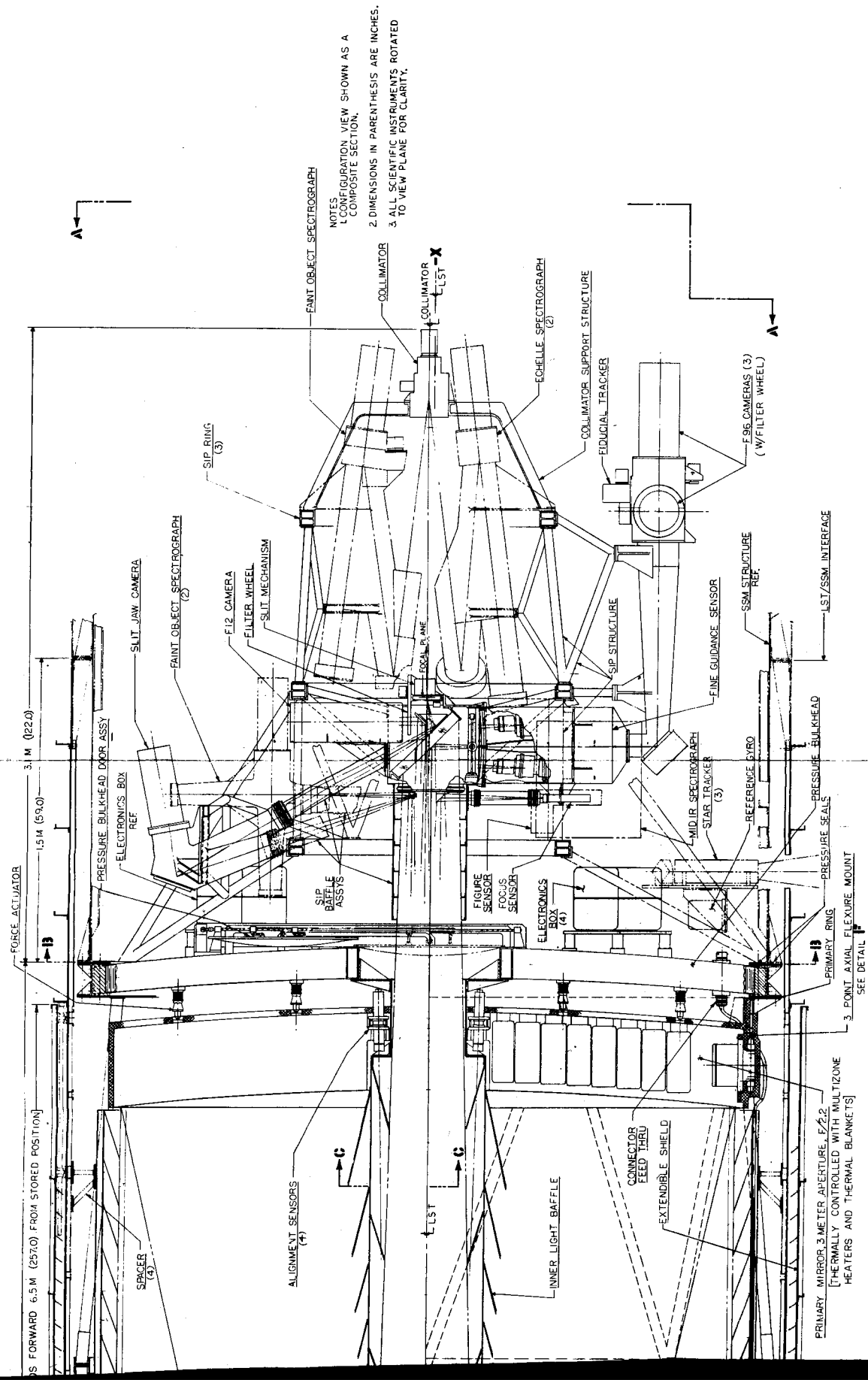
The SSM will control pressurization of the OTA instrument compartment for man-maintenance activities. This atmosphere will consist of the following characteristics:

1. Pressure —  $101.5 \times 10^3 \text{ N/m}^2$  (14.7 psia).
2. Composition — 20-percent oxygen, 80-percent nitrogen.
3. Humidity — < 50 percent.

4. SSM/OTA Electrical Interfaces. The spacecraft system design goal is for the SSM to maintain supervisory control over the receipt and distribution of ground commands to the OTA, and the receipt, storage, and transmission of the diagnostic data generated by the OTA subsystems to the ground data network.



Fold-out #1



Fold-out #2

Figure VI-10. SSM/OTA structural interface.



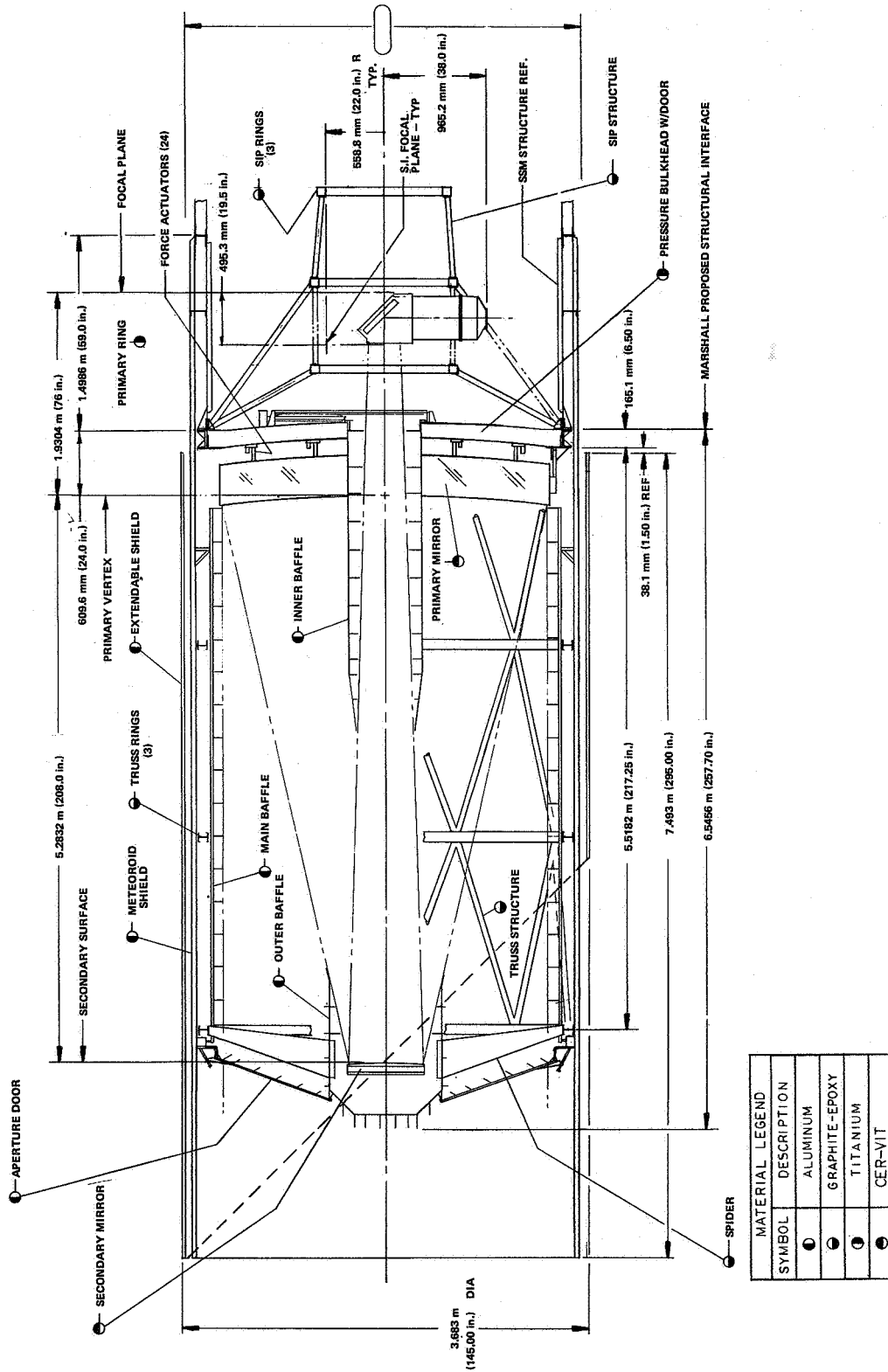


Figure VI-11. SSM/OTA structural provisions.



Although functional requirements differ, the SSM to OTA and SSM to SIP electrical interfaces have been standardized and kept as common as possible. It is intended to maintain constant requirements at the separable electrical interface planes to be defined by the SSM, and yet to permit versatility on the OTA and SIP side of the interface. This is accomplished by standardized, versatile remote units located within the OTA and SIP, but furnished and controlled by the SSM. The separable interfaces are established at the input connectors to the remote units. The simplified diagram shown in Figure VI-12 illustrates the interface concepts and units involved.

The SSM will route to the OTA all operating commands, whether initiated by ground control or by a stored program. These commands will be issued in digital format from an SSM remote command decoder. Up to 256 commands may be sent to the OTA through one command decoder. Including redundancy, two remote command decoders (RCD) are allocated to the OTA.

The OTA will receive the decoded commands and will convert them to analog form and route them to the appropriate OTA subsystem for implementation.

The OTA will generate diagnostic data concerning the status of subsystems and the execution of commands, will precondition analog data to 0- to 5-Vdc, and route the data to a data acquisition unit (DAU) of the SSM. Each DAU can accept 64 analog or bilevel signals, and as many DAUs as required will be assigned to the OTA interface. The SSM will provide all data synchronizing signals required. Data delivered to storage will be limited to a rate of 1.6 kbits/sec. Six DAUs are allocated to the OTA.

The SSM will provide all onboard data storage capacity required.

An average power of 500 W is allocated to the OTA. Short term peak power will be limited to 1000 W.

The spacecraft system guidelines specify that the SSM will furnish all basic electrical power to the OTA via two redundant electrical distribution units (EDUs) located in the OTA, but that are furnished by and under switching control of the SSM. The voltage will be within 28 to 30 Vdc, regulated to 2 percent. Each EDU will automatically isolate an overload fault on its input. It will also provide overvoltage and electromagnetic interference (EMI) protection.

The EDU will consist of two input modules and one or more output modules as required. One of the input modules has a 25-A switch for the large heater load. The inputs are to be standardized for common interfaces

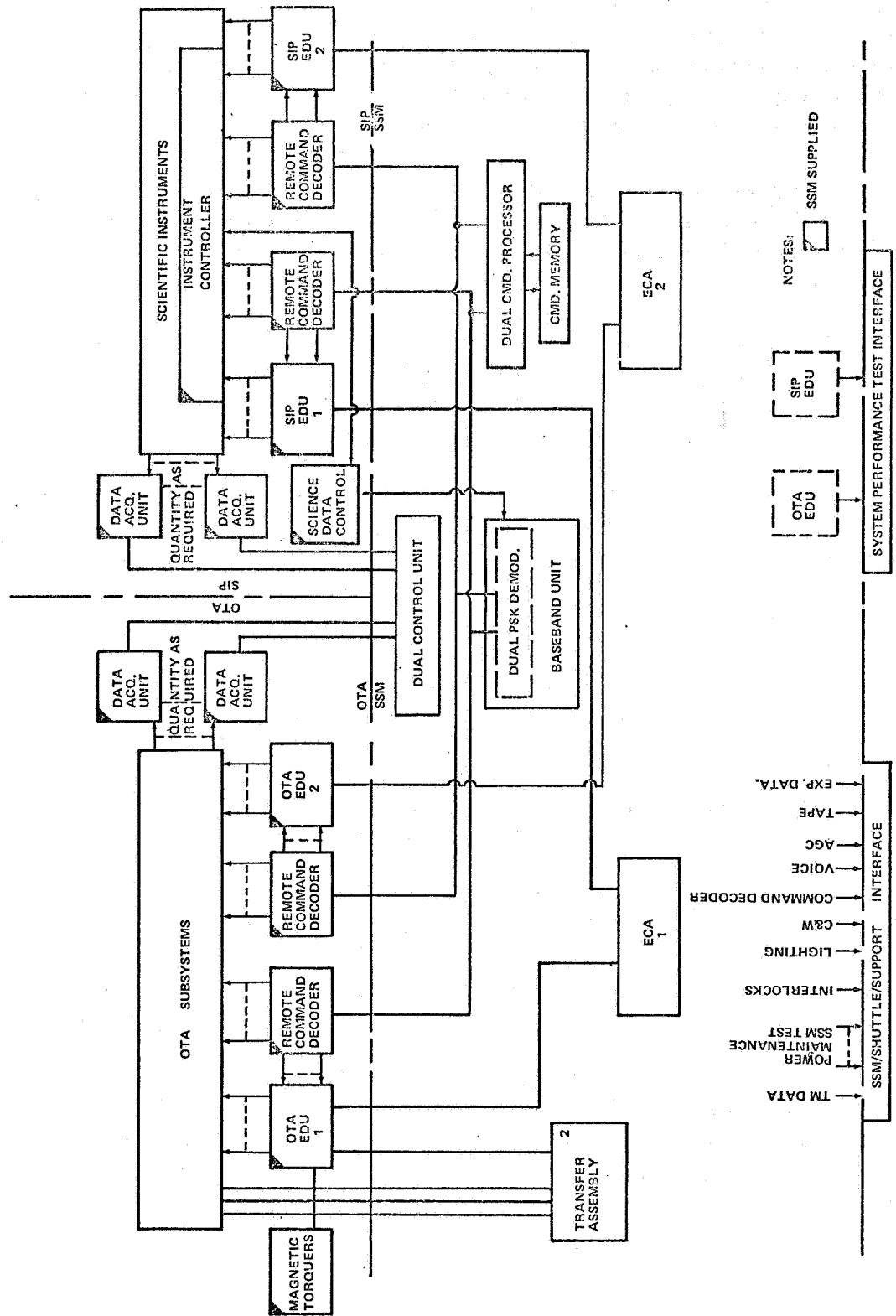


Figure VI-12. SSM electrical interfaces.

with the electrical distribution subsystem. Electrical inputs from electrical control assemblies (ECAs), RCDs, and test cables are provided. Output modules consist of a family of adaptable subassemblies selected to satisfy specific requirements of each subsystem. The modular construction of the EDU is consistent with that of the RCDs and DAUs so that these may be grouped together as one functional assembly when needed.

The power input cable will provide five separate inputs and five ground return lines to each EDU. Four of the inputs will have a 5-A switch rating. The fifth will be rated at 25 A. Thus, the total rating of each EDU will be 1200 W.

The OTA will route the dc power received from the EDUs to the OTA subsystems and will provide internal regulation and overload isolation circuits via five power distribution units. The OTA may also generate any special voltage or frequency required.

Electrical access to external connectors for test and checkout was requested but the specific number of functions and lines was not determined. A 39-pin connector is provided on each EDU for this purpose. Test lines are not to be made redundant. Only one SSM cable to one EDU is presently allocated for OTA tests.

Three pairs of lines are allocated for feedback signals from the OTA fine pointing subsystem to the SSM transfer assemblies. If these are amplified high level analog signals, the same separable connectors designated for EDUs should be used. Coax is recommended if these are high rate digital signals. Several lines are required for the SSM-supplied magnetic torquers to be located on the OTA. Routing is to be determined.

a. Separable Connectors. Connectors allocated for the electrical separation plane between SSM and OTA will be attached to SSM cabling. These cables will be routed near the RCDs, DAUs, and EDUs on the OTA and will have sufficiently free length for mating with these units after the OTA and SSM are assembled.

b. Electromagnetic Control. Both the OTA and SSM equipment are potential sources and recipients of electromagnetic interference. The design of all systems will utilize techniques to minimize EMI susceptibility by proper cable routing, shielding, bonding, and grounding techniques. General requirements for electromagnetic control are given in Section B.2 of this chapter.

5. Pointing Control Interfaces. The system design goal is to have the SSM responsible for coarse pointing the telescope line of sight to command celestial coordinates to  $\pm 4.85\text{-}\mu\text{rad}$  ( $\pm 1\text{-arc sec}$ ) accuracy, while the OTA will perform the final pointing and image stabilization.

The SSM will maneuver the spacecraft to coordinates commanded by ground control to  $\pm 145.5\text{-}\mu\text{rad}$  ( $\pm 30\text{-arc sec}$ ) accuracy in two axes without utilizing data from the OTA.

When the telescope line of sight is within  $\pm 145.5\ \mu\text{rad}$  ( $\pm 30\text{-arc sec}$ ) of the target, the OTA by means of guide star trackers will generate and deliver to the SSM proportional error signals in pitch, yaw, and roll, referred to spacecraft coordinate systems. The SSM will utilize these error signals to reduce the pointing error to  $\pm 4.85\ \mu\text{rad}$  ( $\pm 1\text{ arc sec}$ ).

The OTA will then stabilize the image for the SIP instruments to  $0.49\text{-}\mu\text{rad}$  ( $0.1\text{-arc sec}$ ) accuracy and  $0.024\text{-}\mu\text{rad}$  ( $0.005\text{-arc sec}$ ) stability, using error signals from guide star trackers fed to transducers producing corrective motions of the secondary mirror.

The OTA will send roll error signals and secondary mirror position error signals to the SSM. The SSM will generate torques to reduce these error signals and maintain spacecraft pointing accuracy to  $\pm 4.85\ \mu\text{rad}$  ( $\pm 1\text{ arc sec}$ ).

The pitch, yaw, and roll error signals generated by the OTA will be converted to digital format before transmission to the SSM. Format details will be established during Phase B.

The SSM will forward to the OTA pointing control system commands to position star trackers and to insert velocity aberration corrections.

The SSM will furnish magnetic torquer assemblies to be mounted on the OTA. Operation of these assemblies is controlled by the ACS of the SSM.

## D. SSM/SIP Interfaces

1. Mechanical/Structural Interface. The SIP structural interface is primarily with the OTA; however, the SSM structural design will accommodate the combined requirements of the OTA and SIP.

Structural accommodations will be provided as needed to effect thermal and electrical compatibility between the SSM and SIP.

2. SSM/SIP Contamination Control Interfaces. The contamination control equipment on board the LST provides a class 10 000/100 000 particulate cleanliness and control of hydrocarbons to less than 15 ppm within the SIP/SSM. This design supplies clean air from the Shuttle with nonparticulate contaminants removed. This air is routed through an umbilical connected by the crew through the open hatch to the duct work installed in the SSM of the LST and then through HEPA filters to the SIP and the forward end of the SSM. This procedure provides the cleanest air to the most sensitive parts and then it flows outward to less sensitive regions. Air flow through the SIP is governed by valves which control the pressure so that approximately 0.5 m/sec (100 ft/min) flows through any opening in the SIP cowling.

3. SSM/SIP Thermal Interface. The electrical components contained within the SSM shall be as thermally independent from the SIP as practicable.

Excess heat energy generated within the SIP shall be dissipated to space through the SSM wall areas to which electrical components are not attached.

4. Pointing Control Interfaces. No pointing control interface requirements exist between the SSM and the SIP.

5. SSM/SIP Electrical Interfaces

a. Interface Implementation. The electrical interfaces between the SSM and the SIP are implemented in a manner similar to that for the OTA, as previously indicated by Figure VI-12. Because of the higher data and command requirements for the scientific instruments, the number of interface assemblies differs. Scientific data are also handled differently.

Two addressable RCDs, as described in Section C.4, are to be furnished by the SSM to the SIP. Each has the capability to receive 256 commands. Two additional RCDs are included in the SIP for redundancy.

Twelve DAUs will be furnished by the SSM to provide redundant channels for data.

Two basic EDUs are provided by the SSM for redundant access to power. These EDUs differ from those for the OTA because the 25-A input

module has not been included. The EDU for the SIP, therefore, will have a maximum power rating of 600 W. Each will have five separate, controlled power inputs rated at 5 A each.

b. Separable Connectors. The separable connectors for the electrical separation plane between the SSM and SIP will be attached to SSM cabling. This cabling will be routed near the RCDs, DAUs, and EDUs where interface mating occurs. Cables will have sufficiently free length to permit connection and tiedown after the SIP is installed on the SSM. Power cabling to the EDUs shall include five lines and five ground returns. One 39-line cable in the SSM will be allocated for SIP test and calibration. Routing of cables for scientific data is to be determined.

c. Requirements of SSM and SIP. The SSM shall supply power to the SIP in the form of 28 Vdc, regulated to  $\pm 2$  percent. The SSM shall be capable of furnishing to the SIP 2000 W-h over a 10-hour period with a maximum power capability of 500 W. The SSM shall have the capability to deliver 600-W peak power, not to exceed 15 sec. The SSM +28-V line shall be capable of withstanding a short circuit for 50 msec, as a minimum requirement.

Five separate return lines shall be provided. These will be used by the various separate load groups. High power or transient types of loads will be isolated from the more sensitive ones. Cabling will also have provisions for shielding and coax lines.

The SIP electronics shall be designed such that a single component failure will not cause a short circuit on the +28-V line. In the event of a short circuit, the short circuit condition shall be removed within 20 msec, otherwise, the EDU, or the ECA in the SSM, will remove it in less than 50 msec.

The SIP and the SSM shall conform to specifications given in Section B.2.

The SIP and SSM electronics shall be designed such that transient disturbances of greater than  $\pm 50$  V (such as inductive kickbacks) shall not be generated on the +28-V or ground return lines, and the duration shall not exceed 10  $\mu$ sec. Loads with repetitive transient characteristics will be filtered or suppressed to conform with conducted noise requirements specified. The steady-state noise level should not exceed 5 mV rms.

Each instrument and those mechanisms that are capable of being operated independently will be supplied commands and data services from the SSM via the RCDs and DAUs provided. Sufficient cabling for synchronization, message, and clock lines will be provided to the RCDs and DAUs to meet these requirements. The output modules of the EDUs in conjunction with the RCDs will provide "on-off" power switching commands. Outputs from remote units are to be routed as necessary by the SIP.

The SSM must be capable of accepting 3000 bits of diagnostic information from the SIP. Data for real time transmission will not exceed a rate of 51.2 kbits/sec. Data delivered to the SSM tape system will be recorded at 1.6 kbits/sec. The SSM must be capable of accepting  $10^8$  bits in the scientific data readout messages.

The SIP shall comply with interfaces established with the OTA and the SSM, and with system requirements and standards specified in Section B. The SIP must deliver status and diagnostic data to the DAUs provided. The SIP will condition signals with a 0- to 5-V level. The SIP must conform to the sampling and data rates specified for the SSM-DAUs.

The SIP must be capable of generating the necessary scientific data. The SIP will deliver data in the proper form for acceptance by the SSM communications subsystem.

The SIP must be capable of accepting decoded command messages furnished by the SSM via the RCDs and the scientific instrument controller. The SIP will supply output cables from the scientific instrument controller and will convert command signals into the form necessary for implementing the desired function.

## E. OTA/SIP Interfaces

1. OTA/SIP Optical/Physical Interface. A 2.9-mrad (10-arc min) field of view has been established as a design goal for the telescope to provide to the scientific instrumentation. This field size will cover most of the identified scientific objectives and can be achieved without the use of corrective refractive elements in the optical system.

The telescope field of view outside this central 2.9-mrad (10-arc min) field shall be used for fine pointing the telescope by means of guide stars near the target position. Detectors used for tracking guide stars should not infringe on the space near the focus needed by the scientific instruments.

The OTA will contain a main optics system that will deliver to a principal focus plane a near-diffraction-limited image over a 1.46-mrad (5-arc min) total field of view. The principal focus plane will be located 1.93 m (76 in.) behind the vertex of the primary mirror (Fig. VI-13). The plane will be flat to "TBD" millimeters and perpendicular to the telescope longitudinal axis to "TBD" milliradians.

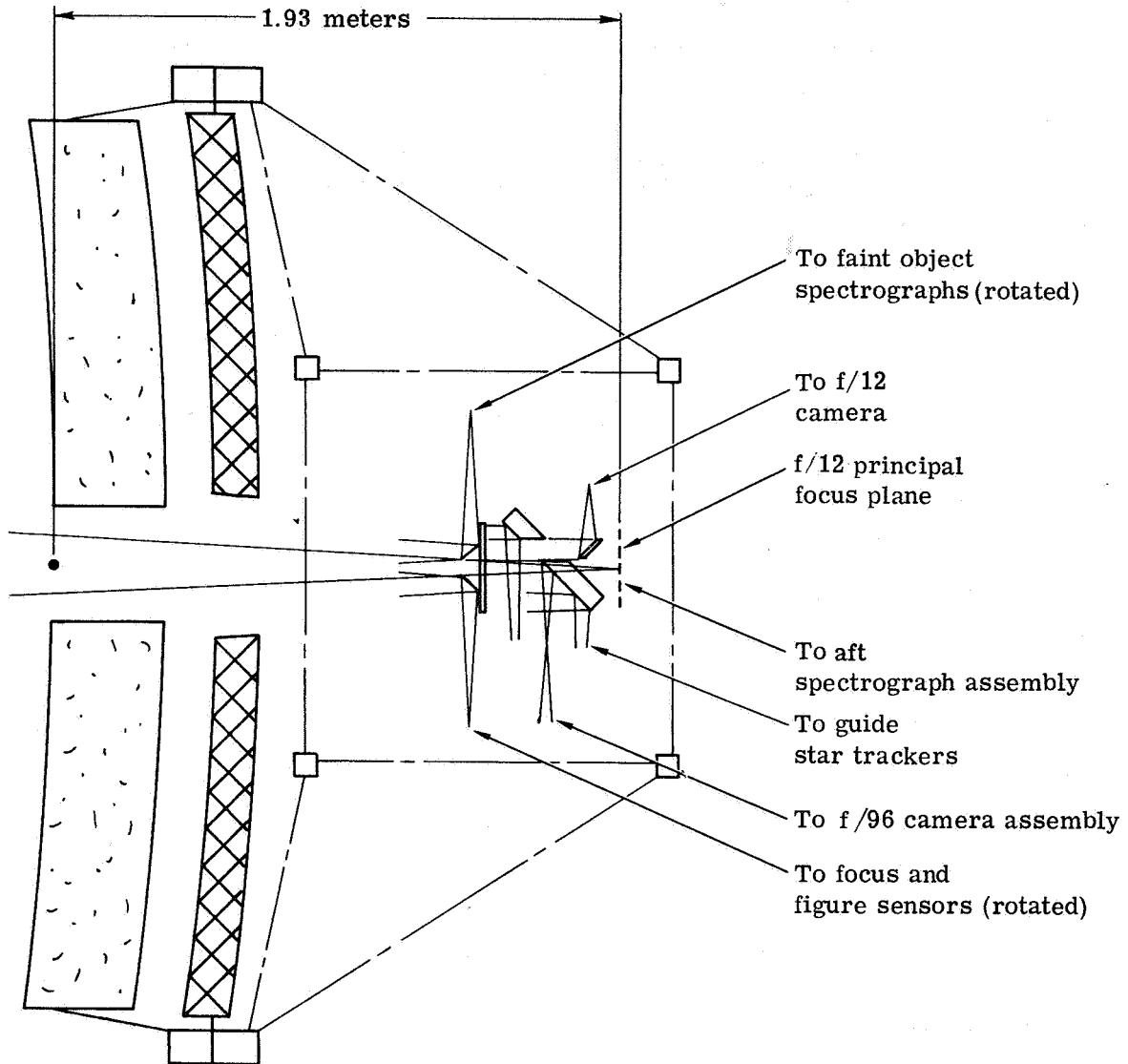


Figure VI-13. Location of f/12 image plane.



The OTA will utilize the telescope field of view from 4.6- to 7.0-mrad (16- to 24-arc min) diameter centered around the central 2.9-mrad (10-arc min) scientific data field for the fine guidance system.

The OTA will position a reflector to fold the guide field to a side area of the instrument compartment. The reflector will be centered 23.9 cm (9.4 in.) forward of the focal plane. The area behind the reflector will be available for SIP instruments.

The OTA will position small fold mirrors within the convergent data beam to route the beam to scientific instruments located within the forward section of the instrument compartment. The arrangement of these mirrors in the image plane will be as shown in Figure VI-14. The data beam for each instrument will be located as follows. The optical characteristics of each of these fold mirrors will be specified by the SIP to match the requirements of the associated instrument.

		Axial Position <sup>a</sup> , m (in.)	Radial Position <sup>b</sup> , rad (degrees)
Spectrograph, 0.22 to 0.66 $\mu\text{m}$	Station	1.43 (56.4)	3.93 (225)
Spectrograph, 0.66 to 1 $\mu\text{m}$	Station	1.43 (56.4)	2.36 (135)
Spectrograph, 1 to 5 $\mu\text{m}$	Station	1.43 (56.4)	5.50 (315)
f/96 Camera Assembly	Station	1.69 (66.6)	0 (0)
f/12 Camera Assembly	Station	1.82 (71.5)	3.14 (180)

- a. Relative to primary mirror vertex at station 0.0.
- b. View looking forward with guidance package at 0 degree.

The OTA will also position fold mirrors for a focus sensor and a figure sensor in the convergent data beam, as indicated in Figure VI-14. The data beam for these instruments will be located as follows.

		Axial Position, <sup>a</sup> m (in.)	Radial Position, <sup>b</sup> rad (degrees)
Focus Sensor	Station	1.43 (56.4)	0 (0)
Figure Sensor	Station	1.43 (56.4)	0.78 (45)

- a. Relative to primary mirror vertex at station 0.0.
- b. View looking forward with guidance package at 0 degree.

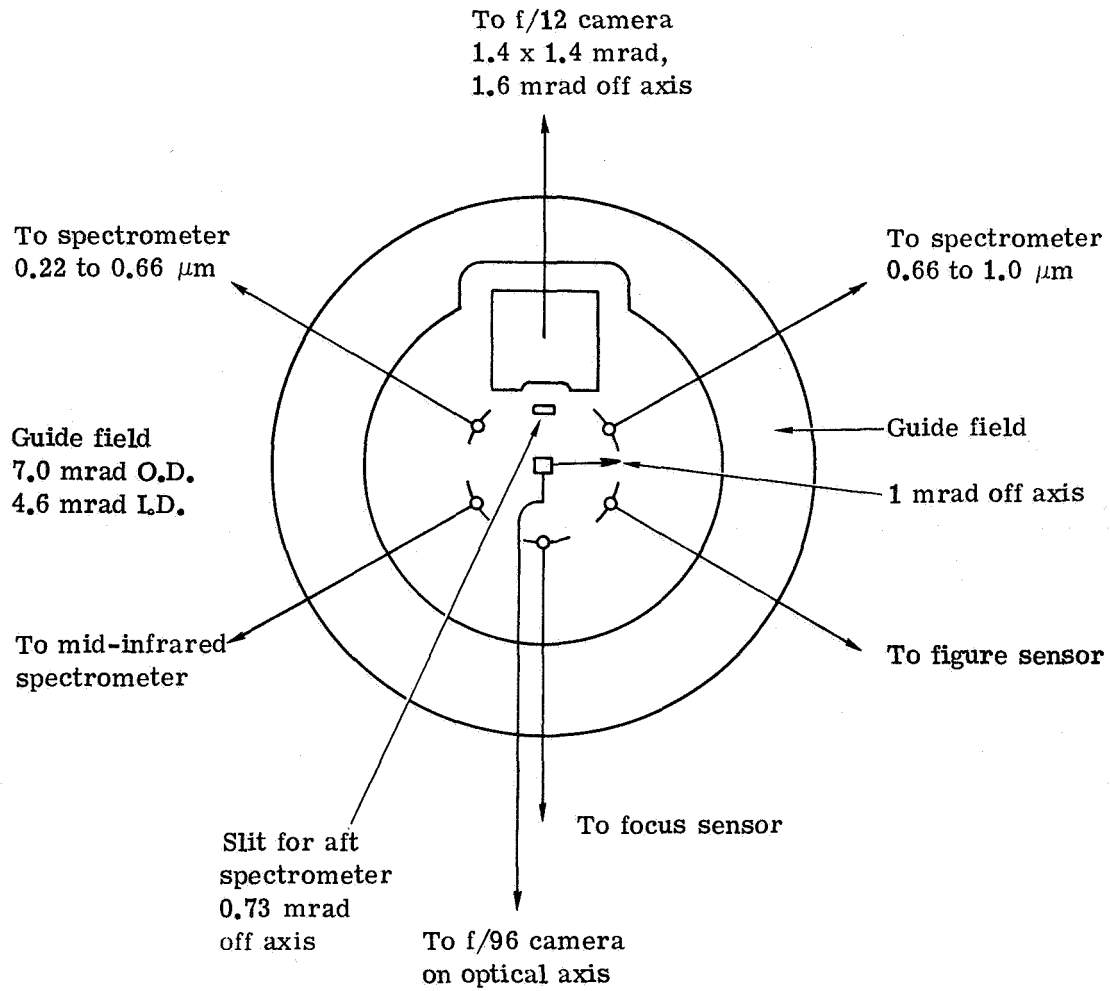


Figure VI-14. f/12 image plane arrangement schematic.

The SIP will mount an ultraviolet spectrograph assembly behind the principal focus plane, with the entrance slit mechanism centered 0.73 mrad (2.5 arc min) off axis at a radial position of 180 degrees.

The SIP will include a slit-jaw camera assembly on the OTA instrument truss. This assembly will view mirrors on the three spectrograph entrance slits.

The reticle plate of the OTA fine guidance assembly will contain lighted fiducial marks. The f/96 camera assembly of the SIP will utilize these marks to maintain alignment of the cameras with respect to the stellar target.

Each SIP instrument will contain all field stops, shutters, filters, and other modifications to the data beam needed by the instruments.

The OTA will include a protective device to prevent incoming light energy in excess of  $10^{-7}$  W/mm<sup>2</sup> at the principal focus from reaching the SIP.

The SIP will be designed to scatter a minimum of light energy back into the fine guidance system or OTA.

2. Structural Interfaces. The OTA will contain a structural assembly for the instrument compartment which will support OTA subsystem equipment and provide a mounting surface for installation of SIP instruments. This OTA instrument structure will be tied to the telescope primary ring for orientation reference. The position of the mounting surface of each instrument of the SIP will be controlled relative to the primary ring. The OTA instrument structure will include a mounting surface within the radial bay for each of the following instruments:

1. f/12 Camera
2. f/96 Camera Assembly
3. Faint Object Spectrograph, 0.22 to 0.66  $\mu$ m

4. Faint Object Spectograph, 0.66 to 1  $\mu\text{m}$
5. Mid-Infrared Spectograph, 1 to 5  $\mu\text{m}$
6. Slit-Jaw Camera Assembly

These mounting provisions will support each instrument centered over the folded optical axis for that instrument within  $\pm 0.4$  mm and the mounting surface plane will be perpendicular to the optical axis within 0.03 mrad (0.1 arc min) when the instruments are installed on the structure. The location of the optical axes are described in Section E.1.

The OTA instrument structures will include a mounting surface for an ultraviolet spectograph assembly containing two Echelle spectographs and a faint object spectograph, 0.115 to 0.22  $\mu\text{m}$ . This surface will be located 1.97 m (77.6 in.) aft of the primary mirror vertex and perpendicular to the telescope data beam axis within 1 arc min. The surface will not decenter more than 0.4 mm when the spectograph assembly is installed with the instrument structure in a horizontal position.

The baseline location of each instrument in the truss is shown in Figure VI-15.

The instruments of the SIP will not exceed the mass and center of gravity (CG) locations listed below.

	Mass, kg (lb)	CG Distance from Mounting Plane, cm (in.)
f/12 Camera	67.1 (148)	10.2 (4.0)
f/96 Camera Assembly	240 (530)	11.4 (4.5)
Faint Object Spectograph, 0.22 to 0.66 $\mu\text{m}$	45.4 (100)	10.2 (4.0)
Faint Object Spectograph, 0.66 to 1 $\mu\text{m}$	44.5 (98)	10.2 (4.0)
Mid-Infrared Spectograph, 1 to 5 $\mu\text{m}$	18.1 (40)	7.6 (3.0)
Slit-Jaw Camera	42.2 (93)	10.2 (4.0)
Ultraviolet Spectograph Assembly	173 (381)	63.5 (25)

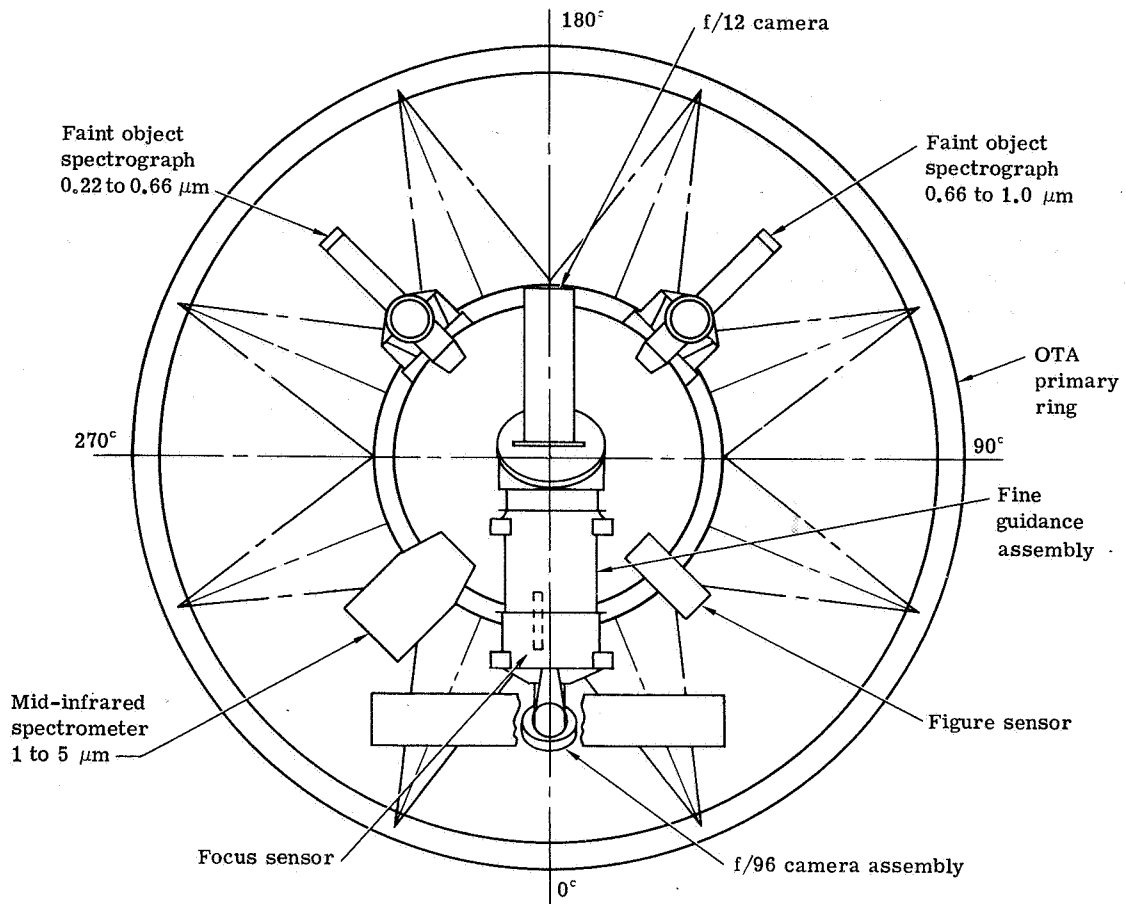


Figure VI-15. Instrument locations in SIP forward truss.

The mounting provisions for the f/96 camera assembly will be located on the fine guidance assembly. The mounting plane will be centered to 0.10 mm and perpendicular to the f/12 data beam routed through the fine guidance assembly to 2.9 mrad (10 arc min).

The coordinate system for the combined OTA/SIP instrument assembly is shown in Figure VI-16.

3. OTA/SIP Thermal and Environmental Interfaces. The interface between the OTA and the SIP, which exists at the pressure bulkhead just aft of the primary ring, is to be as adiabatic as practicable making use of insulation and low conductivity connectors.

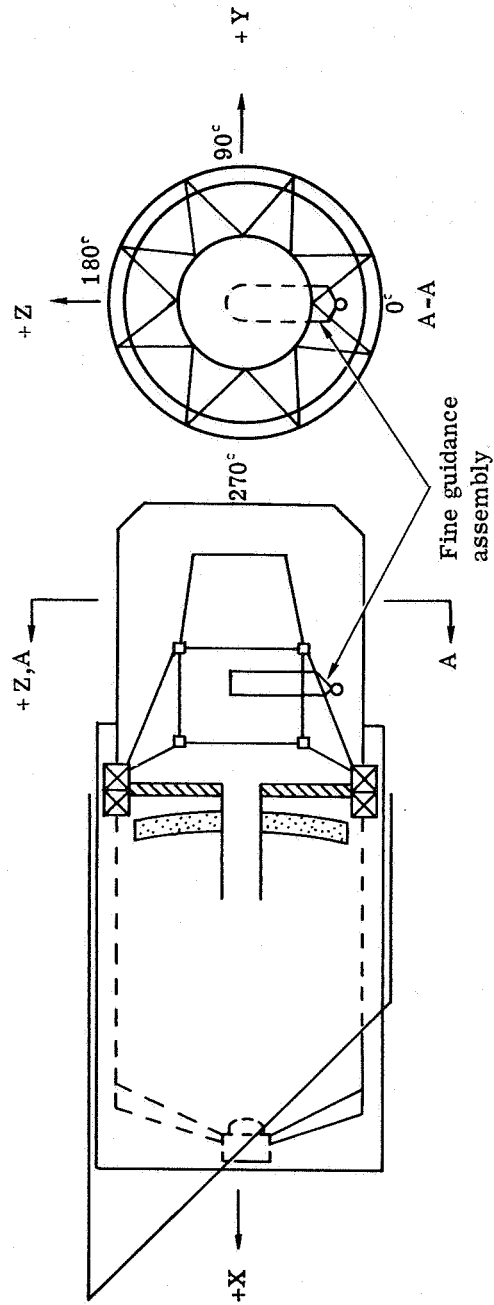


Figure VI-16. OTA/SIP coordinate system.

Both OTA and SIP equipment in the instrument compartment may be sources and recipients of contaminants of optical surfaces. All subsystems will exert design efforts to eliminate sources of contaminant substances.

4. Electrical Interfaces. There are no identified direct electrical connections required between the OTA and the SIP. Each assembly will interface directly with the SSM, which will have supervisory control of the electrical power and data handling circuits.

5. Pointing Control Interfaces. The SIP has no direct interfaces with the OTA image stabilization system that maintains the accuracy and stability of the f/12 image.

The SIP f/96 camera assembly will include a separate image correlation mechanism to maintain the position of a stellar target on the image tube relative to the positions of the guide stars being used for the f/12 image stabilization. This system will utilize fiducial marks on the guide head reticle plate.

6. Compatibility Tests. The OTA contractor will perform an optical beam quality test to verify that a collimated light source is focused the specified distance from the SIP mounting surface to  $\pm$ 'TBD' meters and a concentration instability of not more than 0.254 nm ( $1 \times 10^{-6}$  in.) rms during 10 hours of simulated closed loop operation (including focus sensor and fine pointing) in a temperature range from +19 to +23°C, with a total wavefront error of not more than 0.05  $\lambda$  rms as measured at 632.8 nm.

## F. Mission Control Operations Interface

This section identifies the requirements for support needed by the LST during the mission control operations phase of an LST mission.

These interfaces are principally with a mission control center (MCC) which will have control of the LST through a ground data network (GDN) and the SSM, which transmits data without alteration. Thus, the LST can be viewed as having direct interfaces with the MCC.

The MCC will transmit to the LST commands for setup and operation of all instruments and components to conduct a stellar observation program. The format will be suitable for digital transmission and storage and conversion to analog as needed within the LST.

The MCC will receive from the LST diagnostic data concerning status of the LST system. The MCC will process the data and display it for review by mission support personnel.

The LST will generate sufficient diagnostic data of systems performance to permit mission support personnel to monitor the health of the LST systems. The data will be in a format suitable for display and rapid interpretation.

The GDN will record the diagnostic data received from the spacecraft and transmit via a land line to the MCC with minimum delay.



## CHAPTER VII. LOW COST CONSIDERATIONS



# TABLE OF CONTENTS

	Page
A. Policy Statements and Trends . . . . .	VII-1
1. Design Phase . . . . .	VII-1
2. Implementation Phase . . . . .	VII-2
B. LST Reference Configuration Low Cost Features . . . . .	VII-2
C. Expendable Versus Maintainable LST Program Comparisons . . . . .	VII-16
D. Titan-and Shuttle-Launched LST Comparisons . . . . .	VII-20
1. Configuration . . . . .	VII-20
2. Constraints . . . . .	VII-20
3. Comparison . . . . .	VII-24
4. Low Cost Reference LST Design Summary . . . . .	VII-24
5. Low Cost LST Management Techniques . . . . .	VII-26
6. Low Cost Design Trades . . . . .	VII-26

## LIST OF ILLUSTRATIONS

Figure	Title	Page
VII-1.	Projected composite material costs . . . . .	VII-6
VII-2.	LST reference thermal control system . . . . .	VII-8
VII-3.	LST low cost analysis . . . . .	VII-17
VII-4.	LST flight sharing analysis . . . . .	VII-19
VII-5.	Titan and Shuttle configurations . . . . .	VII-21
VII-6.	LST payload effectiveness trades . . . . .	VII-28
VII-7.	LST payload effectiveness trades matrix . . . . .	VII-29
VII-8.	LST payload effectiveness trades examples . . . . .	VII-30

## LIST OF TABLES

Table	Title	Page
VII-1.	Relaxed System Performance Requirements . . . . .	VII-15
VII-2.	LST Configuration Comparisons . . . . .	VII-22
VII-3.	Titan and Shuttle Constraints . . . . .	VII-23
VII-4.	Effects of a Solid Mirror (Nonlight-Weighted) . . . . .	VII-25

## CHAPTER VII. LOW COST CONSIDERATIONS

### A. Policy Statements and Trends

Among the more recent policy statements on low cost approaches to the space program were those given by Dr. George M. Low, deputy administrator of NASA, at the Shuttle Sortie Workshop held at the Goddard Space Flight Center (GSFC) on July 31, 1972, and a symposium conducted by the National Security Industrial Association and Armed Forces Management Association in Washington on Aug. 16, 1972. Dr. Low's remarks were summarized in the "NASA Activities" publication, Vol. 3, No. 9, dated Sept. 15, 1972, and in the issue of Aviation Week and Space Technology dated Sept. 25, 1972. In these addresses, Dr. Low stressed the fact that NASA's budgetary constraints are very tight and apparently will remain so and that doing something about the high cost of doing business in space is today's biggest challenge. He stated that payloads have become more complex, while launch costs have come down and should continue to do so, particularly with the availability of the Shuttle. Consequently, we should now optimize our payloads for low cost and high reliability rather than for minimum weight and maximum performance. Dr. Low has visited several companies in various segments of the "consumer industry," where costs are a dominant factor, to investigate the applicability of their approaches to the space program and he believes that many of their approaches might be adaptable.

Dr. Low listed several principles of low cost design which are summarized below:

#### 1. Design Phase

1. Don't reinvent the wheel — use the best that is available from other programs.
2. Standardize — use common hardware modules at all levels of hardware complexity, where possible.
3. Design for low cost — involve production engineers in early phases of design to help lower production costs.
4. Design to minimize testing and paperwork — take advantage of reduced weight and volume constraints and use standard parts, larger margins, and larger safety factors.

5. Recognize that different systems can accept differing degrees of risk, and let the costs reflect the greater acceptance of risks where possible.

6. Know your costs — commercial firms, of necessity, have developed this area to a high degree.

7. Trade features for cost — many of our so-called "requirements" really are not that firm and should be stated as "goals" to be re-examined in terms of cost.

8. Pay particular attention to the very few high cost items and try especially to reduce costs in these areas.

## 2. Implementation Phase

1. Know your costs before you start — this perhaps is the most fundamental of all requirements.

2. Set firm cost targets — a firm and absolute cost ceiling should be established for each job.

3. Meet the established cost targets — we have to become more productive in one area if another area exhibits an "unavoidable" cost increase.

## B. LST Reference Configuration Low Cost Features

The LST reference configuration has already incorporated many of the low cost features mentioned herein. Some of the general low cost features in the LST reference are listed as follows with some suggestions of potential future cost reduction areas.

### 1. Present Features

a. Modularity/Standardization

b. Commonality with High Energy Astronomy Observatory

(HEAO)

- c. Maintenance with Shuttle
  - d. Shared Launches
  - e. Man-Rating Impacts Reduced
  - f. Apollo/Skylab "Man" Experience and Hardware
  - g. Intravehicular Activity (IVA) is Backup
  - h. Earth Return is Backup
  - i. Orbital Storage Mode
  - j. Large Margins and Safety Factors
  - k. Growth Potential
  - l. Low Manufacturing Costs
  - m. Reduced Test Program/Common Test Facilities
  - n. Maintenance at "Black Box" Level
  - o. Packaging Flexibility
  - p. Low Cost Design-Consciousness
2. Future (Potential) Considerations
- a. Commonality with Stratoscope
  - b. Reliability Requirements Decrease
  - c. Higher Risk Acceptance in Some Areas
  - d. Reduction in Instruments
  - e. Reassessment of High Cost Areas
  - f. Further Trades of Requirements for Cost

- g. Further Trades of Features for Cost
- h. Lower Materials/Components Costs
- i. Effects of Size Increase
- j. Improvements in Operations
- k. Further Trades of "Closing Loops" On-Orbit Versus On-Ground Concepts.
- l. Optimize Reliability/Maintainability/Mission Sharing

Some of the specific low cost features and future recommendations for the structures and thermal control systems are listed, respectively, as follows (see Fig. VII-1).

- 1. Present Low Cost Design Features of the LST Structure
  - a. Most of Structure is Aluminum
  - b. High Stability Graphite-Epoxy Optical Telescope Assembly/Scientific Instrument Package (OTA/SIP) Structure
    - (1) Permits mostly passive thermal control
    - (2) Reduces heater power requirements
    - (3) Reduces reliability/lifetime requirements of focus/adjust mechanisms
  - c. Reduces Sensitivities to Facilitate Temperature Fluctuations
  - d. Simple Construction
  - e. Materials/Development Commonality/with Other Programs



f. Standardized Sizes and Constant Cross Sections

- (1) Truss members
- (2) Skin panels
- (3) Stringers
- (4) Equipment mounting hardware
- (5) Aperture doors and mechanisms
- (6) Light shield extension/retraction mechanism

2. Future (Potential) Considerations

- a. Lower Materials Costs
- b. Commonality of Development with HEAO and Stratoscope
- c. Greater Margin
- d. Reduced Testing
- e. Greater Baffle Standardization

3. Present Low Cost Design Features of the LST Thermal Control System (TCS)

- a. Mostly Passive System
- b. 21° C Norminal Operating Temperature
  - (1) Grinding
  - (2) Testing
  - (3) Flight operations

- c. Modularity/Standardization
    - (1) Insulation
    - (2) Paint/coatings
    - (3) Louvers
    - (4) Thermal electric devices
  - d. Heater Power Requirements Minimized by High Stability Structure
  - e. Heat Dissipation Margins
    - (1) SIP — 200 W ( 50 %)
    - (2) Support Systems Module (SSM) 700 W (100%).
4. Future (Potential) Considerations
- a. Lower Materials/Components Costs
  - b. Longer Lasting, Less Degrading Paints/Coatings.

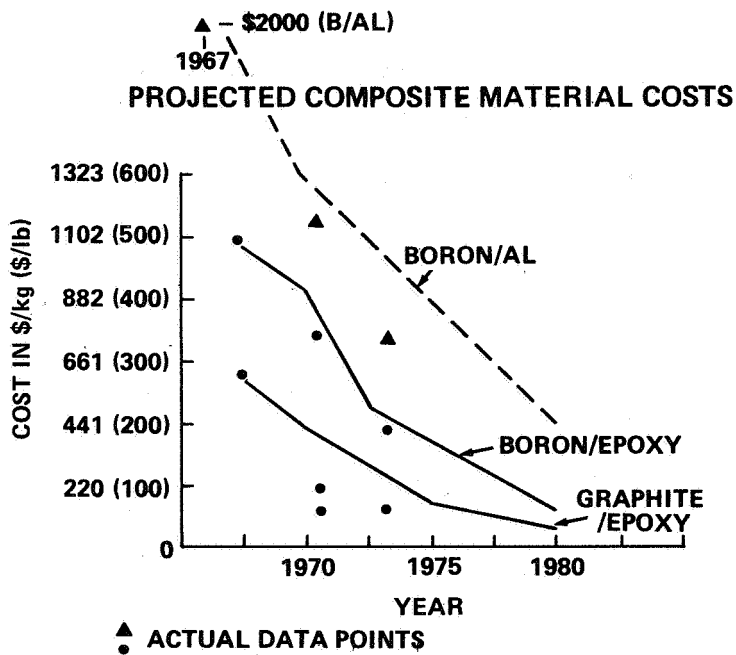


Figure VII-1. Projected composite material costs.

The following list and Figure VII-2 show the design margins in these two systems.

The margins/safety factors are

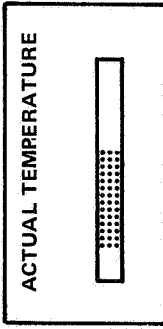
1. LST Structure Sized for 20 Percent Weight Increase Plus
  - a.  $1.4 \times$  Structural Loads (1.25 used in Skylab)
  - b.  $2.0 \times$  Pressure Loads (no cost here — sized by launch loads) (2.0 used in Skylab)
2. Micrometeoroid Protection (sized by paint flaking requirements)
  - a. 0.95 OTA for 5 years
  - b. 0.98 SSM for 5 years
  - c. 0.995 SSM for 5 days When Inhabited.

Design margins will help decrease costs by allowing reduced testing in some instances and a growth in the requirements placed on the systems.

Some of the low cost design features and future recommendations for the other LST systems are listed as follows. (The electrical system design could be more common with the HEAO, but since its load size made it more nearly equivalent to the Apollo Telescope Mount (ATM) and Skylab, it was decided to optimize it along hardware developments in these areas.)

1. Electrical System
  - a. Present Features
    - (1) Modularity/Standardization
      - (a) Solar panels
      - (b) Mechanisms
      - (c) Power distribution
      - (d) Batteries

	INSULATION	COATINGS	HEATERS	LOUVERS	PELTIER DEVICES
OTA	X	X	X		
SIP	X	X	X		
SSM	X	X	X	X	X



OTA

- PRIMARY MIRROR
- SECONDARY MIRROR
- OTA METERING STRUCT.
- SIP PRIMARY STRUCT.

SIP

- COLD PLATES & CAMERA OUTER SURFACES
- PHOTOCATHODES

SSM

- COMM
- DATA MGMT
- SOLAR CELLS
- BATTERIES
- ELECT. PWR
- AS&C

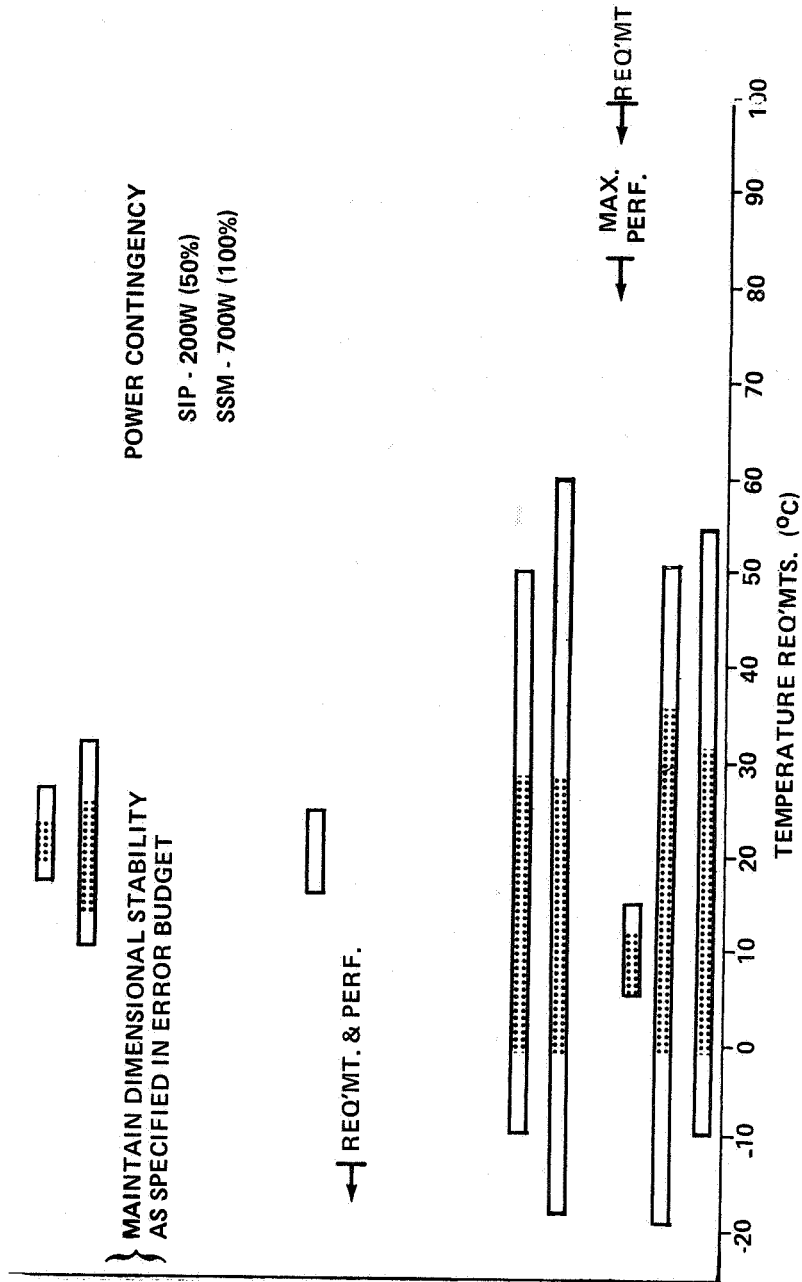


Figure VII-2. LST reference thermal control system.

- (e) Chargers
- (f) Regulators
- (g) Overload protection
- (2) Commonality
  - (a) HEAO hardware — 0 items (0 percent)
  - (b) Other program hardware — 12 items (26.7 percent)
  - (c) Modified HEAO hardware — 10 items (22.2 percent)
  - (d) New hardware — 23 items (51.1 percent)
- (3) Multiple Cross-Strapping and Remote Switching
- (4) Resettable Circuit Breakers
- (5) Standard 28 Vdc Distribution
- (6) Cylindrical Battery Cells
- (7) Rigid Solar Panels
- (8) One-Degree-of-Freedom Array Gimbals
- (9) Power Tracking Regulator/Charger Design
- b. Future (Potential) Considerations
  - (1) Greater Commonality
  - (2) Reliability Requirements Decrease
  - (3) Greater Risk Acceptance
  - (4) Longer Life Batteries

## 2. Communications and Data Management System

### a. Present Features

#### (1) Modularity/Standardization

- (a) Antennas
- (b) Transponders
- (c) Processor
- (d) Remote decoders
- (e) Remote multiplexers
- (f) Tape recorders
- (g) Control units
- (h) Clock
- (i) Software

#### (2) Commonality

- (a) HEAO hardware — 49 items (79 percent)
- (b) Other program hardware — 5 items (8.1 percent)
- (c) Modified HEAO hardware — 7 items (11.3 percent)
- (d) New hardware — 1 item (1.6 percent)

#### (3) Image Integration and Storage on Image Tubes

#### (4) Unified S-Band (USB) System and Ground Stations

#### (5) National Aeronautics and Space Administration Communications Network (NASCOM) Circuits

#### (6) Frequency-Diversity, Switched-Transmitter Communications

- b. Future (Potential) Considerations
  - (1) Commonality Increase
  - (2) Reassessment of High Cost Areas
  - (3) Further Trade of Requirements and Features for  
Cost
  - (4) Improvements in Space Tracking and Data Network  
(STDN) Data Rates and Coverage
  - (5) Improvements in Operations
  - (6) Further Data Relay Satellite Trades
  - (7) Further Trades of "Closing Loops" On-Orbit  
Versus On-Ground

### 3. Attitude Control System (ACS)

- a. Present Features
  - (1) Modularity/Standardization
    - (a) Reaction control system (RCS)
    - (b) Sensors
    - (c) Control moment gyros (CMGs)
    - (d) Transfer assemblies
    - (e) Processors
    - (f) Magnetic torquers
    - (g) Software

- (2) Commonality
  - (a) HEAO hardware, 18 items (47 percent)
  - (b) Other program hardware, 8 items (22 percent)
  - (c) Modified HEAO hardware, 2 items (6 percent)
  - (d) New hardware, 9 items (25 percent)

(3) Backup operational modes

(4) On-orbit storage mode

(5) Onboard magnetometer and computation

(6) Cold gas RCS

b. Future (Potential) Considerations

(1) Commonality increase

(2) Reassessment of high cost areas

(3) Further trades of requirements and features

for cost

(4) Further trades of closing loops on-orbit versus

on-ground

4. Telescope

a. Present Features — Modularity/Standardization

(1) Secondary mirror actuators

(2) Primary mirror actuators

(3) Alignment sensors



- (4) Alignment detectors
- (5) Focus detectors
- (6) Fine guidance mechanism
- (7) Processors
- (8) Pickoff mirrors
- (9) Low cost construction
- (10) Reduced testing

b. Future (Potential) Considerations

- (1) Reassessment of high cost areas
- (2) Further trades of requirements and features
- (3) Lower materials costs
- (4) Improved manufacturing techniques
- (5) Further reduction of testing

for cost

(6) Commonality of development with HEAO (structure) and stratoscope (structure, sensors, fine guidance, and image motion stabilization)

5. Instruments

a. Present Features

- (1) Modularity/Standardization
  - (a) Image tubes
  - (b) Fold mirrors
  - (c) Shutters and mechanisms

- (d) Filter wheels and mechanisms
  - (e) Processors
  - (f) Alignment guiderails
  - (g) Experiment quick-disconnect mounts
- (2) Low cost construction
  - (3) Reduced testing
  - (4) Data storage on image tubes
- b. Future (Potential) Considerations
- (1) Commonality of development with stratoscope  
(image tubes)
  - (2) Reassessment of high cost areas
  - (3) Consolidation of instruments
  - (4) Lower materials costs
  - (5) Further trades of requirements and features for cost.

A summary of some of the relaxed system performance requirements which allow cost savings is given in Table VII-1.

The  $1.01 \times 10^5$  N/m<sup>2</sup> (14.7 psi) atmosphere during maintenance allows flammability hazards to be no greater than those on the ground, thus permitting the man-rating costs to be significantly less than those on the Apollo and Skylab programs. The short lengths of time during which the LST would be inhabited on-orbit, compared with Apollo and Skylab, should also allow considerable reductions in some of the requirements for "man-rating."

TABLE VII-1. RELAXED SYSTEM PERFORMANCE REQUIREMENTS

Requirement Relaxed	Effect
<p>LST Data Per Time (for bright sources only)</p> <p>Heater Power for OTA/SIP Metering Structure (permitted due to high stability graphite-epoxy materials)</p> <p>RCS Requirements (permitted due to Shuttle availability and to LST orbital storage mode)</p> <p>Increased Structural Safety Factor (1.25 to 1.4)</p>	<p>Image buildup and storage on image tubes — eliminates external memory requirement (120 megabits to 1200 megabits).</p> <p>Heaters and heater power reduced by 200 watts. SIP TCS heat dissipation requirements reduced by 40 percent.</p> <p>Allows reduced quantity of hardware and propellant and use of cold gas RCS.</p> <p>Allows reduced testing and less sensitivity to design changes.</p>

An additional hazard-reduction feature of the LST is that the systems will be inactive during maintenance except for the subsequent check-out period during which the LST need not necessarily be inhabited since the checkout consoles are located in the Shuttle. These factors plus the shirt-sleeve environment allow the use of standard quick-disconnect electrical connectors and mounting fasteners, rather than expensive man-rated types of hardware.

### C. Expendable Versus Maintainable LST Program Comparisons

The most significant cost-saving feature of the LST program is the ability to utilize the Shuttle for maintenance rather than having to launch expendable LSTs on expendable launch vehicles to achieve the full mission lifetime of 10 to 15 years. This effect is shown in Figure VII-3, where the cost in "equivalent" LSTs and launch vehicles is shown for a 15 year mission. Assumptions were made that the Shuttle maintenance flights would be shared with Tug missions and that the average flight-shared Shuttle cost to the LST program would be 34 percent of the full Shuttle cost. It was also assumed that the LST would receive a 20 percent update during on-orbit maintenance and a 40 percent update during an earth-return refurbishment. The percentages of update include a considerable margin, based on initial assessments of spares required for a "typical" maintenance mission.

The effect of the loss of science during downtimes has not been accounted for in this comparison but should be done so in later assessments. The value of the loss in science is difficult to weigh. It may be that the costs of downtime for science should not be weighed as heavily as costs which are more tangible, at least as long as the downtime remains only a fairly small portion of the overall mission time. Other effects which have not been accounted for are the benefits of utilizing the initial LST (in the two-payload maintainable LST case) for a ground observatory and for flight spares for the second LST National Astronomical Space Observatory (NASO).

The two payload case offers at least two significant advantages over the one payload cases:

1. Should the initial LST have difficulty meeting cost, schedule, or performance requirements, the requirements might be relaxed rather than implementing costly corrective action if there is a second LST which can achieve the requirements with less impact.
2. Should a catastrophic failure occur on the first one, the program would not suffer as much if there were two LSTs.

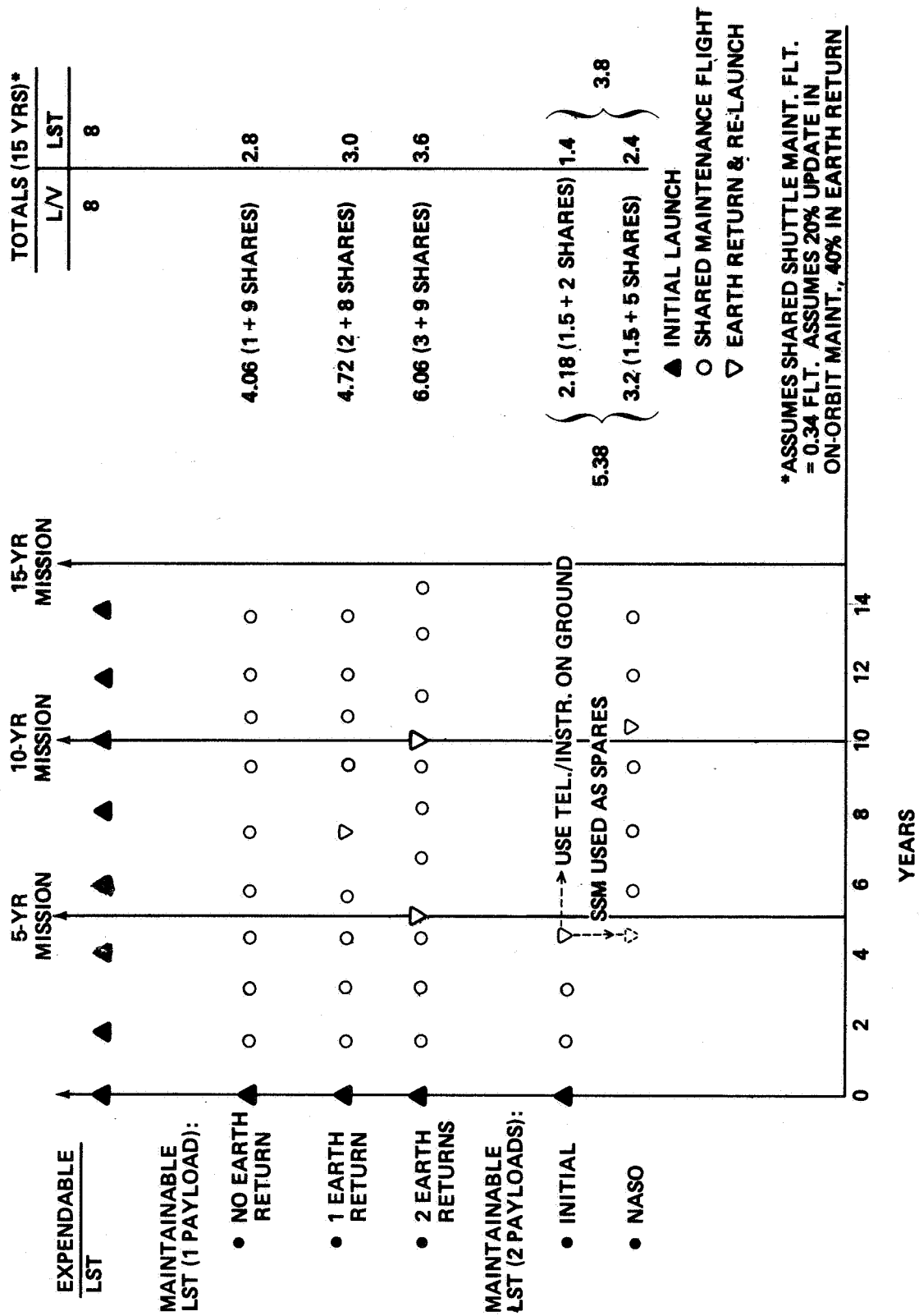


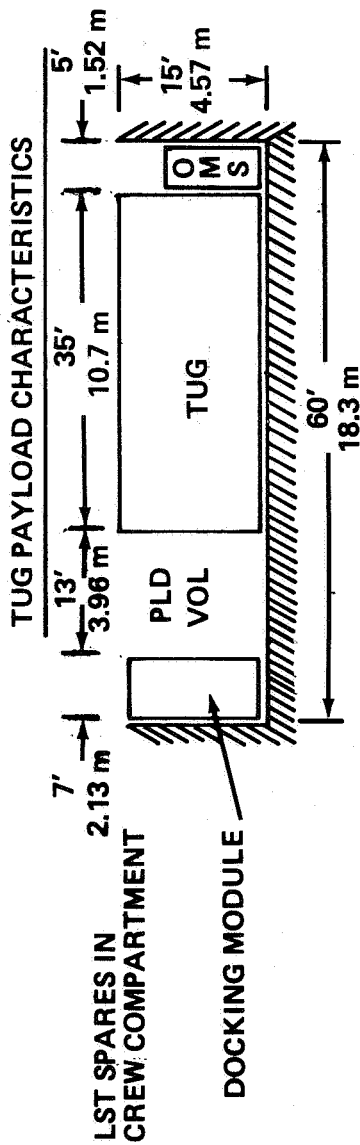
Figure VII-3. LST low cost analysis.

Figure VII-4 shows some of the rationale used in determining the degree of flight sharing of the LST with other payloads. A typical LST maintenance mission load is shown as 7474 kg (16 478 lb) including the orbital maneuvering system (OMS) propellant and docking module. It was assumed that the Tug and LST hardware together would utilize all of the 29 484 kg (65 000 lb) Shuttle capability. The cost to the LST on a weight pro-rata basis would then be about 25 percent of the cost of a Shuttle flight. A factor of 34 percent was utilized in this assessment to provide some margin. Figure VII-4 also shows that the ability of the LST to share flights with other mission hardware is very sensitive to the weight of the LST maintenance mission load. With the LST load shown, the largest Tug payload which could be accommodated is 485 kg (1070 lb), which is less than the 745 kg (1639 lb) "average" Tug payload. Hence, LST maintenance flight weights should be reduced, if possible, to allow greater flexibility in flight sharing, thereby reducing costs.

Launch frequency for the expendable LST cases was set at 2 years since HEAO-C component designs were used in many cases and provided a high reliability for 2 years. The systems have a fairly high probability of operating successfully for longer than 2 years but performance would probably be degraded, particularly of the science instruments. For this assessment, the comparison was made at the undegraded performance lifetime limit of the LST. For the maintainable LST, the design was for a high reliability at the end of 1 year, and differences in redundancy between the 1 year and 2 year cases were identified. Although the high reliability lifetime for the maintainable cases is for 1 year, the launch frequency was set at 1 1/2 years, since the Shuttle launch should be more reliable than the Titan and the Shuttle allows on-orbit checkout and emergency repair after release in orbit, providing a higher initial reliability of the maintainable LST.

This comparison should be extended to assess the impacts of various launch frequencies, the payload design complexity factors for LSTs of different lifetimes, and program cost factors. It is anticipated that the cost data, when plotted against years, will show a minimum somewhere between 1 year and 4 years for each case, with the launch vehicle costs driving more strongly in the cases of higher launch frequency and payload costs driving more strongly in the cases of lower launch frequency.

Commonality with existing hardware is another major area of cost savings. In comparing the difference in redundancy between the expendable (1 year) LST and the maintainable (2 years) LST, it was found that there



MINIMUM	AVERAGE	MAXIMUM
(300#), (7') 136 kg 2.13 m	(2,835#), (14.6') 1286 kg 4.45 m	(18,891#), (32') 8569 kg 9.75 m
(300#), (7') 136 kg 2.13 m	(1,639#), (13.2') 743 kg 4.02 m	(3,545#), (25') 1608 kg 7.62 m

ALL TUG PAYLOADS -----

SYNC. ORBIT TUG PAYLOADS -----

**LST MAINTENANCE MISSION WEIGHT:**

1124 kg ( 2,478 LBS) SPARES  
 5443 kg (12,000 LBS) OMS  
 907 kg ( 2,000 LBS) DOCKING MODULE  
**TOTAL 7474 kg (16,478 LBS)**

SHUTTLE PAYLOAD CAPACITY = 29484 kg ( 65,000 LBS)  
 -7474 kg (-16,478 LBS)  
 PAYLOAD AVAILABLE FOR TUG + PAYLOAD = 22010 kg ( 48,522 LBS)  
 TUG WITH PROPELLANT = -21509 kg (-47,452 LBS)  
**MAXIMUM DELIVERABLE EQ. SYNC. PAYLOAD = 485 kg (1,070 LBS)**

Figure VII-4. LST flight sharing analysis.

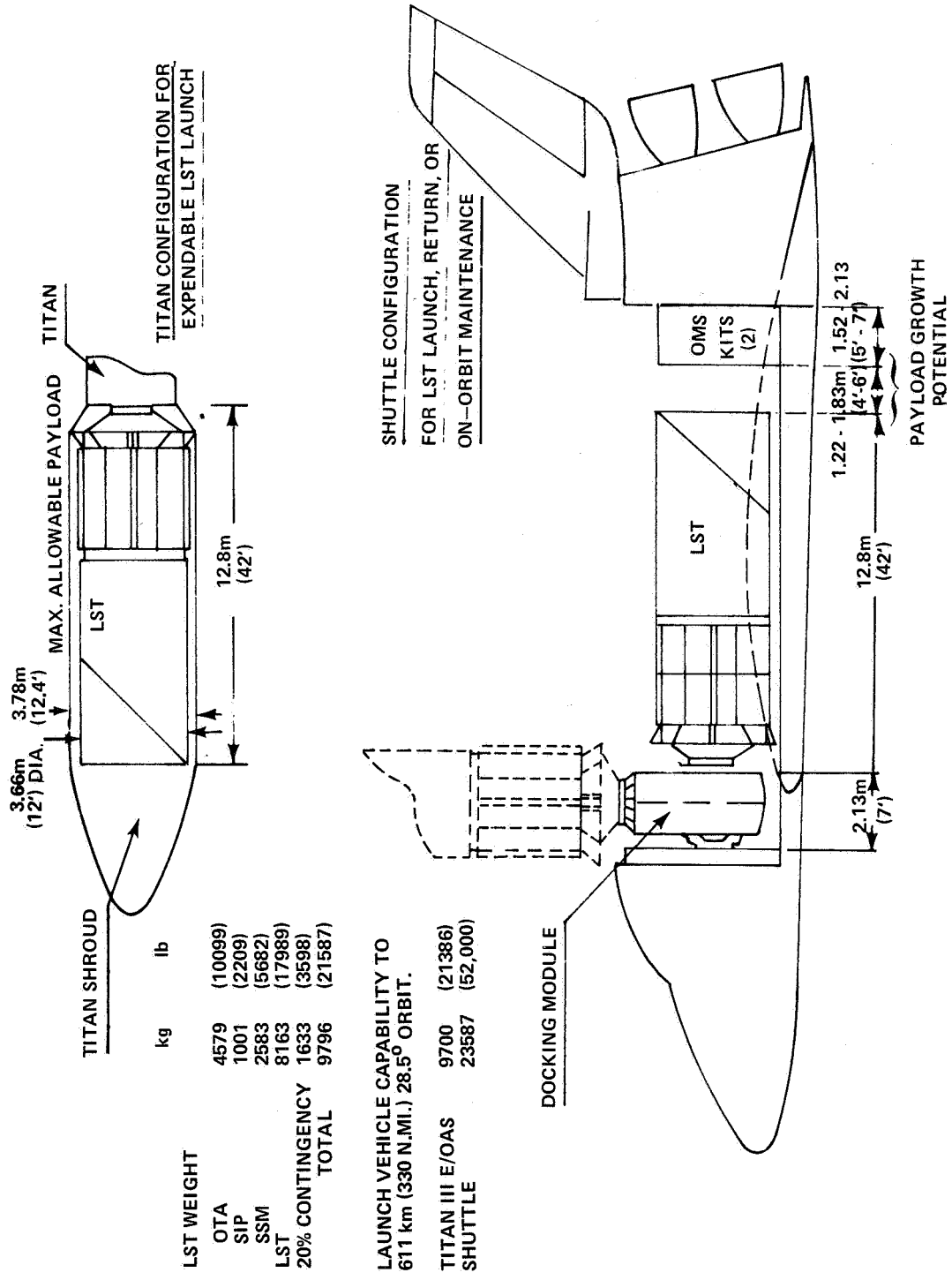
was little significant difference. The primary reason for this is that several factors help determine the quantity of redundancy required, some of which become more dominant than the reliability factors at shorter lifetimes. The principal factors for determining redundancy quantity in the LST are lifetime, reliability, single-point failure criteria, and commonality with other program hardware. This latter factor became more dominant in the shorter lifetime cases. Hence, reduction in reliability and/or lifetime made possible by the Shuttle will provide cost savings, but these will be second-order effects compared with the savings the Shuttle provides in allowing maintenance on the LST.

## D. Titan- and Shuttle-Launched LST Comparisons

1. Configuration. Figure VII-5 depicts the reference LST design installed in the Titan and in the Shuttle. Lengths, diameters, and masses can be seen also in this figure. It can be seen that the Shuttle provides room for growth in each of these areas. There appears to be a trend, however, to charge more of the Shuttle payload provisions to the payload space (such as the addition of the docking module to the cargo bay), which decreases the allowable payload growth. The LST design must continue to retain some margin for such events because the Shuttle is in a definition period itself at the present time. The docking module would be required on a maintenance visit and would probably be required on an initial launch since the capability to perform emergency repairs before release to orbit is one of the more important advantages of the Shuttle in launching payloads. Also, even if the LST did not require the docking module on initial launch, the desire to share Shuttle missions with other payloads would probably require the docking module to be available for maintenance or servicing of other payloads during this same mission. The OMS propellant tank is required in the bay in order for the Shuttle to achieve the 611 km (330 n. mi.) LST orbit with its payload. A tabulation of the masses of the two configurations is shown in Table VII-2. There is a net savings of about 563 kg (1241 lb) for the expendable LST.

2. Constraints. A tabulation of the major Titan and Shuttle constraints on the LST design is provided in Table VII-3. The Shuttle constraints are separated into launch and maintenance columns. The biggest relief provided by the Shuttle is in the area of payload mass. Since it is believed that the reference LST is near optimum in its present configuration, it is not clear that it would benefit significantly from this relief of constraints, but this must be investigated further. Two examples of such relief in the area of mass increases





TITAN SHROUD	
	MAX. ALLOWABLE PAYLOAD
	LST
	TITAN
	TITAN CONFIGURATION FOR EXPENDABLE LST LAUNCH

LST WEIGHT		
	kg	lb
OTA	4579	(10099)
SIP	1001	(2209)
SSM	2583	(5682)
LST	8163	(17989)
20% CONTINGENCY	1633	(3598)
<b>TOTAL</b>	<b>9796</b>	<b>(21587)</b>

**LAUNCH VEHICLE CAPABILITY TO 611 km (330 N.M.I.) 28.5° ORBIT.**

TITAN III E/OAS SHUTTLE	9700	(21386)
	23587	(52,000)

Figure VII-5. Titan and Shuttle configurations.

TABLE VII-2. LST CONFIGURATION COMPARISONS

Consideration	Reference LST Configuration	Expendable LST Configuration
SSM Reliability	0.95 @ 1 Year	0.95 @ 2 Years
Δ Weight		
Systems Redundancy	-	73 kg ( 161 lb)
Docking Hardware	-	-182 kg (- 400 lb)
Contamination Protection (during maintenance)	-	-195 kg (- 429 lb)
Bulkhead and Pressure Hatch	-	-154 kg (- 338 lb)
Micrometeoroid Protection	-	-45 kg (- 100 lb)
Human Factors	-	-61 kg (- 135 lb)
Total	-	<u>-563 kg(-1241 lb)</u>
Total LST Weight <sup>a</sup>	9796 kg (21 587 lb)	8703 kg (19 186 lb)
"Typical" Maintenance Load		-
Spares and Science Update	665 kg (1465 lb)	
Maintenance Support Equipment	<u>460 kg (1014 lb)</u>	
Total	1125 kg (2479 lb)	

a. Includes 20 percent contingency.

TABLE VII-3. TITAN AND SHUTTLE CONSTRAINTS

Constraint	Titan Launch	Shuttle Launch	Shuttle Maintenance
Launch Loads	1.5 g Lateral 6 g Longitudinal	1.3 g Lateral 3.25 Longitudinal	Same as Shuttle Launch Plus 3.5 g Lateral (reentry) 1 g Longitudinal (reentry)
Orbit	611 km (330 n. mi.) (for 5-year life) 28.5 degree Inclination [for Manned Space Flight Network (MSFN) coverage and maximum payload]	Higher or Lower Altitudes and Inclina- tions Available	Same as Shuttle Launch <sup>b</sup>
Reliability/Lifetime	High	Less	Still Less
Size	Weight 9700 kg (21 386 lb) Diameter 3.66 m (12 ft) Length 12.8 m (42 ft)	23 587 kg (52 000 lb) <sup>a</sup> 4.27-4.57 m <sup>a</sup> (14-15 ft) <sup>a</sup> 14-14.6 m (46-48 ft) <sup>a</sup>	Same as Shuttle Launch <sup>b</sup>

a. No strong driver to push the present design towards these limits.

b. Ultimate constraints exist but maximum-payload orbit parameters will enhance flight sharing and smaller spares sizes will enhance maintenance/logistics.

were investigated. An aluminum metering structure with a passive thermal control and thermal stability (orbital transients) equivalent to the present graphite-epoxy structure would have a mass of 10 614 kg (23 400 lb) compared with 82 kg (180 lb). An aluminum metering structure lighter than this could be built but would require an active TCS at some point down the weight scale. The high thermal stability provided by the graphite-epoxy structure allows a savings in electrical heater power (~200 watts) and in heat dissipation area (40 percent). The effects of not light-weighting the primary mirror are tabulated in Table VII-4.

3. Comparison. The major advantages of the Shuttle over the Titan are summarized as follows:

1. Launch Mode
  - a. Less risk (higher reliability launch).
  - b. Checkout and emergency repair or return after release in-orbit.
  - c. Some relief from Titan physical constraints.
2. Maintenance Mode
  - a. More efficient utilization of high cost payload hardware.
  - b. Shared flights — reduced costs per pound to orbit.
  - c. Capability to react quickly — less downtime for science.
  - d. Reduced reliability required in payload design.

4. Low Cost Reference LST Design Summary. The primary conclusions from the low cost assessment of the reference LST design are summarized as follows:

1. The present LST design has many low cost features.
2. Primary contributors to LST low cost are
  - a. Commonality with existing hardware.
  - b. Shuttle maintenance.

TABLE VII-4. EFFECTS OF A SOLID MIRROR (NONLIGHT-WEIGHTED)

120-in. Mirror	Estimated Deflection [ $\mu\text{m}$ ( $\mu\text{in.}$ ) ] ( $\lambda$ )	Weight [kg (lb)]	Figure of Merit (stiffness-to-weight)
Solid Mirror (edge-supported)	4.01 (158) 7.3	9253 (20 400)	0.03
Light-Weighted Mirror (hexagonal cavities, ring-supported at edge)	2.39 (93.9) 5.3	1474 (3 250)	0.03

- SSM structure weight would increase 350 lb.
- Structure would be 33 percent more complex because of additional shear distribution members.
- Mirror would exhibit low stiffness-to-weight ratio.
- More mirror deflection because of its own weight; therefore, more change in contour in 0 g.
- More problems in ground handling, grinding, testing, etc., because of greater weight and greater deflection in 1 g.
- Increased cost in handling, grinding, and testing and a more difficult on-orbit control of mirror contour will offset savings realized from not light-weighting.

3. The primary advantages provided to the LST by the Shuttle are
  - a. Maintainability.
  - b. Lower risk.
4. Secondary advantages provided to the LST by the Shuttle are
  - a. Some decrease in redundancy.
  - b. Larger margins in size and weight.
5. Titan backup for initial LST launch does not significantly constrain the present LST design.
6. These same areas must be reassessed and the conclusions reevaluated in phase B.

5. Low Cost LST Management Techniques. Specific techniques, check points, etc., must be included in the technical management and programmatic management areas to insure that a continuous and effective low cost effort is accomplished and that a low cost LST results from this effort. Some of the techniques which are applicable are

1. Select proper low cost evaluation criteria.
2. Provide cost visibility early to the work breakdown structure level or lower.
3. Establish cost targets to the work breakdown structure level or lower.
4. Establish the organizational responsibilities for costs.
5. Schedule cost reviews as part of design reviews for check points.

6. Low Cost Design Trades. During subsequent phases of the study, an approach which trades overall LST performance against program costs and scientific value must be pursued. The cost versus LST performance trades alone are not sufficient; the science value impacts must be utilized to help determine the real effect of trading performance for cost.

Figure VII-6 shows typical elements of such a trade. Figure VII-7 shows a matrix of the trades at three different levels of design complexity. Optimization across categories and within categories must be made at each level. Figure VII-8 shows examples of data which would be the output from such trades.

Some such approach could insure optimization of the LST for the three basic trades categories of cost, performance, and science value.

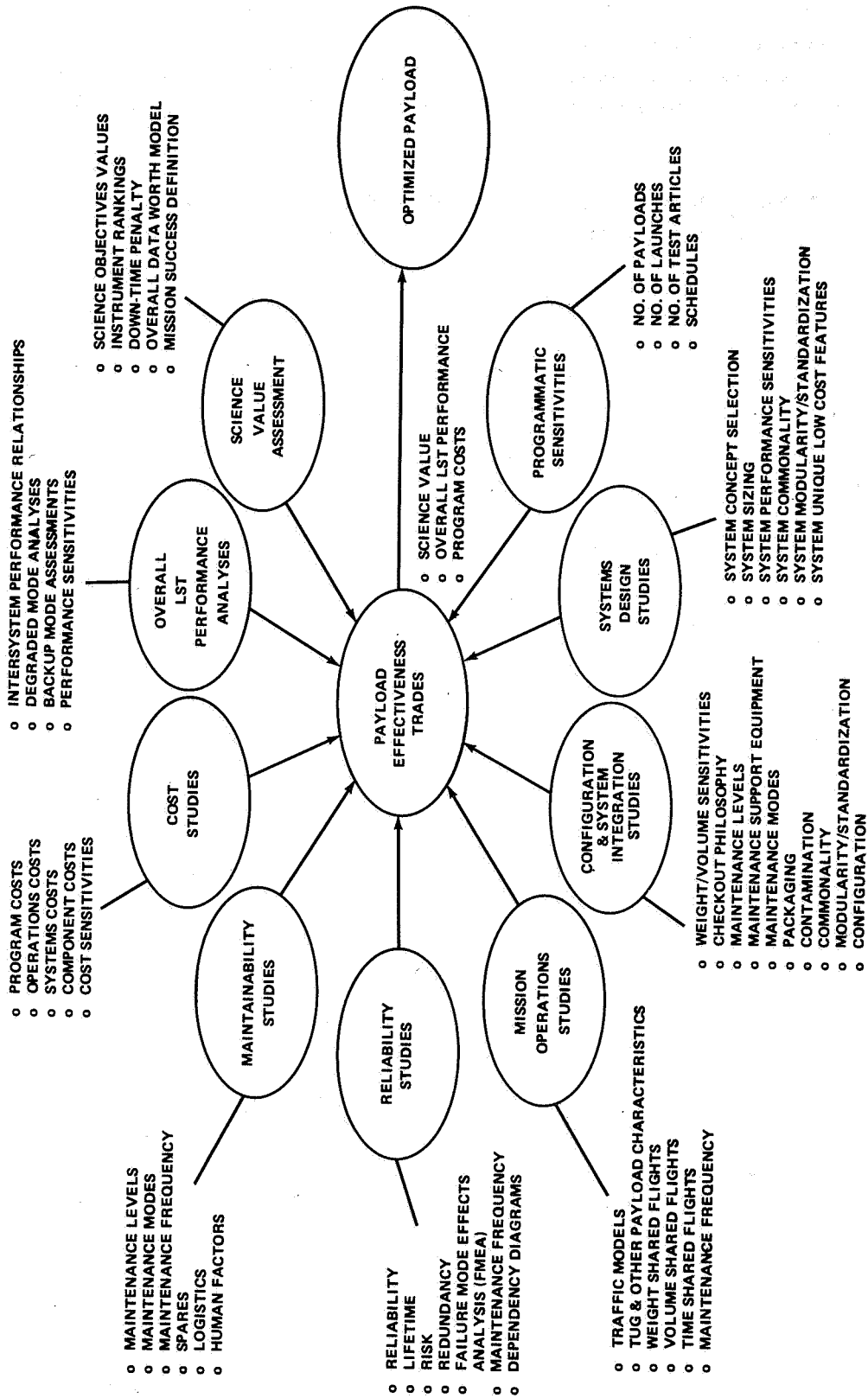


Figure VII-6. LST payload effectiveness trades.



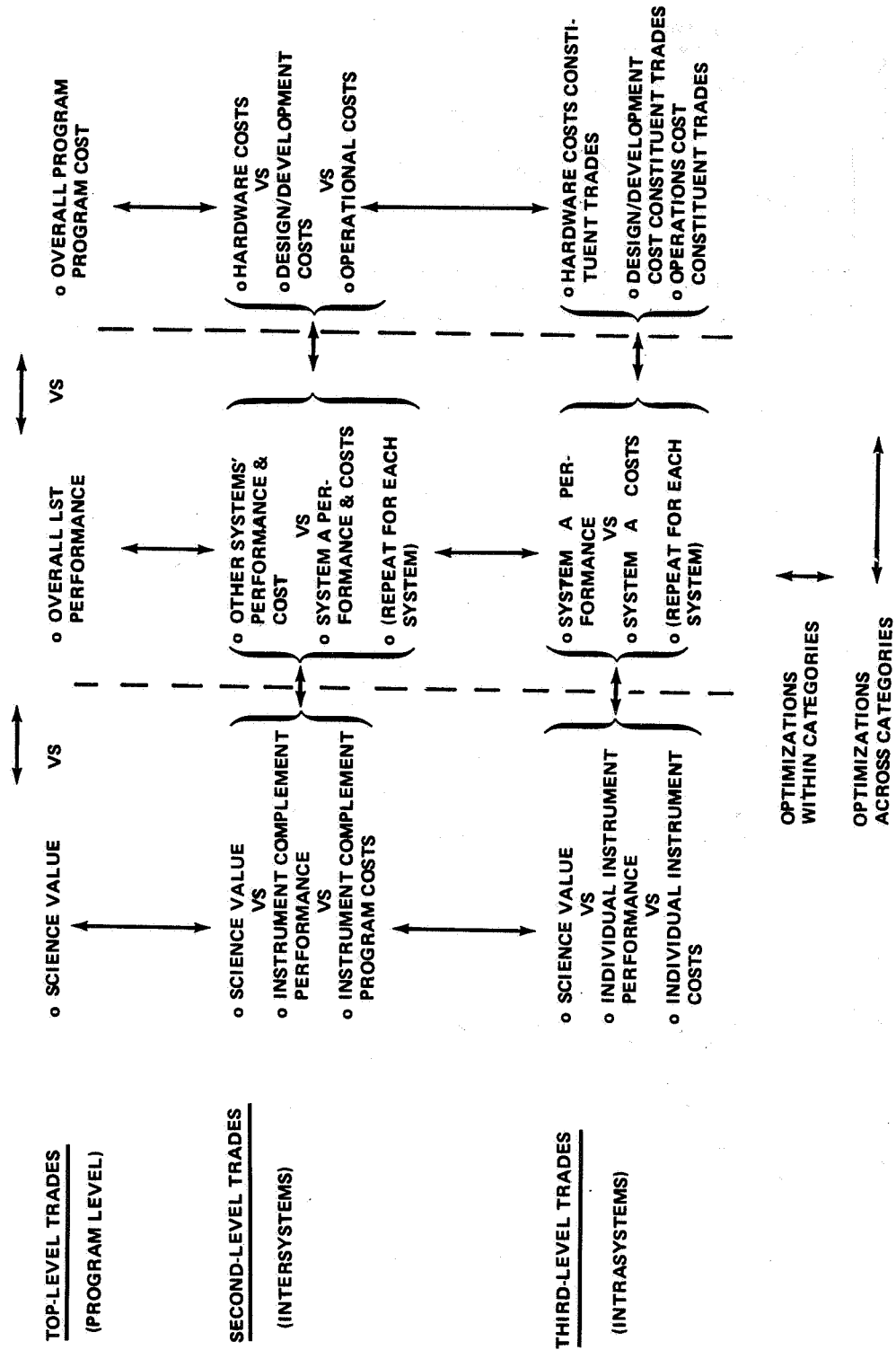
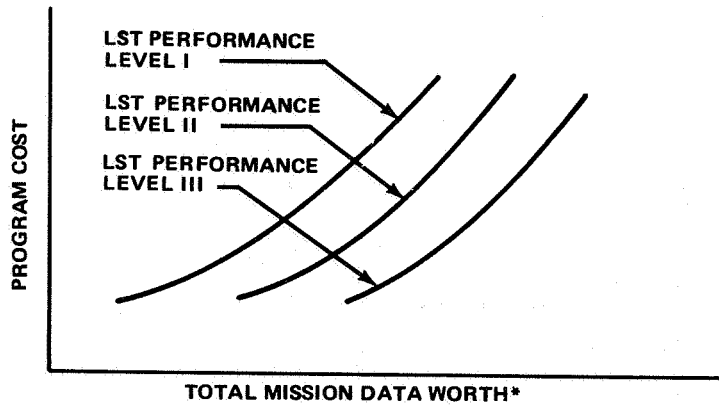
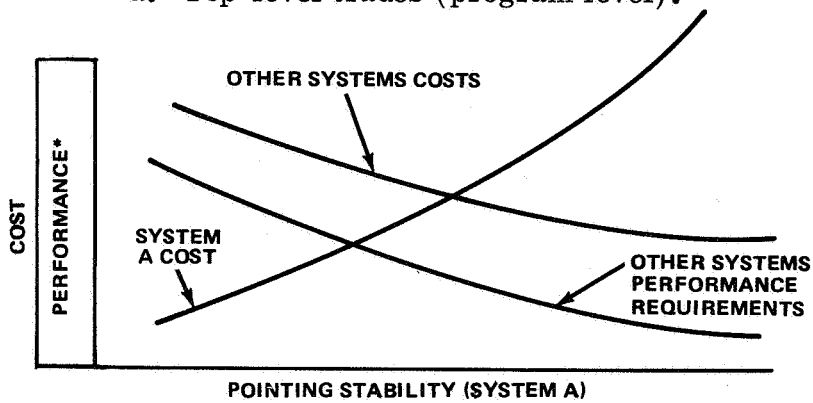


Figure VII-7. LST payload effectiveness trades matrix.



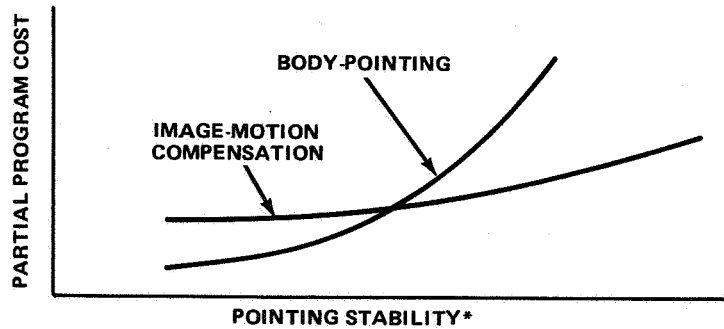
\*Value of data x quantity of data returned (includes degradation probabilities).

a. Top-level trades (program level).



\*Performance expressed in terms of effective image resolution, point spread function, modulation transfer function, and /or star magnitude capability per unit time, etc.

b. Second-level trades (intrasystems).



\*Parametrize for various slew rates.

c. Third-level trades (intrasystems).

Figure VII-8. LST payload effectiveness trades examples.

## CHAPTER VIII. PROGRAM IMPLEMENTATION



# TABLE OF CONTENTS

	Page
A. Introduction . . . . .	VIII-1
B. Project Elements . . . . .	VIII-2
1. Ground Test and Flight LSTs . . . . .	VIII-2
2. Science Instruments . . . . .	VIII-2
3. Optical Telescope Assembly . . . . .	VIII-3
4. Support Systems Module . . . . .	VIII-3
5. Integration and Test . . . . .	VIII-3
6. Thermal Optical Test Facility . . . . .	VIII-3
C. Phased Project Plan . . . . .	VIII-4
D. Project Flow and Schedules . . . . .	VIII-4
1. LST Project Functional Flow Chart . . . . .	VIII-5
2. LST System/Subsystem Functional Flow Diagrams . . . . .	VIII-6
a. OTA Manufacturing and Test Flow Plan . . . . .	VIII-6
b. SSM ACS Design, Verification, and Delivery Flow Charts and Schedule . . . . .	VIII-7
c. SSM Structures Flow Chart . . . . .	VIII-7
d. SSM Thermal Control Flow Chart . . . . .	VIII-7
e. Maintenance Mode Model . . . . .	VIII-7
f. LST Maintenance Support Activities . . . . .	VIII-7

# LIST OF ILLUSTRATIONS

Figure	Title	Page
VIII-1.	LST program schedule . . . . .	VIII-8
VIII-2.	LST project functional flow chart . . . . .	VIII-9
VIII-3.	Project milestones . . . . .	VIII-11
VIII-4.	OTA manufacturing and test flow plan . . . . .	VIII-12
VIII-5.	LST/SSM ACS design, verification and delivery flow chart . . . . .	VIII-13
VIII-6.	ACS preliminary schedule . . . . .	VIII-14
VIII-7.	LST RCS design, verification and delivery flow chart . . .	VIII-15
VIII-8.	SSM structures flow chart . . . . .	VIII-17
VIII-9.	SSM thermal control hardware flow chart . . . . .	VIII-19
VIII-10.	Maintenance mode model . . . . .	VIII-20
VIII-11.	LST maintenance support activities . . . . .	VIII-21

## CHAPTER VIII. PROGRAM IMPLEMENTATION

### A. Introduction

The LST program will be implemented through the accomplishment of a planned sequence of project activities. Preceding sections of this report have described the LST mission objectives and constraints and the planned mission and system characteristics and capabilities. This chapter will outline how these capabilities are to be developed, tested, and then utilized during operational activities. The various tasks and activities are briefly described and time phased.

Implicit in the functional flow chart shown later is the philosophy of the design and development of the optical telescope assembly (OTA) by one contractor, the support systems module (SSM) by a second contractor, and the science instruments (SIs) by a third contractor. Integration could be performed by the SSM contractor or by a NASA center. The electrical/electronic interface units, analogous to those interfacing internal SSM subsystems, would be supplied by the SSM contractor to the OTA/SI contractors to reduce the duplication of design, fabrication, and test efforts among the three contractors and to reduce the variety of maintenance spares required. Two concepts for the division of the design effort between the OTA and SI contractor have been considered, one where the SIs are integrated into a package before being integrated with the OTA and one where the SIs are developed on an individual instrument basis.

From the technical and cost viewpoint, the concept where the OTA contractor interfaces at the individual SIs would be the best. The structure, thermal control, electrical/electronics, etc., design skills required for the OTA design will be the same as those required in designing for SI accommodation at the rear of the OTA. The OTA/SI functional and physical interfaces will be the simplest at the individual SI interface, a necessary condition for considering on-orbit or ground exchange of individual instruments during the program life. The option of having individual instruments provided later in the program by principal investigators and companies originally not related to the program, including those designed and manufactured in foreign countries, would probably be accommodated best through the use of this concept.

The LST program can be considered in two phases, the design, development, integration, and test phase and the flight operation and maintenance phase. The first is unique to the LST program from the standpoint of skills and design capabilities, test equipment and facilities, and developing centers

involved. The second may be very common with other programs that are launched, supported, and maintained through the use of the Shuttle, common ground tracking networks, ground maintenance equipment and facilities, and possibly common ground support personnel. Now that the flight operations and maintenance phase is becoming as long or longer than the first phase, a support operation that contains only a skeleton of the original design and development operation or that shares support operations costs with other programs is very desirable from the total program cost standpoint. Although the question of long-term sustained operations costs is not peculiar to the LST and transcends this program, its final resolution by NASA will probably strongly impact the total LST program cost.

## B. Project Elements

The project elements are defined to include ground test and flight LSTs, the launch vehicle, launch and mission operations; ground and space test, checkout, servicing and maintenance equipment and operations; and overall systems integration and test equipment, facilities, and software.

1. Ground Test and Flight LSTs. The present LST development philosophy involved the fabrication of three LST articles: an engineering model (EM) and two flight units. The engineering model of the LST and its test program is designed to reveal functional incompatibilities early enough to permit appropriate design modifications prior to the fabrication of flight hardware. The engineering model approaches the flight hardware configuration as opposed to breadboard configurations used during the development testing phase. Because of the absence of a qualification model and a "ship queen," the engineering model will be used to accomplish limited verification and qualification tests.

2. Science Instruments. The SIs are comprised of the high spatial resolution camera, f/96; two high resolution spectrographs; three faint object spectrographs; a Fourier interferometer; a wide field camera, f/12, and ancillary subsystems such as the slit jaw camera and the selector mechanisms.

This project element includes the design effort and the hardware fabrication, assembly, debugging, and testing required to build and deliver the engineering model and two flight units of each SI. Included are the detailed engineering, design, and analyses required to define each instrument; the breadboarding and subassembly tests required; the purchase, fabrication, and functional and environmental tests of components, and the assembly, debugging, and functional environmental tests of each instrument assembly before delivery.



3. Optical Telescope Assembly. The OTA consists of the primary optics and associated thermal control and structural subsystems (including those for SI accommodation), light baffles, fine pointing and stabilization subsystems, focal plane structure, automatic alignment and focusing systems, and optical figure sensors. This project element includes the design, breadboarding, fabrication, assembly and subassembly/assembly testing of the principal OTA assemblies, typically including the primary mirror assembly, secondary mirror assembly, diagnostic sensors (alignment, focus, figure), fine guidance error detection system, all major electronic assemblies, the pressure compartment door assemblies, and the aperture door assembly. Included is the assembly and test of the integrated OTA, containing the SI accommodations provisions.

4. Support Systems Module. The SSM consists of an attitude control system (ACS), communications and data handling system (C&DH), thermal control system (TCS), reaction control system (RCS), electrical power system (EPS), and structures system. This project element includes the design, breadboard, fabrication, assembly, and test of each system and the assembly and test of the integrated SSM. The same will be performed for the OTA and SI interfacing electrical/electronics assemblies that are to be physically located within the OTA/SI structures.

5. Integration and Test. The project elements of integration and test, located at different stages of assembly, are required to reveal interface incompatibilities or qualification failures as early as possible before an existing error is submerged within a more complex assemblage where correction would be more difficult and the error might cause damage to other interfacing assemblies. An existing error can then be corrected while the item is geographically located near supporting engineering and test facilities. The paralleling of integration and test operations allows the discovery and correction of errors simultaneously in major elements, thereby reducing the time required to produce the flight qualified LST. Usually precision testing on a subassembly or assembly basis can be accomplished with general-purpose test equipment and facilities where many of the same type of tests at a later point of assemblage would require special-purpose test equipment and facilities of unwieldy complexity.

6. Thermal Optical Test Facility. If end-to-end optical system testing of the assembled LST in a thermal-vacuum environment is required, an elaborate new test facility will be needed. It would be a thermal-vacuum optical test facility capable of enclosing the entire LST with its external shields, the SI bay, and the SSM. Also included as part of this test facility should be a

large 304.8 cm (120 in.) collimating mirror capable of providing simulated stars and star patterns for evaluation of the fine guidance sensor system and for a checkout of the assembled instrument complement. The test facility itself should be isolated from the local seismic and vibration environment to insure that these optical performance and pointing system performance tests can be conducted effectively.

## C. Phased Project Plan

The LST project utilizes the phased approach to the planning, approval, and conduct of the research and development activity. The definition of the time-sequenced phases is as follows:

1. The Phase A effort involves analyzing a proposed objective or mission in terms of alternate approaches or concepts and conducting the research and technology development requisite to support that analysis and to assist in determining whether the proposed technical objective or mission is valid.

2. The Phase B effort involves detailed study, analysis, and preliminary design directed toward the selection of a single project approach from among the alternate approaches resulting from the Phase A activities.

3. The Phase C effort includes the detailed definition of the final project concept, including the system design and the breadboarding of critical systems and subsystems, as necessary to provide reasonable assurance that the technical milestone schedules and resource estimated for the next phase can be met and that definitive contracts can be negotiated for Phase D.

4. The Phase D effort includes the final hardware design and development, fabrication, test, and project operations.

The LST is currently at the end of Phase A of this sequence. It should be noted that phased planning is applied at both the project and system level on a related, but not identical, schedule basis.

## D. Project Flow and Schedules

To assure the readiness of the LST for the 1980 and 1982 missions, a number of interrelated activities must be accomplished. A representative sample of function and hardware flow diagrams and related schedules which have been developed to date is as follows:

1. The LST program schedule (Fig. VIII-1) represents an overall time-phased concept of the main elements of the required activities necessary for mission accomplishment.

2. Supporting the LST program schedule is the LST project functional flow chart (Fig. VIII-2), which identifies the event constraints, interrelationships, and critical paths associated with mission accomplishment. The related schedule of major events on the project functional flow chart is shown in Figure VIII-3.

3. Supporting the project functional flow diagram are the LST systems/subsystems flow diagrams and their related schedules as shown in Figures VIII-4 through VIII-11.

1. LST Project Functional Flow Chart (Fig. VIII-2). This flow chart identifies each program element and its respective subelements. The LST hardware, from design and test as a subsystem or assembly to the overall integration, test, and launch to on-orbit operation and maintenance to final disposal at end-of-life (EOL), is described. The supporting test equipment and facilities are identified. The support operations of the launch vehicle, ground or orbit maintenance, ground control, and science data distribution are shown. The heaviest lines identify the integration and flow of the OTA and SSM subsystems into an LST Integration and Acceptance Test point. Here the SIs are received and integrated before final LST acceptance. The SIs' supporting structures and equipment in the science accommodations volume at the rear of the OTA have undergone thermal, vacuum, shock, vibration, and electromagnetic interference (EMI) tests as an integral part of the OTA integration and test at the preceding point in the OTA flow. Special facilities required in the fabrication and test of the system elements are shown. The most unique facility requirement is the Optical Thermal Vacuum Test Facility, which may be required in support of the LST Integration/Acceptance Tests.

After acceptance, the LST is transported to the Kennedy Space Center (KSC). After receiving inspection and the reassembly of any assemblies removed for shipment, a final calibration and flight readiness test is performed. The major items of required ground support equipment, including optical calibration equipment, can be part of the equipment used for the LST Integration and Acceptance Test just before shipment to KSC, provided it can be dolly mounted or exchanged from one rack to another in such a way as to follow the LST through to launch.

It has been assumed that the Space Shuttle assigned as the LST launch or maintenance support flight vehicle will go through a refurbishment cycle ending with Shuttle preflight checks as a separate entity. Then, the LST peculiar interface, handling, or orbital maintenance and checkout equipment and spares would be installed. The LST would then be loaded and interconnected and prelaunch tests of the launch vehicle with payload would be performed. After launch, orbit attainment, final checks, and deployment, the Shuttle would return and the LST would begin on-orbit operations.

Both on-orbit maintenance and ground-return maintenance modes are shown with the ground operations in support of each indicated. The mock-ups required for maintenance operations analysis, ground verification, and maintenance crew training are also depicted.

Normal LST mission control through the ground tracking network is shown. Engineering and scientific data received during RF contacts are distributed to the Mission Control Station, or in the case of science data, processed and distributed to the principal investigator and scientific community. New data or instrument requirements are provided to an LST operations and engineering support group, which initiates the design, fabrication, assembly, and test of any field modification or new instruments required when existing equipment being flown is inadequate.

## 2. LST System/Subsystem Functional Flow Diagrams

a. OTA Manufacturing and Test Flow Plan (Fig. VIII-4). This plan is of the fabrication and buildup cycle of the OTA and the integration of the OTA with the SI. It identifies the general flow of the fabrication cycle for the OTA, including the fabrication of the primary optical system and the required test optics, and the other principal assemblies, typically including the fine guidance subsystem, the secondary alignment system, and the main structures. The manufacturing test for the OTA consists of a complete checkout and test, including the acceptance level and environmental test for all major subsystems within the OTA. It will include vibration, temperature, altitude, EMI, and acoustical testing of each of the identified subsystems. Assemblies now scheduled for manufacturing test include the primary mirror assembly, secondary mirror assembly, diagnostic sensors (alignment, focus, figure), the fine guidance error detection system, all major harness assemblies, the pressure compartment door assemblies, and the aperture door assembly. For the operation of each of these subsystems, individual test consoles providing a simulation of the electrical-mechanical-optical interface will be designed and fabricated. These test consoles will include appropriate measuring

instrumentation to evaluate the subsystem compatibility with the subsystem requirements. These test data will provide the first positive data base for an evaluation of the engineering model and a comparison with downstream measurements of precursor and mission flight article systems.

b. SSM ACS Design, Verification, and Delivery Flow Charts and Schedule ( Figs. VIII-5 through VIII-7) . The chart and schedule ( Figs. VIII-5 and VIII-6, respectively) identify the time-phased functional flow to be followed in the design, test, and delivery of the ACS and are typical for each electrical/electronic subsystem of the SSM. Figure VIII-7 identifies the flow of work for the SSM RCS.

c. SSM Structures Flow Chart ( Fig. VIII-8) . This chart identifies the time-phased functional flow to be followed in the fabrication, test, and delivery of the SSM structures system.

d. SSM Thermal Control Flow Chart ( Fig. VIII-9) . This chart identifies the sequence of procurement or fabrication, installation, and test of thermal control hardware for the SSM.

e. Maintenance Mode Model ( Fig. VIII-10) . This flow chart relates the major project elements involved in the maintenance mode required for sustained LST operations.

f. LST Maintenance Support Activities ( Fig. VIII-11) . This schedule shows the LST neutral buoyancy simulation milestones. This activity is part of the in-house effort in support of the LST program.

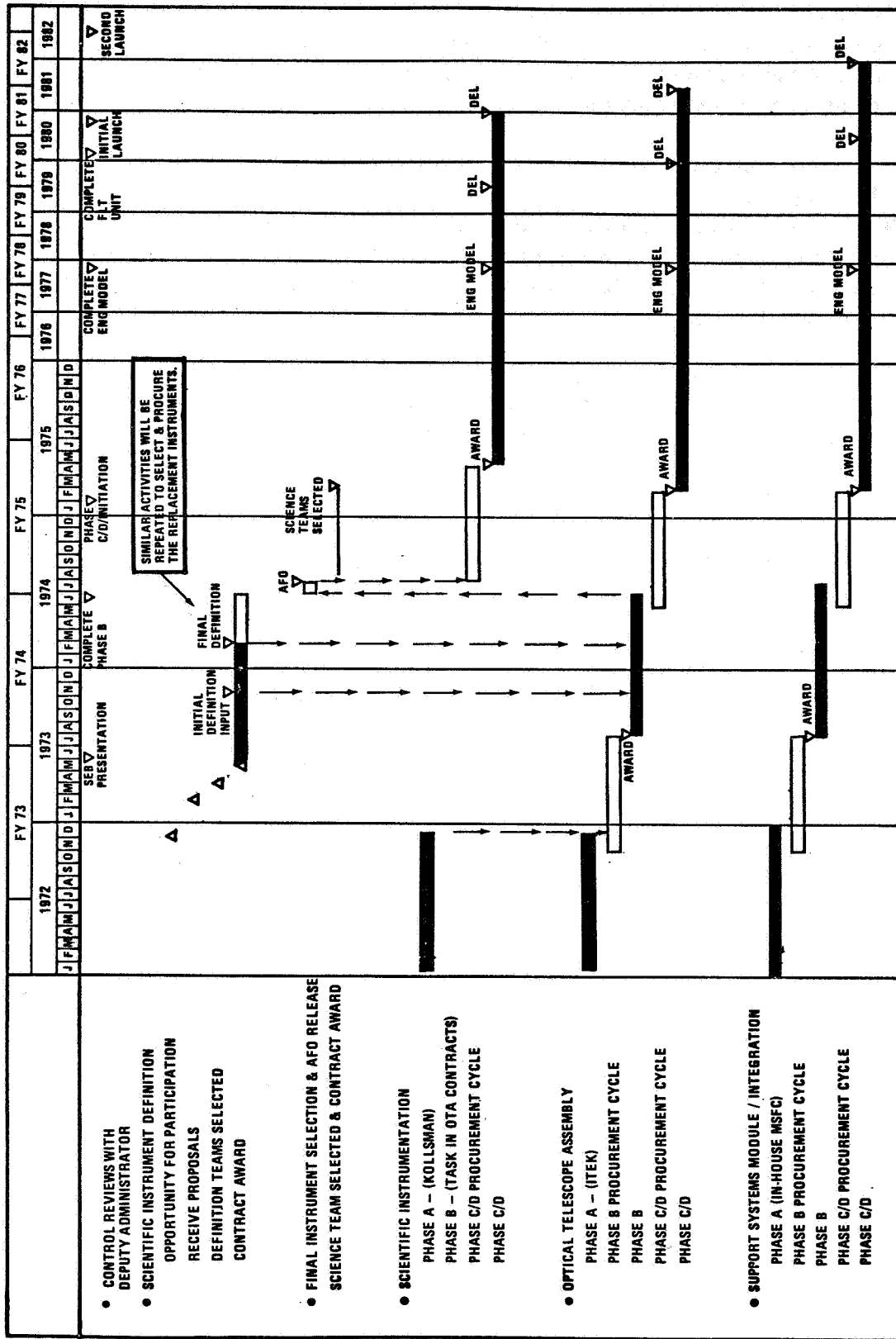


Figure VIII-1. LST program schedule.

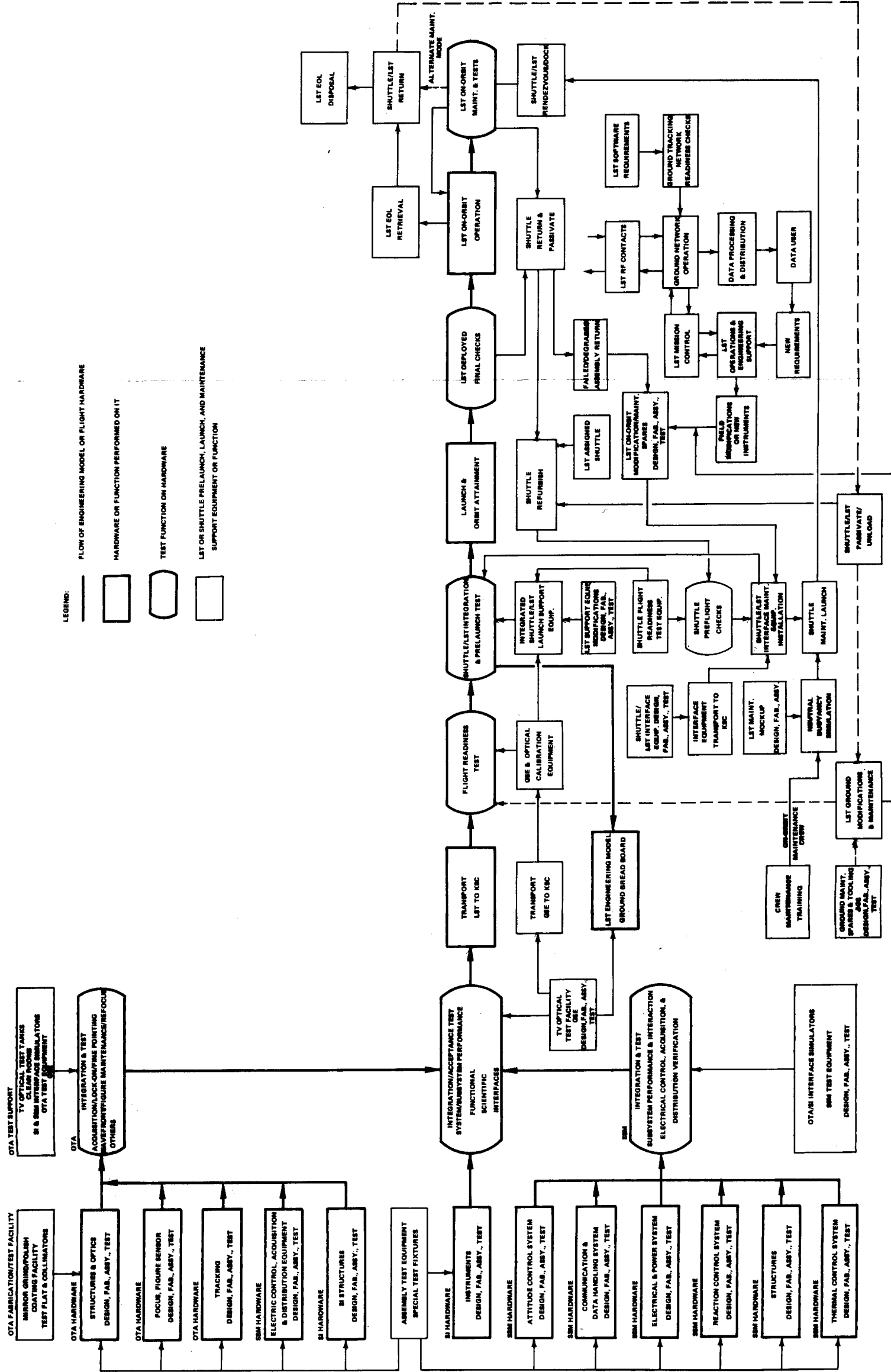


Figure VIII-2. LST project functional flow chart.





PROJECT MILESTONES	1975		1976		1977		1978		1979		1980		1981		1982	
	Q1	Q2	Q3	Q4	Q1	Q2	Q3	Q4	Q1	Q2	Q3	Q4	Q1	Q2	Q3	Q4
PHASE C/D CONTRACT OTA, SI, AND SSM				▽ AWARD												
OTA, SSM, AND SI EM (INTEGRATION, TEST, DELIVERY)				PRELIMINARY DESIGN REVIEW ADVANCED DESIGN		CRITICAL DESIGN REVIEW FABRICATION, TEST	▽									
LST EM (INTEGRATION, GROUND BREADBOARD, TESTING)								▽								
LST EM DELIVERY TO KSC (FACILITY, EQUIPMENT CHECKOUT)										▽						
EM TO GROUND BREADBOARD																
OTA, SSM, AND SI NO. 1 (INTEGRATION, TEST, DELIVERY)				PRELIMINARY DESIGN		(PDR) ADVANCED DESIGN		(CDRI) FABRICATION, TEST								
LST NO. 1 INTEGRATION/ACCEPTANCE TESTS																
LST NO. 1 DELIVERY TO KSC																▽
LST NO. 1 LAUNCH																
OTA, SSM, AND SI NO. 2 (INTEGRATION, TEST, DELIVERY)																
LST NO. 2 INTEGRATION/ACCEPTANCE TESTS																
LST NO. 2 DELIVERY TO KSC																▽
LST NO. 2 LAUNCH																▽

Figure VIII-3. Project milestones.



Figure VIII-4. OTA manufacturing and test flow plan.

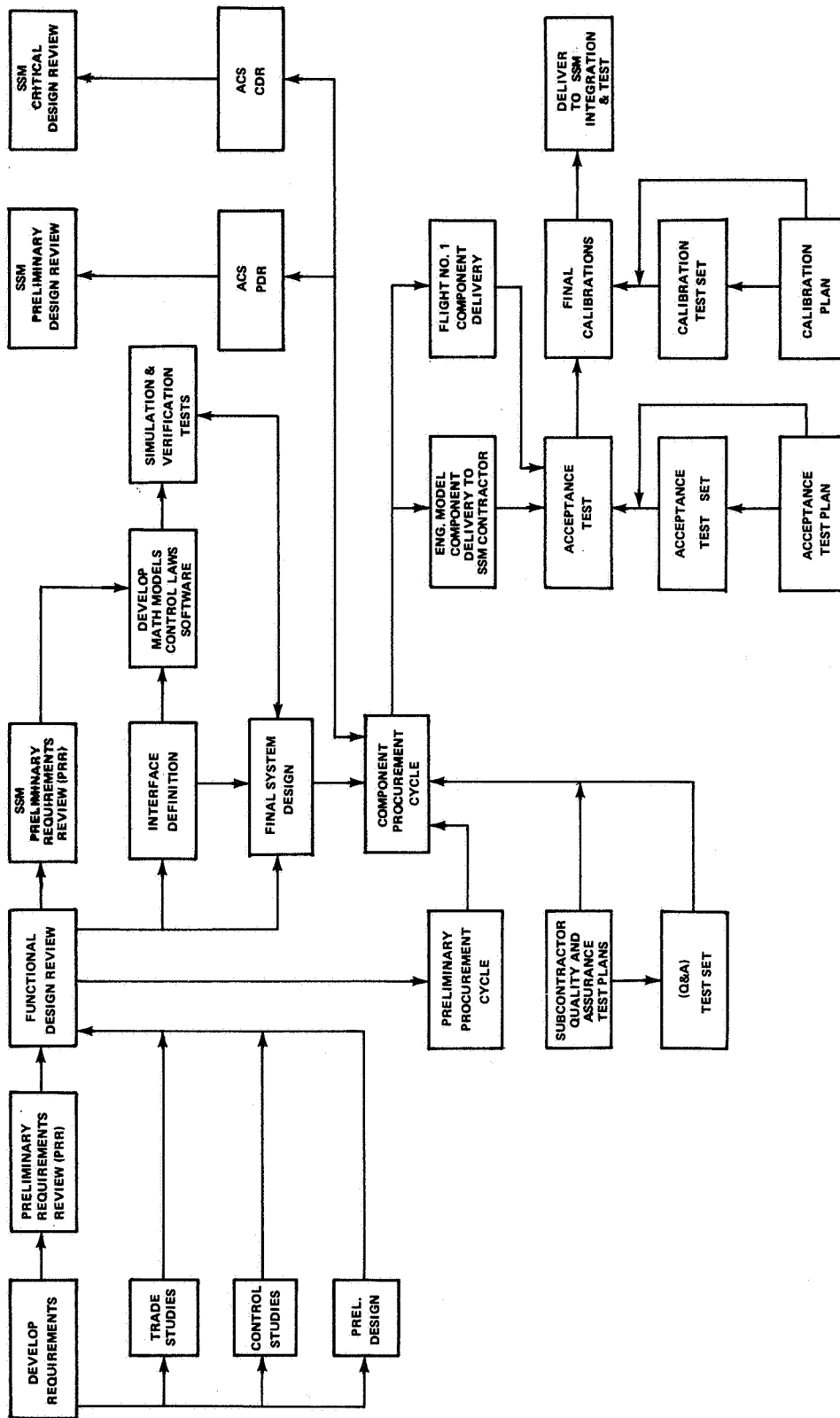


Figure VIII-5. LST/SSM ACS design, verification, and delivery flow chart.

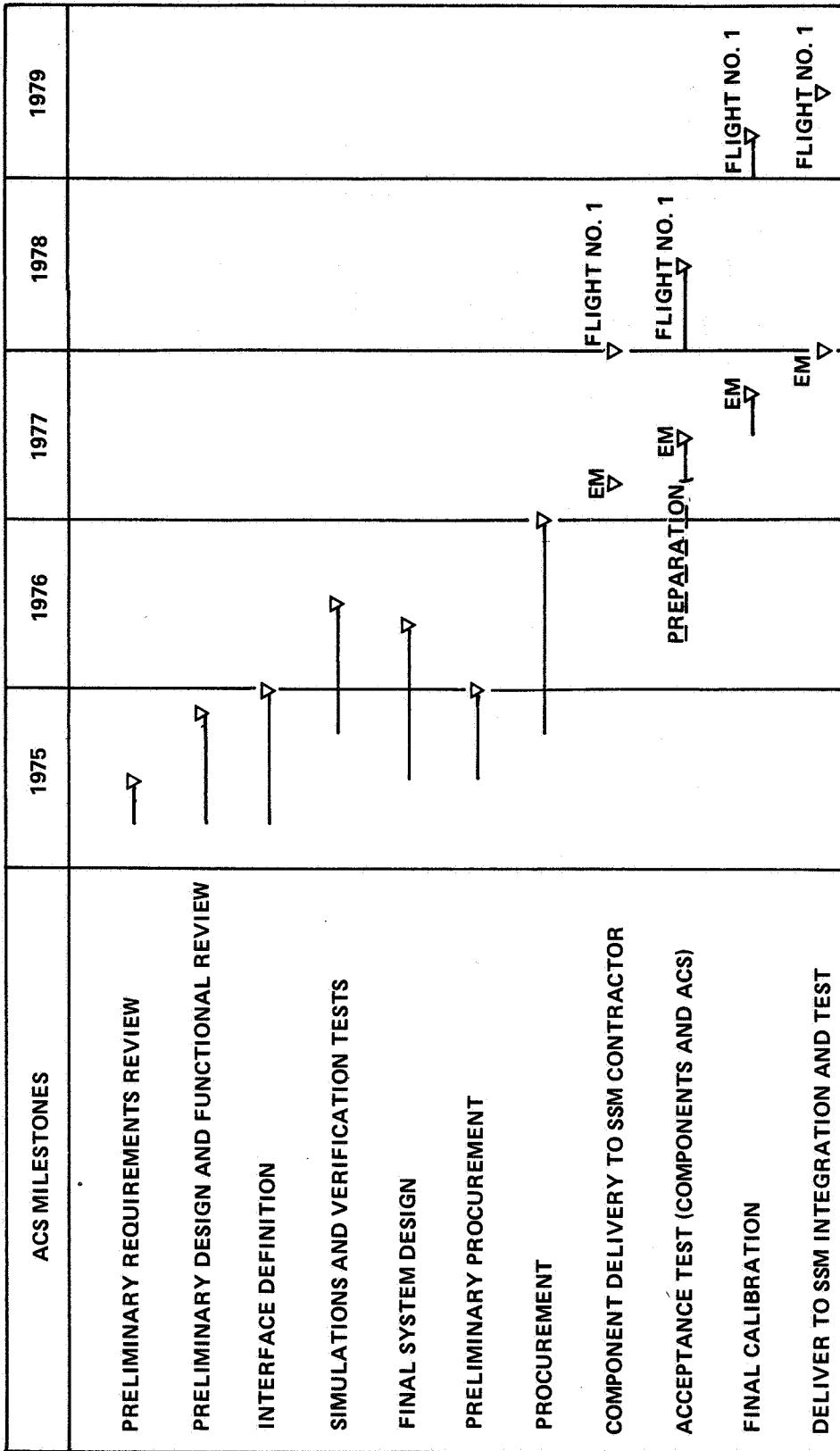


Figure VIII-6. ACS preliminary schedule.

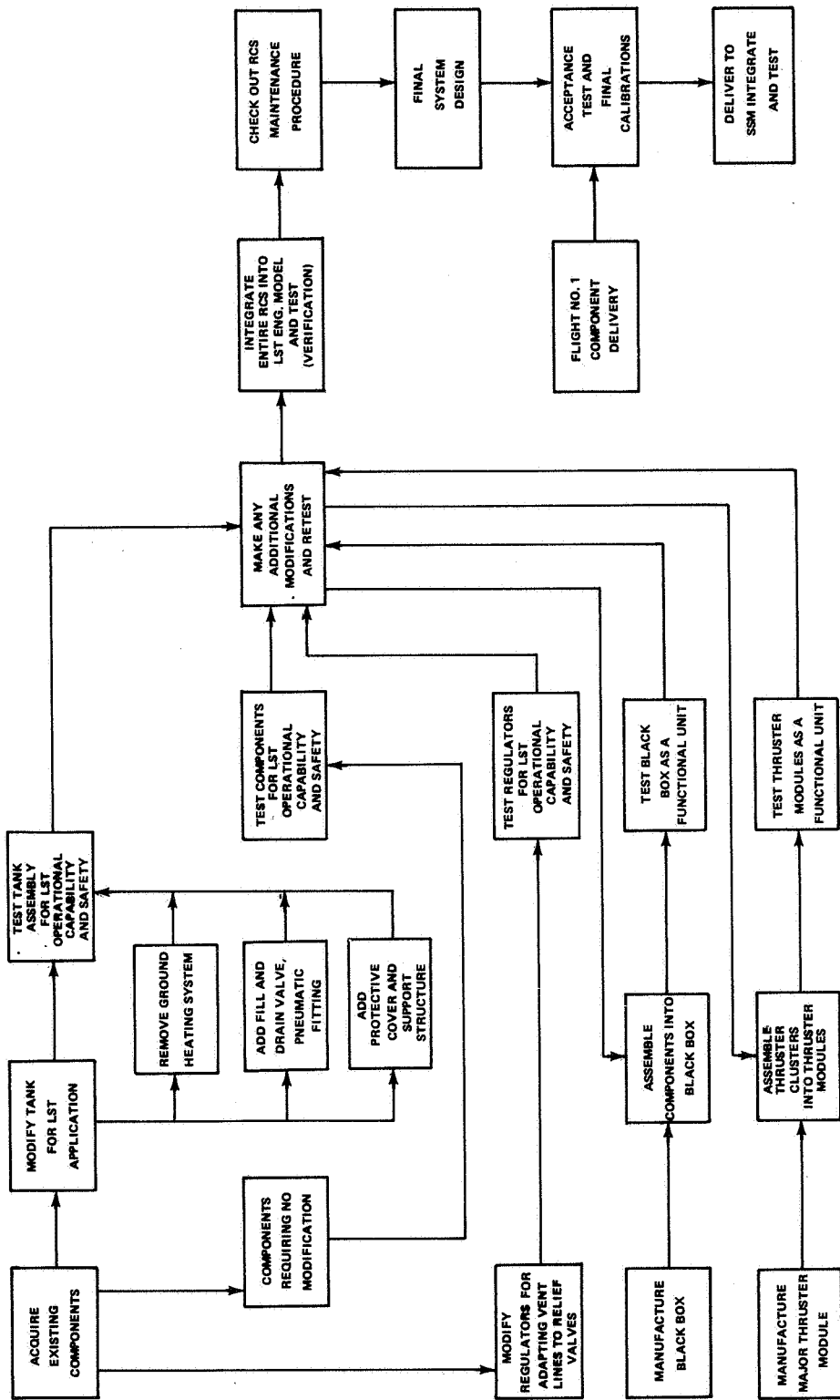


Figure VIII-7. LST RCS design, verification, and delivery flow chart.



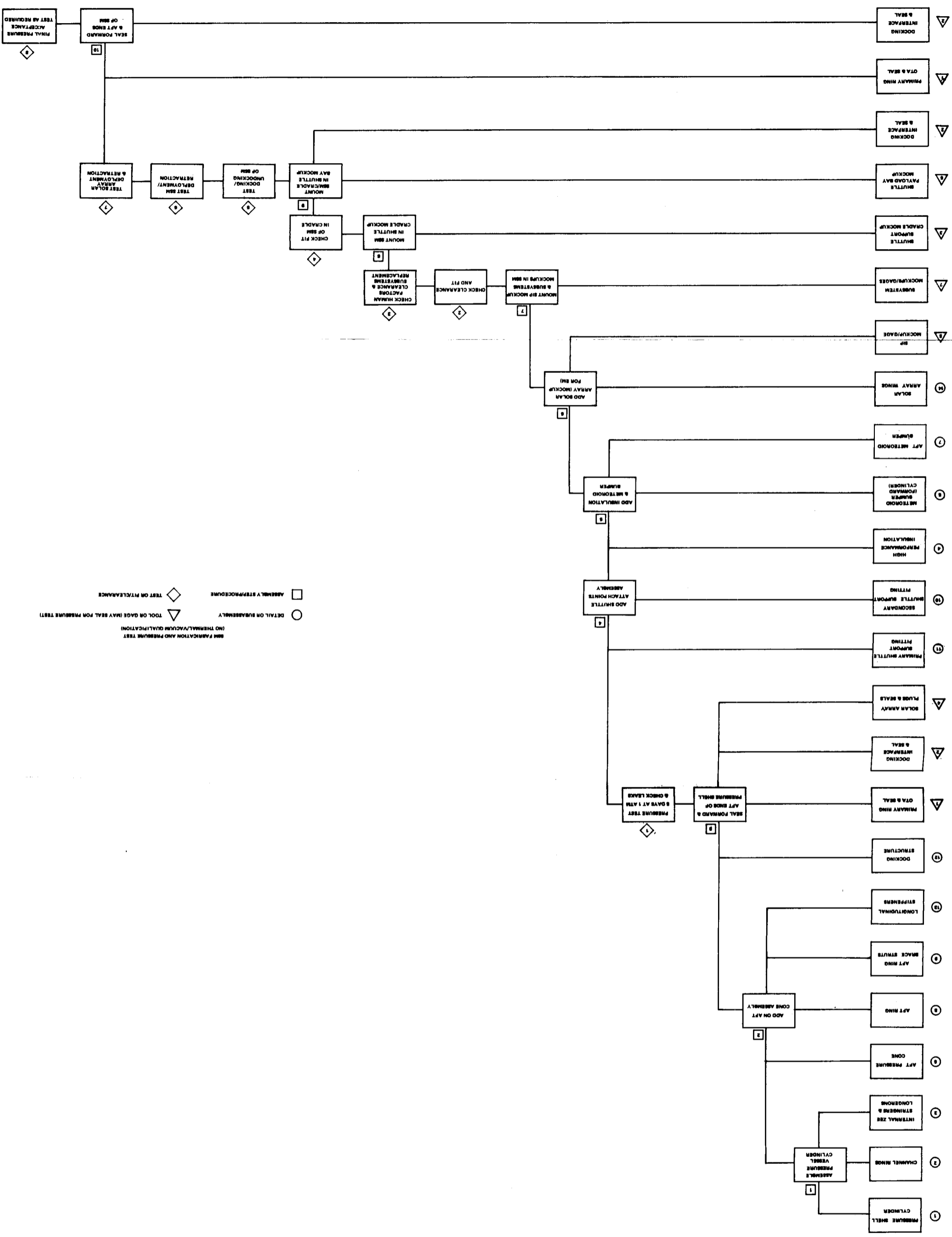


Figure VIII-8. SSM structures flow chart.

□ ASSEMBLY STEPPROCEDURE  
 ○ DETAIL ON SUBASSEMBLY  
 ◇ TEST ON FIT/CLEANANCE  
 ▼ TOOL ON GAUGE (MAY SEAL FOR PRESSURE TEST)  
 (NO THERMAL/VACUUM QUALIFICATION)





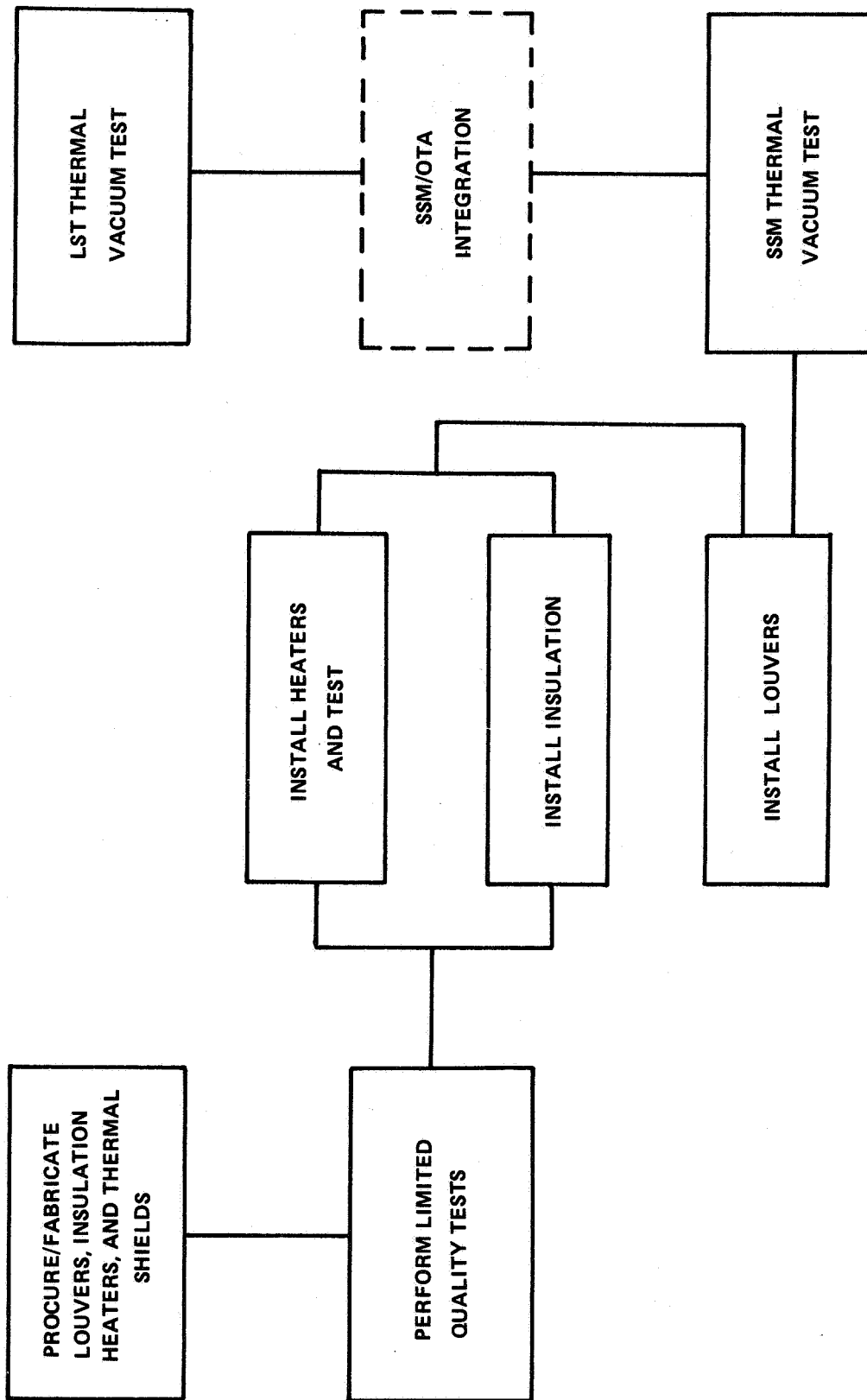


Figure VIII-9. SSM thermal control hardware flow chart.

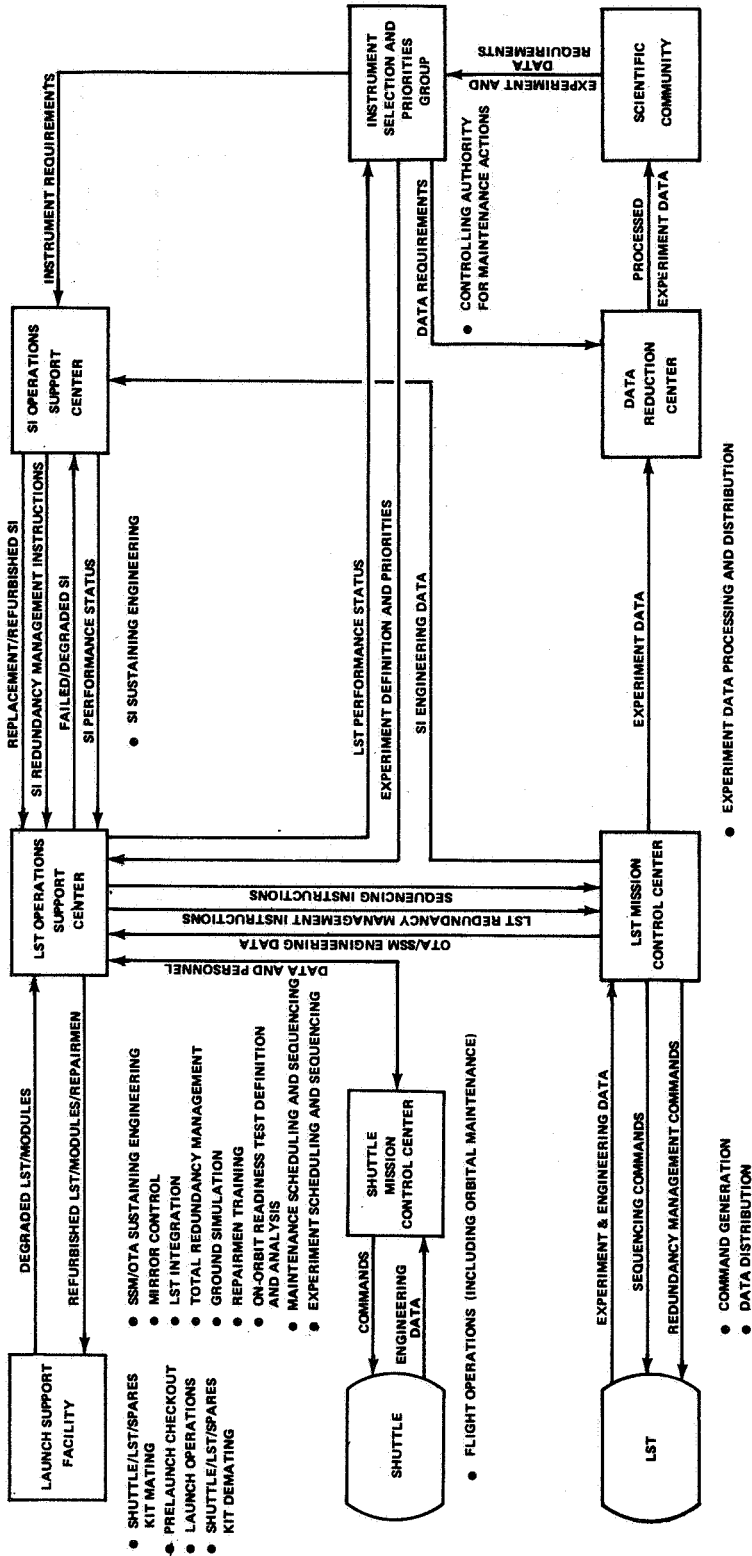


Figure VIII-10. Maintenance mode model.

	CALENDAR YEAR											
	1972	1973	1974	1975	1976	1977	1978	1979	1980	1981	1982	
LST NEUTRAL BUOYANCY SIMULATION MILESTONES												
NEUTRAL BUOYANCY SIMULATION REQUIREMENTS	▲											
MOCKUP FABRICATION												
MOCKUP WITH PRELIMINARY SI		▲										
MOCKUP WITH DETAILED SI		▲										
NEUTRAL BUOYANCY SIMULATION TESTS												
PRELIMINARY SI												
DETAILED SI												
CREW TRAINING												

Figure VIII-11. LST maintenance support activities.

## CHAPTER IX. CONCLUSIONS AND RECOMMENDATIONS



# TABLE OF CONTENTS

	Page
A. Optical Telescope Assembly (OTA) . . . . .	IX-1
B. Scientific Instruments (SI) . . . . .	IX-2
C. Support Systems Module (SSM) . . . . .	IX-3
D. General . . . . .	IX-3

## CHAPTER IX. CONCLUSIONS AND RECOMMENDATIONS

The results of the Phase A study indicate that a 3 m optical telescope can be operated in low earth orbit for 5 or more years. The telescope support requirements can be provided by onboard systems to give near diffraction limited optical performance. The LST spacecraft may be launched by either the Shuttle (primary) or the Titan IIIE/Orbit Adjust Stage (OAS) (alternate) vehicle.

The systems concepts utilized in the reference configuration appear to provide a feasible solution to the requirements. Some of the more critical areas for further study and analysis are fine error sensing, image motion compensation, pointing control, structural stability, imaging sensors and their cooling, large high-precision optics, optical system figure sensing and control, and maintenance.

It is believed that most of the basic technology and much of the systems hardware required by the LST will be available from other programs, thus reducing costs and improving reliability significantly. Other ways must be found to reduce costs and still achieve the scientific objectives of the mission. Our experience in manned space flight, unmanned satellites, and groundbased astronomy must be merged in the LST and from this merger new philosophies and approaches will be developed which will allow a more cost-effective utilization of man and machines in space. The use of man in such unmanned satellite programs as the LST, no matter what the configuration of the LST, can be more effective and accomplished with much less impact on the design of the hardware than we have experienced on the Apollo or Skylab programs. This is because of the differences in the nature of the missions and the experience gained on those programs.

### A. Optical Telescope Assembly (OTA)

An f/12 Ritchy-Cretien version of the Cassegrainian design is recommended over the Gregorian for the OTA because it is clearly superior for the LST application. A primary focal ratio of f/2.2 is recommended upon considerations of overall length, mass, and volume constraints but primarily because it is believed that, using current technology, this is the fastest mirror that can be made that will meet the exacting surface requirements.

It was concluded that a three-bay eight-point mount truss with graphite-epoxy members was a suitable design for the metering truss. A feasible alternate was found to be a graphite-epoxy shell structure which may offer the advantages of a smaller overall diameter and greater stiffness. A three-point axial leaf design is advised for the primary mirror mount. A light shield truncation angle of 45 degrees is recommended as being a good compromise between providing maximum sky coverage and minimizing design problems.

The thermal control concept recommended for the OTA is a combination of active thermal control for the optical elements and passive control for the supporting structure. Since the maximum rate of temperature change in the elements of the metering truss is less than  $4.5^{\circ}\text{C}$  per hour and appears linear, it is concluded that fewer than two refocusing operations per hour will be required.

It is recommended that force isolation rather than a simple actuation system be used for the secondary mirror in order to meet the frequency response requirements of the fine pointing system. Alignment accuracy can be achieved using already developed sensors and suitably designed mechanical actuators.

## B. Scientific Instruments (SI)

The feasibility of design and construction of the SIs that are capable of diffraction-limited imagery and high spectral resolution for a large range of celestial bodies has been established. The instruments can be repaired in orbit and the complement can be changed and upgraded in response to the requirements of the scientific community. Thus the LST is capable of being usable for several decades and of obtaining scientific data not available on the ground.

It should be possible to align instruments replaced during on-orbit maintenance to within the specified tolerances. If these specified replacement tolerances are exceeded, the instruments will still function but performance will be degraded. Replacement of the f/96 camera tubes will require the least precision.



## C. Support Systems Module (SSM)

For the SSM, a conventional pressurized cylindrical structure of simple skin/stringer construction utilizing conventional materials such as aluminum alloys in standard gages was found quite adequate to meet the LST requirements. A passive thermal control system (TCS) is feasible and compatible with a component arrangement to provide adequate clearance for astronaut maintenance.

A solar array reference design, based upon conventional solar panels, can satisfy all power requirements. However, it is a high mass approach with complex storage, deployment, and retraction, and is not a good candidate for in-space maintenance. Therefore, it is recommended that an alternate rollup array be studied and compared for a possibly more cost effective approach.

The feasibility of transmitting to ground more than two frames per orbit of high resolution camera data was established. Data storage in the secondary electron conduction (SEC) vidicon tube permits the use of conventional state-of-the-art hardware to provide a flexible communications and data system that meets or exceeds the LST requirements.

It was found feasible to meet the LST pointing requirements utilizing the design reference attitude control system (ACS) in conjunction with the OTA fine guidance system (FGS). Tip and tilt positioning of the secondary mirror in response to the fine guidance sensor star tracker outputs is required to maintain the 0.005 arc second pointing stability.

## D. General

The concept of unscheduled, on-orbit, manned maintenance utilizing the Shuttle orbiter for support appears to lead toward the more cost effective approach. This allows a reduction in the equipment design lifetime from a goal of 2.5 years to a shorter time. Shuttle flight sharing with other payloads is a prime means of reducing maintenance costs.

There is a high degree of commonality between the reference design and the hardware from other programs. For example, an approximate breakdown of the SSM components is as follows:

1. 42 percent identical to the High Energy Astronomy Observatory (HEAO).
2. 17 percent from other programs.
3. 13 percent could probably be identical if shown to be cost effective.
4. 23 percent new design requiring development but no new technology.

APPENDIX A

ALTERNATE LST STRUCTURAL DESIGN EMPLOYING  
GRAPHITE/EPOXY SHELLS



# TABLE OF CONTENTS

	Page
A. Introduction .....	A-1
B. Orbiting Telescope Assembly Structure Design Description . . .	A-1
1. Structural Design .....	A-1
a. Main Structural Shell .....	A-2
b. Meteoroid Shell Structure .....	A-2
c. Sun Shade Structure .....	A-10
2. Mechanical Deployment Systems .....	A-10
a. The Roller System .....	A-10
b. The Locking Mechanism .....	A-11
c. The Activation System .....	A-11
C. Thermal Analysis .....	A-11
1. Assumptions .....	A-14
2. Analysis Procedure .....	A-14
3. Second Iteration Revisions .....	A-24
D. Structural Analysis .....	A-25
1. Structural Sizing .....	A-26
a. Main Shell Loads .....	A-26
b. Main Shell Instability .....	A-26
c. Secondary Shells .....	A-32
d. Secondary Mirror Support Beams .....	A-32
e. Meteoroid Protection System .....	A-36
2. Finite Element Model .....	A-37
a. Solar Array .....	A-37
b. System Support Module .....	A-37
c. Scientific Instrument Package .....	A-39
d. Pressure Bulkhead .....	A-39
e. Main Mirror .....	A-39
f. Main Shell .....	A-39
g. Micrometeoroid Shield (MMS) .....	A-39
h. Secondary Mirror Structure .....	A-46
i. Aperture Doors .....	A-46
j. Sun Screen .....	A-46
k. Launch Case .....	A-46

## TABLE OF CONTENTS (Concluded)

	Page
3. Distortion Analysis .....	A-46
a. Interior Sun Shade Insulation .....	A-49
b. Exterior Sun Shade Insulation .....	A-52
4. Structural Dynamics Analysis .....	A-58
a. Development of Dynamic Model .....	A-58
b. Results .....	A-59
E. Weight Analysis .....	A-65
F. Conclusions .....	A-69
References .....	A-71

## LIST OF ILLUSTRATIONS

Figure	Title	Page
A-1.	LST general arrangement . . . . .	A-3
A-2.	LST subassembly details . . . . .	A-4
A-3.	LST splice details . . . . .	A-5
A-4.	LST structural sections . . . . .	A-6
A-5.	Alternate secondary mirror main support ring . . . . .	A-7
A-6.	Sunshade locking mechanism . . . . .	A-12
A-7.	LST sunshade actuation system . . . . .	A-13
A-8.	Structural shell inside-wall temperatures — 61st orbit . . . . .	A-18
A-9.	Longitudinal temperature change variation in main shell wall . . . . .	A-20
A-10.	Micrometeoroid shell first ring temperatures — 61st orbit . . . . .	A-21
A-11.	Assumed FEM node point temperatures . . . . .	A-22
A-12.	Time/temperature variation of forward shell rings . . . . .	A-23
A-13.	Temperature/depth variation of main shell rings . . . . .	A-23
A-14.	SSM wall temperature variation . . . . .	A-25
A-15.	Structure of LST . . . . .	A-27
A-16.	Section properties of main shell wall . . . . .	A-30
A-17.	Secondary mirror support beam . . . . .	A-33
A-18.	Beam stress and stiffness diagrams . . . . .	A-35

## LIST OF ILLUSTRATIONS (Continued)

Figure	Title	Page
A-19.	Structural shell thickness as a function of mission time . .	A-36
A-20.	SSM and solar array model . . . . .	A-38
A-21.	SIP truss bars and panels . . . . .	A-40
A-22.	Pressure bulkhead panels . . . . .	A-41
A-23.	Primary mirror panels . . . . .	A-41
A-24.	Main shell bars . . . . .	A-42
A-25.	Main shell panels . . . . .	A-43
A-26.	Primary ring panels . . . . .	A-43
A-27.	Primary ring bars . . . . .	A-44
A-28.	Forward ring model of main shell . . . . .	A-44
A-29.	Meteoroid shell bars and panels . . . . .	A-45
A-30.	Secondary mirror and support beams . . . . .	A-47
A-31.	Aperture door model . . . . .	A-47
A-32.	Sunscreen shell bars and panels . . . . .	A-48
A-33.	Distortion check points . . . . .	A-50
A-34.	Thermally compensating structure . . . . .	A-50
A-35.	Thermally compensating beam structure . . . . .	A-53
A-36.	Primary ring distortion . . . . .	A-55
A-37.	Primary mirror motion . . . . .	A-55



## LIST OF ILLUSTRATIONS (Concluded)

Figure	Title	Page
A-38.	SSM thermal distortion . . . . .	A-56
A-39.	Main shell distortion plot . . . . .	A-56
A-40.	Meteoroid shell distortion plot . . . . .	A-57
A-41.	Sunshade distortion plot . . . . .	A-57
A-42.	Mode 3 — SIP bending at 10.6 Hz . . . . .	A-60
A-43.	Mode 4 — first body bending at 22 Hz . . . . .	A-61
A-44.	Mode 7 — second SIP mode at 28.9 Hz . . . . .	A-62
A-45.	Mode 9 — meteoroid shield at 37.1 Hz . . . . .	A-63
A-46.	Mode 17 — second body mode at 60.1 Hz . . . . .	A-64
A-47.	Structural shell frame weight vs thickness . . . . .	A-69

## LIST OF TABLES

Table	Title	Page
A-1.	Structural Component Thickness and Laminate Description . . . . .	A-9
A-2.	Main Shell Inside-Wall Temperature History for Nodes Nearest Primary Mirror (in °F) . . . . .	A-16
A-3.	Main Shell Inside-Wall Temperature History for Nodes Nearest Secondary Mirror (in °F) . . . . .	A-17
A-4.	Summary of Main Shell Temperature Changes . . . . .	A-19
A-5.	LST Limit Load Factors . . . . .	A-26
A-6.	Component Weights and Center of Gravity Locations . . . . .	A-27
A-7.	Pseudo-Isotropic HMS Graphite/Epoxy [+45, -45, 90, 0 deg] <sub>S</sub> . . . . .	A-28
A-8.	Main Shell Ultimate Applied Loads . . . . .	A-29
A-9.	Beam Optimization (Weight vs Blockage) . . . . .	A-33
A-10.	LST Natural Frequencies . . . . .	A-59
A-11.	Weight Summary of OTA Composite Structure . . . . .	A-66
A-12.	Composite OTA Weight Summary . . . . .	A-68

## APPENDIX A

# ALTERNATE LST STRUCTURAL DESIGN EMPLOYING GRAPHITE/EPOXY SHELLS

### A. Introduction

Advanced composite materials differ greatly from metallic structural materials in basic mechanical and physical behavior and in their optimum structural arrangement capability. Therefore, for comparison purposes, it was decided to generate an alternate LST design which utilized the unique and very desirable properties of graphite/epoxy. The technical approach was to redesign the optical telescope assembly (OTA) metering structure, primary light baffles, micrometeoroid shield, extendable sunshade, and secondary mirror mounting beams to essentially the same criteria (criteria that were defined early in the Phase A effort but are not necessarily valid now) that were used in the reference truss design.

General Dynamics/Convair Aerospace Division was given the task of generating such a design and the following technical discussion is an MSFC-edited excerpt from the final report given in Reference A-1.

### B. Orbiting Telescope Assembly Structure Design Description

1. Structural Design. The structural design of the LST in graphite composite materials has been applied to four major components of the telescope structure: the structural shell, meteoroid protection shell, extendable sun shade, and secondary mirror support assembly.

The main structural shell is the primary element of the structure and serves as a support for the meteoroid shell, sun shade, and secondary mirror support structure. The general arrangement of the structure is shown in Figure A-1. The meteoroid shell is attached to the forward ring of the structural shell which puts the meteoroid shell skin in tension during launch. The aft end of the shell is restrained in a compressible material to restrict side movement of the shield. The sun shade structure is also put in tension during boost by bearing against the forward ring of the structural shell. Torsional and sway stability is provided jointly by the extension rollers and the shear pins in the aft torque box which engage the sun shade in its retracted

position (Fig. A-2). The secondary mirror assembly is supported in a 940 mm (37 in.) diameter ring, which in turn is attached to the forward ring of the structural shell by a system of four spider beams, as shown in Figure A-2.

a. Main Structural Shell. The main structural shell is comprised of 42 ring frames, a forward ring, and the skin panels. The complete cylinder is made up of two cylinders of equal length, each of which contains six panel assemblies. These assemblies consist of the skin panel and 21 frame segments which are spliced together longitudinally as shown in Figure A-3. The ply orientation and total thickness of the skin and frames are shown in Table A-1. The ring frame configuration is shown in Figure A-3. The 0.8 mm (0.032 in.) frame is a tee-section which is 76 mm (3 in.) high with a width of 51 mm (2 in.) at the skin flange. These frames also serve as light baffles and for this reason may require the alternate configuration as shown in Figure A-4. In the alternate configuration, the flange angle would vary, depending on the particular station location of the ring. The main structural member of the shell is the forward torque box ring which is used as the support member for the secondary mirror spider beams, meteoroid shell, and sun shade in the stowed or retracted position. The torque box ring is a closed box measuring 4 in. by 4 in. which is vented through filters into space between the structural shell and the meteoroid shell, thus eliminating the possibility of emitting trapped contamination directly into the optical barrel.

An alternate approach to the closed torque box ring is shown in Figure A-5. In this configuration the ring is an open channel reinforced with intercostals at (0.175 rad) (10 degree) spacing to provide sectional stability. The secondary mirror support spider beams are attached to the inside of the channel by the use of two intercostals at each beam.

b. Meteoroid Shell Structure. The meteoroid shell is a minimum weight structural shell which surrounds the main structural shell, affording it protection against meteoroid damage. The space between the two shells is 51 mm (2 in.) deep, of which 38 mm (1.5 in.) is occupied by the frame height and 13 mm (0.5 in.) by the insulation material which is attached to the outer surface of the structural shell. The 38 mm (1.5 in.) high ring frames are spaced on 20-in. centers and are a simple "T" section with the 38 mm (1.5 in.) base bonded to the skin panels (Fig. A-4).

The meteoroid shell is supported by a zee section attached to the forward torque box ring of the structural shell which pulls the meteoroid shell during boost. The aft end of the shield is supported in a compressible material which eliminates compressive forces in the skin but prevents lateral sway of the shell.

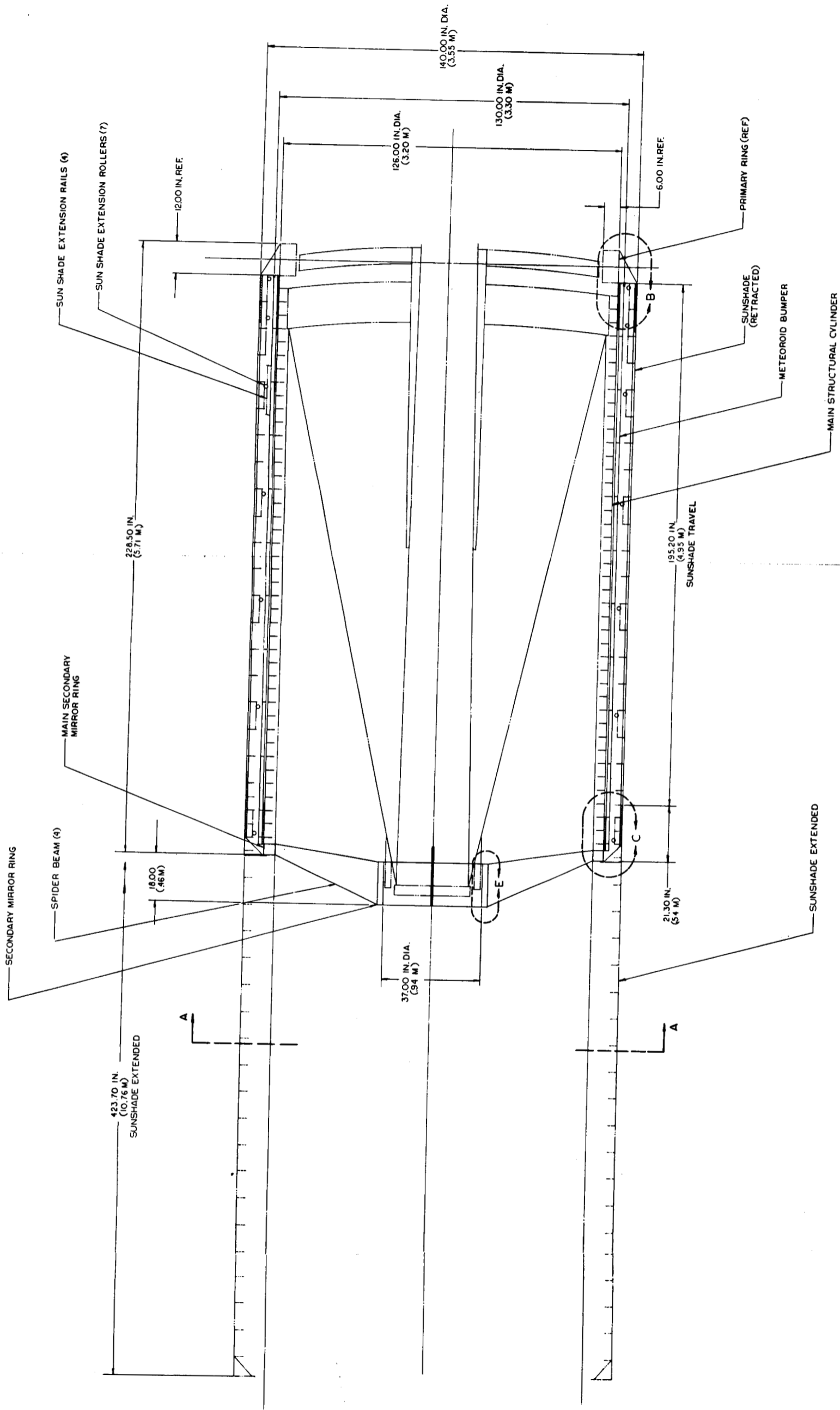
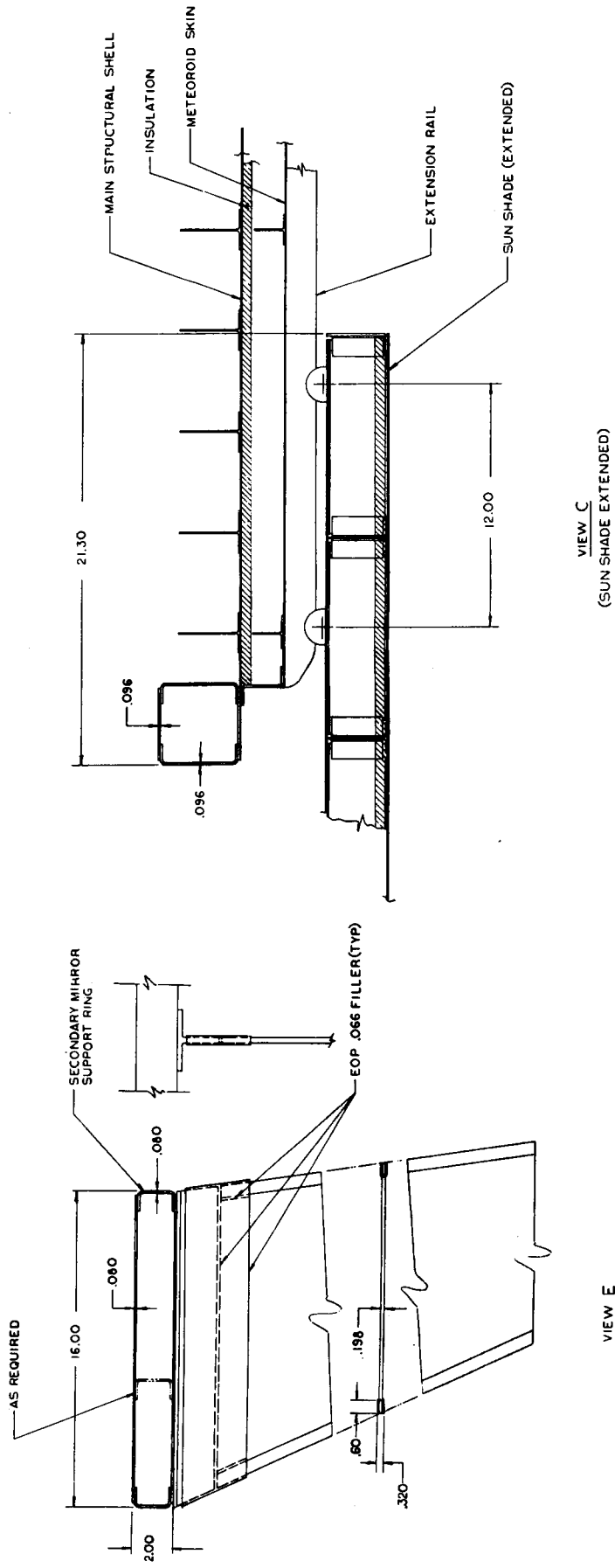
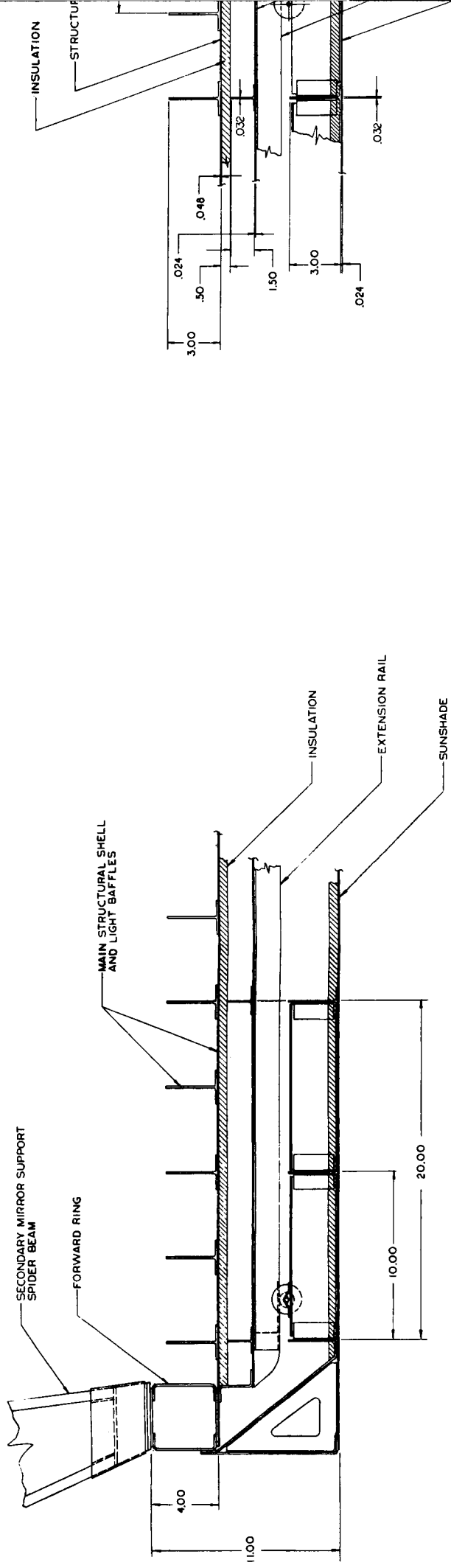
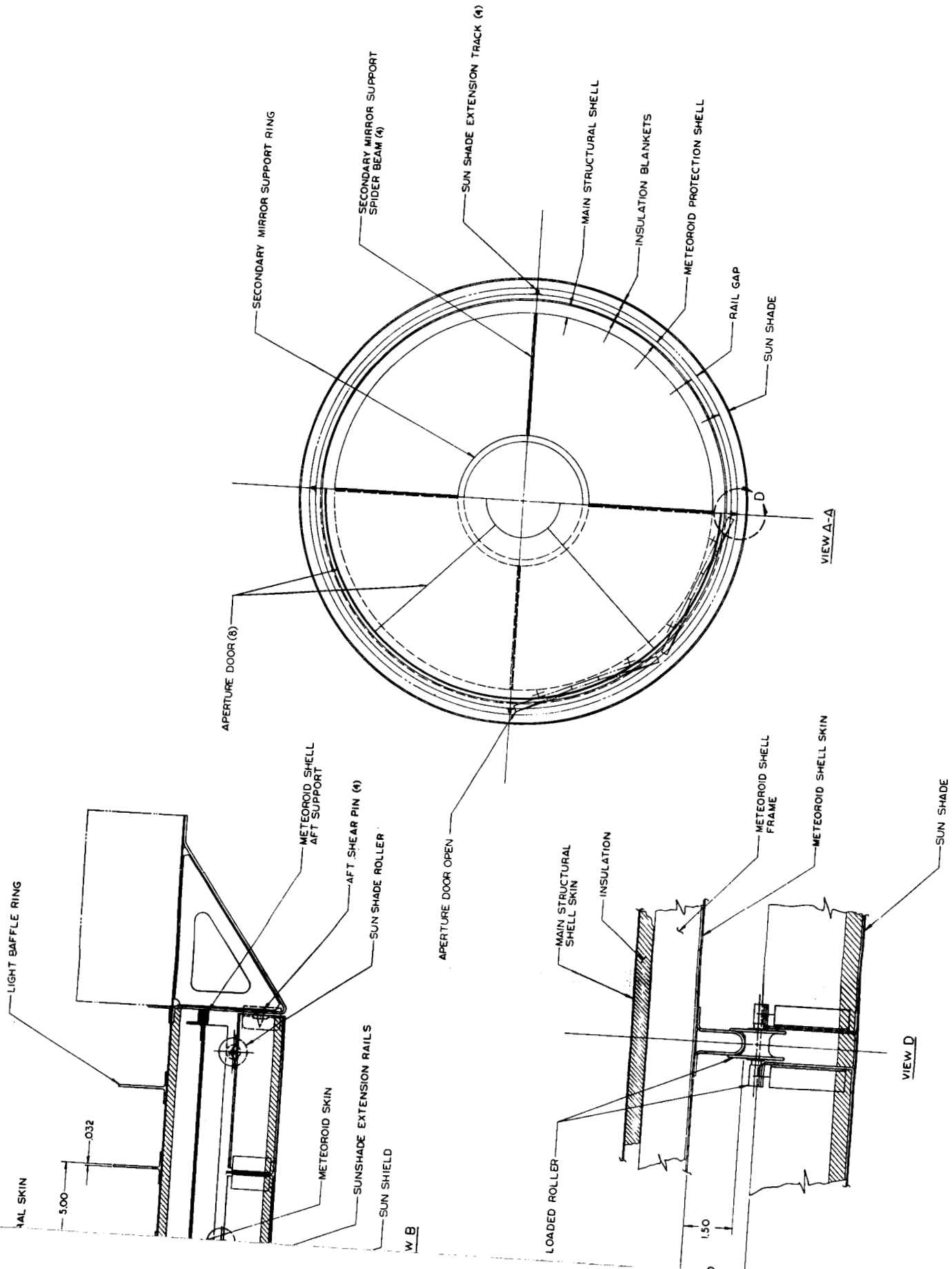


Figure A-1. LST general arrangement.

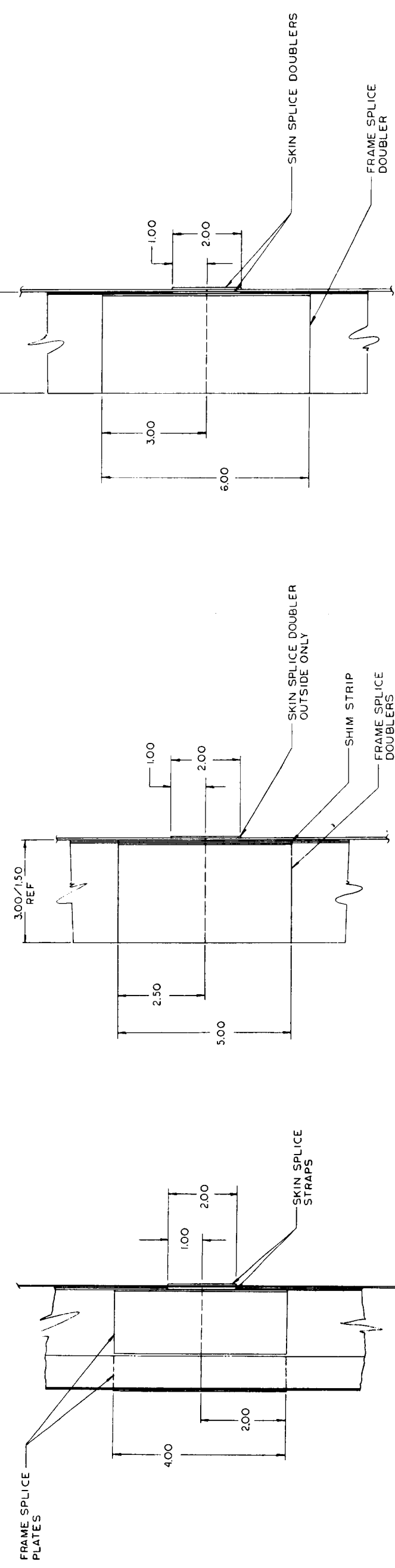
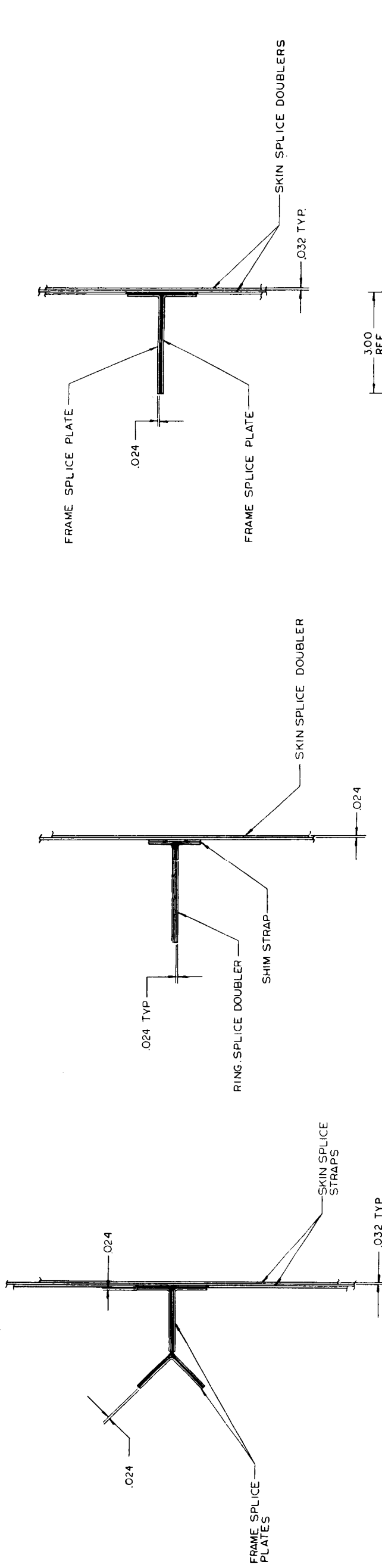


VIEW C  
(SUN SHADE EXTENDED)

Figure A-2. LST subassembly details.



Fold-out #2



STRUCTURAL SHELL  
ALTERNATE RING AND SKIN  
SPLICE DETAIL

SUN SHADE/METEOROID SHELL  
TYPICAL RING AND SKIN  
SPLICE DETAIL

STRUCTURAL SHELL  
TYPICAL RING AND SKIN  
SPLICE DETAIL

Figure A-3. IST splice details.



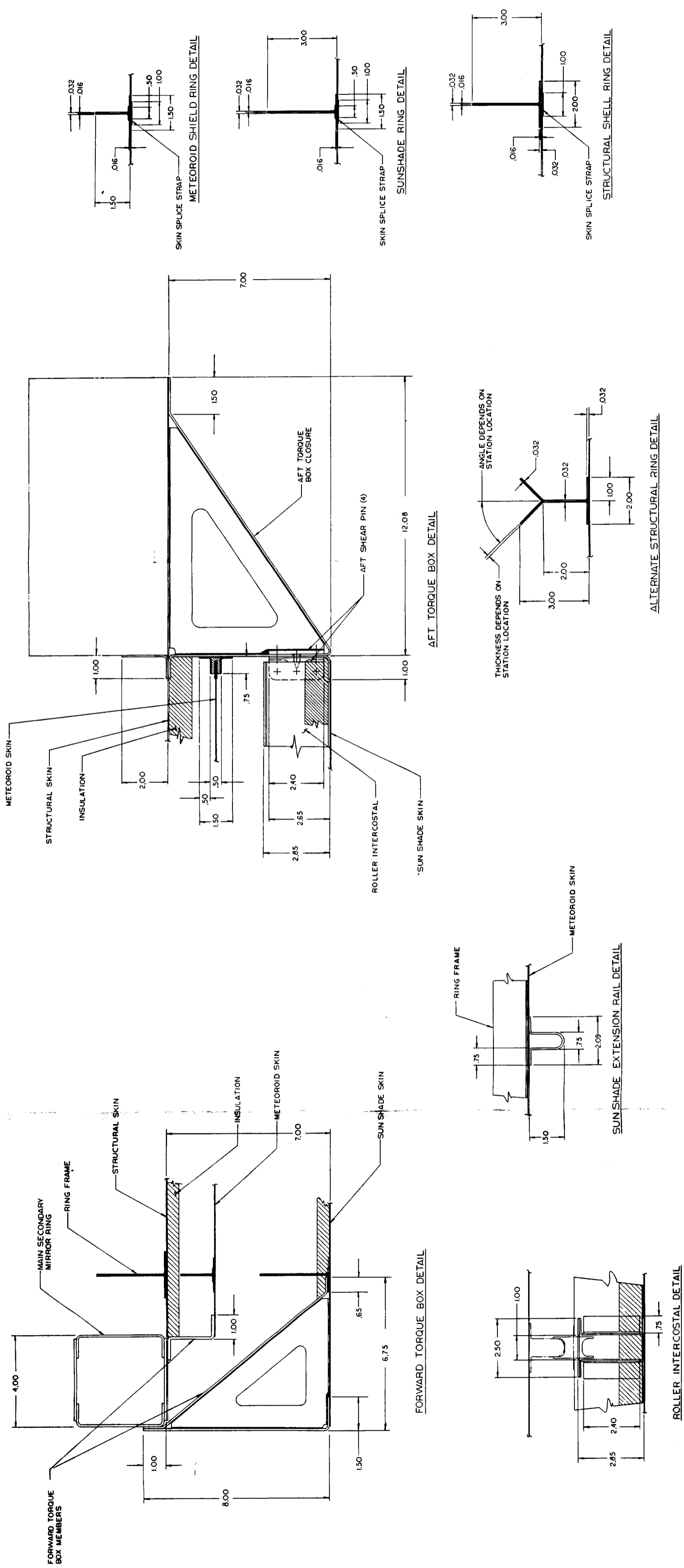


Figure A-4. IST structural sections.

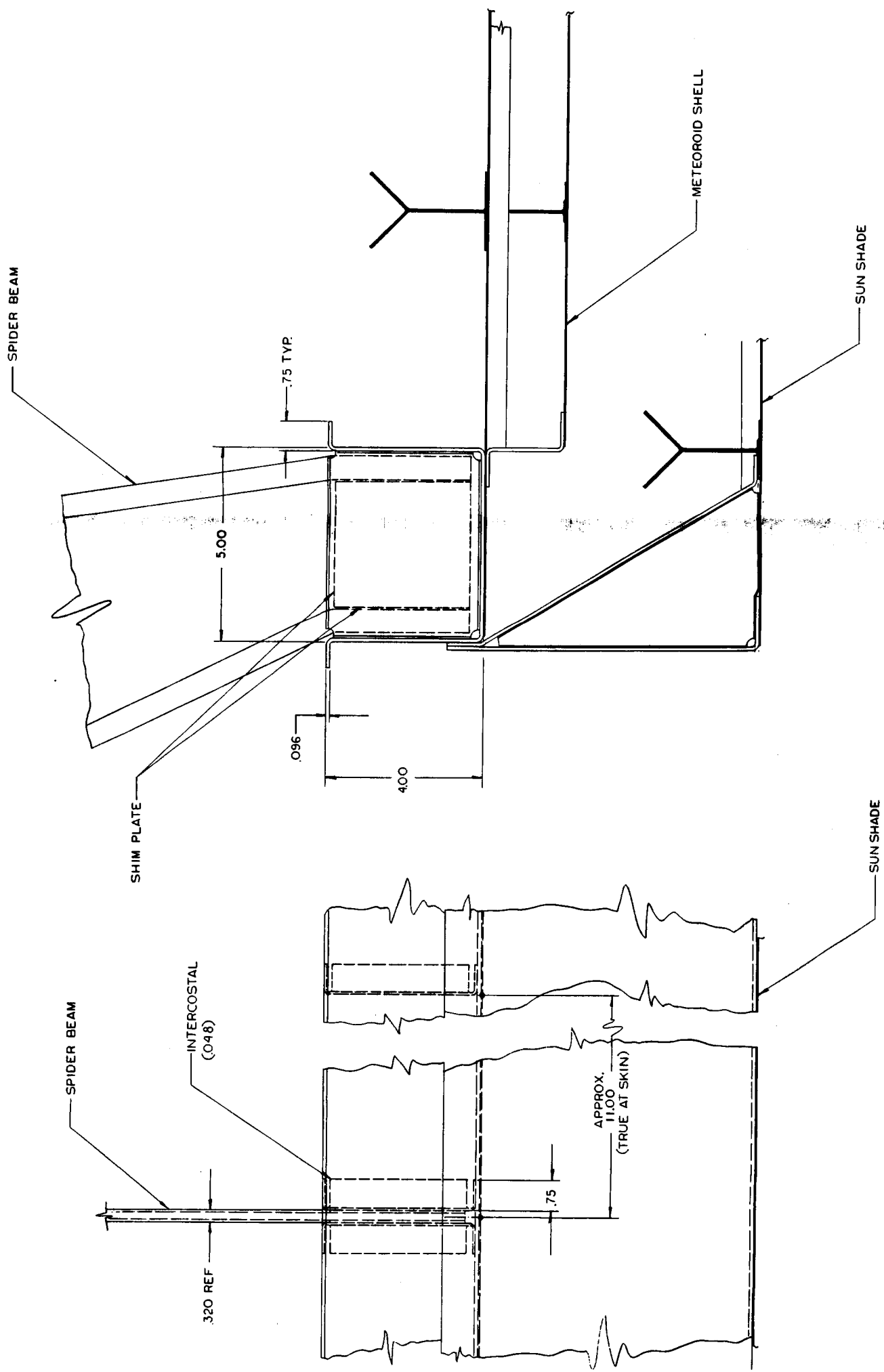
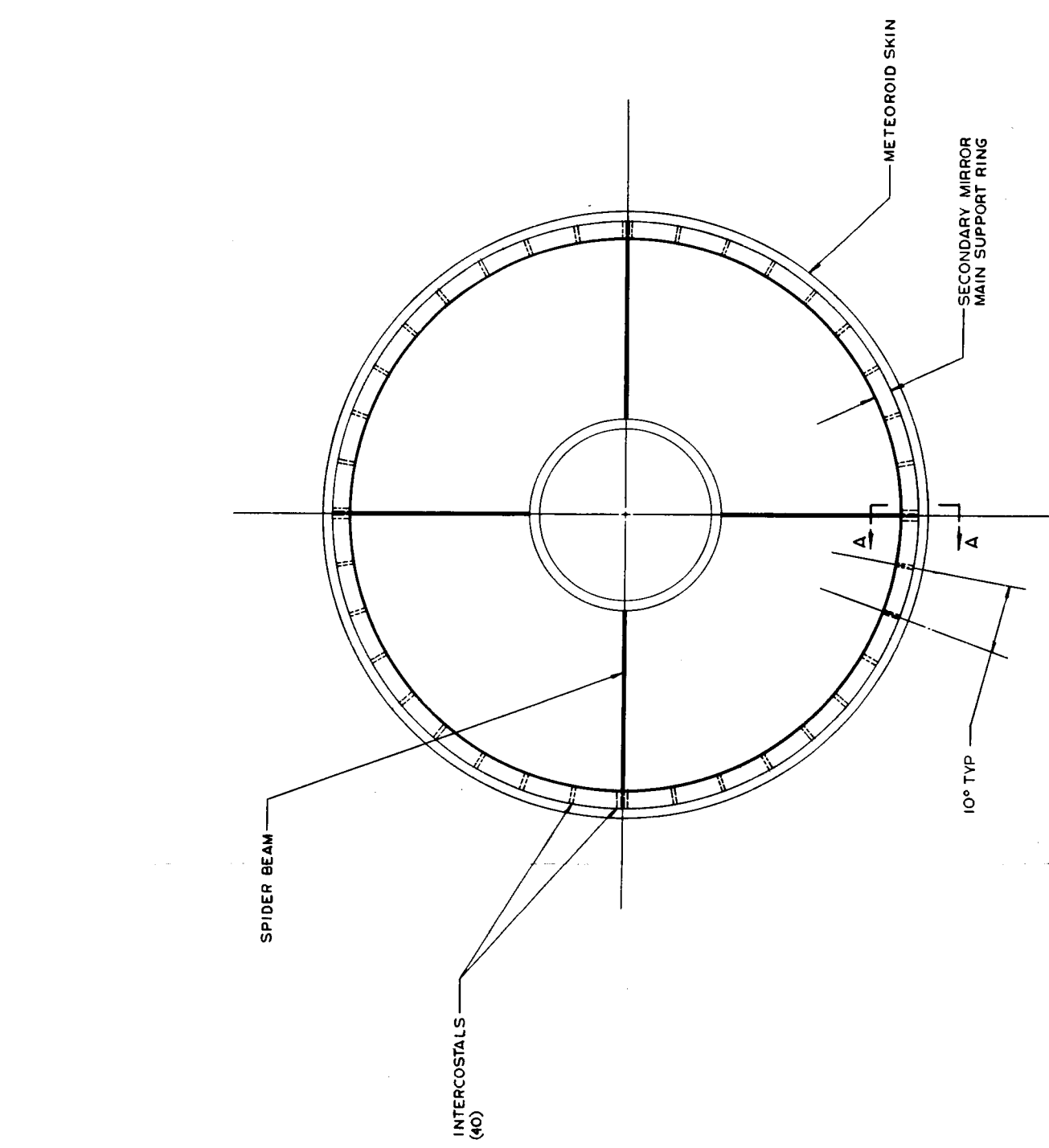


Figure A-5. Alternate secondary mirror main support ring.



TABLE A-1. STRUCTURAL COMPONENT THICKNESS AND LAMINATE DESCRIPTION

Component	Thickness (in.)	Material	Ply Orientation (deg)	Ply Thickness (mils)
<b>Structural Shell</b>				
Skin	0.048	HMS/X-904	[+45, -45, 90, 0] <sub>2S</sub>	3
Frames	0.032	HMS/X-904	[+45, -45, 90, 0] <sub>S</sub>	4
<b>Meteoroid Shell</b>				
Skin	0.024	HMS/X-904	[+45, -45, 90, 0] <sub>S</sub>	3
Frames	0.032	HMS/X-904	[+45, -45, 90, 0] <sub>S</sub>	4
<b>Sunshade</b>				
Skin	0.024	HMS/X-904	[+45, -45, 90, 0] <sub>S</sub>	3
Frames	0.032	HMS/X-904	[+45, -45, 90, 0] <sub>S</sub>	4
Forward Ring	0.096	HMS/X-904	[+45, -45, 90, 0] <sub>2S</sub>	6
Secondary Mirror Ring	0.080	HMS/X-904	[+45, -45, 90, 0] <sub>2S</sub>	5
Aperture Doors	2.00/0.010	Alum/HC	—	
Spider Beams	0.198	HMS/X-904	[+45, -45, 90, 0] <sub>4S</sub>	6
Extension Rails	0.096	HMS/X-904	[+45, -45, 90, 0] <sub>2S</sub>	6
<b>Aft Torque Box</b>				
Ring	0.080	HMS/X-904	[+45, -45, 90, 0] <sub>2S</sub>	5
Web	0.032	HMS/X-904	[+45, -45, 90, 0] <sub>S</sub>	4
<b>Forward Torque Box</b>				
Rings	0.080	HMS/X-904	[+45, -45, 90, 0] <sub>2S</sub>	5
Web	0.032	HMS/X-904	[+45, -45, 90, 0] <sub>S</sub>	4

The shell assembly is constructed in a similar manner as the main shell, with the complete cylinder made of two cylinders, each of which is comprised of six panel assemblies consisting of skins and stub frame sections. Panel splicing is done as shown in Figure A-3.

c. Sun Shade Structure. The sun shade structure surrounds the meteoroid shell when retracted. A space of 5 in. is maintained between the sun shade skin and meteoroid shell skin. This space is utilized to house the 76 mm (3 in.) high frames of the sun shade and the deployment tracks which are bonded to the exterior surface of the meteoroid skin, as shown in View D of Figure A-2.

The 76 mm (3 in.) high ring frames of the sun shade, which are spaced on 255 mm (10 in.) centers, are a "T" section configuration as shown in Figure A-4. The base of the frame is 38 mm (1.5 in.) wide and is bonded to the baffle skin panels. As in the case of the main structural cylinder, an alternate "Y" frame configuration is shown in Figure A-4 should it be needed for light dispersion on further analysis.

Again, as with the main shell and meteoroid shell, the completed cylinder is made up of two cylindrical assemblies, each consisting of six panel subassemblies spliced together (Fig. A-3).

The sun shade is supported by the forward torque box ring of the structural shell during boost and is stabilized against sway and torsional forces by shear pins in the aft closure member as shown in View B of Figure A-2.

2. Mechanical Deployment Systems. The sun shade deployment system consists of three basic parts: the rails and rollers, the actuation system, and the locking mechanism. The three systems were designed to the depth required for dynamic and structural analysis of the complete deployed telescope structure.

a. The Roller System. The sun shade is guided to its extended position by four rails which are bonded to the exterior surface of the meteoroid skin. The rollers are located on the inside of the sun shade, as shown in Figure A-1 and Views B, C, and D of Figure A-2.

The rails are spaced at 1.6 rad (90 degree) intervals with seven rollers traveling on each rail. The rollers are spring mounted to maintain constant pressure on the rails. The forward ends of the four rails are tapered to aid in roller engagement onto the rails during retraction.

The rails do not react any loads from the deployed sun shade due to the locking mechanism used to secure the sun shade. In the retracted position the rollers at the forward end of the rails impart some minor torsion and sway loads into the rails. The rails are primarily loaded by motion during deployment and retraction operations.

The rails are a graphite composite layup, which is described in Table A-1. The rollers are molded graphite composite.

b. The Locking Mechanism. The locking mechanism used to secure the sun shade in its extended position is shown in Figure A-6. The locking system is located in four places adjacent to the forward ends of the rail system.

The lock consists of a dual hook and an eccentric crank pin which is initially passively activated by the forward motion of the hook. Final locking is accomplished by an electric driven screw jack which pulls the eccentric pin up into the hook, removing the weight of the sun shade from the rails and transferring it into the forward torque box ring of the structural shell to which the locking mechanism is attached.

c. The Activation System. Figure A-7 shows a feasible deployment system of minimum weight which eliminates the need for heavy gear tracks and traveling motor systems.

The system utilizes 0.13 mm (5 mil) stainless steel tapes which are stored on two reels, one for the deployment tape and one for the retraction tape. Tension is applied to the appropriate tape by a two-position electric motor and drive gear. Tape slack is controlled by a slip clutch between the two storage drums.

The system consists of two assemblies located 3.15 rad (180 degrees) apart in the aft closeout structure. The motors are synchronized to ensure identical deployment rates from both assemblies. Travel termination is controlled by sensitized inlays on the tapes which are detected by an electronic scanner, which in turn controls the power input to the motor drive system.

## C. Thermal Analysis

A modal temperature analysis was performed by the Marshall Space Flight Center on the selected graphite/epoxy optical telescope assembly (OTA) structure, primary OTA ring, and mirror assemblies. A separate part of

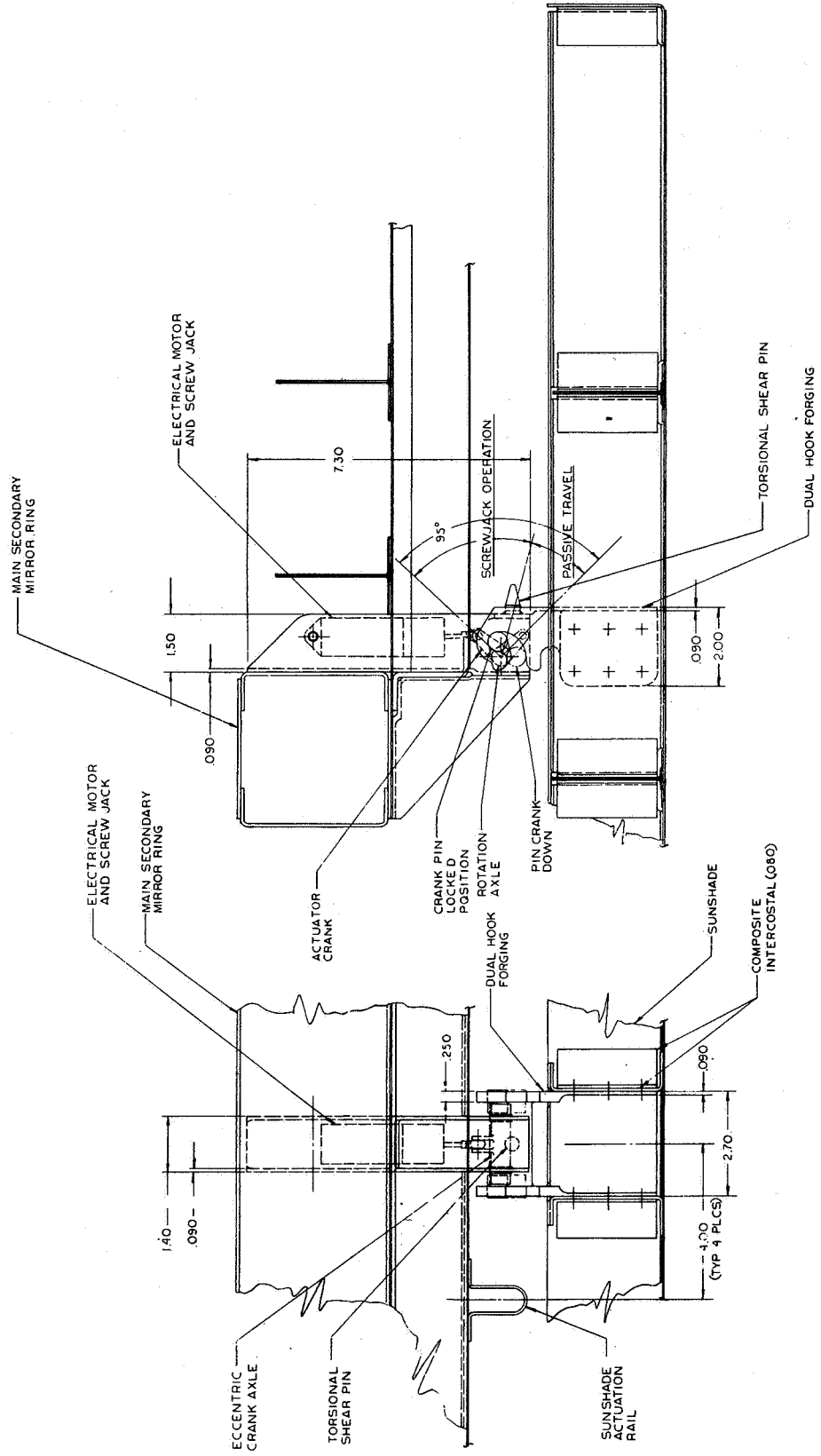


Figure A-6. Sunshade locking mechanism.

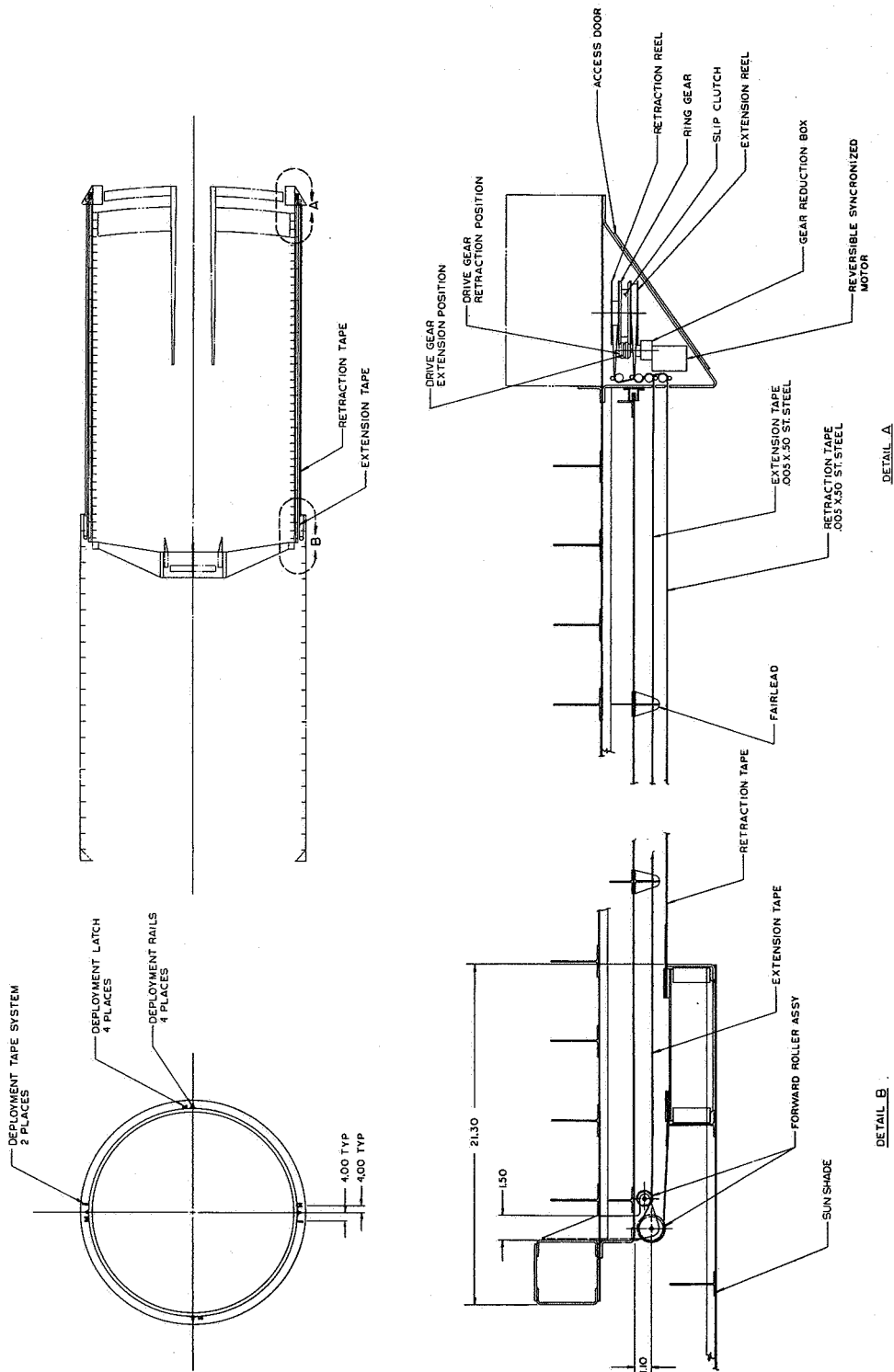


Figure A-7. LST sunshade actuation system.



the analysis produced temperature gradient data for two of the main shell baffle rings, one near the primary mirror support and one near the secondary mirror support. Structural wall temperatures for the support systems module (SSM) were taken from an earlier analysis provided by NASA-MSFC from Reference A-2. The effect of temperature change on structural distortion was investigated for the worst 20-minute time period of orbit 61, assuming a sun inclination angle of 0.91 rad (52 degrees) to the OTA shell structure. The information supplied was converted to temperature change parameters necessary for the NASTRAN structural analysis model by the techniques described in this section.

1. Assumptions. The following assumptions can be made:

1. The critical time span is 20 minutes. (This was approximated to 0.4036 hours to coincide with the computer printout.)
2. The Main Shell wall is the critical component and the particular 20 minute period for analysis is that period during which the main shell wall experiences the maximum temperature change.
3. The temperature changes are symmetrical about a plane containing the longitudinal axis of the structure and the sun. (This assumption permitted the analysis of only two boundary conditions on the quarter model.)
4. The temperature changes in the scientific instrument package (SIP) are identically zero.
5. The inside caps of the baffle rings in the main shell have a longitudinal temperature change ( $\Delta T$  distribution) similar to the main shell wall  $\Delta T$  distribution and a circumferential  $\Delta T$  distribution similar to the circumferential  $\Delta T$  distribution of the sun shade baffles.
6. The forward support ring outside face temperature change is similar to the main shell wall  $\Delta T$  and the inside face  $\Delta T$  is similar to the spider beams  $\Delta T$ .
7. The sun screen and micrometeoroid shield are loosely coupled to the structural shell.

2. Analysis Procedure. The procedure used in the assigning of temperatures to the nodes of the NASTRAN finite element structural model of the LST was as follows. The main shell inside-wall temperatures were

tabulated for the 61st orbit for the ring of eight nodes nearest the primary mirror (Table A-2) and for the ring of eight nodes nearest the secondary mirror (Table A-3). Figure A-8 is a plot of the inside wall, eight nodes near the secondary mirror support. By comparison of the temperature changes during each 0.4 hour time period, it was observed that the critical time span was from 96.4603 hours to 97.0657 hours (the temperatures for 96.4603 hours being assumed equal to the temperatures for 98.2765 hours). The temperatures of the two intermediate rings of nodes on the main shell inside wall and the four rings of nodes on the main shell outside wall were tabulated for  $t = 96.4$  hours and for 97.0 hours. Differences were obtained and averaged about the plane of assumed symmetry. The temperature changes were separated into symmetric and antisymmetric components about the plane of structural symmetry normal to the plane of symmetry containing the sun. This operation is shown in Tables A-2 and A-3 and summarized in Table A-4. The symmetric and antisymmetric components in Table A-3 were plotted versus longitudinal position as shown in Figure A-9 and curves drawn through the points. Temperature changes for the 10 ring stations of the NASTRAN model were scaled from the curves. At this stage, temperature changes were known at 0.39 rad (22.5 degrees) and 1.2 rad (67.5 degrees) from the symmetry plane containing the sun. The NASTRAN model has grid points in 0.26 rad (15 degree) increments from zero to 1.6 rad (90 degrees). The two temperature change components were plotted at each of the 10 stations and a curve was drawn through the points perpendicular to the planes of structural symmetry and through zero for the antisymmetric component at the plane of antisymmetry. The temperature changes for the grid points of the NASTRAN model on the main shell wall were then scaled from these plots.

The sun screen and micrometeoroid shield temperatures were tabulated next. Considerable asymmetry was observed as typified in Figure A-10. It was decided to invoke the assumption of loose coupling and to approximate the asymmetrical temperature change by a symmetrical change. To partially compensate for the unconservatism in the symmetry approximation, the temperature changes selected for application to the model, Figure A-11, were chosen to represent the maximum variations encountered and not the changes occurring during the selected 0.4 hour time period critical on the main shell wall. This selected temperature change distribution was not varied longitudinally since longitudinal variation in the sun screen and micrometeoroid shield can have only a minor effect on the main shell and mirror support structure. The circumferential variation of the selected temperature change was extrapolated to grid points spaced 0.53 rad (30 degrees) apart, separated into symmetric and antisymmetric components, and applied to the grid points of the NASTRAN model.

TABLE A-2. MAIN SHELL INSIDE-WALL TEMPERATURE HISTORY FOR NODES  
NEAREST PRIMARY MIRROR (IN °F)

Sun Angle (deg) Node Time (hr)	-157.5	-112.5	-67.5	-22.5	22.5	67.5	112.5	157.5
	266	265	264	263	262	261	268	267
96. 8639	44. 42142	44. 223279	44. 38959	44. 56957	44. 57130	44. 33094	44. 34139	44. 45609
97. 0657	44. 74844	44. 51341	44. 60416	44. 84503	44. 88855	44. 64001	44. 50604	44. 76489
97. 2675	44. 77157	44. 62295	44. 72450	44. 94233	44. 95156	44. 69818	44. 58556	44. 77051
97. 4693	44. 65486	44. 55083	44. 62755	44. 84322	44. 86198	44. 61802	44. 52318	44. 65776
97. 6711	44. 52207	44. 45230	44. 50795	44. 72201	44. 74999	44. 51862	44. 43224	44. 52771
97. 8729	44. 37465	44. 33168	44. 36500	44. 56828	44. 59979	44. 38649	44. 31296	44. 38016
98. 0741	44. 21010	44. 18633	44. 19987	44. 38864	44. 41737	44. 22012	44. 16673	44. 21466
98. 2765	44. 13650	44. 13192	44. 15013	44. 34025	44. 39516	44. 21160	44. 14753	44. 15621
Maximum ΔT	0. 61194	0. 38149	0. 45403	0. 50478	0. 49339	0. 42841	0. 35851	0. 60868
Average ΔT					0. 49908	0. 44122	0. 37000	0. 61031
Symmetrical					+0. 55469	+0. 40561		
Asymmetrical					-0. 05561	+0. 03561		

TABLE A-3. MAIN SHELL INSIDE-WALL TEMPERATURE HISTORY FOR NODES  
NEAREST SECONDARY MIRROR (IN °F)

Sun Angle (deg) Time (hr)	-157.5	-112.5	-67.5	-22.5	22.5	67.5	112.5	157.5
	Node 290	289	288	287	286	285	292	291
96.8	22.87121	22.82739	22.62477	22.97971	23.28690	22.63720	23.12635	23.06230
97.0	26.16802	26.06715	25.47254	26.25087	26.19616	25.60094	26.05247	26.08721
97.2	26.91838	27.01644	26.63686	27.05249	26.95143	26.43619	26.77119	26.78276
97.4	25.93531	26.00439	25.74074	26.04123	25.99917	25.65945	25.87341	25.86354
97.6	24.50936	24.54584	24.35939	24.59538	24.58869	24.34442	24.46370	24.46225
97.8	23.02575	23.04416	22.92490	23.10655	23.09675	22.91221	22.99187	22.99735
98.0	21.62454	21.65620	21.57265	21.69444	21.67028	21.53441	21.60885	21.59588
98.2	20.89137	20.92460	20.83974	21.07307	21.11495	21.11849	21.15462	20.97400
Maximum ΔT	5.27665	5.14255	4.63280	5.17780	5.08121	4.48245	4.89785	5.11321
Average ΔT					5.12950	4.55762	5.02020	5.19493
Symmetrical					+5.16221	+4.78891		
Asymmetrical					-0.03271	-0.23129		

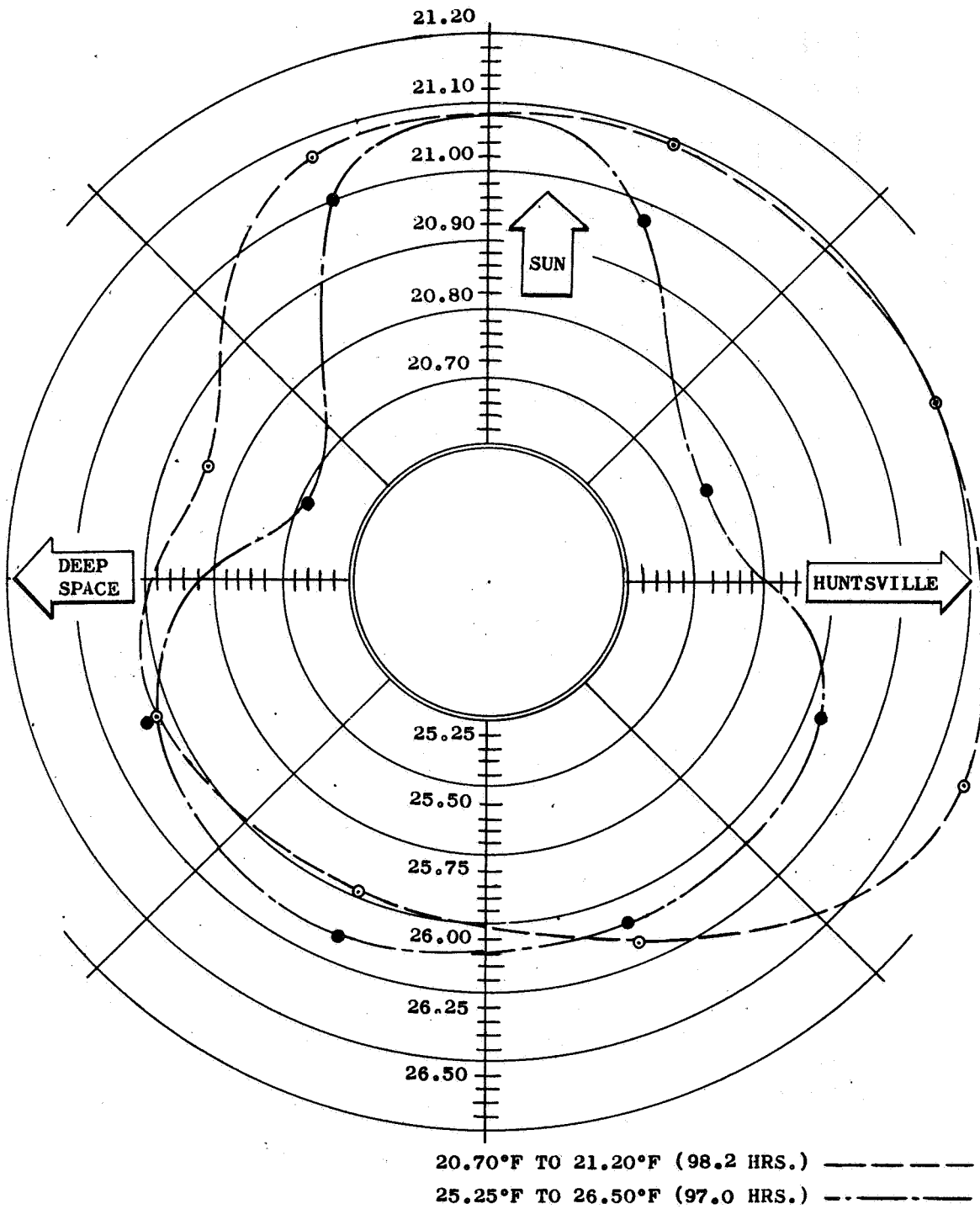


Figure A-8. Structural shell inside-wall temperatures — 61st orbit.

TABLE A-4. SUMMARY OF MAIN SHELL TEMPERATURE CHANGES

Node Ring Location	Temperature Component	Temperature at 22.5 deg Sun Angle (°F)			Temperature at 67.5 deg Sun Angle (°F)		
		Inner Wall	Outer Wall	Average	Inner Wall	Outer Wall	Average
Aft	Symmetric	+0.555	+0.543	+0.549	+0.405	+0.396	+0.400
	Asymmetric	-0.055	-0.063	-0.059	+0.035	+0.034	+0.034
2	Symmetric	+0.657	+0.620	+0.638	+0.587	+0.551	+0.569
	Asymmetric	-0.029	-0.032	-0.030	+0.014	+0.014	+0.014
3	Symmetric	+1.825	+1.743	+1.784	+1.755	+1.672	+1.713
	Asymmetric	-0.142	-0.144	-0.143	-0.043	-0.045	-0.044
Forward	Symmetric	+5.162	+5.032	+5.097	+4.789	+4.647	+4.718
	Asymmetric	-0.033	-0.017	-0.025	-0.231	-0.233	-0.232

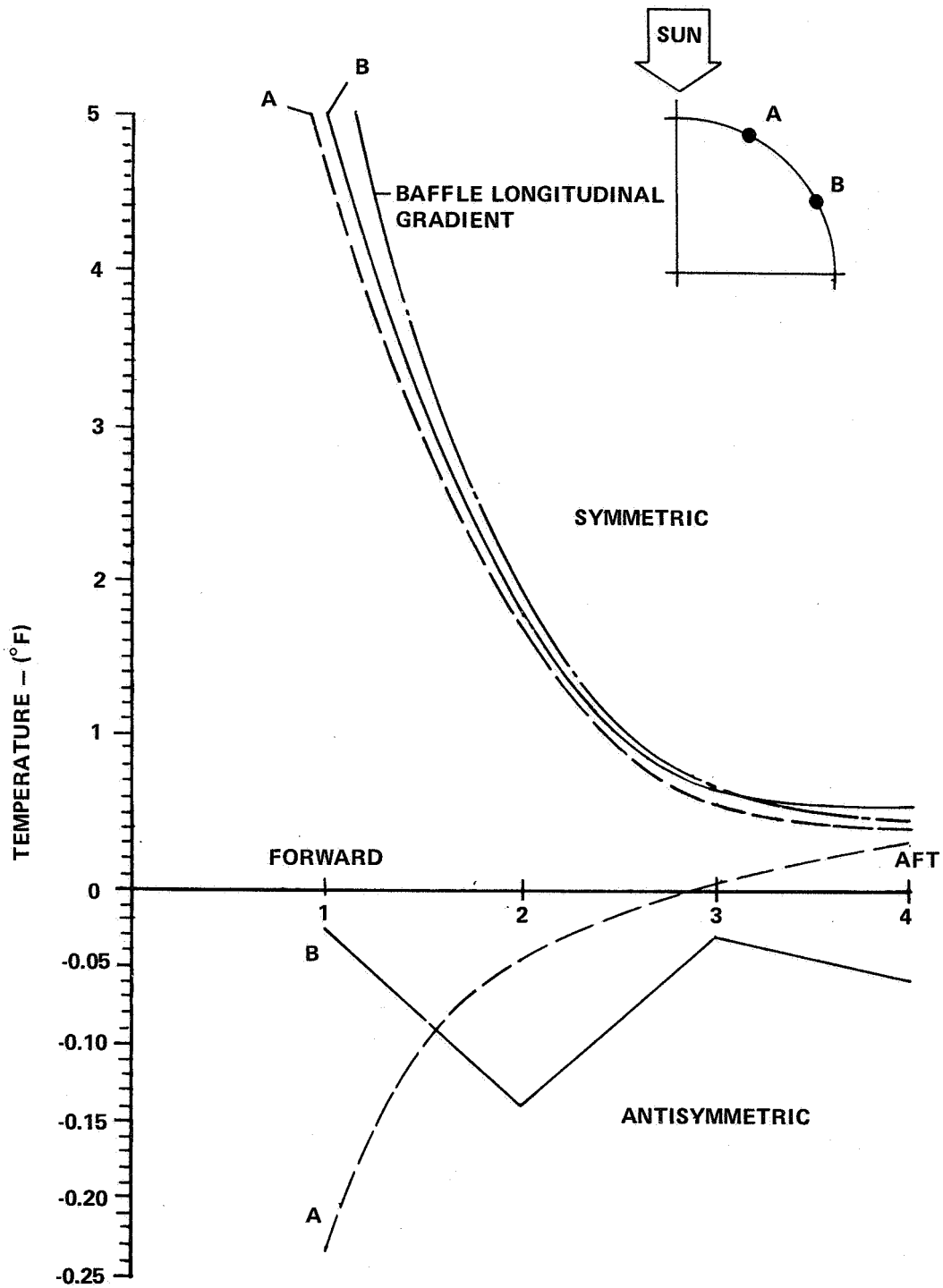


Figure A-9. Longitudinal temperature change variation in main shell wall.

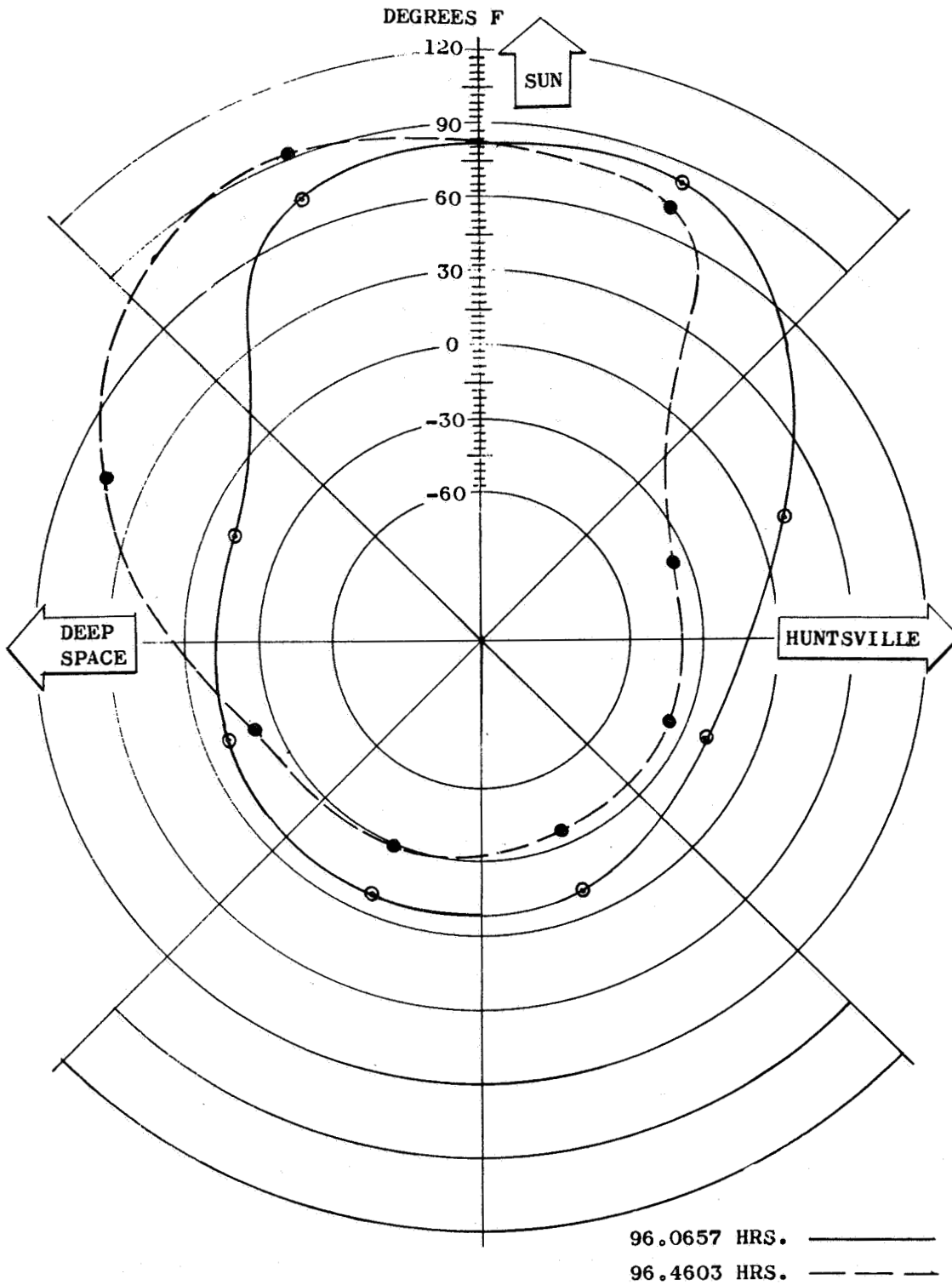


Figure A-10. Micrometeoroid shell first ring temperatures — 61st orbit.



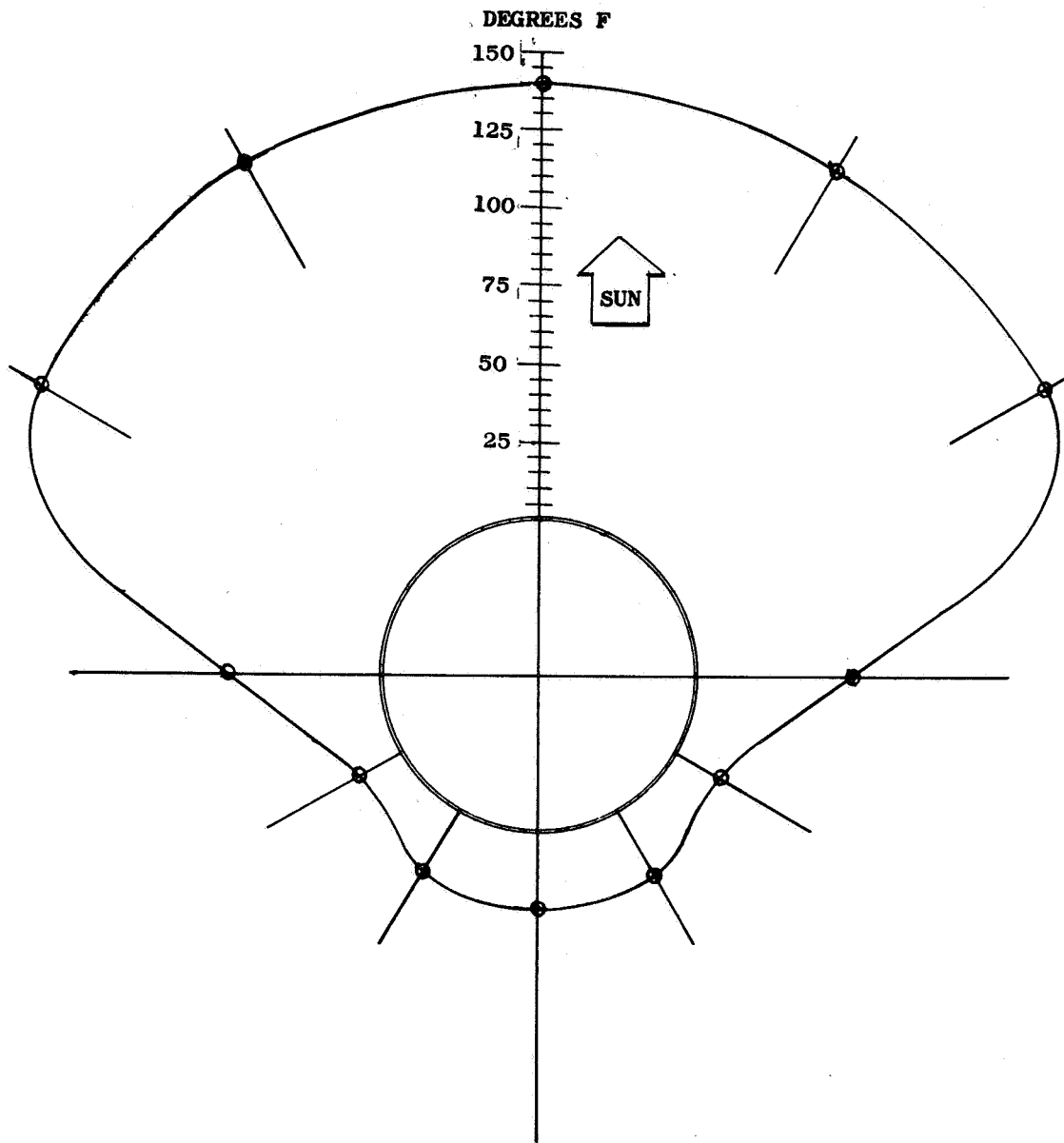


Figure A-11. Assumed FEM node point temperatures.

Temperature information on the caps of the rings in the main shell was obtained from the curves included as Figures A-12 and A-13. Node 10 was assumed typical of caps of the rings. For ring caps near the secondary mirror, the maximum temperature change in 20 minutes (0.33 hour) was found to be

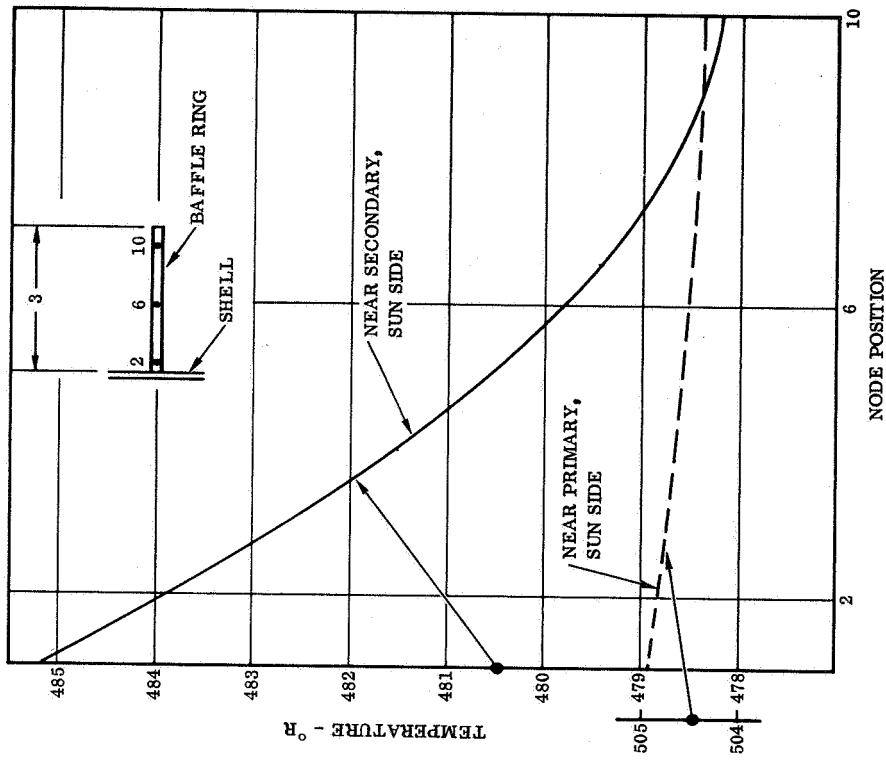


Figure A-13. Temperature/depth variation of main shell rings.

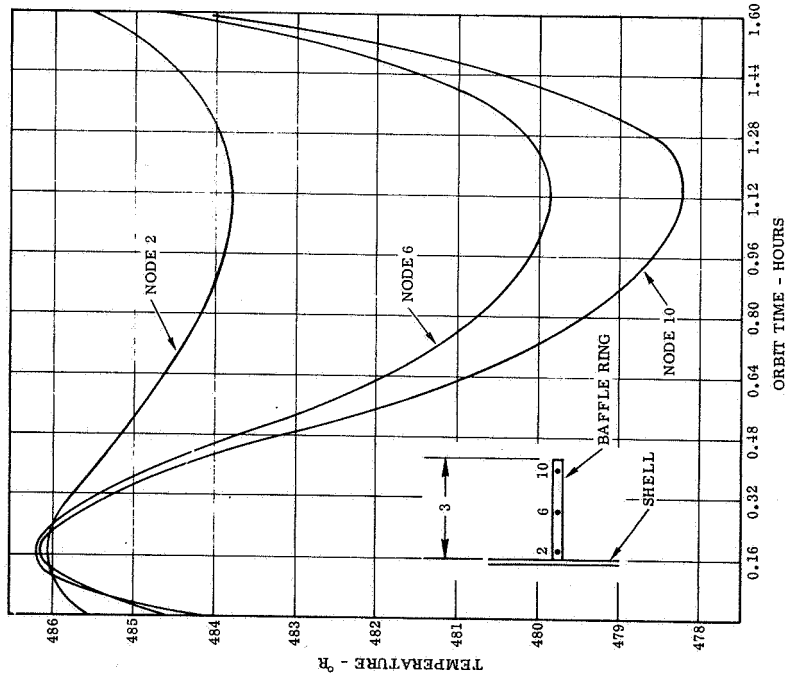


Figure A-12. Time/temperature variation of forward shell rings.

approximately 0.1 rad (5.8 degrees). For ring caps near the primary mirror, the temperature change was obtained by ratioing the 0.1 rad (5.8 degrees) by the ratio of the total gradient of a baffle near the secondary mirror to the total gradient of a baffle near the primary mirror. This gave a variation of 0.2°C (0.47°F). These two temperature change points were added to the plot of wall temperature change longitudinal variation and a similar curve was drawn. Also, in accordance with the assumption in item 57 of Section C.1, the above temperature change was assumed to be a maximum, and a circumferential distribution similar to the sun shade baffle distribution was used. The longitudinally and circumferentially distributed ring cap temperature changes were added to the main shell temperature changes and applied to the grid points of the NASTRAN model.

The temperature changes for the spider beams during the critical time period were obtained directly from the computer printout and were applied to the grid points of the NASTRAN model. The temperature changes were very small and zero longitudinal variation on the height of the spider beams was assumed.

The forward ring on the main shell was assigned temperature changes equal to spider beam temperature changes on the inside face and equal to the main shell wall temperature changes on the outside face.

The SSM wall temperature change was taken from Figure A-14 [A-2]. The maximum temperature change during 20 minutes was scaled as 0.83°C (1.5°F). This was an error because the plot is in degrees centigrade. Any future runs with the model should have the SSM wall variation corrected. Zero longitudinal variation and a circumferential temperature change variation similar to the one selected for the micrometeoroid shield were assumed.

Since the SSM is structurally attached to the ring supporting the primary mirror, it is important that the temperature change applied to the SSM wall be corrected and a better circumferential distribution obtained. This is probably the single largest source of inaccuracy in the current analysis.

3. Second Iteration Revisions. The first thermal distortion analysis employing the node-point temperatures described in Section C.2 was conducted. It was evident that the high temperature changes of the sun shade shell were producing large radial deflections which structurally coupled with the main shell and secondary support beams to induce most of the secondary mirror defocus. It was decided to rerun the distortion analysis for the case of insulation on the exterior wall of the sun shade. For this analysis, the interior surface insulation temperatures of the thermal analysis were applied

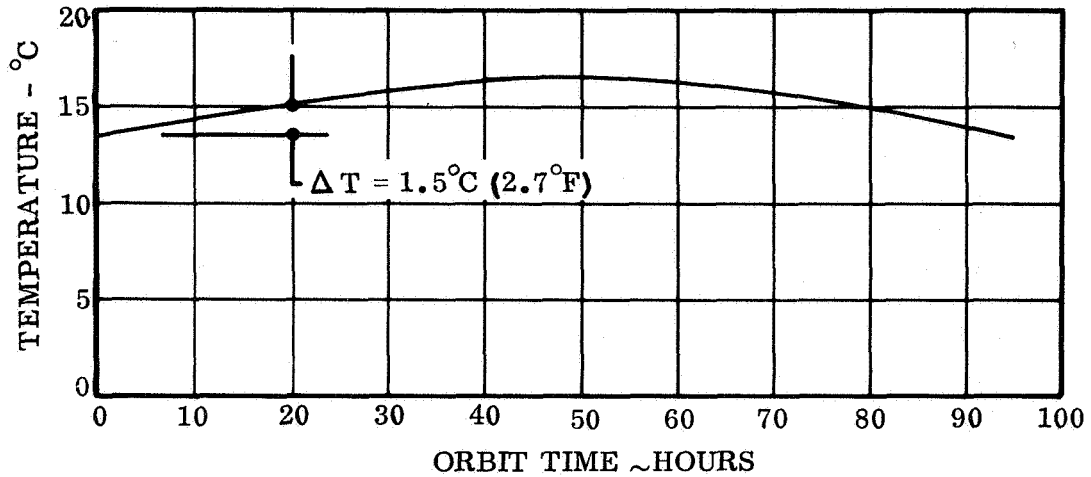


Figure A-14. SSM wall temperature variation.

to the inner structural shell wall of the sun shade. A procedure similar to that described in Section C.2 was used to derive the circumferential symmetric and asymmetric temperature changes.

An additional change was made to the meteoroid shell node-point temperatures of the NASTRAN model in the overlap area (20 in. long) of the sun shade and meteoroid shell. The meteoroid shell temperatures were tapered from the exposed area edge to values corresponding to the inside of the sun shade at the end of the meteoroid shell.

As a final correction, the SSM shell wall maximum temperature change was revised upward from 0.83°C (1.5°F) to 1.5°C (2.7°F) to correct the inadvertent error introduced in the first run.

## D. Structural Analysis

Using the structural design outlined in Section B, the main elements of the structures were sized for load based on the Titan launch and Space Shuttle retrieval load factors. Detail element structural properties were then input to a NASTRAN finite element model and distortion, stress, and dynamic resultants were determined for the orbital condition. The purpose of the analyses was to assess the feasibility of the graphite design and establish the critical areas of the structure. Optimization of the designs was not possible. Therefore the analysis results may be viewed with a certain degree of optimism toward future refinement.

1. Structural Sizing. The limit load factors for all conditions are shown in Table A-5. The structure (Fig. A-15) is assumed supported at the end rings (Points A and B) of the main shell for all loading conditions except for the Titan launch condition, where the structure is cantilevered from the aft end (Plane A). The preliminary estimates of component weights used in the strength sizing analysis are shown in Table A-6. The structural material used was, in the main, a pseudo-isotropic layup of HM-S/X-904 graphite/epoxy. Reduced allowables (from the average of current test data) for this material used in the analysis are shown in Table A-7. A factor of safety of 1.4 on limit loads was used throughout the sizing to derive the ultimate design loads.

TABLE A-5. LST LIMIT LOAD FACTORS<sup>a</sup>

Condition	Forward	Lateral	Vertical
Titan Launch	6.0	±1.5	±1.5
Orbiter Entry	-0.5	±1.0	-3.0 ±1.0
Shuttle Launch	1.4 ±1.6	±1.0	±1.0
End Shuttle Boost	3.0 ±0.3	±0.6	±0.6
Landing	-1.3	±0.5	-2.7 ±0.5
Air Transport	±3.0	±1.5	±3.0

a. Ultimate factor of safety = 1.4.

a. Main Shell Loads. Shell loads and shell equivalent unit loads for the Titan and Space Shuttle Orbiter conditions are given in Table A-8. The Titan launch case is critical for shell stability.

b. Main Shell Instability. The properties of the main shell wall, with baffle ring stiffeners, was calculated as shown in Figure A-16. A general instability analysis of the main shell was performed by the method of Reference A-3. The classical instability value for the shell was calculated (for pure compression) to be

$$N_c = 44.6 \text{ MN/m (255 lb/in.)}$$

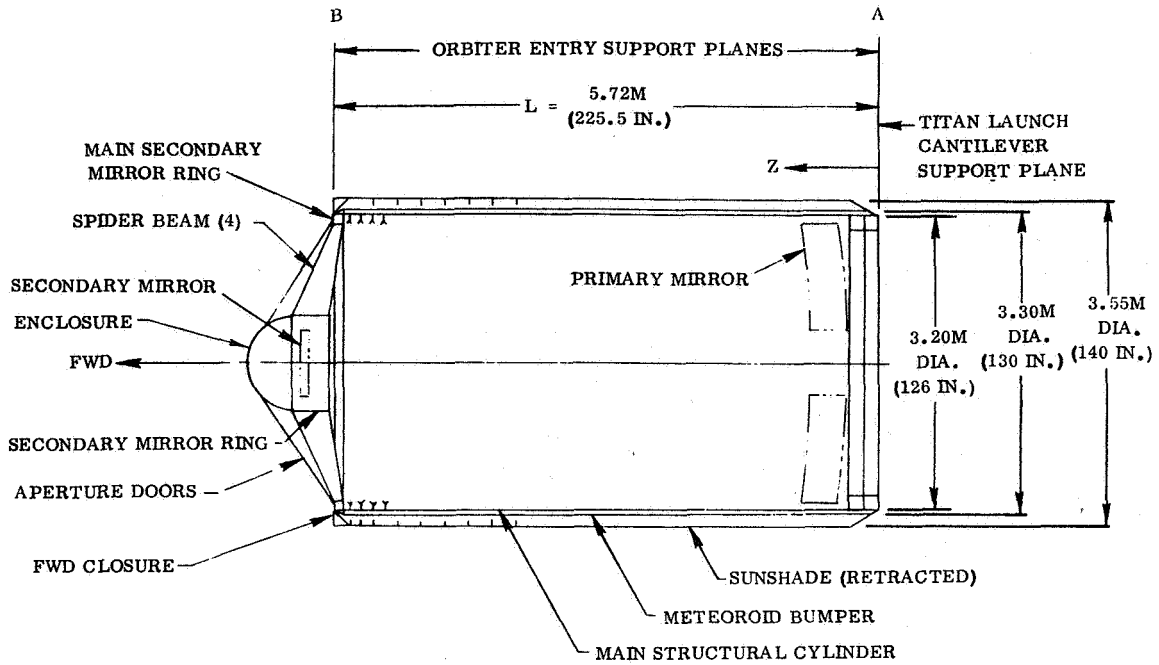


Figure A-15. Structure of LST.

TABLE A-6. COMPONENT WEIGHTS AND CENTER OF GRAVITY LOCATIONS

Code	Component	Weight		Z (C. G.) <sup>a</sup>	
		kg	(lb)	m	(in.)
a	Main Structural Shell (Skin)	112	(248)	2.87	(113)
b	Main Structural Shell (Rings)	51	(112)	2.87	(113)
c	Main Structural Shell (Insulation)	35	(77)	2.87	(113)
d	Meteoroid Bumper (Skin)	61	(134)	2.87	(113)
e	Meteoroid Bumper (Rings)	13	(28)	2.87	(113)
f	Meteoroid Bumper (Rails)	14	(31)	2.87	(113)
g	Sunshade (Skin)	66	(145)	2.87	(113)
h	Sunshade (Rings)	38	(84)	2.87	(113)
i	Forward Torque Box Closure	15	(34)	5.66	(223)
j	Secondary Mirror	36	(80)	6.05	(238)
k	Enclosure	6	(13)	6.43	(253)
l	Aperture Doors	57	(125)	6.05	(238)
m	Main Secondary Mirror Ring	13	(28)	5.69	(224)
n	Secondary Mirror Ring	10	(22)	5.97	(235)
o	Spider Beams (4)	20	(43)	5.89	(232)
p	Sunshade Latch Mechanisms	3.2	(7)	5.60	(220)

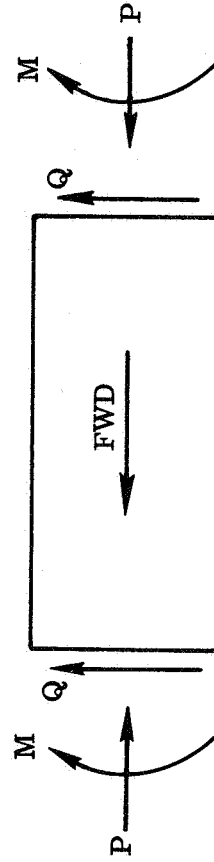
a. Z measured from plane A (Fig. A-15).

TABLE A-7. PSEUDO-ISOTROPIC HMS GRAPHITE/EPOXY [+45, -45, 90, 0 deg]<sub>S</sub>

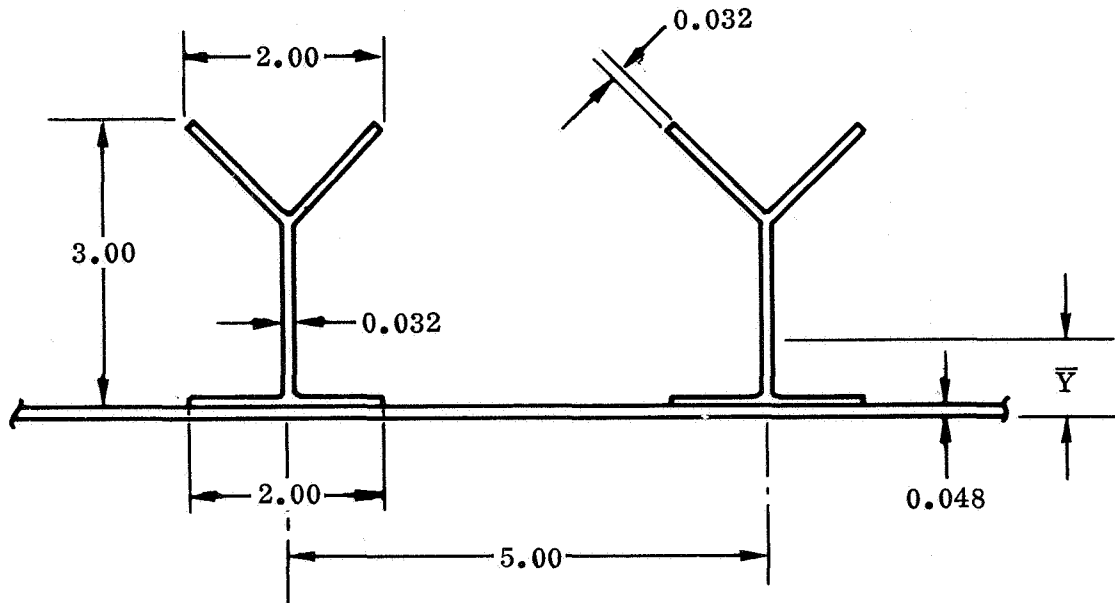
Laminate Thickness (in.)	Ply Thickness (in.)	No. of Plies	$E_{XX}, E_{YY}$ (psi)	$G_{XY}$ (psi)	$\nu_{XY}, \nu_{YX}$	$D_{11}$ (lb-in.)	$D_{12}$ (lb-in.)	$D_{22}$ (lb-in.)	$D_{16}$ (lb-in.)	$D_{26}$ (lb-in.)	$D_{66}$ (lb-in.)
0.024	0.003	8	$10.5 \times 10^6$	$4.0 \times 10^6$	0.32	9.01	7.15	12.04	2.27	2.27	7.52
0.032	0.004	8	$10.5 \times 10^6$	$4.0 \times 10^6$	0.32	21.36	16.96	28.55	5.39	5.39	17.83
0.040	0.005	8	$10.5 \times 10^6$	$4.0 \times 10^6$	0.32	41.71	33.12	55.76	10.53	10.53	34.82
0.048	0.003	16	$10.5 \times 10^6$	$4.0 \times 10^6$	0.32	86.78	45.60	104.98	7.58	7.58	48.50
0.048	0.006	8	$10.5 \times 10^6$	$4.0 \times 10^6$	0.32	72.08	57.23	96.35	18.20	18.20	-60.17
0.056	0.007	8	$10.5 \times 10^6$	$4.0 \times 10^6$	0.32	114.46	90.88	153.00	28.90	28.90	95.55
0.064	0.004	16	$10.5 \times 10^6$	$4.0 \times 10^6$	0.32	205.71	107.99	248.85	17.98	17.98	114.96
0.080	0.005	16	$10.5 \times 10^6$	$4.0 \times 10^6$	0.32	401.78	210.92	486.04	35.11	35.11	224.54
0.096	0.006	16	$10.5 \times 10^6$	$4.0 \times 10^6$	0.32	694.27	364.48	839.88	60.67	60.67	388.00
0.112	0.007	16	$10.5 \times 10^6$	$4.0 \times 10^6$	0.32	1102	579	1334	96	96	616

TABLE A-8. MAIN SHELL ULTIMATE APPLIED LOADS

Case	Location	P (lb)	Q (lb)	M (in.-lb)	Unit Load Resultants			
					Compression (lb/in.)	Bending (lb/in.)	Combined Axial (in. -lb)	Shear
Titan Launch	Forward	6 502	1183	7 445	16.4	0.6	17.0	4.7
	Aft Plane	10 172	2100	377 562	25.7	30.3	56.0	8.3
Orbiter Entry	Forward	—	3153	19 852	—	1.6	1.6	12.5
	Center	—	—	-266 554	—	21.4	21.4	—







AREA = 0.4125 INCH<sup>2</sup>  
 CENTROID (Y) = 0.4178 INCH  
 I ABOUT CENTROID = 0.2667 INCH<sup>4</sup>

Figure A-16. Section properties of main shell wall.

A knockdown factor from Reference A-4 must be calculated and applied to the classical value. The values obtained are

$$\lambda = 0.524 \text{ (compression)}$$

and

$$\lambda = 0.614 \text{ (bending) .}$$

The resulting buckling allowables for general instability are, therefore,

$$\begin{aligned}
 N_{cr} &= 0.524 (44.6) = 23.37 \text{ MN/m (133.6 lb/in.)} \\
 &\text{(compression)}
 \end{aligned}$$

and

$$N_{cr} = 0.614 (44.6) = 27.38 \text{ MN/m (156.6 lb/in.)}$$

(bending) .

The Titan launch condition at Plane A (Fig. A-15), produces the maximum running loads. The margin on general instability for this condition is

$$\text{M.S.} = \frac{1}{R_c + R_b} = \frac{1}{\frac{26}{134} + \frac{30}{157}} - 1 = 1.6 .$$

General instability for shear gives a very high margin of safety.

The shell was also checked for local instability between rings in combined compression, bending, and shear; shear was not critical. The general form of the local instability equation is taken from Reference A-3 as

$$N_{cr} = 0.6 \gamma E \frac{t^2}{R} ,$$

where  $\gamma$  is a knockdown factor. For local instability, the following allowables are calculated:

$$N_{cr} = 7.7 \text{ MN/m (44 lb/in.) (compression)}$$

and

$$N_{cr} = 8.2 \text{ MN/m (80 lb/in.) (bending) .}$$

The margin in combined bending and compression for the Titan launch case is critical:

$$M.S. = \frac{1}{R_c + R_b} - 1 = +0.03 \quad .$$

Thus the shell is appropriately sized for local instability near the base ring. It should be possible, if desired, to reduce the shell weight somewhat by reducing the skin thickness near the forward end. This was not considered in the design, however, in order to provide a uniform protection against micrometeoroid impact over the entire shell. The maximum shell stresses from launch loads are:

$$\begin{aligned} \sigma &= \frac{N_c + N_b}{t} = \frac{98 \text{ MN/m}}{1.21 \times 10^{-3} \text{ m}} \left( \frac{56}{0.048} \right) \\ &= 8.274 \times 10^3 \text{ MN/m}^2 \text{ (1200 psi)} \quad . \end{aligned}$$

c. Secondary Shells. The highest loads on the sun shade and micrometeoroid shells occur during Space Shuttle entry (since these shells are not cantilevered). Both shells show very high margins for general and local instability and were therefore sized for minimum-gage with the micrometeoroid bumper requirements.

d. Secondary Mirror Support Beams. An analysis of these beams indicates them to be critical in torsional instability because of the desire to reduce the frontal area blockage (and therefore the beam cap width) on the primary mirror. A typical beam is shown in Figure A-17. Four combinations of cap/web thickness were checked for instability and weight as shown in Table A-9. The configuration of Case 3 was selected as a reasonable compromise between cap width (blockage) and weight.

The beams are assumed to be restrained against twist at the ends but free to warp. Torsional instability is therefore governed by the following expression (taken from Reference A-3):

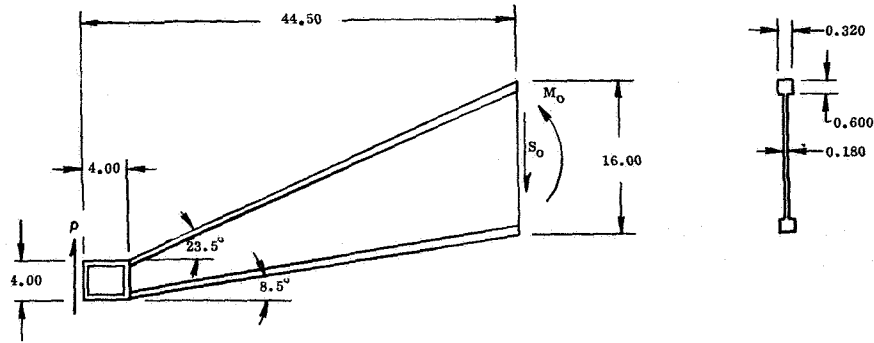
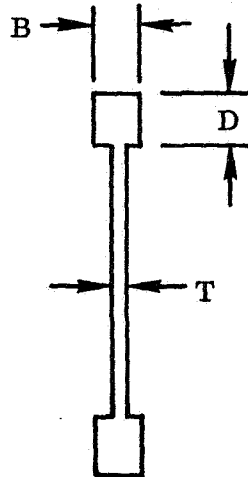


Figure A-17. Secondary mirror support beam.

TABLE A-9. BEAM OPTIMIZATION (WEIGHT VS BLOCKAGE)

Case	B (in.)	D (in.)	T (in.)	Weight (lb)
1	0.520	0.400	0.160	5.9
2	0.400	0.520	0.160	6.6
3	0.320	0.600	0.180	6.2
4	0.280	Full Depth	0.280	8.5



$$\sigma_{cr} = \frac{GJ + \frac{\pi}{L^2} E \Gamma}{I_p} ,$$

where all the nomenclature is familiar except, possibly, the warping constant  $\Gamma$  , given by

$$\Gamma = \frac{h^2}{2}$$

for the compression cap (see Reference A-5).

The simple expression shown above for torsional instability is really applicable only to beams of constant cross section. Thus, for the variable height support beam, an effective height must be determined which represents an equivalent constant beam section.

Figure A-18 includes plots of compressive stress,  $J/I$  , and the warping constant  $\Gamma$  over the length of the beam. The critical stress for instability in this beam geometry is primarily governed by the  $J/I$  ratio, and the critical beam section is the large end. The beam loads and compressive stresses were calculated for the Titan launch condition. The equivalent beam for instability calculations was assumed to have the  $I_p$  ,  $J$  , and  $\Gamma$  values calculated for the large end of the actual beam, with the compressive stress at the large end applied uniformly over the structure. The following numerical values were obtained:

$$\sigma_c = 420 \text{ MN/m (2396 lb/in.) (applied compressive stress) ,}$$

$$I_p = 30 \times 10^6 \text{ mm}^4 \text{ (72 in.}^4\text{) ,}$$

$$J = 17.4 \times 10^3 \text{ mm}^4 \text{ (0.0418 in.}^4\text{) ,}$$

$$\Gamma = 15.68 \times 10^6 \text{ mm}^6 \text{ (0.194 in.}^6\text{) ,}$$

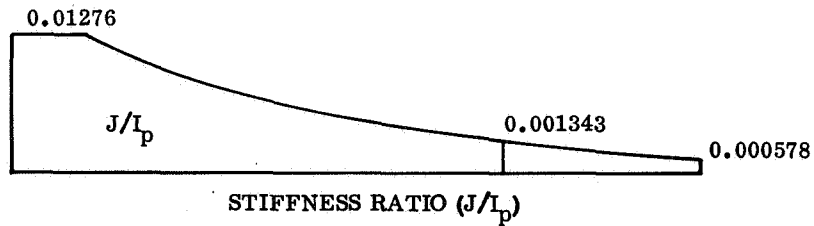
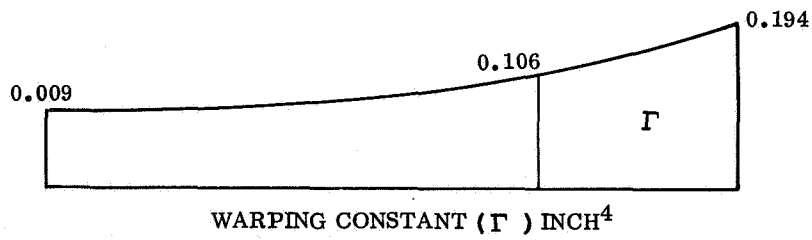
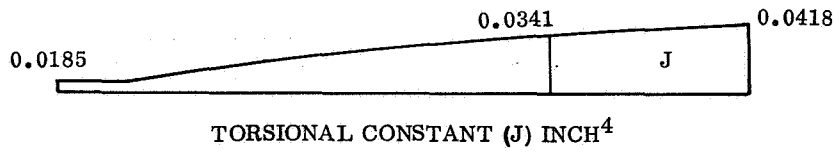
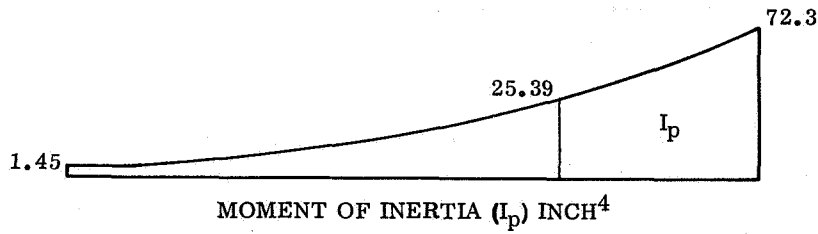
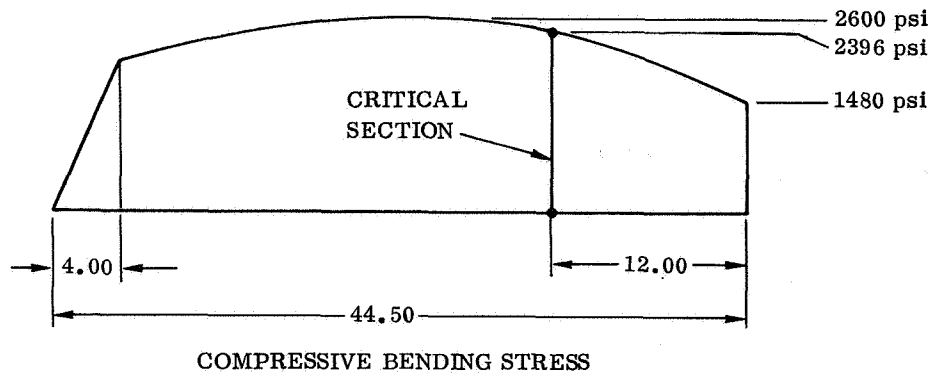


Figure A-18. Beam stress and stiffness diagrams.

and

$$\sigma_{cr} = 430 \text{ MN/m (2461 lb/in.) (critical compressive stress) .}$$

The margin of safety against torsional buckling is

$$M. S. = \frac{2461}{2396} - 1 = + 0.03$$

e. Meteoroid Protection System. An analysis of the required wall thickness for meteoroid protection requirements yields the results shown in Figure A-19. The curves indicate the probability of puncture of the

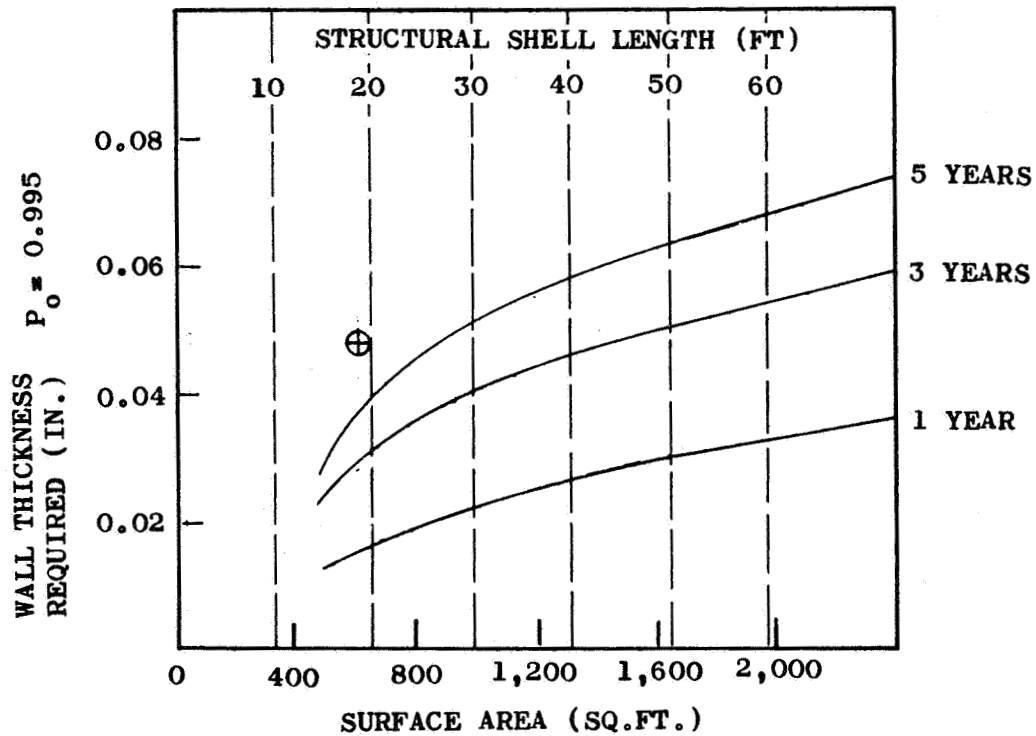


Figure A-19. Structural shell thickness as a function of mission time.

structural shell for 1, 3, and 5 year time spans. The structural wall thickness of 1.22 mm (0.048-in.) is indicated on the graph for the cylinder area of the structural shell, which is 58.27 m<sup>2</sup> (627 ft<sup>2</sup>). The analysis is based on a meteoroid bumper skin thickness of 0.61 mm (0.024 in.).

2. Finite Element Model. The structure of the large telescope was analyzed for thermal distortion and dynamic characteristics using the finite element program, NASTRAN [A-6] operating on a CDC 6400 computer. It was selected as the analysis program because it possessed automated thermal distortion analysis and vibration analysis of a single model. With a single model to be used for both analyses, considerable effort was exerted to model accurately all structure which was important dynamically (because it was heavy and/or flexible) and all structure which would produce distortion of the optical path when that structure was subjected to temperature changes in orbit.

After some effort was exerted in producing a half model with a single plane of symmetry (which the preliminary drawings of the LST indicated the structure possessed), it was decided to develop a more detailed quarter model with two planes of symmetry. This necessitated approximating the three point support of the main mirror with four supports and approximating the assymmetric support of the SIP with doubly symmetric truss structure. It is felt that considerably more accurate data can be obtained from the very detailed quarter model than a less detailed half model which could be handled by the CDC-6400 NASTRAN program. The following paragraphs discuss the procedure and assumptions used in developing the NASTRAN model. Computer plots of each of the substructures are provided to display the modeling technique.

a. Solar Array. The solar array was represented by a single node at the center of gravity of the solar array with a mass and rotary moment of inertia such that the mass and cantilever bar supporting it had a first bending mode of 0.6 Hz and a first torsional mode of 0.66 Hz as supplied by NASA.

b. System Support Module. The SSM was included in the model (1) because it was there, (2) because it has mass and contributed to cantilever bending, and (3) because its main wall was subjected to temperature changes and was directly attached to the main ring supporting the primary mirror. Because the SSM was not of primary interest, it was modeled rather crudely with nodes every 30 degrees on the circumference. The skins are 1.78 mm (0.070 in.) aluminum membrane elements with longerons and rings. The aft ring has a reduced diameter to approximate the center of gravity of the heavy equipment mounted there. The ring and longeron are given increased bending properties where the solar array attaches. Figure A-20 indicates the SSM and solar array bar and plate elements for the quarter model.



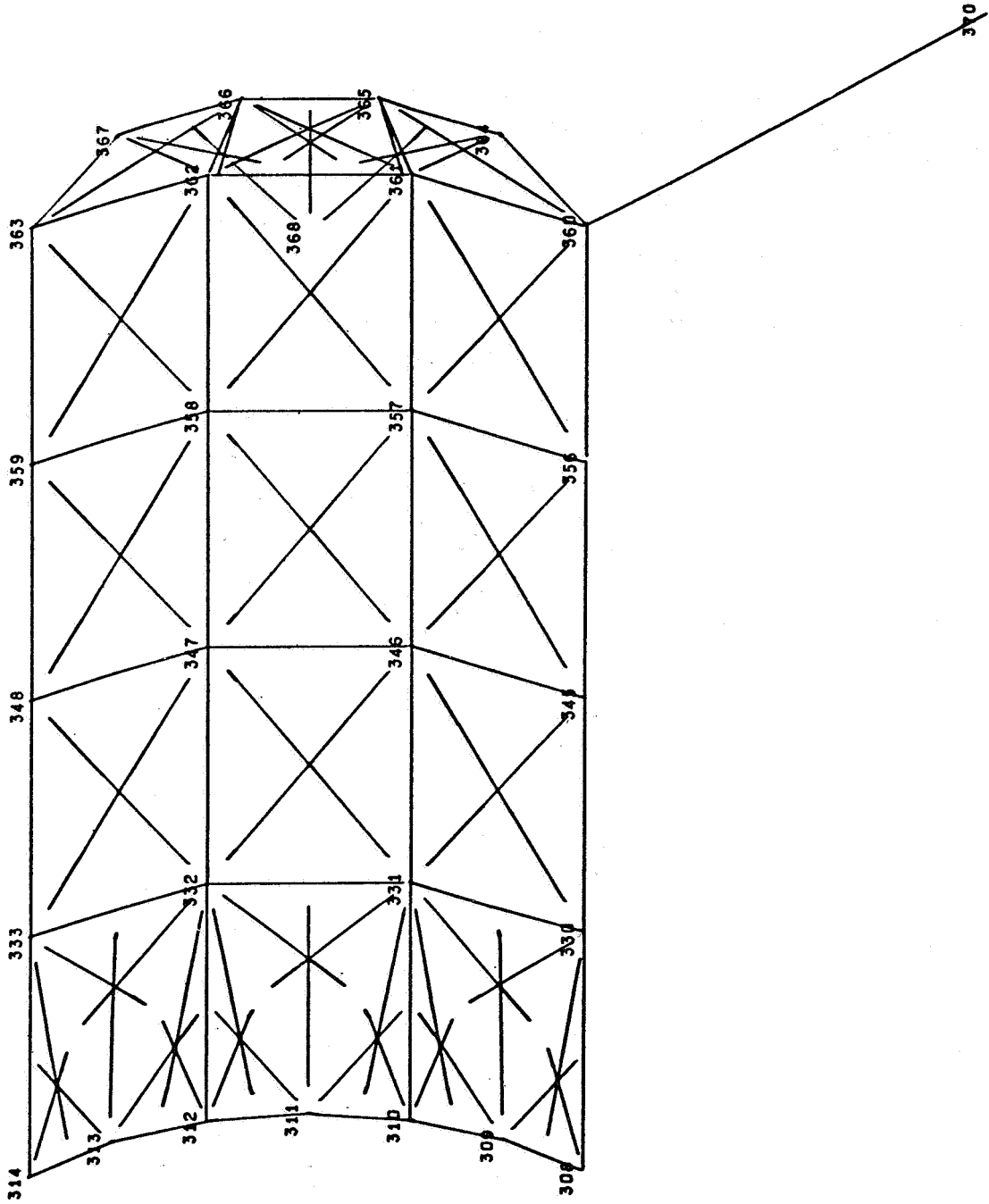


Figure A-20. SSM and solar array model.

c. Scientific Instrument Package. The SIP was included solely for its dynamic influence. The model structure consists of flexural rings and axial rods in the truss area and flexural rings, shear panels, and axial rods in the forward area. It is attached to the inside of the primary ring of the main shell by a substitute doubly symmetric truss structure. Figure A-21 indicates the structural model.

d. Pressure Bulkhead. The pressure bulkhead is modeled with flexural and membrane elements and serves to keep the aft double ring of the main shell round. Figure A-22 shows the bulkhead panels.

e. Main Mirror. The main mirror is modeled with membrane and plate bending elements. Its weight is included for dynamic accuracy. The supports for the main mirror are approximated by four flexural bars rather than three. The bar properties are 75 percent of the properties of the supports. Figure A-23 illustrates the mirror model panels.

f. Main Shell. The main shell is the primary structure of interest in the thermal distortion analysis and was modeled in considerable detail. Grid points were spaced every 0.26 rad (15 degrees) on the circumference and frames were spaced every 508 mm (20 in.) longitudinally. This produced approximately square skin panels which were desired for accuracy. The rings were modeled with inner and outer caps to include any out-of-round effects caused by temperature variation in the light baffles which serve as rings in the structure. The rings on each end of the structure were fully modeled and properties were assigned to most accurately produced torsional and flexural stiffnesses and, somewhat less accurately, axial stiffness. Shear panels were used in the rings and torque boxes because the panel aspect ratios were too large for accurate use of membrane elements. Figures A-24 through A-28 picture in detail the models of the components of the main shell.

g. Micrometeoroid Shield (MMS). The MMS was rather crudely modeled as it is loosely coupled to the main shell. Grid points are spaced every 30 degrees circumferentially and 899 mm (35.4 in.) longitudinally. The structure is represented by membrane elements and flexural rings with flexural longerons at the 0 rad (0 degree) and 1.57 rad (90 degree) points located at the sun screen roller rails. Figure A-29 indicates the shell members. The MMS is attached to the aft main shell ring by radial rods to represent the actual MMS channel support fitting, which is designed to provide zero longitudinal support. The upper end of the MMS is attached to the forward ring of the main shell by two links which provide the radial and longitudinal spring rates provided by the actual zee support. Torsional attachment was by tangent rods in the first modeling and by shear panels in the second modeling.

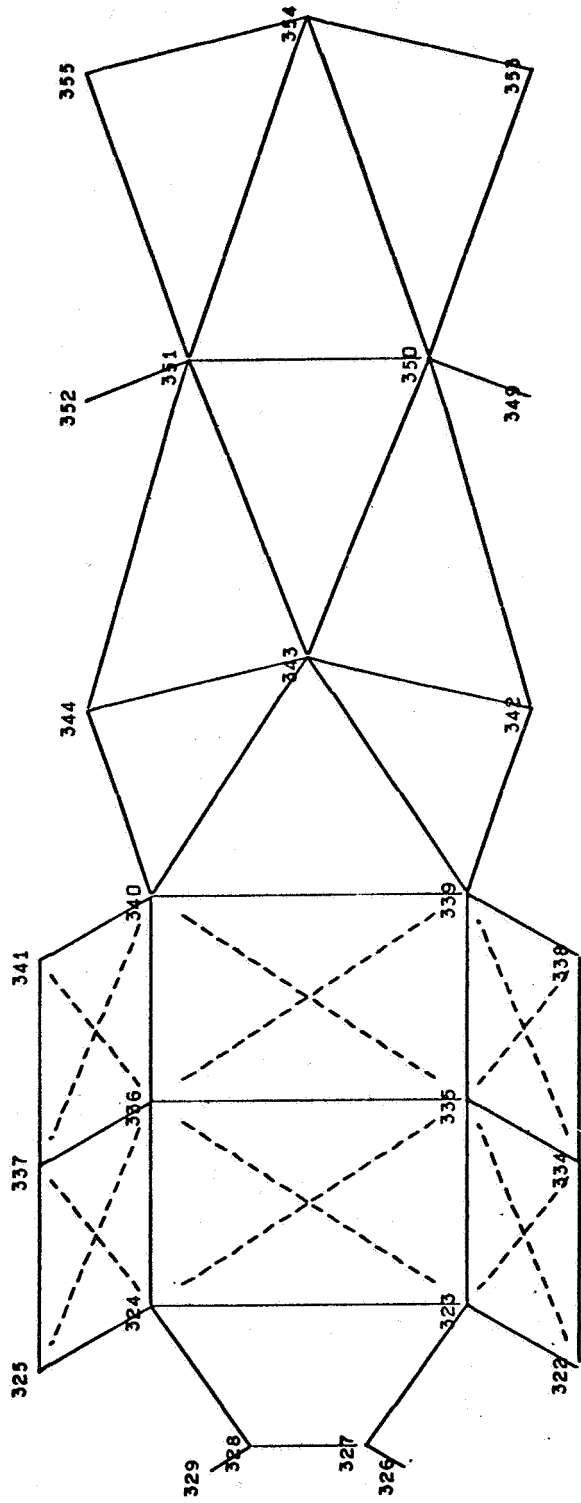


Figure A-21. SIP truss bars and panels.

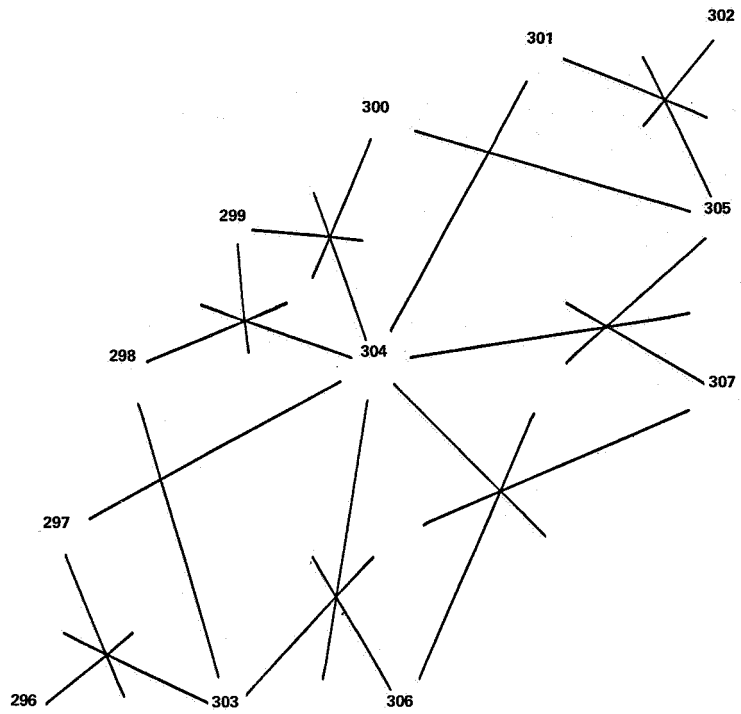


Figure A-22. Pressure bulkhead panels.

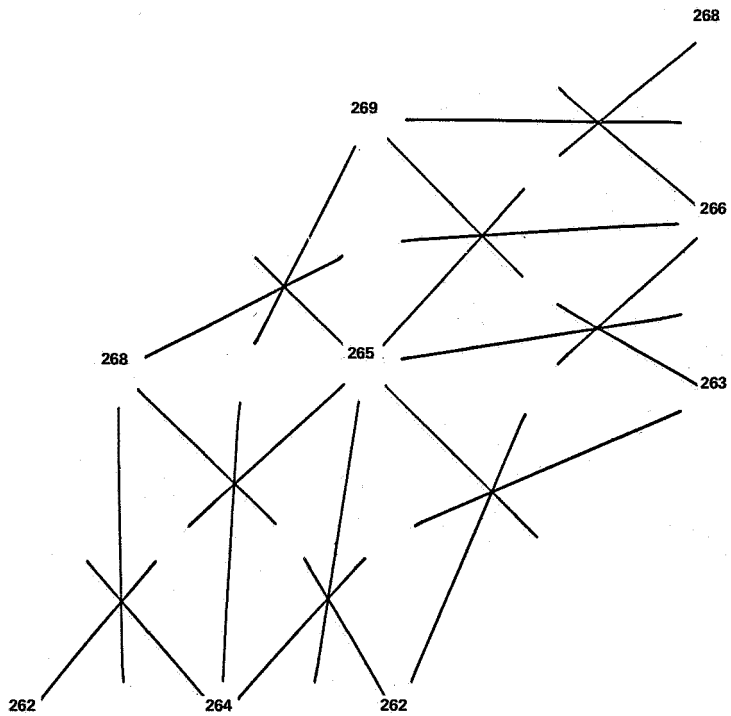


Figure A-23. Primary mirror panels.

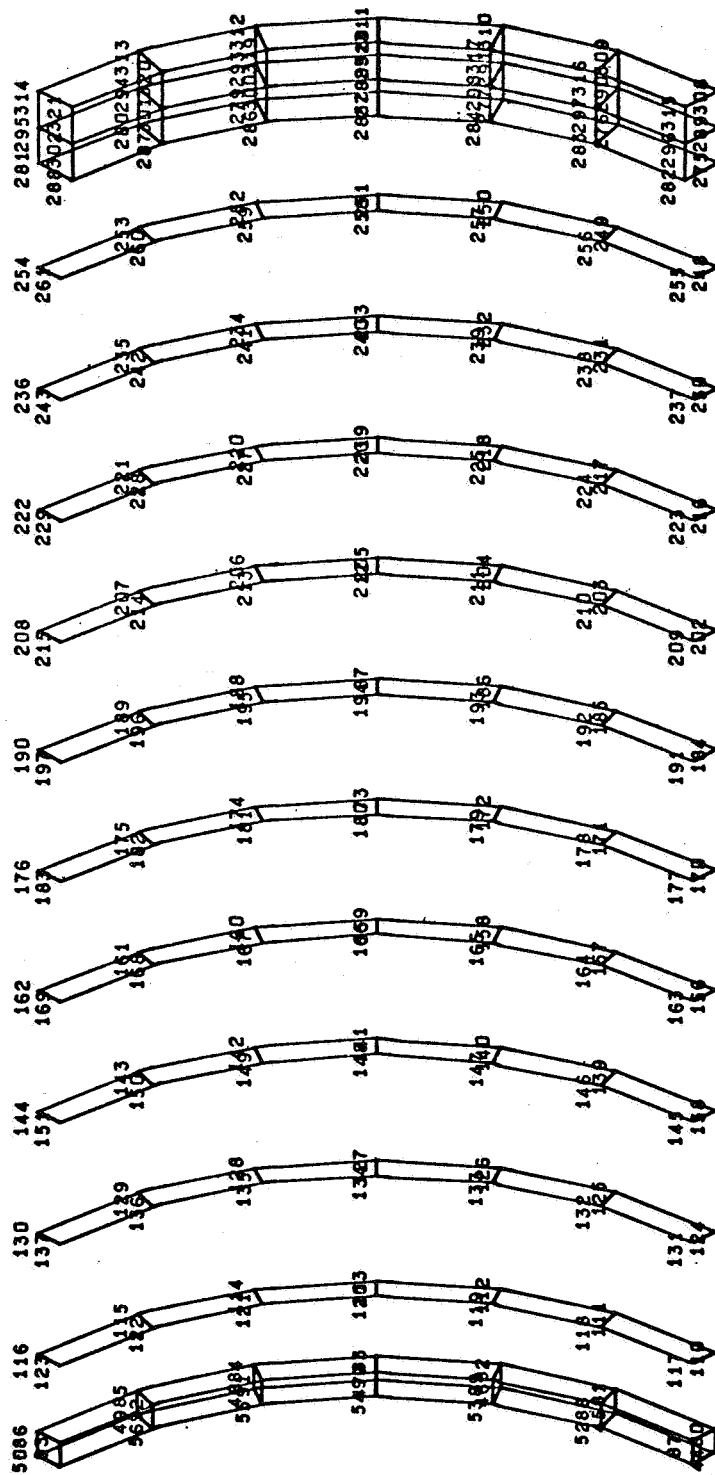


Figure A-24. Main shell bars.

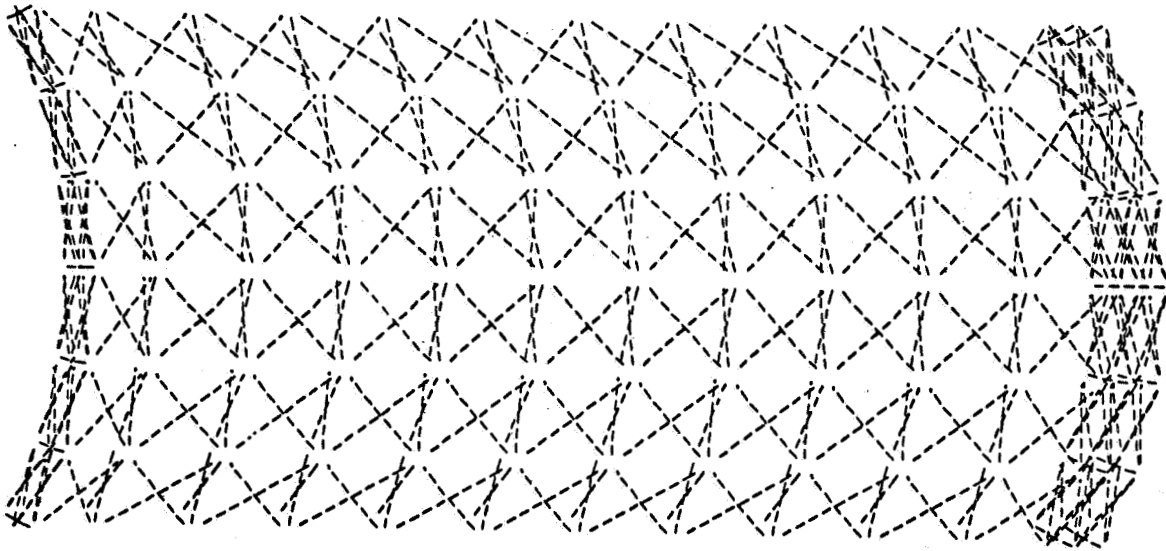


Figure A-25. Main shell panels.

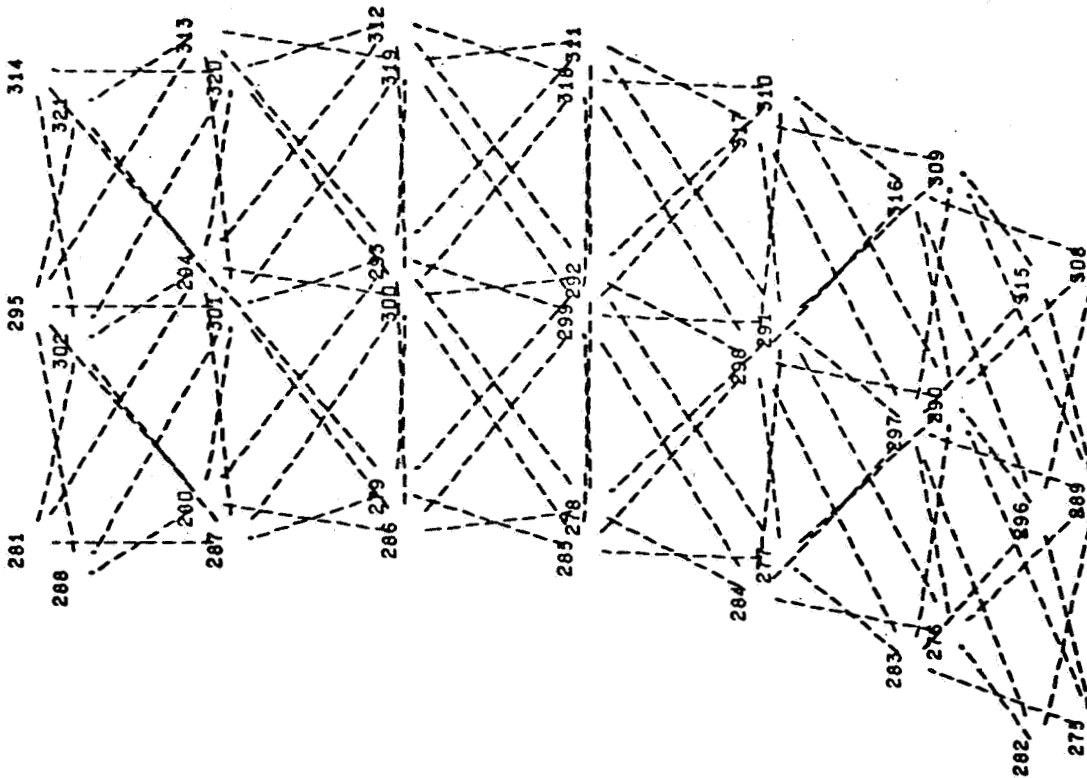


Figure A-26. Primary ring panels.

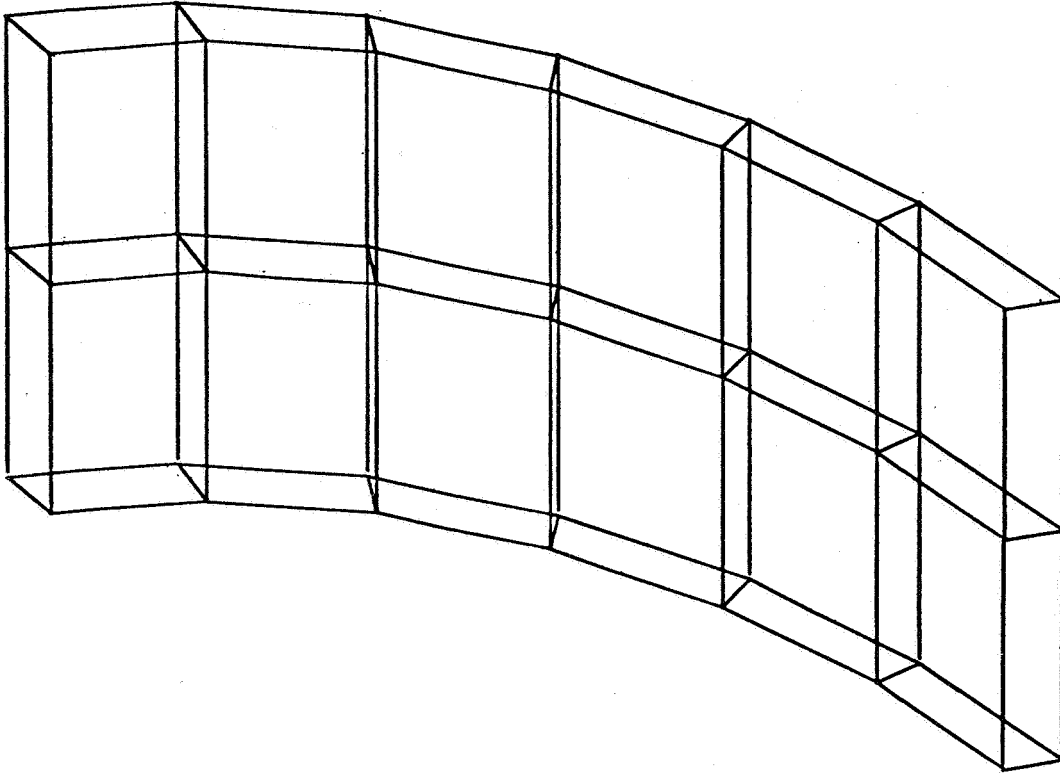


Figure A-27. Primary ring bars.

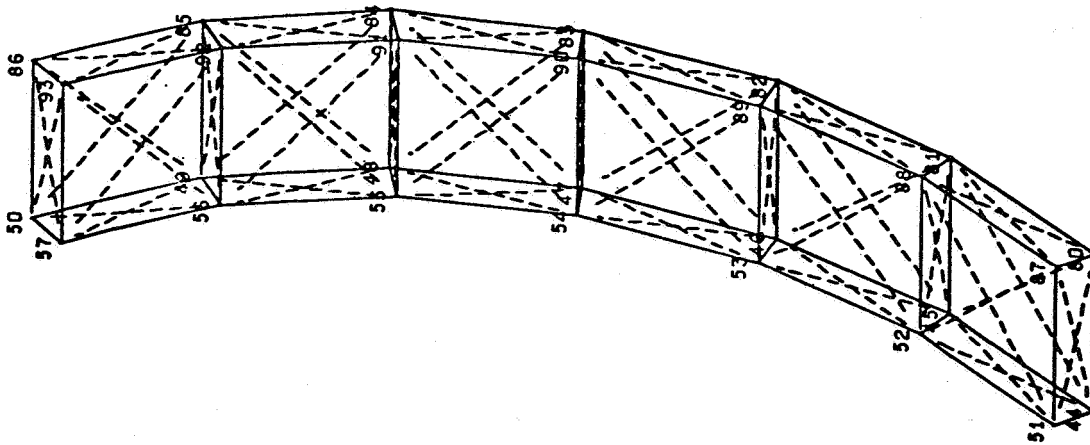


Figure A-28. Forward ring model of main shell.

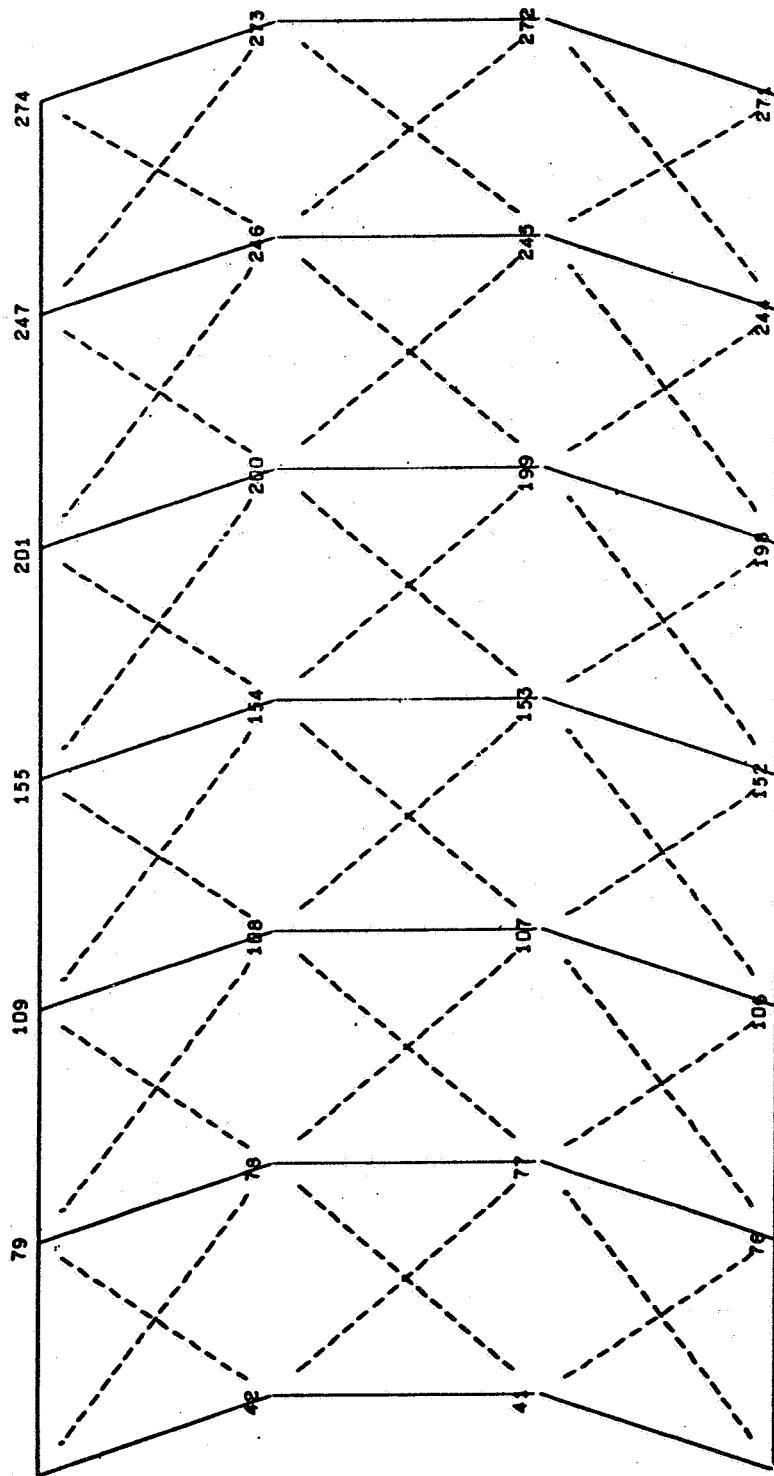


Figure A-29. Meteoroid shell bars and panels.



h. Secondary Mirror Structure. The beams which support the secondary mirror and the structural ring which surrounds it were modeled using bars, bending plates, and shear panels. Considerable effort was expended in this area because the secondary mirror movement caused by main shell distortion is principally dependent on the stiffness and mechanical coupling of this structure. The secondary mirror was supported by 12.7 mm (0.5 in.) diameter rods to a shelf which was hypothesized as closing the top of the ring. Figure A-30 indicates this structure.

i. Aperture Doors. The aperture doors were modeled with single grid points at their centers of gravity. Because of the lack of definition of their support structure, the bars supporting the masses representing the doors were assigned large areas so that the natural frequency of the doors was higher than the range of interest. After the stiffness of the mechanism supporting the doors is determined, the areas of these bars should be corrected. Figure A-31 shows this model.

j. Sun Screen. The sun screen is modeled with grid points 0.53 rad (30 degrees) apart circumferentially and 1113 mm (43.8 in.) longitudinally. The forward part has membrane elements and flexural rings. The aft part has membrane elements with rings and longerons modeled with inner and outer caps. The interior grid points allowed the eccentric attachment to be accurately represented. The model is shown in Figure A-32. The support to the forward ring of the main shell is provided by two bar trusses at the 0 rad (0 degree) and 1.575 rad (90 degree) points. The two bars were sized to represent the stiff attachment mechanism which was designed. It was felt necessary to provide a stiff attachment to prevent low flexural bending frequencies. Torsional attachment was modeled with tangent bars in the initial model but was changed to radial bending bars in the second modeling.

k. Launch Case. Although the current NASTRAN analysis concerned itself only with the orbit configuration of the LST, the same model can be used to study the launch configuration by simply changing the connection of the sun screen support rods and the coordinate system of the sun screen modes. The use of BANDIT, an auxiliary program which examines the connections of a NASTRAN bulk data deck and resequences these connections to minimize the bandwidth of the stiffness matrix, allows the simple remodeling described above to be done without any major penalties in run time.

3. Distortion Analysis. Two models were run to determine thermal distortion. The first and second models were different in the placement of the sun shade insulation, temperature change in the SSM shell, and detail

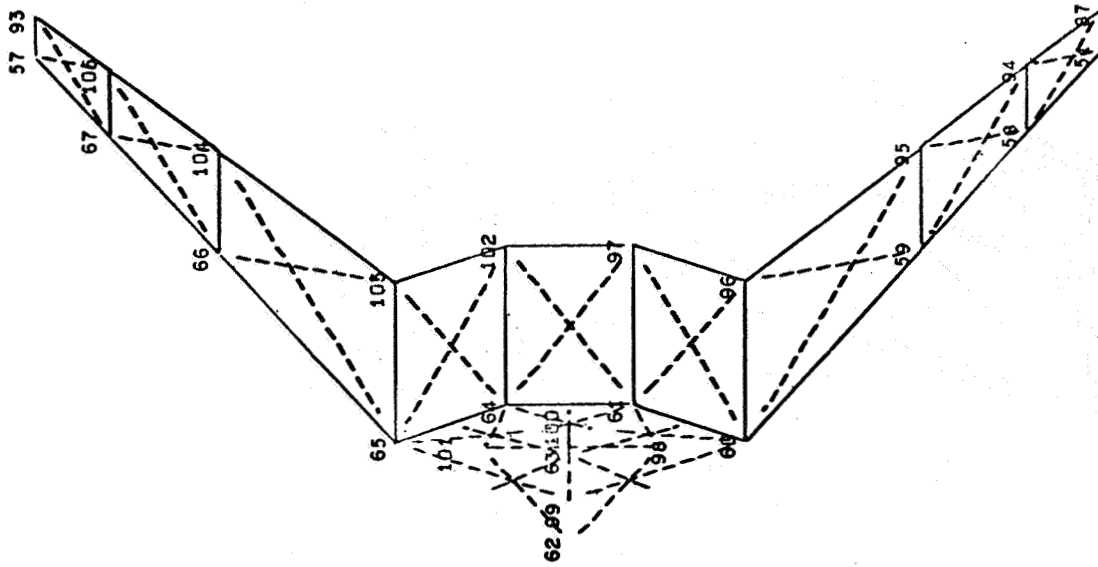


Figure A-30. Secondary mirror and support beams.

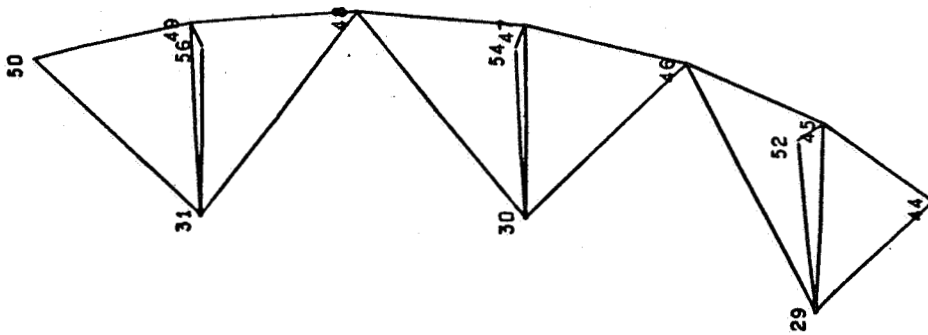


Figure A-31. Aperture door model.

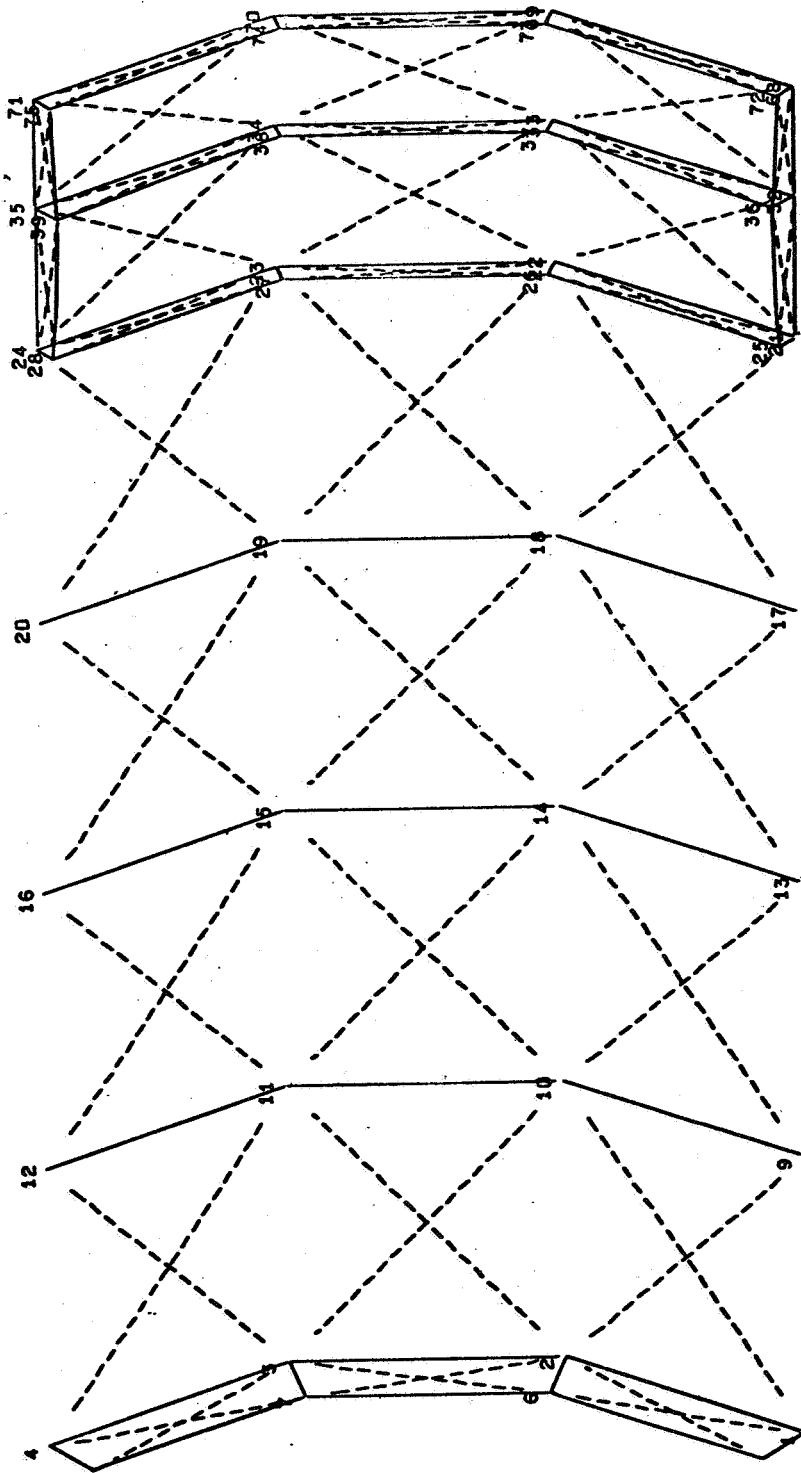


Figure A-32. Sunscreen shell bars and panels.

modeling of the shell coupling bars and panels at the forward end of the main support shell. An inspection of the results of the two runs provides considerable insight into the behavior and critical areas of the various parts of the structure under thermal load. Figure A-33 illustrates the nodes of greatest interest in analyzing the results. Node 99 is at the center of the face of the secondary mirror and nodes 262 and 263 are at the edge of the center hole in the primary mirror. The defocus calculation is, therefore, the sum of the shift of nodes 99 and either 262 or 263. The tilt of the secondary is read directly at node 99.

Node 35 (on the sun shade) and node 50 (on the main shell just below node 35) provide a measure of the optimization of the self-compensating feature of the structure. As illustrated in Figure A-34, an increase in the temperature of the main shell causes the shell to both lengthen and grow in radius at the forward end. Because the beams are at an angle  $\theta$  to the shell radial plane, the radial growth of the shell will cause the beam apex to move aft. If the angle  $\theta$  is properly chosen, the aft motion of the beam apex (which ties directly to the secondary mirror) can exactly compensate for the focal length increase caused by the longitudinal expansion of the main shell.

Nodes 281, 288, 295, and 314, on the primary ring, can be used to visualize the distortion of this ring which drives the longitudinal (or defocus) shift of the primary mirror. A major portion of the defocus distortion of the optical system is due to the movement of the primary mirror.

Two sets of distortions are produced for each model, one for the sunlit side of the shell and one for the shaded side. The largest distortions produced, from either the sun or antisun side, are presented in discussing the results.

a. Interior Sun Shade Insulation. The initial model simulated a design in which the extendable sun shade insulation was mounted on the interior shell wall. While providing a relatively cool surface for radiation to the beams, secondary mirror housing, and other interior features, this design does nothing to alleviate sun shade structure temperature excursions. The resulting node point temperature changes in 24 minutes are as high as 49°C (120°F).

The node point deflections of interest are shown in the following table.

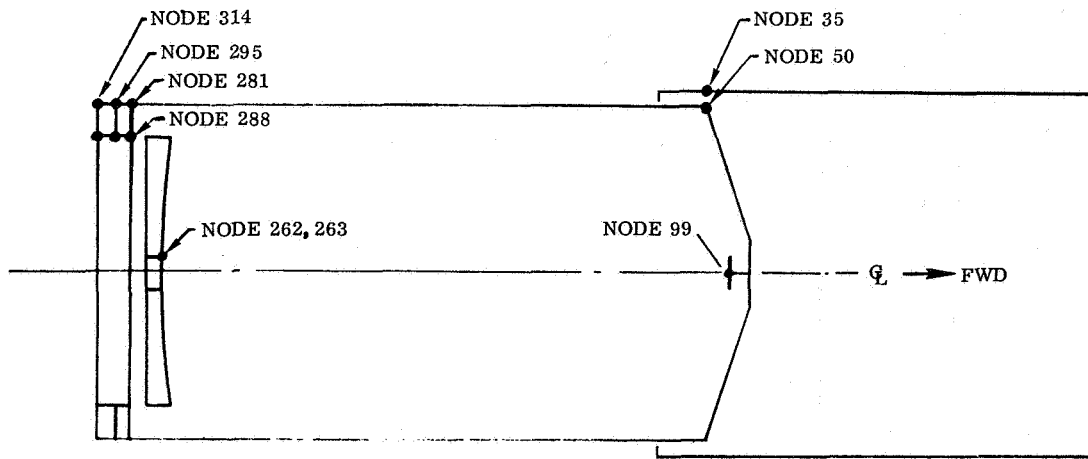


Figure A-33. Distortion check points.

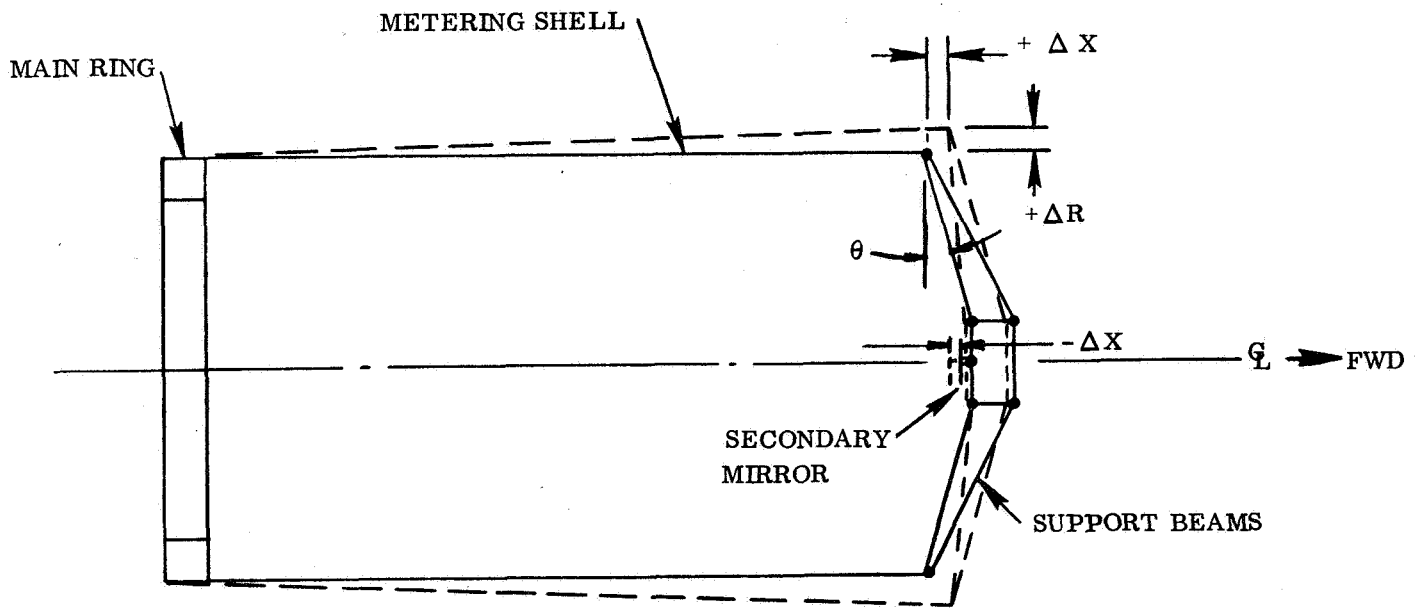


Figure A-34. Thermally compensating structure.

Node Number	Centerline Shift (in. $\times 10^{-5}$ )	Radial Shift (in. $\times 10^{-5}$ )	Tilt (rad $\times 10^{-6}$ )
35	10.38	69.70	—
50	6.21	47.70	—
99	-52.30	25.00	1.42
262	- 2.52	- 0.26	0.07
263	- 2.32	- 0.29	—

Since the axial shift of point 99 (secondary mirror) and point 263 (primary) are of the same sign, the difference between the two values is the axial defocus. This value is

$$\begin{aligned} \text{axial defocus} &= (1328 - 59) 10^{-5} \text{ mm } [(52.30 - 2.32) 10^{-5} \text{ in.}] \\ &= 1269 \times 10^{-5} \text{ mm } (49.9810^{-5} \text{ in.}) \quad . \end{aligned}$$

The error budget for thermal defocus is  $2.0 \times 10^{-3}$  mm, or  $10 \times 10^{-5}$  in. The axial defocus actually calculated, then, is about five times higher than the allowable value.

Similarly, the tilt of the secondary mirror (node 99) is  $1.42 \times 10^{-6}$  rad (0.3 arc seconds). It is not entirely clear what the tilt error budget should actually be, but a dead band value for the tilt sensor of  $2.42 \times 10^{-6}$  rad (0.5 arc seconds) is reported so presumably tilts of less than  $2.42 \times 10^{-6}$  rad (0.5 arc seconds) are acceptable.

The tilt of the secondary is marginally acceptable, but the defocus is far too great. Examination of the axial change of point 50, on the forward end of the main shell, shows a length increase of  $158 \times 10^{-5}$  mm ( $6.21 \times 10^{-5}$  in.), one order of magnitude less than the length change of the secondary and in the opposite direction. The secondary is obviously not driven by the length change of the shell. Instead, the very high radial growth of the sun shade ( $69.70 \times 10^{-5}$  in.) is driving the secondary mirror support apex too far aft, overcompensating for the shell length increase.

Two possible design changes may be solutions to the defocus problem. One approach is to decrease the angle  $\theta$  of the beams (Fig. A-34) to make the secondary less sensitive to shell radial growth. A preferable approach in this case, however, seemed to be to reduce the gross sun shade temperature excursions by moving the insulation to the outside of the shell.

b. Exterior Sun Shade Insulation. The exterior insulation reduces the sun shade structural node point temperature changes to about 27.8°C (50°F), a reduction of over 50 percent. For this iteration, the structural rods connecting the sun shade and main shell were also revised to more nearly represent the actual design of the latch fittings. In addition, the temperature change of the micrometeoroid shell in the area shaded by the sun shade overlap was revised to reflect the sun shade temperature reduction in this area.

The node deflections for this case are shown in the following table.

Node Number	Centerline Shift (in. $\times 10^{-5}$ )	Radial Shift (in. $\times 10^{-5}$ )	Tilt (rad $\times 10^{-6}$ )
35	34.10	40.0	—
50	12.90	4.0	—
99	3.17	1.6	-0.015
262	- 4.69	0.3	-0.016
263	- 4.04	0.3	—

The axial shift of the primary and secondary are now of opposite sign and must be added to obtain the net defocus:

$$\begin{aligned} \text{axial defocus} &= (80.5 + 119) 10^{-5} [(3.17 + 4.69) 10^{-5}] \\ &= 1.98 \times 10^{-6} \text{ mm } (7.86 \times 10^{-5} \text{ in.}) \end{aligned}$$

The tilt of the secondary is much smaller than in the first computation, only  $0.015 \times 10^{-6}$  rad (0.003 arc second).

The axial defocus is now comfortably below the error budget allowance and the tilt is negligible. The reduction in sun shade radial growth (from the prior  $69.7 \times 10^{-5}$  in. to  $40.0 \times 10^{-5}$  in.) and the softer coupling rods to the main shell have decreased the aft tilt of the beam apex. The axial change of the secondary is now considerably less than the shell extension, indicating that the geometry compensation is more nearly optimum. The scale plot of Figure A-35 indicates this compensation.

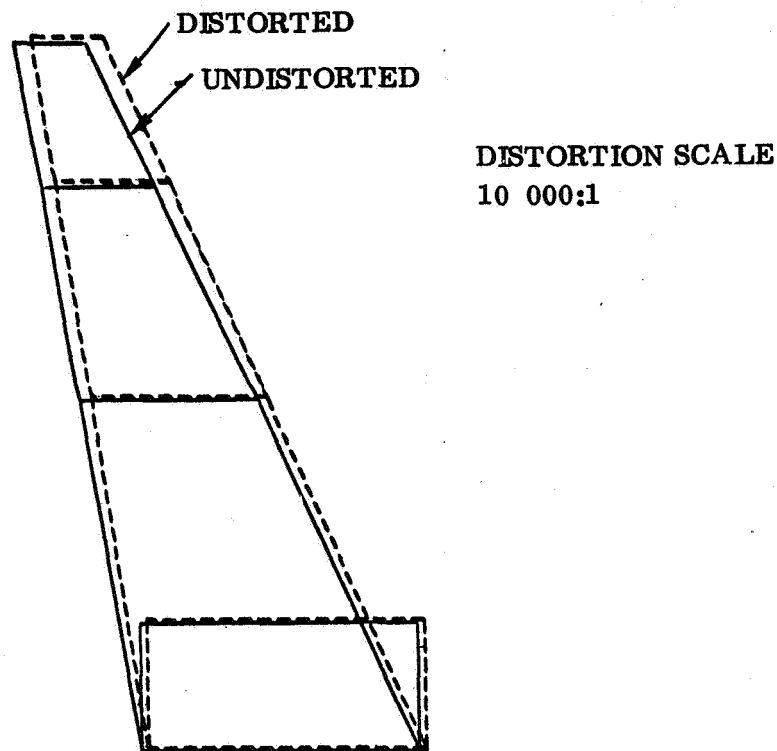


Figure A-35. Thermally compensating beam structure.

It is interesting to note that the axial shift of the primary mirror exceeds the axial shift of the secondary. Since the primary mirror, mirror mounts, and primary mirror support ring are all temperature controlled to 70°F, the distortion is obviously not direct thermal growth. Figure A-36 illustrates the cause of the primary mirror motion. The SSM shell, attached to the ring at node 314, experiences a 1.5°C (2.7°F) temperature change and, since the SSM shell is high expansion aluminum, grows radially



and forces node 314 outboard and slightly forward. Node 288 on the interior forward corner of the ring reacts by rotating inboard and aft. The mirror mounts are located on the ring element defined by nodes 288-302. The main mirror axial shift is a reaction, then, to the tilt of the main mounting ring by thermal expansion of the SSM. A more complete distortion plot of this area is shown in Figure A-37. The distortion of the SSM module is shown in Figure A-38. Note that the heavy primary ring is only slightly affected by the shell expansion. Gross radial deformations occur further aft in the SSM.

Other distortion plots are given in Figures A-39 through A-41 for the main shell, meteoroid shell, and sun shade shell. The distortion scale for these plots is amplified 5000 times.

Several conclusions can be drawn from the thermal distortion analysis. The most satisfying result is the proof that a simple graphite shell structure, protected by a single thin layer of reflective insulation, is sufficiently distortion free to meet the stringent LST requirements.

It can also be concluded that the expansion characteristics, thermal insulation, and connecting rod design of the meteoroid and sun shade shells are very important to the proper design of the OTA structure. It is recommended that further design and analysis be conducted on this local area using only a portion of the full NASTRAN model. The geometry compensation of the support beams should also be checked for other heating cases.

The SSM wall temperatures and forward end insulation should be studied in greater detail because SSM distortion is shown to couple significantly with primary mirror axial shift. The primary ring could also use more study to reduce its driving influence on the mirror. A simple ring tradeoff is the ratio of axial width to radial depth, which will change the reaction rotation of node 288 to node 314. It also appears that active temperature-induced rotation of the main ring could be employed as a vibrationless focus compensation for fine adjustment.

The asymmetric thermal coatings applied to the exterior of the OTA seem to be very effective in reducing circumferential temperature gradients. This conclusion is verified by the close node point deflections of the sun and shade halves of the shells. Other sun incidence angles should be analyzed, however, to find the best overall ratio of coating parameters and the most critical 24-minute time slice.

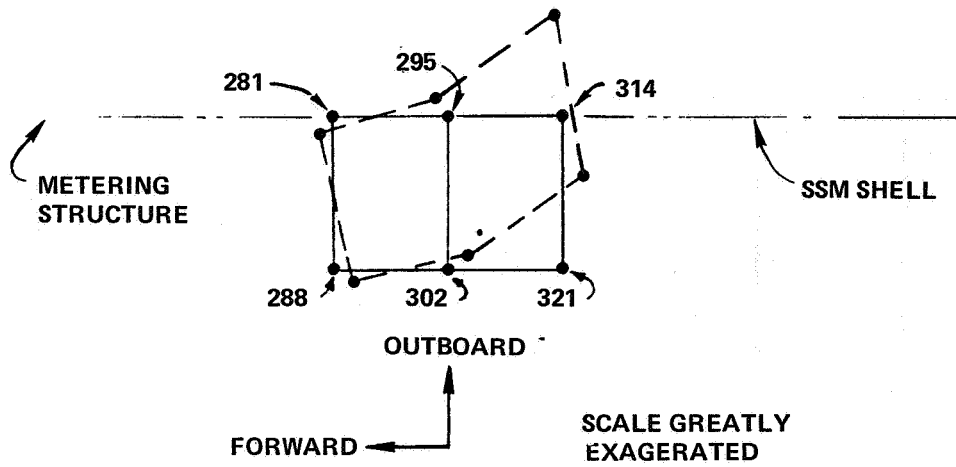


Figure A-36. Primary ring distortion.

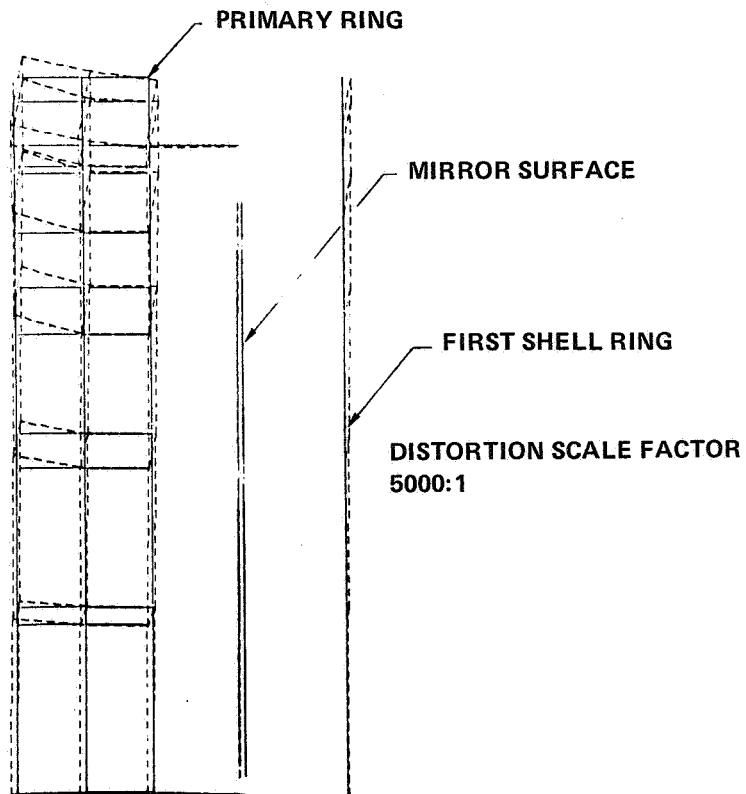


Figure A-37. Primary mirror motion.

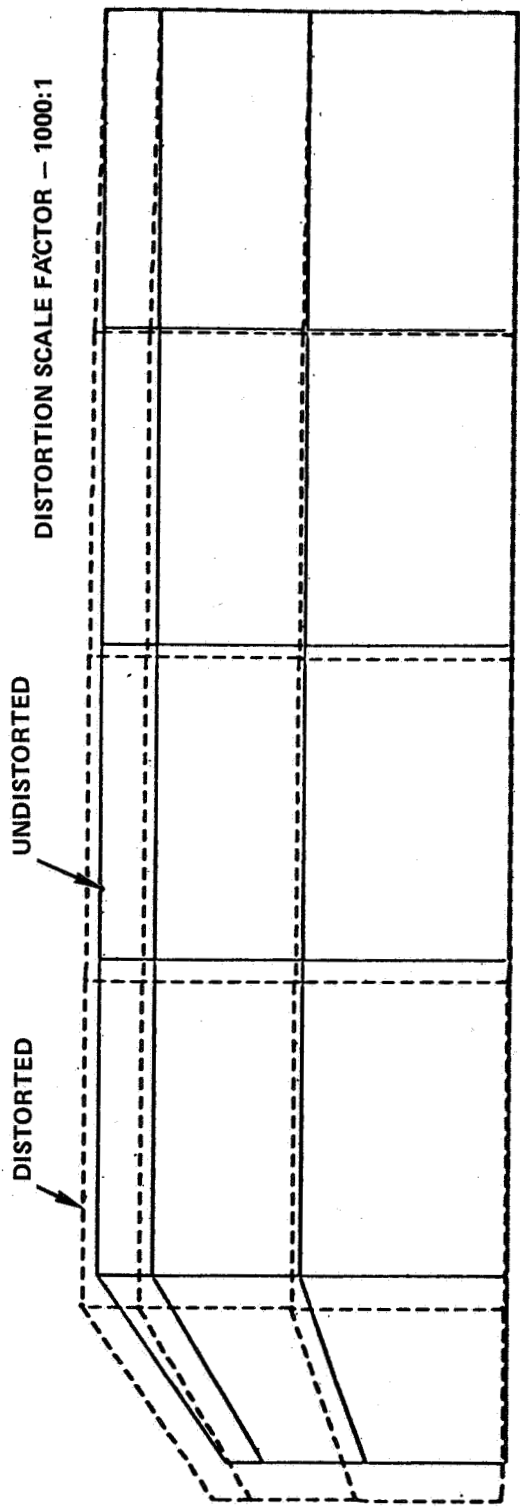


Figure A-38. SSM thermal distortion.

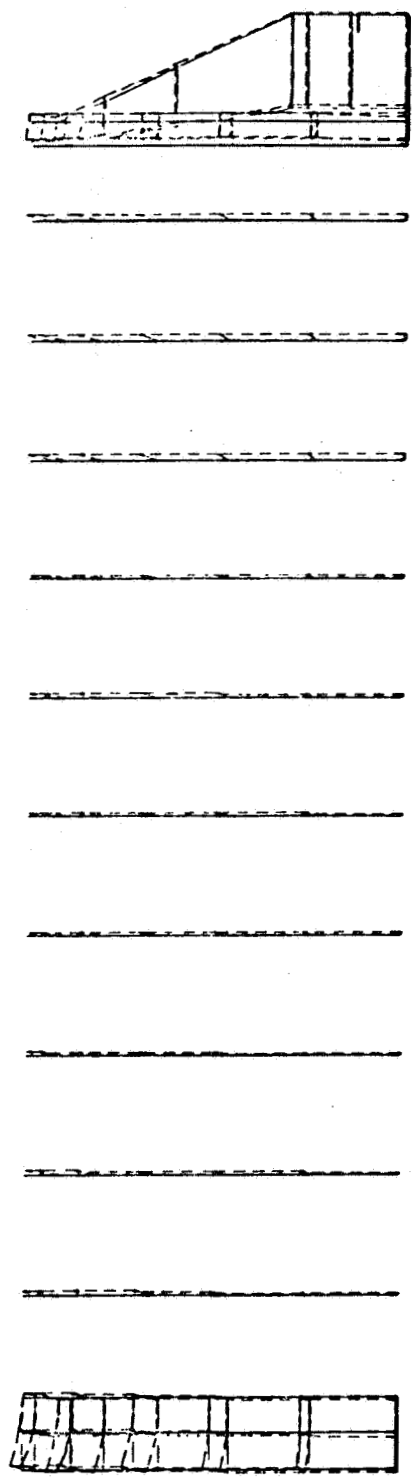


Figure A-39. Main shell distortion plot.

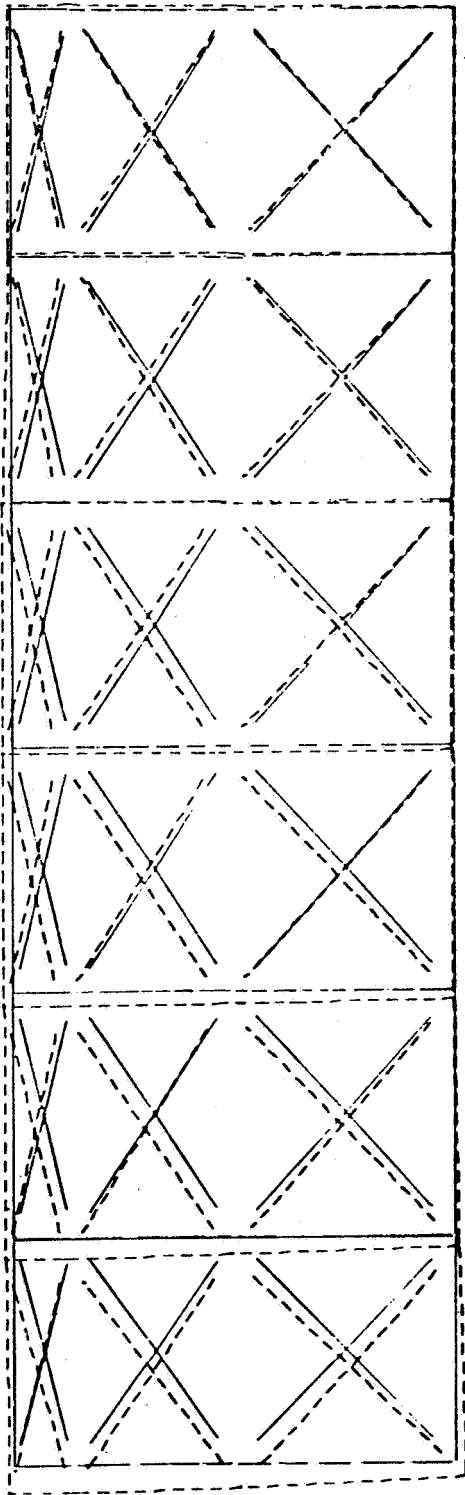


Figure A-40. Meteoroid shell distortion plot.

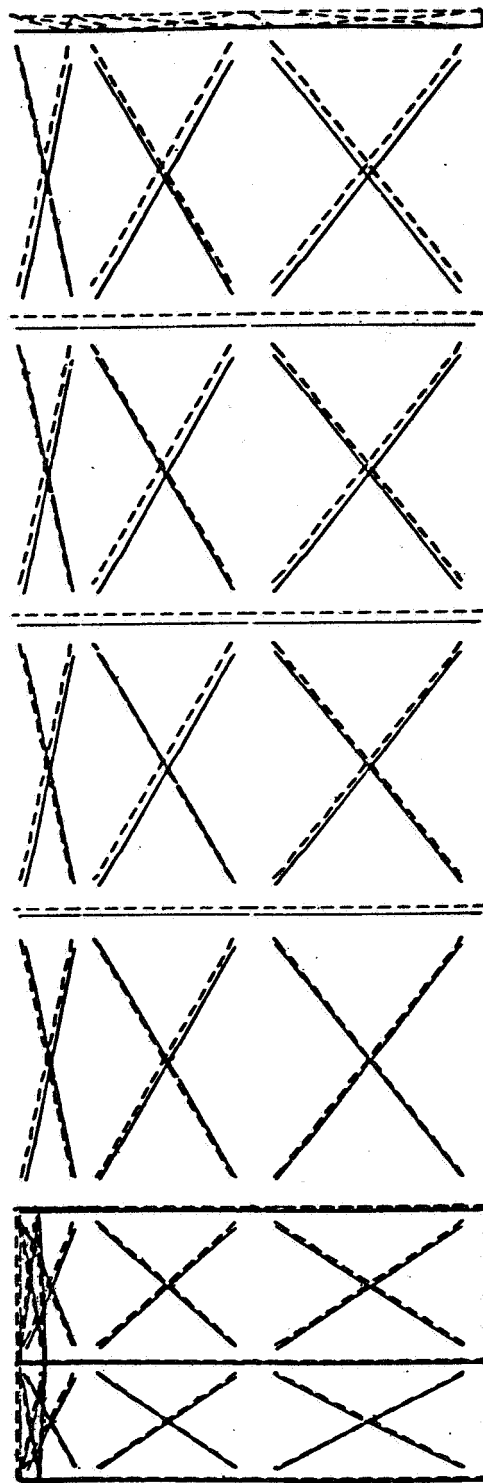


Figure A-41. Sunshade distortion plot.

A final point of interest is the effect of radial temperature gradients in the main shell baffle rings. Both models incorporated ring gradients of about 3.3°C (6°F). Although small ring distortions can be detected, the effect of these distortions appears to be negligible on tile of the secondary. It is concluded that thin rings and high radial temperature gradients are acceptable for the graphite/epoxy design.

4. Structural Dynamics Analysis. An evaluation of the dynamic characteristics of the LST was performed using an analytical dynamic model derived from the detailed structural model used for the thermal distortion analysis of Section D.3.

Symmetric boundary constraints were imposed on the X-Y plane of the quadrant model, while antisymmetric constraints were applied to the X-Z plane. This set of boundary constraints restricts the telescope to lateral motions in the Y-direction, i.e., the motion associated with lateral bending. This selection of boundary conditions was chosen as the more critical of the two boundary conditions used for the thermal distortion analysis. Budgetary considerations precluded the development of additional boundary conditions. Of the four possible combinations of boundary conditions, the one chosen is the most critical. Symmetric-symmetric boundary conditions restrict the system to longitudinal vibrations, which are not considered to be critical. Antisymmetric-symmetric boundary conditions will produce vibration modes and frequencies essentially the same as those obtained in this study. Antisymmetric-antisymmetric boundary conditions permit torsional distortion of the structure. Such behavior was not investigated in this study but it is recommended that it be included in future analyses.

a. Development of Dynamic Model. The analytical model developed for the thermal distortion analysis contained, once the constraints were imposed, some 970 degrees of freedom. Such a large system is well in excess of a practical size for the treatment of the modal evaluation problem. Using the matrix reduction feature of NASTRAN (OMIT cards), the structural model was reduced to 117 degrees of freedom by retaining only 68 of the original 369 grid points.

The selection of the 68 grid points retained was based on an examination of the weight distributions of the model. Grid points carrying large weight concentrations were retained, along with a sparse but uniform distribution of other grid points.

Mass information was originally entered via material density, distributed nonstructural mass values, and concentrated masses. This information was automatically converted into concentrated masses at each of the 369 grid points, then further concentrated by hand to the 68 dynamic model grid points.

The matrix procedure used does not degrade the structural description of the telescope and a recovery of the total displacement vector has been achieved. Modal amplitudes are available at any of the original 369 grid points.

b. Results. The frequencies of vibration obtained in this study are given in Table A-10. Representative mode shape plots are given in Figures A-42 through A-46.

TABLE A-10. LST NATURAL FREQUENCIES

Mode	Frequency (Hz)	Remarks
1	0.66	Solar Panel in Torsion
2	8.87	Secondary Mirror (model error)
3	10.61	SIP Cantilever First Mode
4	22.23	First Body Bending
5	25.31	Local Mode at Doors
6	27.58	Local Mode at Doors
7	28.89	Second SIP Mode

The lowest frequency mode obtained in this analysis is that of the solar panel in a torsional mode about the supporting boom. The solar panel simulation was specifically developed to match the cantilevered natural frequencies supplied by NASA. The low frequency of 0.6 Hz is so far removed from the lowest system frequency that the mode shape remains essentially

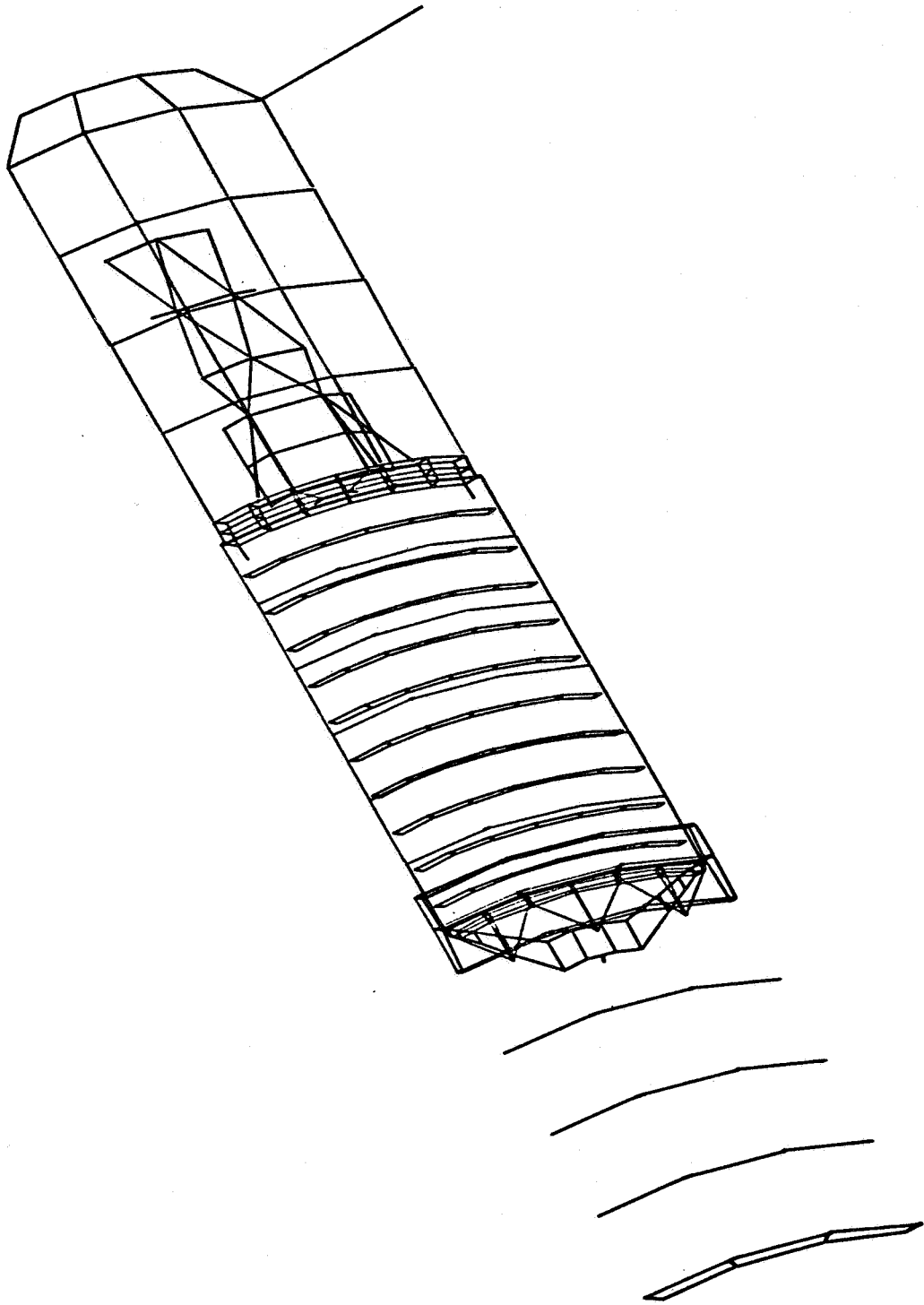


Figure A-42. Mode 3 — SIP bending at 10.6 Hz.

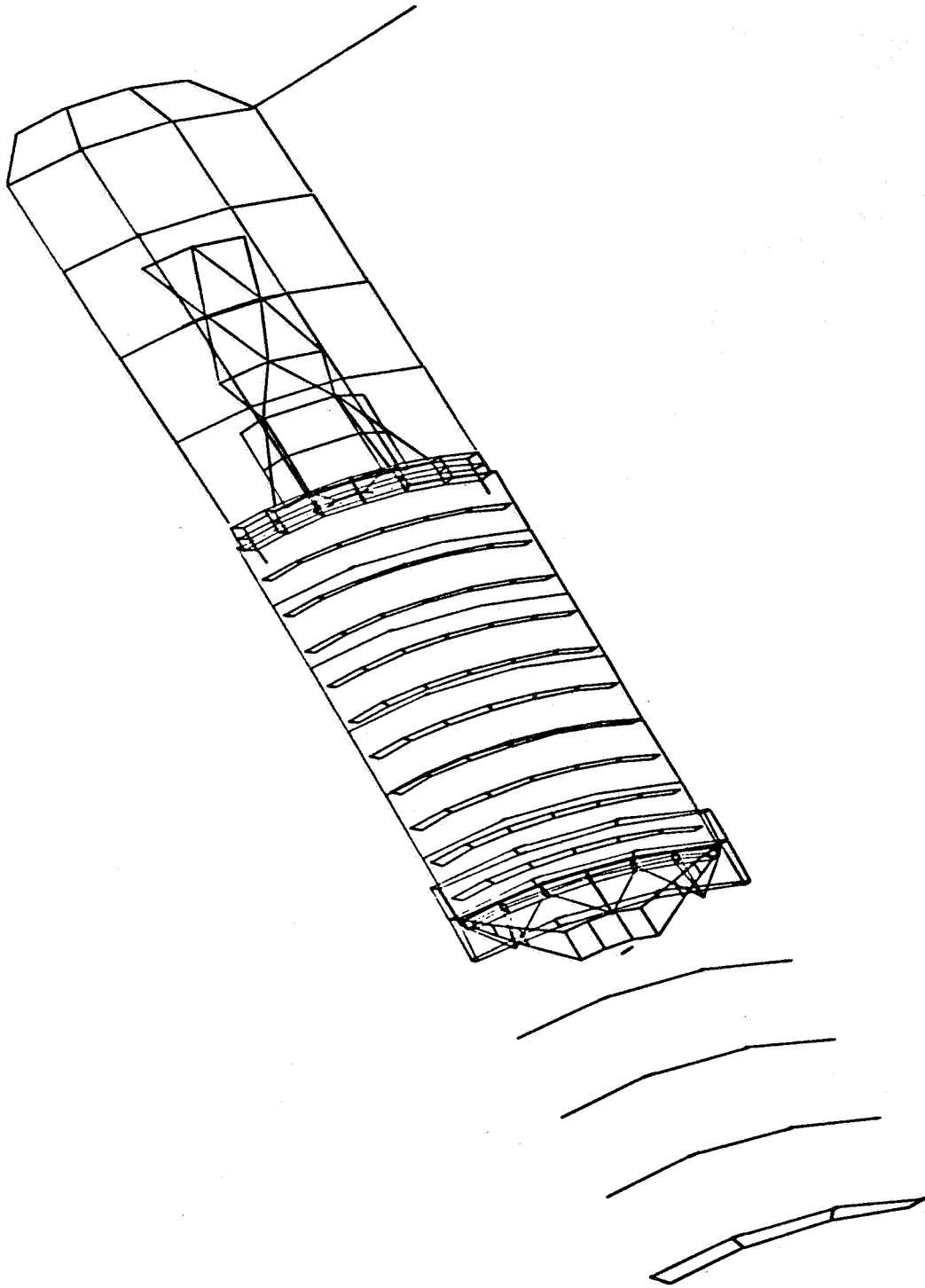


Figure A-43. Mode 4 — first body bending at 22 Hz.



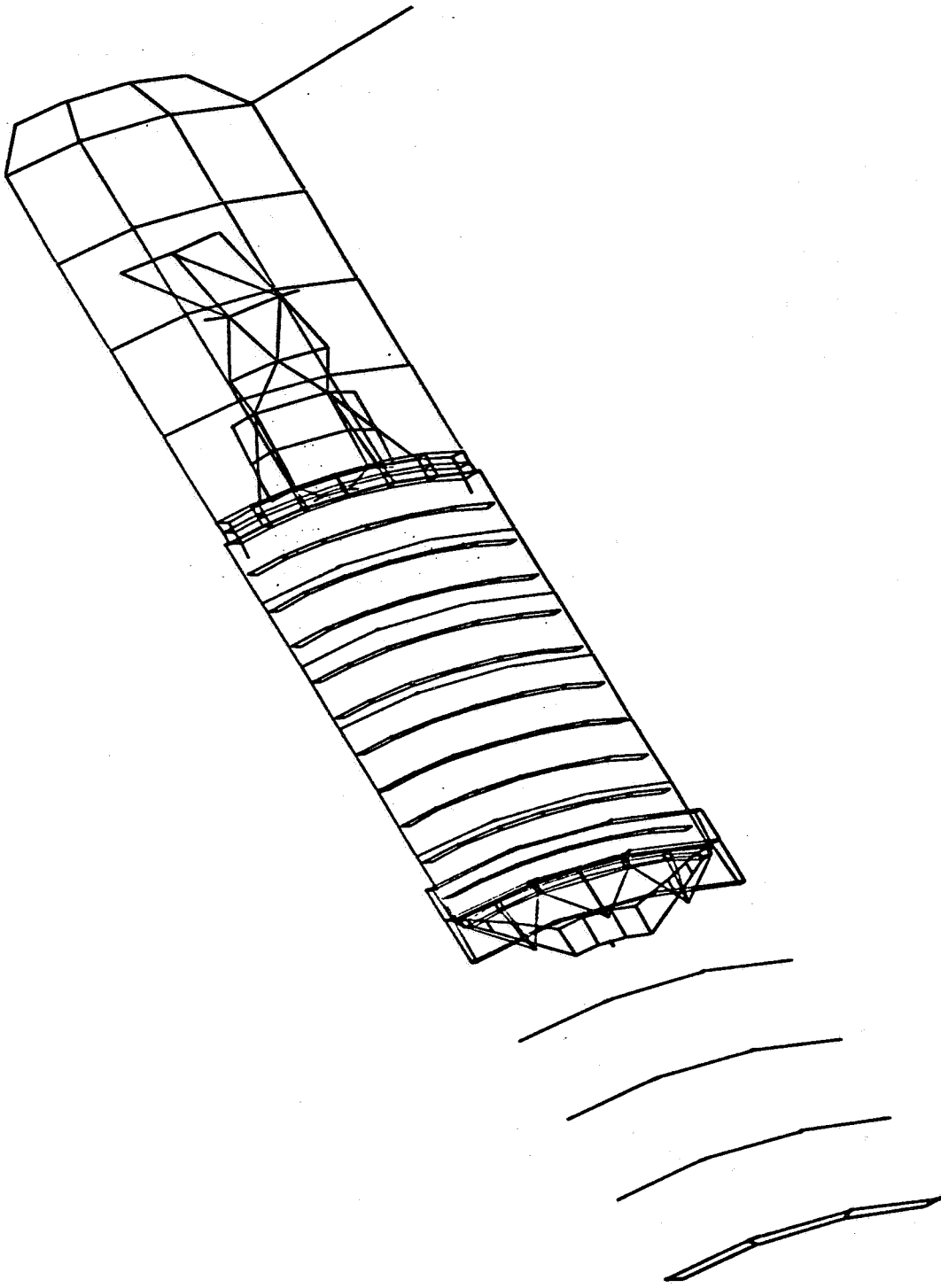


Figure A-44. Mode 7 — second SIP mode at 28.9 Hz.

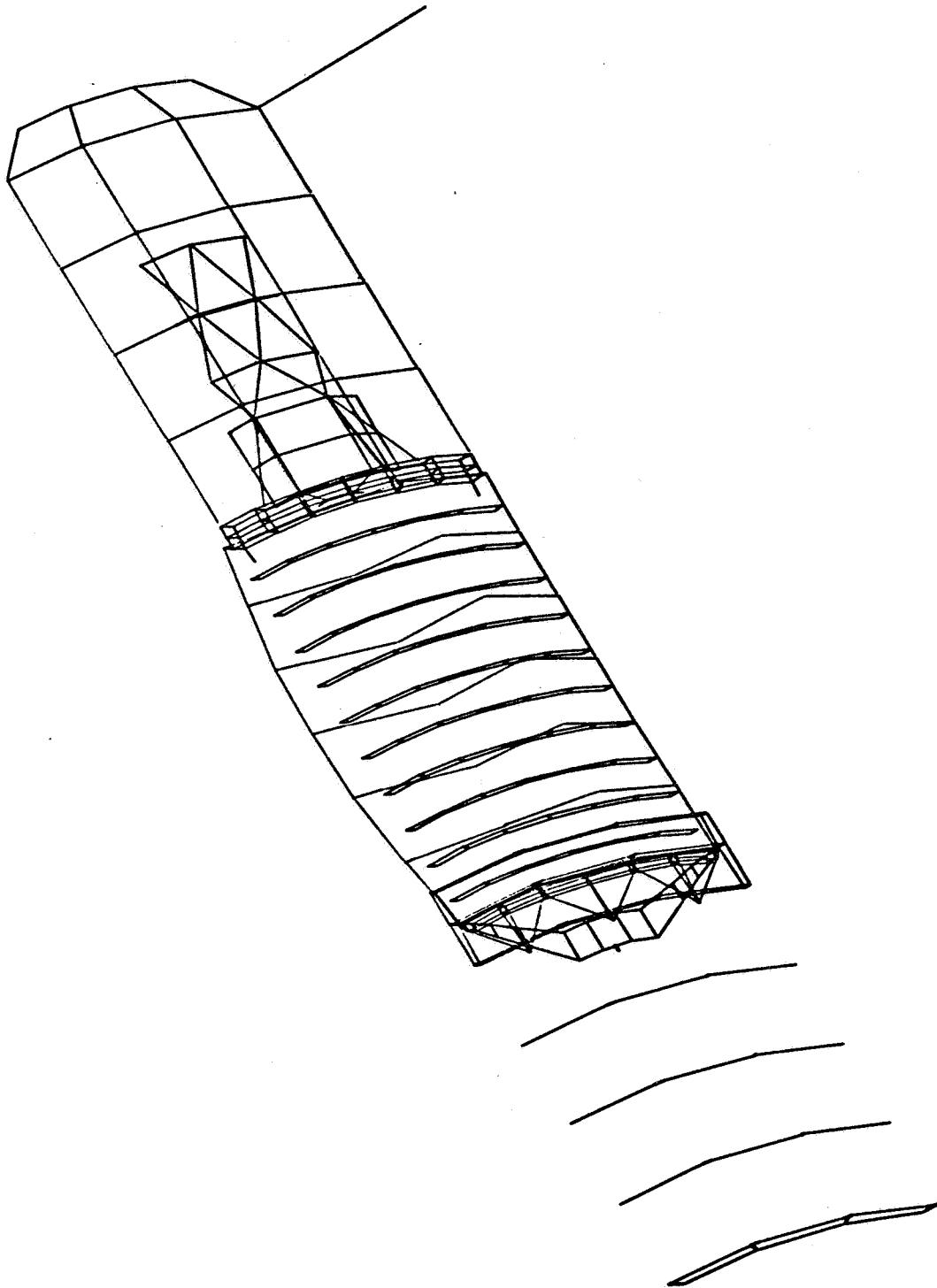


Figure A-45. Mode 9 — meteoroid shield at 37.1 Hz.

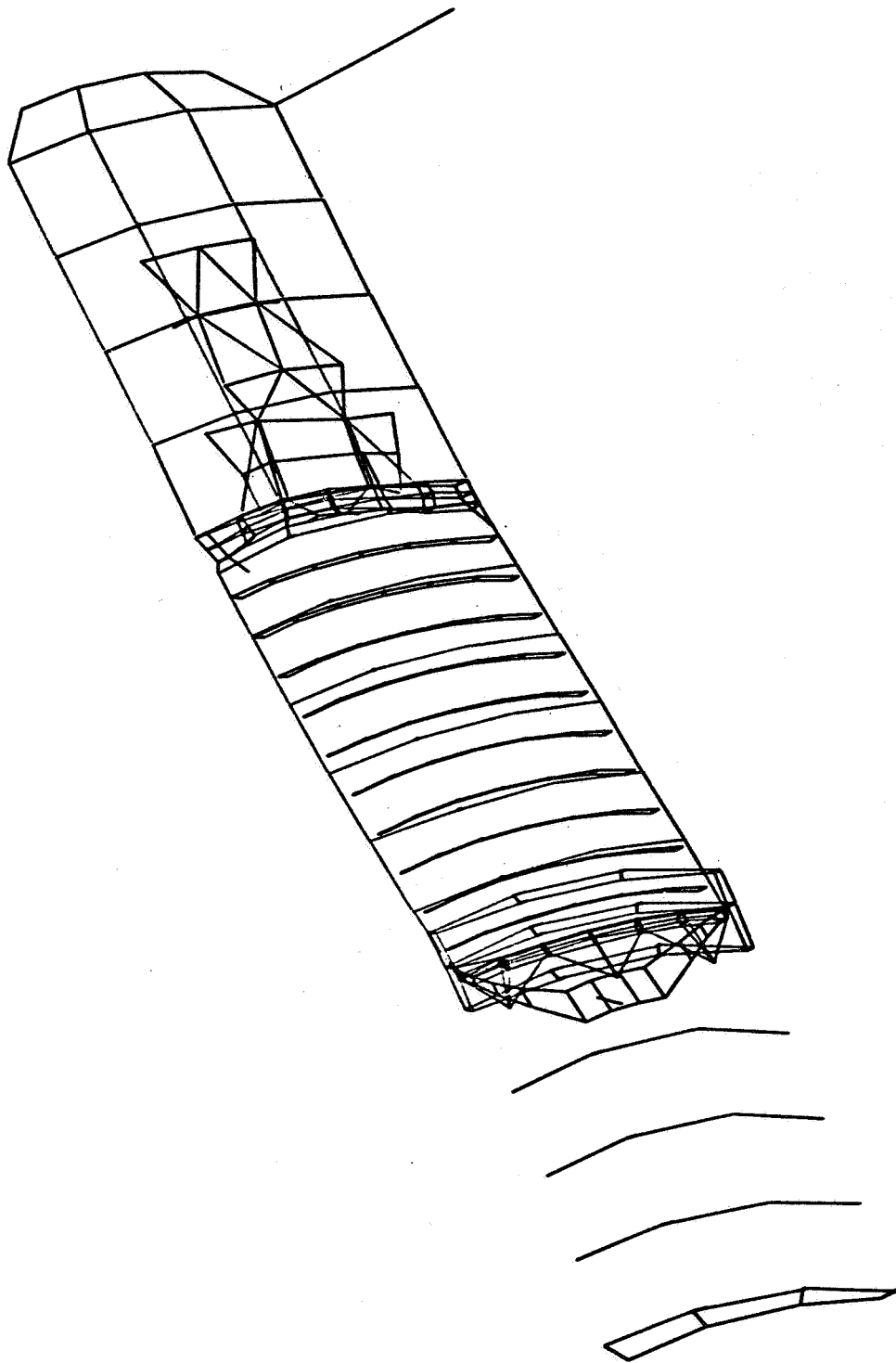


Figure A-46. Mode 17 — second body mode at 60.1 Hz.

solar panel motion only. The second cantilevered solar panel mode is not observed in the results presented here because of a modeling error. Its 6 Hz frequency, along with the results of this study, suggests that it, too, would be uncoupled from responses in the remainder of the structure.

The second mode of vibration, at 8.78 Hz, has been identified as a mode involving the secondary mirror, again without appreciable coupling with the rest of the structure. Examination of the finite element model in this region revealed that the plate system from which the deflecting element is suspended is much too thin. A reasonable thickness will be six orders of magnitude greater, with the result that the resonant frequency of the region will be increased by three orders of magnitude and will not be of concern.

The 10.61 Hz third mode is the response of the cantilevered SIP. The principal concentration of internal energy in this mode is found to be contained in the equipment module itself, rather than its supporting structure. There is very little motion in the remainder of the system except for a slight rigid body response resulting from momentum conservation.

The remaining natural vibration modes, including the first body bending mode, are found in the frequency range above 20 Hz and consequently indicate that the response of the structure caused by external disturbances should not impair control system performance nor produce excessive image plane motion.

## E. Weight Analysis

Mass properties data have been developed for the graphite composite OTA design described in Section B. This section summarizes the detailed weight analysis for both the graphite composite version and the Itek configuration supplied by the NASA contracting office.

Table A-11 presents a detailed weight breakdown of the structure which has been designed in graphite composite materials. Table A-12 summarizes the weights of the complete OTA including the mechanisms, the aperture doors, and the mirrors and their associated mounting structures and mechanisms.

Figure A-47 shows the variation of the total structural shell frame weight versus the frame thickness for the two frame configurations under consideration. The baseline thickness is noted on the curves.

TABLE A-11. WEIGHT SUMMARY OF OTA COMPOSITE STRUCTURE

Item	Weight (lb)
<b>Structural Shell</b>	
Forward Ring	44.11
Frames	157.96
Aft Angle	4.74
Skin	260.20
Longitudinal Skin Splices	7.89
Radial Skin Splices	1.14
Frame Splices	<u>13.06</u>
	489.10
<b>Meteoroid Shell</b>	
Frames	21.34
Aft Angle	1.56
Retainer	3.92
Forward Zee	12.36
Skin	124.89
Longitudinal Skin Splices	3.61
Radial Splices	1.00
Frame Splices	1.14
Rails	<u>21.42</u>
	190.92
<b>Sunshade</b>	
Frames	69.75
Forward Closure Box	40.71

TABLE A-11. (Concluded)

Item	Weight (lb)
<b>Sunshade (Continued)</b>	
Aft Closure Box	41.47
Intercostals	19.59
Skin	137.15
Longitudinal Skin Splices	3.74
Radial Skin Splices	1.26
Frame Splices	<u>3.26</u>
	216.93
<b>Secondary Mirror Support Structure</b>	
Ring	24.57
Spiders	21.73
Fittings	<u>4.60</u>
	50.90
<b>Aperture Doors (Al/Hc)</b>	
Facings	24.29
Core	21.12
Adhesive	<u>2.27</u>
	47.68
<b>Insulation</b>	
Aperture Doors	19.57
Structural Shell	68.00
Sunshade	<u>75.00</u>
	162.57
Contingency	<u>54.50</u>
<b>Total</b>	<b><u>1212.60</u></b>

TABLE A-12. COMPOSITE OTA WEIGHT SUMMARY

Item	lb
Extendable Shield	216.93
Meteoroid Shell	190.92
Structural Shell	489.10
Secondary Mirror Support	50.90
Aperture Doors	47.68
Insulation	162.57
Structural Contingency (5%)	54.50
Truss Structure	—
Truss Rings	—
Secondary Mirror Dome	9.00
Secondary Mirror	80.00
Primary Mirror Assembly	4263.00
Main Mirror Support Ring	372.00
Mirror Mounts	273.00
Pressure Bulkhead	705.00
Mechanisms	180.00
Secondary Mirror Mount	<u>40.00</u>
Total	7134.60

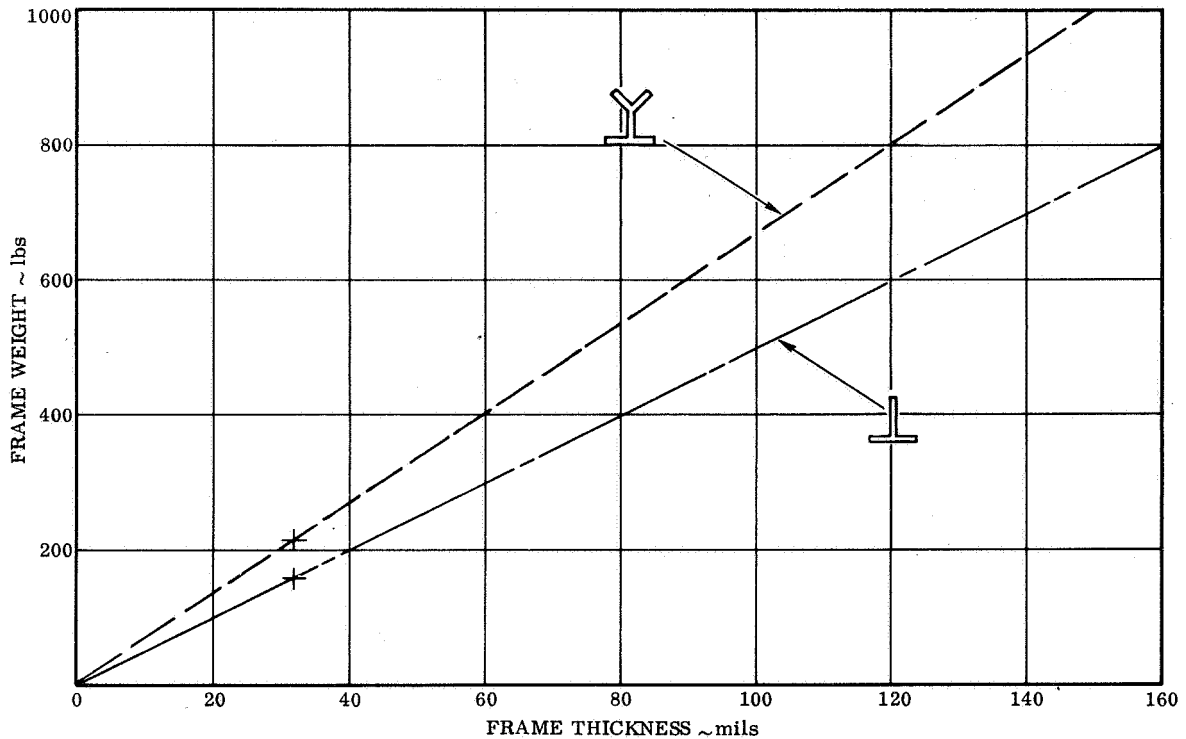


Figure A-47. Structural shell frame weight vs thickness.

## F. Conclusions

The thermal distortion analysis results indicate that the graphite/epoxy OTA structure is adequately stable during the worst 24 minute period of the heating case analyzed. Calculated distortions of the secondary mirror relative to the primary mirror are

Thermal defocus:  $1.9 \times 10^{-6}$  m ( $7.9 \times 10^{-5}$  in.) .

Tilt:  $0.015 \times 10^{-6}$  rad (0.003 arc second) .

The allowable thermal distortion values are

Defocus:  $2 \times 10^{-6}$  m ( $8 \times 10^{-5}$  in.) .

Tilt:  $4.5 \times 10^{-6}$  rad (0.928 arc second) .



The structural dynamics analysis indicates that the composite LST has suitably high natural frequency characteristics. The first few modes in the Orbital Configuration are shown in the following table.

Frequency (Hz)	Characteristics
0.66	Solar Array Torsion
8.9	Aluminum Support Plate Bending
10.6	SIP Structure Bending
22.0	First Body Mode Bending

The weight of the composite structure compared with the other proposed structures is low.

The maximum stress levels in the graphite/epoxy structure occur at the base of the main shell and in the secondary mirror support beams during the Titan launch. These are  $8.27 \text{ MN/m}^2$  (1200 psi) and  $17.93 \text{ MN/m}^2$  (2600 psi), respectively. The maximum thermal stresses during orbit are very low, about  $2.41 \text{ MN/m}^2$  (350 psi). These low stresses are a result of the low thermal expansion of the structure.

## References

- A-1. Research and Applications Modules (RAM) Phase B Study, Technical Data Document, Vol. III — 4.4 Preliminary Design, Appendix F — Application of Advanced Composite Materials to Free-Flying RAM. Report No. GDCA-DDA72-006, Contract NAS8-27539, Convair Aerospace Division of General Dynamics, San Diego, Calif., May 12, 1972.
- A-2. Large Space Telescope (LST) Preliminary Study. Program Development Directorate, George C. Marshall Space Flight Center, Huntsville, Ala., Feb. 25, 1972.
- A-3. Block, D. L.; Card, M. F.; and Milsielus, M. M. Jr.: Buckling of Eccentrically Stiffened Orthotropic Cylinders. NASA TN D-2960, August 1960.
- A-4. Buckling of Thin-Walled Circular Cylinders. NASA SP-8007, 1968.
- A-5. Argyris, J.; and Dunne, P.: Structural Analysis, Structural Principals and Data, Part II. Pitman & Sons, London, 1952.
- A-6. McCormick, Caleb W.: The NASTRAN User's Manual. NASA SP-222, September 1970.

**APPENDIX B**  
**SOLAR SYSTEM OBSERVATIONS**



# TABLE OF CONTENTS

		Page
A.	Introduction .....	B-1
B.	LST Line of Sight (LOS) Travel Rate and Distance .....	B-1
	1. Purpose .....	B-1
	2. Centroid Track of Primary Object .....	B-1
	3. Centroid Track of Satellite .....	B-4
	4. Spot Track .....	B-4
	5. Raster Scan .....	B-4
	6. Stepped Scan .....	B-4
	7. Summary of Maximum LST LOS Travel Distance and Rate .....	B-9
C.	LST Viewing Opportunities .....	B-9
	1. Factors Influencing Capability .....	B-9
	2. Capability of the LST to View the Outer Planets .....	B-11
	3. Capability of the LST to View the Inner Planets .....	B-14
	4. Definition of Parameters Used in Analysis .....	B-20
	a. Viewing Constraints .....	B-20
	b. Viewing Time .....	B-20
	c. Viewing Opportunity .....	B-20
	d. Blind Interval .....	B-20
D.	Solar System Flux and Measurement Capability .....	B-20
	1. Purpose .....	B-20
	2. Flux at the LST Primary Focal Plane .....	B-20
	3. Total Flux at the LST .....	B-23
	4. Flux per Unit Solid Angle at the LST Entrance .....	B-25
	5. Flux at the LST Focal Plane .....	B-25
	6. Comparison of Flux with Typical Instrument Performance .....	B-27
	a. Measurement Capability for the 0.03 to 0.1 $\mu\text{m}$ Range .....	B-31
	b. Measurement Capability for the 0.1 to 10 $\mu\text{m}$ Range .....	B-31
	c. Measurement Capability for the 1.0 to 100 $\mu\text{m}$ Range .....	B-31
	d. Evaluation of LST Measurement Capability .....	B-36
E.	Conclusions and Recommendations .....	B-36

## LIST OF ILLUSTRATIONS

Figure	Title	Page
B-1.	Solar system LST observation line-of-sight travel conditions . . . . .	B-2
B-2.	LST maximum LOS travel due to satellite orbit revolution . . . . .	B-5
B-3.	LST maximum LOS travel due to object rotation . . . . .	B-6
B-4.	LST time to raster-scan object . . . . .	B-7
B-5.	LST available slit frame exposure time for a given object size . . . . .	B-8
B-6.	LST LOS constraints . . . . .	B-10
B-7.	Viewing time for a typical outer planet (Neptune) . . . . .	B-12
B-8.	Viewing opportunities for outer planets . . . . .	B-13
B-9.	Viewing accessibility of the six outer planets . . . . .	B-15
B-10.	Typical viewing opportunities for Venus . . . . .	B-16
B-11.	Elongation angle . . . . .	B-17
B-12.	Typical viewing opportunities for Mercury . . . . .	B-18
B-13.	Using the earth as an occulting disk . . . . .	B-19
B-14.	Viewing accessibility of the two inner planets . . . . .	B-21
B-15.	Flux analysis steps for solar system objects . . . . .	B-22
B-16.	Solar system object maximum total flux at the LST . . . . .	B-24
B-17.	Solar system object radiant flux per unit solid angle collected by the LST effective aperture . . . . .	B-26

## LIST OF ILLUSTRATIONS (Concluded)

Figure	Title	Page
B-18.	Reflectance of LST mirror system . . . . .	B-27
B-19.	Total solar system object flux at the LST primary focal plane . . . . .	B-28
B-20.	LST airy disk size at primary focal plane . . . . .	B-29
B-21.	Solar system object flux in an airy disk at the LST primary focal plane . . . . .	B-30
B-22.	LST measurement capability of solar system objects between 0.03 - 0.1 $\mu\text{m}$ (300 - 1000 $\text{\AA}$ ): spectrometry . . .	B-32
B-23.	LST measurement capability of solar system objects between 0.1 - 1.0 $\mu\text{m}$ : imagery . . . . .	B-33
B-24.	LST measurement capability of solar system objects between 0.1 - 1.0 $\mu\text{m}$ : spectrometry . . . . .	B-34
B-25.	LST measurement capability of solar system objects between 1 - 100 $\mu\text{m}$ . . . . .	B-35
B-26.	Summary of LST measurement capability of solar system object flux . . . . .	B-37

# APPENDIX B

## SOLAR SYSTEM OBSERVATIONS

### A. Introduction

The following material represents the essential parts of a Phase A Boeing study recently completed for MSFC, "An Analysis of the Large Space Telescope (LST) Application to Solar System Observations," Boeing Report No. D180-15232-1, January 1973, NASA Contract NAS8-29182. The purpose of the effort was to examine how the LST can be used for planetary work. An accurate planet tracking capability is necessary to exploit the full potential of the LST for solar system observations.

The Boeing work began about midway of the Phase A LST studies done by ITEK, Kolsman, and MSFC and ended about 2 months later than the others. Therefore, it was impossible to incorporate the results of the Boeing contract into the LST design concepts in the Phase A Report.

### B. LST Line of Sight (LOS) Travel Rate and Distance

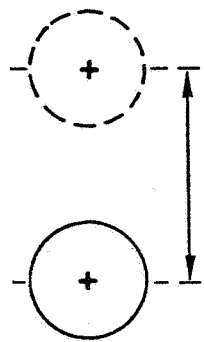
1. Purpose. The purpose of this section is to determine the LST line-of-sight (LOS) travel rate and distance.

Figure B-1 illustrates four conditions that were established for analysis of the telescope motion. Condition I is an LOS track mode where the object is assumed to be a point source. (This condition has two parts as can be seen in Figure B-1.) Condition II applies to a moving spot on a rotating object such as Jupiter. Condition III is a raster scan mode. Condition IV is a stepped scan mode. A spectrometer slit, for example, might be stepped across an object, stopping at each step to collect sufficient flux for a meaningful measurement.

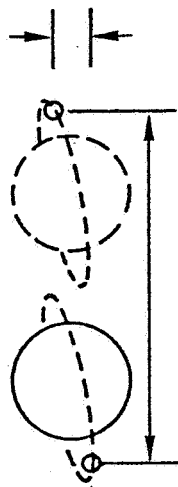
2. Centroid Track of Primary Object. The maximum LOS travel rate and distance for the LST have been calculated. The calculations show that generally the maximum LOS travel rates occur when the target is on the opposite side of the sun from the earth. Certain maximum values are tabulated in Table B-1. The second column in the table gives: (1) the angular LOS travel distance, (2) viewing time per LST orbit, (3) earth to object distance, and (4) object size.



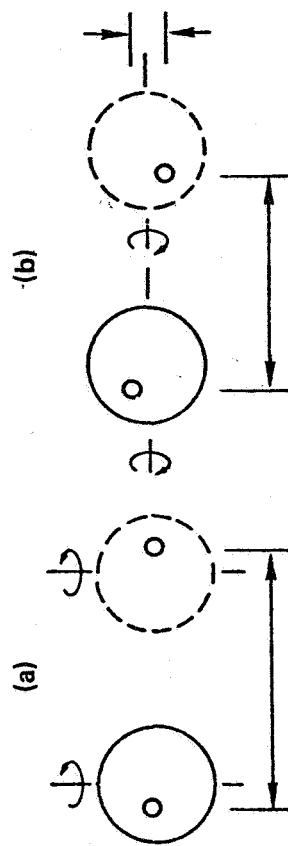
- **CONDITION I:  
(CENTROID TRACK – PRIMARY OBJECT)**



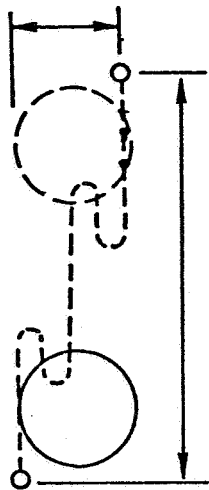
- (CENTROID TRACK – SATELLITE)**



- **CONDITION II:  
(MOVING SPOT TRACK)**



- **CONDITION III:  
(CONTINUOUS SCAN TRACK)**



- **CONDITION IV:  
(STEPPED SCAN TRACK)**

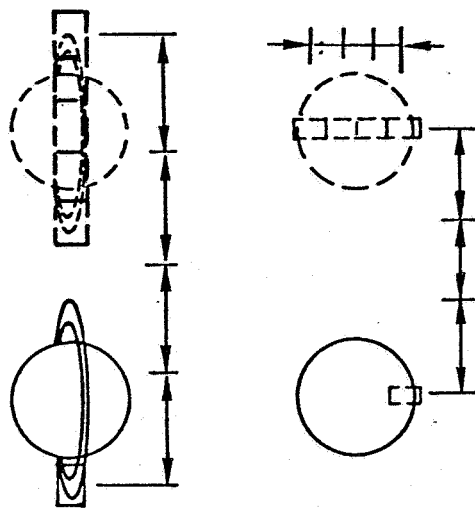


Figure B-1. Solar system LST observation line-of-sight travel conditions.

TABLE B-1. MAXIMUM LST (LOS) RATE AND TRAVEL CONDITIONS

Object	Object Centroid Track Observations		Object Spot Track Observations		Object Raster Scan Track Observations		Object Step Scan Track Observations	
	Maximum LST LOS Rate (arc sec/min)	Maximum LST LOS Travel at Earth Viewing Time Orbit Object Distance Apparent Object Diam. (arc sec-min-AU-arc sec)	Maximum LST LOS Rate = Cen- troid + Object Rotation (arc sec/min)	Maximum LST LOS Travel = Cen- troid + Object Rotation (arc sec)	Maximum LST LOS Rate = Cen- troid + Scan (arc sec/min)	Maximum LST LOS Travel + Object Width + 20 arc sec (arc sec)	Maximum LST LOS Rate During Observation = Centroid (arc sec/min)	Maximum LST LOS Travel = Cen- troid + Object Width (arc sec)
Mercury	4.06	13.4-3.3-0.9-7.5	4.06	13.4	64.1	40.9	4.06	20.9
Venus	3.30	181-55-0.9-19	3.30	181	63.3	220	3.30	200
Mars	2.15	120-56-1.35-6.8	2.16	121	62.2	147	2.16	127
Phobos	2.58	128-56-1.35-	-	-	-	-	-	-
Jupiter	0.57	31-54-5.7-38.5	0.74	40	60.6	89.5	0.74	69.5
Amalthea	1.13	52-54-5.7	-	-	-	-	-	-
Saturn	0.29	16-55-9.9-16.5	0.38	21	60.3	52.5	0.38	32.5
Janus	0.44	23-55-9.9	-	-	-	-	-	-
Rings	-	-	-	-	-	-	0.29	54
Uranus	0.14	7.7-55-19.2-3.7	-	-	60.2	31.4	0.14	11.4
Miranda	0.18	9.3-55-19.2	-	-	-	-	-	-
Nephthys	0.08	4.7-56-30.9-2.2	0.08	4.7	60.1	26.9	0.08	7.0
Triton	-	-	-	-	-	-	-	-
Pluto	0.09	4.7-54-30.9-0.25	0.09	4.7	60.1	24.9	0.09	5.0
Minor Planets	-	-	-	-	-	-	-	-
Ceres	1.16	64-55-3.1-0.33	-	-	61.16	84.3	1.16	64.6
Icarus	24.6	1310-53-0.10-	-	-	-	-	-	-
Comet	-	-	-	-	-	-	-	-
Halley	12.5	690-55-0.4-	-	-	72.5	84.0 <sup>b</sup>	12.5	820 <sup>b</sup>
Encke	8.28	440-57-0.5-	-	-	68.3	620 <sup>c</sup>	8.28	600 <sup>c</sup>

a. Assume 10 arc sec turnaround distance beyond object on each side; total, 20 arc sec.

b. Assume comet head at 130 arc sec.

c. Assume comet head at 160 arc sec.

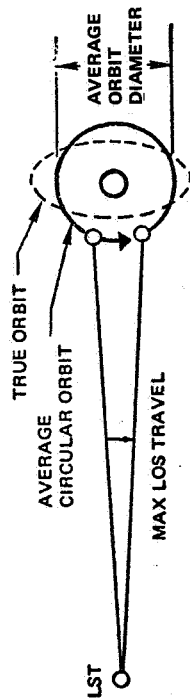
3. Centroid Track of Satellite. Data were developed that give the maximum LST LOS angular travel distance and rate for satellite tracking, assuming the LST and planet to be fixed. Figure B-2 illustrates the maximum effect of satellite motion. Those having the greatest effect on the LOS motions are nearest to the planet. The graphical data provide only maximum values that occur when tracking satellites near their parent body. Using as an example the satellite nearest Jupiter, a maximum LOS travel of 39 arc sec and a rate of about 0.6 arc sec/min are found to exist. This assumes a viewing period of 59 min per LST orbit.

4. Spot Track. Calculations were made to determine the maximum LOS travel distance and rate that occur when tracking a spot on a rotating object. Figure B-3 illustrates these calculations. The data apply to the maximum LOS movement that occurs only when observing near the center of the object. The LOS movement for observation near the limb of the object would approach zero. For example, for Jupiter with a 45-arc sec diameter, the LST LOS maximum travel distance would be approximately 13 arc sec for 50 min of viewing, and the LOS travel rate would be approximately 0.25 arc sec/min.

5. Raster Scan. This analysis was done to establish the total scan time for an object of given size, assuming the object and LST are fixed. Data from this analysis are shown in Figure B-4. These values are based on the following assumptions: a track velocity of 1 arc sec/sec, a turnaround time between scans of 1 min (this accounts for acceleration, deceleration, travel, and dynamic decay time involved in this nondata recording period), and a 10-arc sec turnaround distance beyond the limb. The data show that when using a 2-arc sec aperture, Jupiter can be raster-scanned in approximately 50 min. This is nearly the maximum time for viewing Jupiter during an LST orbit.

6. Stepped Scan. The condition here is the stepping of a slit in the LST science data field across an object, assuming a certain setup time between slit exposures. The data developed are used to establish the available slit exposure time for a given object size. Figure B-5 illustrates these data.

The data are based on an assumed slit setup time of 1.5 min. This time accounts for acceleration, travel, deceleration, and dynamic decay. As an example of the data, consider a 10-arc sec length slit stepped across Jupiter (49-arc sec size) and an LST viewing period of 50 min; this will permit a 9-min exposure time for each of the required five frames.



$$\text{MAXIMUM LST LOS TRAVEL PER VIEWING PERIOD (ARC SEC)} =$$

$$\pi \times \text{AVERAGE ORBIT DIAM.} \times \text{LST VIEWING PERIOD} / \text{SATELLITE ORBIT PERIOD}$$

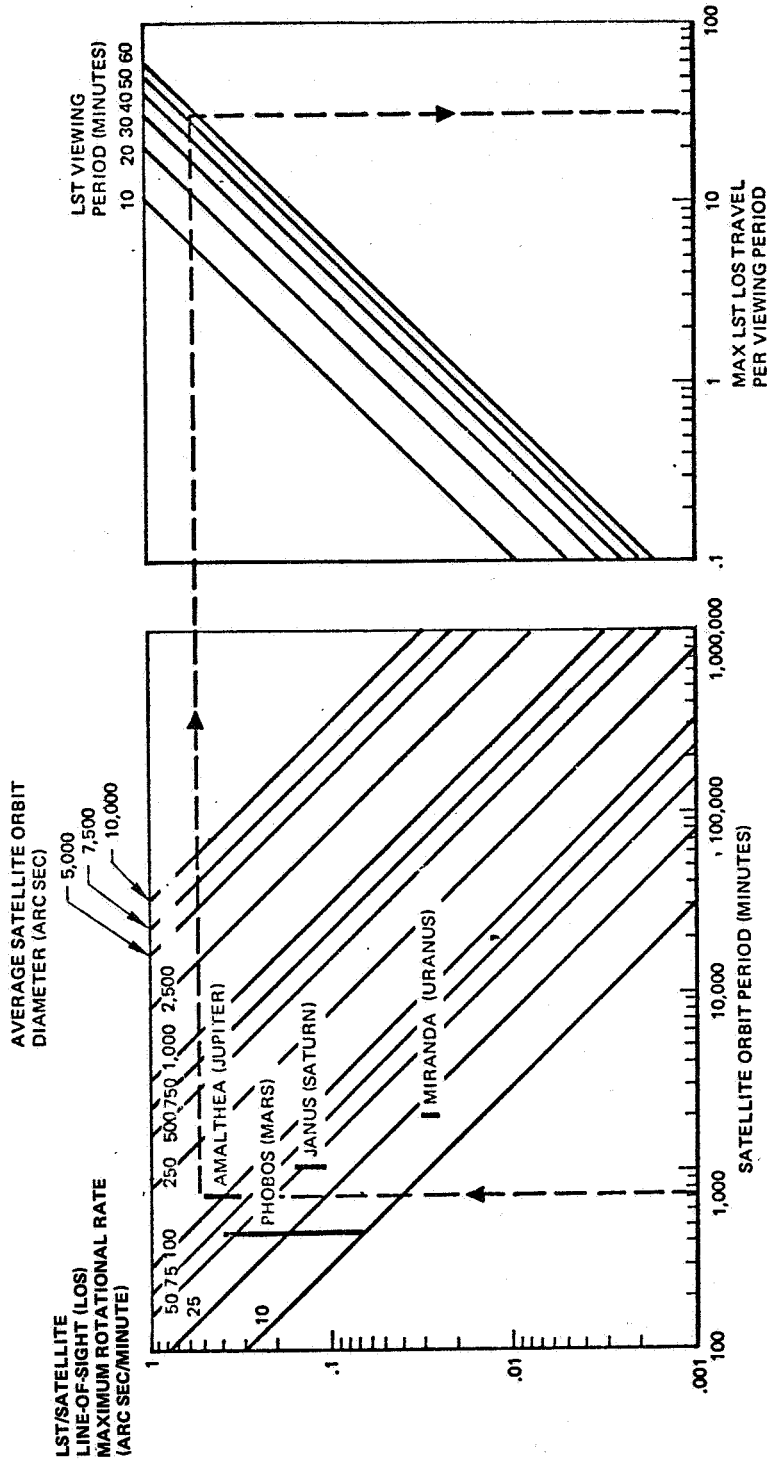


Figure B-2. LST maximum LOS travel due to satellite orbit revolution.

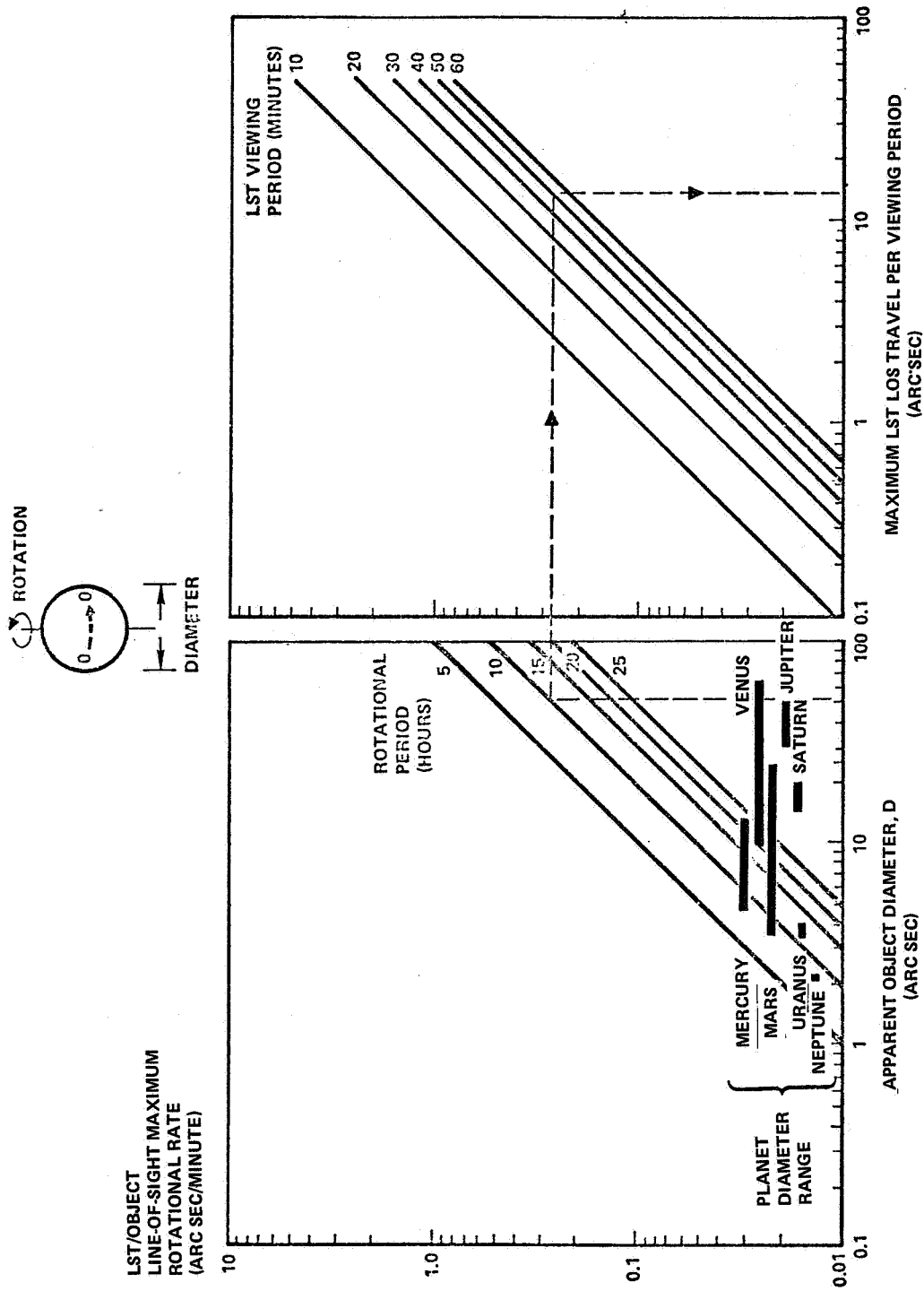
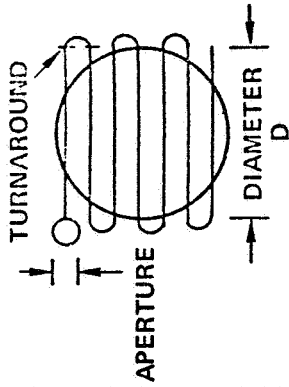


Figure B-3. LST maximum LOS travel due to object rotation.



ASSUMPTIONS:  
 TRACK VELOCITY  
 1 ARC SEC/SEC  
 TURNAROUND TIME:  
 1 MINUTE  
 TURNAROUND DISTANCE:  
 10 ARC SEC BEYOND  
 DIAMETER ON EACH  
 SIDE

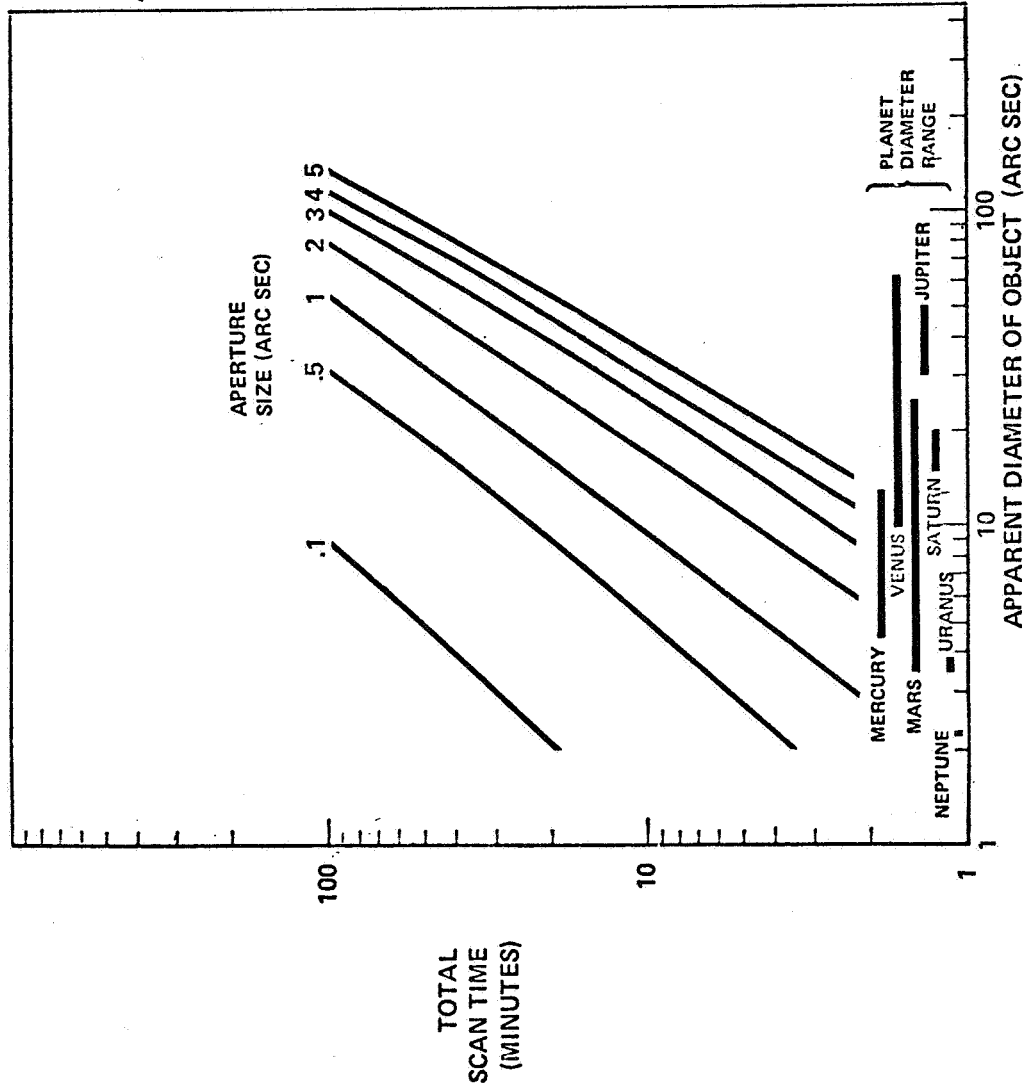


Figure B-4. LST time to raster-scan object.

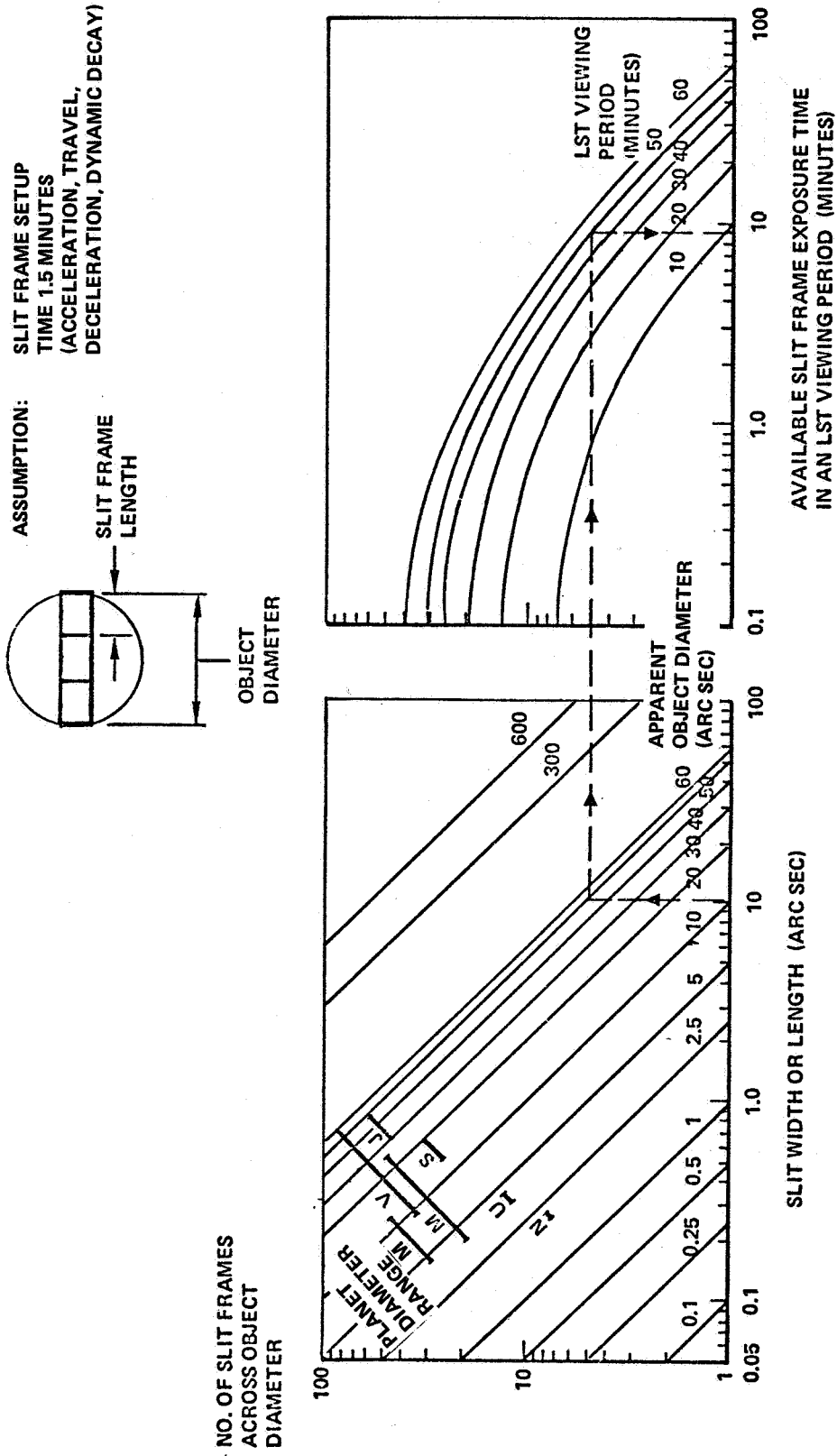


Figure B-5. LST available slit frame exposure time for a given object size.

7. Summary of Maximum LST LOS Travel Distance and Rate. Table B-1 is a compilation of data for the previously described four basic observational conditions. For conditions I and II (centroid and spot tracking) for planets and satellites, Mercury requires the largest LOS tracking rate (approximately 4 arc sec/min) and Venus the largest LOS travel distance (approximately 180 arc sec) during a viewing period. Of the two asteroids considered, Icarus has the largest LOS travel rate and distance (approximately 25 arc sec/min and 1300 arc sec, respectively) for 50 min of viewing.

Of the two comets studied, Halley has the highest LOS travel rate and distance (12.5 arc sec/min and 690 arc sec, respectively) for 55 min of viewing.

For condition III (raster scan), the maximum LOS rates determined for condition I are increased by the previously selected 1 arc sec/sec scan rate. The LOS travel for this condition is determined by adding the scan turnaround distance and object diameter to the maximum values determined in condition I.

For condition IV (step scan), the maximum LOS tracking rate is considered the same as for the largest value of the centroid or spot track conditions. Observation of a local area of the object must be held stationary on the science data field for the duration of the exposure, regardless of object motion. For LOS travel distance, the maximum value is found by adding the centroid travel and the width of the object. In the case of Venus, the maximum travel is about 200 arc sec.

Of the two asteroids studied, Icarus is smaller than the LST spatial resolution size; therefore, a raster scan is not applicable. Ceres is not a large LOS control object because of its small size and degree of centroid track motion.

The two comets studied in the two scan track conditions do require high LOS travel rates and distances (i. e., 73 arc sec/min and 840 arc sec). This is due to the assumed size of the comet head.

## C. LST Viewing Opportunities

1. Factors Influencing Capability. The dominant factor influencing the capability of the LST to view a solar system object is the sun-angle constraint. The influence of this constraint is shown in Figure B-6. As long as the sun angle is greater than 45 degrees, the viewing time is equal to, or



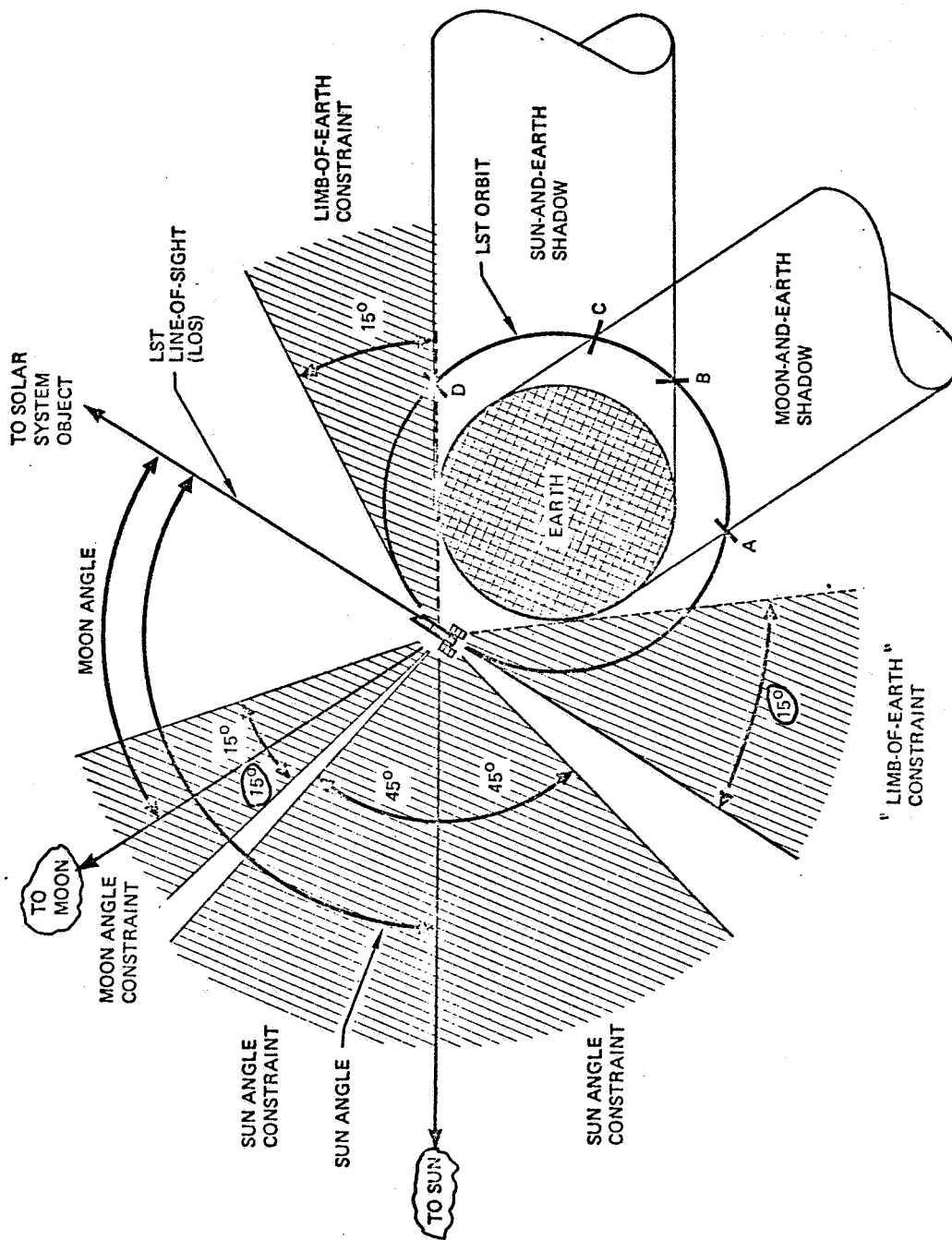


Figure B-6. LST LOS constraints.

greater than, 53.2 min per LST revolution, as in the example for Neptune. As soon as the sun angle drops below 45 degrees, the LST can no longer view the solar system object while the LST is in the sunlight. This results in a steep drop in the viewing time, as plotted in Figure B-7. The viewing time does not drop entirely to zero, because there is still some viewing possible while the LST is in the sun-and-earth shadow. In this case, the LST is using the earth as an occulting disc to block the sunlight while it views the solar system object, allowing viewing of less than 45 degrees. As the sun angle drops further below 45 degrees the viewing time grows shorter and eventually vanishes.

For the Neptune example, the value of 53.2 min derives from the limb-of-the-earth constraint, defined in Figure B-6, and the orbit altitude, chosen for this study as 330 n. mi. The orbit altitude fixes the nodal period of the LST in its orbit at 96.6 min. The solar system object will clearly have the shortest viewing time (sun and moon constraints neglected) if the line of sight from the LST to the object lies in the plane and the LST orbit. When this happens, the limb-of-the-earth constraint of 15 degrees limits the viewing time to 53.2 min per LST revolution. As time passes, the line of sight from the LST to the solar system object departs from the plane of the LST orbit, making an angle ( $\phi$ ) with the orbit plane.  $\phi$  varies in a complicated, oscillatory manner. This variation is due to two factors: (1) the motions of the earth and the solar system object, which cause the direction of the line of sight to change; and (2) the steady gyroscopic precession of the plane of the LST orbit due to the earth's oblateness. As  $\phi$  departs from zero, the viewing time increases; as  $\phi$  returns to zero, the viewing time returns to 53.2 min. This accounts for the oscillation of maximum viewing times with date, as shown in Figure B-7.

The moon-angle constraint has a relatively trivial effect on the capability of the LST to view solar system objects, as shown in Figure B-7. The periodic deep and narrow chasms in the plot of viewing time available are due to the moon-angle constraint.

2. Capability of the LST to View the Outer Planets. The definitions in topic 4 are useful in making a compact presentation of the capability of the LST for viewing outer planets. Figure B-8 shows viewing opportunities and blind intervals for the six outer planets. The data have been continued only long enough to exhibit the almost-periodic variation of viewing capability with calendar date.

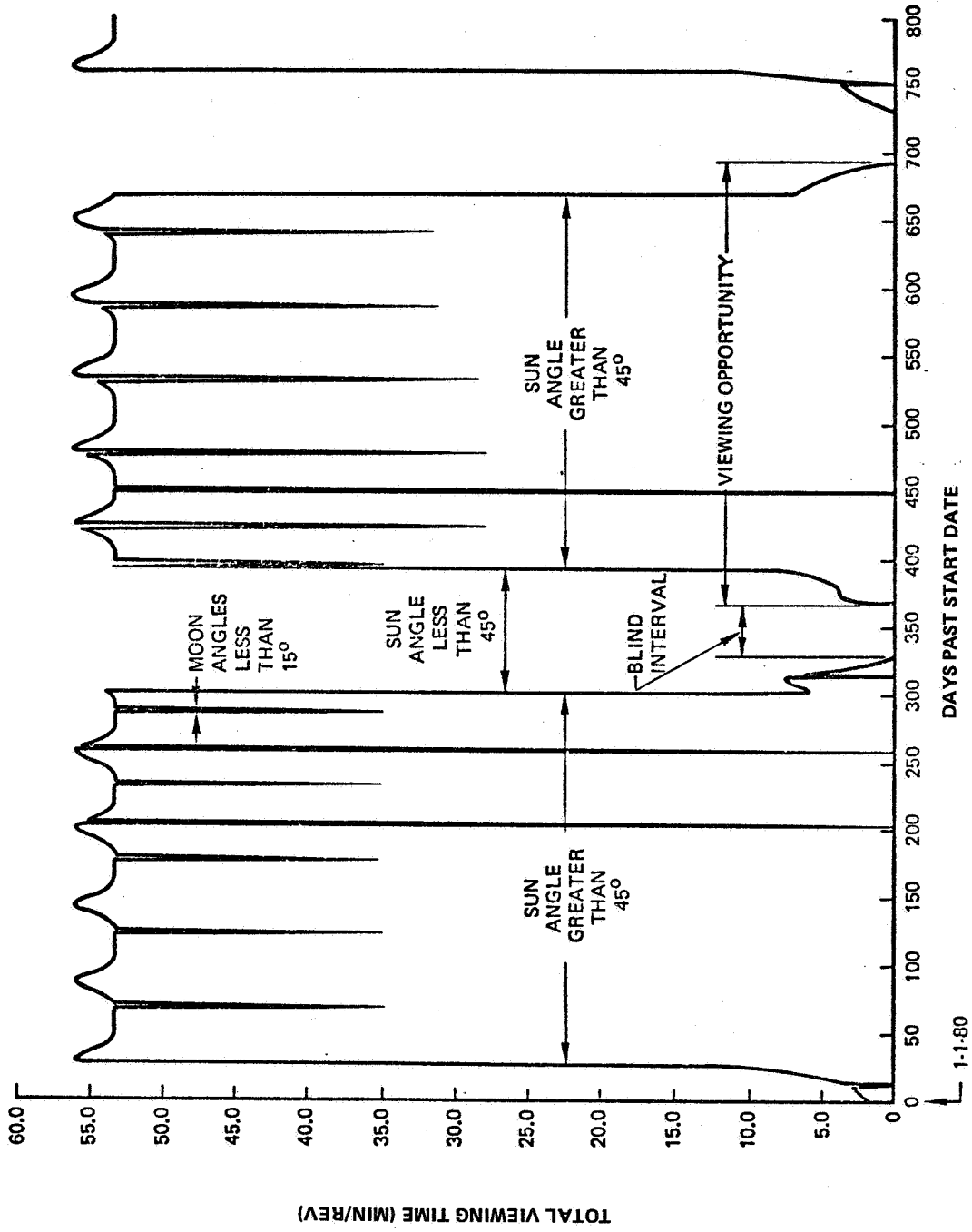


Figure B-7. Viewing time for a typical outer planet (Neptune).

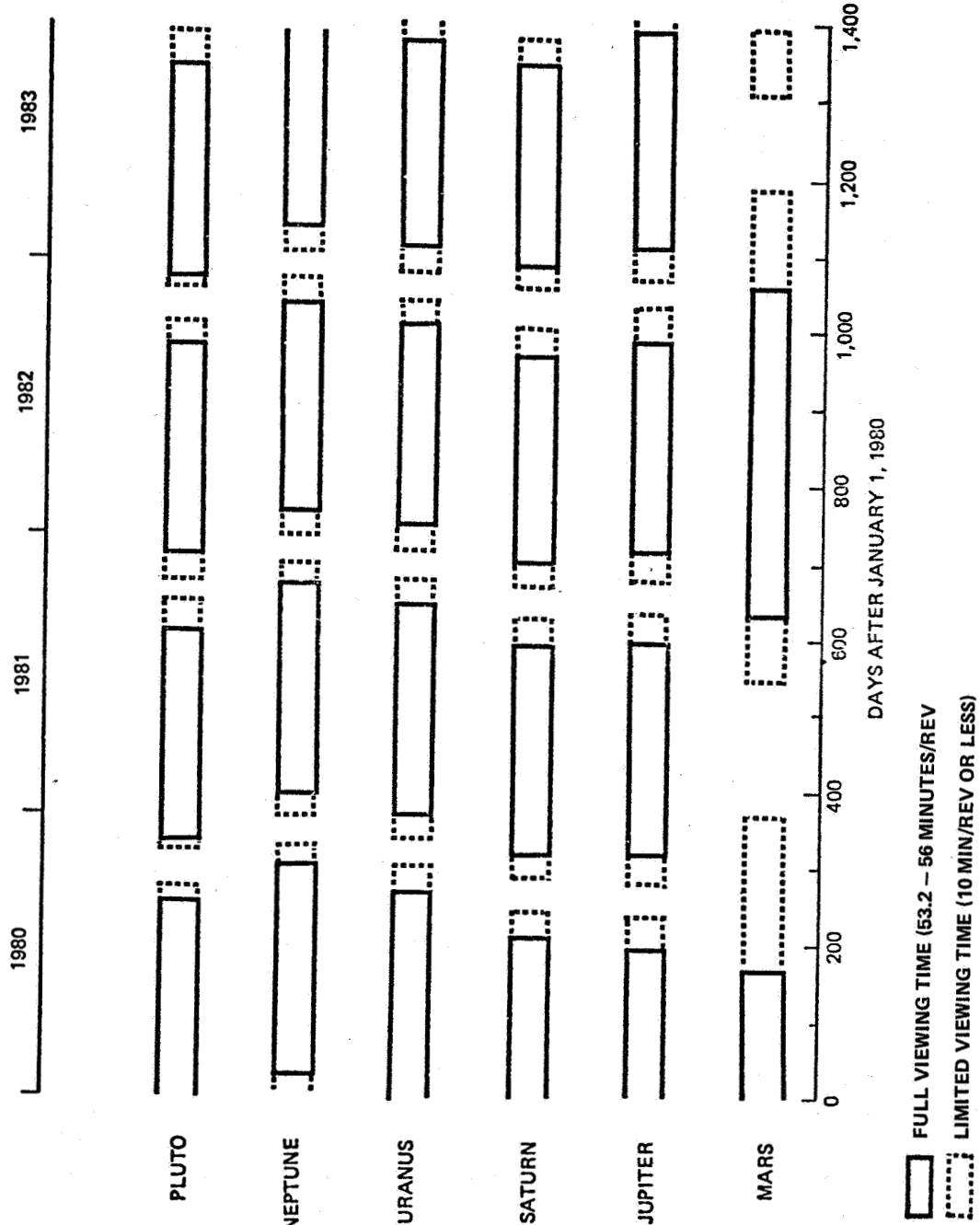


Figure B-8. Viewing opportunities for outer planets.

The viewing opportunities of Figure B-8 are centered about the dates on which the objects and the sun are most nearly opposite when viewed from the earth. The blind intervals are centered on the dates when the objects are near the sun when viewed from the earth, and the 45-degree viewing constraint applies.

Figure B-8 suggests that the LST, on any day, may be used to view several outer planets. Figure B-9 shows the effect of calendar date on the number of planets accessible to viewing by the LST.

3. Capability of the LST to View the Inner Planets. The orbit of Venus lies completely within the orbit of the earth, and the sun angle of Venus defined in Figure B-6 never exceeds 47.2 degrees. Since the sun-angle constraint is 45 degrees, the viewing opportunities in Figure B-10 do not cover as many days as they do for an outer planet (Figure B-7, for example). The spacing of the viewing opportunities in a calendar time is also different. The first viewing opportunity occurs when Venus is near its greatest eastern elongation, defined in Figure B-11. Venus then moves between the earth and the sun, which causes the first blind interval. Venus then approaches its maximum western elongation, providing the next viewing opportunity. Following this geometry Venus passes behind the sun, and the second blind interval occurs.

Eventually Venus returns to near maximum eastern elongation, another viewing opportunity results, and the cycle recurs. (If earth and Venus were in precisely circular, coplanar orbits, the sequence would be exactly periodic.) The passage of Venus from one maximum elongation to the next maximum elongation is greater for the westward trip than for the eastward; this accounts for the alternately shorter and longer blind intervals shown in Figure B-10.

The orbit of Mercury is so close to the sun that the sun angle to Mercury is never greater than 27.8 degrees. Hence, the sun-angle observation constraint is always violated as long as the LST is on the sunlit portion of its orbit. When the LST is in the sun-earth shadow, Mercury can be viewed using the earth as an "occluding disc." Figure B-12 shows typical viewing opportunities of this type, and Figure B-13 illustrates the geometry. The LST at Point A in Figure B-13 has just reached the point on the orbit at which the limb-of-the-earth constraint first permits viewing mercury. At Point B on the orbit, the LST has just emerged from the earth's shadow, and all observation ceases since the sun angle is less than the light shield cutoff angle, as shown in Figure B-13. In this case some sunlight will enter the the telescope tube, as indicated by the dotted line in Figure B-13.

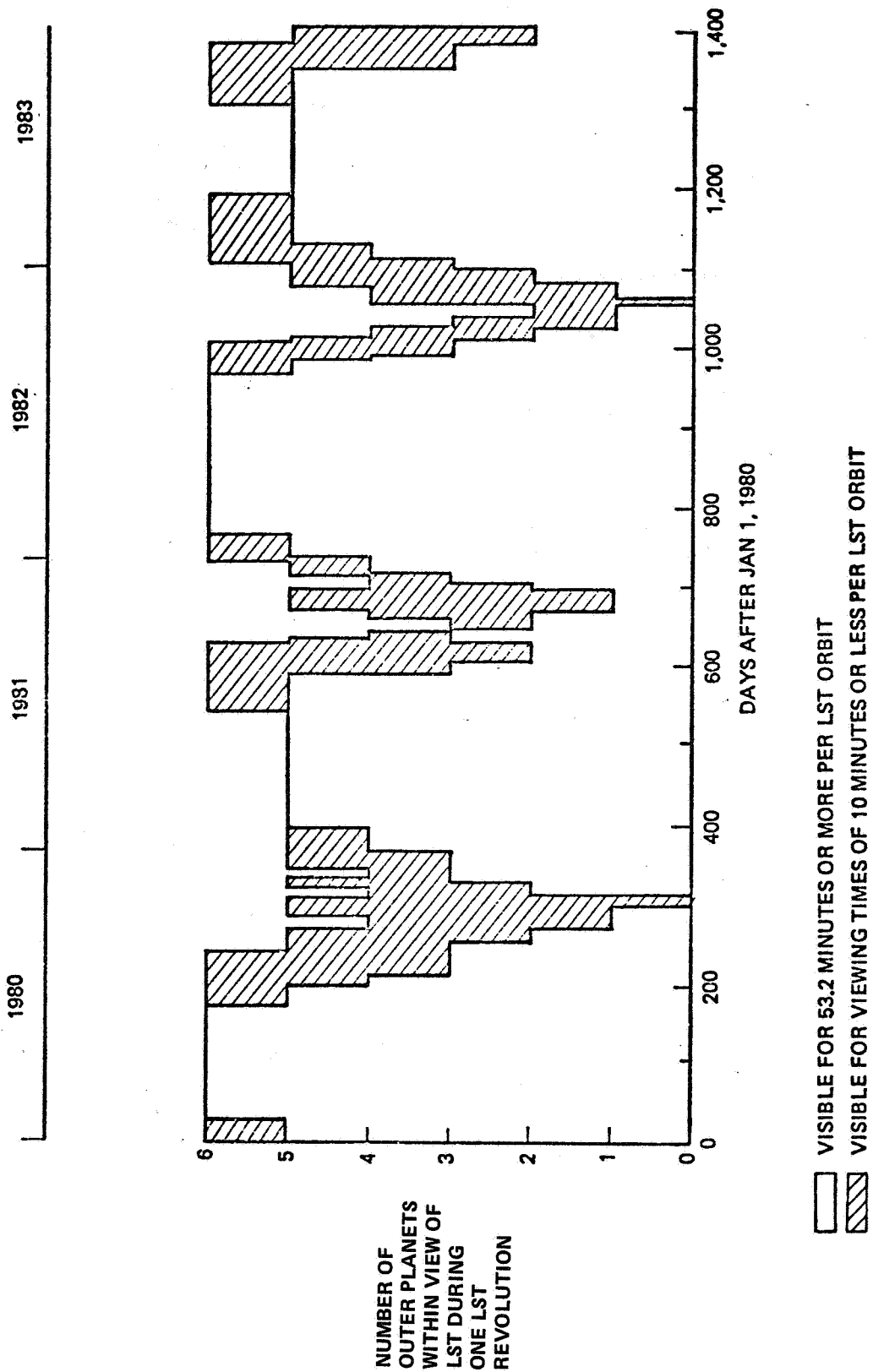


Figure B-9. Viewing accessibility of the six outer planets.

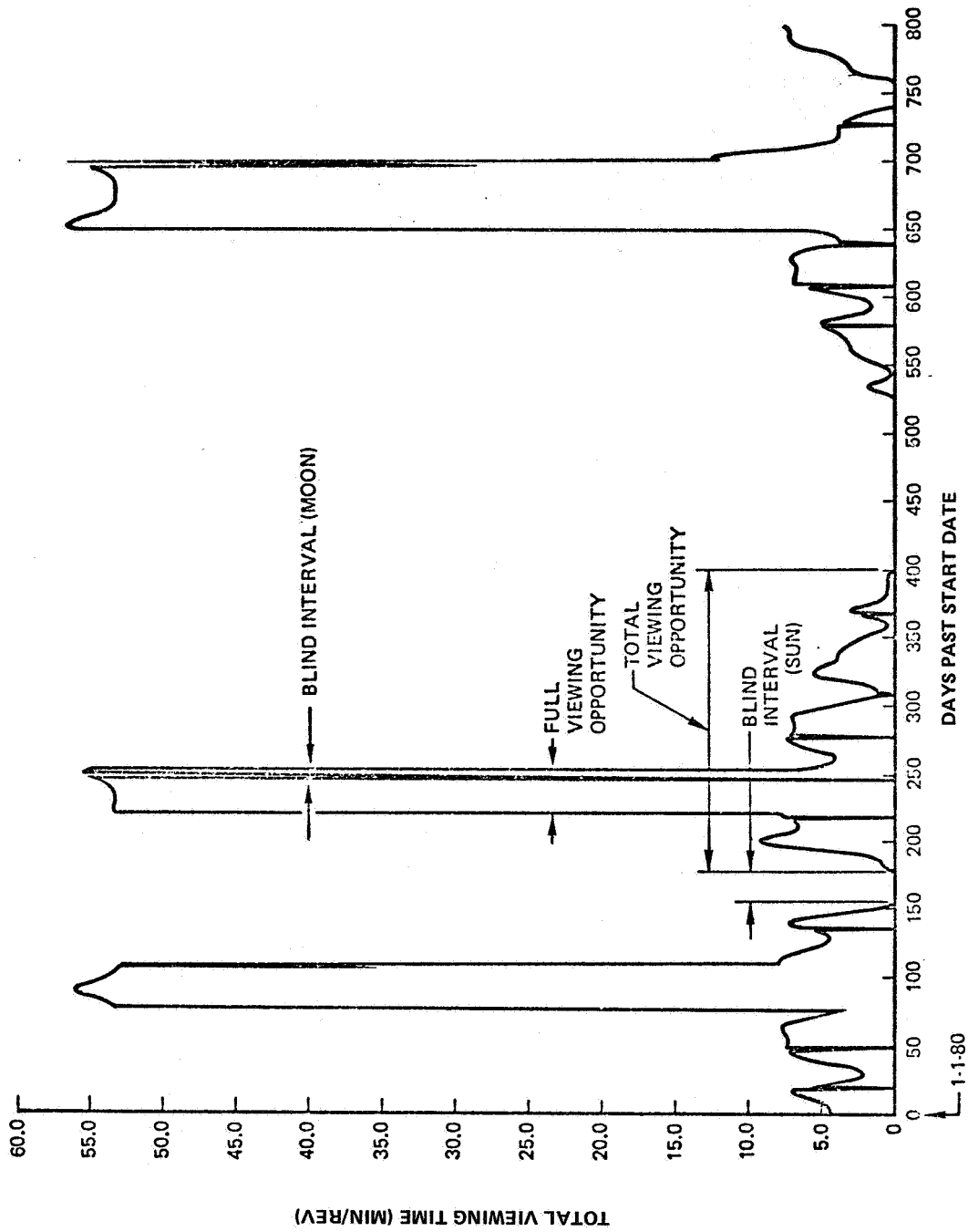


Figure B-10. Typical viewing opportunities for Venus.

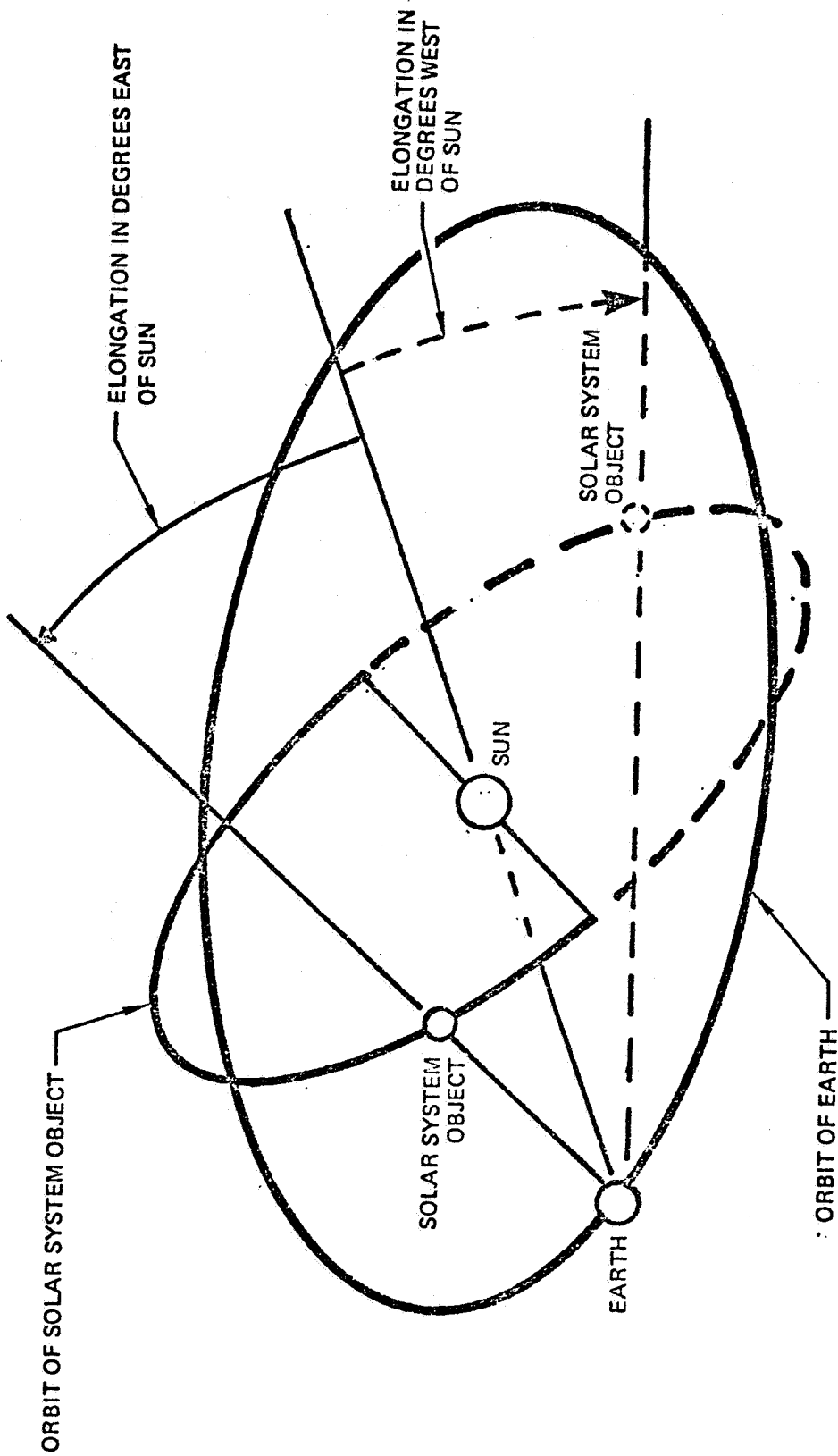


Figure B-11. Elongation angle.



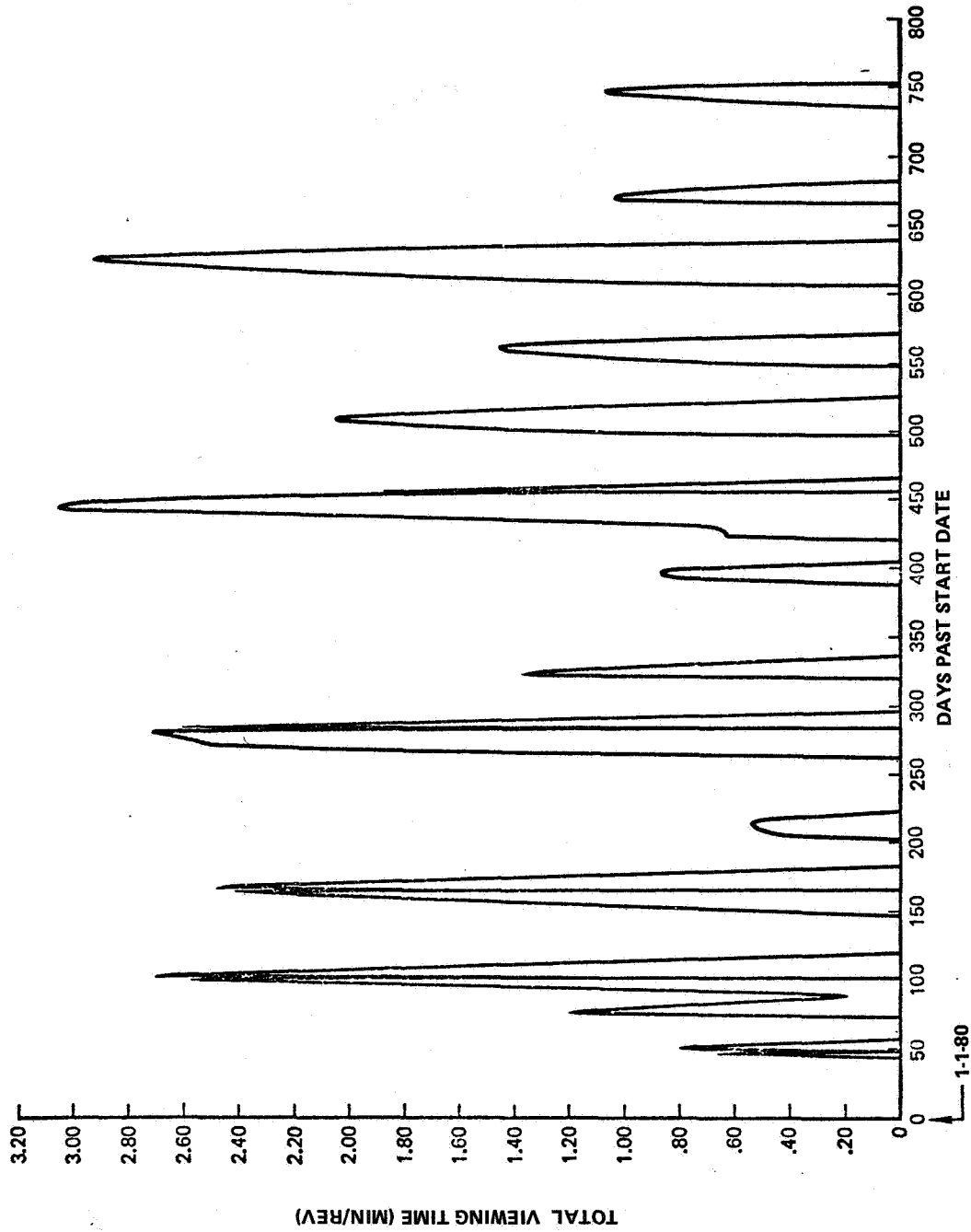


Figure B-12. Typical viewing opportunities for Mercury.

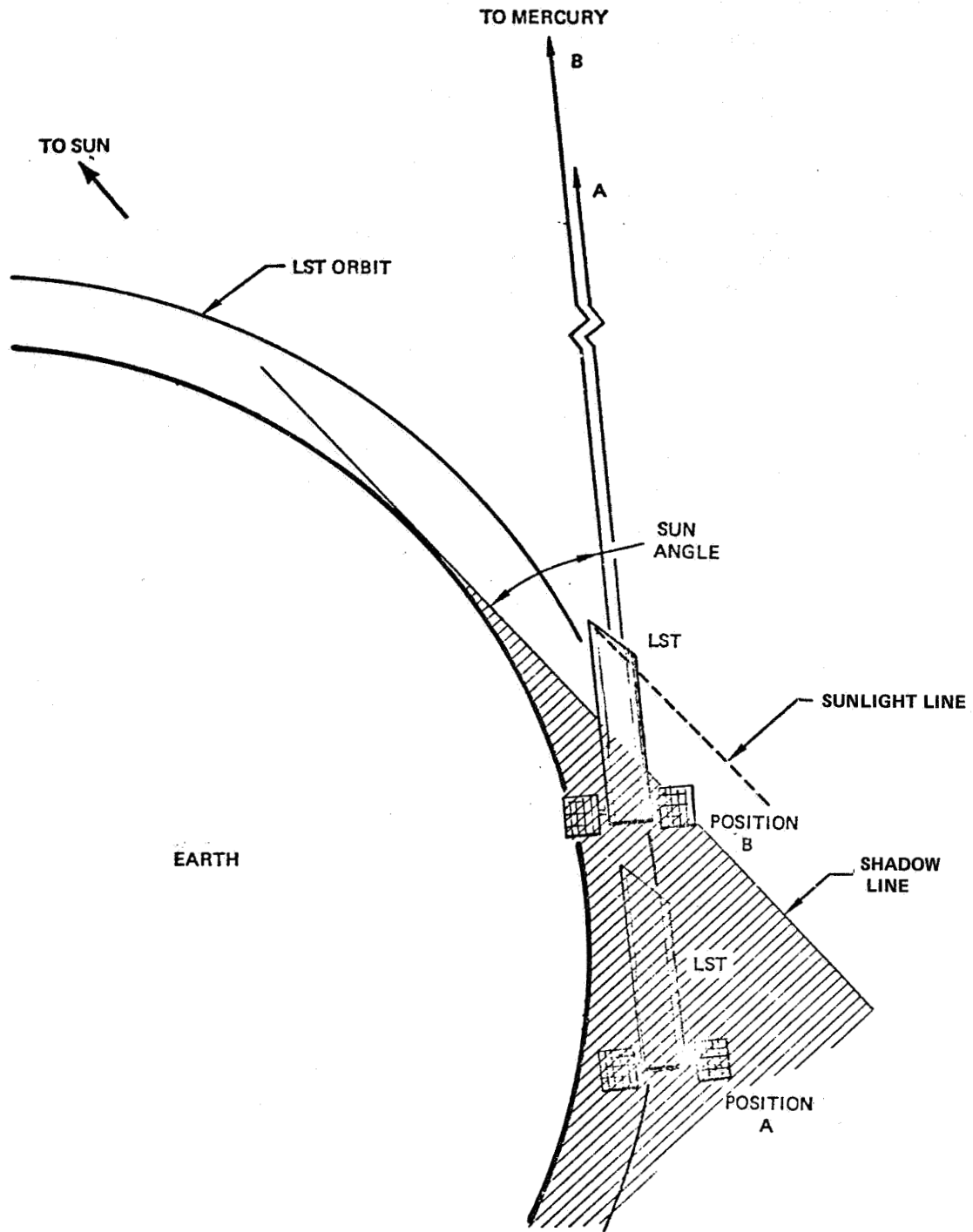


Figure B-13. Using the earth as an occulting disk.

Figure B-14 shows the viewing accessibility of the two inner planets. The limited viewing periods for both planets are when the sun angle is less than 45 degrees and occur when the LST is in the earth shadow.

#### 4. Definition of Parameters Used in Analysis

a. Viewing Constraints. The LST can view a solar system object when the line of sight from the LST to the object lies outside certain geometric or LST system-imposed constraints. The constraints used in the analysis are shown in Figure B-6. The three system-imposed constraints are angular viewing limitations near the sun, moon, and earth.

b. Viewing Time. The definition of viewing time is the number of minutes during which the LST can view the solar system object during one revolution of the LST in its orbit about the earth. Figure B-7 shows the viewing time available for the first 800 days of the time interval from 1980 to 2000 for Neptune. For example, Figure B-7 shows that the viewing time for Neptune is 53.2 min per LST orbital revolution on February 19, 1980 (59 days past start date). This viewing time would occur 14.9 times on that day, since the period of the LST orbit is 96.6 min.

c. Viewing Opportunity. A viewing opportunity is a block of one or more consecutive days. The viewing time is greater than zero during each of these days. For Neptune, Figure B-7 shows one complete viewing opportunity and portions of two more.

d. Blind Interval. A blind interval is a block of consecutive days where there is no viewing time in an LST orbit of revolution. Two blind intervals are shown in Figure B-7.

### D. Solar System Flux and Measurement Capability

1. Purpose. This section gives the flux as a function of wavelength from various solar system sources at the LST aperture and focal plane. These data are then compared with several typical instruments to determine the LST measurement capability.

2. Flux at the LST Primary Focal Plane. Figure B-15 illustrates the steps in the analysis, starting with the flux at the aperture and leading to the primary focal plane. The LST receives flux from an object (sketch a), collects it with the effective aperture of the telescope (sketches b and c), and focuses the energy at the primary focal plane using the primary and secondary mirrors (sketches d and e). The flux available per unit area at the focal plane

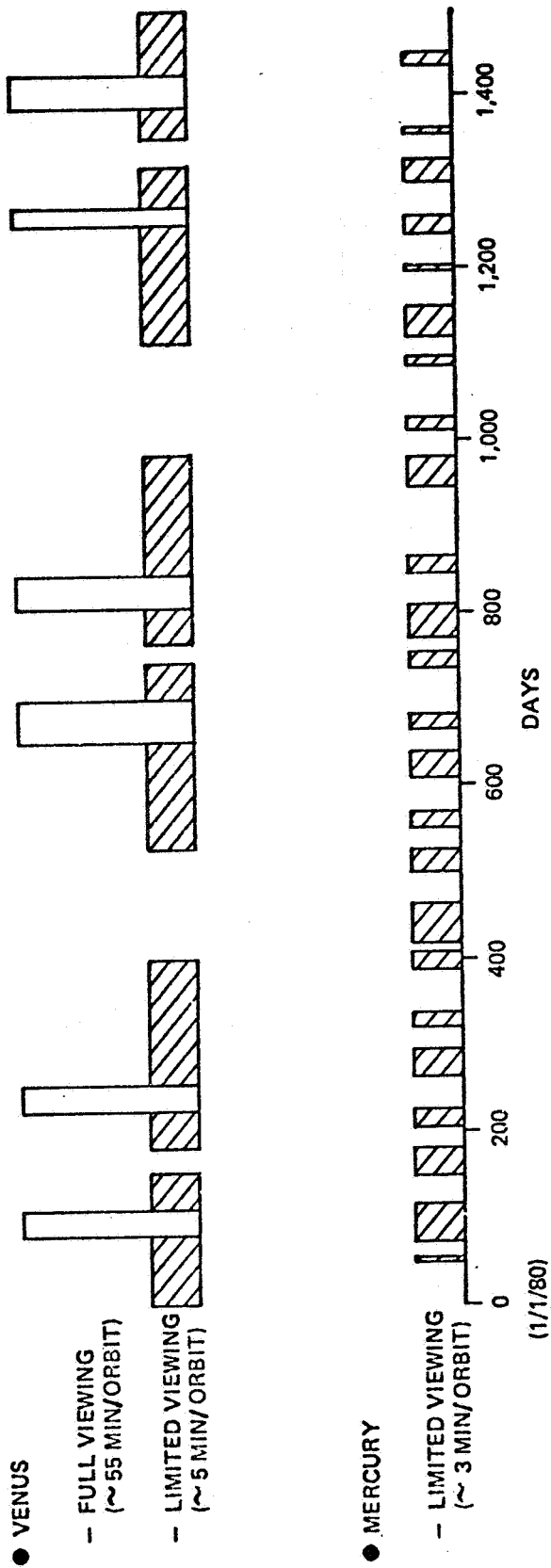
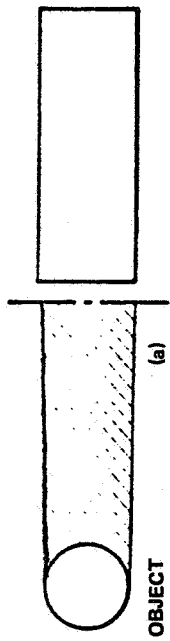
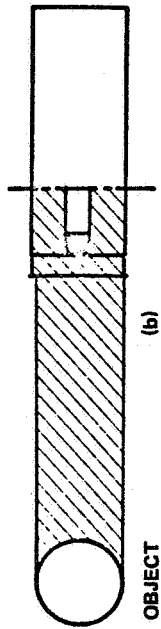


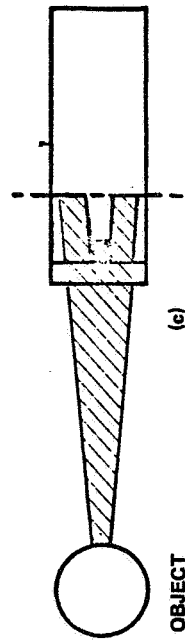
Figure B-14. Viewing accessibility of the two inner planets.



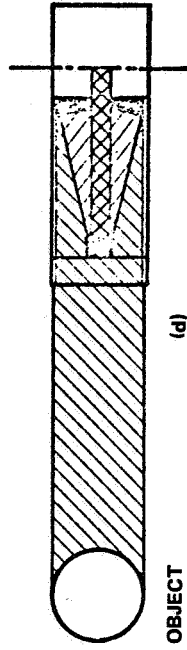
TOTAL OBJECT FLUX PER UNIT AREA AT THE ENTRANCE TO THE LST



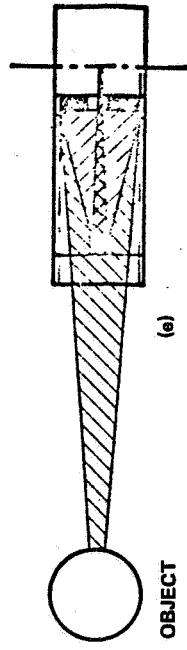
TOTAL OBJECT FLUX COLLECTED BY LST EFFECTIVE APERTURE



FLUX PER UNIT SOLID ANGLE OF OBJECT COLLECTED BY LST EFFECTIVE APERTURE



TOTAL OBJECT FLUX AT THE LST PRIMARY FOCAL PLANE



OBJECT FLUX IN EACH AIRY DISC AREA AT THE LST PRIMARY FOCAL PLANE

Figure B-15. Flux analysis steps for solar system objects.

is important for instrument considerations. The smallest unit area used was equal in size to an airy disk. Flux values could then be increased above this minimum size in multiples of airy disks up to the full object size.

3. Total Flux at the LST. The flux received at the LST from planets and other similar targets is displayed in Figure B-16. This is a plot of incident flux per unit area per unit wavelength at the LST aperture. The right-hand ordinate is the total flux per unit wavelength incident onto the effective LST aperture (left-hand ordinate multiplied by the effective aperture area). At the bottom of the figure are two reference curves of a 20th and 29th magnitude star calculated using the solar spectrum. The dashed lines in this and all subsequent figures indicate calculations, based or estimated, rather than observational data. The flux values assume that the objects are at nearly maximum brightness as seen from the earth.

In Figure B-16 two curves are shown for Mercury. One corresponds to the sunlit side, the other to the shaded side.

The comet curve is for Comet Bennett (1969). It is a bright, long-period comet for which some spectral data exist. Its diameter was assumed to be 200 arc sec.

In the region from 0.2 to 2  $\mu\text{m}$ , the data are mostly taken from NASA reports. Where these data were insufficient, the results from recent observations were used.

In the infrared region, the observational data have been extended with calculated values assuming blackbody radiation based on either observed or calculated brightness temperatures. Notice that for Mercury, because of the low albedo, the peak intensity occurs not in the visible region but rather in the infrared region. In the ultraviolet region, the rapidly falling flux values are caused by the decreasing solar radiation.

Observational albedo data exist in the far ultraviolet down to 0.2  $\mu\text{m}$  for some objects. Below 0.2  $\mu\text{m}$ , the spectral distribution has been estimated in one of two ways. For planets with atmospheres, a constant geometrical albedo is assumed equal to the albedo at the shortest wavelength. For example, from Orbiting Astronomical Observatory (OAO) observations the albedo of Venus has been determined down to about 0.2  $\mu\text{m}$  to be about 0.07. This value then has been used here for all wavelengths shorter than 0.2  $\mu\text{m}$ .

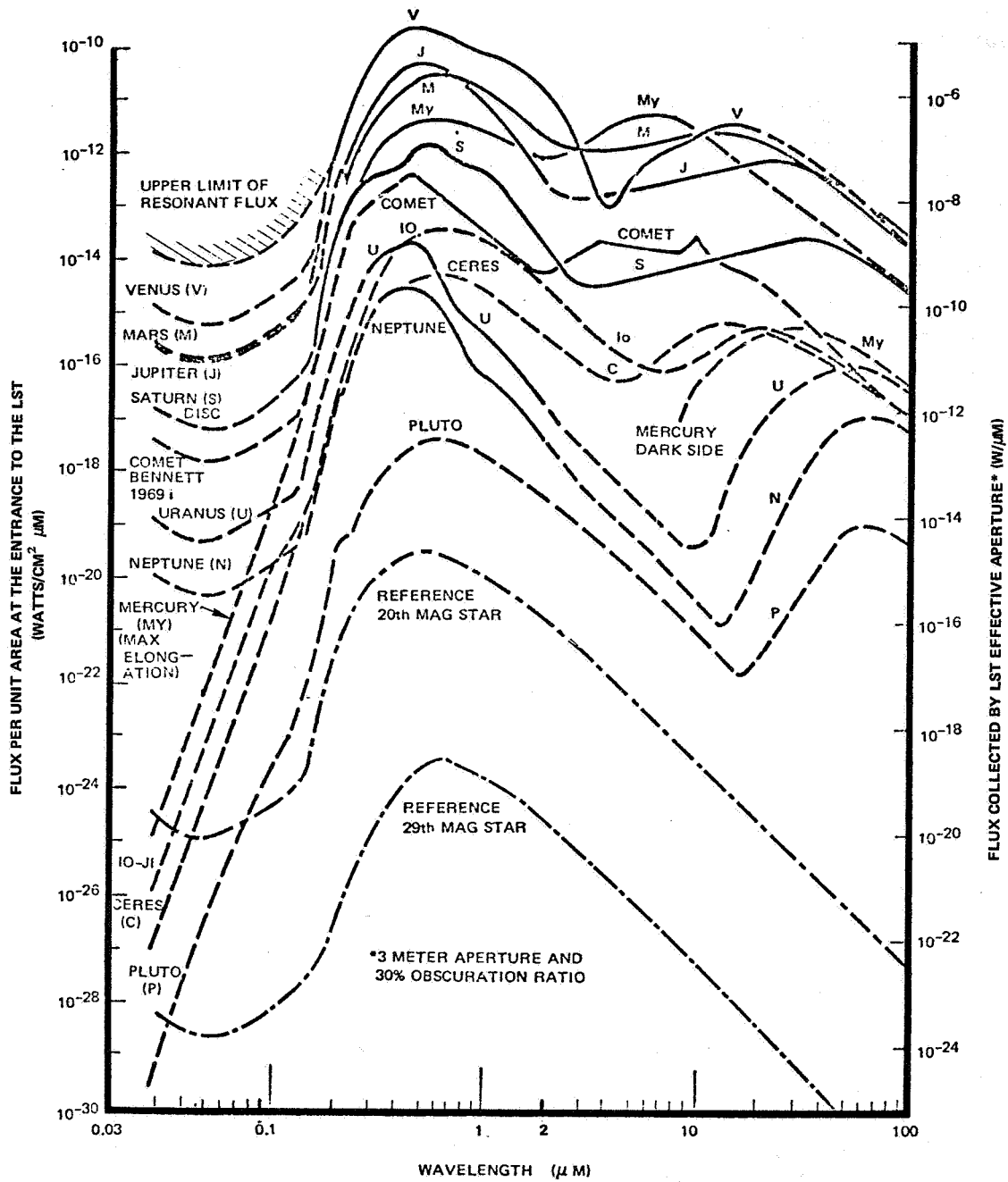


Figure B-16. Solar system object maximum total flux at the LST.

For planets without atmospheres, an albedo value is used based on an expression for the geometric albedo of Mercury. Planets without atmospheres, such as Mercury, have a low surface reflectance in the far ultraviolet.

The dashed line in Figure B-16, and subsequent figures (with the cross-hatching), labeled "upper limit of resonant flux," is an estimate of the maximum resonant flux for Venus.

Many of the solar system objects not shown in Figure B-16 would have much lower intensity values than indicated here; e.g., small satellites, comets, and asteroids.

4. Flux per Unit Solid Angle at the LST Entrance. The data in Figure B-17 were developed by dividing the flux shown in Figure B-16 by the object's solid angle in square seconds of arc. The solid angle used corresponds to near-maximum brightness (size shown in Table B-1). The same objects are shown as in Figure B-16, but the order of listing is now determined by the flux radiating from a unit solid angle of the object rather than the total flux. It is the flux per unit solid angle that is significant when measuring local areas of extended objects. It should be noted that this flux is not particularly sensitive to the object-LST distance.

5. Flux at the LST Focal Plane. The flux at the LST focal plane (Fig. B-15, sketches d and e) can be characterized either as the total flux or as the flux per unit area. The unit area selected is the smallest element of area which the LST primary optics can recognize, an airy disk. Before the flux reaches the focal plane it must undergo reflections from the primary and secondary mirrors. The mirrors are taken to be coated with aluminum and overcoated with a 250-Å thick magnesium fluoride, as might be typical for the LST. Mirrors with such a coating have the reflectance efficiency with wavelength shown in Figure B-18.

To determine the total flux at the focal plane, the reflectance data in Figure B-18 are used along with the total flux collected by the LST effective aperture (Fig. B-16). Figure B-19 shows the total flux collected at the LST primary focal plane.

Note in Figure B-19 how rapidly the flux decreases with decreasing wavelength. This is mainly due to low solar intensity in this region and to the very low reflectance of the mirrors in this region.

The area of the airy disk with wavelength was calculated and is shown in Figure B-20. This calculation assumed diffraction-limited optics beginning at 3000 Å. The number of airy disks in each object for a given wavelength was determined by dividing the airy disk area into the image area of the object. The number of airy disks so determined was then divided into



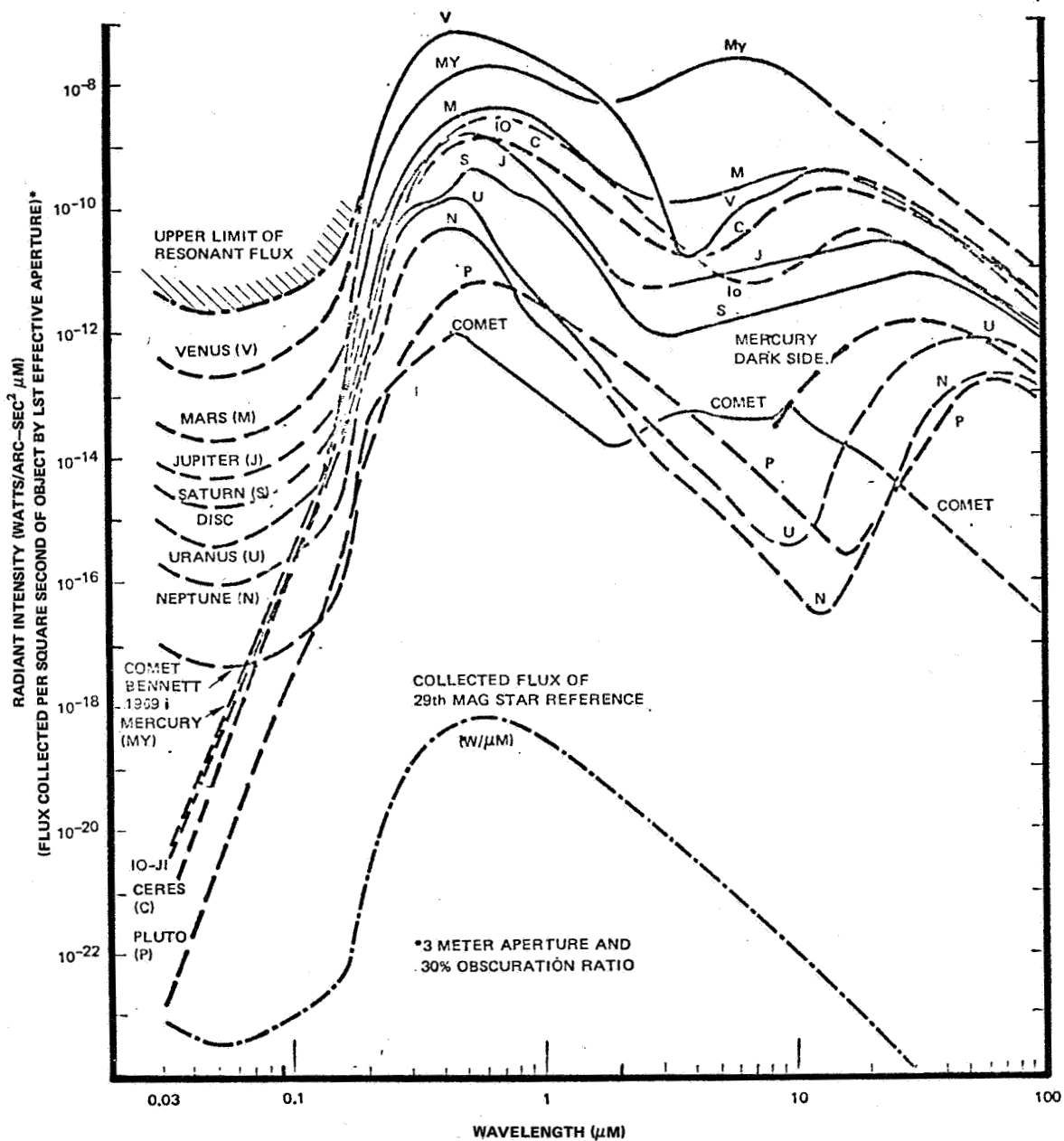


Figure B-17. Solar system object radiant flux per unit solid angle collected by the LST effective aperture.

the total flux at the focal plane as given in Figure B-19. This calculation then gave the flux in an airy disk. This flux was further reduced to account for the fact that no more than about 80 percent of the energy is contained in the central disk of the diffraction pattern. Taking into account the foregoing

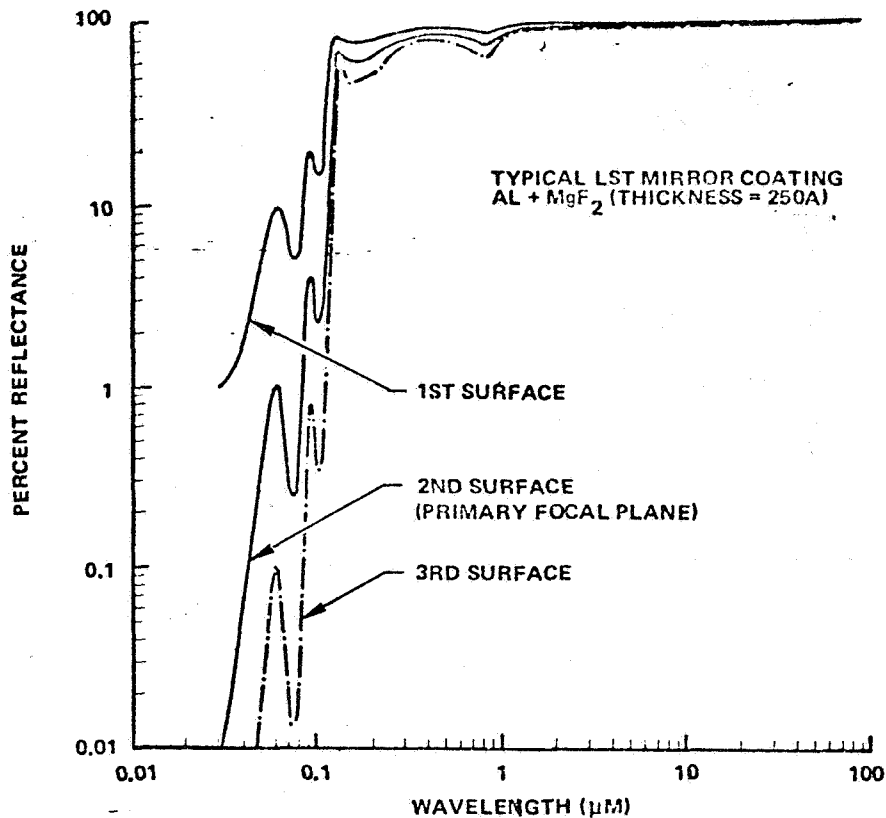


Figure B-18. Reflectance of LST mirror system.

considerations, the flux per airy disk as a function of wavelength was determined and is shown in Figure B-21. In the infrared region, as the airy disk size increases with wavelength, it soon exceeds the size of many of the solar system objects. The wavelength when this occurs is indicated by a closed circle on the curves in Figure B-21.

6. Comparison of Flux with Typical Instrument Performance. To evaluate the LST measurement capability, several typical instrument concepts with an estimated performance for each were identified. This instrument performance was then evaluated with respect to the flux levels at the LST f/12 focal plane. Near-maximum optical performance at the LST focal plane was assumed to exist. By accepting lower optical performance, it may be possible to measure lower flux levels than the data show. However, the unique value of the LST would appear to become less if it is used in a less-than-optimum manner.

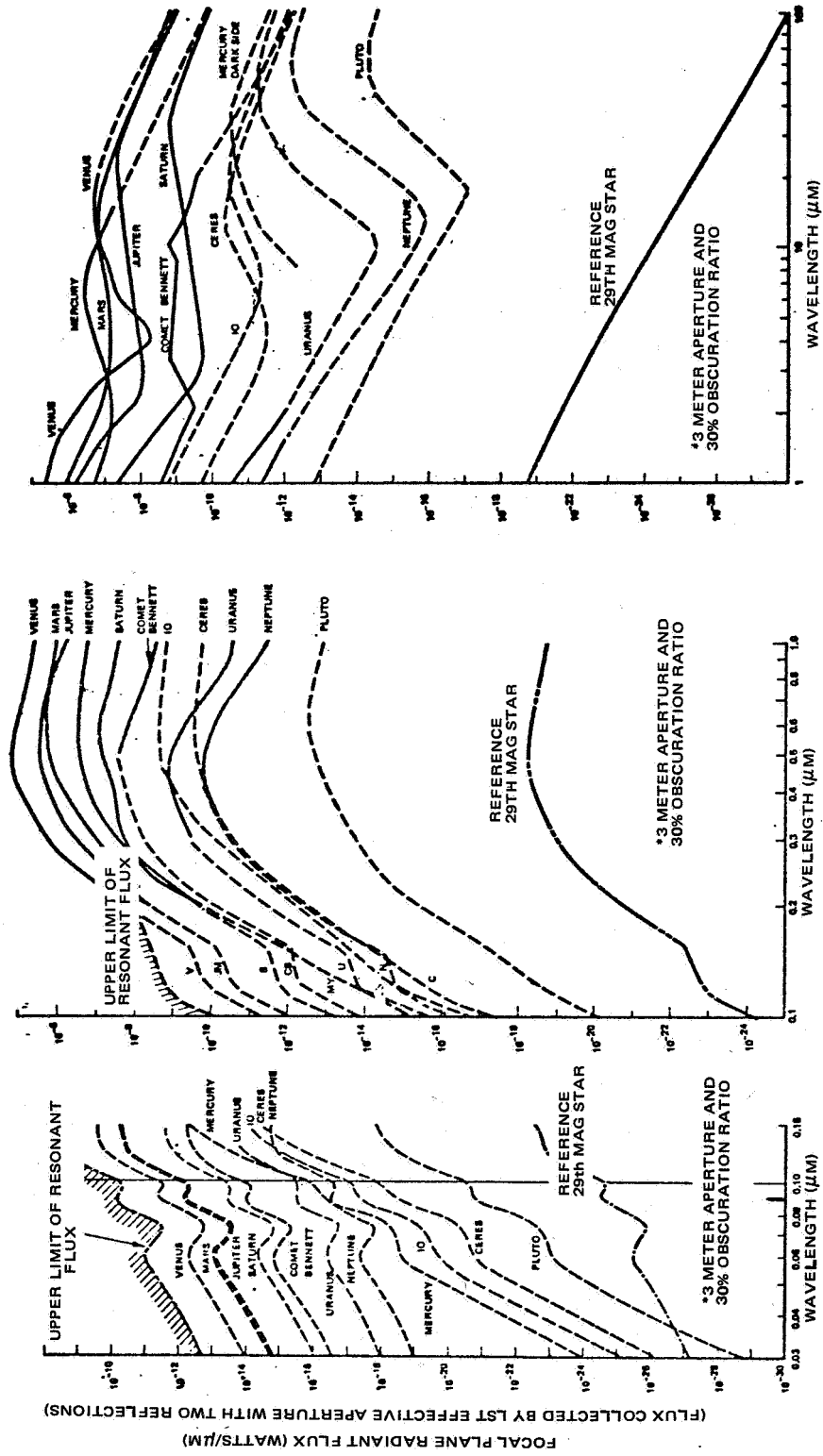


Figure B-19. Total solar system object flux at the LST primary focal plane.

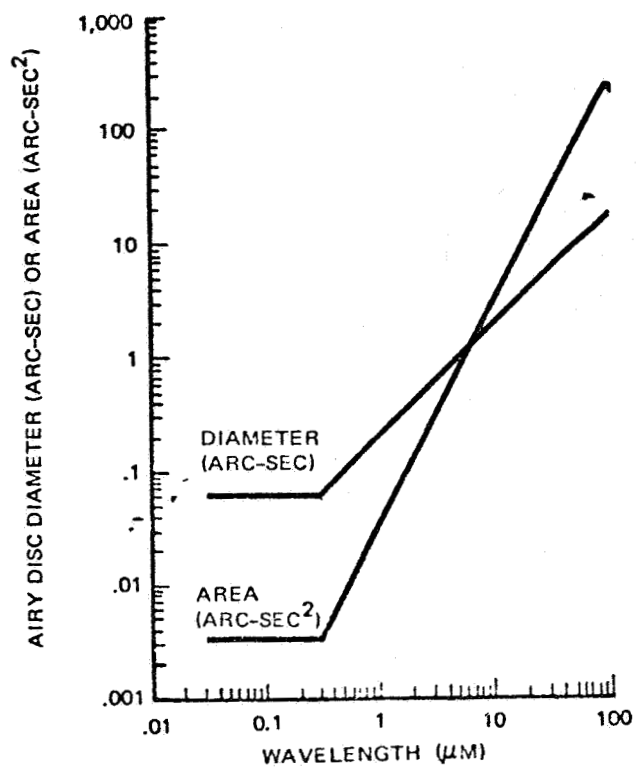


Figure B-20. LST airy disk size at primary focal plane.

Three spectral regions were examined and the minimum flux level levels detectable were established. Factors taken into account in determining the limiting flux levels were:

1. Total flux at the f/12 focal plane (entrance to a typical instrument)
2. Flux in each airy disc at the f/12 focal plane.
3. Instrument optical efficiency.
4. Sensor flux to electrical signal conversion efficiency.
5. Noise magnitude and characteristics.
6. Instrument spectral bandwidth.
7. Measurement exposure time or sampling time.

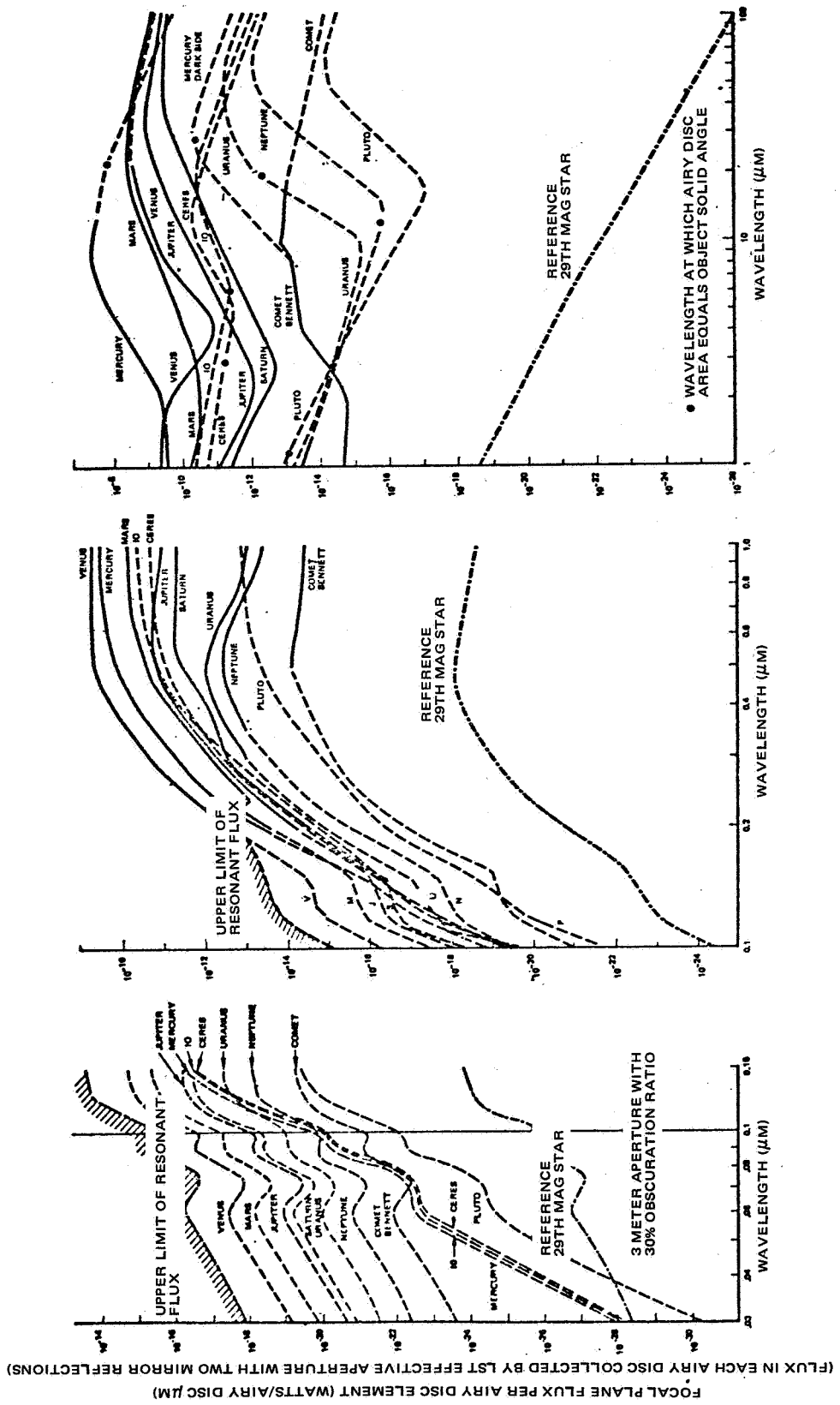


Figure B-21. Solar system object flux in an airy disk at the LST primary focal plane.

8. Measurement error that can be tolerated.

9. Available object viewing time.

a. Measurement Capability for the 0.03 to 0.1  $\mu\text{m}$  Range. By comparing the object flux with the most sensitive and generalized instrument concept for this spectral range, the total flux at the f/12 focal plane is apparently needed for a meaningful measurement. This comparison is illustrated in Figure B-22. The instrument concept is an open-face pulse counting channel detector. The data indicated that solar system objects near the earth (out to Saturn) may be measurable with the LST in this wavelength region.

b. Measurement Capability for the 0.1 to 10  $\mu\text{m}$  Range. The intensity levels in this spectral region are sufficiently high to permit the realization of nearly-full LST optical performance. Therefore, the analysis was made for a size equal to the airy disc area. Two types of measurements were used: imagery and spectrometry. Figures B-23 and B-24 illustrate the results.

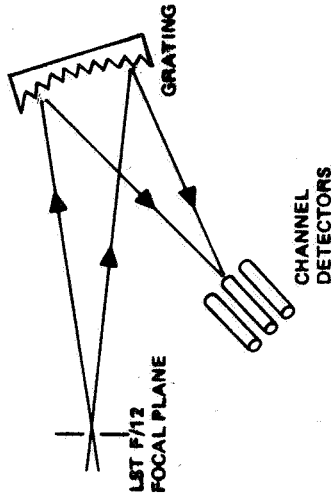
For the imagery (Fig. B-23), the limit lines represent the minimum flux levels detectable assuming a near-diffraction-limited performance for the LST. In the far ultraviolet region the flux for some objects is below the limit lines. These objects may be imaged by reducing the focal ratio which in effect increased the flux intensity incident onto a single sensor element.

In the case of spectrometry, the limit lines occur at higher flux levels than for imagery. This is mainly because less flux is available for measurement since the energy is dispensed into spectral bands. Lower spectrometry limit levels may be obtained by reducing the spectral resolution and by increasing the intensity as above by using a lower focal ratio.

c. Measurement Capability for the 1.0 to 100  $\mu\text{m}$  Range. For this region, because of the available energy, the measurement analysis was made for a size equal to the airy disc area. Two basic types of detectors — uncooled thermal detectors such as pyroelectric or thermistor and cooled photon detectors having greater sensitivity — were examined. For this analysis, a pyroelectric detector was used to illustrate the LST capability. It is a device that requires a minimum of system complexity and resources. Figure B-25 illustrates the LST capability using this detector.

Also shown in Figure B-25 is a curve of the flux at the f/12 focal plane produced by the thermal emission from the primary and secondary

**GENERALIZED INSTRUMENT CONCEPT**



**ASSUMED PERFORMANCE:**

- FLUX FROM TOTAL OBJECT IS COLLECTED BY UV INSTRUMENT, SPECTRALLY DISPERSED, AND PULSE COUNTED UNTIL A GIVEN MEASUREMENT ACCURACY IS REACHED
- TOTAL INSTRUMENT EFFICIENCY: 1% (OPTICS x DETECTOR)
- INSTRUMENT SPECTRAL BANDWIDTH: 10Å
- DARK PULSE NOISE: 0.1 COUNTS/SEC
- SKY BACKGROUND NOISE: NEGLIGIBLE

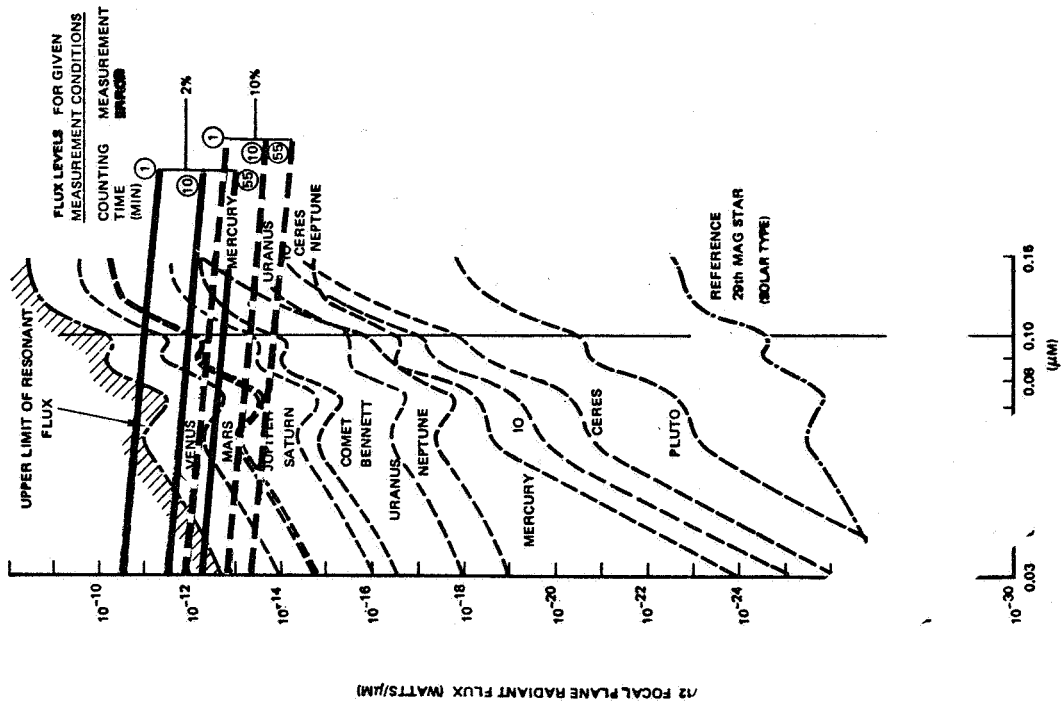
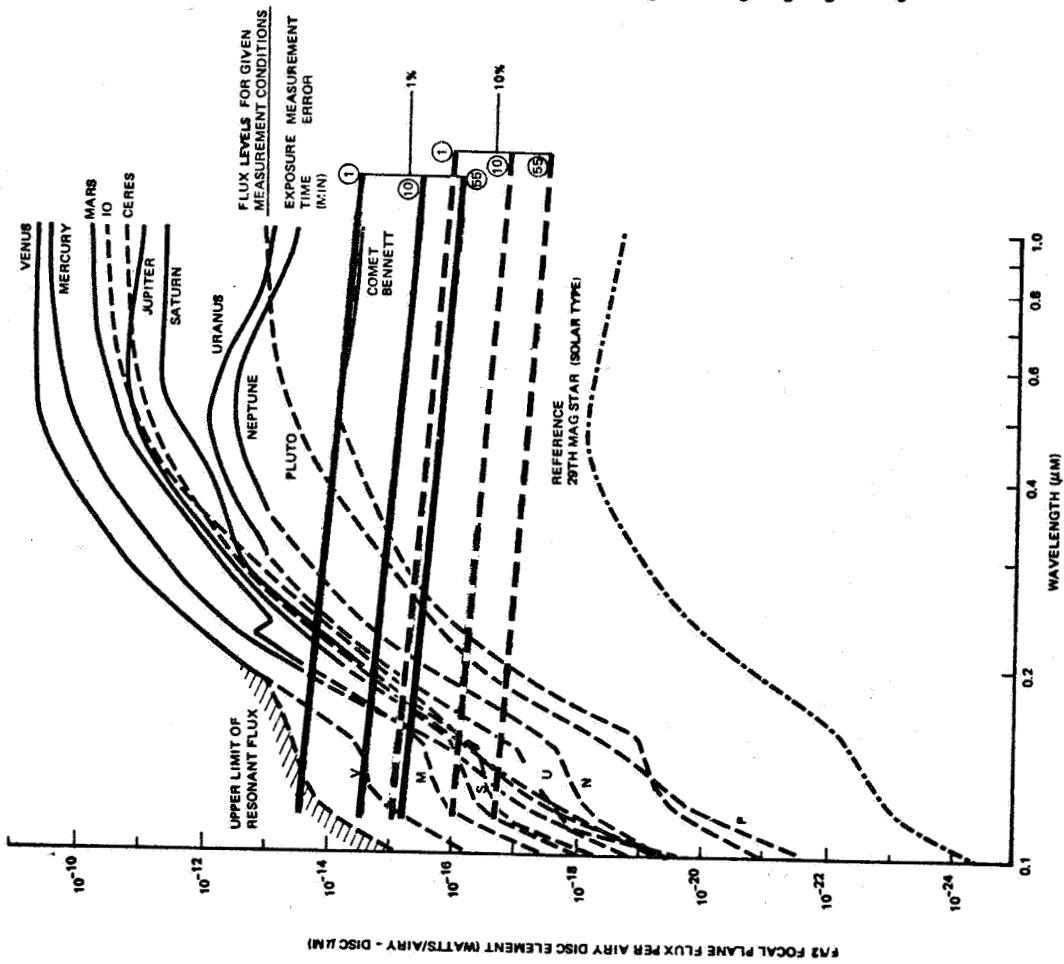
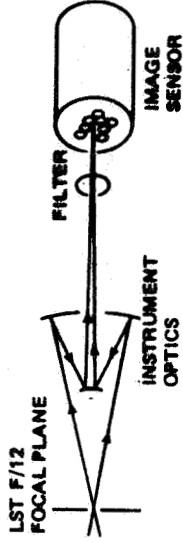


Fig LST measurement capability of solar system objects between 0.03 - 0.1 μm (300 - 1000 Å): spectrometry.



**GENERALIZED INSTRUMENT CONCEPT**



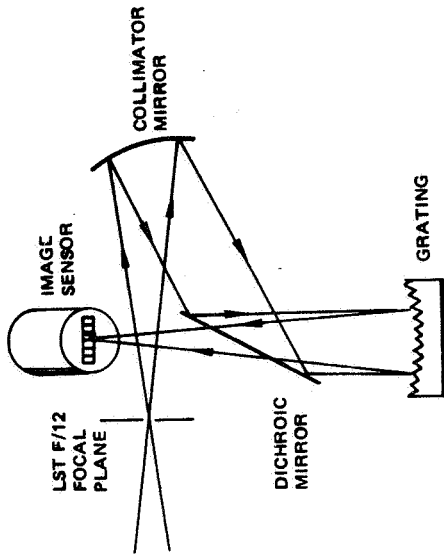
**ASSUMED PERFORMANCE:**

- FLUX FROM A SINGLE AIRY DISC IS IMAGED ONTO 50 SENSOR IMAGE ELEMENTS FOR AN EXPOSURE
- TOTAL INSTRUMENT EFFICIENCY: 10% (SIGNAL ELECTRONS OUT/PHOTONS IN, OPTICS x SENSOR)
- INSTRUMENT SPECTRAL BANDWIDTH: 1000A
- AMPLIFIER READOUT NOISE: 1,000 ELECTRONS/AIRY-DISC
- CATHODE DARK CURRENT NOISE: 1 ELECTRON/MM<sup>2</sup> SEC OR 0.1 ELECTRON/AIRY-DISC SEC
- SKY BACKGROUND NOISE: 1 PHOTON/SEC A ARC-SEC<sup>2</sup> OR 1 ELECTRON/AIRY-DISC SEC

Figure B-23. LST Measurement capability of solar system objects between 0.1 - 1.0  $\mu\text{m}$ : imagery.



GENERALIZED INSTRUMENT CONCEPT



ASSUMED PERFORMANCE:

- FLUX FROM ONE OR MORE AIRY DISCS PASSES THROUGH A SLIT AND IS DISPERSED AND FOCUSED ONTO AN IMAGE SENSOR FOR AN EXPOSURE
- NUMBER OF SENSOR IMAGE ELEMENTS PER SPECTRAL ELEMENT: 50
- TOTAL INSTRUMENT EFFICIENCY: (SIGNAL ELECTRONS OUT / PHOTONS IN, OPTICS x SENSOR) 5%
- INSTRUMENT SPECTRAL BANDWIDTH: 1 Å
- AMPLIFIER READOUT NOISE: 1,000 ELECTRONS/SPECTRAL ELEMENT
- CATHODE DARK CURRENT NOISE: 0.1 ELECTRON/MM<sup>2</sup> SEC OR 10<sup>-2</sup> ELECTRONS/SPECTRAL ELEMENT SEC
- SKY BACKGROUND NOISE: FOR 1 AIRY DISC—NEGLECTIBLE FOR 100 AIRY DISC — 0.05 ELECTRONS/SEC SPECTRAL ELEMENT

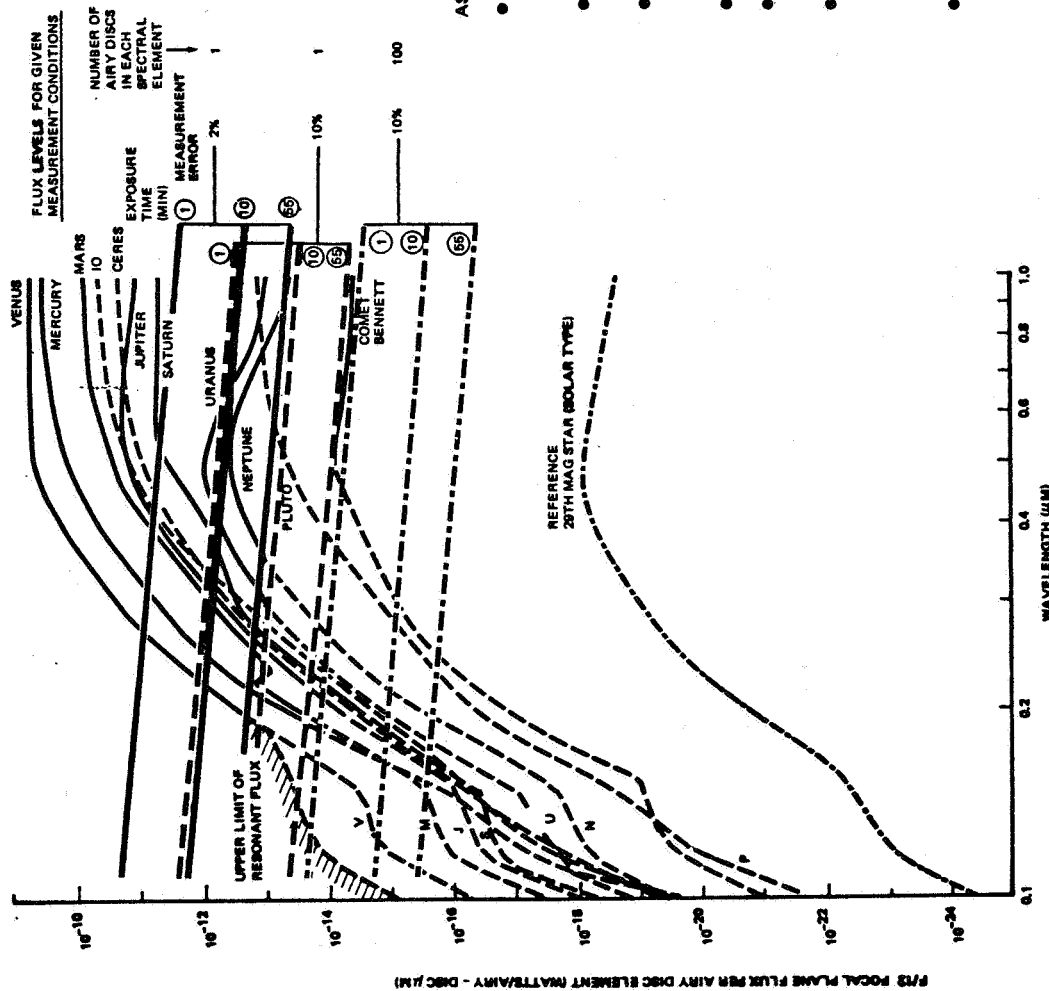
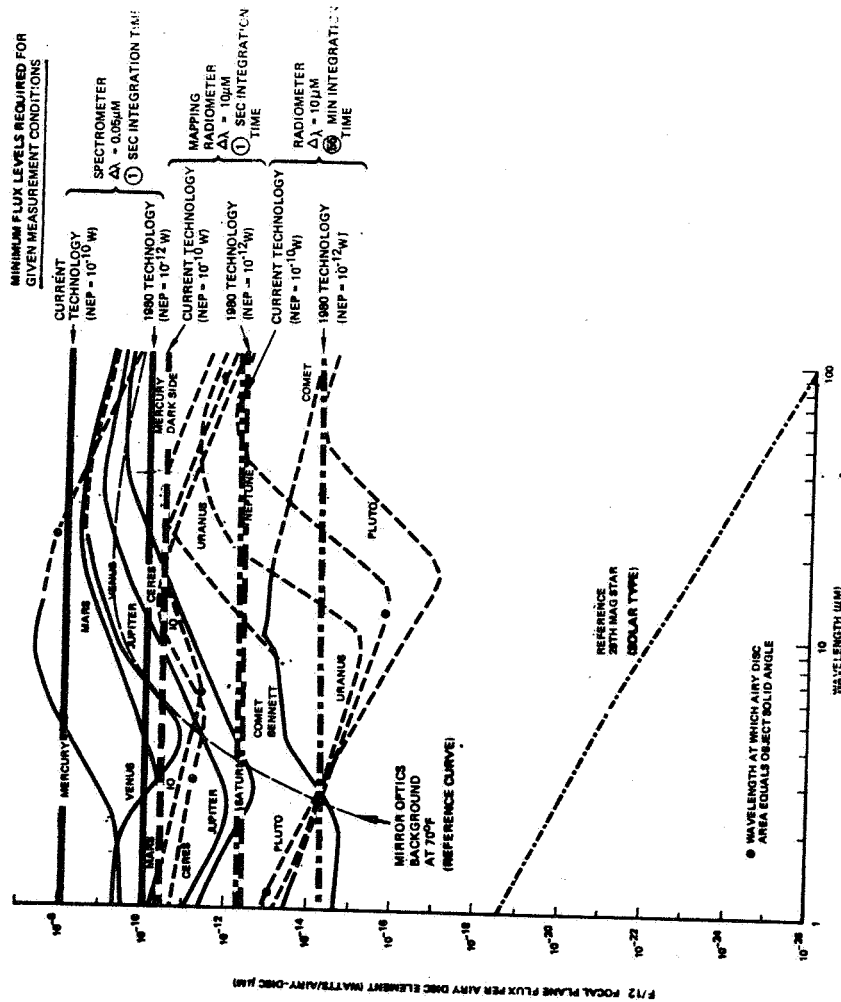
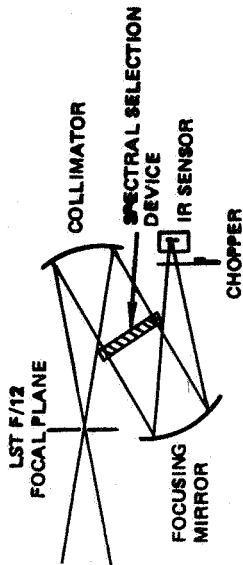


Figure B-24. LST measurement capability of solar system objects between 0.1 - 1.0 μm: spectrometry.



**GENERALIZED INSTRUMENT CONCEPT**



**ASSUMED PERFORMANCE**

- FLUX FROM A SINGLE AIRY DISC IS SPECTRALLY SELECTED AND FOCUSED ONTO A SINGLE IR DETECTOR. A NUMBER OF MEASUREMENTS ARE TAKEN BY SPATIAL SCANNING OF THE LST AT A FIXED WAVELENGTH
- INSTRUMENT OPTICAL EFFICIENCY; 25%
- INSTRUMENT SPECTRAL BANDWIDTH  $\Delta\lambda$ : AS INDICATED
- FREQUENCY BANDPASS: 1 Hz
- SENSOR: THERMAL (PYROELECTRIC) DETECTOR;  
AREA =  $0.2 \text{ MM}^2$   
(0.5 MM DIAMETER)
- SENSOR NOISE EQUIVALENT POWER (NEP):  
AS INDICATED FOR A 1 Hz BANDPASS

Figure B-25. LST measurement capability of solar system objects between 1 - 100  $\mu\text{m}$ .

mirrors at 70° F. This thermal emission plus other instrument fluxes are a part of the total flux that the detector measures. These nonobject flux values can be separated by an onboard calibration using black space. This is accomplished by occasionally looking away from the object and toward space. The black space flux value (which consists almost entirely of the nonobject flux) can then be subtracted from the total value obtained when viewing the object to determine the true object flux.

The data in Figure B-25 indicate that for this spectral range it is possible to use the LST, which is relatively warm (~70° F), for observing most of the solar system objects at near the diffraction-limited performance.

d. Evaluation of LST Measurement Capability. On reviewing the comparison between the flux data and the instrument performance, it is quite evident that the LST has significant measurement capability for solar system objects over a large spectral range. This is illustrated and summarized by Figure B-26. The capability of measuring the flux from solar system objects beyond 0.1  $\mu\text{m}$  down to about 0.03  $\mu\text{m}$  (extreme ultraviolet) and beyond 1.0  $\mu\text{m}$  up to about 100  $\mu\text{m}$  (into the far infrared) appears to require little if any additional system complexity and is therefore a significant bonus.

## E. Conclusions and Recommendations

An area that may impose special requirements on the LST equipment is the line-of-sight (LOS) tracking. Maximum observation times for the planets can require angular travel as large as 220 arc sec and rates as high as 64 arc sec per min. The highest values identified were 1310 arc sec travel and 73 arc sec per min for comets and asteroids. It was concluded from an evaluation of the LST Phase A configuration that it does not have a capability for tracking a moving object. The positional reference system (off-set tracker) in this case appears to be designed for relatively stationary stellar objects and has a very limited range of travel. However, from the results of this study it was determined that an LST positional reference system having the rather large range of travel required for solar system observations might be developed within reasonable resources. Such a positional reference system would also accomplish the requirements for stationary objects.

Minimum flux values needed for adequate signal strength using typical measurement techniques were developed for the 0.03 to 0.12, 0.12 to 1.0, and 1.0 to 100  $\mu\text{m}$  ranges. These values were then compared with the available flux from the solar system objects at the LST primary focal plane. This comparison indicates that the LST has a significant measurement capability across most of the spectral range studied.

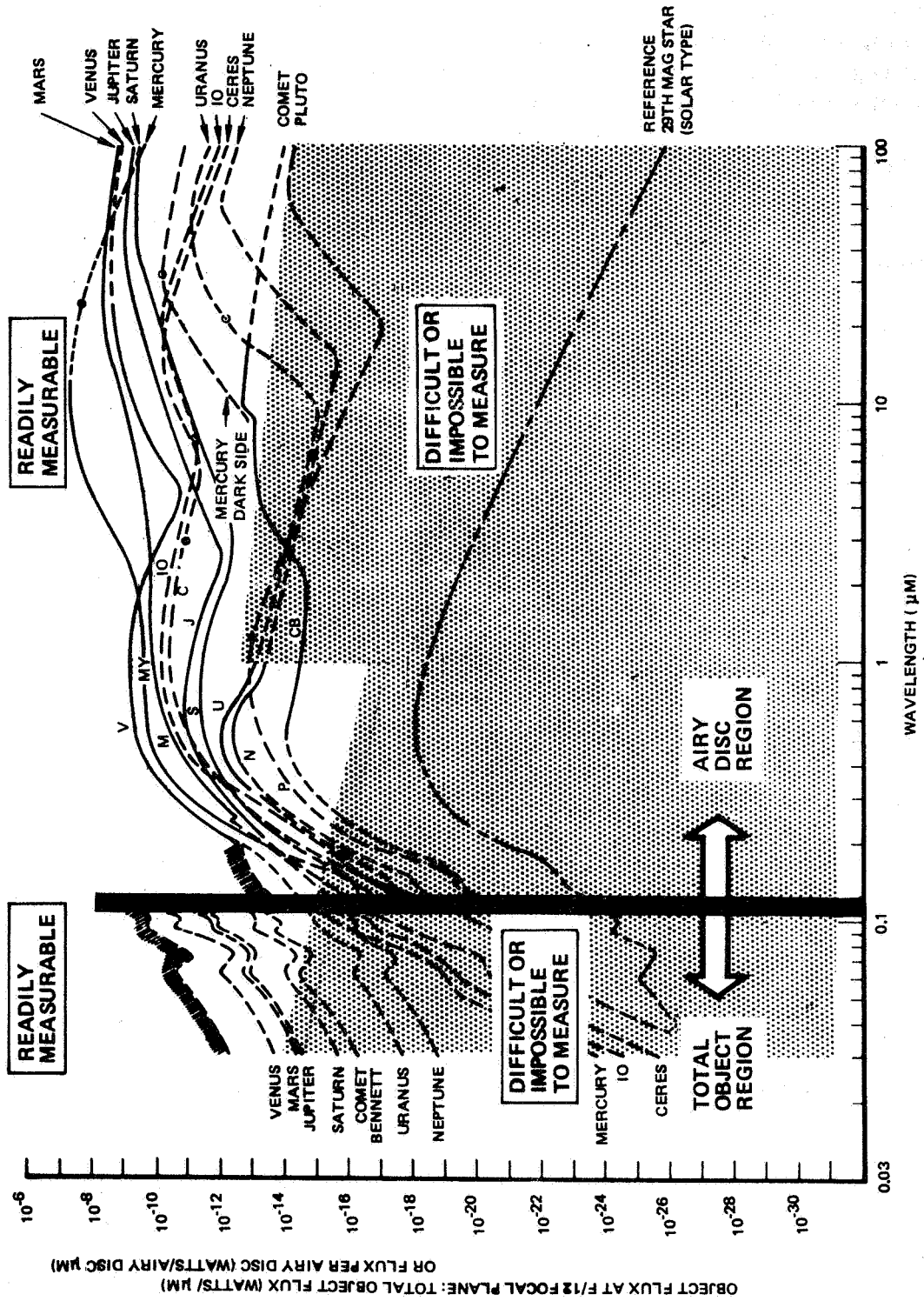


Figure B-26. Summary of LST measurement capability of solar system object flux.

All the object's flux is needed to make a single measurement in the 0.03 to 0.12  $\mu\text{m}$  region. This is because of the low solar flux in this spectral region and, also, the reflectance of LST optical mirrors is low in this spectral region. However, because of the large LST mirror sizes and high instrument sensitivity, fluxes from several near planets may be detectable.

In the 0.12 to 1.0  $\mu\text{m}$  region, adequate flux exists to make imagery and spectrometry measurements near the LST diffraction limit, except in the far ultraviolet region. However, this region may be measured at lower resolution in order to obtain sufficient measurable flux.

By using the extremely accurate control system, most solar system objects can be measured in the 1 to 100  $\mu\text{m}$  region at near full optical resolution using uncooled detectors. By using this control system and raster scanning the object, a diffraction-limited IR image may be obtained with a relatively simple single uncooled detector.

Generally, the viewing capability calculations indicated that the LST can see all solar system objects for about 13 hours per day in 55 min increments, except for objects near the sun. Also, the data indicated that short-duration observation near the sun for such objects as Mercury, comets, and asteroids may be made by observing from the dark side of the earth to avoid sunlight entering the telescope during observations.

The following recommendations are given:

1. An LST system fully capable of making solar system observations should be included in the System Definition (Phase B) program activities. The results of this study indicate that a significant solar system observational capability may be obtained for little additional resources.
2. A tracking system capable of tracking objects at rates up to 73 arc sec per min having a travel capability of at least 220 arc sec during a single tracking period should be considered in the Phase B studies. Also, maximum LST slewing requirements should be based on slewing rates needed at the end of an observational period of viewing for objects near the sun.
3. The sun (45 degrees) and earth (15 degrees) viewing angle constraints should be reviewed for possible reduction in magnitude which would allow increased LST solar system object viewing, particularly near the sun.
4. A science instrumentation system study should be made to determine desirable instrumentation mixes (stellar and solar system) to provide effective LST system usage.

## APPENDIX C

### LST CONFIGURATION CONCEPT COMPARISONS



## LIST OF ILLUSTRATIONS

Figure	Title	Page
C-1.	LST configuration concepts . . . . .	C-2
C-2.	Unpressurized maintenance with small internal packages . . . . .	C-3
C-3.	Concept instrument of replacement using manipulator . . .	C-4
C-4.	Concept of manipulator grasping movements . . . . .	C-5
C-5.	Manipulator grasp of replaceable instrument or support system module package . . . . .	C-6
C-6.	Large external package concept . . . . .	C-7
C-7.	Large external package maintenance concept . . . . .	C-8



## APPENDIX C

### LST CONFIGURATION CONCEPT COMPARISONS

A comparison of several different concepts of the LST was made. Data from other sources was utilized, including the Goddard Space Flight Center (GSFC) LST Preliminary Analysis and Design Report (Revision A) dated December 1971. The concepts which were compared are shown in Figure C-1. The Three broad categories into which the concepts were divided were (1) on-orbit pressurized maintenance, (2) on-orbit unpressurized maintenance, and (3) earth return maintenance. All concepts except the "unpressurized concept with large external packages" which uses heat pipes are based on passive thermal control of the SIP and SSM systems.

The on-orbit pressurized maintenance concept is defined in considerable detail throughout this report. The earth return concept utilized for comparison did not differ significantly from the pressurized concept, either in systems design or overall configuration. Sketches of the on-orbit unpressurized maintenance concept with small internal packages are shown in Figures C-2 and C-3. Here, the basic SSM structure is a shell with cutouts for access to the instruments and systems, with the structure strengthened around the cutouts. Non-load-bearing hinged doors are provided over the instrument cutouts for environmental protection during the mission. Each instrument is replaceable individually, and packaging freedom and growth potential for the instruments are maximized by minimizing the size of the structural packages which must be removable as part of the instrument. The instruments are all removed radially, thus eliminating problems of axial removal. Figures C-4 and C-5 provide a concept of a manipulator end effector which could be used with such packages.

The SSM systems are packaged as individual components or in small groups of components, are mounted on the outer wall, and are removed radially by direct extraction. Environmental protection is provided on the removable plate to which the components are attached. The interior is largely open for packaging and growth optimization and for optimization of thermal control passive radiation. End-effectors to be used with the Shuttle manipulator for this concept should be fairly simple and straightforward. Guide rails and pins must be provided as well as small drogue-probe or other guide-in-and-capture mechanisms for each removable element. This is true for all LST concepts utilizing manipulators. Lights and TV cameras will be necessary on the manipulator boom, and it is assumed that these are standard on the Shuttle manipulator.

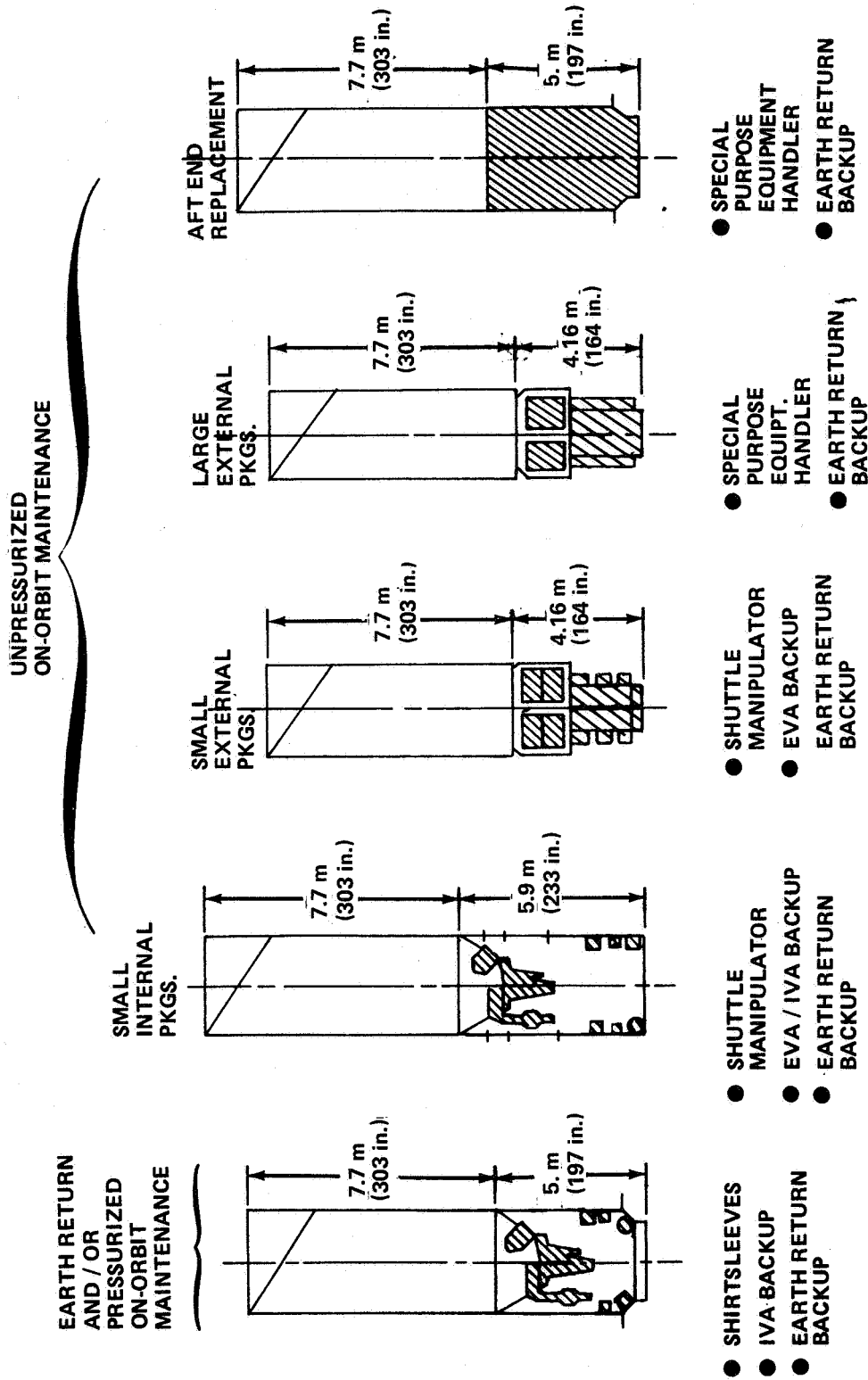


Figure C-1. LST configuration concepts.

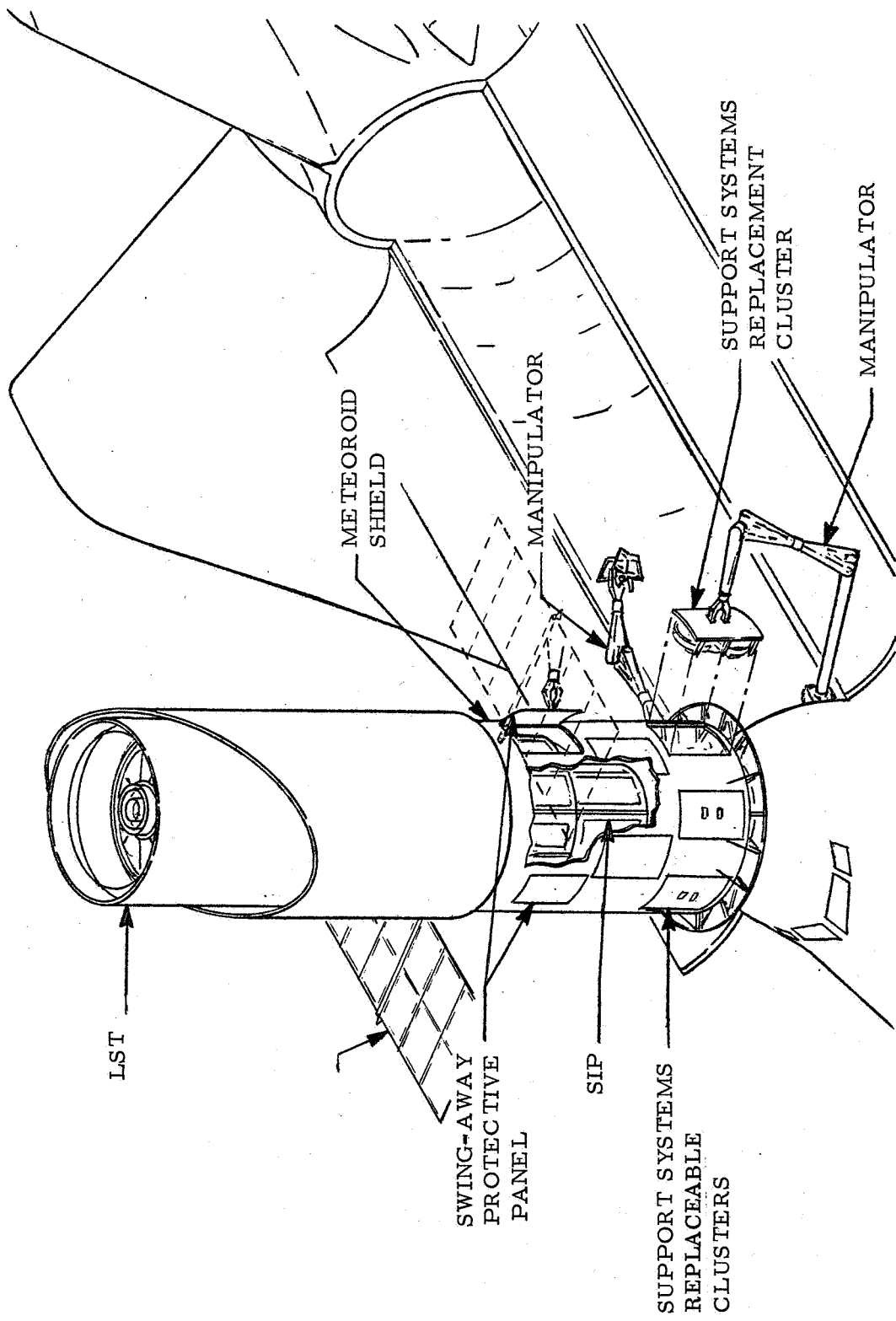


Figure C-2. Unpressurized maintenance with small internal packages.

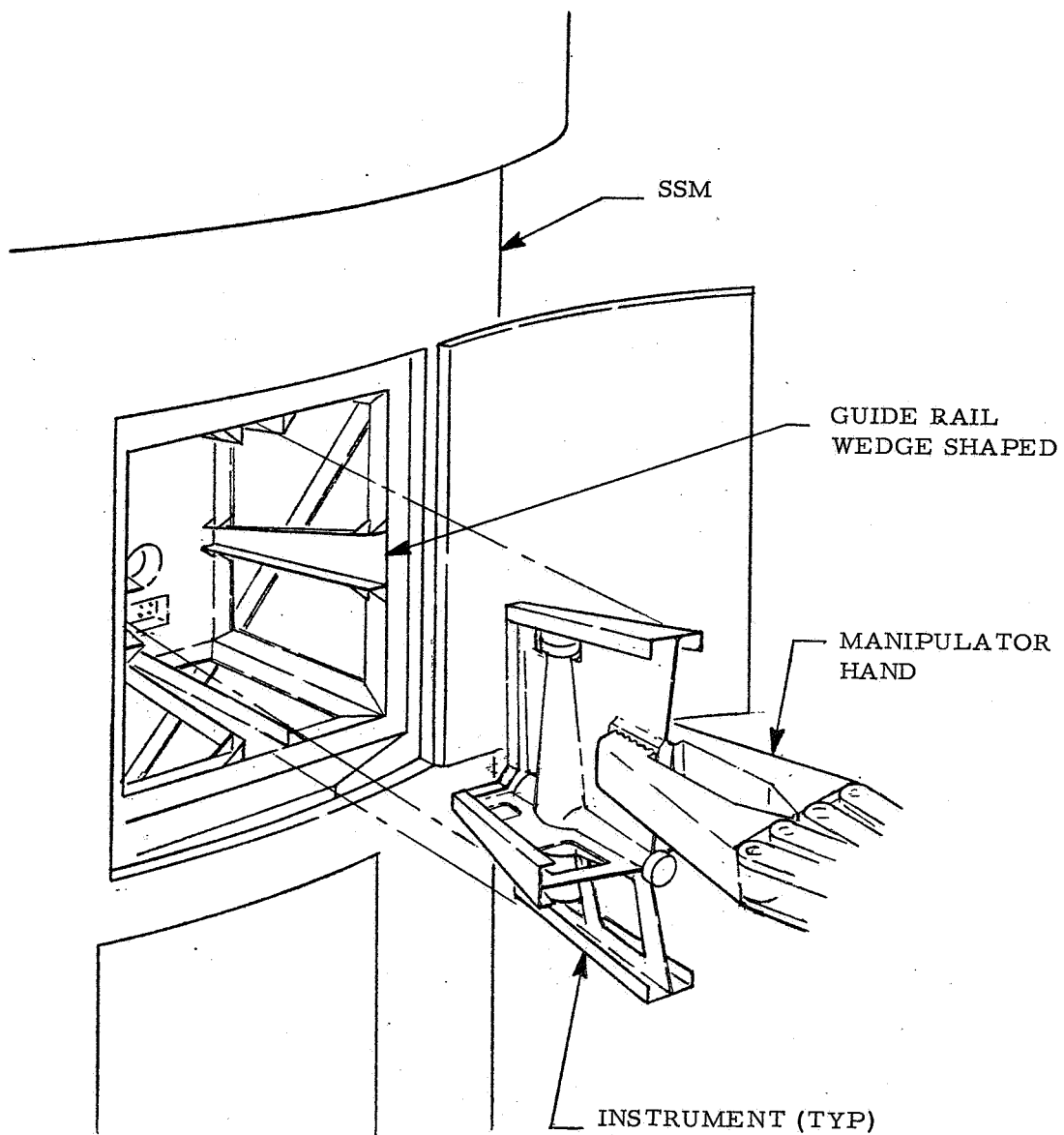
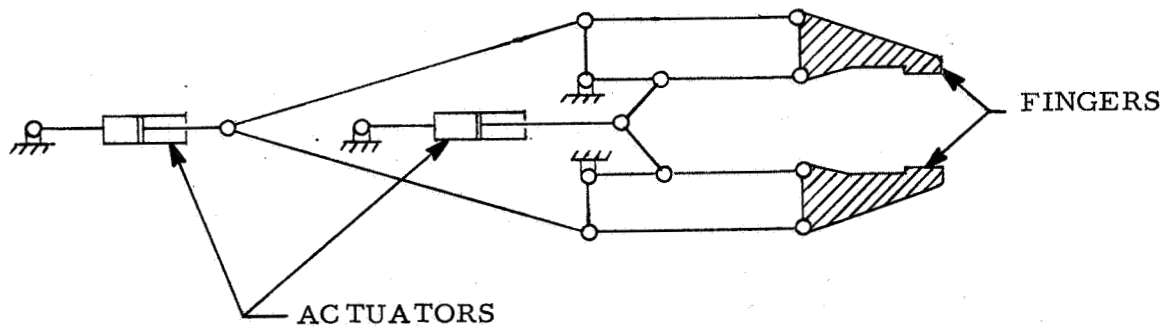
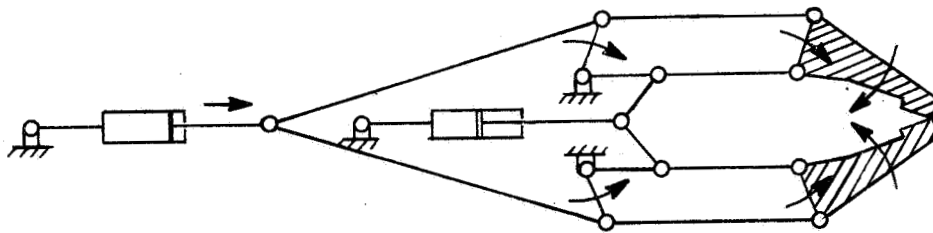


Figure C-3. Concept instrument of replacement using manipulator.

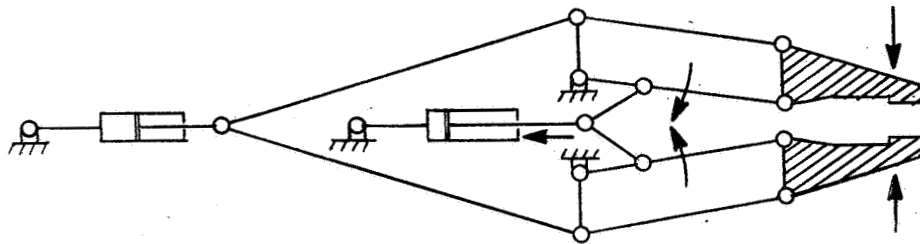
The on-orbit unpressurized concept with large external packages which was utilized in the comparison is shown in Figures C-6 and C-7. There are four instrument packages which are removed radially and one which is removed axially. Four large systems packages are mounted around the sides and are removed radially. Each of the systems and instrument packages is an enclosed



SIDE VIEW



PINCH MOTION



CLAMP MOTION

Figure C-4. Concept of manipulator grasping movements.

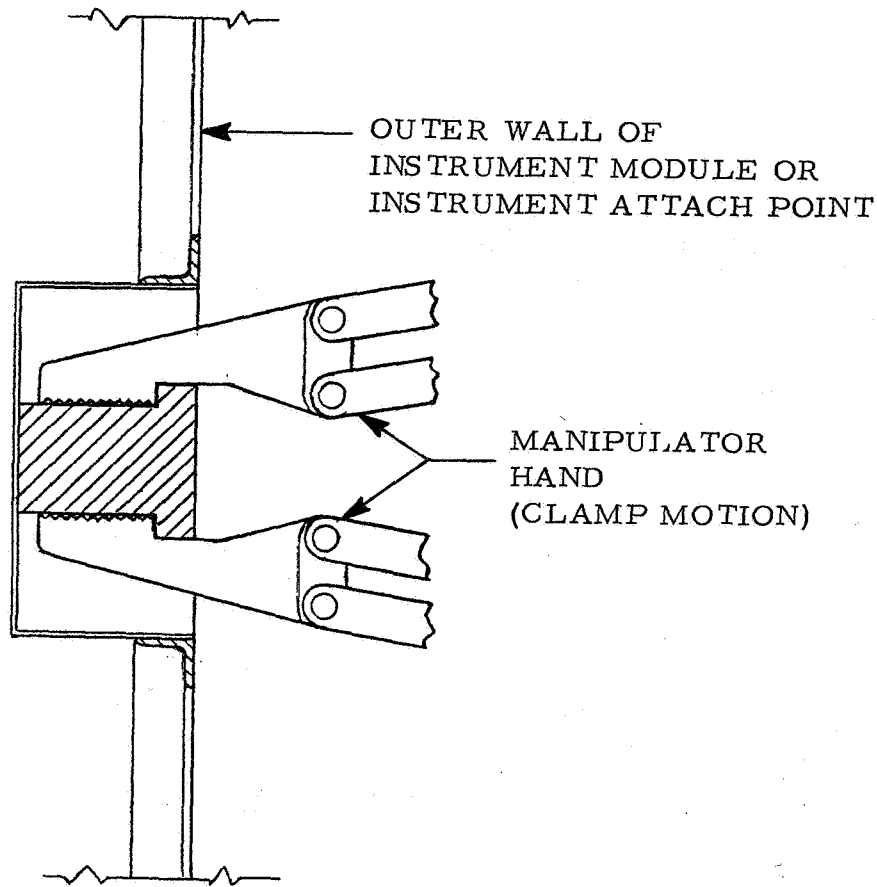


Figure C-5. Manipulator grasp of replaceable instrument or support system module package.

box with its own thermal control and mounting structure. The primary load-carrying structure is separate from these boxes and must be rigid enough to carry their loads and to prevent external loads from being introduced into them. Heat pipes are utilized for thermal control of this concept.

These boxes are large and it is anticipated that the type of end-effector which may be utilized with the Shuttle manipulator may not be adequate to perform removal and replacement of such boxes because of dynamics considerations, the fairly intricate movements required, etc. Instead, a larger, more complex device is assumed to be required; it would be designed to deploy itself and conduct removal and replacement of the packages "automatically." Guide rails, lights, cameras, etc., would be provided as part of such a device. Other concepts of such a device have been generated in the past and have been

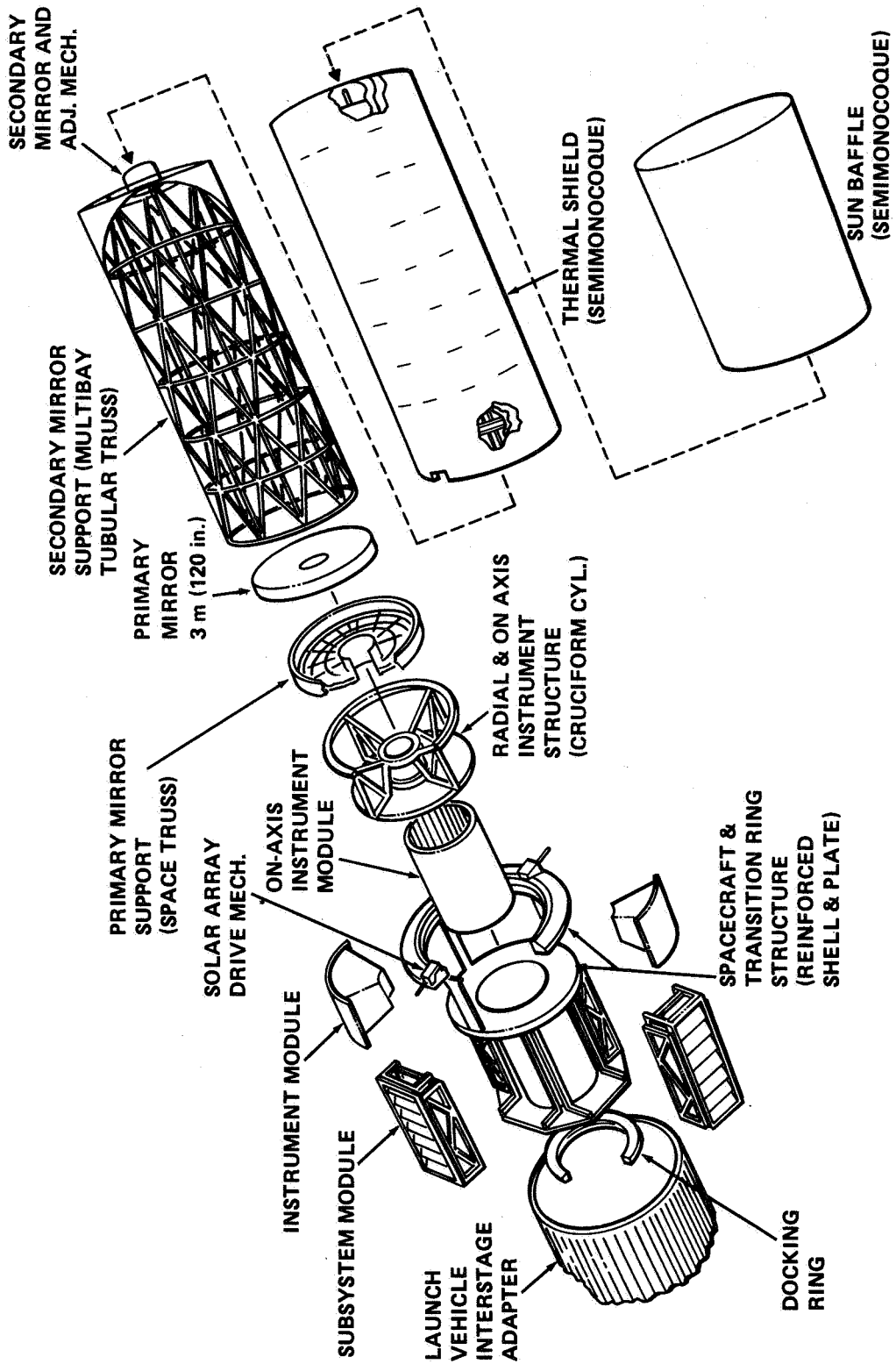


Figure C-6. Large external package concept.

UNPRESSURIZED ON-ORBIT CONFIG. WITH LARGE EXTERNAL PACKAGES.

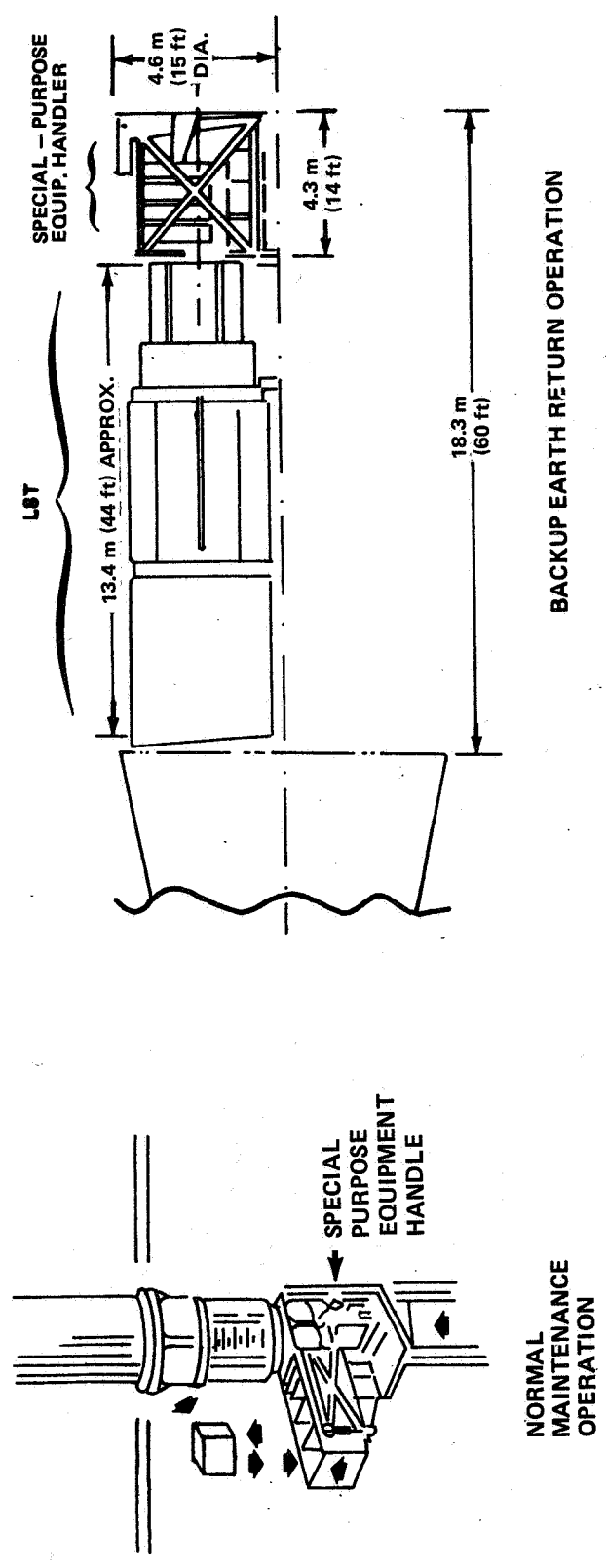


Figure C-7. Large external package maintenance concept.



termed "automated carousels," "end-effector assemblies," etc. The term "special purpose equipment handler (SPEH)" is utilized herein to denote such a device. For this particular LST concept, it is anticipated that two such devices would be required to effect the required maintenance — one for the radial packages and one for the on-axis package. A concept of one for the radial packages is shown in Figure C-7.

The on-orbit unpressurized maintenance concept with small external packages is a hybrid between the two other unpressurized concepts previously described, having some of the advantages and disadvantages of each. It was included primarily to complete the spectrum, and its exact configuration could be anywhere between the two extremes defined by the other two "bounding" concepts.

The aft end replacement concept consists of all the equipment aft of the main ring. Although massive, it requires essentially only one operation to effect the maintenance and, hence, it appears probable that maintenance utilizing this concept could be accomplished with the Shuttle manipulator and a fairly simple end effector. If the dynamics problem proved to be too great for such an operation, possibly an extra-stiff manipulator can be utilized, since intricate maneuvers are not required. At first glance, this concept may be thought to be extravagant in quantity of spares required. However, upon comparing it to the "large external package" concept, it can be seen that the quantity of spares required for that one is essentially the same as this one, with exception of the solar arrays (assuming a separate system in each package, and at least one life-limited component per system) for a scheduled maintenance visit which replaces all life-limited equipment and all instruments. In addition, the two SPEHs are not required, and maintenance consists of one operation rather than having to replace each package separately.

No significant difference in systems configuration or design was found between the on-orbit pressurized and the earth return concepts. The SSM pressure shell is sized by launch loads and not pressure requirements — hence, it would not change in the earth return configuration. The pressure bulkheads could be lightened by only 153 kg (338 lb) in the earth return configuration. (The forward one still must remain stiff enough to contribute shear stiffness to the entire LST and react against the figure adjustment jacks.) In addition, the contamination control and habitability items listed on the Master Equipment List (see Chapter IV of this volume) could be deleted. It was felt that these were fairly minor changes and did not constitute a significant difference in configuration.

The unpressurized on-orbit maintenance concepts provide a spectrum from multiple small systems packages replacement and individual instrument replacement to total aft end (SSM and SIP) replacement.

Table C-1 provides a comparison of the concepts, with the significant strong and weak points of each concept designated. On the basis of this concept comparison and the mission-sharing and maintenance studies documented in Chapter IV, the on-orbit pressurized concept was selected as a reference concept to study in more depth during Phase A.

It is significant to note that some of the key differences between the on-orbit pressurized concept of the LST and the Apollo or Skylab could make the LST significantly less expensive than those programs (see Chapter IV).





FOLD-OUT #3

<p>Shuttle Boatman which is Retained in Orbit (with a Titan Launch). Minimizes Reflections or Interference with Star Tracker FOV. Minimizes Thermal Interactions with SSM Surfaces. Minimizes Congestion in Main Ring Area (For General Pkg. or Replacement of Drive Motors Considerations). Minimizes Vibrations Introduced Near Optics or Instruments. Minimizes Probability of Shuttle RCS Damage or and of Array Damage or Maint. Interference (Arrays Retracted).</p>	<p>Arrays Cannot Remain Retracted, Since Interferes with Maintenance. Mounting Near Main Ring Area Near Aft End Allows Less Interference During Maintenance and Less Probability of Shuttle RCS Contam. of Deployed Arrays.</p>	<p>Arrays Interfere with Star Trackers</p>	<p>Retraction Of Array Is Desired, But Not Required, For Docking</p>	<p>General</p>
<p>Array Retraction or Jettison Req'd for Earth Return.</p>	<p>Emergency Mode Only - Do Not Have To Maintain RCS In Normal Maintenance Operations. Cold Gas Selected At Same Weight Penalty To Reduce Contamination and Corrosiveness Hazard (Leakage or Operations) As To Reduce Hazard to Man. In the Event of Req'd Maintenance, Each Config. Allows for Replacement of Bottles Rather Than Flowing High Pressure Gas, With the Following Differences:</p>	<p>No Fluid Line Connections Broken</p>	<p>Same As Column 1 Except Done On Ground</p>	<p>Same as Press. Maint. for Ground Operations.</p>
<p>Contingency Capability</p>	<p>Man in Shirtsleeves Provides Max. Adaptability to Unexpected Situations. IVA Leaks and Repair Leaks. IVA to do Maintenance (with Special Designs in Certain Areas, Could Fully Utilize as a Normal Mode). EVA to do External Maintenance. Max. Accessibility to EVA Earth Return</p>	<p>Smaller Pkgs. Allow Better Utilization of Man in Contingency. Some or All of Connections Could Be Made By Man in Contingency, or as Normal Mode (To Simplify End-Effector Design)</p>	<p>Earth Return</p>	<p>Earth Return. Note: Volume of Aft End Prevents Earth Return on Same Flight in Event of Contingency.</p>

Basic EVA Capability is Provided by Shuttle - Can Be Used in Emergency in Deploying or Retrieving LST of Any Configuration.

- a. Based on Requirement to use Titan as Backup Launch Vehicle and Shuttle as Primary Launch Vehicle; Logistics Quantities Based on Replacement of all Life-Limited Items and All Instruments.
- b. Man Can Perform Maintenance in IVA Mode (Pressure Suit) as Backup.
- c. Can Be Returned to Earth as Contingency Mode.
- d. Based on Passive Thermal Control System at 120% of Thermal Load.
- e. Light Shield Length can be Changed Somewhat.
- f. Shuttle Cargo Preferred but not Absolutely Required.
- g. Includes Pkg. for Pkg., etc.
- h. Required to be in Shuttle Cabin.
- i. End-Effector is a Device of Minimum-to-Moderate Complexity Which can be Attached to Shuttle Manipulator for Maintenance.
- j. Special-Purpose Equipment Handler (SPEH) is a Device (Probably Automated) of Fairly Major Complexity, such as an Automated Carousel, Which Performs Maintenance Essentially Without Shuttle Manipulators.
- k. Required to be in Shuttle Cargo Bay.

☐ Denotes Major Advantage  
☐☐ Denotes Major Disadvantage